



PhD-FSTC-2014-35
The Faculty of Sciences, Technology and Communication

DISSERTATION

Defense held on 28/10/2014 in Luxembourg

to obtain the degree of

DOCTEUR DE L'UNIVERSITÉ DU LUXEMBOURG EN INFORMATIQUE by Shree Krishna SHARMA

INTERWEAVE/UNDERLAY COGNITIVE RADIO
TECHNIQUES AND APPLICATIONS IN SATELLITE
COMMUNICATION SYSTEMS

Dissertation defense committee

Dr Björn Ottersten, dissertation supervisor
Professor, Université du Luxembourg

Dr Symeon Chatzinotas
Research Scientist, Université du Luxembourg

Dr Ulrich Sorger, Chairman
Professor, Université du Luxembourg

Dr Barry Evans
Professor, University of Surrey, United Kingdom

Dr Jacques Palicot, Vice Chairman
Professor, Supélec, Campus de Rennes, France

Abstract

The demand for precious radio spectrum is continuously increasing while the available radio frequency resource has become scarce due to spectrum segmentation and the dedicated frequency allocation of standardized wireless systems. This scarcity has led to the concept of cognitive radio communication which comprises a variety of techniques capable of allowing the coexistence of licensed and unlicensed systems over the same spectrum. In this context, this thesis focuses on interweave and underlay cognitive radio paradigms which are widely considered as important enablers for realising cognitive radio technology. In the interweave paradigm, an unlicensed user explores the spectral holes by means of some spectrum awareness methods and utilizes the available spectral availabilities opportunistically while in the underlay paradigm, an unlicensed user is allowed to coexist with the licensed user only if sufficient protection to the licensed user can be guaranteed. Starting with a detailed overview of the existing techniques, this thesis provides contributions in both theoretical and the practical aspects of these paradigms. This thesis is structured into two main parts as described below.

One of the important capabilities required for a cognitive radio transceiver is to be able to acquire the knowledge of its surrounding radio environment in order to utilize the available spectral opportunities efficiently. The higher the level of information it can acquire, the better becomes the spectrum utilization. In this context, the first part of this thesis focuses on spectrum awareness techniques such as spectrum sensing, signal to noise ratio estimation and sparsity order estimation which are useful for realizing interweave and underlay based cognitive transceivers as well as a hybrid cognitive transceiver, which overcomes the drawbacks of both the above approaches. The effects of noise and channel correlations, which are often neglected in the existing literature, are considered in our analysis. In the above context, firstly, we propose new sensing thresholds for the eigenvalue based sensing approach using recent results from random matrix theory in order to achieve the improved sensing in correlated scenarios. Then we study the signal to noise ratio estimation problem for both narrowband and wideband transceivers with the help of a detailed theoretical analysis under the signal plus noise hypothesis for a range of correlated scenarios. Subsequently, we study the problem of compressive sparsity order estimation in order to estimate the sparsity order of the carrier occupancy over the wide spectrum using a compressive sensing approach. In addition, we carry out the performance analysis of a hybrid cognitive transceiver which combines the spectrum sensing approach with a power control-based underlay approach.

The second part of this thesis introduces the concept of cognitive satellite communications which is a rather unexplored area in the literature despite its significant benefits to both satellite and terrestrial operators. This concept has been motivated due to the limited availability of the satellite spectrum as well as the continuously increasing demand of broadband multimedia, broadcast and interactive satellite services. Subsequently, we study the applications of various cognitive radio techniques in satellite communication systems focusing on the following two scenarios: (i) Hybrid cognitive satellite communication which deals with the spectral coexistence of satellite systems with the terrestrial systems, and (ii) Dual cognitive satellite communication which deals with the spectral coexistence of two satellite systems operating over the same coverage area. Understanding the characteristics of coexisting systems is of great importance while applying a suitable cognitive radio technique. In this context, this thesis exploits the specific characteristics of satellite systems in order to map a suitable cognitive radio technique to a specific scenario. For hybrid cognitive scenarios, we propose the following enabling techniques: (a) Interference modeling, (b) Harmful interference detection, (c) Cognitive beamforming including both transmit and receive beamforming, and (d) Dual-polarized spectrum sensing. Similarly, for dual cognitive scenarios, we propose the following techniques: (i) Cognitive interference alignment, (ii) Cognitive beamhopping, and (iii) Dual-polarized spectrum sensing. Finally, we provide interesting open research issues in the considered domain.

Acknowledgements

The research work leading to this thesis has been carried out under the valuable guidance of Professor Björn Ottersten and Dr. Symeon Chatzinotas in the Interdisciplinary Centre for Security, Reliability and Trust (SnT), during the years 2011-2014. This work has been supported by the National Research Fund (FNR), Luxembourg under AFR (Aid for Research Training) grant (Reference 3069102) under the framework of private-public partnership with SES, Luxembourg.

First off all, I would like to express my sincere gratitude to my supervisor Professor Björn Ottersten for giving me the opportunity to pursue doctoral studies and providing an excellent work environment. I am very much grateful to your continuous support, insightful suggestions, encouraging feedback and the freedom you provided in choosing the research directions. Likewise, I am highly indebted to my co-supervisor Dr. Symeon Chatzinotas for your excellent technical guidance and quick feedback on my research works. You have always motivated me in selecting valid research problems and modeling them correctly, and provided a lot of freedom in my research activities while also keeping track in good directions. The research work of this quality would not have been possible without your continuous support and guidance.

I would like to express my sincere thanks to Professor Barry Evans for taking your time to serve in my thesis supervisory committee and providing your helpful suggestions and critical comments which always helped to improve the quality of this research work. I would also like to thank Professor Jacques Palicot and Professor Ulrich Sorger for participating in the evaluation committee and providing valuable suggestions on my thesis. I must also thank Mr. Gerald Schlueter for serving as a contact person from SES and providing useful suggestions on practical aspects of the research problems.

I wish to thank my master's thesis supervisor Dr. Mohammad Patwary who encouraged me to pursue my career in scientific research and motivated me towards PhD study. I would like to acknowledge Dr. Sina Maleki, Dr. Joel Grotz, Dr. Jens Krause, Dr. Dimitrios Christopoulos for helpful discussions and suggestions during the course of our joint works. Further, I express my sincere thanks to Dr. Rajesh Kumar Sharma for providing me the opportunity to visit your research group at Ilmeanu university of technology and helpful discussions during our conversations. Many thanks to my colleagues at SnT for their direct and indirect supports during this period. The constant support of the entire administrative and human resource team during this period is greatly appreciated.

Most importantly, I wish to thank all my family members for their constant love and support. Special thanks go to my parents Mr. Hari Narayan and Mrs. Radha for always encouraging and supporting me in my studies and in whatever directions I have chosen in my life. I would like to thank my beloved wife Laxmi for your endless support, love and understanding. Further, I would like to express lots of love to our kids Shreela and Shriyans for making our life beautiful. Finally, I dedicate this thesis to my late grandfather Chop Narayan who always inspired me to work hard since my childhood but unfortunately, I missed him a lot during the course of this study.

Shree Krishna Sharma
Luxembourg, October 2014

Contents

Abstract	i
Acknowledgements	ii
Contents	iii
List of Figures	vii
List of Tables	x
Acronyms	xi
Notations	xiv
1 Introduction	1
1.1 Motivation and Scope	1
1.2 Organization, Problem Statements and Contributions	4
1.3 Research Methodology	15
1.4 Publications	15
2 Cognitive Communications	19
2.1 Background	19
2.2 Cognitive Techniques	20
2.2.1 Spectrum Awareness Techniques	21
2.2.2 Spectrum Exploitation Techniques	24
2.3 Spectrum Sensing	25
2.3.1 Classification and Related Literature	26
2.3.2 Sensing Principle for Cognitive Radio	29
2.3.3 Energy Detection	30
2.3.3.1 Basic Principle	30
2.3.3.2 Literature Review	31
2.3.4 Eigenvalue based Spectrum Sensing	32
2.3.4.1 Basic Principle	32
2.3.4.2 Literature Review	33
2.3.4.3 Existing Approaches	35
2.4 Underlay Techniques	36
2.4.1 Beamforming	36
2.4.1.1 Classification	37
2.4.1.2 Application in Cognitive Radio Networks	38
2.4.2 Interference Alignment	41
2.4.2.1 Interference Alignment Principle	41
2.4.2.2 Classification	42

2.4.2.3	Application in Cognitive Radio Networks	42
2.4.3	Cognitive Resource Allocation	44
2.4.4	Exclusion Zone	45
2.5	Regulatory and Standardization Activities	45
2.5.1	Regulatory Activities	45
2.5.2	Standardization and Development Activities	46
2.6	Chapter Conclusion	47
3	Cognitive Transceiver Design	48
3.1	Background	48
3.1.1	Conventional Sensing Approaches	48
3.1.2	Hybrid Approach	50
3.2	Spectrum Sensing	52
3.2.1	Problem Description	52
3.2.2	Methodology	53
3.2.3	Signal and Channel Model	54
3.2.4	Proposed Signal Condition Number based Sensing	56
3.2.4.1	Analysis	56
3.2.4.2	Sensing Threshold	58
3.2.5	Proposed Maximum Eigenvalue based Sensing	59
3.2.5.1	Analysis	59
3.2.5.2	Derivation of Sensing Threshold	60
3.2.6	Numerical Results	61
3.3	Signal to Noise Ratio Estimation	68
3.3.1	Background and Contributions	68
3.3.2	Analysis under Signal plus Noise Hypothesis	69
3.3.3	Methodology	69
3.3.4	Main Analytical Results	70
3.3.4.1	White Noise and Uncorrelated Channel	70
3.3.4.2	Correlated Noise and Uncorrelated Channel	70
3.3.4.3	Correlated Channel and White Noise	71
3.3.4.4	Correlated Channel and Correlated Noise	71
3.3.5	Proposed Signal to Noise Ratio Estimation Method	71
3.3.6	Numerical Results	73
3.4	Performance Analysis	77
3.4.1	Conventional Approaches	77
3.4.2	Hybrid Approach	79
3.4.2.1	Power Control	80
3.4.2.2	Throughput Maximization	81
3.4.3	Numerical Results	83
3.5	Chapter Conclusion	86
4	Wideband Cognitive Transceiver Design	88
4.1	Introduction	88
4.1.1	Wideband Cognitive Radio Challenges	88
4.1.2	Motivation and Contributions	90
4.1.3	Related Work	91
4.2	Sparsity Order Estimation	92
4.2.1	System and Signal Model	92
4.2.2	Analysis for Constant Power Case	93
4.2.3	Analysis for Varying Power Case	95
4.2.4	Analysis under Correlated Scenario	96

4.2.5	Proposed Compressive Sparsity Order Estimation	97
4.2.6	Numerical Results	99
4.3	Compressive Signal to Noise Ratio Estimation	104
4.3.1	Scenarios and Analysis	104
4.3.2	Correlated Noise Case	104
4.3.3	Correlated Multiple Measurement Vector Case	105
4.3.4	Proposed Approach	105
4.3.5	Numerical Results	105
4.4	Performance Analysis	108
4.4.1	Sweep-tune Approach	108
4.4.2	Filter-bank based Approach	109
4.4.3	Numerical Results	110
4.5	Chapter Conclusion	112
5	Cognitive Satellite Communications	114
5.1	Background	114
5.2	Cognition in Satellite Communication	115
5.3	Related Literature	118
5.3.1	Hybrid/Integrated Satellite-Terrestrial Systems	119
5.3.2	Dual Satellite Systems	120
5.3.3	Spectrum Sharing Techniques	121
5.4	Proposed Cognitive SatCom Scenarios	123
5.4.1	Hybrid Satellite-Terrestrial Coexistence	124
5.4.2	Dual Satellite Coexistence	125
5.5	Scenarios-Techniques Mapping	127
5.5.1	Techniques for Hybrid Coexistence Scenario	128
5.5.1.1	Interweave Techniques	128
5.5.1.2	Underlay Techniques	129
5.5.2	Techniques for Dual Satellite Coexistence	130
5.5.2.1	Interweave Techniques	130
5.5.2.2	Underlay Techniques	130
5.6	Spectrum Regulation and Standards	131
5.6.1	Spectrum Regulation	131
5.6.2	Standards	133
5.7	Discussion	133
5.8	Chapter Conclusion	135
6	Hybrid Cognitive Satellite Communications	137
6.1	Interference Modeling	137
6.1.1	Interference Power Level	138
6.1.2	Techniques Selection	140
6.2	Interference Detection	143
6.2.1	Scenario and Problem Description	143
6.2.2	Problem Formulation	145
6.2.3	Energy Detection-based Interference Detection	146
6.2.4	Numerical Results	147
6.3	Dual Polarized Spectrum Sensing	151
6.3.1	System and Signal Model	152
6.3.2	Energy Detection for Single Antenna Case	153
6.3.3	Proposed Energy Detection Approach for Dual Antenna Case	154
6.3.4	Combining Techniques for Dual Polarized Channel	155
6.3.4.1	Selection Combining	155

6.3.4.2	Equal Gain Combining	156
6.3.5	Numerical Results	157
6.4	Cognitive Beamforming	159
6.4.1	Cognitive Beamforming for Uplink Coexistence Scenario	160
6.4.1.1	Signal Model	160
6.4.1.2	Applicable Techniques	161
6.4.1.3	Proposed Spatial Filtering Approach	162
6.4.1.4	Numerical Results	164
6.4.2	Cognitive Beamforming for Downlink Coexistence Scenario	165
6.4.2.1	Signal Model	166
6.4.2.2	Proposed Techniques	167
6.4.2.3	Numerical Results	169
6.5	Chapter Conclusion	173
7	Dual Satellite Cognitive Communications	174
7.1	Cognitive Interference Alignment	174
7.1.1	Related Literature and Contributions	175
7.1.2	System Model	175
7.1.3	Signal and Channel Model	177
7.1.4	Coexistence Techniques	179
7.1.5	Interference Alignment Types	180
7.1.6	Numerical Results	182
7.2	Cognitive Beamhopping	185
7.2.1	Existing Multibeam Systems	186
7.2.2	Proposed System and Techniques	187
7.2.2.1	System Model	187
7.2.2.2	Applicable Techniques	188
7.2.3	Signal and Channel Model	189
7.2.4	System Performance	190
7.2.4.1	Throughput Analysis	190
7.2.4.2	Power Control Method	191
7.2.4.3	Exclusion Zone Method	192
7.2.5	Results and Discussion	192
7.3	Dual Polarized Sensing	200
7.3.1	System and Signal Model	201
7.3.2	Combining Techniques	202
7.3.3	Results and Discussion	204
7.4	Chapter Conclusion	206
8	Conclusions, Discussion and Future Recommendations	208
8.1	Conclusive Summary	208
8.2	Discussion	211
8.3	Future Recommendations	213
8.3.1	Research Issues (Part I)	213
8.3.2	Research Issues (Part II)	215
A	Random Matrix Theory Preliminaries	219
B	Proofs of Theorems	221
Bibliography		226

List of Figures

2.1	A simplified cognitive cycle	21
2.2	Mapping of spectrum awareness techniques with spectrum exploitation techniques	22
2.3	Illustration of the database approach	23
2.4	Classification of SS techniques	26
2.5	Schematic of the cooperative SS scenario	29
2.6	ED detector (a) Classical approach, and (b) Periodogram approach	31
2.7	Stages involved in eigenvalue based detection	33
2.8	Classification of underlay techniques	37
2.9	Illustration of IA principle in a cellular network	42
2.10	Illustration of EZ approach (SUs are not allowed to reuse primary spectrum inside the EZ)	45
3.1	Secondary frame structure for periodic SS	49
3.2	Secondary frame structure for simultaneous sensing and transmission	49
3.3	Secondary frame structure for the hybrid approach (with periodic SS)	50
3.4	Schematic of the secondary frame structure for the hybrid approach (with simultaneous sensing/Tx) .	50
3.5	Half duplex architecture for a CR transceiver	51
3.6	Full duplex architecture for a CR transceiver	51
3.7	Block diagram of a wideband SDR receiver	52
3.8	Sensing performance of different methods in white and correlated noise scenarios ($\beta = 8, \rho = 0.6, N = 80$)	62
3.9	Sensing performance versus SNR with (3.12) and (3.13) ($\beta = 6, \rho = 0.5, N = 60$)	62
3.10	Sensing performance versus correlation coefficient (SNR = -6 dB, $\beta = 6, N = 60$)	63
3.11	Probability of a false alarm versus correlation coefficient (SNR = -6 dB, $\beta = 6, N = 60$)	63
3.12	Cumulative distribution functions of decision statistics under H_0 hypothesis and thresholds for white and correlated noise scenarios ($\beta = 6, \rho = 0.5, N = 60$)	64
3.13	Probability of correct decision versus number of samples (SNR = -6 dB, $M = 15, \rho = 0.45$)	64
3.14	P_d versus SNR (dB) for MME and EME techniques in channel uncorrelated and correlated scenarios ($\beta = 6, P_f = 0.07, SCN = 3, N = 60$)	65
3.15	Probability of correct decision versus SNR for asymptotic MME method ($\beta = 6, SCN = 3, N = 60$) .	65
3.16	Sensing performance versus fractional sampling rate ($N = 60, \text{SNR} = -5 \text{ dB}$)	66
3.17	Theoretical and simulated c.d.f. plots for different random variables ($N = 300, \beta = 1, \rho = 0.5$) .	66
3.18	False alarm deviation versus ρ ($N = 100, \beta = 2, P_f = 0.001$)	66
3.19	Probability of correct decision versus SNR ($N = 100, \beta = 2, P_f = 0.07, \rho = 0.5$)	67
3.20	Theoretical and simulated eigenvalue distribution of received signal for different cases: (a) uncorrelated channel and white noise, (b) uncorrelated channel and correlated noise, (c) correlated channel and white noise, (d) correlated channel and correlated noise ($\beta = 1, N = 100$)	74
3.21	ME versus SCN of covariance matrix for different cases ($\beta = 1, N = 100, \text{SNR} = 3 \text{ dB}$)	74
3.22	ME versus SNR for different cases ($\beta = 1, N = 100, SCN = 4$)	75
3.23	Normalized MSE versus SNR for SNR estimation using the proposed technique ($N = 100, \beta = 1$) .	75
3.24	Normalized MSE versus SNR with and without knowledge of channel/noise correlation ($\beta = 1, SCN = 4, N = 100$)	76
3.25	Normalized MSE versus SNR for different cases ($\beta = 1, SCN = 4, N = 100$)	77

3.26 Secondary throughput versus sensing time ($I_T = -130$ dBW, $\bar{P}_d = 0.9$, $T = 100$ ms, $\text{SNR}_p = -15$ dB, $\text{SNR}_s = 20$ dB)	84
3.27 Probability of false alarm versus sensing time ($\bar{P}_d = 0.99$, $T = 100$ ms, $\text{SNR}_s = 20$ dB, $I_T = -130$ dBW)	84
3.28 Secondary throughput versus PU interference threshold for different approaches ($\bar{P}_d = 0.9$, $T = 100$ ms, $\text{SNR}_p = -15$ dB, $\text{SNR}_s = 20$ dB, $\tau = 2.5$ ms)	85
3.29 Secondary throughput versus target P_d for different approaches ($I_T = -130$ dBW, $T = 100$ ms, $\text{SNR}_p = -24$ dB, $\text{SNR}_s = 20$ dB, $\tau = 2.5$ ms)	85
3.30 Secondary throughput versus PU SNR for different approaches ($\bar{P}_d = 0.9$, $I_T = -130$ dBW, $T = 100$ ms, $\text{SNR}_s = 20$ dB, $\tau = 2.5$ ms)	85
4.1 Theoretical and simulated eigenvalue distribution of $\hat{\mathbf{R}}_{\mathbf{Y}}(N)$, where $\mathbf{Y} = \mathbf{AU}\sqrt{p}\mathbf{BX} + \mathbf{Z}$ ($\rho = 0.8$, $\sigma = 0.6$, $N = 100$, $M = 100$, $K = 100$, $\text{SNR} = 0$ dB)	100
4.2 Normalized SOEE versus sparsity order with compressive and full measurements for constant received power scenario ($\text{SNR} = 2$ dB, $N = 100$)	100
4.3 Normalized SOEE versus SNR with compressive and full measurements for constant received power scenario ($\sigma = 0.6$, $N = 100$)	101
4.4 Normalized SOEE versus compression ratio ρ ($\text{SNR} = 2$ dB, $\sigma = 0.6$, $N = 100$)	101
4.5 Theoretical and simulated eigenvalue distribution of $\hat{\mathbf{R}}_{\mathbf{Y}}(N)$, where $\mathbf{Y} = \mathbf{AU}\mathbf{P}^{1/2}\mathbf{BX} + \mathbf{Z}$ (DR = 6.02 dB, $N = 100$, $M = 100$, $K = 100$, $\bar{p} = 7.78$ dB)	102
4.6 Normalized SOEE versus sparsity order with compressive and full measurements for varying power scenario (DR = 6.02 dB, $N = 100$, $\bar{p} = 7.78$ dB)	102
4.7 Theoretical and simulated eigenvalue distribution of $\hat{\mathbf{R}}_{\mathbf{Y}}(N)$, where $\mathbf{Y} = \mathbf{AU}\Theta^{1/2}\mathbf{BX} + \mathbf{Z}$ ($\rho = 0.8$, $\sigma = 0.6$, $N = 100$, $M = 100$, $K = 100$, SCN = 4)	103
4.8 Normalized SOEE versus sparsity order with compressive and full measurements for correlated and uncorrelated scenarios (SCN = 4, $N = 100$, $\text{SNR} = 0$ dB)	103
4.9 Theoretical and simulated eigenvalue distributions of $\hat{\mathbf{R}}_{\mathbf{Y}}(N)$ ($\varsigma = 0.6$, $\rho = 0.8$, $\sigma = 0.6$, $N = 100$, $\text{SNR} = 2$ dB) (a) $\mathbf{Y} = \mathbf{AU}\sqrt{p}\Theta^{1/2}\mathbf{BX} + \mathbf{Z}$ (b) $\mathbf{Y} = \mathbf{AU}\sqrt{p}\mathbf{BX} + \Theta^{1/2}\mathbf{Z}$	106
4.10 Normalized MSE versus SNR for the correlated MMV scenario ($\varsigma = 0.6$, $\rho = 0.8$, $\sigma = 0.6$, $N = 100$)	107
4.11 Normalized MSE versus SNR for the correlated noise scenario ($\varsigma = 0.6$, $\sigma = 0.6$, $N = 100$)	107
4.12 Frame structure of periodic SS based CR for wideband scenario	109
4.13 Frame structure of full duplex SS based CR for wideband scenario	109
4.14 Secondary throughput versus sensing time for sweep-tune approach based wideband scenario ($I_T = -130$ dBW, $\bar{P}_d = 0.9$, $T = 100$ ms, $\text{SNR}_p = -24$ dB, $\text{SNR}_s = 20$ dB)	111
4.15 Secondary throughput versus sensing time for filter bank detection based wideband scenario ($I_T = -130$ dBW, $\bar{P}_d = 0.9$, $T = 100$ ms, $\text{SNR}_p = -24$ dB, $\text{SNR}_s = 20$ dB)	111
4.16 Secondary throughput versus interference threshold for sweep-tune approach based wideband scenario ($\tau = 8$ ms, $\bar{P}_d = 0.9$, $T = 100$ ms, $\text{SNR}_p = -24$ dB, $\text{SNR}_s = 20$ dB)	111
4.17 Secondary throughput versus interference threshold for filter bank detection based wideband scenario ($\tau = 2.5$ ms, $\bar{P}_d = 0.9$, $T = 100$ ms, $\text{SNR}_p = -24$ dB, $\text{SNR}_s = 20$ dB)	112
5.1 Different transmission modes for hybrid satellite-terrestrial cognitive scenario	124
5.2 Hybrid satellite cognitive scenario for multiuser link coexistence	125
5.3 Hybrid satellite cognitive scenario for single user coexistence	125
5.4 Dual satellite cognitive scenario for two GEO coexistence	127
5.5 Dual satellite scenario for GEO and MEO/LEO coexistence	127
6.1 Coverage of Europe with multispot beams	138
6.2 Interference power versus latitude and distance	139
6.3 Different co-existence models	142
6.4 Coexistence of FSS satellite downlink and microwave link	143

6.5	Front end of satellite terminal with additional dipole antenna and corresponding desired/interfering links	144
6.6	Probability of detection versus probability of false alarm ($\tau = 2$ ms, $d = 1$ km)	148
6.7	Probability of detection versus distance between FS Tx and FSS terminal ($\tau = 2$ ms, $P_f = 0.01$)	150
6.8	Total signal strengths received by dipole and DVB-S2 chains for different EIRP values	150
6.9	Sample complexity versus noise uncertainty while using the ED technique (target $P_d = 0.9$, target $P_f = 0.01$)	151
6.10	System Model for the considered dual-polarized SS	152
6.11	Block diagram of SC and EGC techniques for SS	155
6.12	P_m versus P_f for different cases (SNR = -4 dB, dof = 60, Number of Monte Carlo realizations ($N = 10^4$)	157
6.13	P_m versus P_f for SC and EGC techniques in MIMO Rayleigh fading channel (SNR = -4 dB, dof = 60, $N = 10^4$)	158
6.14	P_m versus XPR for $P_f = 0.07$ (dof = 60, $N = 2 \times 10^4$)	159
6.15	Layout of the considered scenario (N,W,S and E denote North, West, South and East)	161
6.16	Response versus azimuth angle for LCMV and MVDR beamformers, $M = 20$, $K = 17$	164
6.17	SINR versus Azimuth angles plot of LCMV and MVDR beamformers for the considered scenario, $M = 20$, $K = 17$	165
6.18	SINR versus number of interferers for proposed scenario with beamformers designed for $M = 18$	165
6.19	Hybrid satellite-terrestrial downlink coexistence scenario	166
6.20	Layout of the considered scenario (N,W,S and E denote North, West, South and East)	166
6.21	Beam patterns of different transmit beamforming techniques	171
6.22	SINR comparisons of the modified LCMV and standard LCMV in the considered scenario	171
6.23	Transmit power in the desired direction versus power threshold using optimization problem (6.66)	172
6.24	Worst case SU rate versus PU distance from the BS	172
6.25	Worst case SU rate versus PU distance and angular deviation from the sector of interest	172
7.1	Graphical representation of the considered dual satellite coexistence system	176
7.2	Normalized system rate versus number of SAT2 beams N	184
7.3	Primary to secondary rate ratio versus number of SAT2 beams N	184
7.4	Primary protection ratio versus number of SAT2 beams N	184
7.5	Spectral coexistence scenario of two multibeam satellites in the same geographical region	187
7.6	Throughput comparison of different systems ($K = 3$, $N_b = 19$, $P_{st} = P_{pt}$)	194
7.7	Spectral efficiency versus secondary power in cognitive beamhopping system ($N_b = 37$, $P_{pt} = 10\text{dBW}$)	194
7.8	Primary rate protection ratio versus secondary power in cognitive beamhopping system ($N_b = 37$, $P_{pt} = 10\text{dBW}$)	195
7.9	SE versus number of SUs in cognitive beamhopping system with full frequency reuse ($K = 7$, $N_b = 37$, $P_{pt} = 10\text{dBW}$)	196
7.10	SE versus number of SUs in cognitive beamhopping system with frequency sharing among the SUs ($K = 7$, $N_b = 37$, $P_{pt} = 10\text{dBW}$)	196
7.11	SE versus EZ radius (dB) for cognitive beamhopping system considering single SU in the center of inactive primary beam ($K = 7$, $N_b = 37$, $P_{pt} = P_{st} = 10\text{dBW}$)	197
7.12	Comparison of SE versus EZ radius (dB) for different SU positions (considering multiple SUs within each inactive primary beam) ($K = 7$, $N_b = 37$, $P_{pt} = 10\text{dBW}$, $P_{st} = P_{pt}/4$)	198
7.13	Comparison of power control and EZ methods $K = 7$, $N_b = 37$	198
7.14	Dual satellite cognitive scenario	201
7.15	Block diagram of MRC technique for SS	202
7.16	Block diagram of OPBC technique for SS	203
7.17	Comparison of CROC curves for different combining techniques	204
7.18	Comparison of CROC curves for different values of SNR	205
7.19	Probability of detection versus value of α_p	206

List of Tables

1.1	Causes of channel/noise correlation in multi-dimensional scenarios	5
2.1	List of IA Techniques	43
3.1	Look up table for SNR estimation	73
3.2	Throughput Calculation for Various Cases in the narrowband scenario	83
4.1	Lookup table for sparsity order estimation for the considered scenarios ($\rho = 0.8$)	101
4.2	Lookup table for SNR estimation for correlated MMV scenario ($\varsigma = 0.6, \rho = 0.8, \sigma = 0.6$ SNR = 2 dB)	106
5.1	Possible Frequency bands for spectral coexistence of hybrid satellite-terrestrial and dual satellite networks	116
5.2	Current frequency allocation in Ka band segment (27.5 – 30 GHz uplink, 17.3 – 20.2 GHz downlink)	116
5.3	Possible spectral coexistence scenarios for cognitive SatComs	123
5.4	Conventional approaches and possible cognitive solutions for considered coexistence scenarios	128
6.1	Simulation & Link Budget Parameters	140
6.2	Features of main CR techniques	142
6.3	Simulation and link budget parameters	149
6.4	Sensing time calculation for ED detector	149
7.1	Simulation parameters for capacity results	183
7.2	Simulation and link budget parameters	193
7.3	Throughput comparison for different scenarios in a cognitive beamhopping system	195

Acronyms

ACM	Adaptive Coding and Modulation
ACI	Adjacent Carrier Interference
ADC	Analog to Digital Converter
a.e.p.d.f.	asymptotic eigenvalue probability density function
AWGN	Additive White Gaussian Noise
AGC	Automatic Gain Control
BC	Broadcast Channel
BEM	Block Edge Mask
BPF	Band Pass Filter
BS	Base Station
BSS	Broadcasting Satellite Services
BT	British Telecom
BSRS	Blind Standard Recognition Sensor
CB	Cognitive Beamforming
c.c.s.	complex circularly symmetric
c.d.f.	cumulative distribution function
CD	Cyclostationary feature Detector
CDR	Constant Detection Rate
CDMA	Code Division Multiple Access
CGC	Complementary Ground Component
CR	Cognitive Radio
CS	Compressive Sensing
CSI	Channel State Information
CFAR	Constant False Alarm Rate
CPC	Cognitive Pilot Channel
CROC	Complementary Receiver Operating Characteristics
CRS	Cognitive Radio System
DA	Data-aided
DCN	Demmel Condition Number
DB	Database
DFS	Dynamic Frequency Selection
DoA	Direction of Arrival
DR	Dynamic Range
DSA	Dynamic Spectrum Access
DSP	Digital Signal Processor
DTH	Direct To Home
DVB-S	Digital Video Broadcasting over Satellite
DVB-SH	DVB- Satellite services to Handhelds
DVB-RCS	DVB- Return Channel via Satellite
dof	degree of freedom
DBS	Direct Broadcast Satellite
EC	European Commission
ED	Energy Detection
EIRP	Effective Isotropic Radiated Power

EGC	Equal Gain Combining
EME	Energy to Minimum Eigenvalue
EPFD	Effective Power Flux Density
ETSI	European Telecommunication Standards Institute
EVD	Eigenvalue Decomposition
ESA	European Space Agency
EZ	Exclusion Zone
FBS	Femtocell Base Station
FCC	Federal Communication Commission
FDM	Frequency Division Multiplexing
FDMA	Frequency Division Multiple Access
FDD	Frequency Division Duplex
FPGA	Field Programmable Gate Array
FS	Fixed Service
FSS	Fixed Satellite Services
FFT	Fast Fourier Transform
FBMC	Filter Bank Multi-Carrier
GEO	Geostationary
GSC	Global Standards Cooperation
GLRT	Generalized Likelihood Ratio Test
HAPS	High Altitude Platform Station
HDTV	High Definition Television
HNP	Hidden Node Problem
HP	Hewlett-Packard
IA	Interference Alignment
IC	Interference Channel
IF	Intermediate Frequency
IFFT	Inverse Fast Fourier Transform
i.i.d.	independent and identically distributed
ITU-R	International Telecommunication Union-Radiocommunication
ISP	Intelligent Signal Processing
LCMV	Linearly Constrained Minimum Variance
LoS	Line of Sight
LEO	Low Earth Orbit
LO	Local Oscillator
LTE	Long-Term Evolution
LNA	Low Noise Amplifier
MAC	Medium Access Control
MC	Monte Carlo
MBAN	Mobile Body Area Network
MEO	Medium Earth Orbit
MP	Marchenko-Pastur
MJD	Multibeam Joint Decoding
MUD	Multiuser Detection
MVDR	Minimum Variance Distortionless Response
MMV	Multiple Measurement Vector
ME	Maximum Eigenvalue
MES	Mobile Earth Station
MIMO	Multiple Input Multiple Output
MRC	Maximum Ratio Combining
MME	Maximum to Minimum Eigenvalue
MFPB	Multiple Feeds Per Beam
MSS	Mobile Satellite Services
MSE	Mean Square Error
NDA	Non Data-aided

NGEO	Non Geostationary
NGN	Next Generation Network
NP	Neyman Pearson
OFDM	Orthogonal Frequency Division Multiplexing
OPBC	Optimum Polarization Based Combining
OFCOM	Office of Communications
OSI	Open Systems Interconnection
PC	Personal Computer
PR	Primary Receiver
PT	Primary Transmitter
PU	Primary User
PMSE	Program Making and Special Events
QoS	Quality of Service
RPD	Reconfigurable Polarization Detection
RR	Radio Regulations
RMT	Random Matrix Theory
REM	Radio Environment Map
Rx	Receiver
RF	Radio Frequency
ROC	Receiver Operating Characteristics
SatCom	Satellite Communication
SC	Selection Combining
SCN	Signal Condition Number
SE	Spectral Efficiency
SDMA	Space Division Multiple Access
SLE	Scaled Largest Eigenvalue
SDR	Software Defined Radio
SINR	Signal to Interference plus Noise Ratio
SMV	Single Measurement Vector
SISO	Single Input Single Output
SIMO	Single Input Multiple Output
SFPB	Single Feed Per Beam
SR	Secondary Receiver
ST	Secondary Transmitter
SNR	Signal to Noise Ratio
SS	Spectrum Sensing
SOE	Sparsity Order Estimation
SOEE	Sparsity Order Estimation Error
SU	Secondary User
TDMA	Time Division Multiple Access
TDD	Time Division Duplex
TTC	Telemetry, Tracking and Control
Tx	Transmitter
TVWS	TV White Space
TW	Tracy-Widom
TWC	Tracy-Widom Curtiss
ULA	Uniform Linear Array
UWB	Ultra Wide-Band
VSAT	Very Small Aperture Terminal
WHN	Wireless Heterogeneous Network
WRAN	Wireless Regional Access Network
WRC	World Radio Conference
XPI	Cross Polar Isolation
XPR	Cross Polar Ratio
XPD	Cross Polar Discrimination

Notations

I	Identity matrix
0	Zero matrix
$E[\cdot]$	Expectation
$O(\cdot)$	Order
$(\cdot)^T$	Transpose
\equiv	Equivalent
\leq	Less than or equal
\approx	Approximately equal
\sim	Distributed as
\triangleq	Equal by definition
$ \cdot $	Absolute
\odot	Hadamard product
\otimes	Kronecker product
\mathbb{C}	Complex numbers
$\mathbb{I}_{n \times m}$	$n \times m$ matrix of ones
$(\cdot)^\dagger$	Conjugate transpose
$(\cdot)^*$	Complex conjugate
$(z)^+$	$\max(0, z)$
P_d	Probability of detection
P_f	Probability of false alarm
P_m	Probability of miss detection
H_0	Noise only hypothesis
H_1	Signal plus noise hypothesis
$\mathbf{X}_{i,j}$	(i, j) th element of \mathbf{X}
$f_{\mathbf{X}}(\cdot)$	Eigenvalue distribution function of \mathbf{X}
$\mathbf{R}_{\mathbf{X}}$	Covariance matrix of \mathbf{X}
$\mathcal{S}_{\mathbf{X}}$	Stieltjes transform of \mathbf{X}
$\mathcal{R}_{\mathbf{X}}$	R transform of \mathbf{X}
$\Sigma_{\mathbf{X}}$	Σ transform of \mathbf{X}
$\lambda_{\max}(\cdot)$	Maximum eigenvalue
$\lambda_{\min}(\cdot)$	Minimum eigenvalue
$\lambda_{\text{avg}}(\cdot)$	Average eigenvalue
$\theta_{3\text{dB}}$	3dB beamwidth
I_T	Interference threshold
N_0	Noise power
λ_{th}	Sensing threshold
χ_{cx}	Cross polar ratio (XPR)
${}_1F_1$	Confluent hypergeometric function
$Q_u(\cdot, \cdot)$	Generalized Marcum Q-function
$\Gamma(\cdot)$	Gamma function
$\Gamma(\cdot, \cdot)$	Incomplete Gamma function
J_m	m th order Bessel's function of the first kind

Chapter 1

Introduction

1.1 Motivation and Scope

Radio frequency spectrum is a limited natural resource and needs to be utilized efficiently in order to provide a variety of services to a large number of users with higher data rates. The demand for this precious radio resource is increasing due to a rapidly expanding market of wireless broadband and multimedia users, and applications. However, the available frequency resources are becoming scarce due to spectrum segmentation and the dedicated frequency allocation of the standardized wireless systems. As user demands for broadband services and higher data rates increase rapidly, efficient spectrum usage is becoming a critical issue. On the other hand, several spectrum occupancy measurement campaigns carried out at different parts of the world indicate that a significant amount of the wireless spectrum remains under-utilized over a wide range of radio frequencies in the spatial and temporal domains [1]. Further, Federal Communication Commission (FCC) measurements have indicated that many licensed frequency bands remain unused nearly ninety percent of the time [2]. In this context, Cognitive Radio (CR) communication has emerged as a promising solution to address the spectrum scarcity problem by exploring spectral opportunities in the primary licensed spectrum in several domains, thus facilitating the secondary unlicensed spectrum access. Towards realizing future spectrum aware communications, the CR, firstly proposed in [3], is considered an important candidate as it is aware of its surrounding Radio Frequency (RF) environment and can adjust its operating parameters such as transmit power, modulation and coding scheme etc., dynamically. The FCC has already launched a secondary markets initiative with the aim of removing the regulatory barriers and promoting the development of secondary markets in spectrum usage rights among wireless service providers [4]. As an initial step towards the CR communications, U.S. FCC and U.K. Office of Communications (OFCOM) have already opened up significant parts of the TV spectrum for unlicensed use [5–7] based on a geolocation database approach, and several other regulators are examining the possibilities of using TV whitespaces in different parts of the world [8]. Further, several industry players are putting significant efforts towards the realisation of CR technology. To this end, industries such as Alcatel-Lucent, Ericsson and Motorola from the mobile equipment industry, British Telecom (BT) and Orange from network operators, Hewlett-Packard (HP) and Dell from the computer industry, Philips and Samsung from the consumer electronics industry, and Microsoft and Google from the Internet/software industry etc., carry out active research and development efforts in CR technology [9].

Current wireless networks are characterized by a static spectrum allocation mechanism in which International Telecommunication Union-Radiocommunication (ITU-R) bodies assign frequency bands to the license holders on a long-term basis for the standardized wireless services. Further, in Satellite Communication (SatCom) Systems, frequency bands are allocated statically either in the exclusive basis to a certain service or in the shared basis to different services for large geographical regions. The static allocation of the frequency spectrum in this traditional way does not meet the requirements of

future wireless technologies. Therefore, dynamic spectrum sensing, allocation and management are essential for future wireless networks [10]. Recent technical developments such as Software Defined Radio (SDR), wideband transceivers, increased computation power, etc., have led to the possibility of utilizing the available spectrum in a very dynamic and adaptive manner. Two possible future solutions for addressing the spectrum scarcity problem are: (i) Dynamic Spectrum Access (DSA), and (ii) Spectrum sharing. With the DSA approach, Secondary Transmitters (STs) access the primary licensed spectrum opportunistically by exploiting spectral holes in several domains such as time, frequency and space. With the spectrum sharing approach, secondary and primary systems are allowed to operate in the same spectrum band as long as the STs guarantee the protection of the Primary Receivers (PRs). These approaches can be realized with the help of several spectrum awareness and spectrum exploitation techniques as detailed later in Chapter 2. Depending on the awareness level required by the CR, suitable spectrum awareness techniques such as Spectrum Sensing (SS), database, Signal to Noise Ratio (SNR)/channel/sparsity order estimation, waveform detection, etc. need to be investigated. Further, based on the access technology employed by the secondary system, the available spectrum exploitation paradigms can be categorized into [10]: (i) interweave, (ii) underlay and (iii) overlay. More specifically, the aforementioned spectrum awareness techniques allow the realisation of these CR paradigms. The detailed mapping of these two types of CR approaches is provided in Chapter 2. Out of these approaches, the main focus of this thesis will be on the interweave and the underlay. In the interweave paradigm, an unlicensed user explores the spectral holes by means of some spectrum awareness methods and utilizes the available spectral availabilities opportunistically while in the underlay paradigm, an unlicensed user is allowed to coexist with the licensed user only if sufficient protection to the licensed user can be guaranteed. In CR terminology, Primary (licensed) Users (PUs), also called incumbent users, can be defined as the users who have higher priority or legacy rights on the use of a specific part of the spectrum. On the other hand, Secondary (unlicensed) Users (SUs), also called cognitive users, exploit this spectrum in such a way that they do not cause harmful interference to the normal operation of the PUs. The SU needs to have CR capabilities, such as SS, in order to check whether the spectrum resource is being used by a PU and to adapt its radio parameters in order to exploit the unused part of the spectrum. In the following paragraphs, we briefly highlight our motivation behind the challenges addressed in this thesis. The contributions of the thesis are listed in Section 1.2. This thesis is structured into two main parts as described below.

The first part of this thesis focuses on spectrum awareness techniques such as SS, SNR and sparsity order estimation, which are useful for realising interweave and underlay CRs as well as a hybrid CR. This thesis considers spectrum awareness as a multidimensional problem instead of the widely considered single dimensional approach i.e., SS in the literature. Among many available SS techniques [11, 12], Energy Detection (ED) is the most common SS approach because of its low computational and implementation complexities [13, 14]. Although the ED technique does not require any prior knowledge of the PU's signal and the channel, the performance of this method relies on the accurate knowledge of the noise power [15]. Therefore, it's an important research challenge to investigate blind sensing techniques which do not depend on the primary signal, channel or the noise power. Further, the ED technique can be used effectively to detect independent and identically distributed (i.i.d.) signals but is not optimal for detecting correlated signals [16, 17]. Moreover, most of the existing SS and SNR estimation techniques assume the presence of an uncorrelated channel and white noise [18–20]. However, in practical scenarios, the channel may be correlated due to insufficient scattering in the propagation environment [21] and mutual coupling between antennas [22]. The noise may also be correlated due to imperfections in filtering, pulse shaping and oversampling in the receiver. Therefore, there is a strong need of investigating new SS techniques which provide improved performance in the presence of channel/noise correlation. Additionally, existing spectrum awareness techniques mostly focus on the SS approach. In addition to the SS capability required by a CR, SNR estimation of the primary signals at the CR receiver is crucial in order to adapt its coverage area dynamically using underlay techniques [23]. In the context of CR networks, SNR estimation can be very useful in switching between underlay and interweave modes adaptively as described later in Section 1.2. Further, the PU SNR knowledge

provides channel quality information for the secondary system, which can be further used for implementing adaptive techniques such as adaptive bit loading, handoff algorithms and optimal soft value calculation for improving the performance of channel decoders [24]. Despite its important applications, only a few contributions in the literature address the SNR estimation problem in the context of a CR [19, 20, 25, 26]. Moreover, SNR estimation techniques proposed under the assumption of white noise and uncorrelated channels may not perform well in the presence of channel/noise correlation. The aforementioned issues motivate us to explore blind spectrum awareness approaches which are independent of the noise variance and can perform effectively in the presence of channel/noise correlation.

The available spectrum can be used effectively if the CR is able to find spectrum opportunities over a wideband spectrum. One of the main challenges in implementing a wideband CR is the design of the RF front-end with high Dynamic Range (DR) [27, 28]. To address this challenge, Compressive Sensing (CS) has emerged as an important approach in order to reduce the hardware cost of sensing wideband signals and several sub-Nyquist wideband sensing approaches have been investigated in [29–32]. As detailed later in Section 1.2, an important research problem in implementing CS-based receivers is to acquire the sparsity order of the wideband spectrum accurately in order to adjust the sampling rate dynamically. The above issues motivate us to study the problem of sparsity order estimation for different scenarios as well as the compressive SNR estimation problem. The cognitive spectrum utilization can be further improved by combining interweave and underlay approaches. It can be noted that the interweave approach ignores the interference tolerance capability of the PUs focusing only on the bursty PU traffic whereas the possibility of having secondary transmission with full power is neglected in the underlay based approach [33]. In this context, it's crucial to investigate suitable hybrid spectrum awareness and transmission strategies which can overcome the aforementioned drawbacks and achieve higher secondary throughput while protecting the PUs. This motivates us to study a hybrid cognitive transceiver which combines the SS approach with the power control-based underlay approach with the help of the employed SNR estimation.

The second part of this thesis focuses on the applications of various underlay and interweave techniques in SatCom systems. As in terrestrial wireless systems, one of the main challenges towards realizing the next generation SatCom systems is the spectrum scarcity problem. As detailed later in Section 1.2, there is a strong need to explore innovative spectrum sharing approaches to enhance the spectral efficiency of the usable satellite spectrum. In this direction, this thesis introduces the concept of cognitive SatCom which allows the coexistence of future satellite-terrestrial networks or two satellite networks in the same spectrum. In this thesis, we define the spectral coexistence of satellite-terrestrial networks as “Hybrid Cognitive SatCom” and the spectral coexistence of two satellite networks as “Dual Cognitive SatCom”. In Chapter 5 of this thesis, we provide various possible use cases of the above two scenarios.

The hybrid cognitive SatCom scenarios can be beneficial to both terrestrial and satellite operators depending on whether the secondary system is satellite or terrestrial. In the scenarios, where the satellite links are secondary, satellite operators can take advantage of the licensed terrestrial spectrum whereas in the scenarios, where the terrestrial links are secondary, terrestrial operators can take advantage of the licensed satellite spectrum. This possible reuse of the satellite licensed spectrum by the terrestrial services and the reuse of the terrestrial licensed spectrum by the satellite services is the main motivation behind studying this paradigm in this thesis. As detailed later in Chapter 5, the possible hybrid cognitive SatCom examples on the basis of the operating frequency are: (i) Fixed Satellite Service (FSS)-Fixed Service (FS) coexistence in the Ka band, (ii) FSS-FS coexistence in the Ku band, (iii) multibeam satellite-cellular coexistence in the C-band, and (iv) hybrid/integrated satellite-terrestrial networks in the S-band. The main issues to be considered in these scenarios are: (i) protection of the licensed PRs, and (ii) the Quality of Service (QoS) guarantee of the secondary link. Motivated by these issues, we study the problems of interference modeling, interference detection, dual-polarized SS, and Cognitive Beamforming (CB) for hybrid cognitive SatCom systems.

Towards realizing dual cognitive SatComs, suitable CR techniques can be investigated in order to allow the spectral coexistence of two satellite systems operating in same or different orbits and providing satellite services over the overlapping coverage area. This possible coexistence is motivated from the following aspects: (i) The primary and secondary satellites can be used for providing different services to same/different categories of users, hence enhancing the overall spectral efficiency of the system. As an example, the primary satellite with larger beams can be used to provide high priority broadband multimedia services and the secondary satellite having smaller beams to provide services requiring low QoS. (ii) The Geostationary (GEO) orbit is already being congested due to a significant increase in the number of GEO satellites, leading to the problem of adjacent satellite interference. Further, some portions of the Ka and Ku bands are allocated to both GEO and Non-GEO (NGEO) satellites in the co-primary basis, leading to the inline interference problem in certain regions [34, 35]. In this context, innovative CR techniques can be exploited in order to address these problems. (iii) There may arise a situation where the operator has to launch another satellite that support the existing ones in the same orbital slot in order to meet the increased traffic demand in the same coverage area. (iv) During the replacement phase of the legacy satellites, there may appear the “by default” coexistence of two satellites for a long period [36]. Investigating innovative dual satellite architectures and techniques which can maximize the overall spectral efficiency while providing sufficient protection to the licensed primary spectrum is an important research problem in realizing future dual cognitive SatCom systems. This fact motivates us to explore different CR approaches such as cognitive Interference Alignment (IA), cognitive beamhopping, dual-polarized SS, power control and Exclusion Zone (EZ) for dual cognitive SatComs in this thesis.

1.2 Organization, Problem Statements and Contributions

In this section, we include the outline of the thesis along with the considered problem statements. For each topic, a brief background is provided including the key references and the main contributions are listed using bullet points. The references included within the contributions are author’s own publications. The detailed background is provided in each subsequent part. The first part of this thesis includes Chapters 2, 3 and 4, which deal with interweave and underlay CR techniques in general settings and the second part includes Chapters 5, 6 and 7, which study the applications of several CR techniques in SatCom systems.

Chapter 2: Cognitive Communications

This chapter, firstly, reviews and maps the existing spectrum awareness methods with the spectrum exploitation paradigms. Then it focuses on interweave and underlay CR approaches in detail. Subsequently, the existing SS techniques are classified on different bases and special attention is provided to the ED, and the eigenvalue based techniques. Regarding underlay techniques, classification of the existing approaches is provided and several approaches such as cognitive IA, CB, EZ and resource allocation methods are discussed including their main concepts and the related literature. The contributions to these approaches are provided in several ways in subsequent chapters.

Chapter 3: Cognitive Transceiver Design

This chapter, firstly, discusses the basic design of a hybrid cognitive transceiver utilizing the estimated SNR of the primary signals. Subsequently, it presents our contributions on spectrum awareness approaches such as eigenvalue-based SS, SNR estimation and sparsity order estimation approaches. These techniques can be subsequently used for designing a hybrid transceiver for a CR. Random Matrix Theory (RMT) and statistical signal processing are used as tools for carrying out mathematical

TABLE 1.1: Causes of channel/noise correlation in multi-dimensional scenarios

Cases	Channel Correlation		Noise Correlation	
	Type	Cause	Type	Cause
Multi-antenna SS	Spatial Correlation	Multipath propagation	Filtering	Autocorrelation function of the filter
	Antenna mutual coupling	Transmit/receive Antenna separation		
Oversampled SS	Oversampling	Oversampling operation	Filtering	Autocorrelation function of the filter
	Filtering	Autocorrelation function of filter	Oversampling	Oversampling operation
Cooperative SS	Spatial correlation	Collocated nodes in CR network	Filtering	Autocorrelation function of the filter

analysis. Moreover, this chapter analyses the performance of a hybrid transceiver in terms of the sensing-throughput tradeoff.

Background and Contributions

The SS mechanism plays an important role in CR networks in order to acquire the spectrum awareness required by the CRs. For effective implementation of a CR, it is extremely important to explore efficient SS techniques which can detect the presence of signals reliably. The three main signal processing techniques for sensing the presence of a PU that appear in the literature are matched filter detection, ED and cyclostationary feature detection [10]. Matched filter detection and most of the existing feature detection techniques require prior knowledge about the PU's signal in order to decide about the presence or absence of the PU signal [11]. As mentioned before, the performance of the ED technique is susceptible to the noise covariance uncertainty [15]. Since both the prior knowledge about the PU's signal and the noise variance are unknown to the CRs in practical scenarios, exploring efficient and blind SS techniques for CRs is an important research challenge. In this context, several blind SS techniques have been proposed in the literature [37–40] without requiring the prior knowledge of the PU's signal, the channel and the noise power. Further, the performance of traditional SS techniques is limited by the received signal strength which may be severely degraded in multi-path fading and shadowing environments. To address this issue, various diversity enhancing techniques such as multi-antenna, cooperative and oversampled techniques have been introduced in the literature in order to enhance the SS efficiency in wireless fading channels [18, 41, 42]. Most of these methods use the properties of the eigenvalues of the received signal's covariance matrix and use recent results from advances in RMT [23, 43]. The main advantage of an eigenvalue based SS over other SS techniques is that it does not require any prior information of the PU's signal and it outperforms ED techniques, especially in the presence of noise covariance uncertainty [18].

Several eigenvalue based algorithms have been proposed in the literature [18, 41, 42, 44–48] exploiting RMT methods [23, 43]. In the context of eigenvalue-based SS techniques, the following three practical scenarios are considered in the literature with respect to receive dimensions of the CR node: (i) Cooperative SS scenario [42], (ii) Multiantenna SS scenario [18, 49], and (iii) Oversampled SS scenario [18]. In this thesis, we consider a multi-dimensional framework which can be applicable to all these

scenarios. The main problems that may arise in these practical scenarios are channel correlation and noise correlation due to various causes specified in Table 1.1. The existing eigenvalue-based techniques can be broadly categorized into (i) Signal Condition Number (SCN) based [18, 41, 45], (ii) Maximum Eigenvalue (ME) based [17, 46] and (iii) Scaled Largest Eigenvalue (SLE) based [49–51]. The SCN of a matrix is defined as the ratio of the maximum to the minimum eigenvalue [52] and can be used as a metric to characterize the support of the asymptotic eigenvalue probability distribution function (a.e.p.d.f.) of a random matrix. Furthermore, several SCN based techniques such as asymptotic [44], semi-asymptotic [18] and ratio-based [45] techniques have been proposed utilizing the properties of the eigenvalues of random Wishart matrices. Most of these contributions (detailed later in Section 2.3.4.2) are based on the assumption of additive white noise. In the presence of correlated noise, the parameters of the noise covariance matrix such as SCN, and ME etc., are affected and as a result, the decision metric for the corresponding received signal's covariance matrix is also affected. This leads to a degraded sensing performance while applying the sensing threshold designed for uncorrelated scenarios in the correlated scenarios. In this direction, new sensing thresholds need to be investigated for carrying out SS in the presence of noise correlation.

- We propose new sensing thresholds for the SCN [53, 54] and ME based techniques [55] using recent results from RMT in order to achieve the improved sensing in the correlated noise scenarios.

Furthermore, sampling rate in a CR receiver can be increased beyond the symbol rate, known as fractional sampling (oversampling), to enhance the SS efficiency under fading channel conditions. The fractional sampling technique is commonly used to enhance signal detection reliability [56, 57] and the information throughput [58] in a wireless receiver. From the CR point of view, an fractional sampling receiver can be modeled as a virtual multiple-output system with presumably independent channel fading effects. This technique is especially beneficial in time varying channels with large Doppler spread i.e., small channel coherence time. Another motivation for introducing the fractional sampling concept in the context of a CR is that using more antennas at the receive-side is often impractical and expensive requiring multiple RF chains. In wireless fading environments, fractional sampling introduces diversity and can improve signal detection. However, oversampling operation also results in the colored noise [59] and this phenomenon gradually saturates the performance gain due to fractional sampling [56, 57]. Therefore, it is crucial to determine the operating point for the fractional sampling rate, a design parameter that we can actually configure to find a good trade-off between performance and complexity.

- We study an fractional sampling-based SS in order to enhance the sensing efficiency of a detector and suggest a method for determining the operating point for the fractional sampling rate in terms of the sensing performance and complexity [54].

Moreover, most SS related works focus on a dual hypothesis test to decide the presence or absence of primary on-going transmissions. If the CR is able to estimate the SNR of the primary signals, defined as the ratio of the received primary power to the noise power at the CR receiver, it can dynamically adapt its coverage area using underlay techniques. In this direction, the following two scenarios can be considered. The first scenario assumes duplex mode of transmission for the PUs i.e., each user interchangeably transmits and receives over time. In order to implement underlay techniques such as power control at the CR, we need to know the SNR threshold required for the power control algorithm. If we fix the SNR threshold based on the estimated SNR over multiple time slots, we can also protect the weakest one assuming they have the same interference threshold [60]. The second scenario considers the simplex mode of transmission for the PUs and a short range wireless communication for both primary and secondary systems provided that interference levels from one system to another are at a similar level. In practice, it may be the case that a spectrum resource is completely left unused

within a sufficiently large network coverage area. In this context, the optimal exploitation of spectrum holes depends on the maximally acceptable coverage area of secondary transmission while protecting the primary rate [23]. In such type of systems, it can be assumed that setting SNR threshold for the Primary Transmitter (PT) is a reasonable strategy for protecting the PR as well. In this context, based on the estimated PU SNR, suitable underlay techniques such as exclusion zone [61] can be applied.

Additionally, in CR networks, SNR estimation can be very useful in switching between underlay and interweave modes adaptively. Most of the existing spectrum sharing approaches focus either on interweave or the underlay approach. As mentioned before, the underlay approach is not able to detect the activity or inactivity of the PUs in a particular band and hence does not utilize the idle bands efficiently. On the other hand, the interweave approach does not allow the SUs to transmit in a particular frequency band when the PU is active in that band. Further, in the interweave scheme, the secondary network may have very low throughput specifically in heavily occupied spectrum regions. If the CR node has the capability of estimating the PU SNR along with its sensing ability, the SU can access the channel with full power in case of an idle channel and access the channel with the controlled power in case of an occupied channel, thus enhancing the overall spectrum utilization. This hybrid access approach has been recently important attention in order to address the drawbacks of both SS and underlay approach [33, 62–64]. The employed SNR estimation facilitates the implementation of a hybrid spectrum sharing approach, which combines both interweave and underlay approaches.

- In [53], we derive the a.e.p.d.f. of the received signal's covariance matrix for the signal plus noise case under white and correlated noise scenarios. Based on the derived a.e.p.d.f. expressions, we propose an SNR estimation technique in order to estimate the SNR of the PU signals in the presence of noise correlation. It is shown that the PU SNR can be reliably estimated with the proposed scheme in the presence of the correlated noise.
- In [65], firstly, we evaluate the performance of different eigenvalue-based SS techniques in the presence of channel or/and noise correlation. Secondly, we carry out a detailed theoretical analysis of the signal plus noise hypothesis to derive the a.e.p.d.f. of the received signal's covariance matrix under the following two cases: (i) correlated channel and white noise, and (ii) correlated channel and correlated noise. Subsequently, we use these a.e.p.d.f. expressions in order to estimate the PU SNR in the presence of channel correlation [66] and in the presence of both channel/noise correlation [65]. It is shown that the PU SNR can be reliably estimated when the CR sensing module is aware of the channel/noise correlation.
- In [67], we propose half duplex and full duplex architectures for a hybrid cognitive transceiver with the help of the employed SNR estimation approach. The performance analysis of the hybrid approach is carried out in terms of the sensing-throughput trade-off considering periodic SS and simultaneous sensing/transmission approaches.

Chapter 4: Wideband Cognitive Transceiver Design

This chapter focuses on research challenges for designing a wideband cognitive transceiver and provides our contributions on compressive sparsity order estimation and SNR estimation problems. A CS approach is followed in order to study the considered problems in wideband scenarios. Further, it provides the performance analysis of a wideband cognitive transceiver considering sweep-tune and filter bank based approaches.

Background and Contributions

Existing SS techniques mostly focus on the detection of narrowband signals considering a single radio channel [11, 18]. However, in practical scenarios, the CRs need to detect and acquire information about a wide spectrum band in order to utilize the spectrum efficiently. Further, CRs do not have prior knowledge about the PU's signal and channel. In this aspect, investigating efficient blind wideband spectrum awareness techniques is an important and relevant research challenge. The key challenge of wideband SS is the detection of weak wideband signals hidden in thermal noise with a sufficiently large probability of detection. The sensing RF chain of a CR receiver should be able to receive a wideband signal, sample it using a high speed Analog to Digital Converter (ADC) and perform measurements for the detection of PU signals. The wideband RF signal received by the antenna of an RF front-end includes signals from adjacent and spatially separated transmitters, and from transmitters operating at a wide range of power levels and channel bandwidths. Further, the main limitation in an RF front-end's ability to detect weak signals is its DR. For this purpose, the wideband sensing requires multi-GHz speed ADCs, which together with high resolution (of 12 or more bits) might be infeasible with current technology [68, 69]. As mentioned before, in the above context, CS techniques can play an important role in reducing the acquisition cost at the CR node [70, 71]. According to CS theory, certain signals can be recovered from far fewer samples or measurements than those required by conventional methods [71, 72]. In most of the existing CR-related CS contributions, the original sparse signal is reconstructed generating Nyquist rate samples from the compressed samples and subsequently, SS is carried out [30, 73]. However, the reconstruction process in a CS-based CR requires significant computational complexity [74] and from the SS point of view, it's not necessary to reconstruct the entire sparse signal. In this direction, CS has been applied in [75] and [76] for signal detection purpose using compressed measurements rather than reconstructing the original signal. In contrast to [75] and [76], this thesis focuses on estimating the sparsity order of the wideband spectrum which can be subsequently used for implementing adaptive CS-based CR receivers.

Furthermore, in most of the CS-related contributions, it is assumed that the wideband signal is sparse in some domain and the number of measurements is kept fixed based on the assumed sparsity order. However, in compressive wideband systems, the required number of measurements to achieve a successful recovery rate proportionally varies with the sparsity order of wideband signals [29, 77]. In this context, Sparsity Order Estimation (SOE) is crucial in order to choose the appropriate number of measurements. In addition, in most of the contributions, it is assumed that the sparsity order of the signal is known beforehand. However, in the context of CR networks, this prior information is not available at the CR sensor and has to be estimated. In the above context, a two-step CS algorithm has been proposed recently in [77], in which the sparsity order is estimated in the first step and the total number of collected samples is adjusted in the second step based on the estimated sparsity order. However, the considered estimation approach is based on Monte Carlo simulations and no analytical method has been presented for estimating the sparsity order of the wideband signals. Further, the proposed experimental method for SOE in [77] requires the reconstruction of the original sparse signal. In addition to the SOE problem over a wideband spectrum, estimating the SNR of the PU signals over a wideband spectrum accurately is also crucial in order to fully exploit an under-utilized primary spectrum using underlay CR techniques.

- In [78, 79], we propose a Multiple Measurement Vector (MMV) model to study the sparsity order and SNR estimation problem instead of the Single Measurement Vector (SMV) model considered in the literature. In [78], we derive theoretical expressions for the a.e.p.d.f. of the measured signal's covariance matrix for the following three cases using RMT: (i) constant received power across all active carriers in the considered wideband spectrum [80], (ii) varying received power levels across the carriers, and (iii) correlated MMV scenario where the non-zero entries across multiple measurement vectors are correlated.
- Based on the derived a.e.p.d.f., we use the ME of the measured signal's covariance matrix in order to estimate the sparsity order of the channel occupancy within the considered wideband spectrum [78, 80].
- In [79], we extend the eigenvalue-based SNR estimation problem to the wideband context using the CS approach. For this analysis, we derive the a.e.p.d.f. of the measured signal's covariance matrix for the following two correlated scenarios under compressive settings: (i) correlated MMV, and (ii) correlated noise. Subsequently, the derived a.e.p.d.f. expressions are used for estimating the SNR of the PU signal over a wideband under the considered scenarios. Furthermore, we study a tradeoff between estimation performance and the hardware cost (number of measurements) while using compressive measurements.

Chapter 5: Cognitive Satellite Communications

In this chapter, starting with the importance of SatCom systems, we highlight the main aspects of cognition in SatComs. Then we provide a detailed overview on the existing literature related to the following three categories: (i) hybrid satellite-terrestrial systems, (ii) dual satellite systems, and (iii) spectrum sharing techniques. Further, we propose possible spectral coexistence scenarios for cognitive SatComs considering the following two main categories: (i) hybrid satellite-terrestrial coexistence, and (ii) dual satellite coexistence. Moreover, we provide the mapping of various CR techniques to the considered scenarios. Additionally, we provide the aspects of spectrum regulation and standardization activities for cognitive SatComs. Finally, we provide a discussion on various challenges from technical, regulatory and business perspectives for the effective implementation of cognitive SatComs.

Background and Contributions

As in terrestrial systems, one important aspect to be considered in SatCom systems is the spectrum scarcity problem. The usable satellite spectrum is becoming scarce due to continuously increasing demand for broadcast, multimedia and interactive services. Nowadays, the satellite broadband spectrum demand is mainly driven by video services such as High Definition Television (HDTV). The demand for the satellite spectrum is increasing rapidly not only because of the broadcast applications but also due to multimedia broadband services [81]. Further, there is continued pressure on satellite bands, especially in L and C bands due to the introduction of new terrestrial services such as 3G mobile telephony, WiFi and WiMax services. The FSS satellites commonly use C and K band frequencies while Mobile Satellite Services (MSS) systems use L and S band frequencies due to lower signal attenuation and smaller impact of atmospheric effects [82]. Due to the limitation of available L and S-band frequency resources, higher frequency bands i.e., Ku and Ka bands are already assigned for fixed satellite services and even for MSS systems and the current research is examining the use of Q/V bands for the feeder links. At present, Ku band based MSS systems are available to provide broadband services to many vehicular users such as trains, boats, planes, and cars [82]. In this context, exploring efficient frequency sharing techniques to enhance spectral efficiency while guaranteeing sufficient QoS is a highly relevant and challenging research problem.

In the above context, the next generation SatCom systems target enhanced throughput and higher spectral efficiency. To enhance the system capacity, satellite systems have moved from payloads generating a single beam to multi-beam platform in which a satellite is equipped with multibeam antennas to cover multiple spots over the surface of the Earth [83]. Further, the increased demand for consumer broadband over satellite has led to a number of high throughput Ka-band satellite systems. Multi-beam satellites are being used widely by satellite operators such as KaSat (82 Ka-band spot beams) by Eutelsat, Wildblue-1 and Anik F2 (66 Ka-band spot beams) by Wildblue and Viasat1 (72 Ka-band spot beams) by ViaSat. As in terrestrial cellular systems, multibeam satellite systems use frequency planning and reuse to achieve enhanced capacity. In a multibeam satellite system, by allowing aggressive frequency reuse over a coverage area, the available bandwidth per beam can be increased, at the expense of the increased co-channel interference. Since the system capacity depends on both the available bandwidth and the co-channel interference, enhancing the spectral efficiency of the available bandwidth and exploring advanced interference mitigation techniques in order to mitigate inter/intra-beam interferences are two main challenges towards realizing the next generation Terrabit/s SatComs [84]. Despite the system capacity provided by the multibeam satellites, there is still a large gap to meet the spectral efficiency requirements for realizing the next generation Terabit satellites within the 2020 horizon [85]. In this context, the exploitation of non-exclusive bands in the shared basis can be an important solution to enhance the overall spectral efficiency. Further, it's an important challenge to investigate innovative advanced satellite architectures which can achieve enhanced system throughput by the means of higher spectral efficiency. In this direction, cognitive satellite systems can be considered as innovative and promising satellite architectures which can address the aforementioned challenges.

The spectrum coexistence literature is more mature in the terrestrial context but has received limited attention in the satellite community. The main available literature related to cognitive techniques has considered hybrid or integrated satellite networks [86–90]. The main difference between hybrid and integrated networks lies on whether both space and terrestrial components use a common spectrum and network or not [86], as detailed later in Chapter 5. Recent works exploiting spectrum sharing opportunities in the context of cognitive SatComs include [90–94]. Recently, cognitive SatComs have received interest in different research projects and communities. Examples include ACROSS (Applicability of CR to Satellite Systems) [95], CoRaSat (Cognitive Radio for SatComs) [96, 97], Co²Sat (Cooperative and Cognitive Architectures for Satellite Networks) [98, 99], SeMIGod (Spectrum management and interference mitigation in cognitive radio satellite networks) [67], FREESTONE (Frequency sharing techniques with Other networks or radio services), SatNex (European Network of Experts for SatComs), etc.

- We highlight the important aspects of cognition in SatCom systems and provide a detailed overview on the existing literature related to the following three categories: (i) hybrid/integrated satellite-terrestrial systems, (ii) dual satellite systems, and (iii) spectrum sharing techniques.
- We propose possible spectral coexistence scenarios for cognitive SatComs considering the following two main categories [100]: (i) hybrid satellite-terrestrial coexistence, and (ii) dual satellite coexistence.
- We provide the mapping of various CR techniques to the considered scenarios [100]. Additionally, we provide the aspects of spectrum regulation and standardization activities for cognitive SatComs [101].
- We provide a discussion on various challenges from technical, regulatory and business perspectives for the effective implementation of cognitive SatComs [101].

Chapter 6: Hybrid Cognitive Satellite Communication

This chapter proposes several CR approaches for enabling the hybrid satellite-terrestrial coexistence. First, an interference modeling problem is considered and the criteria for technique selection is provided based on the interference power level. Then a harmful detection problem is tackled by considering the spectral coexistence of FSS-FS coexistence in the Ka band. Further, the performance analysis of an ED-based SS is carried out for a dual polarized fading channel. Finally, the CB problem is studied for the hybrid satellite-terrestrial scenario in both uplink and downlink coexistence scenarios.

Background and Contributions

In the considered hybrid satellite-terrestrial coexistence scenario, investigating suitable spectrum sensing, interference detection and interference mitigation techniques are the key issues to be addressed depending on the considered practical use case. The current literature in this field examines the frequency sharing issues between satellite and terrestrial networks operating in the same spectrum [91, 93, 102–105]. This thesis tackles the problem of interference modeling, harmful interference detection, dual polarized SS and cognitive beamforming motivated by the issues described below.

Interference modeling can be considered as a spectrum awareness approach since it helps to capture the surrounding interference environment created by other systems operating within the same or adjacent spectrum. Furthermore, interference modeling can be used as an important tool to select the best technique among possible CR techniques depending on the cognitive scenario and the geographical region where the technique is to be implemented. Different CR techniques have their own specific requirements and various levels of applicability in the considered scenarios. Therefore, CR techniques suitable in one geographic location and for a certain condition may not be suitable for other locations and conditions. In this context, it is important to select a suitable CR technique for efficient operation of CR networks for allowing the spectral coexistence of satellite-terrestrial networks. By carrying out interference modeling over a large geographical region, we can divide the considered region into low/medium and high interference regions, and then apply suitable CR techniques in those regions as detailed later in Chapter 6.

- We carry out interference modeling in a hybrid satellite-terrestrial scenario in order to estimate the received interference level and subsequently map suitable CR techniques based on the estimated interference power level. It is concluded that the interference level varies over a large geographical area due to the variation in the elevation angle of GEO satellite terminals and different CR techniques are suitable in different geographical regions depending on the received interference level [106].

Among the available CR techniques, SS mechanism is one of the promising techniques in order to acquire spectrum awareness in high interference regions. In the existing terrestrial literature [11, 12], SS is generally studied in the context of sensing primary signals by a CR transmitter. In many cases, a time-slotted half-duplex transmission is assumed meaning that the CR transmitter senses for a certain duration and then transmits its data for the remaining duration of a frame if a vacant PU band is detected [107]. However, in practice, there may arise situations in which the PR is already protected with the help of regulatory limits and we need to mitigate/avoid the interference at the Secondary Receiver (SR) caused by the primary transmission in order to guarantee the QoS of the secondary link. This situation arises in the practical coexistence scenario of FSS-FS links in the Ka band (17.7 – 19.7 GHz) [96]. In this context, it's an important research challenge to explore suitable approaches to detect harmful interference at the SR. The main challenges for implementing an interference detector in the considered scenario are to detect the weak levels of the FS interference, and to define an appropriate sensing threshold in order to decide whether a harmful FS carrier is present or not.

- In order to address the harmful detection problem for the FSS-FS link coexistence in the Ka band (17.7 – 19.7 GHz), we exploit the use of an additional RF chain with a dipole antenna in addition to the existing satellite dish antenna [108]. From the results, it is concluded that the FS harmful interference can be reliably detected with the help of an additional dipole antenna equipped in the satellite terminal. Further, it is shown that this solution can overcome the noise uncertainty problem which arises while sensing with the satellite dish.

Furthermore, the concepts of spectrum sharing in the frequency, time and spatial domains have been considered in various literature but the polarization domain has not been fully exploited. In the existing literature, the polarization domain has been mainly used for diversity and multiplexing purposes [109–111]. The polarization domain can be treated as an additional degree of freedom (dof) in order to explore efficient SS and transmission schemes in the context of cognitive SatComs. Dual polarization plays a significant role in satellite systems to enhance the efficiency of the available bandwidth since two independent signals can be transmitted on the same spectrum by means of two orthogonal polarizations, hence doubling the available spectrum. Furthermore, two orthogonal polarizations can be treated as two different data streams (colors) and dual polarization can be used as an additional color in the frequency planning process of multi-beam satellites and terrestrial cellular networks [112]. From the cognitive point of view, if a primary system is designed to transmit in one polarization, secondary system can be designed to transmit in another polarization using the polarization domain as an interference mitigation tool towards primary systems. Since the dual polarized channel is gaining more importance in cognitive communication [112] [113], there remain challenges to explore suitable SS techniques for this channel.

- We carry out the performance analysis of an ED based SS technique in a dual polarized fading channel in the context of cognitive SatComs [114]. The performances of different combining techniques such as Selection Combining (SC), and Equal Gain Combining (EGC) are analyzed in a dual polarized fading channel considering the Rayleigh fading scenario. Further, we study the effect of cross polar discrimination (XPD) in the sensing performance of the considered combining techniques in a dual polarized Rayleigh fading channel.

Moreover, cognitive beamforming can be considered as an important mechanism for allowing the spectral coexistence of satellite-terrestrial networks. In the context of a CR, beamforming techniques have been investigated for the secondary network for various objectives such as controlling interference [115], capacity maximization [116], and Signal to Interference plus Noise Ratio (SINR) balancing [117]. The beamforming design problem for an underlay CR becomes more challenging since an additional constraint on the primary interference threshold needs to be taken into account. The CB can be considered as an underlay CR technique since it allows the coexistence of two wireless systems by guaranteeing the desired QoS of the SUs while providing sufficient protection to the PRs. In the existing CR literature, the CB techniques have been considered mostly in the coexistence scenarios of two terrestrial networks [115–117]. One important feature of the GEO satellite terminals is that they always point towards the GEO satellites (South if we consider the European continent excluding the regions near to the equator). This special propagation characteristic can be used in investigating suitable CR techniques for the spectral coexistence of satellite and terrestrial networks. Similar scenario was considered in [118] while reusing the satellite broadcast spectrum for terrestrially broadcast signals in the United States and the use of different directional antennas at the user location was proposed to allow the spectrum reuse. In this direction, this thesis focuses on the applications of CB techniques for the spectral coexistence of satellite and terrestrial networks using the above mentioned propagation characteristics of the satellite terminals.

- By exploiting the prior knowledge about the propagation characteristics of the satellite terminals, we apply different receive beamforming techniques such as Linearly Constrained Minimum Variance (LCMV) and Minimum Variance Distortionless Response (MVDR) for the uplink coexistence scenario in [119] and propose different transmit beamforming techniques for the downlink coexistence scenario in [120]. The main differences between the considered approach and commonly applied beamforming approaches in the literature are: (i) the exact locations and the number of the interfering satellite terminals may be unknown to the beamformer, and (ii) we focus on mitigating interference towards/from an specified angular sector instead of distinct angular positions of the interfering/victim terminals. The prior knowledge that all the GEO satellite terminals are pointing south is the cognition that we exploit in our study.

Chapter 7: Dual Satellite Cognitive Communication

This chapter proposes several CR approaches for enabling the dual satellite coexistence. First, cognitive IA problem is studied with the help of theoretical and numerical analysis considering the spectral coexistence scenario of monobeam-multibeam satellites both operating in the normal return mode. Then a novel cognitive beamhopping system is proposed considering the spectral coexistence of two GEO multibeam satellites in the normal forward mode. Finally, the performances of several combining techniques are compared with the polarization-based combining approach in a dual polarized Additive White Gaussian Noise (AWGN) channel in the context of dual cognitive SatComs.

Background and Contributions

Several dual satellite coexistence scenarios are possible as detailed later in Chapter 5. These scenarios can be categorized on the basis of operating frequency, operating mode, satellite orbit, etc. For example, on the basis of the satellite orbit, these scenarios can be categorized into (i) GEO-GEO satellite coexistence, and (ii) GEO-NGEO satellite coexistence. The main issue to be tackled for allowing the dual satellite coexistence is interference management between two satellite systems while guaranteeing the sufficient protection of the PRs.

IA technique has received important attention as an interference mitigation tool in interference-limited wireless systems such as cellular wireless networks, CR systems and ad-hoc networks [121–124]. The concept behind IA is that signals can be designed in such a way that they cast overlapping shadows at the non-intended receivers and remain distinguishable at the desired receivers. This technique can be classified as an underlay CR technique [10] since it deals with interference mitigation towards the primary system in spectral coexistence scenarios. In several literature related to the cellular networks, the IA technique has been shown to a promising solution in order to effectively suppress the cochannel interference [125–130]. In these contributions, the IA is carried out in the spatial domain i.e., antenna dimension. This IA approach does not seem to be applicable in the satellite context due to the complexity of having multiple antennas in the satellite terminals. The multicarrier based IA approach, in which the alignment is carried out over the carrier domain instead of the spatial domain, seem to be applicable in the context of satellite networks due to their multicarrier nature of transmission. In the context of terrestrial multicarrier systems, IA technique has been investigated in different settings [128, 131–133]. Despite various literature about IA in terrestrial cellular networks, only a few studies have been reported about IA in the satellite context. The feasibility of implementing subspace IA in a multibeam satellite system has been studied in [134] and it has been concluded that the SIA using frequency domain is advantageous for a multibeam satellite. Further, IA technique has been applied for CR networks in different settings [135–138]. However, there exist no literature regarding the application of IA in the cognitive satellite scenarios. In this context, it's an important research

challenge to investigate suitable IA techniques in dual satellite cognitive scenarios where two satellites provide coverage to the same area.

- We investigate an underlay spectral coexistence mechanism which exploits an uplink IA in order to mitigate the interference of GEO multibeam satellite terminals towards a GEO monobeam satellite in a monobeam-multibeam dual satellite coexistence scenario [98, 139]. In the proposed IA technique, the IA is carried out over the carrier dimension instead of the spatial dimension considered in most of the literature. The performances of three IA techniques, namely static, uncoordinated and coordinated are evaluated and compared with primary only, resource division and no-mitigation techniques in terms of sum-rate capacity, primary to secondary rate ratio and primary rate protection ratio. With the help of theoretical and numerical analyses, we show that the coordinated IA approach perfectly protects the primary rate while providing the highest sum-rate.

Furthermore, another important issue is to investigate innovative satellite architectures which allow the spectral coexistence of two satellite systems. In the conventional multibeam systems, partial frequency reuse approach can be used to enhance the system capacity. However, it may be impractical to apply the full frequency reuse approach due to excessive co-channel interference which is difficult to remove using existing interference mitigation techniques. A beamhopping satellite system can operate by using the full frequency reuse principle over a certain beamhopping pattern [140]. Several contributions exist in the literature in the context of beamhopping systems [140–143]. The main difference between conventional multibeam and beamhopping systems is that frequency sharing among multiple beams within a cluster takes place in different domains, i.e., frequency and time domains respectively. Since in a beamhopping system, only a single beam of a cluster is active during a particular time slot, there exists an opportunity to reuse the full frequency using smaller beams of another secondary satellite in the same time slot. In this context, it's an important research challenge to investigate advanced satellite cognitive architectures which employ beamhopping techniques.

- We propose a novel cognitive beamhopping system with the objective of enhancing the system spectral efficiency while protecting the primary licensed system [99, 144]. We consider a dual satellite spectral coexistence scenario of two multibeam satellites with a primary satellite having larger beams and a secondary satellite having smaller beams. The cognition is achieved by sharing the beamhopping pattern and the timing information of the primary multibeam system to the secondary multibeam system using a signalling link between their corresponding gateways. The performance of the proposed system is evaluated and compared with the performance of conventional multibeam and beamhopping satellite systems in terms of spectral efficiency (bits/sec/Hz). Further, a power control technique is considered at the secondary satellite to protect the primary satellite terminals using a predetermined interference threshold. Moreover, we apply the EZ principle to investigate the opportunity for secondary transmission in the switched-off regions of the primary satellite system. More importantly, the power control and the EZ techniques are compared in terms of the total system throughput considering the same aggregated secondary interference.
- The sensing performances of several combining techniques such as SC, EGC, Maximum Ratio Combining (MRC) and Optimum Polarization Based Combining (OPBC) are compared in a dual polarized AWGN channel considering a dual satellite coexistence scenario [145]. It is shown that the performance of the OPBC technique provides the better sensing performance than other combining schemes since it optimally combines two signals received from two branches of a dual polarized antenna.

Chapter 8: Conclusions, Discussion and Future Recommendations

This chapter briefly summarizes the thesis, provides overall discussion and open research issues in the considered domain. The detailed concluding remarks are provided at the end of each chapter.

Appendix

The appendix includes RMT preliminaries which are used for carrying out mathematical analysis in our work, and the detailed proofs of the results presented in Chapters 3 and 4.

1.3 Research Methodology

In this thesis, we study and analyze the considered research problems with the help of theoretical as well as numerical analysis. The theoretical analysis is based on widely used tools in the literature. The important tools used in this thesis are signal detection theory from statistical signal processing, RMT, linear algebra and optimization techniques. Detection theory provides several mechanisms in order to detect the presence of a desired wireless signal from the random received signal [16]. In this thesis, binary hypothesis testing is employed in order to distinguish the cases of primary signal presence and the noise only using appropriate decision statistics. Further, RMT is an important tool in order to carry out asymptotic analysis for multidimensional problems since it allows easier approximations and provides closed-form expressions due to the law of large numbers. This tool has been used in the literature in various applications such as asymptotic capacity analysis, modeling transmit/receive correlation in Multiple Input Multiple Output (MIMO) channels and multiuser MIMO fading [23, 43, 146, 147]. Recently, it has received considerable attention in the CR research community, specifically in the eigenvalue-based SS literature [18, 41, 44, 47]. In this thesis, we use this to study eigenvalue based sensing and SNR estimation problems in the multidimensional framework. Moreover, in the recent years, there has been an increasing interest in the use of convex optimization for solving wireless communication problems [148]. In this thesis, we use convex optimization approach in order to solve cognitive beamforming problems.

The numerical analysis carried out in this thesis is based on the Monte Carlo (MC) methods which are based on simulating a large number of realizations of the channel/user/system instances. In each realization, a suitable algorithm is applied and the performance metrics are calculated using numerical methods and averaged in order to estimate the long-term performance of the system. Due to the random nature of user/channel distribution in wireless environments, the use of MC methods has been common in practice for research studies in order to get some preliminary insights on the behavior of the system, as well as to verify the final results of the theoretical analysis. In many cases, final analytical results are compared with the numerical results in order to demonstrate the validity of the analytical studies. The main performance metrics used in this thesis are probability of detection, probability of false alarm, probability of correct decision, sensing time, throughput, primary rate protection ratio, SINR, and the Mean Square Error (MSE).

1.4 Publications

The author's work during his PhD study has been disseminated to related scientific communities through several international scientific conferences, journal papers and book chapters. This work has further created synergies with the Luxembourgish national project "Co²Sat: Cooperative and Cognitive Architectures for Satellite Networks", and the European FP7 project "CoRaSat: Cognitive Radio for

Satellite Communications". The publications resulted during the course of this PhD study are listed below with the following indexes: (i) "J" for the journal paper, (ii) "C" for the peer-reviewed conference paper, (iii) "B" for the book chapter and (iv) "TD" for the temporary document.

1. Contributions Included in the Thesis

- J1. S. K. Sharma, S. Chatzinotas, and B. Ottersten, "Eigenvalue Based Sensing and SNR Estimation for Cognitive Radio in Presence of Noise Correlation", *IEEE Trans. Vehicular Technology*, vol. 42, no. 8, pp. 3671-3684, Oct. 2013.
- J2. S. K. Sharma, S. Chatzinotas, and B. Ottersten, "SNR Estimation for Multi-dimensional Cognitive Receiver under Correlated Channel/Noise", *IEEE Trans. Wireless Commun.*, vol. 12, no. 12, pp. 6392-6405, Dec. 2013.
- J3. S. K. Sharma, S. Chatzinotas, and B. Ottersten, "Interference Alignment for Spectral Coexistence of Heterogeneous Networks", *EURASIP J. Wireless Commun. Networking*, vol. 2013, no. 46, Feb. 2013.
- J4. S. K. Sharma, S. Chatzinotas, and B. Ottersten, "Cognitive Beamhopping for Spectral Coexistence of Multibeam Satellites", *Int. J. Satellite Commun. and Networking*, Mar. 2014, doi: 10.1002/sat.1073.
- J5. S. K. Sharma, S. Chatzinotas, and B. Ottersten, "Compressive Sparsity Order Estimation for Wideband Cognitive Radio Receiver", *IEEE Trans. Signal Process.*, vol. 62, no. 19, Oct. 2014.
- C1. S. K. Sharma, S. Chatzinotas, and B. Ottersten, "Exploiting Polarization for Spectrum Sensing in Cognitive SatComs," in *Proc. 7th Int. Conf. on Cognitive Radio Oriented Wireless Networks (CROWNCOM)*, Stockholm, Sweden, June 2012, pp. 36-41.
- C2. S. K. Sharma, S. Chatzinotas, and B. Ottersten, "Spectrum Sensing in Dual Polarized Fading Channels for Cognitive SatComs", in *Proc. IEEE Global Communications Conference (Globecom)*, Anaheim, California, Dec. 2012, pp. 3419-3424.
- C3. S. K. Sharma, S. Chatzinotas, and B. Ottersten, "Satellite Cognitive Communications: Interference Modelling and Techniques Selection", in *Proc. 6th Advanced Satellite Multimedia Systems Conference (ASMS) and 12th Signal Processing for Space Communications Workshop (SPSC)*, Baiona, Spain, Sept. 2012, pp. 111-118.
- C4. S. K. Sharma, S. Chatzinotas, and B. Ottersten, "The Effect of Noise Correlation on Fractional Sampling based Spectrum Sensing", in *Proc. International Conference on Communications (ICC)*, Budapest, Hungary, June 2013, pp. 2589-2594.
- C5. S. K. Sharma, S. Chatzinotas, and B. Ottersten, "Transmit Beamforming for Spectral Coexistence of Satellite and Terrestrial Networks", in *Proc. 8th Int. Conf. on Cognitive Radio Oriented Wireless Networks (CROWNCOM)*, Washington DC, USA, July 2013, pp. 275-281.
- C6. S. K. Sharma, S. Chatzinotas, and B. Ottersten, "Spatial filtering for underlay cognitive SatComs", in *Personal Satellite Services, ser. Lecture Notes of the Institute for Computer Sciences, Social Informatics and Telecommun. Engg.*, R. Dhaou and et al, Eds. Springer International Publishing, 2013, vol. 123, pp. 186-198.
- C7. S. K. Sharma, S. Chatzinotas, B. Ottersten, "Cognitive Beamhopping for Spectral Coexistence of Multibeam Satellites", in *Proc. Future Network and Mobile Summit (FUNMS)*, Lisbon, Portugal, July 2013, pp. 1-10.
- C8. S. K. Sharma, S. Chatzinotas, B. Ottersten, "Cognitive Radio Techniques for Satellite Communication Systems", in *Proc. IEEE VTC-fall*, Las Vegas, Nevada, Sept. 2013, pp. 1-5.

C9. S. K. Sharma, S. Chatzinotas, B. Ottersten, "Eigenvalue based SNR Estimation for Cognitive Radio in Presence of Channel Correlation", in *Proc. IEEE Globecom*, Dec. 2013, pp. 3419-3424.

C10. S. K. Sharma, S. Chatzinotas, and B. Ottersten, "Compressive SNR Estimation for Wideband Cognitive Radio under Correlated Scenarios", in *Proc. IEEE Wireless Commun. and Networking Conf. (WCNC)*, Istanbul, Turkey, April 2014, pp. 713-718.

C11. S. K. Sharma, S. Chatzinotas, and B. Ottersten, "Maximum Eigenvalue Detection for Spectrum Sensing under Correlated Noise", in *Proc. IEEE ICASSP*, Florence, Italy, May 2014, pp. 4464-4468.

C12. S. K. Sharma, S. Chatzinotas, and B. Ottersten, "Compressive Sparsity Order Estimation for Wideband Cognitive Radio Receiver", in *Proc. IEEE ICC*, Sydney, Australia, June 2014, pp. 1361-1366.

C13. S. K. Sharma, S. Chatzinotas, and B. Ottersten, "A Hybrid Cognitive Transceiver Architecture: Sensing-Throughput Tradeoff", in *Proc. Int. Conf. CROWNCOM*, Oulu, Finland, June 2014.

C14. S. K. Sharma, S. Maleki, S. Chatzinotas, J. Grotz, and B. Ottersten, "Implementation Issues of Cognitive Radio Techniques for Ka-band (17.7-19.7 GHz) SatComs," in *Proc. 7th ASMS/13th SPSC*, Livorno, Sept. 2014.

B1. S. K. Sharma, S. Chatzintoas, and B. Ottersten, "Satellite cognitive communications and spectrum regulation," in *International Regulations of Space Communications: Current Issues*, M. Hofmann, Ed., Larcier, 2013, ch. 11, pp. 201-214.

B2. S. K. Sharma, S. Chatzinotas, and B. Ottersten, "Cognitive Interference Alignment for Spectral Coexistence", in *Cognitive Radio and Networking for Heterogeneous Wireless Networks*, Di Benedetto and et al, Ed., Springer, 2014.

B3. S. K. Sharma, S. Chatzinotas, and B. Ottersten, "Cognitive Beamforming for Spectral Coexistence of Hybrid Satellite Systems", to appear in *Co-operative and Cognitive Satellite Systems*, Elsevier, 2014.

B4. S. K. Sharma, S. Chatzinotas, and B. Ottersten, "Exploiting Polarization for Spectrum Awareness in Cognitive Satellite Communications", in *Software-Defined and Cognitive Radio Technologies for Dynamic Spectrum Access and Management*, IGI Global, 2014.

2. Contributions not Included in the Thesis

J6. S. K. Sharma, S. Chatzinotas, and B. Ottersten, "Inline Interference Mitigation Techniques for Spectral Coexistence of GEO and NGEO Satellites", *Int. J. Satellite Commun. and Networking*, Sept. 2014, doi: 10.1002/sat.1090.

C15. S. Chatzinotas, S. K. Sharma, and B. Ottersten, "Asymptotic Analysis of Eigenvalue based Blind Spectrum Sensing", in *Proc. Int. Conf. Acoustics, Speech and Signal Process. (ICASSP)*, Vancouver, Canada, May 2013, pp. 4464-4468.

C16. S. K. Sharma, S. Chatzinotas, B. Ottersten, "Inline Interference Mitigation Techniques for Spectral Coexistence of GEO and NGEO Satellites", in *Proc. 31st AIAA Int. Commun. Satellite Systems Conf. (ICSSC)*, Florence, Italy, Oct. 2013.

C17. S. Chatzinotas, S. K. Sharma, and B. Ottersten, "Multiantenna Signal Processing for Cognitive Communications", in *Proc. China Summit and Int. Conf. on Signal and Info. Process. (ChinaSIP)*, Beijing, China, July 2013, pp. 293-297.

C18. S. Chatzinotas, S. K. Sharma, and B. Ottersten, “Frequency packing for interference alignment-based cognitive dual satellite systems”, in *Proc. IEEE Vehicular Technology Conf. (VTC-fall)*, Las Vegas, Nevada, Sept. 2013, pp. 1-7 (Selected as one of the best papers of IEEE VTC-fall 2013).

C19. S. K. Sharma, D. Christopoulos, S. Chatzinotas, and B. Ottersten, “New Generation Cooperative and Cognitive Dual Satellite Systems: Performance Evaluation”, in *Proc. AIAA ICSSC*, San Diego, August 2014.

Besides the above dissemination activities, the author’s work has further created synergies with the European COST action IC0902 on “Cognitive Radio and Networking for Cooperative Coexistence of Heterogeneous Wireless Networks” and COST action IC1004 on “Cooperative Radio Communications for Green Smart Environments”. The following contributions have been disseminated through several workshops and technical meetings within these actions.

TD1. S. K. Sharma, S. Chatzinotas, and B. Ottersten, “Exploiting Polarization Domain for Cognitive Coexistence of Satellite-Terrestrial Networks”, *IC0902 COST action 3rd workshop*, Ohrid, September 2012.

TD2. S. K. Sharma, S. Chatzinotas, and B. Ottersten, “Eigenvalue based Blind Spectrum Sensing Techniques”, *COST action IC1004 workshop*, Ilmenau, Germany, May 2013.

TD3. S. Chatzinotas, S. K. Sharma, and B. Ottersten, “Frequency Packing for Cognitive Dual Satellite Systems”, *COST action IC1004 workshop*, Ghent, Belgium, Sep. 2013.

TD4. S. K. Sharma, S. Chatzinotas, and B. Ottersten, “Cognitive Beamforming for Spectral Coexistence of Satellite and Terrestrial Networks”, *COST action IC0902 4th workshop*, Rome, Oct., 2013.

TD5. S. K. Sharma, S. Chatzinotas, and B. Ottersten, “Performance Analysis of a Hybrid Transceiver for Cognitive Radio”, *COST action IC1004 Management Committee and Technical Meeting*, Ferrara, Feb. 2014.

TD6. S. K. Sharma, S. Chatzinotas, and B. Ottersten, “Cooperative Spectrum Sensing for Heterogeneous Sensor Networks”, *COST action IC1004 Management Committee and Technical Meeting*, Aalborg, May 2014.

Chapter 2

Cognitive Communications

This chapter, firstly, reviews and maps the existing spectrum awareness methods with the spectrum exploitation paradigms. Then it focuses on interweave and underlay CR approaches in detail. Subsequently, the existing SS techniques are classified on different bases and special attention is provided to the ED, and the eigenvalue based techniques. Regarding underlay techniques, classification of the existing approaches is provided and several approaches such as cognitive IA, CB, EZ and resource allocation methods are discussed including their main concepts and the related literature. The contributions to these approaches are provided in several ways in subsequent chapters. Some parts of the review work reported in this chapter have been included in [139, 149].

2.1 Background

Cognitive communication is an emerging solution that can overcome the spectrum scarcity problem in future wireless systems. Although this solution started with the idea of a SDR, it comprises a wide variety of techniques and architectures in order to allow the spectral coexistence of the licensed and unlicensed wireless systems. The concept of CR was firstly proposed by J. Mitola in the late 1990's [3]. In [150], he defines the CR as "a really smart radio that would be self-, RF- and user-aware, and that would include language technology and machine vision along with a lot of high-fidelity knowledge of the radio environment". Since its introduction, several industrial/academic/regulatory bodies have provided different definitions of the CR. FCC has defined CR as [4]: "A radio or system that senses, and is aware of its operational environment and can dynamically and autonomously adjust its radio operating parameters accordingly". In an SDR-oriented report, ITU's radio communication study group has provided the following definition of the CR [151]: "A radio or system that senses, and is aware of, its operational environment and can dynamically and autonomously adjust its radio operating parameters accordingly". Further, Global Standards Collaboration (GSC) provides the following definition of the CR [152]: "A radio or system that senses and is aware of its operational environment and can be trained to dynamically and autonomously adjust its radio operating parameters accordingly". Moreover, Qinetiq used the following working definition in its study of CR for OFCOM [153]: "A CR uses Intelligent Signal Processing (ISP) at the physical layer of a wireless system and is achieved by combining ISP with SDR". Additionally, the information theory community defines a CR as [10] "A wireless communication system that intelligently utilizes any available side information about the i) activity, ii) channel conditions, iii) codebooks, or iv) messages of other nodes with which it shares the spectrum. In this thesis, we do not limit the definitions of CR communications to any of the above definitions but define it as "A set of techniques and frameworks which allow the spectral coexistence of primary and secondary systems providing sufficient protection to the PUs while guaranteeing the desired QoS of the SUs".

The FCC has identified a number of CR capabilities such as frequency agility, Dynamic Frequency Selection (DFS), adaptive modulation and transmit power control in order to enable the efficient and flexible usage of the spectrum [2]. Frequency agility is the ability of a radio to change its operating frequency for its adaptation to the radio environment. DFS is a mechanism to detect the signals from other radio systems dynamically and to avoid cochannel operation with them. With the help of adaptive modulation, the CR can reconfigure its transmission characteristics and waveforms in order to exploit spectrum opportunities efficiently. Further, by employing the adaptive transmit power control, the CR node can adapt its transmit power to the allowable limits when needed and to a lower level to allow greater sharing of the spectrum when higher power operation is not required. Moreover, CR technology holds strong potential to unlock spectral gridlock with the help of advanced radio design techniques, powerful encoding and signal processing techniques, and novel protocols [10].

Authors in [154, 155] highlight the following four functions of a CR for realizing a DSA system: (i) SS, (ii) spectrum management, (iii) spectrum sharing, and (iv) spectrum mobility. With the help of SS, a SU should capture information about the available spectrum bands by monitoring them and then identify the spectrum holes in different domains. Based on the available candidate bands, the best available channel should be selected with the help of efficient spectrum management techniques. Further, in the presence of multiple SUs, a suitable multiple access technique should be applied in order to prevent multiple SUs seeking for the same portion of the spectrum, called spectrum sharing. If a specific portion of the spectrum used by the SU is required by a PU, secondary communication should be switched to another vacant portion of the spectrum, called spectrum mobility.

The operation of a CR can be described in the form of a cycle, called cognitive cycle. Several forms of the cognitive cycle exist in the literature [150, 156, 157] and the following tasks are important and common to all available cognitive cycles: (i) Spectrum awareness, (ii) Analysis and decision, and (iii) Spectrum exploitation (adaptation). Any other CR functions can be considered to be just the variants or forms of the above basic tasks. Based on the above tasks, a simplified cognitive cycle is depicted in Fig. 2.1. The first task for a CR is to be aware of its surrounding radio environment i.e, spectrum awareness. This awareness can be obtained with the help of the employed SS mechanism, geolocation database, SNR/sparsity order estimation, etc. as detailed later in Section 2.2.1. The next step is to analyze the acquired information and to take a decision about the best strategy. Subsequently, the CR autonomously adapts its operational parameters such as transmit power, operating frequency, modulation and coding scheme, etc. to any environmental conditions in order to exploit the available spectral opportunities effectively. Further, based on the simplified Open Systems Interconnection (OSI) model presented in [157] in the context of a CR, the following mapping can be made between OSI layers and cognitive capabilities: (i) context awareness for higher layer (application), (ii) inter-operability for intermediate layers (transport and network), and (iii) link adaptation for lower layers (physical and data link). The research problems considered in this thesis are related to the lower layers of this protocol stack.

2.2 Cognitive Techniques

The main functions of a CR are to acquire information about spectral opportunities by monitoring the surrounding radio environments and to exploit those opportunities in an intelligent way while guaranteeing the normal operation of the licensed PUs. In this context, a wide range of cognitive techniques available in the literature can be broadly categorized into: (i) spectrum awareness techniques, and (ii) spectrum exploitation techniques. The first category of techniques are used for acquiring information about the spectral opportunities while the second category deal with the exploitation of the underutilized licensed spectrum in several ways as described later in Section 2.2.2.

In this thesis, we define spectrum awareness problem from multidimensional viewpoint. Depending on the employed techniques at the CR node, different levels of awareness can be achieved. The acquired

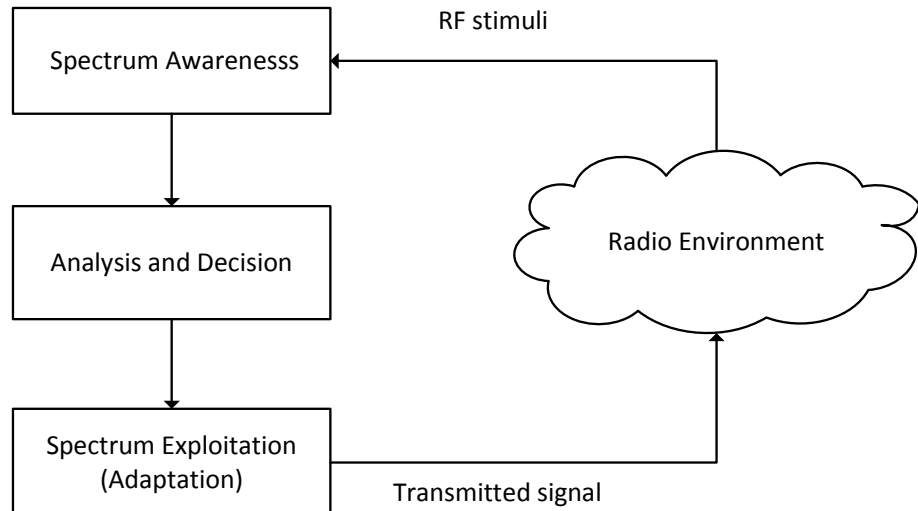


FIGURE 2.1: A simplified cognitive cycle

information can be spectrum occupancy over the available bands, SNR of the PU signal, channel towards the PUs, modulation and coding used by the PUs, pilot/header information in the PU transmit frame, etc. Figure 2.2 presents the mapping of spectrum awareness mechanisms with different spectrum exploitation methods. From the spectrum utilization point of view, the greater the awareness level at the CR node, the better is the spectrum utilization. For example, if the CR node has information only about the spectrum occupancy, it can transmit only in the bands which are not occupied by the PUs at that moment. However, if the CR node can acquire information about the PU SNR, it can even transmit during PU transmission with the controlled power .

2.2.1 Spectrum Awareness Techniques

Depending on the awareness level and the required metric for spectrum exploitation purpose, different spectrum awareness methods can be employed as noted in Fig. 2.2. For acquiring information about the spectrum occupancy, SS, database and beacon transmission-based methods can be applied. Further, for acquiring information about PU SNR and channels, suitable SNR and channel estimation algorithms can be exploited. In addition, the waveform characteristics of the PU signals can be useful for realizing overlay communication as described later in Section 2.2.2. The waveform characteristics are the specific features of the PU signals and may include information about the modulation and coding (modcod) scheme used by the PUs, cyclic frequencies, pilot/header information used in PU transmission, etc. For acquiring these features, suitable modcod detection/classification, frame header/pilot estimation approaches can be utilized. Out of these methods, this thesis focuses on spectrum awareness approaches for interweave and underlay communication, which are briefly described below.

1. Spectrum Sensing: SS is an important mechanism in order to acquire the spectrum occupancy information of the primary spectrum. In other words, it exploits the spectral holes in several domains such as time, frequency, space, polarization, and angular domains. The ST is assumed to be equipped with a RF chain having sensing capability and senses the presence or absence of the PUs with the help of the employed signal processing technique. Depending on the employed signal processing mechanism, there exist several SS techniques [12]. The detailed classification of this approach is provided in Section 2.3.

2. Database: Geolocation database is an alternative spectrum awareness approach to obtain the knowledge of the radio environment and can be used to query various levels of information required by the CRs. In this scheme, spectrum usage parameters of the primary system such as the place, time,

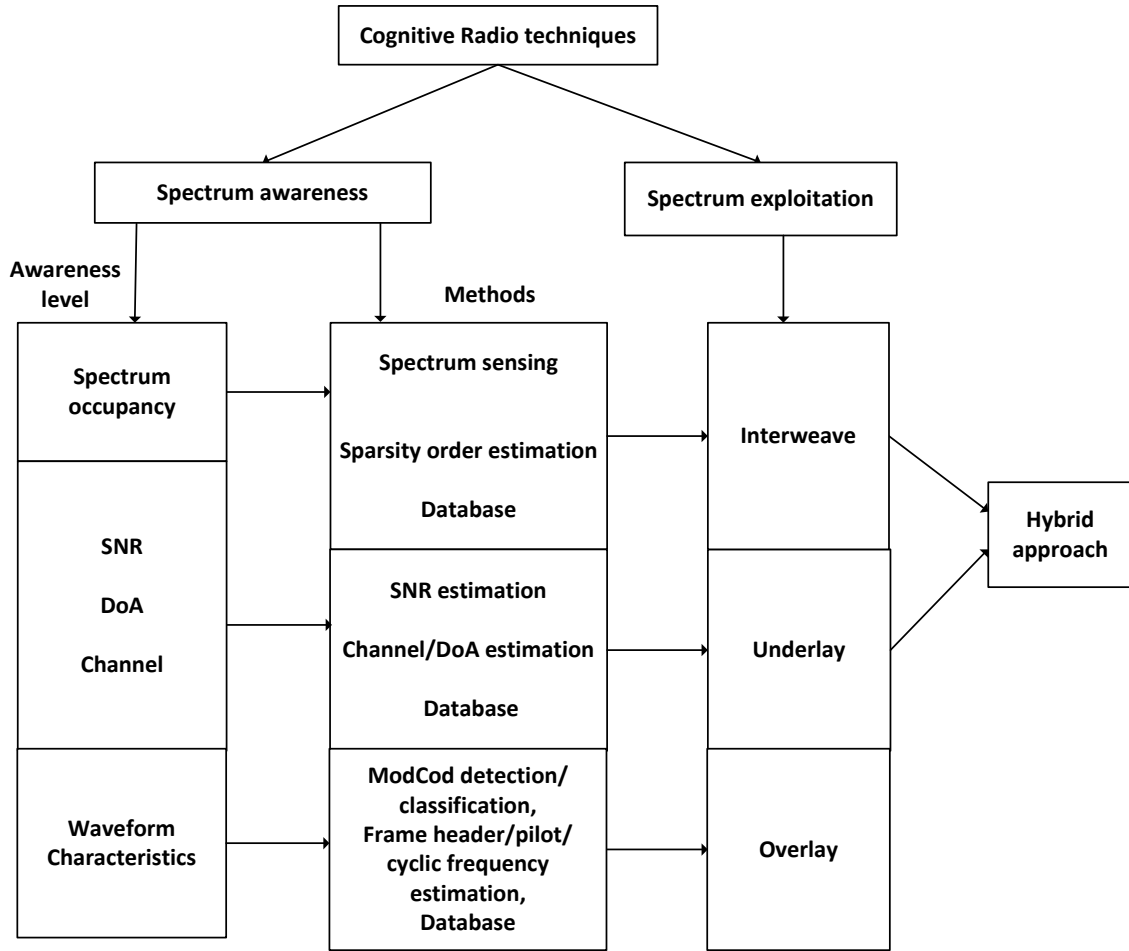


FIGURE 2.2: Mapping of spectrum awareness techniques with spectrum exploitation techniques

frequency, etc. are stored in a centralized database (Fig. 2.3). The SUs who want to reuse the primary spectrum have to make a request to the database system and based on the availability of the unoccupied channels in that location and for the requested period, the database system can grant access to those channels. A CR can also use the database approach including history information and prediction methods to make the operation more efficient. This approach is based on maintaining a frequently updated and centrally located database with information about the regional spectrum usage, including location of PTs, coverage areas, frequencies of operation, transmission powers, radio technologies, etc. This scheme is quite static and the dynamicity of this scheme depends on the how fast the primary spectrum usage information is updated in the database. The database may also store the pre-computed signal levels, waveform characteristics, channel quality information which can be estimated by suitable propagation, prediction and estimation methods. As noted in Fig. 2.2, the database approach can be useful for all interweave, underlay and overlay spectrum exploitation approaches (detailed later in Section 2.2.2) depending on the awareness level of the stored information.

Radio Environment Maps (REMs) are becoming a promising architectural concept for storing environmental information for use in CR networks [158]. In [158], it has been shown that the enhancement of the REM by means of spatial statistics and models can be obtained through a topology engine, which is an agent collecting and processing spatial information about the environment for storage in the REM. One of the sensing and measuring schemes is the Wireless Regional Area Network (WRAN) system based on REM as proposed in [159], which can be considered as an integrated database. REM enabled WRAN system has been proposed in [160] and it has been shown that it can better realize different functions at the same time to ensure the protection of the PUs. As an example, in case of cognitive access to TV white space scenario, based on CR's geolocation data and specific service requirements,

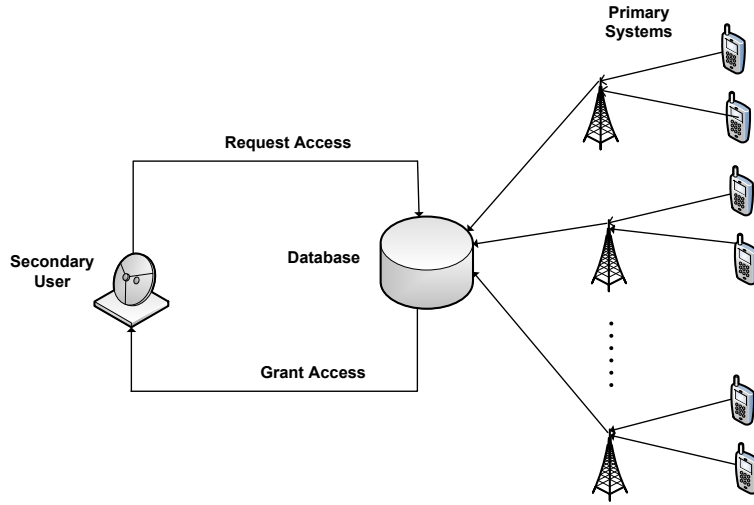


FIGURE 2.3: Illustration of the database approach

the secondary BS queries a central database for channel availability [161]. The database then returns information about various operating parameters such as number of channels, centre frequency and associated power levels available for secondary use in that location. REM makes the adaptation of a CR to a new environment easier where regulations may be different [162]. Existing REM construction techniques can be broadly put into two categories: (i) spatial statistics based methods [163] and (ii) transmitter location determination based methods [164], which are also referred to as direct and indirect methods respectively.

3. Beacon Signals: This awareness method is based on the regional broadcasting of the beacon signals in appropriate signalling channels by the primary systems and the detection of these signals by the CR users in order to obtain information about the spectrum occupancy. The beacon signals may carry the information about the spectrum usage of the primary system, traffic trends, and future frequency usage etc. [165] and also the information from the database in database-assisted systems. This approach requires an agreement between secondary and primary system operators in order to share the real time spectrum usage information of the primary network with the secondary network. The above interaction may require additional modifications in the primary legacy radio systems, which might be difficult to implement in practice. In this context, Cognitive Pilot Channel (CPC) has received important attention as a signalling channel in the scenarios of primary-secondary coexistence [166, 167]. Although the original concept of CPC was to transmit information from the network to the mobile terminals in order to make them aware of surrounding environment and available radio access technologies, it can act an enabler for radio systems coexistence [166]. One of the important aspect in designing CPC channel is the selection of operating frequency. Various in-band and out of band approaches have been suggested in the literature for this purpose.

4. Sparsity Order Estimation: Sparsity order can be defined as the ratio of the occupied carriers to the total carriers over the band of interest. This actually provides information about how much percentage of the licensed band is available for the secondary usage. This awareness is helpful in implementing CS-based wideband sensing as mentioned in Chapter 1. Since the sparsity order is time varying parameter and is not known to the CR receiver beforehand, it needs to be estimated in practice. If the information about the sparsity order is available to the wideband CR transceiver, it can dynamically adapt its sampling rate in order to fully exploit the advantages of the CS technique as detailed later in Chapter 4.

5. SNR/Channel/DoA Estimation: This is the additional level of awareness that a CR needs to have for controlling its power/radiation in order to protect the cochannel PUs. If the CR node can acquire information about SNR and channel of the primary signals, different underlay techniques such as EZ, and power control (described later in Section 2.4) can be employed. As mentioned earlier in Chapter 1, based on the estimated SNR, the CR can control its power in order to enhance its throughput while

protecting the PUs at the same time. An accurate estimation of SNR further helps in link adaptation and iterative decoding. For SNR estimation problem in wireless communications literature, several techniques have been reported (see [168, 169] and references there in). The existing SNR estimation algorithms can be broadly categorized into [169]: (i) data-aided (DA), and (ii) non-data-aided (NDA). The NDA estimators derive the SNR estimates directly from the unknown, information-bearing portion of the received signal while the DA estimators predict the SNR values using known data, for example, training sequences (pilots) provided for synchronization and equalization. In general, DA estimators are more accurate than NDA estimators but may require higher bandwidth and NDA estimators are useful in the applications where data may be unknown. Further, in the context of satellite systems, the authors in [170, 171] propose an SNR estimation algorithm for advanced digital video broadcasting return channel via satellite (DVB-RCS) systems using Adaptive Coding and Modulation (ACM). However, in the context of CR networks, there exist only a few SNR estimation related works [19, 20, 25, 26]. Moreover, if the CR node has information on the DoA of the primary terminals either through database or through some DoA estimation algorithms, it can employ suitable beamforming based underlay approaches in order to mitigate interference towards/from the PRs/PTs.

Out of the aforementioned spectrum awareness approaches, this thesis focuses on SS, SNR estimation and sparsity order estimation problems. Furthermore, on the basis of spectrum sharing policy, spectrum awareness techniques can be categorized into [172]: (i) vertical spectrum sharing, and (ii) horizontal spectrum sharing. Horizontal spectrum sharing provides same right to all the terminals or networks in order to access a particular spectrum band whereas in vertical spectrum sharing, one wireless system i.e., the owner of the spectrum license, has a higher priority to access the spectrum over the rest of the systems. In CR communication, vertical spectrum sharing takes place between PUs and SUs whereas horizontal spectrum sharing occurs among secondary systems.

2.2.2 Spectrum Exploitation Techniques

Based on the access technology of the SUs, the existing spectrum exploitation techniques can be broadly categorized into interweave, underlay, and overlay techniques [10]. Different researchers have diverse opinions about the classification of CR techniques and on the use of terminologies “interweave”, “underlay” and “overlay” [10, 173]. In this thesis, we follow the classification provided by A. Goldsmith, and et al in [10]. The main distinction between these terms in the context of this thesis lies on the following points: (i) interweave paradigm allows secondary transmission only in the spectral holes of the primary spectrum, (ii) underlay paradigm allows the simultaneous operation of primary and secondary systems with the transmit power constraint on the secondary transmission in such a way that interference level at the PR remains below an acceptable limit, and (iii) overlay paradigm allows the concurrent transmission of primary and secondary systems by mitigating interference with the help of advanced coding and transmission strategies at the STs. These exploitation approaches are briefly discussed in the following paragraphs.

1. Interweave: This paradigm encompasses interference avoidance or opportunistic techniques which require SUs to communicate opportunistically using spectral holes in space, time, and frequency which are not occupied by the PUs. Therefore, there occurs no interference in the ideal case [10]. This technique does not impose any restrictions on the transmit power of the SUs but is limited by the range of available spectral holes. Although space, time and frequency are common dimensions used for interweave communication, polarization and angular dimensions can also be considered as additional dimensions for spectrum exploitation purpose. As depicted in Fig. 2.2, the awareness techniques such as SS, database and beacon signals facilitate the interweave communication. The main drawback of this approach is that it needs to correctly identify the spectral holes or the presence of the PU activity in order to avoid harmful interference to the PUs. It should be noted that when the PU reappears in a certain licensed channel, the secondary system should instantly vacate the channel and be switched to another unoccupied channel. Depending on the type of the employed awareness mechanism, this exploitation scheme can be dynamic or static. For example, if the SS is used, this approach can

effectively utilize the spectrum holes as the primary spectrum utilization varies over the time while with the database approach, the spectrum utilization efficiency varies based on the update frequency of the database. In practice, one or the combination of two or more spectrum awareness methods can be used. The combination of SS with a simple database seems to be an effective approach from the perspective of reducing the sensing overhead in large CR networks.

2. Underlay: Underlay networks are characterized by strict constraints on the interference that may be caused by the STs to the PRs. In this paradigm, the coexistence of primary and secondary systems is allowed, only if the interference caused by STs to the PRs can be controlled and managed properly [174]. The maximum allowable interference level at the PR can be modeled by the concept of interference temperature, as defined by the FCC Spectrum Policy Task Force in [175]. This metric is also termed as interference threshold which guarantees the reliable operation of the PUs regardless of the SU's spectrum utilization [176]. The STs utilizing the shared band must guarantee that their transmissions added to the existing interference must not exceed the interference threshold at the PR. As depicted in Fig. 2.2, side information about primary system such as PU SNR, channels, DoAs are useful for realizing the underlay techniques. Further, underlay communication can be realized with the help of one or many of the following methods: (i) beamforming with the help of multiple antennas (See Section 2.4.1), (iii) dynamic resource allocation (carrier/power) at the ST (See Section 2.4.3) , (ii) spread spectrum approaches by spreading the secondary signal below the noise floor and then de-spreading at the CR, (iv) interference management using IA approach (See Section 2.4.2), (v) by using EZ principle (See Section 2.4.3).

3. Overlay: Overlay networks are characterized by the mitigation of interference with the help of advanced coding and transmission strategies at the STs. In this paradigm, the SU can transmit simultaneously with the PU and the interference caused by the ST to the PR can be offset by using a part of the SU's power to relay the PU's message [10]. In this scheme, the SU transmits the PU signal along with its own signal. A two user interference channel where the ST has knowledge of the PU's message can be considered as a simplistic example of an overlay CR network. The cognitive transmitter should have knowledge of the PU's channel gains, codebooks and possibly its messages as well. Different Pre-coding techniques such as Gel'fand-Pinsker binning and dirty paper coding in Gaussian channels can be applied to overlay networks [177] [178]. In [179], an overlay SU signal over a satellite communication channel occupied by a PU has been considered, the SU is allowed to transmit data symbols as a fraction of the PU's symbol rate. In [180], a linear search based approach is proposed to optimally allocate the transmit power and design the beamformers in an overlay CR channel with a single primary and a single cognitive user, where the cognitive user causally obtains primary message knowledge at its transmitter. Overlay techniques are the most suitable techniques for integrated systems where there is a high degree of cooperation between satellite and terrestrial networks. In practice, this paradigm is difficult to implement due to a high level of cognition required between primary and secondary systems. In this context, the possible way is to acquire the wave characteristics of the PU signal by using estimation approaches such as modcod classification/detection, frame header/pilot/cyclic frequencies estimation, etc. as depicted in Fig. 2.2 and use these waveform characteristics in order to design advanced transmission strategies at the ST.

2.3 Spectrum Sensing

The SS problem for a CR is different from normal detection in the following ways [181, 182]: i) no prior knowledge of the signal structure i.e., statistics, noise variance value etc., ii) the detection of PU signal is expected in the shortest possible time, iii) primary SNR may be very low due to fading and multi-path phenomenon, iv) noise/interference power varies with time in practical scenarios giving rise to noise/interference power uncertainty, and v) Noise uncertainty may be non-Gaussian. Further, noise uncertainty can be categorized into the following two types: a) receiver device noise uncertainty caused by components in the RF chain, and b) environmental noise uncertainty caused by

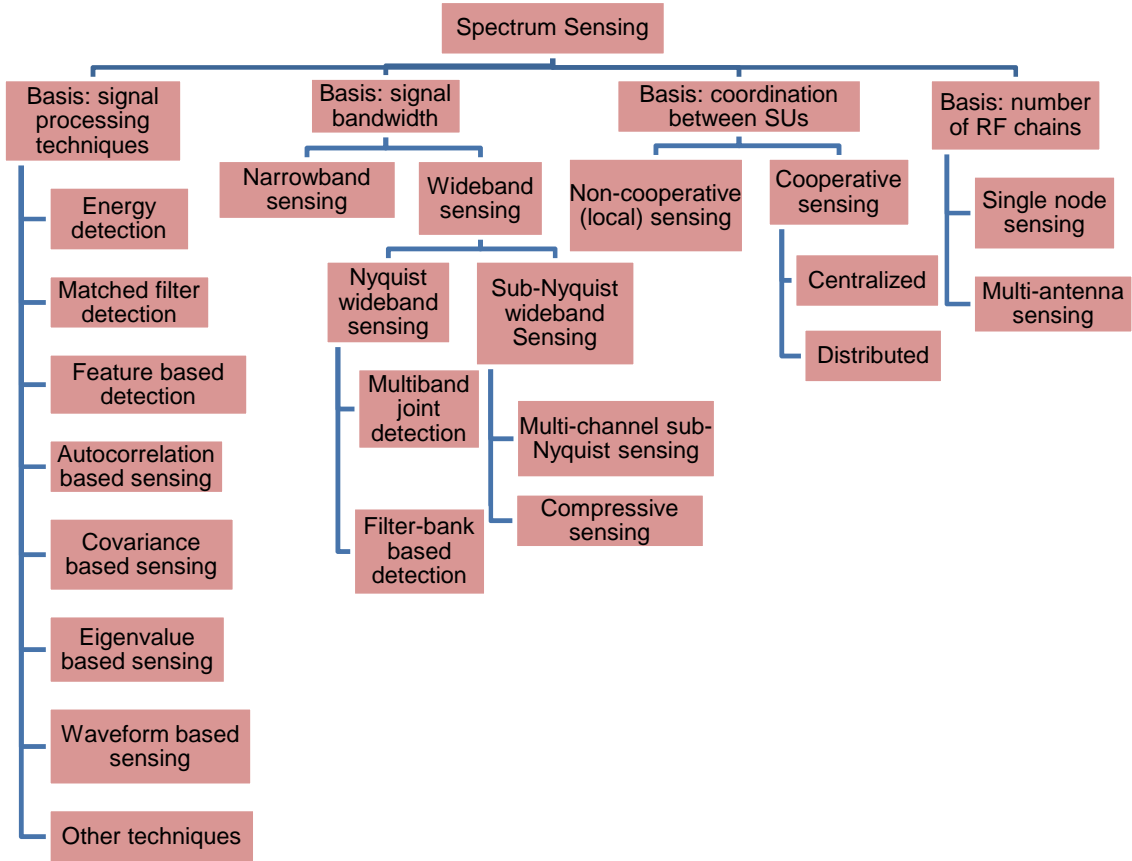


FIGURE 2.4: Classification of SS techniques

the surrounding environment. The inaccurate estimation of noise power may lead to degradation in the sensing performance. In the following subsections, we summarize different types of SS techniques.

2.3.1 Classification and Related Literature

Different SS techniques have their own operational requirements, advantages and disadvantages from the practical perspectives. The available CR techniques can be categorized based on different bases as reflected in Fig. 2.4. The detailed survey of the existing SS techniques can be found in [11, 12]. Further, the reference [29] focuses on the review of existing wideband sensing schemes. According to the employed signal processing mechanisms, SS techniques can be categorized into the following.

1. Energy Detection: ED is the most common way of SS because of its low computational and implementation complexities [13, 14, 183, 184]. With this technique, the PU signal can be detected by comparing the output of the energy detector with a threshold which depends on the noise floor. This method is simple to implement but suffers from different drawbacks such as noise variance uncertainty, inability to differentiate interference from PUs and the noise, and poor performance under low SNR values [28]. The detailed description of this approach is provided in Section 2.3.3.

2. Matched Filter based Detection: Matched-filtering is known as the optimum method for detection of PUs when the transmitted signal is known [185]. The main advantage of the matched filter is that it requires less time to achieve a certain target probability of false alarm or probability of miss detection as compared to other methods due to its coherent nature [182]. This approach has the following two drawbacks: (i) it needs a dedicated receiver for each PU class [186], and (ii) it requires perfect synchronization between transmitter and receiver, which is difficult to achieve in practice since primary and secondary networks may be administered by two different operators. The benefit of optimal coherent processing comes at the cost of perfect synchronization required to demodulate the pilot. In case of the frequency offsets, the coherent pilot-based detection provides limits on the sensing time

as well as on the detectable signal levels [183]. The implementation complexity of the sensing unit with this approach becomes impractically large and power consumption also increases.

3. Feature based Detection: Cyclostationary Detection (CD) is the most widely studied feature detection technique in the literature and this technique detects the active PU transmissions by exploiting the cyclostationary features of the received signals [187]. During signal transmission, modulated signals are generally coupled with different pulses such as sine wave carriers, pulse trains, cyclic prefixes etc., resulting in built in periodicity. These modulated signals are characterized as cyclostationary since their statistics, mean and autocorrelation exhibit periodicity [188]. Cyclostationary features are caused by the periodicity in the signal or in its statistics like mean and autocorrelation or they can be intentionally induced to assist spectrum sensing [189]. In addition to detecting PU signal from the noise, the CD algorithms are capable of distinguishing among different types of signals transmitted by multiple PUs. This approach is robust against noise variance uncertainty and it can reject the effect of adjacent channel interference. However, the computational complexity of this method is high, and a large number of samples are required to exploit the cyclostationarity behavior of the received signal. Further, this detector is very sensitive to cyclic frequency mismatch caused due to clock/oscillator or other errors [190]. Although the original work [188] based on cyclostationary feature requires the prior knowledge about the features of the primary signal, recent works [191–193] have shown that cyclostationary detection based on the proposed estimators can be fully blind.

In addition to CD, other feature detection techniques such as blind standard recognition, feature vectors based detection have been studied in the literature [194, 195]. Authors in [196, 197] introduced the concept of a Blind Standard Recognition Sensor (BSRS) which realizes the fusion of information from several sensors in order to detect the employed standard. The BSRS is a fundamental example among the set of Sensorial Radio Bubble (SRB) sensors introduced in [157]. Further, in [194], the BSRS is implemented on a Universal Software Radio Peripheral (USRP) platform in order to discriminate standard-like signals. The operation of the BSRS is basically composed of the following three steps: (i) band adaptation, (ii) extraction of different features from the received signal, and (iii) information fusion. Moreover, authors in [198] proposed a blind feature learning algorithm and subsequently, a feature template matching algorithm using learned features for the SS purpose. In the similar context, a multiple feature matching algorithm has been proposed in [195] and it has been claimed that the proposed method does not require the prior knowledge of the PU signal feature.

4. Autocorrelation based Sensing: Autocorrelation based detectors exploit the difference between the signal and noise spectrums over the sensing bandwidth. This difference arises due to the higher autocorrelation of the signal which may arise due to the use of practical modulation schemes as well as the presence of RF channel guard bands [199]. In this context, authors in [199] propose a simple correlation sum (CorrSum) detector exploiting both energy and correlation parameters for the improved sensing performance assuming that correlation is real and extend to the scenario with the knowledge of correlation distribution information in [200]. Further, a Constant False Alarm Rate (CFAR) detection algorithm has been studied in [201] using the estimated autocorrelation of the received signal and its performance is shown to be better than the the covariance detector and the cyclic autocorrelation detector.

5. Covariance based Sensing: This approach is based on the sample covariance matrix of the received signal at the CR node and exploits the difference in the statistical covariances of the received signal and the noise. It does not require any a priori information of the signal, channel, and noise power and further no synchronization is needed [202]. The authors in [202] proposed covariance absolute value and generalized covariance based detection algorithms for a CR. Further, authors in [203] study the distribution of the test-statistic for the covariance based detection and propose analytical expressions for calculating detection and false alarm probabilities.

6. Eigenvalue based Detection: Several diversity enhancing techniques such as multi-antenna, cooperative and oversampled techniques have been introduced in the literature to enhance the SS efficiency in wireless fading channels [18, 48, 204, 205]. In most of these methods, the properties of the eigenvalues of the received signal's covariance matrix have been considered using the recent results from advances in RMT. Some of the eigenvalue based SS techniques do not require any prior information

of the PU's signal and they outperform ED techniques, especially in the presence of noise covariance uncertainty. The detailed description of this approach is provided in Section 2.3.4.

7. Waveform based Sensing: In wireless systems, known patterns can be utilized to assist synchronization or for other purposes. Such patterns include preambles, midambles, regularly transmitted pilot patterns, spreading sequences etc. In the presence of a known pattern, sensing can be performed by correlating the received signal with a known copy of itself. This method is only applicable to systems with known signal patterns, and is termed as waveform-based sensing or coherent sensing. Measurement results presented in [183] show that waveform-based sensing requires short measurement time, however, its performance is susceptible to synchronization errors.

8. Other Techniques: Another alternative technique for obtaining the presence of the active PU is external sensing, where an external agent performs the sensing and broadcasts the channel occupancy information to the CRs. The main advantages of external sensing are overcoming hidden PU and the uncertainty due to shadowing and fading. Furthermore, as the CRs do not spend time for sensing, spectrum efficiency is increased. Other alternative spectrum sensing methods include information theoretic based spectrum sensing, fast sensing, radio identification based sensing, multi-taper spectral estimation, wavelet transform based estimation, Hough transform, and time-frequency analysis [12].

In practical wireless fading channels, the SS efficiency of the aforementioned techniques may be degraded due to the Hidden Node Problem (HNP), path loss, shadowing, multipath fading and receiver noise/interference uncertainty issues. The HNP arises when a CR user experiences a deep fade or shadowing from the PT and can not detect the presence of the PU signal, leading to the missed detection, and hence the harmful interference to the PR. In this context, cooperative SS, in which several nodes cooperate with each other in order to enhance the overall sensing performance, has been considered as a promising approach [206–208]. A general schematic of the cooperating SS scenario is depicted in Fig. 2.5. The main concept behind cooperative SS is to enhance the sensing performance by exploiting the observations captured by spatially located CR users. The cooperation can be among the CR nodes or external sensors can be deployed to build a cooperative sensing network. In the former case, the cooperation can be implemented in the following ways [207]: (i) centralized, (ii) distributed, and (iii) relay-assisted. In the centralized approach, a central unit collects sensing information from cognitive devices, identifies the available spectrum, and broadcasts this information to other CRs or directly controls the CR traffic whilst in the distributed approach, cognitive nodes share information among each other but they make their own decisions regarding which part of the spectrum they can use. Distributed sensing is more advantageous than the centralized sensing since it does not require a backbone infrastructure and it has reduced cost. In the relay-assisted approach, a CR user with a strong sensing channel and a weak report channel can cooperate with a CR user observing a weak sensing channel and a strong report channel in order to improve the overall sensing performance.

The cooperative sensing gain is achieved by sharing the information gathered by the cooperating users, thus making the combined decision more reliable than the individual decisions. Besides the cooperative gain, cooperative sensing results in relaxed receiver sensitivity and higher throughput if the sensing time can be reduced with the help of cooperation [206]. Despite the aforementioned advantages, cooperative SS requires a control channel for each cooperating node to report its sensed information to the Fusion Center (FC) and this channel is usually bandwidth limited [209]. Thus, cooperation burden can be a critical issue from a practical perspective. This refers to additional resources required for signalling, any additional sensing time, delay, energy, and other operations devoted to cooperative sensing compared to the non-cooperative SS [206]. The detailed survey on existing cooperative SS can be found in [206, 207].

Furthermore, depending on the amount of knowledge required at the receiver, sensing techniques can be broadly categorized into: (i) knowledge-based, (ii) semi-blind, and (iii) blind. For example, the matched filter and the CD can be considered as knowledge-based techniques since they require the knowledge about the PU signal's characteristics, the ED can be considered as semi-blind since this technique does not require the knowledge about the PU signal and channels but requires the accurate knowledge of the

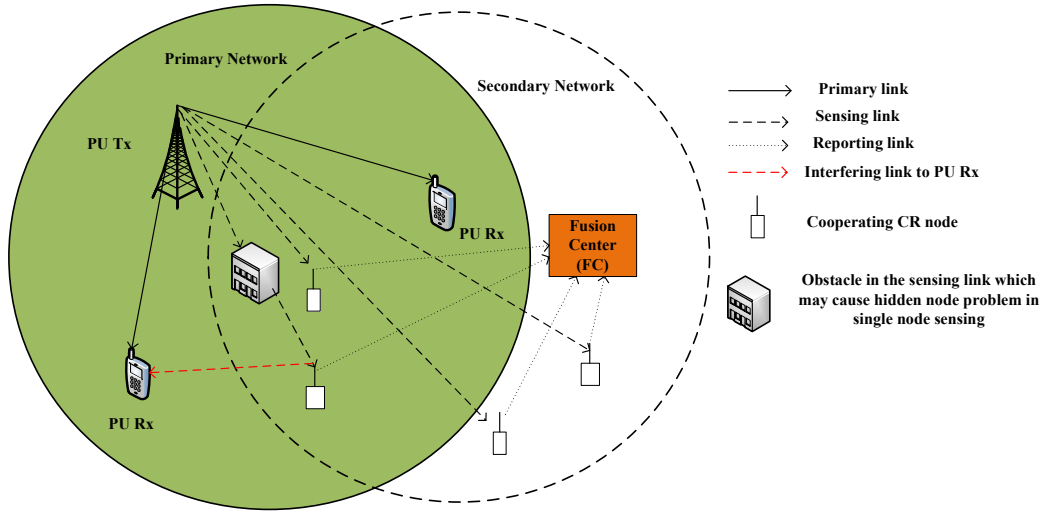


FIGURE 2.5: Schematic of the cooperative SS scenario

noise variance. On the other hand, the MME technique can be considered as a blind technique [18] since it neither needs the knowledge of PU signal and channels nor the noise variance.

Moreover, based on the bandwidth of the channel to be sensed, the SS techniques can be narrowband and wideband. Most of the aforementioned techniques are narrowband and can be extended for wideband context using complex hardware circuitry. Existing wideband sensing techniques include Tunable Filter Method [30], Wavelet transform method [210], Multibeam joint detection [211], Spatial-spectral joint detection [212], and CS [30, 213]. Further, collaborative wideband sensing has been discussed in several literature for enhancing the detection performance in the presence of fading [32, 212]. The collaboration among multiple spatially distributed CRs can relax the sensitivity constraint on the RF front-end by enhancing the detection signal energy at the fusion center and may even broaden the frequency range of SS. The CS technique performs sampling at a rate less than the Nyquist rate and reconstructs the original signal back from significantly lower number of compressive measurements. The sparseness may appear in different scenarios such as communication signals, acoustic signals, slowly varying chirps, smooth signals, piecewise smooth signals etc. In the field of wireless communications, sparse signals may appear in different applications such as transmissions with a frequency-hopping modulation scheme that switches a sinusoidal carrier among many frequency channels according to a predefined sequence, transmissions with narrowband modulation where the carrier frequency is unknown but could lie anywhere in a wide bandwidth. In addition, different signal processing operations such as detection, estimation and filtering can be carried out directly from compressive measurements without the requirement of full signal recovery, hence reducing the sensing hardware cost significantly [74]. Several hardware architectures have been proposed and implemented in the literature enabling the compressive samples to be acquired in practical settings. Some of the examples are [29]: (i) Random Filtering, (ii) Compressive multiplexer, (iii) Random convolution, (iv) Random demodulator, (v) Modulated wideband converter.

2.3.2 Sensing Principle for Cognitive Radio

In this section, we formulate the PU signal detection problem and present its generic principle which is later applied for the energy and eigenvalue-based detectors considered in this thesis. Herein, we present a narrowband detection problem with a single CR node for the simplicity purpose.

Let us consider a frequency band W with the center carrier frequency f_c and we are interested in detecting the presence or absence of the PU signals in this band. We denote the hypotheses of the PU absence and the PU presence by H_0 (noise only hypothesis) and H_1 (signal plus noise hypothesis)

respectively. Let us consider that the received signal at the CR receiver is sampled at the sampling frequency of f_s and N number of samples are acquired for the decision process. Then the sensing time (τ) is given by; $\tau = N/f_s$. Under the H_1 hypothesis, the discrete received signal at the CR receiver can be represented as

$$y(n) = x(n) + z(n), \quad (2.1)$$

where $x(n)$ is the transmitted signal at the n th time instant and $z(n)$ denotes the AWGN. Similarly, under the H_0 hypothesis, the above equation reduces to

$$y(n) = z(n). \quad (2.2)$$

Herein, the detection problem is to distinguish the cases of the PU presence and the PU absence. This is known as a binary hypothesis testing problem since we need to choose between two hypotheses. This can be formulated in terms of the binary hypothesis testing problem in the following way [16]

$$\begin{aligned} H_0 : y(n) &= z(n), & \text{PU absent} \\ H_1 : y(n) &= x(n) + z(n), & \text{PU present.} \end{aligned} \quad (2.3)$$

In order to test the above hypothesis, we need to find a decision statistic whose distribution sufficiently differs under the H_0 and the H_1 hypotheses. The decision threshold can be energy for an ED approach (see Section 2.3.3.1), ME for ME-based detection (see Section 2.3.4.3), etc. The sensing threshold is usually calculated from the distribution of the decision statistics i.e., received energy in ED, under the H_0 hypothesis. If the hypothesis H_0 is satisfied, then it can be decided that the PU signal over a certain band is absent and then the SU can utilize this band in the secondary basis. Whereas, if the hypothesis H_1 is satisfied, the decision is the presence of the PU signal and the secondary transmission should be switched to another band. In case, other bands in the available bandwidth range are not available or their quality is not better enough, the secondary transmission should be moved to the exclusive band. These decisions are to be taken centrally by the network management system based on the feedback it receives by the secondary terminals.

Two general approaches for the hypothesis testing are the classical approach based on the Neyman-Pearson (NP) theorem and the Bayesian approach based on the minimization of the Bayes risk [16]. The difference between these two approaches is that Bayesian methods employ the prior knowledge about the probabilities of occurrence of the hypotheses but the NP approach does not assume this prior knowledge. In this thesis, we follow the NP approach for studying the considered detection problems. There may occur two types of errors in the above hypothesis testing problem. These are: (i) probability of false alarm (P_f) (called Type I error in statistics) and (ii) probability of miss detection (P_m) (called as Type II error in statistics). The false alarm occurs if we decide H_1 when H_0 is true and the miss detection occurs if we decide H_0 when H_1 is true. If we denote the probability of deciding H_i when H_j is true by $Pr(H_i, H_j)$ with $\{i, j\} \in \{0, 1\}$, then $P_f = Pr(H_1, H_0)$, and $P_m = Pr(H_0, H_1)$. Similarly, the probability of detection (P_d) is given by; $P_d = 1 - P_m = Pr(H_1, H_1)$. The performance of a detector is commonly expressed in terms of the Receiver Operating Characteristics (ROCs), which is the plot of P_d versus P_f or Complementary ROC, which is the plot of P_m versus P_f . The sensing threshold can be defined according to the CFAR or the Constant Detection Rate (CDR) methodologies based on the detection problems which may require either the target P_f or the target P_d , respectively.

2.3.3 Energy Detection

2.3.3.1 Basic Principle

In this approach, the decision (test) statistics is the energy of the received signal. The presence or absence of the PU signal is decided by comparing the received energy with the noise floor which is calculated based on a suitable noise variance estimation method. This method is a suboptimal and

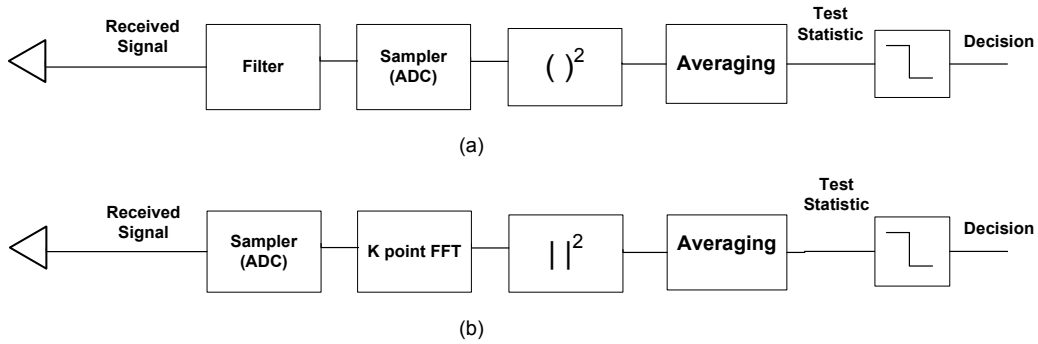


FIGURE 2.6: ED detector (a) Classical approach, and (b) Periodogram approach

simple approach and can be applied to any signal type [183]. An energy detector can be implemented by the following two methods. In the first approach, the received signal is passed through a band pass filter in order to reject out of band signals and noise, then sampled with the help of ADC at the Nyquist rate and subsequently passed through a square law device and an integrator or averaging device (See Fig. 2.6 (a)). The output of the integrator is decision statistics for this detector and is compared with the threshold in order to take a decision on the presence or absence of the PU. This approach requires the filter bandwidth to be matched with the given signal bandwidth. In the second approach, a periodogram can be used to estimate the spectrum by squaring and averaging the frequency bins obtained by Fast Fourier Transform (FFT) process (See Fig. 2.6 (b)). This approach is more flexible in the fact that the frequency resolution of the FFT increases with the number of points K , which is equivalent to changing the filter bandwidth in the first approach and increasing the number of spectral averages improves the detection performance.

Let us consider that the transmitted PU signal $x(n)$ is an i.i.d. random process with mean zero and variance $E[x(n)]^2 = \sigma_x^2$ and the noise $z(n)$ is a Gaussian i.i.d. random process with zero mean and variance $E[z(n)]^2 = \sigma_z^2$. Furthermore, we assume that the PU signal $x(n)$ is independent of the noise $z(n)$. The test statistic for the ED technique is given by

$$T_{ED} = \frac{1}{N} \sum_{n=1}^N |y(n)|^2. \quad (2.4)$$

It can be noted that the test statistic T_{ED} is a random variable and under the H_0 hypothesis, its p.d.f. follows a Chi-squared distribution with $2N$ dofs for the complex valued case [13]. For very large values of N , the p.d.f. of T_{ED} can be approximated by a Gaussian distribution with mean $\mu = \sigma_z^2$ and the variance $\sigma_0^2 = \frac{1}{N}[E[z(n)]^4 - \sigma_z^2]$ [107]. Then using binary hypothesis testing, the expressions for P_f and P_d can be computed by [16]

$$\begin{aligned} P_f &= \Pr(T_{ED} > \lambda_{th} | H_0), \\ P_d &= \Pr(T_{ED} > \lambda_{th} | H_1), \end{aligned} \quad (2.5)$$

where λ_{th} is the sensing threshold. The number of samples N required to satisfy a desired P_d and P_f constraints in the low SNR regime scales as $O(1/\text{SNR}^2)$ for the ED approach while the value of N scales as $O(1/\text{SNR})$ for the matched filter detection [183]. Therefore, the sensing time in an ED detector becomes longer in comparison to the matched filter based detector.

2.3.3.2 Literature Review

The ED problem was first studied in [13] for deterministic signals transmitted over a flat band-limited Gaussian noise channel. The performance of SS methods degrades due to fading effects in a wireless channel. In this context, the ED problem for the signals transmitted over a variety of fading channels

has been considered in [14, 184] using different receive diversity schemes. In practical scenarios, the total fading involves the combined effect of two independent processes: small-scale fading and large scale fading i.e., multi-path and shadowing effects [214].

The performance of the ED technique deteriorates in the scenarios where the PU activity status changes during the sensing period. In many cases, it is assumed that the PU activity remains constant during the sensing time. This assumption is valid for the scenarios like TV Whitespace (TVWS) where the PU spectrum becomes occupied or available for the longer time. However, in the dynamic scenarios, the PU may appear at any time and the detection performance deteriorates. In this context, adaptive detectors have been proposed in the literature [215, 216] considering the PU activity while setting the sensing threshold. However, monitoring the activity of the PU activity is really an issue to implement in practice. Furthermore, as noted in several literature [15, 217, 218], an energy detector is sensitive to the noise variance uncertainty, and there exists an SNR wall below which this detector can not guarantee a certain detection performance. In this context, the current research is examining the ways of tackling the noise uncertainty problem in various settings [218, 219]. In [219] a PU prediction-based adaptive ED algorithm has been proposed in which two thresholds are utilized based upon the average energy received from the PU during the sensing interval. Recently, authors in [218] have proposed a max-min SNR signal energy based SS algorithm under noise variance uncertainty. In this approach, the ratio of the signal energy corresponding to the maximum and minimum SNRs is proposed as a test statistics of the energy detector and it is shown that the proposed algorithm is robust to noise variance uncertainty. Moreover, several ED approaches based on the estimation of the noise variance are studied in [220, 221]. The performance of the ED with the estimated noise power is analyzed in [222] and it is shown that estimation of the noise can avoid the SNR wall if the estimate is consistent with the sensing interval. Further, researchers have studied the combination of the ED technique with other detectors such as cyclostationary detector in order to improve the sensing performance in the low SNR region [223, 224].

2.3.4 Eigenvalue based Spectrum Sensing

2.3.4.1 Basic Principle

In general, this method is based on the Eigenvalue Decomposition (EVD) of the received signal's covariance matrix. Depending on the employed decision statistics, there exist several eigenvalue based techniques. We present its generic principle below. In this approach, different eigenvalue properties of the received signal's covariance matrix can be exploited to perform sensing. For implementing this technique, the CR node has to collect the received samples in the $M \times N$ matrix form with M being the receive dimension. This receive dimension can be either the number of fractional sampled branches, multiple antennas or the cooperating nodes. A single CR node can implement an eigenvalue-based technique independently if it employs fractional sampling on the received signal and/or is equipped with multiple antennas.

After collecting N samples using different receive dimensions, the $M \times N$ received signal matrix \mathbf{Y} can be written as

$$\mathbf{Y} = \begin{bmatrix} y_1(1) & y_1(2) & \dots & y_1(N) \\ y_2(1) & y_2(2) & \dots & y_2(N) \\ \vdots & \vdots & \ddots & \vdots \\ y_M(1) & y_M(2) & \dots & y_M(N) \end{bmatrix}. \quad (2.6)$$

We define the sample covariance matrices of the received signal and the noise as: $\hat{\mathbf{R}}_{\mathbf{Y}}(N) = \frac{1}{N} \mathbf{Y} \mathbf{Y}^\dagger$ and $\hat{\mathbf{R}}_{\mathbf{Z}}(N) = \frac{1}{N} \mathbf{Z} \mathbf{Z}^\dagger$. Under the H_0 hypothesis, the sample covariance matrix of the received signal becomes equal to the sample covariance matrix of the noise i.e., $\hat{\mathbf{R}}_{\mathbf{Y}}(N) = \hat{\mathbf{R}}_{\mathbf{Z}}(N)$.

From the EVD of $\hat{\mathbf{R}}_Y(N)$, several decision statistics such as ME [17], MME or SCN¹ [18], EME [18], Scaled Largest Eigenvalue (SLE) [49], etc. can be derived. It should be noted that the eigenvalue distributions of the sample covariance matrices differ under the H_0 and H_1 hypotheses and in turn, the distributions of aforementioned decision statistics vary under these hypotheses. By exploiting this difference, eigenvalue based techniques take decision about the presence or the absence of the PU signal. In practice, the knowledge about the PU signals and channels is unknown to the detector i.e., the distribution under the H_1 hypothesis is not known. Therefore, most of the sensing techniques derive the sensing threshold based on the distribution of the decision statistics under the H_0 hypothesis. However, in practice, the noise distribution also may not be known to the detector and there may occur noise covariance uncertainty. As mentioned before, the simplest ED technique suffers from SNR wall problem in the presence of noise covariance uncertainty. Further, it should be noted that out of a wide range of available eigenvalue based techniques, some of the techniques such as ME, trace based detector etc. suffer from the noise covariance uncertainty problem and other techniques, which are based on the ratio of the parameters, such as MME, SLE etc. are invariant to this uncertainty.

The block diagram in Fig. 2.7 represent the stages involved in the eigenvalue based detection. It should be noted that the complexity of the total process mainly comes from the first two blocks i.e., sample covariance matrix computation and EVD operation. Furthermore, these two stages and the last stage are common to any of the eigenvalue based methods unless any indirect methods have been applied to compute it e.g., trace, ME based on iterative procedure. Depending on the computational overhead of the test statistic computation in the third stage, these techniques might have different implementation complexities.

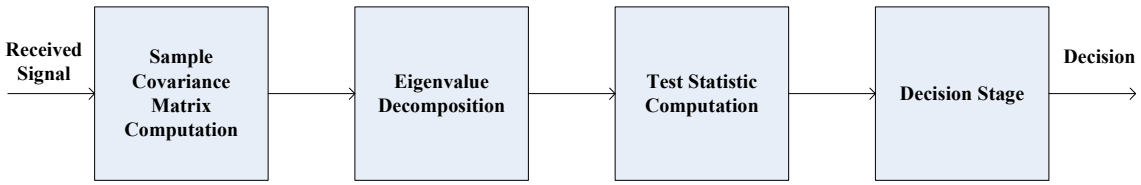


FIGURE 2.7: Stages involved in eigenvalue based detection

2.3.4.2 Literature Review

In this subsection, we provide an overview of the existing works related to eigenvalue based sensing. In [226], authors propose two information theoretic criteria, namely, Akaike's Information Criterion (AIC), and Minimum Description Length (MDL), in order to detect the free bands present over the considered spectrum band based on the number of the independent eigenvectors of a given covariance matrix of the received signal. Further, several eigenvalue-based sensing techniques have been proposed exploiting the properties of Wishart random matrices [17, 18, 49]. The authors in [44] use the Marchenko-Pastur (MP) law to test a binary hypothesis assuming the presence of white noise. In [18], semi-asymptotic Maximum to Minimum Eigenvalue (MME) and Energy to Minimum Eigenvalue (EME) algorithms for SS have been proposed using the combination of the MP based and Tracy-Widom (TW) distribution based approaches and in [45], a ratio based technique has been proposed using the Tracy-Widom Curtiss (TWC) distribution. In [18], the TW distribution is used as a statistical model for the largest eigenvalue and a combination of the TW based and the MP-based approaches is used to find the approximate distribution of random SCN. Subsequently, this distribution is used to derive the relationship between an expression for P_f and the threshold. The difference between MP-based approach and TW approach is that MP-based approach uses deterministic asymptotic bounds for the a.e.p.d.f. support while the TW approach uses the pdf of the maximum/minimum eigenvalue for finite dimensions. Further, in [45], a more accurate model considering the TWC model has been considered by using the distribution of

¹The terms MME and SCN are used interchangeably in this thesis.

the smallest eigenvalues of Wishart random matrices. However, the TW distribution and the Curtiss' ratio of variates formula are highly involved functions, which are hard to evaluate numerically and non tractable to find the support of a.e.p.d.f. [227].

In [42], an approximation of the threshold function is derived for systems having equal number of receiving antennas and samples. Additionally, in [225], the p.d.f. of the eigenvalue ratio has been derived using the expression of the joint distributions of an arbitrary subset of ordered eigenvalues of complex Wishart matrices. In this scenario, the receiver should be provided with a lookup table in order to calculate the proposed inverse cumulative distribution function (c.d.f.) of the second-order TW distribution. The exact distribution of the condition number of a complex Wishart matrix has been used to calculate the threshold expression in [42] without the need of a lookup table. However, the calculated threshold expression in terms of P_f in [42] is based on the exact density of the condition number of complex Wishart matrix considering the noise only case and it is only valid in case of white noise measurements. For the correlated noise scenarios, the sample covariance matrix does not follow the properties of Wishart random matrices.

In [227], the exact distribution of SCNs of dual Wishart random matrices has been used and it is argued that the proposed method requires only tens of samples and outperforms all the RMT based techniques. However, the authors in [227] considered the Wishart random matrix model for signal plus noise case for simplicity and did not address the fact that during the presence of signal and correlated noise, the sample covariance matrix may no longer be a Wishart random matrix. In [228], non-asymptotic behavior of eigenvalues of random matrices has been considered using the spectral properties of random sub-Gaussian matrices of fixed dimensions. A cooperative SS algorithm using double eigenvalue threshold has been proposed in [229], which considers two maximum eigenvalues for the noise only and the signal plus noise cases through analysis of sample covariance matrix of the received signals using RMT approach. In [47], the effect of spatial correlation in the performance of predicted eigenvalue threshold based spectrum sensing is analyzed and it is shown that the detection performance improves in the presence of spatial correlation at the multi-antenna SU considering white noise.

Recently, the distribution of the SCN of Wishart matrices has been considered in signal detection for a CR [52]. In this context, two types of condition numbers i.e., SCN and Demmel Condition Number (DCN) (the ratio of the matrix trace to the minimum eigenvalue) have been considered. In [52], a general framework for the c.d.f. of the SCN of different classes of Wishart matrices has been presented. In [230], the exact distribution of the DCN for random matrices with arbitrary dimensions has been presented. In [231], analytical expressions for the p.d.f. and c.d.f. of the ratio of the largest eigenvalue to the trace of complex Wishart matrices with arbitrary dimensions have been derived and the derived analytical results are used to find the decision threshold for a blind Generalized Likelihood Ratio Test (GLRT) detector. Besides, free probability theory, which is a valuable tool for describing the asymptotic behavior of multiple systems, has also received attention in the SS literature [232, 233]. Besides, in our contribution [234], asymptotic analysis of eigenvalue-based blind SS techniques such as SLE, SCN, John's detection, spherical test based detection has been carried out and the performance of these techniques has been evaluated in the presence of noise correlation numerically. Moreover, the contribution in [60] uses the RMT in order to estimate the transmit power of multiple signal sources blindly in multiantenna fading channels.

Moreover, most of the multi-dimensional SS techniques proposed in the literature do not consider the effect of channel correlation. Some contributions in the literature have analyzed the performance of the ED technique with correlated multiple antennas. In [235], the authors analyzed the sensing performance of an energy detector when multiple antennas are correlated and it was verified that the sensing performance of the energy detector is degraded when the channels are spatially correlated and the performance degradation is proportional to the level of correlation. In [236], the detection performance of an ED based SS in a CR with multi-antenna correlated channels has been investigated in Nakagami-m fading channel.

2.3.4.3 Existing Approaches

In the following subsections, we briefly describe the existing eigenvalue based approaches.

1. Maximum Eigenvalue (ME)

The decision statistic for this method is the ratio of the ME to the noise variance, also called Roy's largest root test in the literature [237]. The performance analysis of this detector has been carried out in [237] under white noise scenarios and it has been shown that this detector outperforms the ED technique for Gaussian signals. Let λ_{ME} be the sensing threshold used for the decision process. The decision rule based on the binary hypothesis test for the ME method can be expressed as

$$\text{decision} = \begin{cases} H_0, & \text{if } \frac{\lambda_{\max}(\hat{\mathbf{R}}_Z(N))}{\sigma_z^2} \leq \lambda_{ME} \\ H_1, & \text{otherwise} \end{cases} \quad (2.7)$$

where $\lambda_{\max}(\hat{\mathbf{R}}_Z(N))$ denotes the ME of $\hat{\mathbf{R}}_Z(N)$.

2. Signal Condition Number (SCN)

The decision statistic for this method is the ratio of the ME to the minimum eigenvalue i.e., SCN. Based on the distribution used for analyzing the bounds for the maximum and the minimum eigenvalues, this technique can be categorized into the following sub-techniques.

a. Asymptotic SCN: In this approach, both the maximum and the minimum eigenvalues are calculated based on the asymptotical properties of Wishart matrices. The minimum and the maximum eigenvalues of $\hat{\mathbf{R}}_Y(N)$ asymptotically converge almost surely to $a = (1 - \sqrt{\beta})^2$ and $b = (1 + \sqrt{\beta})^2$ respectively, in the limit $M, N \rightarrow \infty$ with ratio index $\beta = N/M$ [43]. The parameters a and b can be regarded as the bounds of the MP distribution and based on these MP bounds, the absence or presence of a PU signal can be decided under the white noise scenario [44]. Under white noise scenarios, the decision statistic can be calculated using the MP law as

$$\text{decision} = \begin{cases} H_0, & \text{if } \frac{\lambda_{\max}(\hat{\mathbf{R}}_Y(N))}{\lambda_{\min}(\hat{\mathbf{R}}_Y(N))} \leq \frac{b}{a} \\ H_1, & \text{otherwise} \end{cases} \quad (2.8)$$

where $\lambda_{\min}(\hat{\mathbf{R}}_Y(N))$ denotes the minimum eigenvalue of $\hat{\mathbf{R}}_Y(N)$.

b. Semi-asymptotic SCN: This MME approach is semi-asymptotic in nature since the bound for the ME is calculated based on the TW distribution instead of the asymptotic distribution while the minimum eigenvalue is evaluated based on asymptotic analysis [45]. The binary hypothesis testing problem for this technique can be written as:

$$\text{decision} = \begin{cases} H_0, & \text{if } \frac{\lambda_{\max}(\hat{\mathbf{R}}_Y(N))}{\lambda_{\min}(\hat{\mathbf{R}}_Y(N))} \leq \lambda_{\text{SCN}} \\ H_1, & \text{otherwise} \end{cases} \quad (2.9)$$

where λ_{SCN} is the decision threshold for MME method, which can be written as [45]

$$\lambda_{\text{SCN}} = \frac{b}{a} \cdot \left(1 + \frac{(\sqrt{N} + \sqrt{M})^{-2/3}}{NM^{1/6}} F_{TW2}^{-1}(1 - P_f) \right), \quad (2.10)$$

where F_{TW2}^{-1} is the inverse Tracy-Widom c.d.f. of order 2.

3. Energy with Minimum Eigenvalue (EME)

The average power of the received signal is nearly same as the average eigenvalue (λ_{avg}) of the received signal's covariance matrix [18]. The binary hypothesis testing problem based on the EME technique can be written as

$$\text{decision} = \begin{cases} H_0, & \text{if } \frac{\lambda_{\text{avg}}(\hat{\mathbf{R}}_Y(N))}{\lambda_{\min}(\hat{\mathbf{R}}_Y(N))} \leq \lambda_{\text{EME}} \\ H_1, & \text{otherwise} \end{cases} \quad (2.11)$$

where λ_{EME} is the decision threshold for the EME method, which is given by [18]

$$\lambda_{\text{EME}} = \left(\sqrt{\frac{2}{MN}} Q^{-1}(P_f) + 1 \right) \frac{N}{(\sqrt{N} - \sqrt{M})^2}, \quad (2.12)$$

where Q^{-1} represents the inverse Q-function with $Q(t) = \frac{1}{\sqrt{2\pi}} \int_t^\infty e^{-u^2/2} du$.

4. Scaled Largest Eigenvalue (SLE)

The decision for SLE method can be made on the basis of the following binary hypothesis testing [51]

$$\text{decision} = \begin{cases} H_0, & \text{if } \frac{\lambda_{\max}(\hat{\mathbf{R}}_{\mathbf{Y}}(N))}{\frac{1}{M} \text{tr}\{\hat{\mathbf{R}}_{\mathbf{Y}}(N)\}} \leq \lambda_{\text{SLE}} \\ H_1, & \text{otherwise} \end{cases} \quad (2.13)$$

where $\text{tr}\{\hat{\mathbf{R}}_{\mathbf{Y}}(N)\}$ denotes the trace of $\hat{\mathbf{R}}_{\mathbf{Y}}(N)$, and λ_{SLE} denotes the sensing threshold for the SLE method.

5. Spherical Test (ST) Method

The test statistic for this method is calculated as the ratio of the geometric and arithmetic mean of all eigenvalues [48] in the following way

$$T_{\text{ST}} = \frac{\left(\det(\hat{\mathbf{R}}_{\mathbf{Y}}(N)) \right)^{1/M}}{\frac{1}{M} \text{tr}(\hat{\mathbf{R}}_{\mathbf{Y}}(N))} = \frac{\left(\prod_{i=1}^M \lambda_i \right)^{1/M}}{\frac{1}{M} \sum_{i=1}^M \lambda_i}. \quad (2.14)$$

The binary hypothesis testing based on this method can be expressed as

$$\text{decision} = \begin{cases} H_0, & \text{if } T_{\text{ST}} \geq \lambda_{\text{ST}} \\ H_1, & \text{otherwise} \end{cases} \quad (2.15)$$

where λ_{ST} represents the sensing threshold for the ST method.

6. John's Detection (JD) Method

The test statistic for this method is given as the ratio of the quadratic mean over the arithmetic mean of all eigenvalues [48] i.e., $T_J = \frac{\sqrt{\sum_{i=1}^M \lambda_i^2}}{\sum_{i=1}^M \lambda_i}$. The binary hypothesis testing based on this method can be expressed as

$$\text{decision} = \begin{cases} H_0, & \text{if } T_J \leq \lambda_J \\ H_1, & \text{otherwise} \end{cases} \quad (2.16)$$

where λ_J represents the sensing threshold for the JD detector.

2.4 Underlay Techniques

Figure 2.8 provides the classification of the existing underlay CR techniques. The underlay approach comprises the following two categories of techniques: (i) Interference mitigation techniques, and (ii) Resource allocation techniques. The subcategories of these techniques are discussed in the following subsection providing their basic principles and the related literature. The cognitive beamhopping technique will be detailed in Chapter 7 and hence is not described in this section.

2.4.1 Beamforming

Beamforming is a spatial filtering technique which is capable of separating signals that have overlapping frequency content but originate from different locations [238]. A beamformer consists of a processor

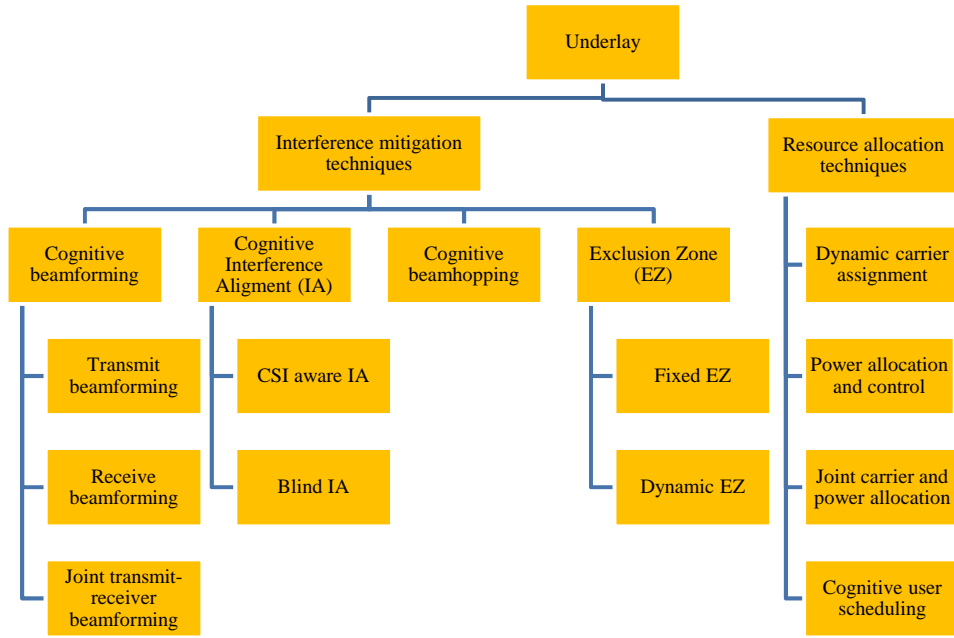


FIGURE 2.8: Classification of underlay techniques

in conjunction with an array of antennas which directs its most of energy to the desired direction and produces nulls in the interfering directions. Its main principle lies in providing each antenna the right delay and weight and then adding the signals i.e., pointing the antenna array and shaping the beam. Although the term “forming beam” seems to indicate the radiation of energy, beamforming can be used for radiation as well as the reception of energy. The main objective of a beamformer is to achieve improved SINR in multiuser scenarios. The improved SNR is usually achieved by focusing the main lobe of the array pattern in desired direction of transmission/reception and the improved SINR can also be achieved by placing beampattern nulls towards the interfering directions. Due to reciprocity principle, the antenna patterns of the array are the same when transmitting or receiving and thus an antenna array can act as a receive or a transmit beamformer following the same principle.

Over the last few decades, beamforming has been widely used in different fields of radio applications such as communications, radar, surveillance, audio and sonar. The traditional beamformers were analog and they were very expensive, and sensitive to component tolerances and drifts. Due to advancements in high speed ADCs and digital processors, it has been possible to use digital beamforming in the aforementioned applications with the advantages of improved dynamic range, and the capability of creating multiple beams with better amplitude and phase control. In both analog and digital domains, the most commonly used methods used to create the desired beams are based on time delay and phase shift of the impinging RF wave [239]. Interested readers can refer to [238, 239] for the detailed description of narrowband and wideband beamforming solutions.

2.4.1.1 Classification

There are several array signal processing techniques used for beamforming purpose [238–240]. Existing techniques can be classified based on different bases and are presented in detail in our contribution [149]. Herein, we present the summary of this classification below. On the basis of beamforming weight generation, beamforming techniques can be categorized into [238, 240] (i) Data independent beamforming, (ii) Statistically optimum beamforming. The data independent beamforming can be further categorized into (i) Classical beamforming, and (ii) General data independent response design. Similarly, statistical optimum beamforming can be further divided into (i) Multiple side-lobe canceller (MSC), (ii) Use of reference signal, (iii) SINR maximization, and (iv) LCMV beamforming. In addition, based on the robustness, the beamforming techniques can be non-robust and robust methods. The

traditional adaptive beamforming techniques such as minimum variance beamforming lack robustness even in the presence of small mismatches in the array response vector [241].

To address the above issue, several contributions have proposed robust techniques based on deterministic worst-case model [242, 243] and probability-constrained or stochastic model [244, 245]. The techniques based on deterministic worst-case approach aim at optimizing the output SINR assuming that the array operates under the worst conditions irrespective of the probability of such worst-case scenario whilst the techniques based on stochastic models model the steering vector mismatch as a random vector and maintain the distortionless constraint with a fixed probability [245]. Further, the beamforming can be employed based on the following different objectives: (i) Sum-rate maximization [246], (ii) SINR/rate balancing [247], (iii) Power minimization [248, 249], and (iv) Interference Minimization [250, 251]. Moreover, based on the location information awareness, beamforming techniques can be (i) purely SNR based, and (ii) SNR and DoA information based. The first category is applicable to wireless environments, where it may be difficult to obtain a clear Line of Sight (LoS) path between the array antenna and the desired/interfering users due to multipath scattering and fading while the second category is suitable for the conditions where there exist LoS paths between Uniform Linear Array (ULA) and desired/interfering users. In Chapter 6 of this thesis, we study the application of the second category of beamformers such as MVDR and LCMV for the spectral coexistence of hybrid satellite-terrestrial networks.

2.4.1.2 Application in Cognitive Radio Networks

In the CR literature, beamforming has been applied as an underlay CR technique in order to maximize the SINR towards the desired user while guaranteeing the aggregate interference to the PUs to be below the interference threshold. The main difference between a conventional beamforming problem and the CB problem is the introduction of interference constraints imposed by primary network while designing the beamformer. These constraints may greatly increase the complexity of the corresponding beamforming and rate allocation techniques. Recently, CB approaches have been widely studied with different secondary network optimization objectives, e.g., sum rate maximization [252], SINR/rate balancing [253, 254], and power minimization with QoS constraints [255–257]. In the following paragraphs, we mention different applications/approaches of beamforming in the context of CR networks.

1. Interference Reduction: In an underlay CR network, additional constraints on the total interference on the PUs need to be taken into account while designing downlink beamforming for the underlay CRN. In this context, suitable transmit beamforming techniques can be used at the STs in order to mitigate interference towards the PRs. In the downlink coexistence of a CR network with a primary cellular network, each cognitive BS can employ beamforming to communicate with the intended user while ensuring that the aggregate interference received by the PRs does not exceed the interference threshold [258, 259]. The contribution in [258] proposes an efficient transmit beamforming technique combined with user selection in order to maximize the downlink throughput and satisfy the SINR constraint while limiting interference to the PU. It is shown that the proposed user selection algorithm combined with zero forcing beamforming strategy is able to achieve high system throughput, interference mitigation, and the complexity reduction.

By increasing the number of antennas in the BS antenna array, the spatial directivity of the signal energy can be increased resulting in higher SINR and the lower average interference towards the PUs. On the other hand, increasing the number of PUs while keeping the constant number of antennas creates a reverse effect. Thus, there exists a tradeoff between the above parameters in a CR network coexisting with a primary network. In this context, authors in [260] show that it's possible to create negligible or zero interference to the PUs by employing as many antennas in the cognitive transmitter as the number of PRs. In the similar context, the contribution in [250] considers the problem of designing beamforming vector in such a way that it maximizes the desired signal power at its corresponding receiver while minimizing the total interference caused to all PRs and the noise at that receiver. Further,

the contribution in [261] considers the problem of downlink CB with interference constraints and it has been shown that a dual virtual uplink problem can be derived, yielding identical beamformers as for the original problem.

2. Beamforming and Power Control: Transmit power control in conjunction with the beamforming has shown a strong potential to suppress interference in multi-user cellular systems. The contribution in [259] studies a joint beamforming and power allocation problem for the Single Input Multiple Output (SIMO) multiple access channel based CR network considering the sum-rate maximization and SINR balancing problems. Both problems have been considered under the peak power constraints for the SUs as well as interference power constraints for the PUs. In the similar context, the contribution in [262] considers a resource allocation problem in order to minimize the total power at the cognitive BS subject to (i) a SINR constraint on all cell-edge PUs and the SUs within a cognitive cell, and (ii) total interference control on the other outer-cell PUs located outside the cognitive cell. It is assumed that cell-edge PUs' data are available to the cognitive BSs through reliable backhaul links between the primary and cognitive BSs. Further, the contribution in [257] considers the problem of joint transceiver cognitive beamformer design to minimize the transmit power of the secondary BS while simultaneously targeting lower bounds on the received SINR for the SUs and imposing upper limits on the PUs' interference thresholds.

In the context of CR networks, the contribution in [263] proposes various CB schemes considering the CR transmit power constraint and a set of interference power constraints at the PR terminals, under the assumption that the CR transmitter knows perfectly all the channels over which it interferes with PR terminals. However, in practice, the perfect knowledge of this channel information may not be available. In this context, authors in [264] considers the problem of joint transmit precoding and power control in order to effectively balance between avoiding interference at the primary terminals and optimizing performance of the CR link without assuming the perfect Channel State Information (CSI). Consequently, the contribution has proposed the idea of effective interference channel, which can be efficiently learned at CR transmitter through blind/semiblind estimation over the received primary signals.

3. Beamforming and User Scheduling: In multiuser CR networks, beamforming in conjunction with user scheduling can be used in order to select the best SU to be served by the designed beamformer. In this context, most of the contributions in the literature consider the problem of designing an efficient scheduling algorithm for the SUs in order to maximize the throughput of the secondary system while minimizing interference to the PUs. In this context, the contribution in [258] studies the above problem by pre-selecting SUs whose channels are nearly orthogonal to the PU channel so as to minimize interference to the PU. Consequently, the M best SUs, whose channels are mutually near orthogonal to each other are scheduled from the preselected cognitive users and a ZF beamforming is applied to cancel the interference among these selected candidates. In the similar context, the contribution in [265] studies an scheduling scheme for both primary and cognitive users in order to improve the sum-rate performance of the entire network considering the case of multiple SUs and multiple PUs and availability of CSI for all the users. However, in practice, obtaining full CSI may be difficult when the number of SUs is high and when the Frequency Division Duplex (FDD) mode is used. In this context, a two phase scheduling scheme based on opportunistic beamforming has been proposed in [266]. In the proposed scheme, a ST generates a set of beamforming matrices consisting of B orthogonal beams and then sends this set to the PU which selects the best beamforming matrix that minimizes interference to it. Subsequently, the index of the selected beamforming matrix is fed back to the cognitive transmitter. In the second step, the cognitive transmitter transmits the beams of the best matrix (selected in the first step) to all SUs and each SU calculates its SINR corresponding to each beam and feeds back its maximum SINR and the corresponding beam index to the cognitive transmitter. The cognitive transmitter then selects the SU having the highest SINR for transmission. This two phase scheme requires cooperation between SUs and the primary system. This cooperation has been exploited in the literature in different contexts [267, 268].

4. Cooperative Distributed Beamforming: It can be noted that most of the above beamforming

approaches consider multiple antennas in an SU in order to realize a beamformer. However, it is impractical to equip them with multiple antennas due to cost and complexity issues. An alternative way of realizing a beamformer is by utilizing a virtual antenna array in cooperative networks, where each node is equipped with a single antenna [269]. In cooperative distributed beamforming, each distributed user is equipped with a single antenna and a number of such users collaboratively transmit the signal by adjusting the carrier phase of each transmitter in such a way that the aggregate interference to the PU is reduced. In other words, two or more information sources simultaneously transmit a common message and control the phase of their transmissions so that the signals constructively combine at an intended destination [270]. The main advantage of the distributed beamforming approach is improvement in range, rate, and energy efficiency and it may also provide benefits in terms of security and interference reduction since less transmit power is scattered in unintended directions. The contribution in [270] provides an extensive review of the contributions in the areas of distributed beamforming and challenges from practical perspectives.

In distributed beamforming, imperfect phase synchronization may cause a significant problem in realizing the beamforming gain since the phase of each node determines the overall beampattern of the CR network. In this context, in [271], the authors have studied the effects of the phase noise in practical oscillators on the performance of distributed beamforming. It has been noted that for a given number of users, the phase offset has a significant impact on the main lobe and a negligible effect on the side-lobes. In the similar context, the contribution in [272] analyzes the effect of phase error on the performance of distributed beamformer and the primary protection. It has been shown that the imperfect phase synchronization may reduce the far-field power in the direction of the SR and decrease the primary protection rate.

5. Robust Cognitive Beamforming: Similar to conventional beamformers, the cognitive beamformer should be robust to the array response vector mismatch and channel uncertainties. As in non-cognitive scenarios, the robust optimization is usually addressed by either a stochastic or a worst case approach. Most of the contributions in the literature are largely based on the assumption of the perfect CSI at the SU transmitter, which is usually difficult to achieve due to limited training, less cooperation between SU and PU, and quantization issues. In this context, several contributions in the literature have studied the aspects of robust CB considering the imperfect CSI [252, 255, 273, 274]. In the context of Multiple Input Single Output (MISO) networks, several robust cognitive beamformer designs have been developed in order to provide robustness against channel uncertainty, where the imperfect CSI of all relevant channels is modeled using an Euclidean ball-shaped uncertainty set [255, 256, 275, 276].

6. Multicast Cognitive Beamforming: Multicast beamforming has been considered an important technique for the next generation cellular wireless services [277]. In a cognitive multicast network, a ST equipped with multiple antennas transmits the same information-bearing signal to several SRs, each equipped with a single antenna. The objective of a beamformer in such networks is to find an optimal beamforming weight vector which minimizes the total radiated power under the constraints of (i) acceptable lower bound of SNR at each SR, and (ii) allowable upper bound of interference level caused to the PRs [278]. The contribution in [278] shows that the rank-one solutions for non-convex quadratically constrained optimization problems, which is generally the case in multicast beamforming [255], are not always obtained in general. Furthermore, it is shown that the approximate solutions picked up from the randomization techniques may be far from the optimal ones. Moreover, the contribution in [279] considers a robust secondary multicast beamformer design problem for spectrum sharing in a MIMO CR network. In [279], two randomized approximation algorithms have been proposed for the robust CR multicast downlink beamforming problem which can provide better approximation accuracies than the previous method proposed in [255]. Besides above contributions, several contributions [280, 281] have recently contributed in solving beamforming problems in the context of multicast beamforming for CR networks.

2.4.2 Interference Alignment

2.4.2.1 Interference Alignment Principle

In wireless interference networks, only a subset of the transmitted symbols are desired by a particular receiver. The remaining symbols, which carry information for other receivers, are undesired at that particular receiver creating interference to the desired signal. In this context, IA can be used as an interference mitigation tool which aligns interference in space, time or frequency domain using precoding techniques. Signals transmitted by all users can be designed in such a way that the interfering signals fall into a reduced dimensional subspace at each receiver. Each receiver can then apply an interference removal filter to project the desired signal onto the interference free subspace. Due to this phenomenon, the number of interference-free signalling dimensions of the network are substantially increased [282]. In MIMO networks, IA can be applied by using the spatial dimension offered by multiple antennas for alignment while in multicarrier systems, interference can be aligned over the carrier dimension.

The dof is an important concept behind IA. It is an important capacity approximation method and may be interpreted as the number of resolvable signal space dimensions. It can also be defined as the number of signaling dimensions, each dimension corresponding to one interference-free AWGN channel with the SNR that increases proportionally with the total transmit power P as $P \rightarrow \infty$ [282]. Let $R(P)$ denotes the sum capacity, then the dof metric, let us denote by η , is given by

$$\eta = \lim_{P \rightarrow \infty} \frac{R(P)}{\log(P)}. \quad (2.17)$$

The above expression can be equivalently written as $R(P) = \eta \log(P) + O(\log(P))$, where the term $O(\log(P))$ is some function $f(P)$ which satisfies the following relation [282]

$$\lim_{P \rightarrow \infty} \frac{f(P)}{\log(P)} = 0. \quad (2.18)$$

For example, a point to point MIMO channel with M transmit and N receive antennas has $\min(M, N)$ dof, whereas it's Single Input Single Output (SISO) counterpart has only 1 dof [283]. The dof regions are characterized for several wireless channels such as MIMO Broadcast Channel (BC), Interference Channels (ICs), including X and multihop ICs, and the CR channels [284]. The dof metric has been extensively used for interference mitigation and alignment objectives in various wireless networks such as interference mitigation in multicell networks [129, 285], interference mitigation in two-cell MIMO interfering BCs [286], IA in CR networks [138, 287].

The IA technique allows many interfering users to communicate simultaneously over a small number of signaling dimensions i.e., number of antennas or carriers. The disadvantage of this approach is that filtering at the non-intended receiver removes the signal energy in the interference subspace. Let us consider an interference network with K number of transmitters, each trying to send one information symbol. To resolve the 1 symbol desired by a particular receiver, K signalling dimensions are generally required [282]. If there are K number of receivers, each with access to a different set of K linear equations formed by its linear channel to the transmitters and interested in a different symbol, a total number of K signalling dimensions will be sufficient to recover the desired symbol by all the K receivers. In this case, the total signalling dimensions are shared among the K users so that each user can communicate using $1/K$ fraction of it like a cake-cutting bandwidth allocation. If all the available receiving dimensions are spanned by interference beams, the desired signal will lie within the interference space as well and cannot be resolved. However, if the signals can be designed in such a way that the interference beams can be consolidated into a smaller subspace i.e., they do not span the entire available signal space at the receiver, and the desired signal beam can avoid falling into the interference space, then the receiver becomes able to recover its desired symbol. The advantage of this mitigation approach is that this alignment does not affect the randomness of the signals and the

available dimensions with respect to the intended receiver. The fundamental assumptions which make IA feasible are that there are multiple available dimensions (space, frequency, time or code) and that the transmitter is aware of the CSI towards the non-intended receiver.

To illustrate the IA principle, we present the spectral coexistence scenario of a primary and a secondary cellular networks in Fig. 2.9. The STs apply precoding using a predefined or coordinated alignment vector before transmitting so that the interfering signals are all aligned at the PR at a certain direction. Then the received signal at the PR is filtered out by using suitably designed filter so that the interference is filtered out, only leaving the desired signal at the output. The main drawback of IA technique from practical perspectives is that it requires the global or local CSI knowledge depending on the applied techniques. The CSI for IA operation can be obtained basically by the following two methods [288]: (i) CSI through reciprocity and (ii) CSI through feedback.

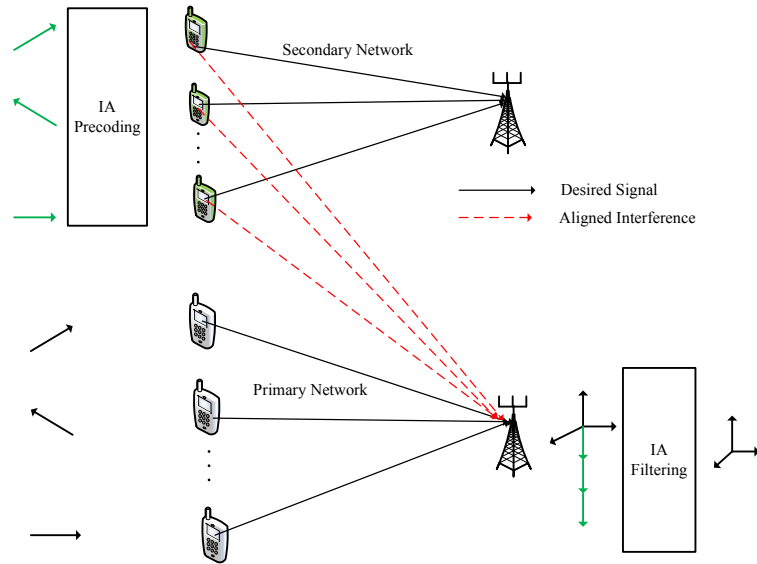


FIGURE 2.9: Illustration of IA principle in a cellular network

2.4.2.2 Classification

The IA technique was firstly proposed in [121] and this technique has been shown to achieve the dofs for a range of interference channels [122, 289, 290]. The IA technique has been investigated in the context of cellular networks in several literature [125–128], showing that it can effectively suppress cochannel interference. IA can be broadly classified into two categories: signal level alignment and signal space alignment [291]. The signal level alignment leads to the tractability to dof characterization while the signal space alignment provides an attractive way to realize IA in practice. The signal space can be generated in several ways such as by concatenating time symbols, frequency bins, or space domain. Several IA techniques have been reported in the literature based on the availability of CSI knowledge at the transmitter, number of signal dimensions used for aligning the interference, and interference removal methods applied at the desired receiver. Existing IA techniques are listed in Table 2.1 along with the corresponding references and are described in [149].

2.4.2.3 Application in Cognitive Radio Networks

The IA technique can be classified as an underlay CR technique [10] since it deals with interference mitigation towards the primary system in spectral coexistence scenarios. In the context of coexistence

TABLE 2.1: List of IA Techniques

IA	CSI	Signal Dimensions	Interference Removal	References
Linear IA	perfect/delayed	single	Filtering	[291] [292]
Subspace	perfect	multi	Filtering	[126] [293]
Distributed IA	local	single	Filtering	[294]
Blind	No	single	Filtering	[295] [296]
Ergodic IA	perfect/delayed	single	Filtering	[297] [298]
Asymptotic IA	perfect	single	Filtering	[296]
Retrospective IA	delayed	single	Filtering	[298, 299]
Lattice Alignment	Perfect	single	Decoding	[300, 301]
Symbol extensions	multiple channel uses	fractional	Filtering	[290]
IA and Cancelation	Perfect	single/multi	Filtering and Decoding	[302]
Opportunistic IA	perfect	single/multi	Filtering	[303] [304]
Asymmetric Complex Signalling	complex	two	Filtering	[305]

of macrocell and the small cells, authors in [306] have applied the IA technique in order to mitigate the interference from small cells towards the macrocell BS. Similarly, the authors in [307] proposed Vandermonde-subspace FDM for the downlink in order to null out the interference of small cells towards primary macro users. In the coexistence of macro/femto networks, authors in [308] have recently studied a joint opportunistic interference avoidance scheme with Gale-Shapley spectrum sharing based on the interweave paradigm in order to mitigate both tier interferences. In the proposed scheme, femtocells opportunistically communicate over available spectrum with minimal interference to macrocells while the femtocells are assigned orthogonal spectrum resources to avoid intratier interference. Considering the dof perspective, the PU does not fully utilize the dof it can achieve and the primary radio resources are underutilized. In other words, there are dof holes in the primary radio resources [138]. As an example, a PU with 1 transmit and 1 receive antenna, who transmits 2 symbols every 3 time slots only utilizes 2/3 dof while the maximum dof it can get is 1. So, it is possible for the SUs to access the 1/3 dof to improve the total dof of the wireless system.

In the context of CR networks, IA techniques can be broadly classified into noncooperative and cooperative. Several contributions in the literature have investigated an opportunistic IA scheme in non-cooperative scenarios. The ergodic IA can be considered as an opportunistic scheme that exploits the existence of complementary channel states in equal proportions to achieve IA [135]. The primary CR link can be modeled by a single user MIMO channel since it must operate free of any additional interference caused by secondary systems. Then, assuming perfect CSI at both transmitter and receiver ends, capacity can be achieved by implementing a water filling power allocation scheme over the spatial directions. It can be noted that even if the PTs maximize their transmission rates, some of their spatial directions are unused due to power limitations. These unused spatial dimensions can therefore be reused by another system operating in the same frequency band in an opportunistic way. An opportunistic ST can send its own data to its respective receiver by processing its signal in such a way that the interference produced on the primary link impairs only the unused spatial dimensions. Using the above principle, authors in [304] consider the opportunistic IA considering same number of antennas and same power budget on both primary and secondary devices while authors in [135] consider the opportunistic IA with a general framework where devices have different antennas. Furthermore, authors in [136] extend the contribution of [135] considering multiple SUs.

In the context of cooperative IA technique, authors in [309] study the femto-macro coexistence scenario in order to manage the uplink interference caused by the macrocell users at the Femtocell BS (FBS). By means of coordination between multiple FBSs and the macrocell users, the received signals from macrocell users can be aligned in a lower dimensional subspace at multiple FBSs simultaneously. Then the remaining dofs are exploited to improve the performance of the femtocell users. Similarly, the contribution in [310] considers a cooperative approach to address the interference problem in femtocell networks by allowing the FBSs to perform IA cooperatively in order to reduce their mutual interference and improve the overall performance. Given a number of FBSs deployed over an existing macrocell network, a cooperative strategy is proposed in [310], where the mutual interference inside a coalition of FBSs is aligned in a subspace which is orthogonal to each desired signal. The remaining part of the

network, which is non-cooperative, contributes with non-aligned interference on each of the receiver's subspaces.

Furthermore, several IA based cognitive schemes have been proposed in [137] in order to exploit the free spatial dimensions left by the PU. In these schemes, the precoding matrices of the SUs are jointly designed so that no interference is generated at the PR. Additionally, each SR does not experience any interference from the primary transmission or from the other SUs. The upper bound of the dof for a SU (with a single transmitter and receiver) with M_1 antennas at the transmitter and N_1 antennas at the receiver operating in the presence of a PU having d_0 active streams has been found to be [138] $d_1 < \min\{(M_1 - d_0)^+, (N_1 - d_0)^+\}$. Subsequently, for the multiple SUs, each with M number of antennas, the achievable dof has been found as $(M - d_0)^+$. This bound is the best known bound for cognitive systems without user cooperation [138]. It indicates that each SU can asymptotically access half the dof holes. In [138], it is shown that each cognitive user can almost get the whole dof holes by properly designing their beamforming vectors. According to [138], the number of dof of the secondary network is given by

$$\max_{\mathcal{D}} \sum_{i=1}^K d_i = K \min(1/2, 1 - d_0), \quad (2.19)$$

where \mathcal{D} is the dof region for the cognitive network and K is the number of SUs. Further, partial and full aided IA schemes can be applied based on the cooperation benefits provided to the PUs.

2.4.3 Cognitive Resource Allocation

The resource allocation problem in CR networks differs from the resource allocation in the conventional wireless systems in a way that CR transmissions should guarantee the interference constraints of the PUs. The cognitive resource allocation problem has been studied in different settings [311–314]. Dynamic resource allocation is an important aspect for CRs in order to deploy their transmission strategies to maximize the secondary network throughput. In this direction, authors in [311, 312] provide an overview of the existing results on resource allocation over space, time, and frequency for CR networks. Depending on the type of allocated resources, the resource allocation techniques can be categorized into (i) carrier allocation, (ii) power allocation, and (iii) joint carrier and power allocation. Furthermore, power allocation based on PU activity has been studied in [313] and sub-carrier allocation problem has been studied in [315] for OFDM based CR networks. A joint subcarrier and power allocation algorithm for cooperative multiuser OFDM CR systems has been investigated in [314].

Several game-theoretical resource allocation mechanisms have been studied in the literature [316–318]. Further, an auction theory, a branch of economics which provides important tools to model, analyze, and optimize allocation of radio resources, has been applied in the context of CR networks [319]. Radio resources such as subchannel, time slot, and transmit power can be allocated among licensed and unlicensed users in the system using an auction based on the market laws. In this context, the authors in [319] provides a survey on auction theory and describe its applications in CR systems. Medium Access Control (MAC) has an important role in several CR functions: spectrum mobility, channel sensing, resource allocation, and spectrum sharing. In MAC strategies, available resources are scheduled (dynamic spectrum allocation) improving the coexistence between users belonging to heterogeneous systems (dynamic spectrum sharing) and may allow cognitive users to vacate selected channels when their quality becomes unacceptable (dynamic spectrum mobility) [320]. In this direction, authors in [320] provide an overview on MAC strategies for CR networks. Several literature have considered the aspect of spectrum scheduling in CR networks [321, 322]. A cognitive scheduler must consider the diversity among the queues of the CRs and channel capacities in terms of the number of bits and the channel switching cost from one frequency to another. In this context, an energy efficient heuristic scheduler has been proposed recently in [322] which allocates each idle frequency to the CR that attains the highest energy efficiency at this frequency.

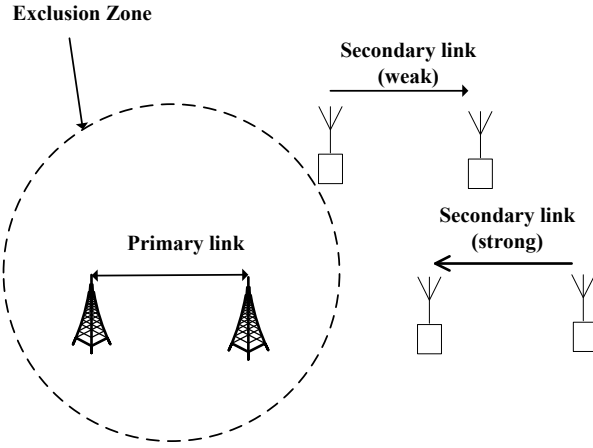


FIGURE 2.10: Illustration of EZ approach (SUs are not allowed to reuse primary spectrum inside the EZ)

2.4.4 Exclusion Zone

In the primary-secondary coexistence scenario (Fig. 2.10), an exclusion zone is generally designed around the PR based on its interference threshold, within which SUs aren't allowed to reuse the primary spectrum². Depending on the size of the EZ, there exists a tradeoff between PU protection and the available spectral opportunities for the secondary system. If the radius of EZ is too small, there occurs the higher chance of the PU being interfered whereas if the EZ radius is too large, less spectral opportunities are available to the secondary system. By employing power control with this EZ approach, the radius of the EZ can be reduced, hence increasing the spectral opportunities for the secondary system while guaranteeing PU protection at the same time. In this combined approach, the SUs which are outside this zone but are very near to the EZ may be allowed to reuse the primary spectrum with power control and the SUs which are sufficiently far from the EZ are allowed to reuse the spectrum with the full power. In this way, secondary system can reuse the primary spectrum by guaranteeing the sufficient protection of the PUs. The EZ approach has been investigated in the literature in various settings ([61, 325, 326]).

In practice, the interference may occur in both directions i.e., from the PTs to the SR and from the STs to the PR. Depending on the scenarios and the level of interference between these two systems, EZs can be created around one of these receivers or both. In the situations where EZs need to create around both receivers, the most restrictive ones need to be considered during implementation in order to guarantee the successful operation of both primary and secondary systems. Further, the shapes of EZs can be optimized considering the antenna patterns of both interfering sources and the victim receiver.

2.5 Regulatory and Standardization Activities

2.5.1 Regulatory Activities

During the last few years, there has been significant developments in the spectrum policy and regulatory domains in the direction of realizing CR technology. The important ones are [327]: (i) publication of national broadband plan, (ii) the publication of the final rules for the unlicensed bands in TV bands,

²Other terminologies related to this concept are: (i) “coordination area” which defines an area within which a more detailed evaluations of the interference potential need to be performed in order to find the possibility of spectrum sharing within this area [323] and (ii) “cognitive zone” which denotes the region in which CR techniques need to be applied in order to meet the interference thresholds set by the ITU” CoRaSat Deliverable D3.2. [324].

and (iii) ongoing proceeding for the secondary use of 2360 – 2400 MHz band for medical body area networks.

Regarding current CR regulations, the World Radio Conference (WRC) 2012 provides the following recommendation on the use of CR technology [101]: (i) any radio system implementing CR System (CRS) technology needs to operate in accordance with the provisions of the radio regulations, (ii) the use of CRS does not exempt administrations from their obligations with regard to the protection of stations of other administrations operating in accordance with the radio regulations, and (iii) CRSs are expected to provide flexibility and improved efficiency to overall spectrum use, recommends that administrations participate actively in the ITU-R studies conducted under Resolution ITU-R 58, taking into the account of first two points.

The database approach has been widely discussed in the CR community in the context of TVWSs for enhancing the usage of the licensed spectrum [5–7]. As mentioned in Chapter 1, FCC and OFCOM have already provided the permission of using significant parts of TVWS for the secondary usage. By implementing a database approach, radios can take the first step towards efficiently utilizing the idle spectrum at any given point in time. This approach can be applied for all spectrum bands, enabling priority driven, lease-based access to maximize the spectrum usage efficiency [328].

2.5.2 Standardization and Development Activities

Several standardization bodies such as Institute of Electrical and Electronics Engineers (IEEE), European Telecommunications Standards Institute (ETSI), and Ecma International are involved in the standardization of CR technologies. Several IEEE standards such as IEEE 802.22, IEEE 802.11af have been already developed in order to allow secondary systems to operate in the TVWSs. The first one is for WRANs in order to have broadband access in the TVWSs whereas the later one is for Wi-Fi services in TVWSs, also called “Super Wi-Fi” or “White Wi-Fi” [329]. Further, the ECMA standard specifies a MAC sub-layer and a physical layer for personal/portable cognitive wireless networks operating in TV bands [330]. Additionally, IEEE DySPAN standards committee is working on developing standards for dynamic spectrum access radio systems and networks with the focus on the improved use of spectrum and IEEE 802.19 develops standards for coexistence between wireless standards of unlicensed devices. Moreover, ETSI Reconfigurable Radio Systems (RRS) committee is responsible for reconfigurable radio system standardization including CR systems and software defined radio in the European level [95]. Besides the database assisted CR approach for TVWSs, there has been an increasing interest in standardizing the SS interfaces and architectures for realizing DSA [331, 332]. In addition, ETSI Specialist Task Force (STF) 386 is dedicated on defining methods, parameters and test procedures for cognitive interference mitigation techniques for Program Making and Special Events (PMSE) devices in order to achieve the spectral coexistence of PMSE devices with other radio services.

Several recent and ongoing research projects such as “Cognitive Radio Experimentation World (CREW)”, “Cognitive Radio Standardization-initiative (CRS-i)”, “Flexible and spectrum-Aware Radio Access through Measurements and modeling In cognitive Radio systems (FARAMIR)”, “Co²Sat”, “CoRaSat”, “COGnitive radio systems for efficient sharing of TV white spaces in European context (COGEU)”, etc. [333] have focussed on analysis and the realization of CR technology in a wide variety of scenarios ranging from TVWSs to SatComs. Further, the concept of CR is applicable for several emerging CR applications, ranging from smart grid, public safety and broadband cellular to medical applications [327]. Some of the widely used CR development platforms are Cognitive Radio Learning Platform (CORAL) from the communications research centre Canada [334] and Wireless open Access Research Platform (WARP) from the Rice university [335].

2.6 Chapter Conclusion

This chapter has provided an overview of the existing contributions in the fields of interweave and underlay CR communication. In Section 2.1, existing spectrum awareness methods have been mapped with the spectrum exploitation paradigms in order to illustrate the relation between these two CR aspects. It has been depicted that depending on the awareness level required by the CRs and the allowable complexity level, different spectrum awareness approaches can be employed which can be subsequently used for realising the corresponding exploitation paradigm. Further, in Section 2.3, the classification of the existing SS techniques has been presented in the following bases: (i) signal processing techniques, (ii) signal bandwidth, (iii) coordination between SUs, and (iv) number of the RF chains. Among several SS techniques, ED-based detection and eigenvalue-based detection have been reviewed in detail with their principles and related literature.

Moreover, Section 2.4 has provided the classification of underlay CR techniques considering the following two main categories: (i) interference mitigation, and (ii) resource allocation. In the existing literature, there exist the following techniques under the first category: (i) CB, (ii) cognitive IA, and (iii) EZ. Similarly, under the second category, there exist the following approaches: (i) dynamic carrier assignment, (ii) power allocation and control, (iii) joint carrier and power allocation, and (iv) cognitive user scheduling. These techniques have been reviewed by referring to the current state of the art. The contributions to several approaches such as ED-based detection, eigenvalue-based SS, cognitive IA, CB, EZ, cognitive beamhopping, and power control are provided in several ways in subsequent chapters. Besides, current CR status and standardization activities have been briefly reviewed in Section 2.5. It can be noted there is an increasing interest in different research communities and standardization/regulatory bodies in implementing CR technology effectively in order to fulfill the spectral efficiency demands of future wireless systems.

Chapter 3

Cognitive Transceiver Design

First, this chapter presents a practical framework in which SS and SNR estimation techniques are applicable. To this end, a hybrid spectrum sharing approach is considered. Subsequently, this chapter provides our contributions on eigenvalue based sensing and SNR estimation problems. Finally, it evaluates the performance of a hybrid cognitive transceiver considering a power control-based underlay scheme. The research work reported in this chapter has been published in [53–55, 65–67].

3.1 Background

Several interweave and underlay approaches exist in the literature as mentioned in Chapter 2. The interweave approach is useful in finding spectral holes in the primary spectrum while the underlay scheme is useful in managing interference between primary and secondary systems. Herein, we highlight the importance of SS and SNR estimation in designing a cognitive transceiver. A cognitive transceiver should be able to sense the activity of the primary signals and based on this activity, it should be able to adjust its operating parameters such as transmit power, duty cycle etc. The research work presented in this section is motivated from the hybrid approach of spectrum exploitation, which has received important attention in the recent literature [33, 62–64]. The hybrid spectrum exploitation approach overcomes the drawbacks of both interweave and underlay approaches as detailed later in Section 3.1.2. In this scheme, a CR is allowed to transmit with full power in a particular band if that band is found to be idle and it can also transmit with the controlled power even if that band is found to be occupied. In the following subsections, we present the conventional sensing approaches¹ appeared in the literature and the hybrid approach based on the combination of SS and underlay schemes.

3.1.1 Conventional Sensing Approaches

1. Periodic Spectrum Sensing

In this approach, the CR operates in a time-slotted mode i.e., the CR sensing module performs SS for a short duration, let us denote by τ and transmits data for the remaining $(T - \tau)$ duration, T being the frame duration [107]. The interweave communication in general consist of several phases such as filtering, detection, characterization, decision and insertion [173]. In Fig. 3.1, we present a simplified frame structure with all the sensing functionalities (mainly detection and decision phases) within the slot of τ duration. It is assumed that the PU activity remains constant during one frame period. In practice, either synchronization is required between primary and secondary transmissions or the SU frame must be much shorter than the PU frame for the above assumption to be true. This

¹It should be noted that any of the SS techniques discussed in Chapter 2 can be considered under these approaches.

scheme can also be referred as a half duplex SS scheme since the SUs do not perform sensing and data transmission simultaneously. Further, the SUs are not able to detect the PU's status when the SUs are transmitting, hence causing interference to the PUs. In this frame structure, there exists an inherent tradeoff between sensing time and the secondary throughput as noted in various literature [107, 336, 337]. Subsequently, there exists an optimum sensing time which yields the highest secondary throughput and finding this for different coexistence scenarios is an open issue [107]. As the sensing time increases, the value of P_d increases and the value of P_f decreases, resulting in better PU protection and the improved utilization of the spectrum. On the other hand, the increase of sensing time causes a decrease in the data transmission time, hence resulting in the reduced throughput.

2. Simultaneous Sensing and Transmission: The frame structure of a CR with simultaneous sensing

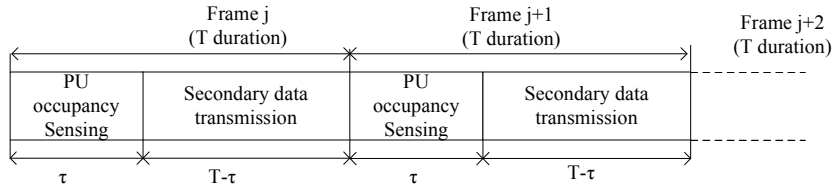


FIGURE 3.1: Secondary frame structure for periodic SS

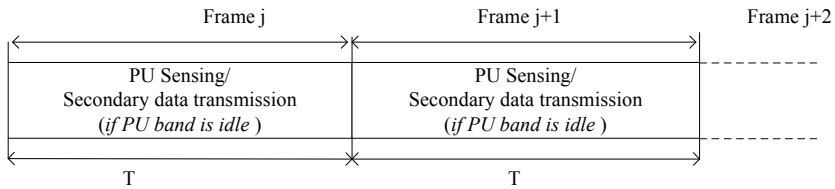


FIGURE 3.2: Secondary frame structure for simultaneous sensing and transmission

and transmission is shown in Fig. 3.2. In this case, we can consider the following two scenarios

- It can be assumed that a CR transmits and receives interchangeably over the time. When a CR is operating in the receive mode, it receives the combination of the PU signals as well as the SU signal. The received signal is decoded at the CR receiver in order to extract the secondary signal and the residue part is the PU signal plus the noise. By comparing residual with the predefined threshold (calculated based on the desired probability of a false alarm), the CR takes the decision about the presence or the absence of the PU activity and can use this decision to transmit or not in the next frame [338]. However, in this case, we should make an assumption that the PU activity does not change during the duration of twice the frame period i.e., $2T$.
- Another scenario is a full duplex scenario in which the CR transmission is non-time slotted as considered in [339]. In this case, two RF chains are required at the CR receiver as depicted in Fig. 3.6. This scheme can accommodate the condition that the PU may change its state during a single SU frame period. Since the full duplex transmission in wireless communications has recently received important attention [340, 341], this concept seems to be promising for full duplex CR nodes of future wireless communications. The full duplex communication can be realized by combining the antenna cancelation, RF interference cancellation and the digital interference cancelation techniques [340, 341].

In both of the above scenarios, the sensing and data transmission take place for the whole duration of the secondary frame and no sensing-throughput tradeoff exists. Since continuous sensing can be achieved under this scheme, finding an optimal sensing time is no longer an issue. Further, better protection of PUs can be achieved due to lower probability of false alarm and higher secondary throughput can be achieved due to a longer data transmission period as compared to the periodic SS [338].

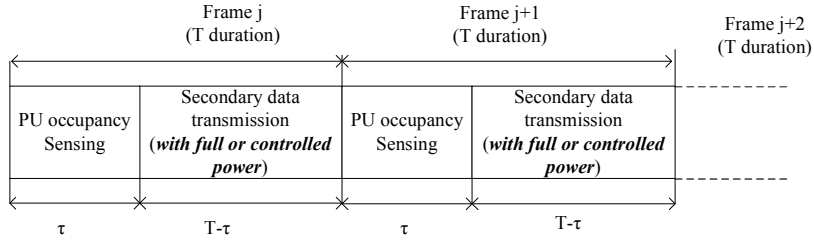


FIGURE 3.3: Secondary frame structure for the hybrid approach (with periodic SS)

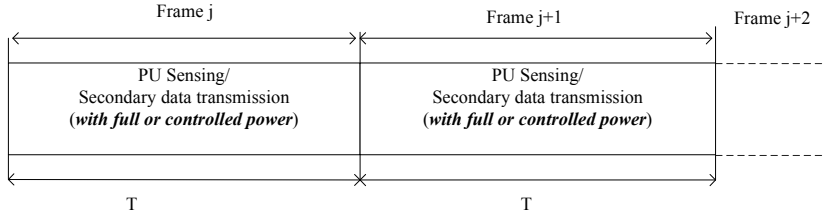


FIGURE 3.4: Schematic of the secondary frame structure for the hybrid approach (with simultaneous sensing/Tx)

3.1.2 Hybrid Approach

The SS approach ignores the interference tolerance capability of the PUs focusing only on bursty PU traffic whereas the possibility of having secondary transmission with full power is neglected in the underlay based approach [33]. More specifically, the underlay approach is not able to detect the activity or inactivity of the PUs in a particular band and hence does not utilize the idle bands efficiently. On the other hand, the SS approach does not allow the SUs to transmit in a particular frequency band when the PU is active in that band. To address this, it is crucial to investigate suitable hybrid spectrum awareness and transmission strategies which can overcome the drawbacks of both the techniques and achieve higher secondary throughput while protecting the PUs. In the context of this hybrid approach, the contribution in [62] studies the transmission mode selection with channel switching in hybrid underlay/overlay systems based on the achievable throughput ratio between underlay and SS transmissions and the PU traffic statistics. In the similar context, the recent contribution in [33] proposes a hybrid strategy, which combines SS and underlay schemes and utilizes a double energy-threshold method in order to switch between full and partial access modes dynamically. In this section, we provide half duplex and full duplex hybrid architectures for a CR transceiver which combines the aforementioned advantages of both SS and underlay techniques. The frame structures of secondary transmission for the hybrid approach with the periodic SS and simultaneous SS/Tx approach are shown in Figs. 3.3 and 3.4 respectively.

Figure 3.5 presents an architecture for the CR transceiver with a single RF chain. Since this architecture consists of a single RF chain, it is capable of either sensing or transmitting data during a single time slot, hence, can be considered as a half duplex transceiver in general. However, if a pair of CR nodes i.e., a CR transmitter and a CR receiver, operates in a half duplex communication mode in such a way that they transmit and receive interchangeably over a time, this half duplex structure can function in a simultaneous sensing/Tx framework as mentioned in Section 3.1.1. In the proposed architecture in Fig. 3.5, the received signal is first passed through a Low Noise Amplifier (LNA) before further processing in the receiver. Subsequently, the amplified signal is passed through a filter, a sampler and then a sensing unit. Based on the sensing requirements and the availability of knowledge about PU signal, channel and the noise variance, the sensing unit may implement any one of the detection techniques mentioned in Chapter 3. In this work, we focus on the ED technique, which is same as trace-based detection in terms of eigenvalue based techniques, due to its low complexity and realize it using SNR estimation and sensing decision blocks as shown in Figs. 3.5 and 3.6. The SNR of the received PU signal can be estimated with the help of various power spectrum and SNR estimation

techniques [25, 53, 65, 168, 342]. Subsequently, based on the estimated PU SNR, let us denote by γ_{est} , the sensing unit takes a decision about the presence or absence of the PU and the decision can trigger the power control block directly in order to transmit with full power in its data transmission slot if the H_0 hypothesis is selected. Alternatively, it can trigger the power control block along with the information about the estimated SNR if the H_1 hypothesis is selected. Based on the estimated SNR, the power control technique calculates the amount of the transmit power while considering the interference constraint of the PU as described later in Section 3.4.2.1.

Figure 3.6 presents the proposed sensing structure for the full duplex scenario. This structure functions in the similar way as the half duplex structure shown in Fig. 3.5 except the fact that it contains two separate RF chains in order to sense and transmit data simultaneously.

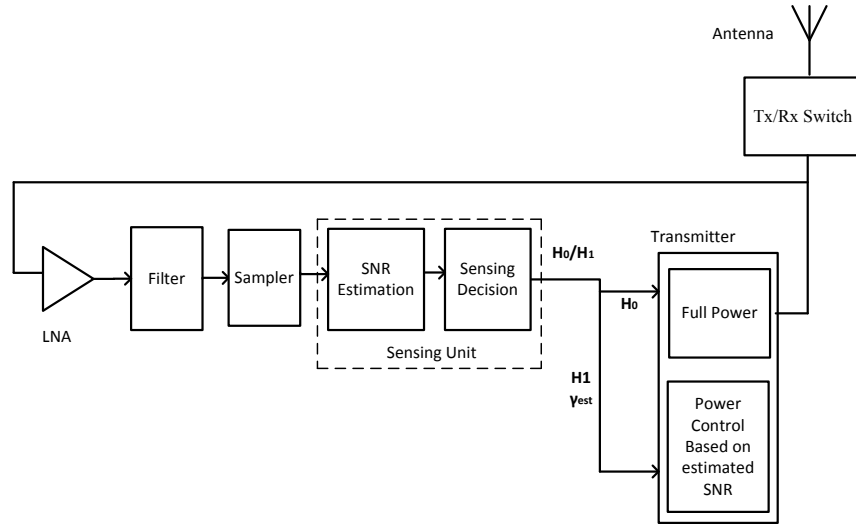


FIGURE 3.5: Half duplex architecture for a CR transceiver

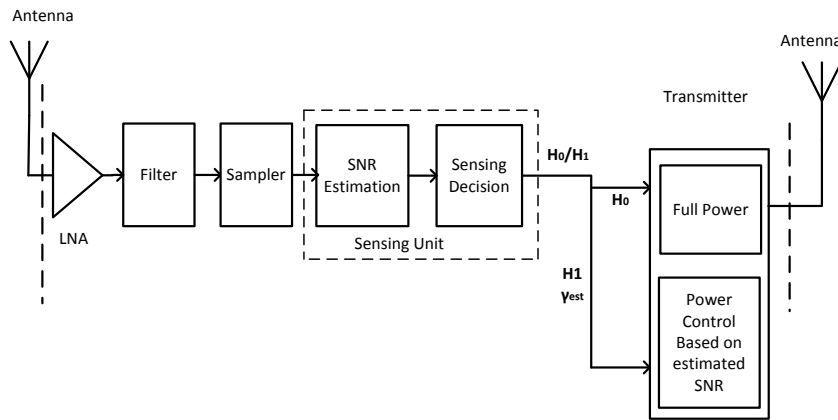


FIGURE 3.6: Full duplex architecture for a CR transceiver

For realizing the hybrid approach, we consider a power control-based underlay scheme, which selects secondary transmit power based on the interference constraints of the PUs. It should be noted that the CR estimates the received PU power, which is transmitted from the PT. However, in practice, we need to protect the PRs from harmful interference caused by the ST. For this purpose, we can consider the following practical cases.

- The first scenario considers the beacon-based sensing, in which a PR is assumed to send a beacon signal on a control channel [343]. In this context, the SUs can detect the presence of a PR as well

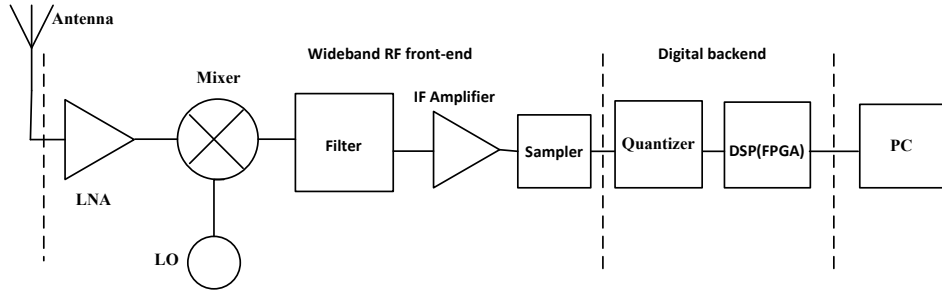


FIGURE 3.7: Block diagram of a wideband SDR receiver

as estimate the power of the beacon signal. Subsequently, based on the strength of the beacon signal and interference threshold of the PU, the SU can adjust its transmit power in order to protect nearby primary receivers.

- The second case assumes duplex transmission mode for the PUs i.e., each user interchangeably transmits and receives over time. If we estimate the path loss based on the strongest SNR over multiple time slots, we can also protect the weakest link assuming they have the same interference threshold. The same explanation applies for the case of multiple PU links as well. If the link with the strongest power is protected, then all the other PU links can be protected.
- The third scenario considers the simplex mode of transmission for the PUs and a short range wireless communication for both primary and secondary systems provided that interference levels from one system to another are at a similar level. In practice, this case arises when a spectrum resource is left completely unused within a sufficiently large network coverage area [23]. In this case, fixing secondary transmit power based on the received signal from the PT is a reasonable strategy for protecting the PR as well.
- In the fourth scenario, the protection of the PRs can be provided by including a detection margin in defining the coverage region of a CR [343]. For example, let r_p and r_s denote the maximum communication range of the primary system and the interference range of the CR. In this case, the CR should be capable of detecting any active PT within a radius of $r_p + r_s$ in order to guarantee that no active PRs exist within its interference range.

The performance evaluation of the proposed architecture as well as the employed power control will be described later in Section 3.4.

3.2 Spectrum Sensing

Among several SS techniques discussed in Chapter 2, the focus of this work is on eigenvalue-based SS as described in the following subsections.

3.2.1 Problem Description

The eigenvalue based SS techniques using RMT have been well investigated in various literature [41, 42, 44, 45, 227, 228, 232]². However, most of these contributions assume the presence of white noise at the CR terminal. In practical implementation of a CR, the received signal should pass through a pulse shaping filter before further processing. As an example, a typical block diagram of a wideband

²The detailed review of the existing eigenvalue-based approaches is provided in Section 2.3.4.

SDR receiver has been shown in Fig. 3.7 [344]. It mainly consists of three parts: wideband RF front-end, digital back-end and control part with processor. In practical implementation of a CR, noise and channel may be correlated due to various reasons, which are summarized in Table 1.1. Depending on the considered multi-dimensional scenario, the causes of channel and noise correlation may be different. We briefly describe these causes below.

1. *Causes of Noise correlation:* The noise correlation in the receiver may arise due to the following reasons.

a) Filtering: In practice, the received signal is passed through a pulse shaping filter before further processing in the CR receiver. In this case, the noise which is added to the signal before the filter is also filtered out and it becomes affected by the autocorrelation function of the filter. With reference to Fig. 3.7, the noise added to the received signal such as environmental noise and contributions from the other receive components such as antenna, LNA and mixer, etc. is affected by the autocorrelation function of the filter. For example, when a white noise input process with power spectral density $N_0/2$ is the input to a RC filter with time constant RC , the noise is affected by the autocorrelation function of the RC filter and it becomes colored.

b) Oversampling: Let the pulse shaping filter has a bandwidth of W Hz, which is usually equal to the bandwidth of the signal. If we sample at a rate higher than the Nyquist rate i.e., $2W$ Hz, the noise process in the output becomes correlated even if the input noise process is white.

2. *Causes of Channel correlation:* The channel correlation in MIMO/Single Input Multiple Output (SIMO) systems depends on the following two components.

a) Spatial Correlation: In wireless multipath environments, the channels are not always independent from each other but can be correlated due to insufficient scattering in the propagation path. This type of correlation can be referred as spatial correlation. In such environments, multipath signals tend to leave the transmit antenna array in a range of angular directions and tend to arrive at the receive antenna array from a range of angular directions rather than a single angular direction. The rich scattering in the propagation path decreases the spatial correlation by spreading the signal such that multipath components are received from many different spatial directions [21]. The smaller spacing between antennas in the transmit and receive sides increases the spatial correlation since adjacent antennas receive similar signal components.

b) Antenna Mutual Coupling: Channel correlation also arises due to mutual coupling between the transmit and/or receive antenna elements [22, 345]. In the transmitter antenna array, antenna mutual coupling causes the input signals to be coupled with the neighbouring antennas. Similarly, the channel correlation may arise due to antenna mutual coupling effect in the receiving antenna arrays.

c) Filtering and oversampling: In addition to noise correlation, filtering and oversampling operations may also cause channel correlation since the received signal passes through the same filter and the same oversampling operation.

Since the value of decision statistics in the presence of noise correlation deviates from its value in uncorrelated scenarios, a sensing threshold proposed for the uncorrelated scenario may not be suitable for sensing in the presence of noise correlation. This will be illustrated with the help of numerical results in Section 3.2.6. In this context, exploring new sensing techniques which can provide better sensing efficiency in the presence of noise correlation is an important research challenge. Motivated by this aspect, we propose new SCN-based decision bounds and new sensing threshold for ME-based detection in order to improve the sensing performance in the presence of noise correlation with the help of theoretical analysis and numerical evaluation under the noise only hypothesis.

3.2.2 Methodology

Due to the absence of knowledge about the channel and the PU signal, coherent receivers such as matched filter i.e., receive part of root raised cosine filter) are not suitable for the SS applications. Active RC filters with tunable cut off frequencies has been proposed in the literature for CR applications

[346, 347]. When a white noise input process with power spectral density $N_0/2$ is the input to a RC filter with time constant RC , the noise is colored after filtering. The RC filter transforms the input autocorrelation function of white noise into output autocorrelation function given by [348]: $R_y(\nu) = \frac{N_0}{4RC} e^{-\frac{|\nu|}{RC}}$. Since the autocorrelation function of output process of RC filter resembles the exponential model, we consider an exponential correlation model³ in this work. Since the same signal after being amplified through an Intermediate Frequency (IF) filter passes to the ADC (with reference to block diagram shown in Fig. 3.7), the correlation which may occur due to oversampling operation at the receiver gives rise to a similar correlation function as in case of the shaping filter.

We study and analyze both the SS and SNR estimation problems in the presence of noise or/and channel correlation with the same methodology. To study the eigenvalue-based SS problem, we carry out analysis under the H_0 hypothesis while to study the eigenvalue-based SNR estimation problem, we perform analysis under the H_1 hypothesis as illustrated later in Section 3.3. To analyze the sensing performance in the presence of noise correlation, we consider probability of correct decision as a performance metric by taking account of correct decisions under both hypotheses. For modeling the noise and/or channel correlation, we consider one-sided correlation model and then we use an exponential correlation model to define the components of the correlation matrix. Moreover, for our considered fractional sampling based sensing example, we use a simple linear model to vary the level of correlation with the fractional sampling rate. For carrying out theoretical analysis, we use an asymptotic approach as carried out in several literature [44, 232, 233, 349]. In this context, we use two important theorems⁴ in Section 3.2.4.1 from the RMT literature. These theorems are applied to find the a.e.p.d.f. of the received signal's covariance matrix under the noise only hypothesis for white noise and correlated noise scenarios. The crossing points of these a.e.p.d.f.s with the x-axis provide the decision bounds under considered scenarios.

3.2.3 Signal and Channel Model

We consider a single PU for simplicity of analysis. Let N be the number of samples analyzed by the cognitive user for the decision process and τ the sensing duration. Let M be the number of receive dimensions in the cognitive receiver. From a system-model point of view, this factor can be considered to be the number of antennas in a multiantenna based CR receiver, number of cooperative users with single antenna RF chain in a cooperative sensing CR system⁵ and the number of oversampled branches in an oversampling based sensing model as considered in [18, 45]. The $M \times N$ received signal matrix \mathbf{Y} in the considered multi-dimensional framework can be written as

$$\mathbf{Y} = \begin{bmatrix} \mathbf{y}_1 \\ \mathbf{y}_2 \\ \vdots \\ \mathbf{y}_M \end{bmatrix} = \begin{bmatrix} y_1(1) & y_1(2) & \dots & y_1(N) \\ y_2(1) & y_2(2) & \dots & y_2(N) \\ \vdots & \vdots & \ddots & \vdots \\ y_M(1) & y_M(2) & \dots & y_M(N) \end{bmatrix}. \quad (3.1)$$

The presented signal model is generic and can be applicable to all the considered multi-dimensional scenarios.

The PU transmitted signal may suffer from slow or fast fading depending on the nature of wireless fading channel. Further, the channel effect on the transmitted symbol may remain constant or vary depending on the transmit data rate and the sampling rate applied at the CR receiver. Moreover, a constant symbol or random symbols may appear in the receiver depending on the relation between sensing duration τ and transmitted symbol duration T_s . Depending on the appearance of constant or

³In practice, a suitable correlation model can be applied depending on the transfer function of the employed filter.

⁴The details on these theorems can be found in [43] and [147] and are not included in this thesis.

⁵In this context, we consider the PU signal detection phase of the cooperative system assuming perfect reporting channels as in [45].

random symbol and the nature of wireless channels, the following cases can be considered for modeling the received PU signal at a cognitive terminal. In our analysis, the channel coefficient resulted from uncorrelated scattering is denoted by h and the channel coefficient resulted from correlated scattering is denoted by \hat{h} . Similarly, z denotes the sampled value of the AWGN and \hat{z} denotes the sampled value of the correlated noise.

Case 1: $\tau \leq T_s$ and channel coefficients vary across receive (i.e., spatial) dimensions but remain constant across temporal dimension: In this case, the $M \times N$ received signal matrix can be written as: $\mathbf{Y} = \sqrt{ps}\hat{\mathbf{h}}^T \cdot \mathbf{1} + \hat{\mathbf{Z}}$, where $\hat{\mathbf{h}}$ is an $1 \times M$ correlated channel⁶ vector i.e., $\hat{\mathbf{h}} = [\hat{h}_1, \hat{h}_2, \dots, \hat{h}_M]$, $\hat{\mathbf{Z}} \triangleq [\hat{\mathbf{z}}_1^T, \hat{\mathbf{z}}_2^T, \dots, \hat{\mathbf{z}}_M^T]^T$ is an $M \times N$ correlated noise matrix with $\hat{\mathbf{z}}_m \triangleq [\hat{z}_m(1) \ \hat{z}_m(2) \ \dots \ \hat{z}_m(N)]$ with $m = 1, 2, \dots, M$, s is a constant transmitted symbol, p is the power of transmitted symbol, $\mathbf{1}$ is an $1 \times N$ vector with all elements being 1. Since we assume normalized noise variance, $\text{SNR} \equiv p$.

Case 2: $\tau \leq T_s$ and channel coefficients vary across both (spatial and temporal) dimensions: In this case, the $M \times N$ received signal matrix can be written as: $\mathbf{Y} = \sqrt{ps}\hat{\mathbf{H}} + \hat{\mathbf{Z}}$, where $\hat{\mathbf{H}} \triangleq [\hat{\mathbf{h}}_1^T, \hat{\mathbf{h}}_2^T, \dots, \hat{\mathbf{h}}_M^T]^T$ with $\hat{\mathbf{h}}_m \triangleq [\hat{h}_m(1) \ \hat{h}_m(2) \ \dots \ \hat{h}_m(N)]$.

Case 3: $\tau > T_s$ and channel coefficients vary across spatial dimension but remain constant across temporal dimension: In this case, the $M \times N$ received signal matrix can be written as: $\mathbf{Y} = \sqrt{p}\hat{\mathbf{h}}^T \mathbf{s} + \hat{\mathbf{Z}}$, where \mathbf{s} is an $1 \times N$ PU transmitted signal vector.

Case 4. $\tau > T_s$ and channel coefficients vary across both dimensions: In this case, the $M \times N$ received signal matrix can be written as: $\mathbf{Y} = \sqrt{p}\hat{\mathbf{H}}\mathbf{S}_d + \hat{\mathbf{Z}}$, where \mathbf{S}_d is an $N \times N$ diagonal transmitted signal matrix with the diagonal $\mathbf{s} = [s(1), \dots, s(N)]$.

We are interested in analyzing cases 2 and 4 in this work⁷. For our analysis, we assume that transmitted symbols are i.i.d. complex circularly symmetric (c.c.s.) symbols. For case 2, the covariance of the transmitted signal can be written as: $\mathbf{R}_s = E[s^2] = 1$. Similarly, for case 4, $\mathbf{R}_{\mathbf{S}_d} = E[\mathbf{S}_d \mathbf{S}_d^\dagger] = \mathbf{I}$ assuming that for each sample we get an i.i.d. c.c.s. symbol with $E[s^2] = 1$. We denote the hypotheses of the presence and absence of the PU signal by H_1 and H_0 respectively. A binary hypothesis testing problem for multi-dimensional sensing techniques can be formulated as

$$\begin{aligned} H_0 : \mathbf{Y} &= \hat{\mathbf{Z}} \\ H_1 : \mathbf{Y} &= \sqrt{p}\hat{\mathbf{H}}\mathbf{s} + \hat{\mathbf{Z}}, \quad \text{Case 2} \\ &= \sqrt{p}\hat{\mathbf{H}}\mathbf{S}_d + \hat{\mathbf{Z}}, \quad \text{Case 4} \end{aligned} \quad (3.2)$$

Assuming that the source signal is independent from the noise, the covariance matrix of received signal \mathbf{R}_Y can be calculated as

$$\begin{aligned} \mathbf{R}_Y &= E[\mathbf{Y}\mathbf{Y}^\dagger] = E\left[(\sqrt{p}\hat{\mathbf{H}}\mathbf{s})(\sqrt{p}\hat{\mathbf{H}}\mathbf{s})^\dagger\right] + E[\hat{\mathbf{Z}}\hat{\mathbf{Z}}^\dagger] \\ &= pE[\hat{\mathbf{H}}\hat{\mathbf{H}}^\dagger] + \mathbf{R}_{\hat{\mathbf{Z}}}, \end{aligned} \quad (3.3)$$

where $\mathbf{R}_{\hat{\mathbf{Z}}} = E[\hat{\mathbf{Z}}\hat{\mathbf{Z}}^\dagger]$. Let us define the sample covariance matrices of the received signal and the correlated noise as: $\hat{\mathbf{R}}_Y(N) = \frac{1}{N}\mathbf{Y}\mathbf{Y}^\dagger$ and $\hat{\mathbf{R}}_{\hat{\mathbf{Z}}}(N) = \frac{1}{N}\hat{\mathbf{Z}}\hat{\mathbf{Z}}^\dagger$. In the following paragraphs, we provide the modeling of noise and channel correlation used for carrying out theoretical analysis.

1. *Noise Correlation Modeling*: To analyze the noise correlation, we consider noise correlation across the receive dimensions and not across the temporal dimension. To model this scenario, we consider the one-sided noise correlation model as in [53]. We model the correlated noise as: $\hat{\mathbf{Z}} = \Theta^{1/2}\mathbf{Z}$, where \mathbf{Z} is an $M \times N$ matrix with c.c.s. i.i.d. Gaussian entries with zero mean and unit variance, representing the white noise and $\Theta^{1/2}\Theta^{1/2} = \Theta = E[\hat{\mathbf{Z}}\hat{\mathbf{Z}}^\dagger]$. It can be noted that since $\mathbf{Z} \sim \mathcal{CN}(0, \mathbf{I})$, $\mathbf{Z}\mathbf{Z}^\dagger$ follows an uncorrelated Wishart distribution i.e., $\mathbf{Z}\mathbf{Z}^\dagger \sim \mathcal{W}_M(\mathbf{R}_Z, N)$. To ensure that Θ does not affect the noise

⁶By the term “correlated channel”, we mean a channel resulted from uncorrelated scattering in the propagation path.

⁷Cases 1 and 3 involve unit rank Wishart matrices which are straightforward to analyze.

power, the normalization $(1/M)\text{trace}\{\Theta\} = 1$ is considered. We define the components of Θ using an exponential covariance model, which is given by [146]

$$\theta_{ij} \sim \begin{cases} \varsigma^{(j-i)}, & i \leq j \\ (\varsigma^{(i-j)})^*, & i > j \end{cases} \quad (3.4)$$

where θ_{ij} is the (i, j) th element of Θ and $\varsigma \in \mathbb{C}$ is the correlation coefficient with $|\varsigma| \leq 1$.

2. Channel Correlation Modeling: As in [147], we use the one-sided correlation model to model channel correlation. In this work, we focus on the correlation across channel receive dimensions and not on the temporal correlation⁸. We model the channel as: $\hat{\mathbf{H}} = \Phi^{1/2}\mathbf{H}$, where \mathbf{H} is an $M \times N$ matrix with c.c.s. i.i.d. Gaussian entries with zero mean and unit variance and $\Phi^{1/2}\Phi^{1/2} = \Phi = E[\hat{\mathbf{H}}\hat{\mathbf{H}}^\dagger]$. It can be noted that since $\mathbf{H} \sim \mathcal{CN}(0, \mathbf{I})$, $\mathbf{H}\mathbf{H}^\dagger$ follows uncorrelated Wishart distribution i.e., $\mathbf{H}\mathbf{H}^\dagger \sim \mathcal{W}_M(\mathbf{R}_H, N)$. To ensure that Φ does not affect the channel power, we consider the following normalization: $(1/M)\text{trace}\{\Phi\} = 1$, where each component of Φ is modeled with the exponential covariance model given by (3.4).

3.2.4 Proposed Signal Condition Number based Sensing

3.2.4.1 Analysis

Herein, we state two RMT based theorems which are going to be used in defining our decision statistics.

Theorem 3.2.1. [43] Consider an $M \times N$ matrix \mathbf{F} whose entries are independent zero-mean complex (or real) random variables with variance $\frac{1}{N}$ and fourth moments of order $O(\frac{1}{N^2})$. As $M, N \rightarrow \infty$ with $\frac{N}{M} \rightarrow \beta$, the empirical distribution of the eigenvalues of $\frac{1}{N}\mathbf{F}\mathbf{F}^\dagger$ converges almost surely to a non-random limiting distribution with density given by

$$f_\beta(\lambda) = (1 - \beta)^+ \delta(\lambda) + \frac{\sqrt{(\lambda - a)^+(b - \lambda)^+}}{2\pi\beta\lambda}, \quad (3.5)$$

where $a = (1 - \sqrt{\beta})^2$, $b = (1 + \sqrt{\beta})^2$, $\delta(\cdot)$ is a Dirac delta function and $(1 - \beta)^+ \delta(\lambda)$ represents the cardinality of zero eigenvalues which can occur if $M > N$. The parameters a and b define the support of the distribution and correspond to λ_{\min} and λ_{\max} respectively and the ratio b/a defines the SCN of $\frac{1}{N}\mathbf{F}\mathbf{F}^\dagger$. The above limiting distribution is the MP law with ratio index β .

□

Remark 3.2.1. In practice, we can have only a finite number of samples and the sample covariance matrix $\hat{\mathbf{R}}_{\mathbf{Y}}(N)$ may deviate from the covariance matrix $\mathbf{R}_{\mathbf{Y}}$. The eigenvalue distribution of $\hat{\mathbf{R}}_{\mathbf{Y}}(N)$ becomes complicated due to requirement of consideration of finite parameters in the analysis. This makes the choice of the threshold difficult for SS purpose and the performance of SS algorithms becomes sensitive to the choice of threshold at low values of SNR. We consider asymptotic analysis as a first step towards analyzing the effect of noise correlation on sensing performance since asymptotic analysis provides less complex solution than finite analysis and it is more tractable [349]. Furthermore, it can be noted in [44] and [349] that the asymptotic analysis provides good approximation to the finite analysis even with a small number of samples.

In this noise only case, $\hat{\mathbf{R}}_{\mathbf{Y}}(N)$ becomes equal to $\hat{\mathbf{R}}_{\hat{\mathbf{Z}}}(N)$ and can be written as:

$$\hat{\mathbf{R}}_{\mathbf{Y}}(N) = \hat{\mathbf{R}}_{\hat{\mathbf{Z}}}(N) = \Theta^{1/2}\mathbf{Z}\mathbf{Z}^\dagger\Theta^{1/2}. \quad (3.6)$$

⁸ The analysis presented here can be straightforwardly extended to the time correlated noise/channel case assuming the exponential correlation model still holds. In this case, the one-sided correlation model can be applied on the right hand side of the noise/channel matrix instead of left hand side.

It can be noted that $\hat{\mathbf{R}}_{\mathbf{Y}}(N)$ converges to $\mathbf{R}_{\mathbf{Y}}$ for $N \rightarrow \infty$ [45] and asymptotic analysis provides a good approximation of the finite analysis even with small values of N [44]. Furthermore, the sample covariance matrix under the white noise scenarios i.e., $\hat{\mathbf{R}}_{\mathbf{Z}}(N) = \frac{1}{N} \mathbf{Z} \mathbf{Z}^\dagger$ is an uncorrelated Wishart matrix but the sample covariance matrix under correlated noise scenarios i.e., $\hat{\mathbf{R}}_{\hat{\mathbf{Z}}}(N) = \frac{1}{N} \hat{\mathbf{Z}} \hat{\mathbf{Z}}^\dagger$ becomes a correlated Wishart matrix. More specifically, an uncorrelated Wishart matrix is the result of the uncorrelated noise i.e., \mathbf{Z} whereas the correlated Wishart matrix is the result of the correlated noise i.e., $\hat{\mathbf{Z}}$.

To calculate the threshold for the SS purpose, we need the support of a.e.p.d.f. of \mathbf{Y} , namely, λ_{max} and λ_{min} . Due to noncommutative nature of random matrices, it is not straightforward to calculate the eigenvalue distribution of \mathbf{Y} by knowing the eigenvalue distribution of Θ and \mathbf{Z} . Using free probability analysis, the asymptotic spectrum of the product or sum can be obtained from the individual asymptotic spectra without involving the structure of the eigenvectors of the matrices under a asymptotic freeness condition [43]. The asymptotic eigenvalue distribution of $\frac{1}{N} \mathbf{Y} \mathbf{Y}^\dagger$ in this context can be obtained by applying multiplicative free convolution property of Σ transform in the following way [350]

$$\Sigma_{\hat{\mathbf{R}}_{\mathbf{Y}}}(z) = \Sigma_{\Theta}(z) \cdot \Sigma_{\hat{\mathbf{R}}_{\mathbf{Z}}}(z), \quad (3.7)$$

where Σ_{Θ} and $\Sigma_{\hat{\mathbf{R}}_{\mathbf{Z}}}$ are the Σ transforms of the densities of eigenvalues of Θ and $\hat{\mathbf{R}}_{\mathbf{Z}}$ respectively. Since Θ is a square matrix, $\Theta^{1/2} \mathbf{Z} \mathbf{Z}^\dagger \Theta^{1/2}$ and $\Theta \mathbf{Z} \mathbf{Z}^\dagger$ have identical eigenvalues [43]. Since $\hat{\mathbf{R}}_{\mathbf{Z}}$ follows the MP law, its Σ transform is given by (A.7) and then the Σ transform of $\hat{\mathbf{R}}_{\mathbf{Y}}$ can be written as

$$\Sigma_{\hat{\mathbf{R}}_{\mathbf{Y}}}(z) = \Sigma_{\Theta}(z) \frac{1}{z + \beta}. \quad (3.8)$$

The Σ transform of corresponding asymptotic eigenvalue distribution $\Sigma_{\Theta}(z)$ can be obtained by choosing a proper model for noise correlation. The asymptotic density of eigenvalues of Θ can be described as a tilted semicircular law [147], which is a close approximation for the exponential model and is analytically tractable. This density can be described using the following theorem.

Theorem 3.2.2. [147] Let Θ be a positive definite matrix which is normalized as: $(1/M)\text{trace}\{\Theta\} = 1$, and whose asymptotic spectrum has the p.d.f.

$$f_{\Theta}(\lambda) = \frac{1}{2\pi\mu\lambda^2} \sqrt{\left(\frac{\lambda}{\sigma_1} - 1\right) \left(1 - \frac{\lambda}{\sigma_2}\right)} \quad (3.9)$$

with $\sigma_1 \leq \lambda \leq \sigma_2$ and $\mu = \frac{(\sqrt{\sigma_2} - \sqrt{\sigma_1})^2}{4\sigma_1\sigma_2}$. If \mathbf{F} is an $M \times N$ standard complex Gaussian matrix as defined in Theorem 3.2.1, then as $M, N \rightarrow \infty$ with $\frac{N}{M} \rightarrow \beta$, the asymptotic distribution of $\mathbf{W} = \Theta^{1/2} \mathbf{F} \mathbf{F}^\dagger \Theta^{1/2}$ has the following p.d.f.

$$f_{\mathbf{W}}(\lambda) = (1 - \beta)^+ \delta(\lambda) + \frac{\sqrt{(\lambda - \tilde{a})^+ (\tilde{b} - \lambda)^+}}{2\pi\lambda(1 + \lambda\mu)}, \quad (3.10)$$

where

$$\begin{aligned} \tilde{a} &= 1 + \beta + 2\mu\beta - 2\sqrt{\beta} \sqrt{(1 + \mu)(1 + \mu\beta)} \\ \tilde{b} &= 1 + \beta + 2\mu\beta + 2\sqrt{\beta} \sqrt{(1 + \mu)(1 + \mu\beta)} \end{aligned} \quad (3.11)$$

The parameters \tilde{a} and \tilde{b} correspond to λ_{min} and λ_{max} respectively and the ratio \tilde{b}/\tilde{a} defines the SCN of \mathbf{W} . □

The eigenvalue spread of Θ is related to the degree of noise correlation i.e., a zero eigenvalue spread corresponds to a zero-correlation model $\Theta = \mathbf{I}_M$ and higher spreads are associated with higher correlation modes. In (3.10), the parameter μ controls the degree of noise correlation and varies the support

of the distribution i.e., for $\mu = 0$, $\tilde{a} = a$ and $\tilde{b} = b$. For the exponential correlation model as stated in [147], the parameter μ is related to correlation coefficient ρ with the following relation: $\mu = \frac{\rho^2}{1-\rho^2}$. Furthermore, the SCN is related to ρ with the relation $\text{SCN} = \frac{1+\rho}{1-\rho}$. To calculate μ in a practical cognitive receiver, the value of ρ can be determined from fractional sampling rate based on some empirical model constructed from measurements. In our results, we employ a simple linear model to study the effect of noise correlation as the fractional sampling rate increases.

It can be noted that MP law can be used as a theoretical prediction under the H_0 hypothesis with white noise [44]. The support of the eigenvalues of the sample covariance matrix under the H_0 hypothesis is finite independently of the distribution of the noise. To decide the absence or presence of signal under white noise scenario, the deviations of distribution of eigenvalues from the normal bounds a and b of MP law can be used. If the eigenvalues appear outside these bounds, then it can be decided that there is presence of PU signal and if all the eigenvalues lie within the bounds of MP law, it can be decided that there is absence of PU signal. In case of noise correlation, the bounds of eigenvalue distribution of sample covariance matrix become different than the bounds obtained in white noise scenarios and MP law no longer applies. The new bounds (\tilde{a}, \tilde{b}) depend on the noise correlation parameter μ . We present a sensing example with new bounds for fractional sampling scenario in the following subsection.

3.2.4.2 Sensing Threshold

The parameter μ depends on the sampling rate applied in the receiver since noise correlation increases along with the sampling rate. Sampling rate can be varied from the symbol rate to some order of the symbol rate and the effect of sampling rate on sensing performance can be evaluated by varying the correlation level. Let us consider that both noise distribution and noise variance are unknown to the detector to reflect the practical scenario. It can be noted that value of the SCN under the H_0 hypothesis does not depend on the noise variance. Under white noise scenario, the decision statistic for MP law can be calculated as [44]

$$\text{decision} = \begin{cases} H_0, & \text{if SCN} \leq \frac{b}{a} \\ H_1, & \text{otherwise} \end{cases} \quad (3.12)$$

It can be noted that the values of the supports a and b can be determined from the closed form of the a.e.p.d.f. provided in Theorem 3.2.1. More specifically, the values of these supports can be calculated by finding out the crossing points of the a.e.p.d.f. with the x-axis. Similar analysis can be applied for sensing in presence of the correlated noise. Equation (3.10) from Theorem 3.2.2 provides the a.e.p.d.f. for the received signal's covariance matrix in presence of noise correlation. By finding out the crossing points of this a.e.p.d.f. with the x-axis, the supports \tilde{a} and \tilde{b} of eigenvalue distribution in presence of noise correlation can be determined. Then the decision about the presence or absence of the PU signal under correlated noise scenarios can be made on the basis of the following condition

$$\text{decision} = \begin{cases} H_0, & \text{if SCN} \leq \frac{\tilde{b}}{\tilde{a}} \\ H_1, & \text{otherwise} \end{cases} \quad (3.13)$$

When fractional sampling rate M is applied at the CR, M rows of sample covariance matrix become correlated. Since the value of ρ varies from 0 to 1, the relation between the fractional sampling rate M and the correlation coefficient ρ is considered as a simple linear model⁹ as shown below

$$\rho = \varepsilon \left(\frac{1}{\beta} - \frac{1}{N} \right), \quad (3.14)$$

⁹This is a simple analytical example and the same method can be applied to more exact relation models which can be acquired through measurements on the CR equipment.

where ε is a parameter defining the slope of the linear dependence. The above equation provides a linear relation between ρ and M . Since $\beta = \frac{N}{M}$, $\rho = 0$ for $M = 1$ i.e., symbol rate sampling and $\rho = 1$ for $M = \frac{N}{\varepsilon} + 1$. Equation (3.14) is a specification of the model used in (3.4) and is used to jointly alter the level of the correlation with the fractional sampling rate.

3.2.5 Proposed Maximum Eigenvalue based Sensing

While applying the sensing threshold designed for the uncorrelated scenario in correlated scenarios, the value of P_f deviates from the target P_f value used for calculating the sensing threshold, resulting in a degraded sensing performance. To address this issue, we consider the problem of detecting the PU's signal in the presence of noise correlation at the CR receiver. We analyze the considered correlated scenario using a tilted semicircular distribution for modeling the noise covariance matrix as in [147], which resembles the exponential covariance model considered in [146]. Further, we use recent RMT results on the universality of the ME of a class of sample covariance matrices from [351] in order to derive the expression for the sensing threshold. Subsequently, the proposed threshold is used for sensing the presence of a PU signal in practical scenarios where noise correlation is always present. Moreover, the performance of the proposed approach is evaluated in terms of the false alarm deviation and probability of correct decision.

3.2.5.1 Analysis

Let $\bar{\mathbf{R}}_{\mathbf{Z}}(N) = \frac{N}{\sigma_z^2} \hat{\mathbf{R}}_{\mathbf{Z}}(N)$ denote the normalized sample covariance matrix under the white noise scenario. Under the assumption $N, M \rightarrow \infty$ with $N/M \rightarrow \beta$ and under white noise (complex) scenarios, the random variable $\frac{\lambda_{\max}(\bar{\mathbf{R}}_{\mathbf{Z}}(N)) - \nu}{\sigma}$ with $\sigma = (\sqrt{M} + \sqrt{N})(1/\sqrt{M} + 1/\sqrt{N})^{\frac{1}{3}}$ and $\nu = (\sqrt{M} + \sqrt{N})^2$ converges to the Tracy-Widom distribution of order 2 (TW₂) [18, 45, 352], which can be stated as

$$\frac{\lambda_{\max}(\bar{\mathbf{R}}_{\mathbf{Z}}(N)) - \nu}{\sigma} \xrightarrow{\text{TW}_2} \text{TW}_2. \quad (3.15)$$

The TW₂ distribution can be defined as [353]

$$F_2 = \exp \left(- \int_s^{+\infty} (x - s) q^2(x) dx \right), \quad (3.16)$$

where $q(s)$ is the solution of the Painlevé II differential equation $q''(s) = sq(s) + 2q^3(s)$ satisfying the condition $q(s) \sim -Ai(s)$ (the Airy function) for $s \rightarrow +\infty$. Due to involvement of a nonlinear differential equation, it is generally complex to evaluate the TW distribution. However, due to its important application in RMT, this distribution has been widely studied and tables for the functions are available in the literature [352]. The contributions in [17, 18] have exploited the above result in order to derive the expression for sensing threshold in terms of P_f . In this work, we are interested in finding out a theoretical expression for the sensing threshold as a function of P_f in the presence of noise correlation for the case of the ME detector using recent RMT results obtained in [351].

Under the H_0 hypothesis, the sample covariance matrix $\hat{\mathbf{R}}_{\mathbf{Y}}(N)$ in the presence of noise correlation can be written as

$$\hat{\mathbf{R}}_{\mathbf{Y}}(N) = \hat{\mathbf{R}}_{\hat{\mathbf{Z}}}(N) = \frac{1}{N} \boldsymbol{\Theta}^{1/2} \mathbf{Z} \mathbf{Z}^\dagger \boldsymbol{\Theta}^{1/2}. \quad (3.17)$$

To model the distribution of the noise covariance matrix $\boldsymbol{\Theta}$, we use tilted semicircular distribution, which can be written as [147]

$$f_{\boldsymbol{\Theta}}(\lambda) = \frac{1}{2\pi\mu\lambda^2} \sqrt{\left(\frac{\lambda}{\sigma_1} - 1\right) \left(1 - \frac{\lambda}{\sigma_2}\right)}, \quad (3.18)$$

with $\sigma_1 \leq \lambda \leq \sigma_2$ and $\mu = \frac{(\sqrt{\sigma_2} - \sqrt{\sigma_1})^2}{4\sigma_1\sigma_2}$.

Let us define the normalized sample covariance matrix under the correlated noise scenario as: $\bar{\mathbf{R}}_{\hat{\mathbf{Z}}}(N) = \frac{1}{\sigma_z^2} \mathbf{R}_{\hat{\mathbf{Z}}}(N)$. From [Theorem 1.5, [351]], the normalized sample covariance matrix $\hat{\mathbf{R}}_{\hat{\mathbf{Z}}}(N)$ ¹⁰ follows the TW₂ distribution in the following way

$$N^{2/3} \left(\frac{\lambda_{\max}(\bar{\mathbf{R}}_{\hat{\mathbf{Z}}}(N)) - \nu_c}{\sigma_c} \right) \Rightarrow TW_2, \quad (3.19)$$

where $\sigma_c^3 = \frac{1}{c^3} \left(1 + \frac{1}{\beta} \int \left(\frac{\lambda c}{1 - \lambda c} \right)^3 dF_{\Theta}(\lambda) \right)$, and $\nu_c = \frac{1}{c} \left(1 + \frac{1}{\beta} \int \frac{\lambda c}{1 - \lambda c} dF_{\Theta}(\lambda) \right)$. The value of c in the above expressions can be obtained by solving the following equation [351, 354]

$$\int \left(\frac{\lambda c}{1 - \lambda c} \right)^2 dF_{\Theta}(\lambda) = \int \left(\frac{\lambda c}{1 - \lambda c} \right)^2 f_{\Theta}(\lambda) d\lambda = \beta. \quad (3.20)$$

It should be noted that the value of c is unique in the range $c \in [0, 1/\lambda_{\max}(\Theta)]$. Substituting the distribution of Θ from (3.18) in (3.20) yields the following expression

$$\int \left(\frac{\lambda c}{1 - \lambda c} \right)^2 \frac{1}{2\pi\mu\lambda^2} \sqrt{\left(\frac{\lambda}{\sigma_1} - 1 \right) \left(1 - \frac{\lambda}{\sigma_2} \right)} - \beta = 0. \quad (3.21)$$

Furthermore, the ratio σ_2/σ_1 in (3.18) can be written as [147]: $\frac{\sigma_2}{\sigma_1} = \frac{(1+\rho)^2}{(1-\rho)^2}$. Using the above relation and $\sigma_1\sigma_2 = 1$, the values of σ_1 and σ_2 can be written as: $\sigma_1 = \frac{1-\rho}{1+\rho}$, $\sigma_2 = \frac{1+\rho}{1-\rho}$. Substituting the values of σ_1 and σ_2 in (3.21) and taking integration limits from σ_1 to σ_2 , (3.21) can be written as:

$$\frac{c^2}{2\pi\mu} \int_{\sigma_1}^{\sigma_2} \frac{1}{(1 - \lambda c)^2} \sqrt{-\lambda^2 - 1 + 2\lambda\mu_1} d\lambda - \beta = 0, \quad (3.22)$$

where $\mu_1 = (1 + \rho^2)/(1 - \rho^2)$. Similarly, the expressions for ν_c and σ_c^3 can be written as

$$\nu_c = \frac{1}{c} \left(1 + \frac{c}{2\pi\mu\beta} \int_{\sigma_1}^{\sigma_2} \frac{1}{(1 - \lambda c)\lambda} \sqrt{-\lambda^2 - 1 + 2\lambda\mu_1} d\lambda \right), \quad (3.23)$$

$$\sigma_c^3 = \frac{1}{c^3} \left(1 + \frac{c^3}{2\pi\mu\beta} \int_{\sigma_1}^{\sigma_2} \frac{\lambda}{(1 - \lambda c)^3} \sqrt{-\lambda^2 - 1 + 2\lambda\mu_1} d\lambda \right). \quad (3.24)$$

3.2.5.2 Derivation of Sensing Threshold

In this section, we derive an analytical expression for the sensing threshold for the considered ME detection following the approach used in [17, 18]. In practice, a CR receiver should be able to detect the presence of PU signals with higher P_d and lower P_f . However, there exists a tradeoff between these two parameters and the sensing threshold should be selected to meet the required value of P_f . Since it's not practical to set a threshold based on the value of P_d due to absence of the knowledge about the PU signal, the threshold is usually determined based on the predefined value of P_f . The contribution in [17] proposes a sensing threshold for the ME detection for the white noise case, which can be written as [17, 45]

$$\lambda_{th} = \frac{(\sqrt{N} + \sqrt{M})^2}{N} \left(1 + \frac{(\sqrt{N} + \sqrt{M})^{-2/3}}{(NM)^{1/6}} F_2^{-1}(1 - P_f) \right). \quad (3.25)$$

¹⁰This normalization is used by considering the fact that the sample covariance matrix of the form (3.17) with variance $1/N$ follows Theorem 1.5 in [351].

In correlated noise scenarios, the detection with the threshold in (3.25) may not provide perfect sensing performance. For this purpose, we propose a new threshold for the ME detector using the analysis presented in Section 3.2.5.1. The probability of false alarm of the ME based detection is given by

$$\begin{aligned} P_f &= P(\lambda_{\max}(\hat{\mathbf{R}}_{\hat{\mathbf{Z}}}) > \lambda_{cth}\sigma_z^2) = P(\sigma_z^2\lambda_{\max}(\bar{\mathbf{R}}_{\hat{\mathbf{Z}}}) > \lambda_{cth}\sigma_z^2), \\ &= P\left(N^{2/3}\frac{\lambda_{\max}(\bar{\mathbf{R}}_{\hat{\mathbf{Z}}}) - \nu_c}{\sigma_c} > N^{2/3}\frac{\lambda_{cth} - \nu_c}{\sigma_c}\right), \end{aligned} \quad (3.26)$$

where λ_{cth} denotes the sensing threshold under the correlated scenario. Subsequently, using the condition (3.19), (3.26) can be written as

$$P_f = 1 - F_2\left(N^{2/3}\left(\frac{\lambda_{cth} - \nu_c}{\sigma_c}\right)\right). \quad (3.27)$$

Equivalently, the above expression can be written as

$$N^{2/3}\left(\frac{\lambda_{cth} - \nu_c}{\sigma_c}\right) = F_2^{-1}(1 - P_f). \quad (3.28)$$

Subsequently, the value of γ_c can be calculated as

$$\lambda_{cth} = \frac{\sigma_c F_2^{-1}(1 - P_f) + N^{2/3}\nu_c}{N^{2/3}}. \quad (3.29)$$

3.2.6 Numerical Results

1. *Performance Metrics:* For evaluating the performance of eigenvalue-based SS techniques in the presence of noise and/or channel correlation, we use the following performance metrics: (i) probability of correct decision, (ii) P_d , and (iii) P_f . These metrics can be defined in the following way. Let $P(H_i; H_j)$ indicate the probability of deciding hypothesis H_i when hypothesis H_j is true with $\{i, j\} \in \{0, 1\}$. The metric P_d can be defined as: $P_d = P(H_1; H_1)$ and the P_f as: $P_f = P(H_1; H_0)$ [16]. Then the probability of correct decision is defined as: $(P(H_1; H_1) + P(H_0; H_0))/2$ i.e., $(P_d + (1 - P_f))/2$. In other words, it depicts how many correct decisions are made out of the total considered realizations under both hypotheses. In the presented simulation results, 10^3 realizations were considered. We consider Rayleigh fading channel in our simulation model and the coefficients of uncorrelated channel \mathbf{H} are generated from random complex numbers whose real and imaginary components are i.i.d. Gaussian variables. Further, the correlated channel $\hat{\mathbf{H}}$ is generated by applying the covariance matrix Φ .
2. *SCN-based SS:* Firstly, we plot the performance of MME and EME techniques proposed in [18] and the MP based asymptotic approach proposed in [44] in the presence of noise correlation in Fig. 3.8. From the figure, it can be noted that noise correlation degrades the sensing performance of the considered detectors. The performance of the proposed sensing scheme has been analyzed in white and correlated noise scenarios. In case of white noise scenarios, it has been noted that the eigenvalue distribution of the received signal's covariance matrix follows the MP law and the distribution is limited to the bounds given by this law. Therefore, the decision rule in (3.12) is used for sensing of the PU signal under white noise scenarios. However, in the presence of noise correlation, the eigenvalue distribution deviates from the distribution under white noise scenario (Fig. 2, [146]) and a new decision rule proposed in (3.13) is considered.

To compare the sensing performance with MP based threshold and new proposed threshold, the probability of correct decision versus SNR for $\rho = 0.5, \beta = 6, N = 60$ is depicted in Fig. 3.9. It can be observed that sensing with (3.13) outperforms than sensing with (3.12) in correlated noise scenarios. Figure 3.10 shows the sensing performance versus correlation coefficient at the SNR value of -6 dB and $\beta = 6$ and it can be noted that with the increased amount of noise correlation, the sensing with MP bounds decreases drastically and sensing with (3.13) gives better performance up to some value of

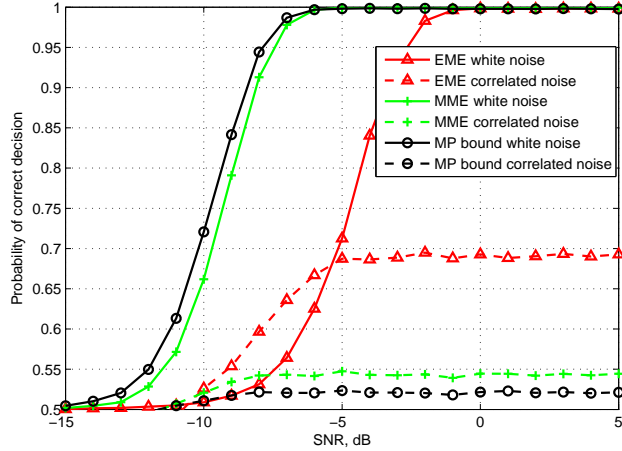


FIGURE 3.8: Sensing performance of different methods in white and correlated noise scenarios ($\beta = 8, \rho = 0.6, N = 80$)

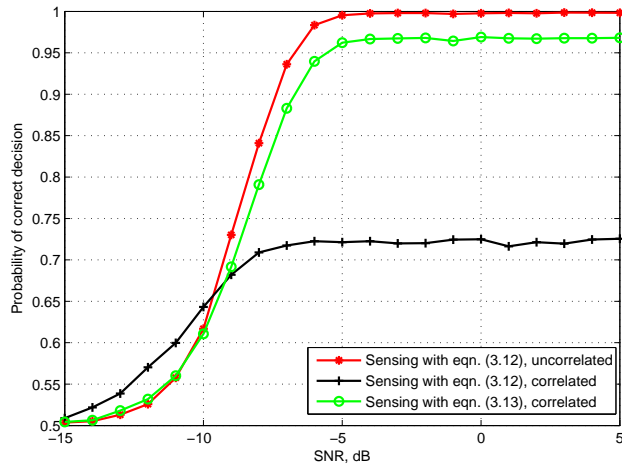
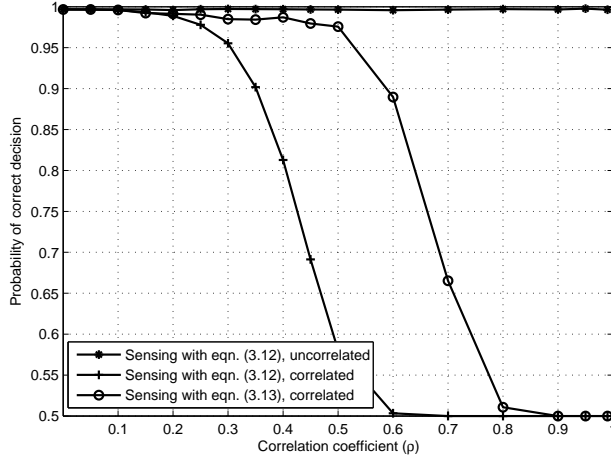
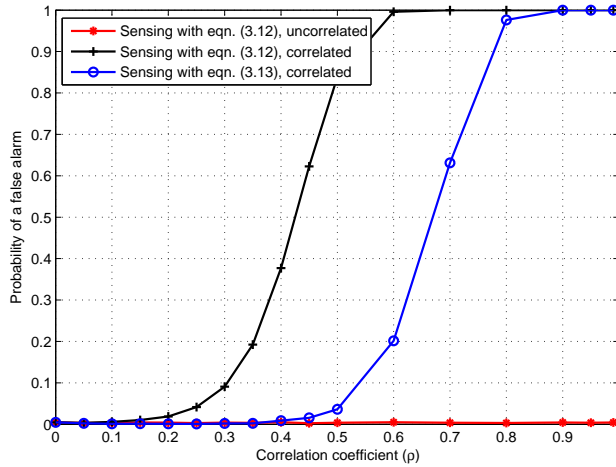


FIGURE 3.9: Sensing performance versus SNR with (3.12) and (3.13) ($\beta = 6, \rho = 0.5, N = 60$)

correlation. Moreover, it has been noted that new bounds also do not provide better sensing at high correlation region. This is due to the fact that the threshold increases and the asymptotic eigenvalue support of H_1 is subsumed in the one of H_0 at this region.

Figure 3.11 depicts the P_f versus correlation coefficient for $\text{SNR} = -6 \text{ dB}, \beta = 6, N = 60$. It can be noted that the value of P_f differs for sensing in white noise and correlated noise scenarios. The value of P_f is very small for sensing with (3.12) in white noise scenarios but it varies with the value of ρ for sensing in correlated noise scenarios. In correlated noise scenarios, the value of P_f with the increase in the value of ρ becomes worse for sensing with (3.12) than for sensing with (3.13). This has been further illustrated by the plots of c.d.f. curves and thresholds in Fig. 3.12. From these results, it can be noted that overall sensing performance is improved with the proposed bounds since we get lower P_f while sensing with the proposed bounds than with the MP bounds up to a certain level of correlation. The c.d.f. curves for white noise and correlated noise scenarios in Fig. 3.12 were plotted by accumulating the decision statistics over 10^3 iterations for $\beta = 6, \rho = 0.5, N = 60$.

Figure 3.13 depicts the probability of correct decision versus number of samples (N) for $\text{SNR} = -6 \text{ dB}, M = 15, \rho = 0.45$. It can be noted that the probability of correct decision increases with the increase in the number of samples and the performance of the proposed bounds in the correlated noise case meets the performance of the MP based bounds at the white noise scenarios at $N = 80$ for the given set of parameters. Further, another interesting aspect to be noted is that these asymptotic bounds can

FIGURE 3.10: Sensing performance versus correlation coefficient (SNR = -6 dB, $\beta = 6$, $N = 60$)FIGURE 3.11: Probability of a false alarm versus correlation coefficient (SNR = -6 dB, $\beta = 6$, $N = 60$)

achieve good detection performance even for small number of samples (sample size greater than 60 for the considered parameters) as noted in [44] for the case of MP based bounds.

Figure 3.14 shows the performance of MME and EME techniques for correlated channel and white noise case in terms of P_d versus SNR (SCN = 3). For the comparison of MME and EME techniques in the presence of channel correlation, the fixed false alarm rate of 0.07 was considered and the detection threshold was calculated using (2.10) and (2.12) respectively. Then the value of P_d was calculated numerically based on the calculated thresholds for different SNR values in the considered range (from -15 dB to 5 dB). From the figure, it can be noted that the detection performance improves in the presence of channel correlation as concluded in [47].

Figure 3.15 shows the performance of the asymptotic MME technique for different cases with the MP bounds i.e., $[a, b]$ and the new bounds i.e., $[\tilde{a}, \tilde{b}]$ in terms of probability of correct decision. The decision for the MME technique using the MP bounds was calculated based on (3.12). Similarly, the decision for the MME technique using new bounds was calculated using \tilde{b}/\tilde{a} , obtained from the supports of (3.10), as the decision threshold instead of b/a in (3.12). From the figure, it can be noted that the MP bounds do not perform well in presence of noise correlation and new bounds provide better sensing performance in this scenario. In the presence of spatial correlation, the sensing performance improves with the MP bounds and the performance becomes slightly worse with new bounds. Furthermore, it can be noted that the sensing with new bounds increases sensing performance in the presence of both channel/noise correlation. Similar to the performance results obtained in [47], we note that the performance of the

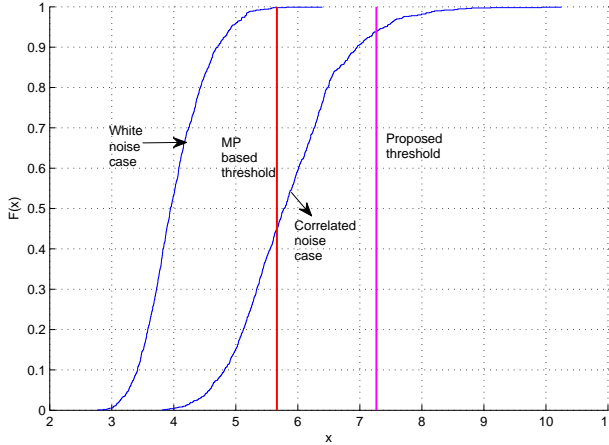


FIGURE 3.12: Cumulative distribution functions of decision statistics under H_0 hypothesis and thresholds for white and correlated noise scenarios ($\beta = 6, \rho = 0.5, N = 60$)

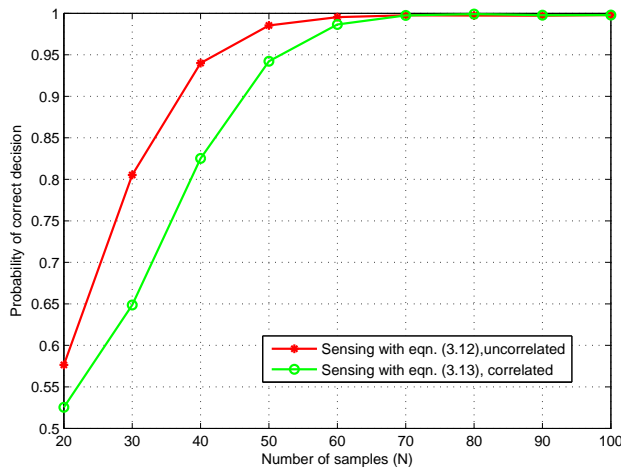


FIGURE 3.13: Probability of correct decision versus number of samples (SNR = -6 dB, $M = 15, \rho = 0.45$)

considered eigenvalue-based techniques improve in the presence of spatial correlation. This is due to the reason that the presence of spatial correlation strengthens the eigenvalues of the received signal's matrix under the H_1 hypothesis compared to the uncorrelated case. Since the contribution of the signal eigenvalues is improved in comparison to the noise eigenvalues in the presence of spatial correlation, the P_d improves in the presence of spatial correlation in eigenvalue-based techniques.

3. Fractional Sampling Operating Point: Figure 3.16 shows the probability of correct decision versus fractional sampling rate for $\varepsilon = 3.5$. The fractional sampling rate has been increased from 1 to 11 and noise correlation has been calculated using (3.14) for different values of M . It can be noted that the sensing performance increases with the fractional sampling rate for white noise scenario. However, at the same time, noise becomes correlated due to fractional sampling and increasing the sampling rate does not monotonically increase the performance. From Fig. 3.16, it can be noted that for $N = 60$, $\text{SNR} = -5$ dB, the performance increases up to the fractional sampling rate of $M = 8$ and for $M > 8$, the sensing with (3.13) saturates. It can be observed that increasing sampling rate enhances the sensing performance up to a certain fractional sampling rate, however, this also increases the complexity in the receiver. Thus it can be concluded that optimum sampling rate should be chosen at the receiver without increasing further complexity since larger sampling rate does not enhance the performance due to noise correlation.

4. ME-based Sensing: We analyze the performance of the proposed sensing approach in terms of

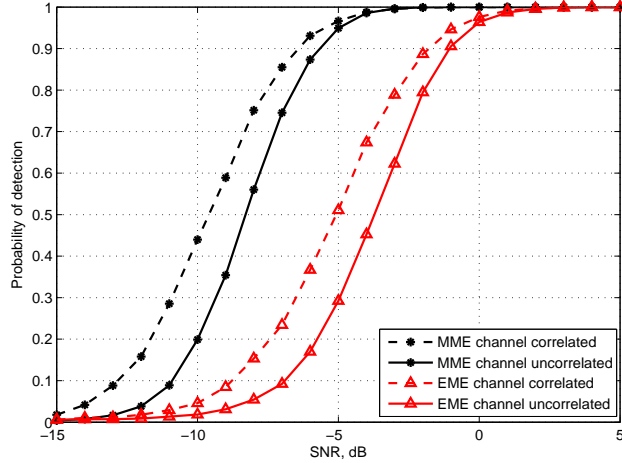


FIGURE 3.14: P_d versus SNR (dB) for MME and EME techniques in channel uncorrelated and correlated scenarios ($\beta = 6, P_f = 0.07, \text{SCN} = 3, N = 60$)

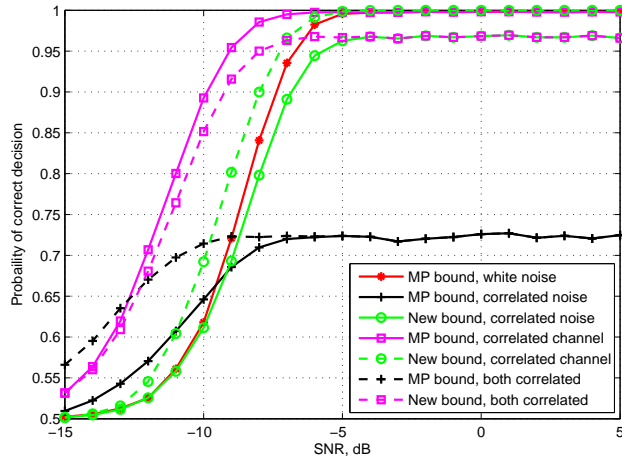


FIGURE 3.15: Probability of correct decision versus SNR for asymptotic MME method ($\beta = 6, \text{SCN} = 3, N = 60$)

false alarm deviation and the probability of correct decision. The false alarm deviation is defined as: $|P_{ft} - P_{fs}|$, where P_{ft} is the target value of P_f , which is usually chosen based on the sensing requirements of a wireless standard and P_{fs} is the simulated value of P_f observed during the decision process. We assume perfect knowledge of the noise variance as in [17]. In practice, this knowledge can be acquired by using noise covariance estimation techniques as in [220].

In order to validate the theoretical analysis presented in Section 3.2.5, we present c.d.f. plots for the following cases in Fig. 3.17: (i) Theoretical TW_2 distribution from (3.16), (ii) Scaled theoretical TW_2 for the uncorrelated case, obtained by scaling the TW_2 distribution based on (3.15), (iii) Scaled theoretical TW_2 for the correlated case, obtained by scaling the TW_2 distribution based on (3.19), (iv) Simulated uncorrelated case, obtained by considering 10^3 realizations of $\lambda_{\max}(\mathbf{R}_Z(N))$, and (v) Simulated correlated case, obtained by taking 10^3 realizations of $\lambda_{\max}(\mathbf{R}_{\hat{Z}}(N))$. From the figure, we note that the c.d.f. of $\lambda_{\max}(\mathbf{R}_Z(N))$ matches perfectly with the theoretical TW_2 distribution, scaled based on (3.15) and the c.d.f. of $\lambda_{\max}(\mathbf{R}_{\hat{Z}}(N))$ matches perfectly with the theoretical TW_2 distribution, scaled based on (3.19). From this result, it can be concluded that the TW_2 distribution can be used for deriving the sensing threshold under the considered correlated scenario considering the mean and variance expressions derived in Section 3.2.5.1.

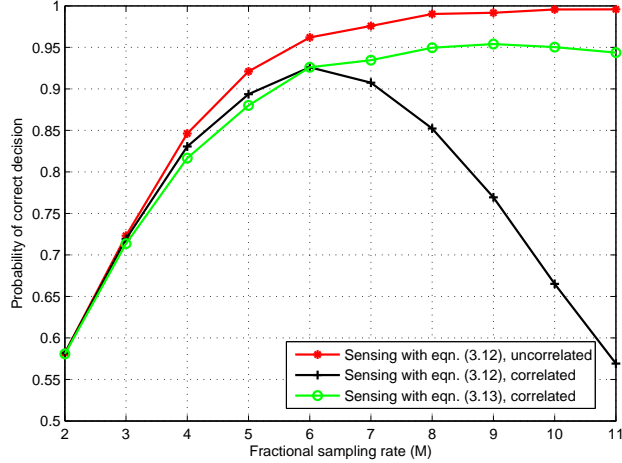


FIGURE 3.16: Sensing performance versus fractional sampling rate ($N = 60$, $\text{SNR} = -5$ dB)

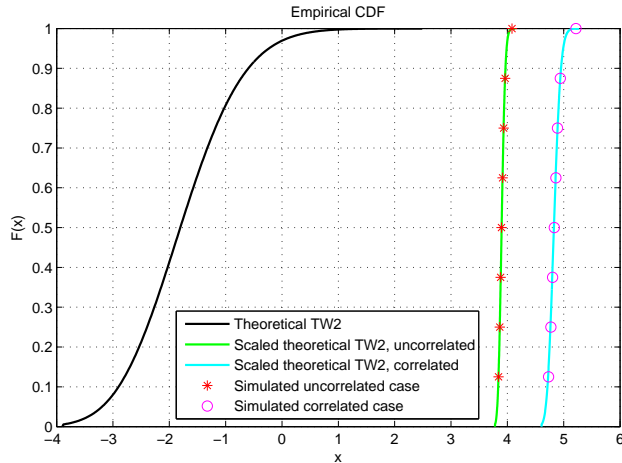


FIGURE 3.17: Theoretical and simulated c.d.f. plots for different random variables ($N = 300$, $\beta = 1$, $\rho = 0.5$)

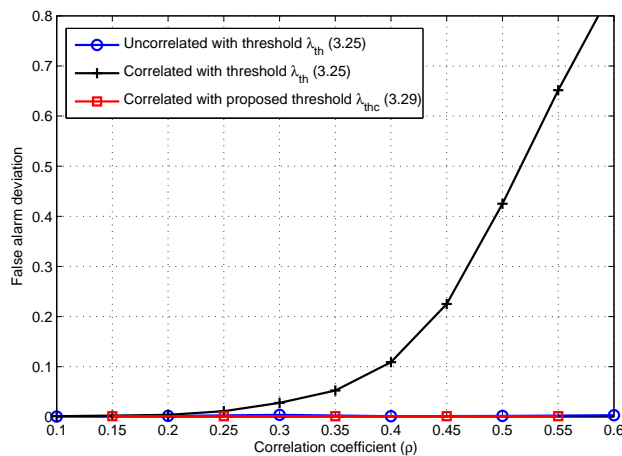


FIGURE 3.18: False alarm deviation versus ρ ($N = 100$, $\beta = 2$, $P_f = 0.001$)

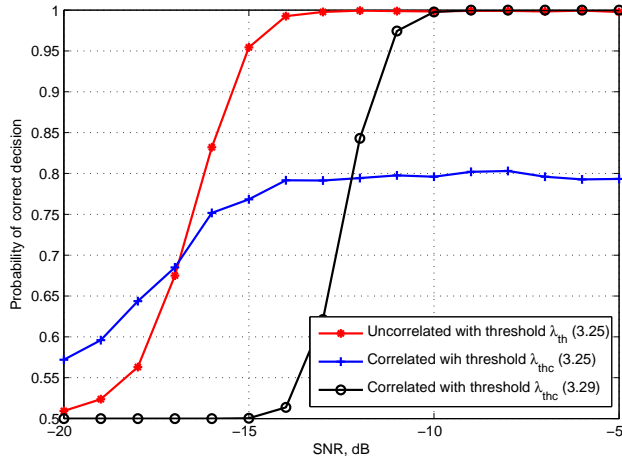


FIGURE 3.19: Probability of correct decision versus SNR ($N = 100, \beta = 2, P_f = 0.07, \rho = 0.5$)

While using the sensing threshold λ_{th} , given by (3.25), under the correlated noise case, the value of P_f deviates from that of the target value used in determining the sensing threshold. This has been illustrated in Fig. 3.18, which shows the false alarm deviation versus correlation coefficient. From the figure, it can be noted that the proposed threshold λ_{thc} , given by (3.29), compensates for this deviation and the difference in P_f is almost zero as in the uncorrelated case while using the sensing threshold λ_{th} .

Figure 3.19 depicts the probability of correct decision versus SNR at a fixed false alarm rate of $P_f = 0.07$ for 3 different cases with parameters ($N = 100, \beta = 2, \rho = 0.5$). From the figure, we note that although the correlated case with the threshold λ_{th} performs better for low SNR values, it can not achieve the perfect sensing performance (even at higher SNR values). The perfect sensing is the condition in which there occur no false alarm and no miss detection. The correlated case with the proposed threshold λ_{thc} improves the sensing performance and achieves the perfect sensing performance above the SNR value of -10 dB. Therefore, it can be concluded that the proposed threshold for the ME based detection can be used for sensing under correlated noise scenarios.

5. Discussion: In this work, the performance of eigenvalue-based SS techniques has been studied in the presence of noise/channel correlation. It has been noted that noise correlation degrades the performance while the channel correlation enhances the performance of the SCN-based SS techniques. A new SCN-based threshold has been proposed for improved sensing in the presence of noise correlation. Further, the performance of an fractional sampling-based SS technique is studied and it has been noted that SS efficiency increases with the fractional sampling rate up to a certain limit and it does not provide performance advantage beyond this limit. Therefore, it can be concluded that an optimal operating point for the fractional sampling rate should be selected to maintain a good tradeoff between performance and complexity. Further, the ME-based detection was studied for sensing the PU signal under correlated noise scenarios. Using recent RMT results on the distribution of the maximum eigenvalue for a class of sample covariance matrices, an expression for the sensing threshold has been derived in terms of the P_f and system parameters. From the simulation results, it has been noted that the P_f for the considered correlated case increases with the increase in the correlation level and the proposed threshold compensates for this deviation.

3.3 Signal to Noise Ratio Estimation

3.3.1 Background and Contributions

Several methods based on the eigenvalue distribution of the received signal's covariance matrix usually focus on interweave CR meaning that an SU transmits only when no PU signal is present [18, 41]. However, if side information is available about the primary SNR, advanced underlay transmission schemes could be employed at the CRs. In practical scenarios, it would be advantageous to estimate the primary SNR in order to decide the transmission strategy of the cognitive transmitter. Depending on the estimated primary SNR level, different underlay transmission strategies (e.g., cognitive resource allocation) can be implemented at the cognitive transmitters to allow the coexistence of primary and secondary systems.

In CR networks, SNR estimation can be very useful in switching between underlay and interweave modes adaptively. In an interweave approach, the SUs are not allowed to access a particular PU channel when the channel is found to be occupied. In this scheme, the secondary network may have very low throughput specifically in heavily occupied spectrum regions. If the CR node has the capability of estimating the PU SNR along with its sensing ability, the SU can access the channel with full power in case of an idle channel and access the channel with controlled power in case of the occupied channel. Based on the link budget analysis and the interference constraint, proper SNR threshold can be determined to guarantee the protection of the PU rate. Subsequently, by comparing the estimated SNR with the SNR threshold, power control mechanism can be implemented at the CR to adjust its coverage area. More specifically, in the SS only techniques, the noise only hypothesis is decided if $\text{SNR} \leq \lambda_1$, λ_1 being the decision threshold and the signal plus noise hypothesis is decided if $\text{SNR} > \lambda_1$. When we combine SS with the SNR estimation, we can introduce another threshold λ_2 under the signal plus noise hypothesis in the following way. If $\text{SNR} \leq \lambda_2$, then the CR can transmit in the same channel using the power control algorithm based on the interference threshold of the PU and the CR must stop its transmission when $\text{SNR} > \lambda_2$.

Despite its important applications, only a few contributions in the literature address the SNR estimation problem in the context of a CR [19, 20, 25, 26]. In [19], an SNR estimation method has been proposed for ultra-wideband CR systems using computer simulations and this method is specific only for multiband orthogonal frequency division multiplexing-based systems. In [25], a pseudo bit error rate based SNR estimation has been proposed for the ED scheme. The contribution in [20] utilizes the priori knowledge of SNR, which can be obtained using estimation techniques, for realizing the adaptive SS techniques. Similarly in [26], a cooperative SS scheme has been proposed based on the SNR estimation and the energy combining method, where the combining weights for the received energies of cooperative sensors are determined at the fusion center for making the final decision.

Further, the SNR estimation techniques proposed under the assumption of white noise and uncorrelated channel scenario may not perform well in the presence of channel/noise correlation. Taking the above into account, exploring efficient SNR estimation techniques in the presence of channel/noise correlation is an important research challenge. Motivated by this aspect, we carry out detailed theoretical analysis under signal plus noise hypothesis to obtain the a.e.p.d.f. of the received signal's covariance matrix for white and correlated noise scenarios. Based on this a.e.p.d.f. of the received signal's covariance matrix, we propose an SNR estimation method for estimating the SNR of the PU signal using the ME.

The theoretical analysis carried out in this section has been inspired by the multi-dimensional eigenvalue-based SS model and it has been applied for SNR estimation application by carrying out analysis under the signal plus noise hypothesis. We study the SNR estimation problem in the presence of noise and/or channel correlation. For this purpose, we need the expressions for a.e.p.d.f. of the received signal's covariance matrix under the aforementioned scenarios. However, these expressions are not available in the literature. In this context, we derive the expressions for the a.e.p.d.f. of the received signal's

covariance matrix under the considered scenarios using RMT. Further, we use these a.e.p.d.f. expressions in order to estimate the PU SNR based on the ME. Moreover, the performance of the proposed technique is evaluated in terms of normalized MSE.

3.3.2 Analysis under Signal plus Noise Hypothesis

Theorem 3.2.2 is applicable for noise covariance matrix Θ in case of noise correlation and for channel covariance matrix Φ in case of channel correlation. The eigenvalue spread of Θ or Φ is related to the degree of noise or channel covariance i.e., a zero eigenvalue spread corresponds to a zero-covariance model and higher spreads are associated with higher covariance models. In (3.10), the parameter μ controls the degree of covariance and varies the support of the distribution i.e., for $\mu = 0$, $\tilde{a} = a$ and $\tilde{b} = b$, where $a = (1 - \sqrt{\beta})^2$ and $b = (1 + \sqrt{\beta})^2$ are the supports of the MP distribution [43]. For the exponential covariance model as stated in [147], the parameter μ is related to the correlation coefficient ς with the following relation: $\mu = \frac{\varsigma^2}{1 - \varsigma^2}$. Furthermore, the SCN is related to ς with the relation $\text{SCN} = \frac{1 + \varsigma}{1 - \varsigma}$. To calculate μ in a practical cognitive receiver, the value of ς for noise correlation case can be determined based on some empirical model constructed from measurements such as [53] and its value for channel correlation case can be determined using channel estimation techniques like [355]. The received signal matrix under the correlated channel and white noise case can be written as

$$\mathbf{Y} = \sqrt{p}\Phi^{\frac{1}{2}}\mathbf{H}\mathbf{S}_d + \mathbf{Z}. \quad (3.30)$$

Assuming that signal and noise are independent, for very large value of N , the sample covariance matrix of the received signal under considered scenario in the presence of channel correlation can be approximated as

$$\lim_{N \rightarrow \infty} \hat{\mathbf{R}}_{\mathbf{Y}}(N) \approx p\Phi^{\frac{1}{2}}\mathbf{H}\mathbf{H}^{\dagger}\Phi^{\frac{1}{2}} + \hat{\mathbf{R}}_{\mathbf{Z}}. \quad (3.31)$$

3.3.3 Methodology

The a.e.p.d.f. of the received signal's covariance matrix under the H_1 hypothesis can be used to estimate the PU SNR by a CR. To calculate the a.e.p.d.f. of $\hat{\mathbf{R}}_{\mathbf{Y}}(N)$, we need to know the Stieltjes transform of its asymptotic density function. In this subsection, we provide a generalized methodology to derive the a.e.p.d.f. for $\hat{\mathbf{R}}_{\mathbf{Y}}(N)$ in the presence of channel correlation referring to the case considered in (3.31).

Due to noncommutative nature of random matrices, it's not straightforward to calculate the eigenvalue distributions of the received signal \mathbf{Y} by knowing the eigenvalue distribution of covariance matrices of Φ , \mathbf{H} and \mathbf{Z} in (3.31). Using free probability analysis, the asymptotic spectrum of the sum or product can be obtained from the individual asymptotic spectra without involving the structure of the eigenvectors of the matrices [43] under a asymptotic freeness condition. The asymptotic eigenvalue distribution of \mathbf{Y} in our context can be obtained by applying Σ transform and R transform [43]. In (3.31), since Φ is a deterministic matrix and $\mathbf{H}\mathbf{H}^{\dagger}$ is a Wishart random matrix, they are asymptotically free (see Example 2.34, [43]). As a result, the combined a.e.p.d.f. of the term $p\Phi^{\frac{1}{2}}\mathbf{H}\mathbf{H}^{\dagger}\Phi^{\frac{1}{2}}$ in (3.31) can be obtained by applying multiplicative free convolution property of Σ transform in the following way [350]

$$\Sigma_{p\hat{\mathbf{R}}_{\mathbf{H}}}(z) = \Sigma_{\Phi}(z) \cdot \Sigma_{p\hat{\mathbf{R}}_{\mathbf{H}}}(z), \quad (3.32)$$

where Σ_{Φ} and $\Sigma_{p\hat{\mathbf{R}}_{\mathbf{H}}}$ are the Σ transforms of the densities of eigenvalues of Φ and $p\hat{\mathbf{R}}_{\mathbf{H}}$ respectively. Since Φ is a square matrix, $\Phi^{1/2}\mathbf{H}\mathbf{H}^{\dagger}\Phi^{1/2}$ and $\Phi\mathbf{H}\mathbf{H}^{\dagger}$ have identical eigenvalues [43]. Furthermore, $\Phi\mathbf{H}\mathbf{H}^{\dagger}$ and $\mathbf{Z}\mathbf{Z}^{\dagger}$ are independent and $\mathbf{Z}\mathbf{Z}^{\dagger}$ is a Wishart matrix. As a result, $\Phi\mathbf{H}\mathbf{H}^{\dagger}$ and $\mathbf{Z}\mathbf{Z}^{\dagger}$ are asymptotically free due to unitarily invariance [23]. Then the combined R transform of $\hat{\mathbf{R}}_{\mathbf{Y}}$ can be found from the R transforms of $\hat{\mathbf{R}}_{\mathbf{Z}}$ and $p\hat{\mathbf{R}}_{\mathbf{H}}$ using additive free convolution property of R transform

in the following way [356]

$$\mathcal{R}_{\hat{\mathbf{R}}_{\mathbf{Y}}}(z) = \mathcal{R}_{\hat{\mathbf{R}}_{\mathbf{Z}}}(z) + \mathcal{R}_{p\hat{\mathbf{R}}_{\mathbf{H}}}(z). \quad (3.33)$$

Since $\hat{\mathbf{R}}_{\mathbf{Z}}$ follows MP law, its R transform can be written as the R transform of the MP law and is given by (A.5). Using the transformations as described in the preliminaries, we get the Stieltjes transform of $\hat{\mathbf{R}}_{\mathbf{Y}}$ (See Appendix B for detailed procedure). The Stieltjes transforms obtained for different correlated scenarios are provided in Section 3.3.4. The a.e.p.d.f. of $\hat{\mathbf{R}}_{\mathbf{Y}}$ is then obtained by determining the imaginary part of the Stieltjes transform $\mathcal{S}_{\hat{\mathbf{R}}_{\mathbf{Y}}}$ for real arguments in the following way

$$f_{\hat{\mathbf{Y}}}^{\infty} = \lim_{y \rightarrow 0^+} \frac{1}{\pi} \text{Im}\{\mathcal{S}_{\hat{\mathbf{R}}_{\mathbf{Y}}}(x + jy)\}. \quad (3.34)$$

3.3.4 Main Analytical Results

In this section, we present the main results of our analysis for the considered cases in the form of theorems. The detailed proofs of these theorems are postponed to the appendix (Appendix B) to improve the continuity of this thesis.

3.3.4.1 White Noise and Uncorrelated Channel

Theorem 3.3.1. The Stieltjes transform $\mathcal{S}_{\hat{\mathbf{R}}_{\mathbf{Y}}}$ of the asymptotic distribution of eigenvalues of $\frac{1}{N}\mathbf{Y}\mathbf{Y}^{\dagger}$ where $\mathbf{Y} = \mathbf{H}\mathbf{S}_d + \mathbf{Z}$ can be obtained for any $z \in \mathbb{C}$ by solving a cubic polynomial having the following coefficients

$$\begin{aligned} c_0 &= 1, \\ c_1 &= (1 - \beta)(1 - p) + z, \\ c_2 &= p(-2\beta + z + 1) + z, \\ c_3 &= pz, \end{aligned} \quad (3.35)$$

where c_n is the n th order coefficient of the polynomial, $\beta = \frac{N}{M}$ and p is the SNR of the transmitted PU signal.

Proof. The proof is included in Appendix B. \square

3.3.4.2 Correlated Noise and Uncorrelated Channel

Theorem 3.3.2. The Stieltjes transform $\mathcal{S}_{\hat{\mathbf{R}}_{\mathbf{Y}}}$ of the asymptotic distribution of eigenvalues of $\frac{1}{N}\mathbf{Y}\mathbf{Y}^{\dagger}$ where $\mathbf{Y} = \mathbf{H}\mathbf{S}_d + \hat{\mathbf{Z}}$ can be obtained for any $z \in \mathbb{C}$ by solving a quartic polynomial with the following coefficients

$$\begin{aligned} c_0 &= 1 + \mu, \\ c_1 &= 2p(1 + \mu(1 - \beta)) + z(1 + 2\mu) - \beta(1 + p) + 1, \\ c_2 &= p^2(\mu(1 - \beta)^2 + 1 - \beta) + 2p(1 + z + \mu z(2 - \beta)) + z - 3p\beta + z^2\mu, \\ c_3 &= 2z\mu p(z - p\beta) + p^2(1 + 2z\mu + z - 2\beta) + 2zp, \\ c_4 &= zp^2(1 + \mu z), \end{aligned} \quad (3.36)$$

where $\mu = \frac{\varsigma^2}{1 - \varsigma^2}$, defines the degree of covariance of the noise covariance matrix Θ .

Proof. The proof is provided in Appendix B. \square

3.3.4.3 Correlated Channel and White Noise

Theorem 3.3.3. The Stieltjes transform $\mathcal{S}_{\hat{\mathbf{R}}_{\mathbf{Y}}}$ of the asymptotic distribution of eigenvalues of $\frac{1}{N}\mathbf{Y}\mathbf{Y}^\dagger$ where $\mathbf{Y} = \hat{\mathbf{H}}\mathbf{S}_d + \mathbf{Z}$ can be obtained for any $z \in \mathbb{C}$ by solving a quartic polynomial with the following coefficients

$$\begin{aligned} c_0 &= 1 + \mu, \\ c_1 &= 2\mu(z + 1 - \beta) - \beta(p + 1) + p + z + 2, \\ c_2 &= p(z - 3\beta + 2) + \beta(\mu(\beta - 2z - 2) - 1) + \mu(z(z + \mu) + 1) + 2z, \\ c_3 &= -2p(\beta - z) + 2z\mu(1 - \beta + z) + p + z, \\ c_4 &= z(p + \mu z), \end{aligned} \tag{3.37}$$

where the parameter μ defines the degree of covariance of the channel covariance matrix Φ .

Proof. The proof is presented in Appendix B. \square

3.3.4.4 Correlated Channel and Correlated Noise

Theorem 3.3.4. The Stieltjes transform $\mathcal{S}_{\hat{\mathbf{R}}_{\mathbf{Y}}}$ of the asymptotic distribution of eigenvalues of $\frac{1}{N}\mathbf{Y}\mathbf{Y}^\dagger$ where $\mathbf{Y} = \hat{\mathbf{H}}\mathbf{S}_d + \hat{\mathbf{Z}}$ can be obtained for any $z \in \mathbb{C}$ by solving a quartic polynomial with the following coefficients

$$\begin{aligned} c_0 &= \mu(\mu + 2)(\mu + 1)^2, \\ c_1 &= -\mu(\mu + 1)((-4\mu^2 - 8\mu - 2)z + (1 + p)((2\beta - 2)\mu - 3 + 2\beta)), \\ c_2 &= \mu(6z^2\mu^3 - 2z((2p + 2)\beta - 6z - 3(p + 1))\mu^2 + \mu(5z^2 + (-2(1 + p)(-5 + 2\beta))z \\ &\quad + (p - 1)^2\beta^2 + (p + 1)^2(1 - 2\beta) + p) + p^2(1 - \beta) + (3z - 6\beta + 4)p + 3z + 1 - \beta), \\ c_3 &= \mu p^2(1 + z(1 + 2\mu) - 2\beta) + \mu^2\beta(-2z(1 + p)^2 - 2z^2\mu(1 + p)) \\ &\quad + \mu z(1 + 4z\mu(1 + 3p)) + 2 + \mu^2 z^2((1 + p)(5 + 6\mu) + 4\mu^2 z), \\ c_4 &= z^2\mu^2((1 + p)^2 + p + 2z\mu) + z\mu p(p + 2z^2\mu^2 + 1) + z^4\mu^4, \end{aligned} \tag{3.38}$$

where the parameter μ defines the degree of covariance of the noise covariance matrix Θ and the channel covariance matrix Φ .

Proof. The proof is included in Appendix B. \square

Remark 3.3.1. We can find the roots of the above polynomials (3.36), (3.37) and (3.38) in closed forms. The closed form is not specifically provided because it includes many terms which provide no further insight. In practice, we can just solve these polynomials with a mathematical software for finding the Stieltjes transforms under considered scenarios.

3.3.5 Proposed Signal to Noise Ratio Estimation Method

Based on the analysis presented in the above section, firstly, we present the SNR estimation method for estimating the PU SNR in the presence of noise and/or channel correlation. Then for evaluating the SNR estimation performance, we consider the following four cases: (i) uncorrelated channel plus

white noise, (ii) uncorrelated channel plus correlated noise, (iii) correlated channel plus white noise, and (iv) correlated channel plus correlated noise.

Based on the polynomials of the Stieltjes transforms specified in the above section, the supports for the corresponding a.e.p.d.f. are obtained using (3.34)¹¹. The support for the a.e.p.d.f. of $\hat{\mathbf{R}}_{\mathbf{Y}}$ under uncorrelated channel plus correlated noise case is calculated based on (3.36). Similarly, for correlated channel plus white noise case is obtained using polynomial (3.37) and for both correlated case is obtained using polynomial (3.38). It can be noted that the value of ς for correlated channel can be found with channel estimation methods such as [355] and its value for correlated noise can be found by carrying out measurements in the sensing module like [53]. Since we know the value of β and we can measure the value of ς , we can estimate the value of p by sensing the ME of $\hat{\mathbf{R}}_{\mathbf{Y}}$. Further, it can be noted that the parameters M, N and ς are assumed as operating parameters of the CR sensing module.

For convenience, a lookup table (Table 3.1) is provided in order to estimate the PU SNR (see Section 3.3.6). In the lookup table, we present the MEs of the received signal's covariance matrix for the above four cases for different values of SNR and β . With the help of this table, we can estimate the PU SNR based on the ME of the received signal's covariance matrix. Based on this estimated SNR, we could potentially design suitable underlay transmission strategy for secondary transmission as described in Section 3.3.1. In Section 3.3.6, we provide the normalized MSE versus SNR plot to evaluate the performance of this estimation technique. To clarify the above process, we include algorithms for lookup table formation and for PU SNR estimation below.

Algorithm for lookup table formation

1. Select N, M and calculate $\beta = N/M$.
2. Find ς using channel estimation and noise measurement methods like [355] [53].
3. Calculate $\mu = \frac{\varsigma^2}{1-\varsigma^2}$.
4. Select p range e.g., -10 dB to 5 dB.
5. Evaluate $\mathcal{S}_{\mathbf{R}_{\mathbf{Y}}}$ using (3.37).
6. Find $\lambda_{\max}(\mathbf{R}_{\mathbf{Y}})$ using (3.34).
7. Store all $\lambda_{\max}(\mathbf{R}_{\mathbf{Y}})$ and corresponding p e.g., Table 3.1

Algorithm for SNR estimation

1. Calculate instantaneous $\hat{\mathbf{R}}_{\mathbf{Y}}(N) = \frac{1}{N} \mathbf{Y} \mathbf{Y}^\dagger$.
2. Calculate $\lambda_{\max}(\hat{\mathbf{R}}_{\mathbf{Y}})$.
3. Find p corresponding to λ_{\max} from lookup table.
4. Use suitable interpolation for any intermediate λ_{\max} .

¹¹We select the imaginary root which complies with the definition and properties of Stieltjes transform (See Appendix A).

TABLE 3.1: Look up table for SNR estimation

SCN	β	SNR (dB)	Case I $\lambda_{\max}(\mathbf{H}\mathbf{S}_d + \mathbf{Z})$	Case II $\lambda_{\max}(\mathbf{H}\mathbf{S}_d + \hat{\mathbf{Z}})$	Case III $\lambda_{\max}(\hat{\mathbf{H}}\mathbf{S}_d + \mathbf{Z})$	Case IV $\lambda_{\max}(\hat{\mathbf{H}}\mathbf{S}_d + \hat{\mathbf{Z}})$
2	1	4	10.77	10.78	11.03	11.15
2	1	2	7.45	7.47	7.58	7.73
2	1	0	5.59	5.65	5.65	5.82
2	1	-2	4.70	4.79	4.71	4.88
2	1	-4	4.29	4.38	4.29	4.43
2	1	-6	4.08	4.19	4.08	4.21
2	1	-8	3.96	4.07	3.96	4.09
2	1	-10	3.90	4.01	3.90	4.01
3	1	4	10.77	10.82	11.45	11.77
3	1	2	7.45	7.52	7.82	8.19
3	1	0	5.59	5.75	5.75	6.18
3	1	-2	4.70	4.93	4.75	5.17
3	1	-4	4.29	4.55	4.30	4.68
3	1	-6	4.08	4.35	4.08	4.42
3	1	-8	3.96	4.24	3.97	4.29
3	1	-10	3.90	4.18	3.90	4.20
4	1	4	10.77	10.83	11.86	12.38
4	1	2	7.45	7.57	8.05	8.65
4	1	0	5.59	5.86	5.86	6.55
4	1	-2	4.70	5.08	4.78	5.45
4	1	-4	4.29	4.72	4.31	4.92
4	1	-6	4.08	4.52	4.08	4.63
4	1	-8	3.96	4.42	3.97	4.48
4	1	-10	3.90	4.35	3.90	4.39

3.3.6 Numerical Results

To evaluate the performance of the proposed SNR estimation method in the presence of noise or/and channel correlation, normalized MSE is used and is defined as

$$\text{MSE} = \frac{E[(\hat{p} - p)^2]}{p^2}, \quad (3.39)$$

where \hat{p} is the estimated SNR with the proposed method and p is the actual SNR.

Table 3.1 shows the lookup table for different values of SCN of the channel/noise covariance matrix and SNRs. For all the considered cases, the ME corresponding to the particular value of SNR was obtained by solving the polynomial expressions provided in Section 3.3.4 with the help of a mathematical software. This table can be used to estimate the PU SNR on the values of SCN and β for all the considered cases. For example, if the value of SCN is 2, β is 1 and the ME of the received signal's sample covariance matrix i.e., $\frac{1}{N}\mathbf{Y}\mathbf{Y}^\dagger$ is 4.79 in case II, we can then estimate that PU SNR is -2 dB and intermediate values can be calculated through interpolation.

Analysis under H_1 hypothesis case was considered by taking the combination of signal and noise under both scenarios. Figure 3.20 (a) shows the theoretical and simulated eigenvalue distribution of covariance matrix of received signal i.e., $\frac{1}{N}\mathbf{Y}\mathbf{Y}^\dagger$ for SNR = -2 dB and $\beta = 1$ under white noise scenarios. The histograms of the eigenvalues were created by accumulating the eigenvalues over 10^3 iterations. The theoretical result was obtained by evaluating the polynomial given by (3.35). Similarly, Fig. 3.20 (b) shows the eigenvalue distribution of covariance matrix of received signal for SNR = -2 dB, SCN = 3 and $\beta = 1$ under correlated noise. In this case, theoretical result was obtained by evaluating the polynomial given by (3.36). From Fig. (3.20), it can be observed that the theoretical and simulated density functions match perfectly for all the considered cases.

Figure 3.21 shows the ME of the received signal's covariance matrix versus SCN of the noise covariance matrix for different cases ($\beta = 1$, $N = 100$, SNR = 3 dB). From the figure, it can be noted that the ME increases with the SCN for all correlated cases and the rate of increase for both channel/noise correlated case is higher than other two individually correlated cases. Furthermore, the rate of increase

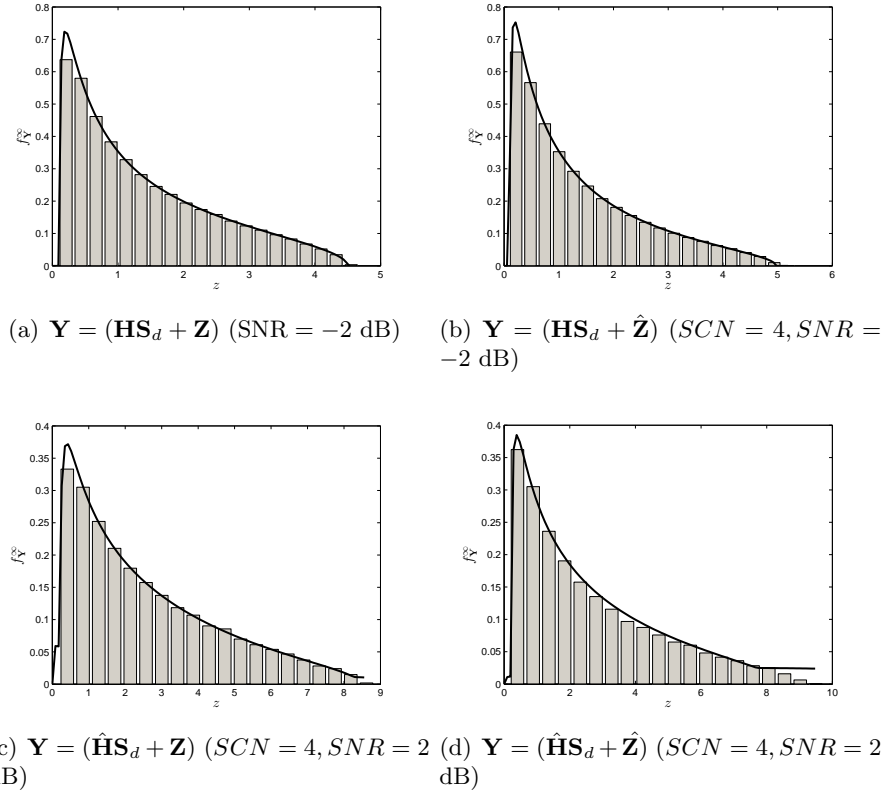


FIGURE 3.20: Theoretical and simulated eigenvalue distribution of received signal for different cases: (a) uncorrelated channel and white noise, (b) uncorrelated channel and correlated noise, (c) correlated channel and white noise, (d) correlated channel and correlated noise ($\beta = 1, N = 100$)

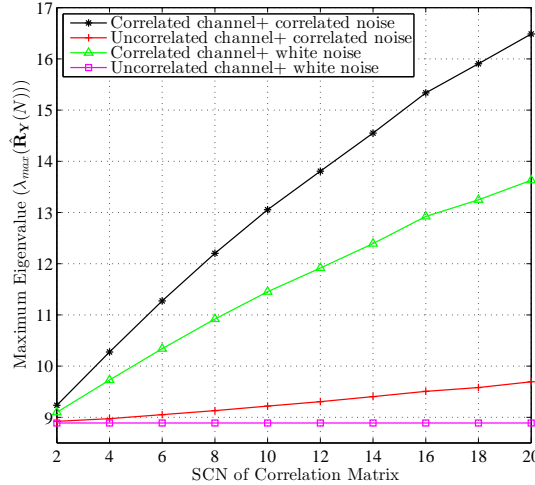
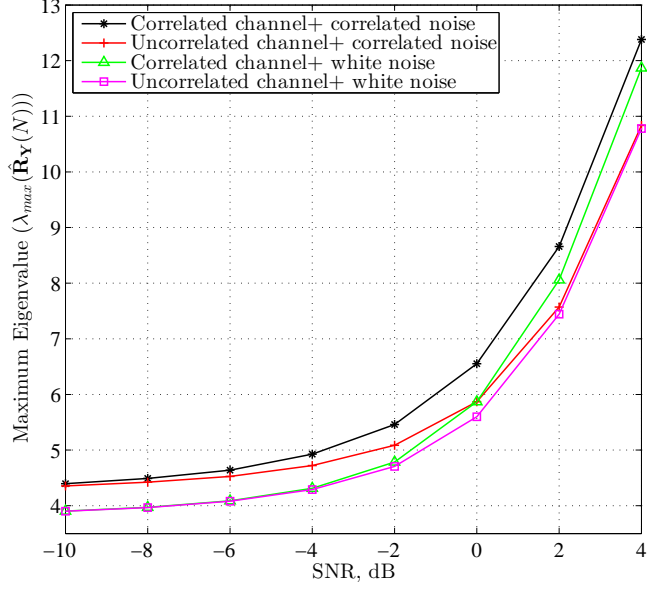
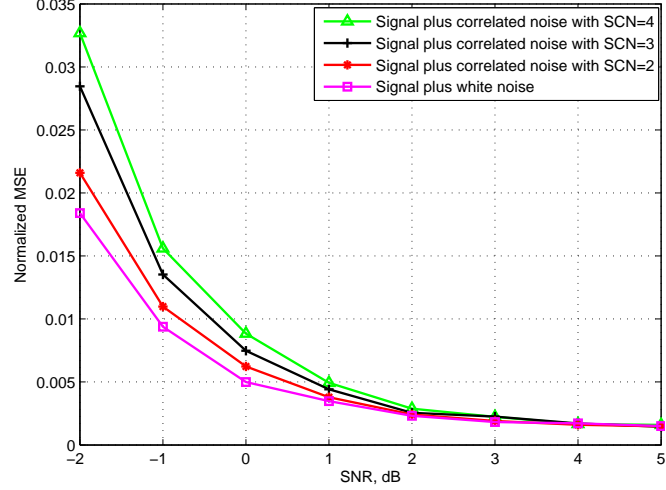


FIGURE 3.21: ME versus SCN of covariance matrix for different cases ($\beta = 1, N = 100, \text{SNR} = 3 \text{ dB}$)

of the ME is higher for the channel correlated case than the noise correlated case at SNR value of 3 dB. Figure 3.22 shows the ME versus SNR for different cases ($\beta = 1, \text{SCN} = 4, N=100$). From the figure, it can be noted that the ME increases with the SNR for all considered cases with the higher rate in the high SNR region. Furthermore, the rate of increase is higher for both correlated case than other cases. From the curves for correlated channel plus white noise case and uncorrelated channel plus correlated noise case, it can be noted that the effect of noise correlation is dominant at lower values of SNR and the channel correlation effect becomes more than that of noise correlation at high SNR values (after 0

FIGURE 3.22: ME versus SNR for different cases ($\beta = 1, N = 100, \text{SCN} = 4$)FIGURE 3.23: Normalized MSE versus SNR for SNR estimation using the proposed technique ($N = 100, \beta = 1$)

dB in Fig. 3.22). Furthermore, it can be noted that at the value of $\text{SNR} = 0 \text{ dB}$ i.e., $p = 1$, effects of channel correlation and noise correlation are equivalent for identical ς .

Figure 3.23 shows the normalized MSE versus SNR plot for white noise and correlated noise scenarios for different SCNs of the noise correlation matrix. From the figure, it can be observed that for all considered cases, normalized MSE decreases with the SNR. In case of white noise scenario, we can estimate the PU SNR with less than 0.5 % normalized MSE up to 0 dB and with less than 1 % normalized MSE up to -1 dB. Similarly, in case of correlated noise scenarios, we can estimate the SNR with less than 1 % normalized MSE up to 0 dB for all considered values of SCN, with less than 2 % normalized MSE up to -1 dB and after SNR values of 3 dB, SNR in all the cases can be estimated with almost 0.2 % normalized MSE. Furthermore, it can be noted that the normalized MSE performance decreases with the increase in the value of SCN at lower SNR values and it becomes almost stable if we go to higher SNR values beyond 3 dB. From this result, it can be concluded that the proposed technique can be used to estimate the PU SNR reliably in the presence of correlated noise and noise correlation mostly affects the SNR estimation performance at lower SNR values.

Figure 3.24 shows the normalized MSE versus SNR with and without the knowledge of noise or/and channel correlation ($\beta = 1$, $SCN = 4$, $N = 100$). In this case, we consider the correlated case with the presence of both channel/noise correlation. In this simulation setting, we generate the instances of \mathbf{Y} according to case IV shown in Table 3.1 and we evaluate the knowledge of correlation on the PU SNR estimation performance using (3.39). To evaluate the knowledge of noise correlation only, we use case II of the table and to evaluate the knowledge of channel correlation only, we use case III. Similarly, to evaluate performance without knowledge of both channel/noise correlation, we use case I and to evaluate the knowledge of both channel/noise correlation, we use case IV of the table. From the figure, it can be noted that the performance is optimal assuming the knowledge of both channel/noise correlation. Moreover, the MSE performance with knowledge of noise correlation becomes better than with the knowledge of channel correlation at lower SNR values and the phenomenon reverses for higher SNR values (> -1 dB SNR in the figure). Therefore, it can be concluded that the PU SNR can be reliably estimated if we have the perfect knowledge of both channel/noise correlation at the CR sensing module.

Furthermore, to evaluate the performance of the proposed technique in case of the imperfect correlation model, we consider 10% static deviation in the considered value of the correlation coefficient for both the channel and noise correlation. Subsequently, we carry out SNR estimation based on the procedure mentioned in Section 3.3.5 and evaluate the performance using (3.39) in terms of the normalized MSE versus SNR plot shown in Fig. 3.24. From the figure, it can be noted that the PU SNR can be estimated with less than 2.5% normalized MSE error up to the SNR value of 0 dB while considering 10 % imperfect correlation knowledge. At the same value of SNR i.e., 0 dB, the normalized MSE error is about 0.8 % while considering perfect knowledge of both channel/noise correlation. Thus the normalized MSE performance degradation in case of 10 % imperfect correlation knowledge is about 1.7 % at the SNR value of 0 dB. Moreover, it can be noted that this performance degradation increases for lower SNR values and decreases for higher SNR values following performance of the perfect correlation knowledge case beyond the SNR value of 3 dB.

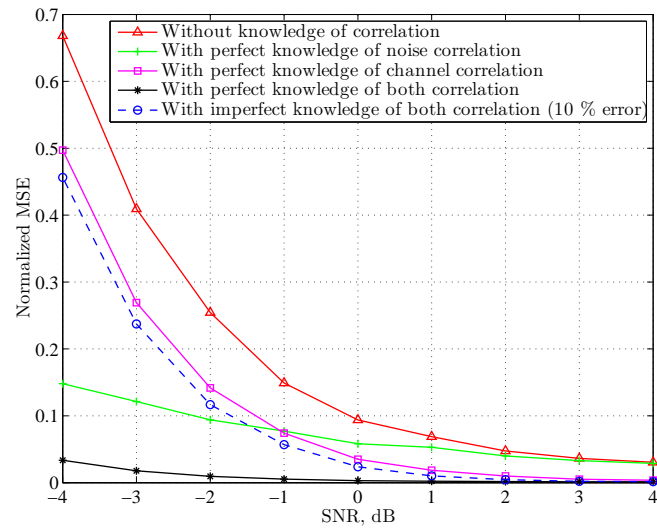
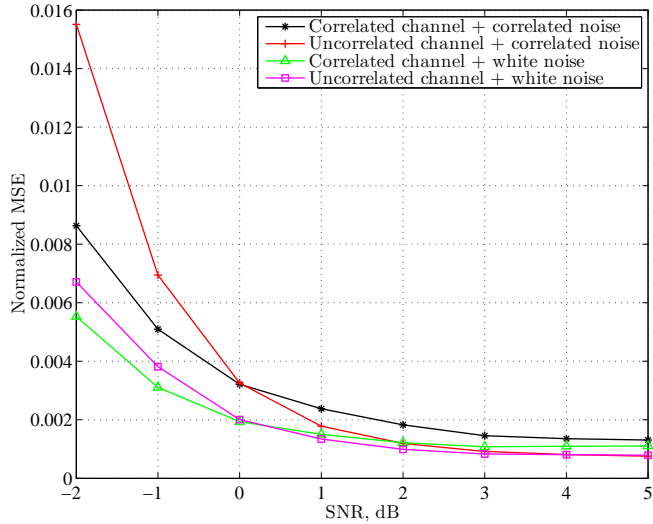


FIGURE 3.24: Normalized MSE versus SNR with and without knowledge of channel/noise correlation ($\beta = 1$, $SCN = 4$, $N = 100$)

Figure 3.25 shows the normalized MSE versus SNR for considered cases with the simulation parameters ($\beta = 1$, $SCN = 4$ and $N = 100$). In this simulation setting, we generate instances of \mathbf{Y} according to the considered case and we evaluate the MSE performance with (3.39) by considering the same case from the table. From the figure, it can be noted that the value of normalized MSE decreases with the increase in the SNR for all the cases. It can be noted that the SNR for all the cases can be reliably estimated with almost 0.1 % normalized MSE after 3 dB. Furthermore, SNR for both channel uncorrelated and correlated cases can be estimated with 0.2 % normalized MSE after SNR value of 0 dB at SCN value

FIGURE 3.25: Normalized MSE versus SNR for different cases ($\beta = 1$, SCN = 4, $N = 100$)

of 4. For the case of presence of both channel/noise correlation, SNR can be estimated with 0.9 % normalized MSE at -2 dB and with 0.5 % normalized MSE at -1 dB. Moreover, it can be noted that at lower SNR values, noise correlated case has higher normalized MSE than other cases and at higher values of SNR, noise correlated case provides better MSE performance than channel correlated case and both correlated case.

Discussion: In this work, SNR estimation problem in the presence of channel/noise correlation has been considered in the context of a CR. Theoretical expressions for a.e.p.d.f of the received signal's covariance matrix have been derived under the signal plus noise hypothesis for the four considered cases. Further, an eigenvalue-based SNR estimation technique has been proposed in order to estimate the PU SNR in the presence of channel and/or noise correlation. From the presented numerical results, it can be concluded that the PU SNR can be reliably estimated using the proposed technique when the CR sensing module is aware of the channel/noise correlation.

3.4 Performance Analysis

In this section, we analyze the performance of the conventional and hybrid approach considering an ED based detection and the power control method. This analysis can be easily for other detectors whose closed from expressions for the P_d and the P_f are deducible.

3.4.1 Conventional Approaches

The test statistic T_{ED} in (2.4) is related to the estimated SNR (γ_{est}) depicted in Figs. (3.5) and (3.6) as follows: $T_{ED} = \gamma_{\text{est}}\sigma_z^2$. From the central limit theorem, the decision statistics of energy detector for a large number of samples follows Gaussian distribution. In this context, the expressions for P_d and P_f can be written as

$$P_d(\lambda_{th}, \tau) = Q \left(\left(\frac{\lambda_{th}}{N_0} - \gamma_p - 1 \right) \sqrt{\frac{\tau f_s}{2\gamma + 1}} \right), \quad (3.40)$$

$$P_f(\lambda_{th}, \tau) = Q \left(\left(\frac{\lambda_{th}}{N_0} - 1 \right) \sqrt{\tau f_s} \right), \quad (3.41)$$

where τ denotes sensing time, f_s denotes the sampling frequency, λ_{th} denotes the sensing threshold of the ED technique, γ_p is the PU SNR measured at the secondary sensor, N_0 is the noise variance. Let

\bar{P}_d be the target P_d required by the detector. Combining (3.40) and (3.41), the expression for P_f in terms of \bar{P}_d can be expressed as:

$$P_f(\tau) = Q(\sqrt{2\gamma + 1}Q^{-1}(\bar{P}_d) + \sqrt{\tau f_s} \gamma) \quad (3.42)$$

The above analysis holds for a large number of samples. However, it is necessary to make a sensing decision within a very short time i.e., using a small number of samples in practical scenarios.

a. Periodic Sensing: Let C_1 and C_0 be the throughput of the secondary network in the presence and the absence of the PU respectively. Further, let γ_s and γ_p be the SNRs of the received power of the SU and the PU respectively and are defined as $\gamma_s = \frac{P_s}{N_0}$ and $\gamma_p = \frac{P_p}{N_0}$, where P_s is the received power of the SU and P_p is the interference power of the PU measured at the SR. Then C_0 and C_1 can be defined as

$$\begin{aligned} C_0 &= \log_2(1 + \gamma_s), \\ C_1 &= \log_2 \left(1 + \frac{\gamma_s}{1 + \gamma_p} \right). \end{aligned} \quad (3.43)$$

We define $P(H_0)$ as the probability of the PU being inactive, and $P(H_1)$ as the probability of the PU being active in such a way that $P(H_0) + P(H_1) = 1$. When there is perfect detection under the H_0 hypothesis, i.e., $P_f = 0$, then the throughput of the secondary link is given by $\frac{T-\tau}{T}C_0$. Since in practice, we do not have perfect detection and there always exists some probability of false alarm P_f , the probability of having perfect detection under the H_0 hypothesis is given by $(1 - P_f(\lambda_{th}, \tau))P(H_0)$ [107]. Similarly, in case of miss detection under the H_1 hypothesis, the throughput of the secondary link is given by $\frac{T-\tau}{T}C_1$ and the probability of having such a situation can be written as: $(1 - P_d(\lambda_{th}, \tau))P(H_1)$.

Taking the above definitions into account, the average throughput for the secondary network is given by

$$R(\lambda_{th}, \tau) = R_0(\lambda_{th}, \tau) + R_1(\lambda_{th}, \tau), \quad (3.44)$$

where the values of $R_0(\lambda_{th}, \tau)$ and $R_1(\lambda_{th}, \tau)$ can be calculated using the following expressions

$$\begin{aligned} R_0(\lambda_{th}, \tau) &= \frac{T - \tau}{T} (1 - P_f(\lambda_{th}, \tau)) P(H_0) C_0, \\ R_1(\lambda_{th}, \tau) &= \frac{T - \tau}{T} (1 - P_d(\lambda_{th}, \tau)) P(H_1) C_1. \end{aligned} \quad (3.45)$$

b. Simultaneous Sensing/Transmission In this scenario, the sensing duration is T instead of τ in the periodic SS approach as described in the previous subsection. For a target \bar{P}_d , the P_f expression in (6.6) for the ED technique can be written as

$$P_f(T) = Q \left(\sqrt{(2\gamma_p + 1)} Q^{-1}(\bar{P}_d) + \sqrt{T f_s} \gamma_p \right). \quad (3.46)$$

Therefore, the total throughput of the simultaneous sensing and transmission approach can be written as [338]

$$R(\lambda_{th}, T) = R_0(\lambda_{th}, T) + R_1(\lambda_{th}, T), \quad (3.47)$$

where the values of $R_0(\lambda_{th}, T)$ and $R_1(\lambda_{th}, T)$ can be calculated using the following expressions

$$\begin{aligned} R_0(\lambda_{th}, T) &= (1 - P_f(\lambda_{th}, T)) P(H_0) C_0, \\ R_1(\lambda_{th}, T) &= (1 - P_d(\lambda_{th}, T)) P(H_1) C_1. \end{aligned} \quad (3.48)$$

3.4.2 Hybrid Approach

In this approach, SU transmission strategy is based not only on the sensing decision but also on the power control-based underlay mechanism. For the power control purpose, the sensing unit provides information about the estimated SNR to the power control block if the H_1 hypothesis is decided as noted in Figs. 3.5 and 3.6. We describe the considered power control mechanism in detail in Section 3.4.2.1. In this section, we derive expressions for the total achievable throughput for the considered scenario considering both periodic and simultaneous sensing/Tx approaches.

Let λ_{th} be the sensing threshold, and P_{est} be the estimated power i.e., $P_{est} = \gamma_{est}\sigma_z^2$, which can be obtained based on suitable power spectrum or SNR estimation techniques [25, 53, 65, 168, 342]. We assume that the SUs have the knowledge of the interference threshold of the PUs, which can be known based on the technical standards and regulations. We employ the following transmission strategy for secondary transmission. Under the H_0 hypothesis,

- if the hypothesis is satisfied i.e., $P_{est} < \lambda_{th}$, the SUs transmit with a full power level, let us denote by P_{full} .
- if the hypothesis is not satisfied i.e., $P_{est} > \lambda_{th}$, the SUs transmit with a reduced power level, let us denote by P_{red} , which is calculated based on the power control mechanism described later in Section 3.4.2.1. In this case, even if the PU is inactive, the SU assumes the active state of the PU and transmits with P_{red} .

Similarly, under the H_1 hypothesis,

- if the hypothesis is satisfied i.e., $P_{est} > \lambda_{th}$, the SUs transmit with the reduced power level P_{red} .
- if the hypothesis is not satisfied i.e., $P_{est} < \lambda_{th}$, the SUs transmit with the full power level P_{full} . In this case, even if the PU is active, the SU assumes the inactive state of the PU and transmits with P_{full} , hence causing interference to the PU. This interference is usually handled by regulations and standard as described later in Section 3.4.2.1.

Based on the above proposed hybrid strategy, we derive the total achievable throughput based on the widely used Shannon formula. Let's introduce a new rate for the secondary link, which arises due to the partial access of the PU spectrum by the SU using the reduced power level. We denote the rate of the secondary link under the reduced power level as C_2 and define as

$$C_2 = \log_2 \left(1 + \frac{\gamma_{sr}}{1 + \gamma_p} \right), \quad (3.49)$$

where $\gamma_{sr} = \frac{P_{red}}{N_0}$. It should be noted that in (3.49), we assume perfect estimation of interference at the CR receiver and in the presence of interference and channel uncertainties, the performance outage constraints should be taken into consideration. In this case, our results provide upper bound on the achievable throughput. Subsequently, the total throughput for periodic sensing case can be calculated as

$$R(\lambda_{th}, \tau) = R_0(\lambda_{th}, \tau) + R_1(\lambda_{th}, \tau) + R_2(\lambda_{th}, \tau), \quad (3.50)$$

where the values of $R_0(\lambda_{th}, \tau)$, $R_1(\lambda_{th}, \tau)$ and $R_2(\lambda_{th}, \tau)$ can be calculated using the following expressions

$$\begin{aligned} R_0(\lambda_{th}, \tau) &= \frac{T - \tau}{T} (1 - P_f(\lambda_{th}, \tau)) P(H_0) C_0, \\ R_1(\lambda_{th}, \tau) &= \frac{T - \tau}{T} (1 - P_d(\lambda_{th}, \tau)) P(H_1) C_1, \\ R_2(\lambda_{th}, \tau) &= \frac{T - \tau}{T} P_d(\lambda_{th}, \tau) P(H_1) C_2 + \frac{T - \tau}{T} P_f(\lambda_{th}, \tau) P(H_0) C_2. \end{aligned} \quad (3.51)$$

It should be noted that authors in [107] and [338] have not considered the case of R_2 in their analysis. Similarly, the achievable throughput for the simultaneous sensing/Tx case can be calculated using the following expression

$$R(\lambda_{th}, T) = R_0(\lambda_{th}, T) + R_1(\lambda_{th}, T) + R_2(\lambda_{th}, T), \quad (3.52)$$

where the values of $R_0(\lambda_{th}, T)$, $R_1(\lambda_{th}, T)$, and $R_2(\lambda_{th}, T)$ can be calculated as

$$\begin{aligned} R_0(\lambda_{th}, T) &= (1 - P_f(\lambda_{th}, T))P(H_0)C_0, \\ R_1(\lambda_{th}, T) &= (1 - P_d(\lambda_{th}, T))P(H_1)C_1, \\ R_2(\lambda_{th}, T) &= P_d(\lambda_{th}, T)P(H_1)C_2 + P_f(\lambda_{th}, T)P(H_0)C_2. \end{aligned} \quad (3.53)$$

It should be noted from (3.51) and (3.53) that the achievable throughput for the simultaneous sensing/Tx case is higher than the achievable throughput for the periodic sensing case, which is illustrated with the help of numerical results in Section 3.4.3.

3.4.2.1 Power Control

The aggregate secondary interference towards the PR should be below the tolerable interference threshold of the PR in order to provide sufficient primary protection. Let us denote the tolerable interference threshold of the PR by I_T . Under the proposed framework, the ST may interfere with the PR in the following two cases

1. Transmission under the H_1 hypothesis with probability $P(H_1)(1 - P_d)$ as in [338].
2. Transmission under the H_1 hypothesis with probability $P(H_1)P_d$ under the proposed hybrid framework.

More specifically, for a target \bar{P}_d , there exist the following constraints for restricting interference towards the PU.

$$P(H_1)(1 - \bar{P}_d)\alpha P_{\text{red}} \leq I_T, \quad (3.54)$$

$$P(H_1)\alpha \bar{P}_d P_{\text{red}} \leq I_T, \quad (3.55)$$

where α denotes the path loss between ST and the PR. If we look carefully at the first constraint, when a SU misses the detection of the PU, it assumes the H_0 state and transmits with full power instead of implementing any power control. This constraint is usually handled by the regulations and standards by defining the desired P_d for the secondary system in order to coexist with a particular primary system so that the primary system is able to tolerate the outage for the duration of the miss detection. For example, IEEE 802.22 Wireless Regional Area Network (WRAN) defines the desired P_d as 0.9 for detecting the primary signals of -20 dB [357]. Therefore, we focus on the second constraint in our power control mechanism as follows

$$P_{\text{red}} \leq \frac{I_T}{\alpha P(H_1)\bar{P}_d}. \quad (3.56)$$

The path loss α between ST and the PR can be estimated with the help of the estimated PU SNR and the Effective Isotropic Radiated Power (EIRP) of the primary system. The received PU SNR can be obtained by using suitable power spectrum or SNR estimation algorithms. Further, the EIRP for the primary system can be obtained based on the power class of the primary terminals, which is known based on the specifications of wireless standards such as LTE, GSM/GPRS, EDGE etc. For this purpose, we assume that the power class of the primary terminals is known to the CR. As an example, denoting EIRP for the PT by EIRP_p , the path loss between the ST and the PR can be calculated using

the Friis transmission formula as

$$\alpha(\text{dB}) = \text{EIRP}_p(\text{dBW}) + G_r(\text{dB}) - P_{\text{est}}(\text{dBW}), \quad (3.57)$$

where G_r is the gain of the CR receive antenna. Subsequently, based on this path loss or attenuation and the interference threshold of the PU receiver, the ST adapts its transmit power based on (3.56).

It should be noted that the CR estimates the received PU power, which is transmitted from the PT and hence the path loss using (3.57) denotes the path loss between the CR receiver and the PT. However, in practice, we need to protect the PRs from harmful interference caused by the ST.

If there exist multiple PUs in the system, we need to consider the worst case i.e., minimum path loss α in order to calculate the transmit power based on (3.56). For a number of PUs under a given power class, if the PU with the minimum path loss i.e., strongest estimated power is protected, all other PUs under that class can be protected at the same time. The problem with the above worst case approach is that it may not be possible to estimate the received SNR of all the PUs. In this context, another solution to address the problem of multiple PUs protection can be the design of a power control algorithm based on the aggregate received power instead of the highest received power. This solution is simpler to implement than the previous solution since it is easier to estimate the total primary received power instead of estimating individual PU's received power separately in order to find the worst case scenario.

3.4.2.2 Throughput Maximization

In this section, we formulate an optimization problem for the throughput maximization of the proposed hybrid approach. In this formulation, we are interested in finding out the optimum sensing time and the controlled power for the underlay transmission in order to maximize the total throughput of the proposed hybrid technique subject to the following constraints: (i) P_d is greater than or equal to the target P_d , and (ii) total interference caused to the primary receiver is less than the interference threshold of the primary receiver. This formulation for the periodic SS-based approach can be written in the following form

$$\begin{aligned} \max_{\tau, P_{\text{red}}} R(\tau) &= R_0(\lambda_{th}, \tau) + R_1(\lambda_{th}, \tau) + R_2(\lambda_{th}, \tau), \\ &\text{subject to } P_d(\lambda_{th}, \tau) \geq \bar{P}_d, \\ &P(H_1)P_dP_{\text{red}}\alpha \leq I_T, \end{aligned} \quad (3.58)$$

where the values of $R_0(\lambda_{th}, \tau)$, $R_1(\lambda_{th}, \tau)$ and $R_2(\lambda_{th}, \tau)$ are given by (3.51). In (3.51), it can be noted that the value of $R_0(\lambda_{th}, \tau)$ is comparatively higher than the value of $R_1(\lambda_{th}, \tau)$. Furthermore, the first term is dominant over the second term in the expression of $R_2(\lambda_{th}, \tau)$. This is due to the requirement of the higher value of P_d and lower value of probability of false alarm in practical scenarios. Applying the above conditions and using (3.51) and (6.6), the optimization problem in (3.58) can be written as

$$\begin{aligned} \max_{\tau, P_{\text{red}}} R(\tau) &= \left(1 - \frac{\tau}{T}\right) \left(C_0 P(H_0) \left(1 - Q\left(\sqrt{2\gamma + 1} Q^{-1}(P_d(\lambda_{th}, \tau)) + \sqrt{\tau f_s \gamma}\right)\right) + P_d(\lambda_{th}, \tau) P_{\text{red}} P(H_1) C_2\right) \\ &\text{subject to } P_d(\lambda_{th}, \tau) \geq \bar{P}_d \\ &P(H_1)P_d(\lambda_{th}, \tau)P_{\text{red}}\alpha \leq I_T, \end{aligned} \quad (3.59)$$

where \bar{P}_d is the target P_d . In practice, this is defined by ensuring that the primary users are sufficiently protected. In the above optimization problem, for a fixed value of τ , the value of $R(\tau)$ becomes maximum when the equality constraint holds for the second constraint i.e., $P(H_1)P_d(\lambda_{th}, \tau)P_{\text{red}}\alpha = I_T$. This comes from the fact that as the value of I_T increases i.e., interference tolerance of the primary receiver increases, the cognitive transmitter can transmit with higher power while guaranteeing the sufficient PU protection. If we substitute the value of $P_{\text{red}} = \frac{I_T}{P(H_1)P_d(\lambda_{th}, \tau)\alpha}$ in the objective function

of (3.59), the third term becomes a constant term i.e., $\frac{C_2 I_T}{\alpha}$. Then the optimization problem (3.59) becomes equivalent to the following problem

$$\max_{\tau} \bar{R}(\tau) = \left(1 - \frac{\tau}{T}\right) \left(C_0 P(H_0) \left(1 - Q\left(\sqrt{2\gamma + 1} Q^{-1}(P_d(\lambda_{th}, \tau)) + \sqrt{\tau f_s} \gamma\right)\right) \right) \\ \text{subject to } P_d(\lambda_{th}, \tau) \geq \bar{P}_d. \quad (3.60)$$

It can be noted that the optimum sensing time for the optimization problem (3.59) is same as the optimum sensing time provided by the solution of problem (3.60). Furthermore, the maximum throughput for the hybrid approach is equal to the maximum throughput given by (3.60) plus some constant term i.e., $\frac{C_2 I_T}{\alpha}$. This has been further validated by numerical results in Section 3.4.3.

The optimization problem (3.60) has been discussed in [107] and it has been proved that the maximum secondary throughput is achieved when the equality constraint i.e., $P_d(\lambda_{th}, \tau) = \bar{P}_d$ is satisfied. For the sake of completeness, we briefly illustrate the reason behind this solution below. Let us choose a decision threshold λ_{th} such that $P_d(\lambda_{th}, \tau) = \bar{P}_d$ and another decision threshold λ_1 in such a way that $P_d(\lambda_1, \tau) > \bar{P}_d$. In this context, the relation between the corresponding false alarm probabilities is $P_f(\lambda_1, \tau) > P_f(\lambda_{th}, \tau)$. If we apply these conditions in the objective function of the optimization problem (3.60) and use (3.51), we get $R(\lambda_1, \tau) < R(\lambda_{th}, \tau)$.

As stated before, we are further interested in finding the optimal sensing time and the optimal controlled power for the considered hybrid approach. In order to derive the optimum controlled power, we proceed as follows. For a given target \bar{P}_d , let I_T be the interference threshold in such a way that $P(H_1)\bar{P}_d P_{\text{red}}\alpha = I_T$ and let $I_{T1} < I_T$ be another interference threshold with $P_{\text{red}1}$ being the corresponding controlled power. Since $I_{T1} < I_T$, it's obvious that $P_{\text{red}1} < P_{\text{red}}$. Then from (3.49), the value of C_2 corresponding to P_{red} becomes higher than the value of C_2 with $P_{\text{red}1}$. If we substitute these values of C_2 in the objective function of (3.59), the value of $R(\lambda_{th}, \tau)$ becomes higher for the case of P_{red} . Therefore, the optimum value of the controlled power is given by $P_{\text{red}} = \frac{I_T}{P(H_1)\bar{P}_d\alpha}$.

Another problem is to obtain optimal sensing time for the considered optimization problem. Authors in [107] have proved that there indeed exists an optimum sensing time for maximizing the secondary throughput with respect to the constraint $P_d(\lambda_{th}, \tau) \geq \bar{P}_d$. Here, we use similar methodology in order to prove the existence of the optimal sensing time for the proposed hybrid approach. Differentiating the objective function of (3.59) with respect to τ , we get

$$R'(\tau) = C_0 P(H_0) \left(\frac{\gamma \sqrt{f_s} (1 - \frac{\tau}{T})}{2\sqrt{2\pi\tau}} \exp\left(-\frac{(\sqrt{2\gamma + 1} Q^{-1}(\bar{P}_d) + \sqrt{\tau f_s} \gamma)^2}{2}\right) \right. \\ \left. - \frac{1}{T} + \frac{1}{T} Q(\sqrt{2\gamma + 1} Q^{-1}(\bar{P}_d) + \sqrt{\tau f_s} \gamma) \right) - \frac{1}{T} \bar{P}_d P_{\text{red}} P(H_1) C_2. \quad (3.61)$$

Subsequently, the limiting values of $R'(\tau)$ can be written as

$$\lim_{\tau \rightarrow T} R'(\tau) < C_0 P(H_0) \left(-\frac{1}{T} + \frac{1}{T} Q(\sqrt{2\gamma + 1} Q^{-1}(\bar{P}_d) + \sqrt{\tau f_s} \gamma) \right) - \frac{1}{T} \bar{P}_d P_{\text{red}} P(H_1) C_2 < 0. \quad (3.62)$$

$$\lim_{\tau \rightarrow 0} R'(\tau) = +\infty. \quad (3.63)$$

From (3.62) and (3.63), it can be noted that there exists an optimum sensing time within the interval $(0, T)$ which maximizes $R(\tau)$ for the proposed periodic SS-based hybrid approach as observed in the periodic SS only approach. In this context, in [107], it has been shown that the value of $P_f(\tau)$ is decreasing and convex for the range of τ in which $P_f(\tau) \leq 0.5$ and $R\tau$ is concave within this range which justifies the uniqueness of the maximum point of $R\tau$ within the interval $(0, T)$. The similar analysis applies in the considered wideband context as well.

3.4.3 Numerical Results

In this section, we evaluate the performance of the proposed hybrid approach with the help of numerical results. We use achievable secondary throughput as a performance metric and present the variation of this metric with respect to sensing time, PU interference threshold, received PU SNR and the target P_d . We consider the carrier bandwidth and sampling frequency to be 6 MHz. Let us consider $P(H_1) = 0.2$ and the target detection probability be 0.9 as in [107]. In practice, the value of \bar{P}_d should be close to but less than 1, especially in the low SNR region. As an example, the IEEE 802.22 cognitive WRAN standard requires the receiver sensitivity of -20 dB for sensing Digital Television (DTV) signals with 90 % P_d [357]. Furthermore, we consider received secondary SNR as $\text{SNR}_s = 20$ dB and we evaluate the throughput performance in low primary SNR region. Let us consider the frame duration to be $T = 100$ ms. In the presented simulation results, we consider a fixed channel attenuation of 10 dB for the channel between a SU and the PR as in [338]. For simulating this scenario, we consider a single radio channel of 6 MHz bandwidth. Table I provides references to the throughput expressions used for evaluating performance of different cases in the narrowband scenario. Figure 3.26 presents throughput versus sensing time for different approaches with parameters ($I_T = -130$ dBW, $\bar{P}_d = 0.9$, $T = 100$ ms, $\text{SNR}_p = -15$ dB, $\text{SNR}_s = 20$ dB). In this figure, we have provided the theoretical and simulated results. During simulation, the decision threshold was calculated to achieve a target P_d of 0.9 considering 15000 Monte Carlo realizations and this decision threshold was used for calculating the value of P_f for a certain sensing time. From the figure, it can be noted that there exists a tradeoff between throughput and sensing time for the periodic sensing approach as noted in [107]. It can be depicted that for both conventional and the proposed hybrid approaches, the optimum sensing time is 2.5 ms and the proposed hybrid approach with periodic sensing achieves higher throughput in comparison to the conventional periodic sensing approach for all the considered values of the sensing duration. For example, at the sensing time of 2.5 ms, the proposed hybrid approach with periodic sensing achieves 5.6 bits/s/Hz throughput, whereas the conventional periodic sensing approach achieves only about 5.3 bits/s/Hz i.e., 0.3 bits/s/Hz increased throughput, which is a considerable gain. Moreover, while considering the simultaneous sensing/Tx case, the proposed hybrid approach achieves 5.76 bits/s/Hz throughput whereas the conventional approach achieves 5.45 bits/s/Hz throughput. Therefore, it can be concluded that the proposed hybrid approach performs better than conventional approaches for both periodic sensing and simultaneous sensing/Tx cases.

TABLE 3.2: Throughput Calculation for Various Cases in the narrowband scenario

Case	Reference
Conventional Approach with Periodic Sensing	Eqn. (3.44)
Conventional Approach with Simultaneous Sensing/Tx	Eqn. (3.47)
Proposed Hybrid Approach with Periodic Sensing	Eqn. (3.50)
Proposed Hybrid Approach with Simultaneous Sensing/Tx	Eqn. (3.52)

Figure 3.28 presents the secondary achievable throughput versus PU interference threshold with parameters ($I_T = -130$ dBW, $\bar{P}_d = 0.9$, $T = 100$ ms $\text{SNR}_p = -15$ dB, $\text{SNR}_s = 20$ dB). From the figure, it can be noted that the achievable throughput with the proposed hybrid approach in both the cases (periodic sensing and simultaneous sensing/Tx) is higher than that of the conventional approach. It can be depicted that while increasing the interference threshold, the secondary throughput increases for both the proposed hybrid approaches. It means that if the PU can tolerate more interference from the secondary system, secondary transmit power can be increased by guaranteeing the sufficient PU protection, hence resulting in the increased secondary throughput. Since conventional approaches do not consider achievable throughput from the underlay approach, no variation is observed on the secondary throughput with respect to the PU interference threshold.

Figure 3.29 depicts the secondary throughput versus target P_d (\bar{P}_d) for all the considered approaches with ($I_T = -130$ dBW, $T = 100$ ms, $\text{SNR}_p = -24$ dB, $\text{SNR}_s = 20$ dB). From the figure, it can be noted that the throughput decreases with an increasing value of \bar{P}_d for the considered value of SNR. During

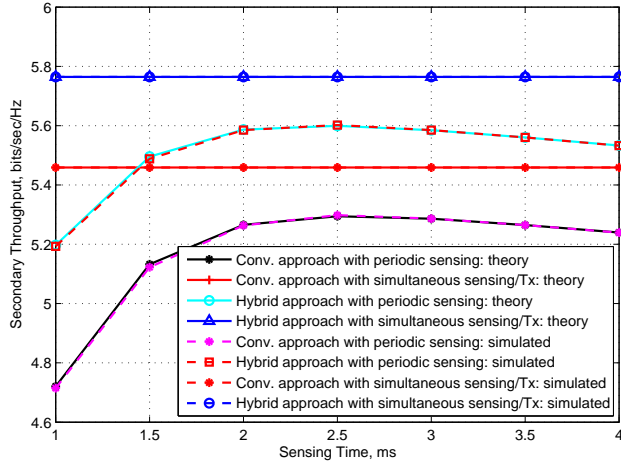


FIGURE 3.26: Secondary throughput versus sensing time ($I_T = -130$ dBW, $\bar{P}_d = 0.9$, $T = 100$ ms, $\text{SNR}_p = -15$ dB, $\text{SNR}_s = 20$ dB)

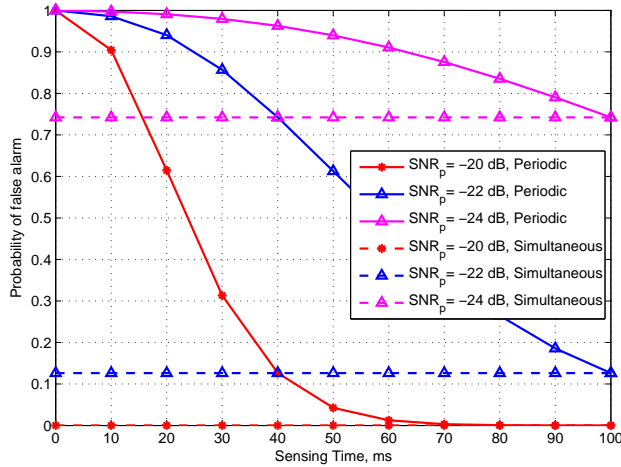


FIGURE 3.27: Probability of false alarm versus sensing time ($\bar{P}_d = 0.99$, $T = 100$ ms, $\text{SNR}_s = 20$ dB, $I_T = -130$ dBW)

simulation, it has been noted that the rate of throughput decrease with respect to \bar{P}_d increases as the received PU SNR decreases. Figure 3.30 shows secondary achievable throughput versus PU SNR for all the considered approaches with parameters ($I_T = -130$ dBW, $T = 100$ ms, $\text{SNR}_s = 20$ dB, $\tau = 2.5$ ms). From the figure, it can be noted that the secondary throughput increases with the increase in the received PU SNR for both the conventional and proposed hybrid approaches with the periodic sensing whereas for both the conventional and the proposed hybrid approaches with simultaneous sensing/Tx, the secondary throughput remains constant after some value of the received PU SNR. Furthermore, from the simulation results, it can be noted that as the value of the received PU SNR increases, the performance gap between periodic sensing and simultaneous sensing/Tx decreases. Therefore, it can be concluded that at higher SNR regime, the periodic sensing scheme is advantageous from practical perspectives due to its lower complexity in comparison to the simultaneous sensing/Tx scheme.

3. Discussion: A hybrid cognitive transceiver, which can overcome the drawbacks of SS only and underlay only approaches, has been studied. In this approach, the SU first estimates the PU SNR and then makes the sensing decision based on the estimated SNR. Subsequently, under the H_0 hypothesis, the SU transmits with the full power and under the signal plus noise hypothesis, the SU transmits with the controlled power which is calculated based on the estimated PU SNR and the interference constraint of the PU. The performance of this approach has been evaluated in terms of the achievable throughput considering the periodic sensing and simultaneous sensing/transmission schemes in narrowband and wideband scenarios. From the numerical results, it has been noted that the hybrid

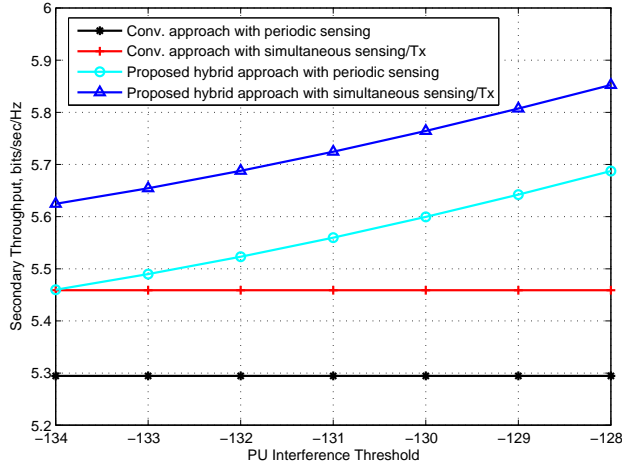


FIGURE 3.28: Secondary throughput versus PU interference threshold for different approaches ($\bar{P}_d = 0.9$, $T = 100$ ms, $\text{SNR}_p = -15$ dB, $\text{SNR}_s = 20$ dB, $\tau = 2.5$ ms)

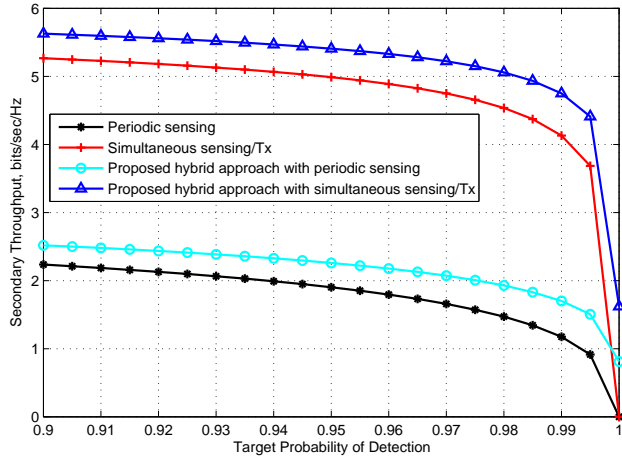


FIGURE 3.29: Secondary throughput versus target P_d for different approaches ($I_T = -130$ dBW, $T = 100$ ms, $\text{SNR}_p = -24$ dB, $\text{SNR}_s = 20$ dB, $\tau = 2.5$ ms)

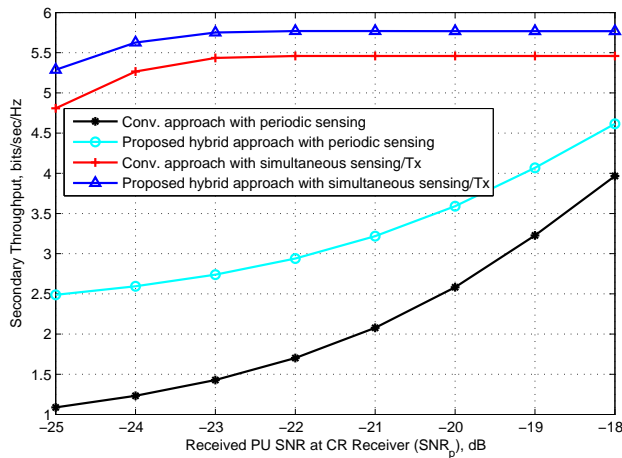


FIGURE 3.30: Secondary throughput versus PU SNR for different approaches ($\bar{P}_d = 0.9$, $I_T = -130$ dBW, $T = 100$ ms, $\text{SNR}_s = 20$ dB, $\tau = 2.5$ ms)

approach for the periodic sensing case operates under a sensing-throughput tradeoff as it happens in the conventional periodic sensing approach. Further, it can be concluded that the hybrid scheme achieves significantly higher throughput than the conventional SS approaches.

3.5 Chapter Conclusion

With regard to the SS in general settings, the performance of eigenvalue-based SS techniques has been studied in the presence of noise/channel correlation in Section 3.2. It has been noted that noise correlation degrades the sensing performance while the channel correlation enhances the performance of the SCN-based SS techniques. Further, new sensing thresholds for the SCN and ME based techniques have been proposed and it has been shown that the proposed thresholds can achieve better sensing performance in the correlated noise scenarios. Using recent RMT results on the distribution of the ME for a class of sample covariance matrices, an expression for the sensing threshold has been derived in terms of the P_f and system parameters. From the simulation results, it has been noted that the P_f for the considered correlated case increases with the increase in the correlation level and the proposed threshold compensates for this deviation. Further, the performance of an fractional sampling-based SS has been studied and it has been noted that SS efficiency increases with the fractional sampling rate up to a certain limit and beyond this limit, the performance advantage is not obvious. It can be concluded that there exists an optimal operating point for the fractional sampling rate in order to enhance the sensing efficiency of a single node sensor.

Furthermore, in Section 3.3, an SNR estimation problem has been studied for a CR in the presence of channel and/or noise correlation considering a multidimensional framework. The considered multi-dimensional framework is applicable for the following scenarios: (i) single node-based sensing (single antenna) with the oversampling operation, (ii) single node-based sensing for a CR node equipped with multiple antennas, and (ii) cooperative sensing scenario with each node equipped with single/multiple antenna. With the help of the RMT tool, analytical expressions for Stieltjes transforms of the received signal's covariance matrix (which are subsequently used for evaluating the a.e.p.d.f.) have been derived under the signal plus noise hypothesis for the following four considered cases: (i) uncorrelated channel and white noise, (ii) uncorrelated channel and correlated noise, (iii) correlated channel and white noise, and (iv) correlated channel and correlated noise. The validity of the derived expressions have been verified with the help of numerical simulations. Based on the these expressions, an eigenvalue-based SNR estimation technique has been proposed in order to estimate the PU SNR in the aforementioned scenarios. From the presented numerical results, it can be concluded that the PU SNR can be reliably estimated using the proposed technique when the CR sensing module is aware of the channel/noise correlation. Further, the performance of the proposed technique has been evaluated in the case of imperfect correlation model and it has been noted that the PU SNR can be estimated with 2.5 % normalized MSE up to the SNR value of 0 dB while considering 10 % imperfect correlation knowledge. Moreover, it can be noted that this performance degradation increases for lower SNR values and decreases for higher SNR values following performance of the perfect correlation knowledge case beyond the SNR value of 3 dB. In addition, while comparing the effects of channel and noise correlation on the estimation performance, it has been noted that the effect of channel correlation dominates at higher SNR values while the effect of noise correlation dominates at low SNR values.

Moreover, in Section 3.4, the performance of a hybrid transceiver, which can overcome the drawbacks of SS only and underlay only approaches, has been studied considering periodic SS and simultaneous SS/Tx approaches. The performance of the half duplex and full duplex transceivers have been evaluated in terms of the sensing-throughput tradeoff in narrowband and wideband contexts. It has been noted that the hybrid approach for the periodic sensing case operates under a sensing-throughput tradeoff as it happens in the conventional periodic sensing approach. Furthermore, it can be concluded that the hybrid scheme achieves significantly higher throughput than the conventional SS approaches. From the theoretical and simulation results, it has been noted that the hybrid approach provides about 0.3

bits/s/Hz gain in the throughput in comparison to the conventional periodic sensing approach. Further, it has been depicted that the secondary throughput increases with the PU interference threshold for both the considered periodic sensing and simultaneous SS/Tx hybrid approaches. In addition, the secondary throughput decreases with the target detection probability and increases with the received PU SNR for both conventional and hybrid schemes. While comparing the performances of the periodic SS and simultaneous SS/Tx with respect to the received PU SNR, it has been observed that the performance gap between these schemes decreases at the higher SNR regime and hence the periodic sensing seems to be advantageous from practical perspectives due to its lower implementation complexity.

Chapter 4

Wideband Cognitive Transceiver Design

Spectrum sensing and SNR estimation approaches proposed in Chapter 3 are based on the assumption of narrowband channels. However, in practice, the CR may need to explore spectral opportunities over a wideband of spectrum in order to enhance the utilization of the available spectrum. In this context, this chapter focuses on challenges for designing a wideband cognitive transceiver and provides our contributions on compressive sparsity order estimation and SNR estimation. More specifically, this chapter studies the compressive sparsity order estimation and SNR estimation problems using the CS approach. The contributions included in this chapter have been published in [78–80].

4.1 Introduction

Existing SS techniques mostly focus on the detection of narrowband signals considering a single radio channel [11, 18]. However, in practical scenarios, the CRs need to detect and acquire information about a wide spectrum band in order to utilize the spectrum efficiently. Further, CRs do not have prior knowledge about the PU’s signal and channels. In this aspect, investigating wideband blind spectrum awareness techniques is an important and relevant research challenge. In the following subsections, we present the main challenges in implementing a wideband CR transceiver and highlight the main contributions of our work.

4.1.1 Wideband Cognitive Radio Challenges

One of the key challenges of SS for a CR is the detection of weak signals hidden in thermal noise with a very small probability of miss detection. An SS technique requires the radio to receive a wideband signal through an RF front-end, sample it by a high speed ADC, and subsequently perform measurements for the detection of the PU signals. Some of the physical layer challenges unique to the CR system identified in [27, 28] are summarized below. The main challenges for realizing wideband sensing schemes in a CR are: (i) achieving sufficient RF sensitivity for wideband signals, and (ii) accurately detecting dissimilar, frequency band-dependent PU signals at varying received power levels. After acquiring information about the PU vacant band, a CR should be able to adapt to the best modulation scheme that can provide the best spectrum utilization and the capacity while guaranteeing sufficient protection of the PRs. Additionally, the CR transmission scheme should be flexible in order to assign any available band to any SU, and should be scalable with the number of the SUs and operating spectrum bands. This flexible wideband CR transmission can be realized with the help of digital domain waveform synthesis where a set of parameters specify transmission bands and power control in the ideal case.

In this context, the main challenge for a wideband CR transceiver is to generate a signal that can adaptively change the occupied bandwidth without the need of external analog filters while providing sufficient protection to the active PUs. For this purpose, a wideband CR transceiver must have higher sensitivity and wideband frequency agility than the conventional radios. From the SS point of view, the main issues can be summarized as follows: (i) exploring low complexity wideband sensing solutions, (ii) acquisition of different PU signal types with varying power levels, and (iii) channel uncertainty between the CR and the PU. Similarly, from the transmission point of view, the main issues are: (i) wideband transmission, (ii) dynamic adaptation of frequency bands and powers, and (iii) interference avoidance to the PUs.

1. Wideband Signal Acquisition: As highlighted in Chapter 1, one of the main challenges in implementing a wideband CR is the design of an RF front-end [27, 28]. Further, the main limitation in an RF front-end's ability to detect the weak signal levels is its DR i.e., the requirement for number of bits in an ADC. For this purpose, a wideband CR transceiver requires a multi-GHz speed ADC, which together with high resolution (of 12 or more bits) might be infeasible with current technology [68, 69]. The wideband RF signal presented at the antenna of such a front-end may include signals from close and spatially separated transmitters, and from transmitters operating at varying power levels and channel bandwidths. One method of reducing the DR is by filtering the strong PU signal which is not of interest by using a notch filter. However, the strong PU signals may be located anywhere in the spectrum band and may need tunable filters, resulting in higher complexity [27]. Another solution could be to use a spatial filter using multiantenna processing techniques. In this case, the multiantenna processing should be applied before the Automatic Gain Control (AGC) circuits that would properly amplify the reduced DR signal for the best utilization of number of bits in the ADC.

For the implementation of wideband SS, a CR transceiver needs to have a wideband antenna, a wideband filter and a high speed ADC. The solutions of wideband antennas and wideband filters have been reported in the literature [358, 359], however, the development of ADC technology is relatively behind [68, 69]. The conventional wideband SS techniques based on the standard ADC could lead to unaffordable high sampling rate or implementation complexity. To address this issue, many researchers have considered CS technique for wideband SS assuming some sparsity basis. The important advantage of the CS approach for wideband signal acquisition is that it can increase the overall DR of the acquisition system [213]. In contrast to conventional Nyquist rate sampling systems, CS-based ADCs provide an important benefit in reducing the required sampling rate in order to represent the same spectrum. Further, fewer quantization operations are required in CS-based receivers due to the reduction in the number of acquired measurements, thus resulting in significant power savings [360].

2. Wideband Transmission: Orthogonal Frequency Division Multiplexing (OFDM) transmission scheme has been considered as one of the suitable physical layer candidates for CR systems [28] since it allows the easy generation of signal waveforms that can fit into discontinuous and nonuniform spectrum segments. Besides, an OFDM scheme has other advantages such as inherent multiple access mechanism, simplicity in channel equalization and the benefits of frequency diversity and coding. In this scheme, the assignment of non-zero data to Inverse FFT (IFFT) inputs corresponds to the free sub-carriers to be used by a particular SU while the assignment of zeros corresponds to channels occupied by the PUs or other SUs. Despite various advantages of the OFDM transmission, the conventional OFDM scheme may not be suitable solution due to the presence of relatively large side-lobes and such lobes may result in the signal power leakage among the bands of different users [361]. For CR applications, several spectrum shaping techniques such as introducing guard bands, windowing and power control per sub-carrier can be applied to improve this spectral leakage problem. To address the issue of large side-lobes in an OFDM scheme, current research is examining the application of Filter Bank Multicarrier (FBMC) technique [361–363]. Although there exist several studies on filter bank based multicarrier systems in the literature [364], its potential merits over OFDM and possible implementation challenges in practical channels and impairment conditions require further investigation.

4.1.2 Motivation and Contributions

The focus of the present work is on signal acquisition over a wideband and the aspects of wideband transmission are not further addressed in this work. Towards reducing the acquisition cost at the CR node, CS can be considered a prominent solution [70, 71]. According to CS theory, certain signals can be recovered from far fewer samples or measurements than those required by conventional methods [72, 365]. Most of the CS literature has focused on improving the speed and accuracy of recovering the original sparse signal from compressive measurements [366–368]. In the context of CR networks, CS techniques are suitable for acquiring the spectrum usage information in a wide spectrum band as in many cases the spectrum occupancy is sparse in the frequency and time domains [1].

The wideband signal detection using CS can be carried in the following two ways: (i) reconstructing the original sparse signal spectrum from compressed samples using CS recovery algorithms and taking decision based on the reconstructed signal spectrum, and (ii) signal detection directly from the compressive measurements. Examples for the first approach include [73, 369] where, first, an estimate of the original sparse signal spectrum is made and then the decision about the free bands is taken based on the reconstructed signal spectrum. However, the reconstruction process in a CS-based CR requires significant computational complexity [74] and from the SS point of view, it is not necessary to reconstruct the entire sparse signal. In this context, recently, the later approach has received important attention [76, 370] where CS has been applied for signal detection purpose using compressed measurements rather than reconstructing the original sparse signal. In contrast to the signal detection problem considered in [76, 370], we are interested in estimating the sparsity order of the wideband spectrum which can be subsequently used for implementing adaptive CS-based CR receivers.

Further, in most of the CS-related contributions, it is assumed that the wideband signal is sparse in some domain and the number of measurements is kept fixed based on the assumed sparsity order. However, in compressive wideband systems, the required number of measurements to achieve a successful recovery rate proportionally varies with the sparsity order of wideband signals [29, 77]. In this context, Sparsity Order Estimation (SOE) is crucial in order to choose the appropriate number of measurements. In addition, in most of the contributions, it is assumed that the sparsity order of the signal is known beforehand. However, in the context of CR networks, this prior information is not available at the CR sensor and has to be estimated. In the above context, a two-step CS algorithm has been proposed recently in [77], in which the sparsity order is estimated in the first step and the total number of collected samples is adjusted in the second step based on the estimated sparsity order. However, the considered estimation approach is based on Monte Carlo simulations and no analytical method has been presented for estimating the sparsity order of the wideband signals. Further, the proposed experimental method for SOE in [77] requires the reconstruction of the original sparse signal.

To address the above issues, we provide the following contributions.

1. We propose a MMV model to study the SOE problem. To estimate the sparsity order, we consider an eigenvalue-based approach using the eigenvalues of the CS measurement vector since it requires no prior information about the PU signals neither the knowledge of channel nor the noise covariance [53]. Our theoretical analysis differs from [371] since our analysis is based on the MMV model instead of the SMV model considered in [371].
2. We derive theoretical expressions for a.e.p.d.f. of the measured signal's covariance matrix for three different scenarios using asymptotic RMT. In the first case, we consider a simple case of constant received power across all active carriers in the considered wideband spectrum. However, in practice, the transmitted power is different across multiple carriers due to spatial separation of PUs and frequency selective channels. To address this scenario, we also study the case where the received power levels across the carriers are different but follow a specific distribution. Further, the non-zero entries across the multiple measurement vectors may be correlated in practice due to channel correlation or imperfections in frequency selective filters present at the CR node. To

address this specific issue, we consider the correlated MMV scenario where the non-zero entries across multiple measurement vectors are correlated.

3. Based on the derived a.e.p.d.f. expressions, we propose a technique in order to estimate the sparsity order of the channel occupancy within the considered wideband spectrum. In this context, we consider multiple subbands within the considered wideband spectrum and represent each subband with a center carrier frequency.
4. We study a tradeoff between estimation performance (expressed in terms of SOE Error (SOEE)) and the hardware cost (number of measurements).

4.1.3 Related Work

1. *CS-based Signal Acquisition*: Various sub-Nyquist wideband sensing techniques have been proposed in the literature assuming sparse spectrum occupancy over a wideband spectrum [30, 31, 372, 373]. In [30], CS theory has been applied to the CRs for acquiring wideband signals using sub-Nyquist sampling rates considering the sparseness of the signal spectrum in open-access network. The contribution in [372] proposes several methods for low-rate sampling of continuous-time sparse signals in shift-invariant spaces. A multi-rate sub-Nyquist sampling system has been proposed in [31] to perform wideband SS considering several sub-Nyquist sampling branches in each sensing node. The authors in [373] study the blind sub-Nyquist sampling of multiband signals, whose unknown frequency support occupies only a small portion of a wide spectrum. In [374], a sequential CS approach has been proposed where observations are available in a sequence and can be stopped as soon as there is reasonable certainty of correct reconstruction.

2. *Signal Recovery Algorithms and Hardware Architectures*: The basic CS theory starts with the SMV problem and is extensively applied in magnetic resonance imaging, underwater acoustic channel estimation and DoA estimation [375, 376]. Several algorithms have been developed for solving the SMV problem including Orthogonal Matching Pursuit (OMP) [366] and its variants, sparse reconstruction by separable approximation (SpaRSA) algorithm [377], l_1 regularized least squares (l_1 -LS) [378], focal undetermined system solve (FOCUSS) class of algorithms [379], and least square absolute shrinkage and selection operator (LASSO) algorithm [380]. In comparison to the SMV case, the support recovery rate can be significantly enhanced using the MMV method [381]. Several MMV algorithms have been proposed in the literature including M-OMP [382], M-FOCUSS, l_1/l_2 minimization [381], and Multiple Sparse Bayesian Learning (M-SBL) [383]. Further, several hardware architectures have been proposed and implemented in the literature enabling the acquisition of compressive samples in practical settings [373, 384, 385].

3. *Support Recovery Techniques*: Several contributions focus on the support recovery problem instead of recovering the original sparse signal [371, 386–390]. The contributions [387] and [386] focus on necessary and sufficient conditions for exact recovery of the sparsity pattern. In [388], the support recovery problem is studied in the context of the MMV model and it is shown that the structure of the matrix formed by the nonzero entries has a significant role in the performance limits of the support recovery. The contribution in [389] investigates a tradeoff between sampling rate and the detection error focusing on the high-dimensional setting. In addition, [390] provides sufficient conditions for stable recovery assuming the prior knowledge of the partial support information. Moreover, the recent contribution in [371] studies a sparse support recovery problem using an asymptotic RMT approach.

4.2 Sparsity Order Estimation

4.2.1 System and Signal Model

Let us consider a total bandwidth of W Hz with N number of carriers each having W/N channel bandwidth. Since all the carriers may not be occupied all the time [1], we assume sparse channel occupancy in the considered wideband spectrum. We define sparsity order, let us denote by σ , as the ratio of the number of the occupied carriers to the total number of carriers over the considered wideband spectrum. Further, we define another parameter ρ as the compression ratio, which depends on the number of measurements as discussed later. The signal model used in this work has been inspired from the model used in [371] which focuses on the input-output mutual information and the support recovery rate in the asymptotic limit. For our analysis, we extend the SMV model of [371] into the MMV model as described below.

Let us consider the following complex valued observation model for the SMV problem as considered in [371]

$$\mathbf{y} = \mathbf{AUXb} + \mathbf{z}, \quad (4.1)$$

where \mathbf{A} is an $N \times N$ diagonal matrix with independent and identically distributed (i.i.d.) Bernoulli distributed elements i.e., $\mathcal{P}[\mathbf{A}_{i,i} = 1] = \rho = 1 - \mathcal{P}[\mathbf{A}_{i,i} = 0]$, where $\rho = \frac{1}{N}E_{\mathbf{A}}[M] = \frac{1}{N}\bar{M}$ denotes the average fraction of non-zero diagonal elements of \mathbf{A} to the total number of diagonal elements and is equivalent to the ratio of the dimensions of the measurement matrix considered in [74], \mathbf{U} is an $N \times N$ random matrix having i.i.d. elements with zero mean and variance $1/N$, and an $N \times N$ combined matrix \mathbf{AU} denotes the compressed sensing matrix. Further, $\mathbf{X} = \text{diag}(\mathbf{x})$, with \mathbf{x} being an $1 \times N$ complex Gaussian vector having i.i.d. elements with zero mean and variance $1/N$, \mathbf{b} is an $N \times 1$ vector with i.i.d. complex components b_i distributed with Bernoulli distribution i.e., $\mathcal{P}[b_i = 1] = \sigma = 1 - \mathcal{P}[b_i = 0]$ with its non-zero elements defining the support of Bernoulli-Gaussian vector \mathbf{Xb} , whose sparsity (average fraction of non-zero elements) is equal to $\sigma = \frac{1}{N}E_{\mathbf{b}}[M]$, and \mathbf{z} is an i.i.d. complex Gaussian $N \times 1$ vector with components $z_i \sim \mathcal{CN}(0, 1)$. It should be noted that \mathbf{Xb} denotes the sparse vector considered for the standard CS formulation in the literature [74]. In model (4.1), the non-zero diagonal elements of \mathbf{A} define the components of the product \mathbf{UXb} for which a noisy measurement is acquired and the parameter ρ indicates the sampling rate i.e., average fraction of the observed components. Further, as in [371], we consider the covariance $\mathbf{U}^\dagger \mathbf{A}^\dagger \mathbf{AU}$ to be free from any deterministic Hermitian matrix [43].

In contrast to the above SMV problem, we are interested in analyzing the MMV scenario, where the combination of concatenated multiple measurement vectors has been represented in the form of a matrix \mathbf{Y} . We consider $N \times N$ sensing matrix \mathbf{AU} consisting of $\bar{M} = \rho N$ number of non-zero rows. This is equivalent to the scenario with a CR node equipped with \bar{M} number of frequency selective filters considered in [32], where \bar{M} filters are used to measure \bar{M} different linear combinations of the received signals of all N carriers. In practice, the frequency selective surfaces can be used to realize frequency filtering by designing a planar periodic structure with a unit element size around half wavelength of the frequency of interest. Further, the bandwidth of a subband can be dealt by finding a suitable shape of the unit elements through the initial test procedure [32]. Let N also be the number of samples collected by a sensor during the measurement process and therefore each measurement vector of \mathbf{Y} contains N number of samples. We assume that the channel occupancy status remains unchanged during the period of measurement. In this context, we extend the SMV problem (4.1) into the following MMV model

$$\mathbf{Y} = \mathbf{AUP}^{1/2} \boldsymbol{\Theta}^{1/2} \mathbf{BX} + \mathbf{Z} = \mathbf{AUP}^{1/2} \boldsymbol{\Theta}^{1/2} \mathbf{S} + \mathbf{Z}, \quad (4.2)$$

where $\mathbf{B} = \text{diag}(\mathbf{b})$ is an $N \times N$ diagonal matrix with the diagonal having i.i.d. Bernoulli distributed elements i.e., $\mathcal{P}[\mathbf{B}_{i,i} = 1] = \sigma = 1 - \mathcal{P}[\mathbf{B}_{i,i} = 0]$, \mathbf{X} is an $N \times N$ random matrix having i.i.d. entries with zero mean and variance $1/N$. The definitions of matrices \mathbf{A} and \mathbf{U} are same as the ones defined earlier in the SMV model. Further, \mathbf{P} is an $N \times N$ diagonal matrix and its diagonal entries correspond to the varying power levels received across different carriers within the considered spectrum, and $\boldsymbol{\Theta}^{1/2}$ is the

square root of the correlation matrix Θ and its elements are drawn from an exponential correlation model given by (3.4). The $N \times N$ matrix $\mathbf{S} = \mathbf{B}\mathbf{X}$ is a sparse signal matrix with uniform sparsity (sparsity order σ) across all the columns. It can be noted that \mathbf{Y} contains $\bar{M} = \rho N$ number of non-zero rows and each non-zero row contains N number of samples. We assume that the matrices \mathbf{A} , \mathbf{U} , \mathbf{B} , \mathbf{X} and \mathbf{Z} are mutually independent. The sensing matrix \mathbf{AU} is assumed to be known by the receiver.

Assuming that the source signal is independent from the noise, the covariance matrix of the measured signal, denoted by \mathbf{R}_Y , can be calculated as

$$\mathbf{R}_Y = E[\mathbf{Y}\mathbf{Y}^\dagger] = E\left[(\mathbf{A}\mathbf{U}\mathbf{P}^{1/2}\Theta^{1/2}\mathbf{B}\mathbf{X})(\mathbf{A}\mathbf{U}\mathbf{P}^{1/2}\Theta^{1/2}\mathbf{B}\mathbf{X})^\dagger\right] + E[\mathbf{Z}\mathbf{Z}^\dagger]. \quad (4.3)$$

In this research work, we are interested in finding out the eigenvalue distribution $f(\lambda)$ of \mathbf{R}_Y . Since all the matrices \mathbf{A} , \mathbf{U} , \mathbf{B} , \mathbf{X} and \mathbf{Z} are square, $f_{\mathbf{R}_Y}(\lambda) = f_{\bar{\mathbf{R}}_Y}(\lambda)$, where $\bar{\mathbf{R}}_Y = \mathbf{P}\Theta E\left[\mathbf{U}^\dagger\mathbf{A}^\dagger\mathbf{A}\mathbf{U}\mathbf{B}\mathbf{X}\mathbf{X}^\dagger\mathbf{B}^\dagger\right] + E[\mathbf{Z}\mathbf{Z}^\dagger] = \mathbf{P}\Theta\mathbf{R}\mathbf{R}_1 + \mathbf{R}_Z$ with $\mathbf{R} = E\left[\mathbf{U}^\dagger\mathbf{A}^\dagger\mathbf{A}\mathbf{U}\right]$, $\mathbf{R}_1 = E\left[\mathbf{B}\mathbf{X}\mathbf{X}^\dagger\mathbf{B}^\dagger\right]$ and $\mathbf{R}_Z = E[\mathbf{Z}\mathbf{Z}^\dagger]$. In practice, the covariance matrix \mathbf{R}_Y is not available and we have to rely on the sample covariance matrix. Let us define the sample covariance matrices of the measured signal and noise as: $\hat{\mathbf{R}}_Y(N) = \frac{1}{N}\mathbf{Y}\mathbf{Y}^\dagger$ and $\hat{\mathbf{R}}_Z(N) = \frac{1}{N}\mathbf{Z}\mathbf{Z}^\dagger$. Similarly, let $\hat{\mathbf{R}}$ and $\hat{\mathbf{R}}_1$ be the sample covariance matrices corresponding to the covariance matrices \mathbf{R} and \mathbf{R}_1 respectively. It can be noted that $\hat{\mathbf{R}}$ and $\hat{\mathbf{R}}_1$ are asymptotically free from any deterministic matrix for the considered \mathbf{X} and \mathbf{U} [371]. As mentioned in Section 4.1.2, we are interested in studying the following three specific cases.

Case 1: Constant Power: We consider equal received power across all the carriers and uncorrelated non-zero entries across the multiple measurement vectors of \mathbf{Y} . In this case, the observation model (4.2) reduces to the following

$$\mathbf{Y} = \mathbf{A}\mathbf{U}\sqrt{p}\mathbf{B}\mathbf{X} + \mathbf{Z}, \quad (4.4)$$

where p denotes the constant power across all the carriers. Since we assume normalized noise variance, $\text{SNR} \equiv p$. The value of SNR is assumed to be known and it can be acquired through SNR estimation techniques like in [53]. The detailed analysis of this case is presented in Section 4.2.2.

Case 2: Varying Power: The received power levels across all the carriers vary but are assumed to follow a known distribution. Further, we consider uncorrelated non-zero entries across the multiple measurement vectors of \mathbf{Y} . In this case, the observation model (4.2) reduces to the following

$$\mathbf{Y} = \mathbf{A}\mathbf{U}\mathbf{P}^{1/2}\mathbf{B}\mathbf{X} + \mathbf{Z}, \quad (4.5)$$

where \mathbf{P} is an $N \times N$ diagonal matrix with its diagonal entries corresponding to the varying power levels received across different carriers as defined earlier. The detailed analysis of this case is presented in Section 4.2.3.

Case 3: Correlated MMV: We consider the correlated scenario in which the non-zero entries across the multiple measurement vectors are correlated and assume that the received power across each carrier is constant. In this case, the observation model (4.2) reduces to the following

$$\mathbf{Y} = \mathbf{A}\mathbf{U}\Theta^{1/2}\sqrt{p}\mathbf{B}\mathbf{X} + \mathbf{Z}, \quad (4.6)$$

where $\Theta^{1/2}$ represents the square root of the correlation matrix Θ and its elements are drawn from an exponential correlation model. The detailed analysis of this case is presented in Section 4.2.4.

4.2.2 Analysis for Constant Power Case

Assuming that signal and noise are uncorrelated with each other, for large values of N , the measured signal's sample covariance matrix can be written using the following asymptotic approximation

$$\lim_{N \rightarrow \infty} \hat{\mathbf{R}}_Y(N) \approx p\hat{\mathbf{R}}\hat{\mathbf{R}}_1 + \hat{\mathbf{R}}_Z. \quad (4.7)$$

For the considered constant received power case, the a.e.p.d.f. of the measured signal's sample covariance matrix given by (4.7) can be used to estimate the sparsity order over the considered wideband spectrum as illustrated later in Section 4.2.5. In this context, our aim is to find the a.e.p.d.f. of $\hat{\mathbf{R}}_{\mathbf{Y}}(N)$. However, due to noncommutative nature of random matrices (Example 2.33, [43]), it's not straightforward to calculate the eigenvalue distribution of $\hat{\mathbf{R}}_{\mathbf{Y}}(N)$ by knowing the individual eigenvalue distributions of $\hat{\mathbf{R}}$, $\hat{\mathbf{R}}_1$ and $\hat{\mathbf{R}}_{\mathbf{Z}}$. Using free probability analysis, the asymptotic spectrum of the sum or product can be obtained from the individual asymptotic spectra without involving the structure of the eigenvectors of the matrices (Section 2.4, [43]). According to free probability theory of random matrices, Σ transform follows the multiplicative free convolution property [350] while the \mathbf{R} transform follows the additive free convolution property [356]. In this context, the free convolution properties of Σ and \mathbf{R} transforms can be used to find out the eigenvalue distribution of $\hat{\mathbf{R}}_{\mathbf{Y}}(N)$ as illustrated later in the Appendix B. By applying these properties in (4.7) and with the help of Theorems A.3, A.4 and A.8 (in Appendix A), the Stieltjes transform of asymptotic density function of $\hat{\mathbf{R}}_{\mathbf{Y}}(N)$ can be obtained. Subsequently, the derived Stieltjes transform is used to find the a.e.p.d.f. of $\hat{\mathbf{R}}_{\mathbf{Y}}(N)$ using (3.34), which is then subsequently used to estimate the sparsity order in our considered problem.

From [43, Theorem 2.39], the η transform of $\hat{\mathbf{R}}$ satisfies the following relation

$$1 = \frac{1 - \eta_{\hat{\mathbf{R}}}(z)}{1 - \eta_{\mathbf{F}}(z\eta_{\hat{\mathbf{R}}}(z))} \quad (4.8)$$

with $\mathbf{F} = \mathbf{A}^\dagger \mathbf{A}$. Since \mathbf{A} is diagonal with Bernoulli i.i.d. diagonal elements, its η transform can be written as [371]

$$\eta_{\mathbf{F}}(z) = \eta_{\mathbf{A}}(z) = 1 - \rho + \frac{\rho}{1 + z}. \quad (4.9)$$

Using (4.9) in (4.8), the η transform of $\hat{\mathbf{R}}$ is given by the positive solution of the following polynomial

$$z\eta_{\hat{\mathbf{R}}}(z)^2 - ((1 - \rho)z - 1)\eta_{\hat{\mathbf{R}}}(z) - 1 = 0. \quad (4.10)$$

Using the similar procedure, the η transform of $\hat{\mathbf{R}}_1$ is given by the positive solution of the following polynomial

$$z\eta_{\hat{\mathbf{R}}_1}(z)^2 - ((1 - \sigma)z - 1)\eta_{\hat{\mathbf{R}}_1}(z) - 1 = 0. \quad (4.11)$$

Equation (4.10) corresponds to the η transform of the $\mathbf{H}\mathbf{H}^\dagger$ with $N \times \rho N$ random matrix \mathbf{H} with i.i.d. elements having zero mean and variance $1/N$. Similarly, (4.11) corresponds to the η transform of the $\mathbf{H}\mathbf{H}^\dagger$ with \mathbf{H} of dimension $N \times \sigma N$. Since the $\mathbf{H}\mathbf{H}^\dagger$ follows the MP law given by Theorem 3.2.1 in Appendix A, the Σ transforms of $\hat{\mathbf{R}}$ and $\hat{\mathbf{R}}_1$ can be written as [43]

$$\Sigma_{\hat{\mathbf{R}}}(z) = \frac{1}{\rho + z}, \Sigma_{\hat{\mathbf{R}}_1}(z) = \frac{1}{\sigma + z}. \quad (4.12)$$

Based on the detailed analysis presented in Appendix B, we derive the following theorem for the Stieltjes transform of the $\hat{\mathbf{R}}_{\mathbf{Y}}(N)$.

Theorem 4.2.1. The Stieltjes transform $\mathcal{S}_{\hat{\mathbf{R}}_{\mathbf{Y}}}(z)$ of the asymptotic distribution of eigenvalues of $\frac{1}{N} \mathbf{Y} \mathbf{Y}^H$, where $\mathbf{Y} = \mathbf{A} \mathbf{U} p^{1/2} \mathbf{B} \mathbf{X} + \mathbf{Z}$ for arbitrary value of p can be obtained for any $z \in \mathbb{C}$ by solving a polynomial

with the following coefficients

$$\begin{aligned}
c_0 &= -p^2, \\
c_2 &= p^2(\rho\sigma - 1 - z) - p^3(\rho + \sigma) + p^4, \\
c_3 &= -p^3(\rho + \sigma)(z + 1) + 2p^2(\rho\sigma - z + zp^2), \\
c_4 &= zp^4(2 - z) - 2zp^3(\rho + \sigma) - p^2(z - \rho\sigma), \\
c_5 &= 2z^2p^4 - zp^3(\rho + \sigma), \\
c_6 &= p^4z^2,
\end{aligned} \tag{4.13}$$

where c_n is the n th order coefficient of the polynomial, ρ and σ denote the compression ratio and sparsity order respectively, and p is the common receive SNR of all the PU signals.

Proof. By applying multiplicative and additive free convolution properties of Σ and \mathbf{R} transforms and then using the relation (A.4), the polynomial in (4.13) is obtained. For detailed proof, see Appendix B. \square

The a.e.p.d.f. of $\hat{\mathbf{R}}_{\mathbf{Y}}$ can be obtained using Stieltjes inversion formula (3.34).

4.2.3 Analysis for Varying Power Case

Using the similar arguments as in Section 4.2.2, the measured signal's sample covariance matrix for large values of N can be written using the following asymptotic approximation

$$\lim_{N \rightarrow \infty} \hat{\mathbf{R}}_{\mathbf{Y}}(N) \approx \hat{\mathbf{R}}\mathbf{P}^{1/2}\hat{\mathbf{R}}_1\mathbf{P}^{1/2} + \hat{\mathbf{R}}_{\mathbf{Z}}. \tag{4.14}$$

To model the received power, uniform distribution over a certain power range would be the most suitable choice but it is analytically intractable because its transforms include logarithmic functions. To overcome this, we use modified semicircular distribution since it is symmetric around a non-zero mean and analytically tractable. The standard semicircular law is given by [43]

$$f_S(z) = \frac{1}{2\pi} \sqrt{4 - z^2}, \quad -2 < z < 2. \tag{4.15}$$

We extend (4.15) in the following form to allow for non-zero power mean and scalable dynamic range of the power profile.

$$f_{MS}(z) = \frac{g}{2\pi} \sqrt{4 - g^2(z - \bar{p})^2}, \quad \bar{p} - \frac{2}{g} < z < \bar{p} + \frac{2}{g}. \tag{4.16}$$

where \bar{p} denotes the mean of the considered distribution and g denotes the scaling factor of the dynamic range with $g \geq 2/\bar{p}$. Let $[a, b]$ denote the support of the considered distribution, then the parameters \bar{p} and g can be expressed as: $\bar{p} = \frac{a+b}{2}$ and $g = \frac{4}{b-a}$. The dynamic range of power variation across the carriers can be defined as: $DR = 10\log \frac{b}{a}$.

Lemma 4.2.1. The Stieltjes transform of the modified semicircular law (4.16) is given by

$$\mathcal{S}_{\mathbf{P}}(z) = \frac{1}{2}g[-g(z - \bar{p}) + \sqrt{g^2(z - \bar{p})^2 - 4}]. \tag{4.17}$$

Proof. By definition of the transform and integration over (4.16). \square

Lemma 4.2.2. The Σ transform of the modified semicircular law (4.16) is given by

$$\Sigma_{\mathbf{P}}(z) = \frac{1}{2} \frac{g(gc + \sqrt{g^2\bar{p}^2 - 8 - 4z})}{z}. \tag{4.18}$$

Proof. By definition of the transform and (4.17). \square

Lemma 4.2.3. The Stieltjes transform of the asymptotic distribution of eigenvalues of $\hat{\mathbf{R}}\mathbf{P}^{1/2}\hat{\mathbf{R}}_1\mathbf{P}^{1/2}$, let us denote by \mathbf{W} , can be obtained for any $z \in \mathbb{C}$ by finding roots of the equation

$$\mathcal{S}_{\mathbf{W}}(z)(\rho - z\mathcal{S}_{\mathbf{W}}(z) - 1)(\sigma - z\mathcal{S}_{\mathbf{W}}(z) - 1) + \frac{1}{2}g^2\bar{p} + \frac{1}{2}g\sqrt{g^2\bar{p}^2 + 4z\mathcal{S}_{\mathbf{W}}(z) - 4} = 0. \quad (4.19)$$

Proof. By applying the multiplicative free convolution property of Σ transform and using the definitions of the transforms. \square

Theorem 4.2.2. The Stieltjes transform $\mathcal{S}_{\hat{\mathbf{R}}_{\mathbf{Y}}}(z)$ of the asymptotic distribution of eigenvalues of $\frac{1}{N}\mathbf{Y}\mathbf{Y}^H$, where $\mathbf{Y} = \mathbf{A}\mathbf{U}\mathbf{P}^{1/2}\mathbf{B}\mathbf{X} + \mathbf{Z}$ can be obtained for any $z \in \mathbb{C}$ by finding roots of the equation

$$\mathcal{S}_{\hat{\mathbf{R}}_{\mathbf{Y}}}^{-1}(z) = z(\rho - z\mathcal{S}_{\mathbf{W}}(z) - 1)(\sigma - z\mathcal{S}_{\mathbf{W}}(z) - 1) + \frac{1}{2}g^2\bar{p} + \frac{1}{2}g\sqrt{g^2\bar{p}^2 + 4z\mathcal{S}_{\mathbf{W}}(z) - 4} + \frac{1}{1-z}, \quad (4.20)$$

where g is the scaling factor of the dynamic range, ρ and σ denote the compression ratio and sparsity order respectively, and \bar{p} is the mean SNR of the considered distribution.

Proof. By applying multiplicative and additive free convolution properties of Σ and \mathbf{R} transforms and then using the definitions of the transforms. For detailed proof, see Appendix B. \square

4.2.4 Analysis under Correlated Scenario

In this case, we consider correlation across the non-zero entries of the multiple measurement vectors. To model this scenario, we consider the one-sided noise correlation model. We model the correlated sparse signal matrix as: $\hat{\mathbf{S}} = \Theta^{1/2}\mathbf{S}$, where $\Theta^{1/2}\Theta^{1/2} = \Theta = E[\hat{\mathbf{S}}\hat{\mathbf{S}}^H]$. To ensure that Θ does not affect the received signal power, the normalization $(1/N)\text{trace}\{\Theta\} = 1$ is considered. We model the components of the covariance matrix Θ using an exponential correlation model given by (3.4). A similar correlation model has been applied in [391] for sparse support recovery in the presence of correlated multiple measurements. Using the correlation model in (3.4), the observation model is given by (4.6).

For correlation analysis, we consider that the correlation matrix Θ follows the tilted semicircular law¹ as in [147], which is given by

$$f_{\Theta}(z) = \frac{1}{2\pi\mu z^2} \sqrt{\left(\frac{z}{\delta_1} - 1\right) \left(1 - \frac{z}{\delta_2}\right)}, \quad (4.21)$$

where $[\delta_1, \delta_2]$ defines the support of the distribution and $\mu = \frac{(\sqrt{\delta_2} - \sqrt{\delta_1})}{4\delta_1\delta_2}$ with $\mu > 0$. The parameter μ controls the degree of correlation and varies the support of the distribution. The Signal Condition Number (SCN) of the $N \times N$ correlation matrix Θ is related to μ as: $\mu = \frac{\text{SCN}-1}{\text{SCN}+1}$. As stated in [147], the parameter μ is related to ς as: $\mu = \frac{\varsigma^2}{1-\varsigma^2}$. In this work, we are interested in carrying out SOE for different levels of correlation across the non-zero entries of the MMV model. For this purpose, we need the a.e.p.d.f. of $\hat{\mathbf{R}}_{\mathbf{Y}}(N)$ under the correlated scenario. Using the similar arguments as in earlier sections, the measured signal's sample covariance matrix for large values of N can be written using the following asymptotic approximation

$$\lim_{N \rightarrow \infty} \hat{\mathbf{R}}_{\mathbf{Y}}(N) \approx p\hat{\mathbf{R}}\Theta^{1/2}\hat{\mathbf{R}}_1\Theta^{1/2} + \hat{\mathbf{R}}_{\mathbf{Z}}. \quad (4.22)$$

¹It can be noted that this law closely approximates the exponential correlation model given by (3.4).

Theorem 4.2.3. The Stieltjes transform $S_{\hat{\mathbf{R}}_{\mathbf{Y}}}(z)$ of the asymptotic distribution of eigenvalues of $\frac{1}{N}\mathbf{Y}\mathbf{Y}^H$ where $\mathbf{Y} = \mathbf{A}\mathbf{U}\Theta^{1/2}\sqrt{p}\mathbf{B}\mathbf{X} + \mathbf{Z}$ can be obtained for any $z \in \mathbb{C}$ by solving a polynomial with the following coefficients

$$\begin{aligned} c_0 &= p\mu(1 + p\mu), \\ c_1 &= 2p\mu(zp\mu - p^2) + p^2(\mu(\rho + \sigma) - 1) + p\mu(z - \rho\sigma + 1), \\ c_2 &= (\rho + \sigma)(p^2\mu + zp^2\mu - p^3) + p\rho\sigma(p - 2\mu) + 2zp\mu(p\mu + 1 - 2p^2) - p^2(1 + z - z^2\mu^2), \\ c_3 &= 2zp^2(\mu(\rho + \sigma) - z\mu(p - \mu) + p^2 - 2p\mu - 1) - p^3(z + 1)(\rho + \sigma) + p(\rho\sigma(2p - \mu) + z\mu), \\ c_4 &= zp^2\mu(\rho + \sigma) - 2zp^3(\rho + 1) + p^2(z^2(\mu^2 - 4p\mu + p^2) + \rho\sigma - z + 2zp^2), \\ c_5 &= 2z^2p^3(p - \mu) - zp^3(\rho + \sigma), \\ c_6 &= z^2p^4, \end{aligned} \tag{4.23}$$

where c_n is the n th order coefficient of the polynomial, ρ and σ denote the compression ratio and sparsity order respectively, μ defines the correlation degree of Θ , and p is the common receive SNR of all the PU signals.

Proof. By definitions of the transforms and using multiplicative and additive free convolution properties of Σ and \mathbf{R} transforms respectively. For detailed proof, see Appendix B. \square

4.2.5 Proposed Compressive Sparsity Order Estimation

The SOE is the process of identifying the number of non-zero elements of a sparse vector and does not need to have the exact knowledge of their amplitudes or positions. The proposed compressive SOE can be applicable in general settings. In this thesis work, this problem is mainly motivated by wideband CR scenarios where compressive SOE is the main issue for determining the suitable sampling rate at the receiver. To determine the suitable sampling rate at the CR receiver, most existing CS literature implicitly assumes that the sparsity order of the considered wideband spectrum is known beforehand. However, in practical CR applications, the actual sparsity order corresponds to the instantaneous spectrum occupancy of wireless users and it varies dynamically as the spectrum occupancy changes. Hence, the sparsity order is often unknown and only its upper bound can be measured based on the maximum spectrum utilization observed statistically over a time period. In practice, the determination of the sampling rate based on the upper bound can cause unnecessarily high sensing cost since the sampling rate depends on the sparsity order [77]. From the above discussion, it can be noted that it is crucial to adapt the sampling rate in accordance to the sparsity variation of the spectrum occupancy and thus tracking the instantaneous sparsity order is an important issue. In this context, we propose an eigenvalue-based blind SOE method which is based on the ME of the measured signal's sample covariance matrix.

Based on the polynomials of the Stieltjes transforms specified in the above sections, the support range of the corresponding a.e.p.d.f. is obtained using (3.34). For convenience, a lookup table (Table 4.1) is provided in order to illustrate the SOE method in the considered scenarios (see Section 4.2.6). In the lookup table, we present the maximum eigenvalues of $\hat{\mathbf{R}}_{\mathbf{Y}}$ for the considered three different cases and the corresponding values of σ . For SOE purpose, we select K number of sampling slots and calculate $\bar{\lambda}_{\max} = E_K[\lambda_{\max}(\hat{\mathbf{R}}_{\mathbf{Y}}(N))]$ over these slots. Subsequently, $\bar{\lambda}_{\max}$ is compared with the values of λ_{\max} stored in the lookup table and the corresponding value of σ is obtained. Further, for any intermediate values of $\bar{\lambda}_{\max}$, a suitable interpolation method can be applied for estimating the corresponding value of σ . To clarify the above process, we include procedures for lookup table formation and sparsity order estimation considering the constant power scenario (Section 4.2.2) below.

In all the considered cases, the parameter ρ is assumed as an operating parameter of the CR sensing module and its value depends on how much compressed measurements we want to carry out in order to

reduce the hardware costs at the expense of some estimation error. The Stieltjes transform of $\hat{\mathbf{R}}_{\mathbf{Y}}$ for the constant power case is calculated using polynomial (4.13). In this case, the value of p is assumed to be known and in practice, its value can be obtained by using SNR estimation techniques like in [53]. Since we know the value of ρ and p in (4.13), we can estimate the value of σ by sensing the $\bar{\lambda}_{\max}$ of $\hat{\mathbf{R}}_{\mathbf{Y}}$, where $\mathbf{Y} = \mathbf{A}\mathbf{U}p^{1/2}\mathbf{B}\mathbf{X} + \mathbf{Z}$, obtained using (4.13) and (3.34). Similarly, the Stieltjes transform for the varying power case is obtained using (4.20). In this case, the support of the considered power distribution i.e., $[a, b]$ is assumed to be known and based on this support, the values of g and \bar{p} can be calculated as mentioned in Section 4.2.3. As we know the value of g , \bar{p} and ρ in (4.20), we can estimate the sparsity order i.e., σ by evaluating $\bar{\lambda}_{\max}$ of $\hat{\mathbf{R}}_{\mathbf{Y}}$, where $\mathbf{Y} = \mathbf{A}\mathbf{U}p^{1/2}\mathbf{B}\mathbf{X} + \mathbf{Z}$, obtained using (4.20) and (3.34).

In the similar way, the Stieltjes transform for the correlated case is obtained using the polynomial (4.23). In this case, the value of ς is assumed to be known and in practice, its value can be found using different noise correlation models such as in [53, 391] or measurement methods. Based on the value of ς , the value of μ can be calculated as mentioned in Section 4.2.4. Since we know the value of p , ρ and μ in (4.23), we can estimate the value of σ by calculating the ME of $\hat{\mathbf{R}}_{\mathbf{Y}}$, where $\mathbf{Y} = \mathbf{A}\mathbf{U}\Theta^{1/2}\sqrt{p}\mathbf{B}\mathbf{X} + \mathbf{Z}$, obtained using (4.23) and (3.34). For example, for Scenario 4.2.6, if the value of $\bar{\lambda}_{\max}$ of the $\hat{\mathbf{R}}_{\mathbf{Y}}$ is 6.67 under compressive measurement scenario with $\rho = 0.8$, it can be estimated that the sparsity order of the considered wideband spectrum is 0.5. Based on this estimated sparsity order, we could potentially fix the optimum sampling rate of the CS acquisition system in order to reduce the sensing hardware cost. In Section 4.2.3, we provide the normalized SOEE versus sparsity order plots to evaluate the performance of this estimation technique.

Procedure for lookup table formation

1. Select the operating parameter ρ .
2. Select the value of p based on SNR estimation techniques like in [53].
3. Evaluate $\mathcal{S}_{\hat{\mathbf{R}}_{\mathbf{Y}}}(z)$ using (4.13).
4. Find $\lambda_{\max}(\hat{\mathbf{R}}_{\mathbf{Y}})$ using (3.34).
5. For each value of σ in $(0, 1)$, repeat steps 3 and 4.
6. Store all $\lambda_{\max}(\hat{\mathbf{R}}_{\mathbf{Y}})$ and corresponding σ e.g., Table 4.1 (Scenario I).

Procedure for sparsity order estimation

1. Select the number of sampling slots K .
2. Calculate instantaneous $\hat{\mathbf{R}}_{\mathbf{Y}}(N) = \frac{1}{N}\mathbf{Y}\mathbf{Y}^H$ in each sampling slot.
3. Calculate $\bar{\lambda}_{\max} = E_K[\lambda_{\max}(\hat{\mathbf{R}}_{\mathbf{Y}}(N))]$ over K number of sampling slots.
4. Find σ corresponding to $\bar{\lambda}_{\max}$ from the lookup table.
5. Use suitable interpolation for any intermediate value of $\bar{\lambda}_{\max}$.

4.2.6 Numerical Results

To evaluate the performance of the proposed SOE method for the considered scenarios, the metric normalized SOE Error (SOEE) is used, which is expressed in terms of root mean square error normalized to the true sparsity order and defined by

$$\text{SOEE} = \frac{\sqrt{E[(\hat{\sigma} - \sigma)^2]}}{\sigma}, \quad (4.24)$$

where $\hat{\sigma}$ is the estimated sparsity order with the proposed method and σ is the actual sparsity order. In our numerical results, we run 10^3 number of Monte Carlo realizations in order to obtain the value of normalized SOEE in (4.24) and each Monte Carlo realization includes steps (2) and (3) from the SOE procedure specified in Section 4.2.5.

The total error in our estimation process results from the two sources. The first error comes from the randomness of the ME which is used as an input parameter for the estimator and the second error is the residual error resulting from the interpolation process. In practice, the second error can be minimized by having a dense look up table and the first error can be minimized by increasing the number of sensing slots over which the mean eigenvalue i.e., $\bar{\lambda}_{\max}$ is calculated. However, in practice, the number of sampling slots are limited due to the limited sampling time required to capture the dynamicity of the time varying sparsity order. If the spectrum occupancy changes too rapidly i.e., the sparsity order varies at a faster rate, the number of sampling slots should be small. To take this fact into account, we use only $K = 30$ number of sampling slots in our results.

In the following subsections, we present numerical results for SOE for the considered three different scenarios. In the numerical results, we compare the performance of the proposed SOEE technique in compressive and full measurement cases. The compressive measurement case corresponds to the signal model given by (4.2) while the full measurement case for the constant power scenario corresponds to the following signal model $\mathbf{Y} = \sqrt{p}\mathbf{B}\mathbf{X} + \mathbf{Z}$ and the following sample covariance matrix $\hat{\mathbf{R}}_{\mathbf{Y}} = p\hat{\mathbf{R}}_1 + \hat{\mathbf{R}}_Z$. From practical perspectives, the difference between full measurement and compressive measurement cases is that the former considers all the measurements across the carriers whereas the later case considers the sparse linear combinations of carrier measurements.

1. Constant Power Scenario: To validate our theoretical analysis presented in Section 4.2.2, we plot the theoretical and simulated eigenvalue distributions of $\hat{\mathbf{R}}_{\mathbf{Y}}(N)$ in Fig. 4.1 with parameters $\rho = 0.8$, $\sigma = 0.6$, $N = 100$, $\text{SNR} = 0\text{dB}$. The theoretical a.e.p.d.f. in this case was obtained by solving the polynomial given by (4.13) and using the Stieltjes inversion formula in (3.34). From the figure (Fig. 4.1), it can be noted that the theoretical curve perfectly matches with the simulated one.

For SOE purpose, we provide a lookup table (Table 4.1, Scenario I), where the MEs of $p\hat{\mathbf{R}}\hat{\mathbf{R}}_1 + \hat{\mathbf{R}}_Z$ are provided for different values of σ for compressive and full measurement cases. The value of σ can be estimated using this table based on the SOE method described in Section 4.2.5. For example, if the value of $\bar{\lambda}_{\max}$ is 6.05 for the compressive measurement case, it can be estimated that the sparsity order of the occupancy of the considered wideband spectrum is 40 %. Figure 4.2 presents the normalized SOEE versus sparsity order for compressive and full measurement cases for $\text{SNR} = 2\text{ dB}$. From this figure, it can be noted that the normalized SOEE is higher for the compressive case than for the full measurement case. For $\text{SNR} = 2\text{ dB}$ as shown in Fig. 4.2, the normalized SOEE for the compressive case is slightly less than 2.9 % and for the full measurement case is nearly about 2.4 % at the sparsity order of 0.5. On the other hand, the advantage is that we have used the compression of 80 % i.e., 20 % saving can be achieved in terms of hardware resources, which is a considerable gain. Furthermore, Fig. 4.3 presents the normalized SOEE versus SNR considering a fixed sparsity order of 0.6. Our simulation results show that at lower values of SNR, the compressive case performs better than the full measurement case in terms of the normalized SOEE (below the SNR value of -0.5 dB in Fig. 4.3). An intuitive explanation is that in the full measurement case, the contribution of the noise in the a.e.p.d.f. becomes dominant with a faster rate compared to the compressed measurement case.

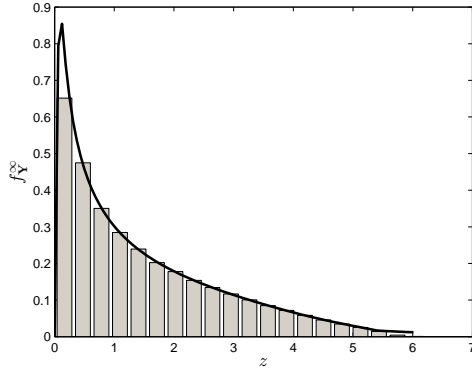


FIGURE 4.1: Theoretical and simulated eigenvalue distribution of $\hat{\mathbf{R}}_Y(N)$, where $\mathbf{Y} = \mathbf{AU}\sqrt{p}\mathbf{BX} + \mathbf{Z}$ ($\rho = 0.8, \sigma = 0.6, N = 100, M = 100, K = 100, \text{SNR} = 0\text{dB}$)

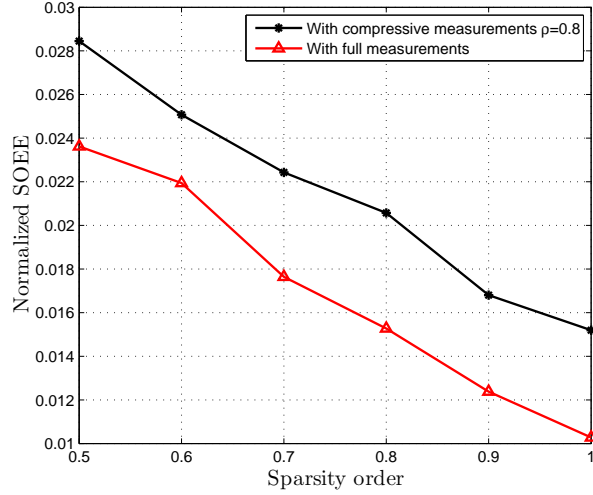


FIGURE 4.2: Normalized SOEE versus sparsity order with compressive and full measurements for constant received power scenario (SNR = 2dB, $N = 100$)

Figure 4.4 presents the estimation error in terms of the normalized SOEE versus compression ratio ρ for the SNR value of 2 dB. In this simulation settings, the value of σ was considered as 0.6 and the estimation error for each ρ was calculated by interpolating the value of $\bar{\lambda}_{\max}$ with the provided set of the values of σ and λ_{\max} for the considered value of ρ . It can be noted that $\rho = 1$ corresponds to no-compression and the estimation error in terms of normalized SOEE increases as ρ decreases (Fig. 4.4) i.e., with the increase in the compression. It can be depicted that by using the smaller value of compression ratio ρ , we are saving sampling resources in one hand but on the other hand, we have to sacrifice some estimation performance. Therefore, in practice, there exists a tradeoff between the number of measurements (hardware cost) and the estimation performance.

2. Varying Power Scenario: Under this scenario, received power levels across the carriers within the considered wideband spectrum vary but they are assumed to follow a known distribution as mentioned in Section 4.2.3. The main advantage of the applied approach is that we do not need to have information of all the individual channel powers in order to estimate the sparsity order. In order to validate the theoretical analysis presented in Section 4.2.3, we provide the theoretical and simulated distributions of $\hat{\mathbf{R}}_Y(N)$ in Fig. 4.5. The theoretical curve was obtained by evaluating (4.20) and using the Stieltjes inversion formula in (3.34). It can be noted that the theoretical and simulated results match perfectly.

In order to estimate the sparsity order under this scenario, the lookup table (Table 4.1, Scenario II) can be used, where the MEs of $\hat{\mathbf{R}}_Y\hat{\mathbf{R}}_Y^T + \hat{\mathbf{R}}_Z\hat{\mathbf{R}}_Z^T$ are provided for different values of σ for compressive and full measurement cases. For example, if the value of $\bar{\lambda}_{\max}$ is 9.36 for the compressive case, it

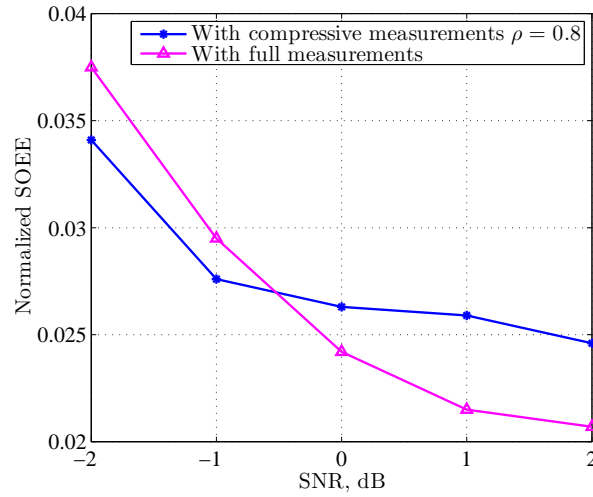


FIGURE 4.3: Normalized SOEE versus SNR with compressive and full measurements for constant received power scenario ($\sigma = 0.6, N = 100$)

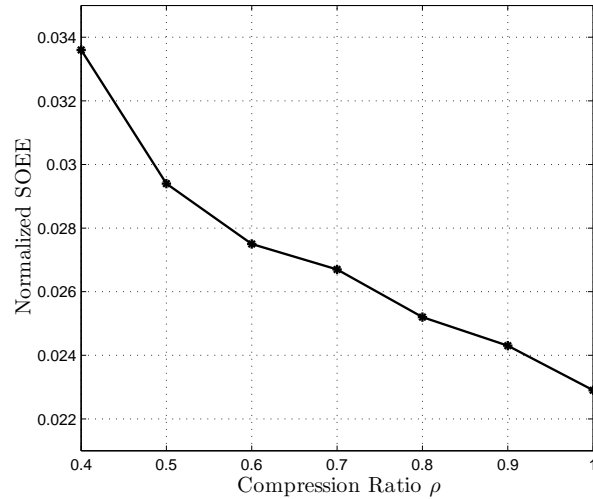


FIGURE 4.4: Normalized SOEE versus compression ratio ρ (SNR = 2 dB, $\sigma = 0.6, N = 100$)

TABLE 4.1: Lookup table for sparsity order estimation for the considered scenarios ($\rho = 0.8$)

Scenarios	I SNR=2 dB Compressive	I SNR=2 dB Full	II DR=6.02 dB Compressive	II DR=6.02 dB Full	III SCN=4 SNR=0 dB Compressive	III SCN=4 SNR=0 dB Full
Sparsity Level						
1	9.63	7.44	12.80	10.19	6.93	5.86
0.9	9.03	7.14	11.80	9.58	6.53	5.65
0.8	8.41	6.83	11.03	9.08	6.17	5.44
0.7	7.85	6.53	10.22	8.60	5.80	5.24
0.6	7.26	6.21	9.36	8.08	5.43	5.02
0.5	6.67	5.88	8.42	7.44	5.08	4.81
0.4	6.05	5.52	7.51	6.84	4.74	4.60
0.3	5.44	5.15	6.63	6.24	4.43	4.40
0.2	4.85	4.76	5.66	5.57	4.17	4.20
0.1	4.25	4.31	4.69	4.80	3.96	4.00
0	3.79	3.79	3.79	3.79	3.79	3.79

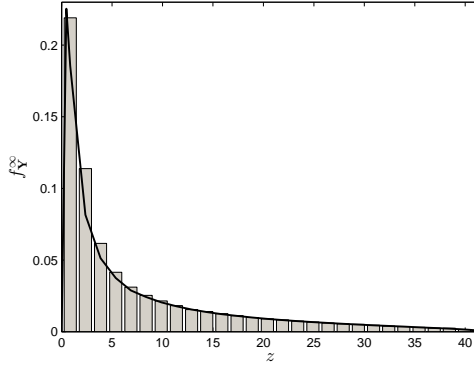


FIGURE 4.5: Theoretical and simulated eigenvalue distribution of $\hat{\mathbf{R}}_{\mathbf{Y}}(N)$, where $\mathbf{Y} = \mathbf{A}\mathbf{U}\mathbf{P}^{1/2}\mathbf{B}\mathbf{X} + \mathbf{Z}$
(DR = 6.02 dB, $N = 100$, $M = 100$, $K = 100$, $\bar{p} = 7.78$ dB)

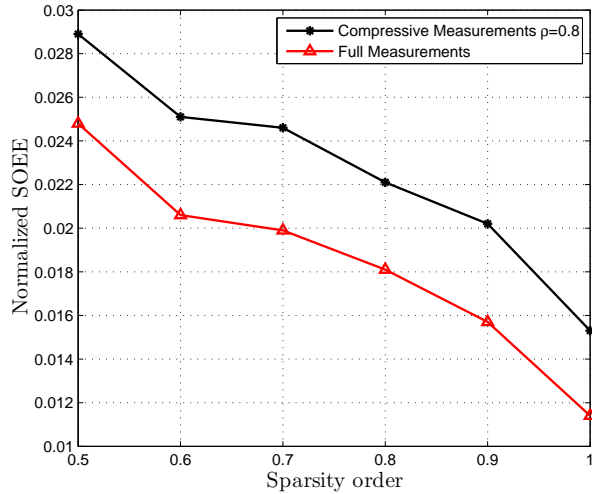


FIGURE 4.6: Normalized SOEE versus sparsity order with compressive and full measurements for varying power scenario (DR = 6.02 dB, $N = 100$, $\bar{p} = 7.78$ dB)

can be estimated that the sparsity order of the occupancy of the considered wideband spectrum is 60 %. Figure 4.6 presents the comparison of the normalized SOEE versus sparsity order for full and compressive measurement cases with parameters (DR = 6.02 dB, $N = 100$, $\bar{p} = 7.78$ dB). From the figure, it can be noted that sparsity order up to 0.5 can be estimated with less than 2.9 % estimation error for the compressive case and with less than 2.5 % estimation error for the full measurement case. Furthermore, it can be noted that we have to tolerate a small amount of additional error while using compressive measurements. On the other hand, we are saving 20 % hardware resources using 20 % less measurements.

3. Correlated MMV Scenario: Under this scenario, we consider correlated MMVs as mentioned in Section 4.2.4. To validate the our theoretical analysis, we present the theoretical and simulated eigenvalue distributions of the measured signal's covariance matrix given by (4.22) in Fig. 4.7 with parameters ($\rho = 0.8$, $\sigma = 0.6$, $N = 100$, SCN = 4). The theoretical plot was obtained by solving the polynomial (4.23) and using the Stieltjes inversion formula in (3.34). From the figure, it can be noted that the theoretical and simulated results match perfectly. In order to estimate the sparsity order, we can use the λ_{\max} of the a.e.p.d.f. obtained from the Stieltjes transform given by polynomial (4.23). Since we assume the value of ρ , μ to be known in (4.23), the value of σ can be estimated based on the procedure described in Section 4.2.5. For convenience, we provide a lookup table (Table 4.1, Scenario III). Figure 4.8 shows the normalized SOEE versus sparsity order comparison for compressive and full measurement cases for the correlated MMV scenario with parameters (SCN = 4, $N = 100$, SNR = 0 dB). From the figure, it can be noted that the full measurement case performs better than the compressive measurement case with $\rho = 0.8$. The sparsity order can be estimated with less than 3 % for the compressive

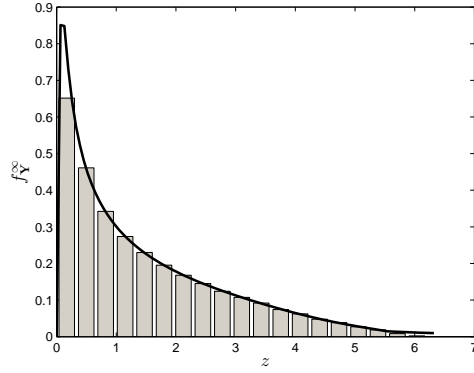


FIGURE 4.7: Theoretical and simulated eigenvalue distribution of $\hat{\mathbf{R}}_{\mathbf{Y}}(N)$, where $\mathbf{Y} = \mathbf{A}\mathbf{U}\boldsymbol{\Theta}^{1/2}\mathbf{B}\mathbf{X} + \mathbf{Z}$
($\rho = 0.8, \sigma = 0.6, N = 100, M = 100, K = 100, \text{SCN} = 4$)

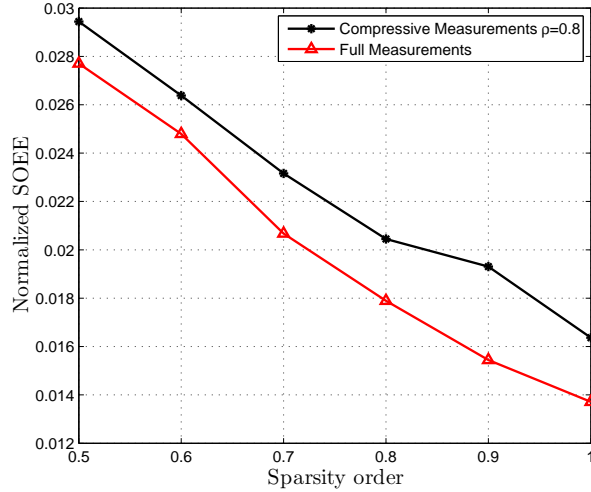


FIGURE 4.8: Normalized SOEE versus sparsity order with compressive and full measurements for correlated and uncorrelated scenarios ($\text{SCN} = 4, N = 100, \text{SNR} = 0 \text{ dB}$)

measurement case and with less than 2.8 % for the full measurement case up to the sparsity order of 0.5 (as depicted in Fig. 4.8). As in previous scenarios, it can be concluded that we need to sacrifice some amount of performance in terms of the estimation error in order to save the sensing hardware resources.

4. Discussion: In practical applications, it may be difficult to acquire the sparsity order knowledge over a wideband spectrum since it requires a lot of hardware resources in acquiring full measurements. In this context, compressive sparsity estimation is important in order to acquire the sparsity order knowledge. This prior knowledge helps CS based CR systems in applying a correct sampling rate in order to fully exploit the advantages of these systems. In this direction, a novel technique has been proposed for estimating the sparsity order of the spectrum occupancy within a wideband spectrum in the context of a wideband CR. First, the theoretical expressions for a.e.p.d.f. of the measured signal's covariance matrix have been derived for three different scenarios using RMT-based methods. More specifically, the following different scenarios have been considered: (i) constant received power scenario, (ii) varying received power scenario, and (iii) correlated MMV scenario. Then the performance of the proposed method was evaluated in terms of the normalized SOEE for the considered scenarios. From the results, it can be concluded that the proposed technique can reliably estimate the sparsity order for a range of scenarios even with compressive measurements. Further, it has been noted that there exists a tradeoff between hardware sensing cost and the estimation error while using compressive measurements.

4.3 Compressive Signal to Noise Ratio Estimation

In this work, we study an eigenvalue-based SNR estimation problem over a wideband spectrum using the CS approach instead of the narrowband context considered in the existing literature. We consider the following two correlated scenarios: (i) correlated MMV, and (ii) correlated noise. As stated before, in practice, the correlated MMV case may arise due to channel correlation or imperfections in frequency selective filters present at the CR node [391] and the correlated noise case may arise due to filtering and oversampling operations. We derive the a.e.p.d.f. expressions for the above two cases based on the MMV model using asymptotic RMT. Subsequently, based on the derived a.e.p.d.f. expressions, we apply the eigenvalue based SNR estimation technique proposed in Chapter 3 in order to estimate the PU SNR over a wideband spectrum using compressive measurements and evaluate its estimation performance in terms of the normalized MSE. For this analysis, we use the signal model used for SOE in Section 4.2.1 and the exponential correlation model presented in 3.2.3. The considered scenarios are briefly described below.

4.3.1 Scenarios and Analysis

Herein, we are interested in studying the following two correlated scenarios considering equal expected received power across all the carriers.

4.3.2 Correlated Noise Case

The signal model in this case can be written as

$$\mathbf{Y} = \mathbf{AU}\sqrt{p}\mathbf{BX} + \boldsymbol{\Theta}^{1/2}\mathbf{Z} = \mathbf{AU}\sqrt{p}\mathbf{BX} + \hat{\mathbf{Z}}, \quad (4.25)$$

where $\hat{\mathbf{Z}} = \boldsymbol{\Theta}^{1/2}\mathbf{Z}$ denotes the correlated noise. The detailed analysis of this case is presented below.

Assuming that signal and noise are uncorrelated with each other, for large values of N , the following approximation can be written for the this scenario

$$\lim_{N \rightarrow \infty} \hat{\mathbf{R}}_{\mathbf{Y}}(N) \approx p\hat{\mathbf{R}}\hat{\mathbf{R}}_1 + \boldsymbol{\Theta}^{1/2}\hat{\mathbf{R}}_{\hat{\mathbf{Z}}}\boldsymbol{\Theta}^{1/2}. \quad (4.26)$$

In the above expression, the p.d.f. of the term $\boldsymbol{\Theta}^{1/2}\hat{\mathbf{R}}_{\hat{\mathbf{Z}}}\boldsymbol{\Theta}^{1/2}$ i.e., $\hat{\mathbf{R}}_{\hat{\mathbf{Z}}}$ follows the Theorem 2.41 of [43] and its Stieltjes transform of $\hat{\mathbf{R}}_{\hat{\mathbf{Z}}}$ can be written as [147]

$$\mathcal{S}_{\hat{\mathbf{R}}_{\hat{\mathbf{Z}}}}(z) = \frac{z + 2z\mu + 1 - \beta + \sqrt{[z - (1 + \beta)]^2 - 4\beta(1 + \mu z)}}{2z(1 + \mu z)}. \quad (4.27)$$

In the next step, the corresponding R transform is calculated using (A.4) and is given by

$$\mathcal{R}_{\hat{\mathbf{R}}_{\hat{\mathbf{Z}}}}(z) = -\frac{1}{2} \frac{(z - 1 + \sqrt{(z^2 - 2z + 1 - 4\mu\beta z)})}{\mu z}. \quad (4.28)$$

Since $\hat{\mathbf{R}}$ and $\hat{\mathbf{R}}_1$ follow the MP distribution, the Σ transform of the product of the $\hat{\mathbf{R}}$ and $\hat{\mathbf{R}}_1$ can be written as

$$\Sigma_{\hat{\mathbf{R}}\hat{\mathbf{R}}_1}(z) = \frac{1}{\rho + z} \cdot \frac{1}{\sigma + z}. \quad (4.29)$$

Subsequently, the corresponding η , Stieltjes and R transforms are calculated using (A.3), (A.8) and (A.4) respectively, with the similar procedure described in Section 4.3.2. Then the R transform of $\hat{\mathbf{R}}_{\mathbf{Y}}$ in (4.26) is calculated using the additive free convolution property of the R transform in the following way

$$\mathcal{R}_{\hat{\mathbf{R}}_{\mathbf{Y}}}(z) = p\mathcal{R}_{p\hat{\mathbf{R}}\hat{\mathbf{R}}_1}(pz) + \mathcal{R}_{\hat{\mathbf{R}}_{\hat{\mathbf{Z}}}}(z). \quad (4.30)$$

The Stieltjes transform $\mathcal{S}_{\hat{\mathbf{R}}_{\mathbf{Y}}}(z)$ of the asymptotic distribution of eigenvalues of $\hat{\mathbf{R}}_{\mathbf{Y}}$ in this case can be found by using (4.30) and (A.4). Then the corresponding a.e.p.d.f. can be obtained using the Stieltjes inversion formula (3.34).

4.3.3 Correlated Multiple Measurement Vector Case

The signal model in this case can be written as

$$\mathbf{Y} = \mathbf{AU}\sqrt{p}\Theta^{1/2}\mathbf{BX} + \mathbf{Z}, \quad (4.31)$$

where p denotes the constant power across all the carriers, $\Theta^{1/2}$ represents the square root of the correlation matrix Θ and its elements are drawn from an exponential correlation model. Since we assume normalized noise variance, $\text{SNR} \equiv p$.

Using similar arguments in the previous section, the measured signal's sample covariance matrix can be written using the following asymptotic approximation

$$\lim_{N \rightarrow \infty} \hat{\mathbf{R}}_{\mathbf{Y}}(N) \approx p\hat{\mathbf{R}}\Theta^{1/2}\hat{\mathbf{R}}_1\Theta^{1/2} + \hat{\mathbf{R}}_{\mathbf{Z}}. \quad (4.32)$$

The a.e.p.d.f. of $\hat{\mathbf{R}}_{\mathbf{Y}}$ given by (4.32) can be used to estimate the SNR for the considered case. This case resembles to that of the correlated scenario considered in Section 4.2.4 and we use the Stieltjes transform provided by (4.23) for finding the a.e.p.d.f. and subsequently, in estimating the SNR as described in Section 4.3.4.

4.3.4 Proposed Approach

In this section, we apply an eigenvalue-based SNR estimation method proposed in Section 3.3.5 under compressive settings based on the ME of the measured signal's covariance matrix. Based on the polynomials of the Stieltjes transform obtained using the procedure mentioned in the above sections, the support range of the corresponding a.e.p.d.f. is obtained using (3.34). For convenience, we provide a lookup table (Table 4.2) in order to illustrate the compressive SNR estimation method in the considered scenarios (See Section 4.3.5). In the lookup table, we present the MEs of $\hat{\mathbf{R}}_{\mathbf{Y}}$ for the correlated MMV case and the corresponding values of p i.e., SNR. For any instantaneous ME (λ_{\max}) of $\hat{\mathbf{R}}_{\mathbf{Y}}$, its value is compared with the values of λ_{\max} stored in the lookup table and the corresponding value of p is obtained. Furthermore, for any intermediate values of λ_{\max} , suitable interpolation methods can be applied for estimating the corresponding value of p .

The Stieltjes transform of $\hat{\mathbf{R}}_{\mathbf{Y}}$ for the correlated MMV case is calculated using the polynomial (4.23) and the corresponding Stieltjes transform for the correlated noise case is obtained using the procedure described in Section 4.3.2. The value of σ is assumed to be known and in practice, its value can be obtained by using SOE techniques such as in [77]. Further, the value of ς for the correlated MMV case can be found with channel estimation methods such as in [355] and its value for the correlated noise can be found by carrying out measurements in the sensing module. Moreover, the parameter ρ is assumed as an operating parameter of the CR module and its value depends on how much compressed measurements we want to carry out in order to reduce the hardware costs at the expense of some estimation error. Considering an example of the correlated MMV in (4.23), since we know the value of ρ and σ , we can estimate the value of p by sensing the ME of $\hat{\mathbf{R}}_{\mathbf{Y}}$, where $\mathbf{Y} = \mathbf{AU}\sqrt{p}\Theta^{1/2}\mathbf{BX} + \mathbf{Z}$, obtained using (4.23) and (3.34).

4.3.5 Numerical Results

We evaluate the performance of the proposed SNR estimation for the considered scenarios under compressive settings using the normalized MSE, which is given by (3.39). In our numerical results, we compare the performance of the considered SNR estimation technique in compressive and full measurement cases. The compressive measurement case for the correlated MMV scenario corresponds to the signal model given by (4.2) while the corresponding full measurement case is given by $\mathbf{Y} = \sqrt{p}\Theta^{1/2}\mathbf{BX} + \mathbf{Z}$.

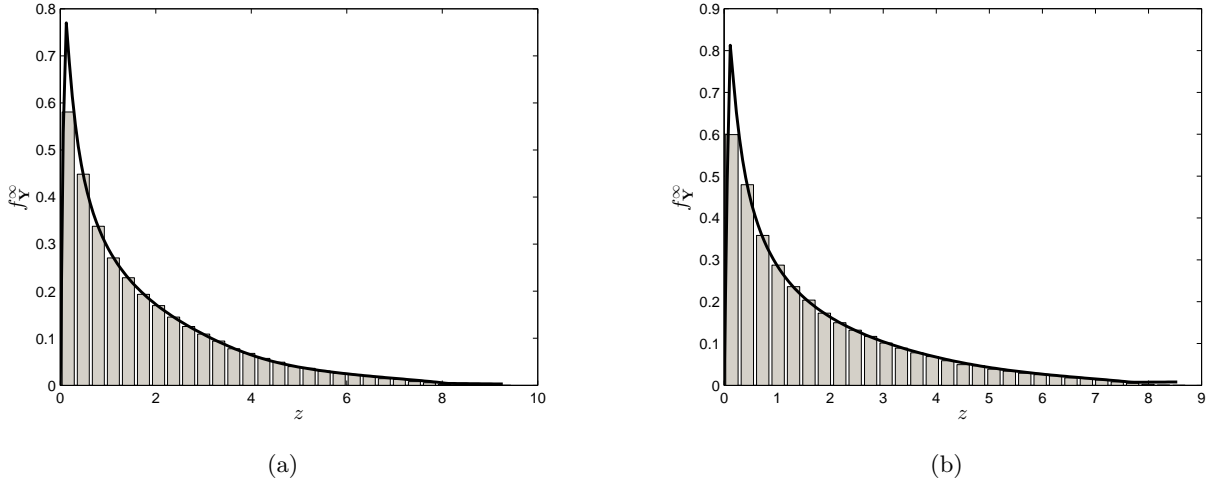


FIGURE 4.9: Theoretical and simulated eigenvalue distributions of $\hat{\mathbf{R}}_Y(N)$ ($\varsigma = 0.6, \rho = 0.8, \sigma = 0.6, N = 100, \text{SNR} = 2 \text{ dB}$) (a) $\mathbf{Y} = \mathbf{AU}\sqrt{p}\Theta^{1/2}\mathbf{BX} + \mathbf{Z}$ (b) $\mathbf{Y} = \mathbf{AU}\sqrt{p}\mathbf{BX} + \Theta^{1/2}\mathbf{Z}$

TABLE 4.2: Lookup table for SNR estimation for correlated MMV scenario ($\varsigma = 0.6, \rho = 0.8, \sigma = 0.6, \text{SNR} = 2 \text{ dB}$)

SNR, dB	$\lambda_{\max}(p\hat{\mathbf{R}}\Theta\hat{\mathbf{R}}_1 + \hat{\mathbf{R}}_Z)$	$\lambda_{\max}(p\Theta\hat{\mathbf{R}}_1 + \hat{\mathbf{R}}_Z)$
5	13.03	10.83
4	10.64	8.91
2	7.26	6.31
0	5.28	4.91
-2	4.38	4.34
-4	4.06	4.08
-6	3.95	3.97

To validate our theoretical analysis presented in Section 4.3.3 and Section 4.3.2, we plot the theoretical and simulated eigenvalue distributions of $\hat{\mathbf{R}}_Y(N)$ in Fig. 4.9 (a) for the correlated MMV scenario and (b) for the correlated noise scenario with parameters $\rho = 0.8, \sigma = 0.6, N = 100, \text{SNR} = 2 \text{ dB}$. The theoretical a.e.p.d.f. for the correlated MMV scenario was obtained by using (4.23) and (3.34), and for the correlated noise case was found by using the Stieltjes transform obtained using the procedure mentioned in Section 4.3.2. It can be noted that the theoretical curve perfectly matches with the simulated one for both the cases. For compressive SNR estimation purpose, we provide a lookup table for the correlated MMV case, where the MEs of $\hat{\mathbf{R}}_Y$ are provided for different values of p for compressive and full measurement cases. Then the value of p can be estimated using this table based on the SNR estimation method described in Section 4.3.4. For example, if the ME of an instantaneous $\hat{\mathbf{R}}_Y$ is 7.26 for the compressive measurement case, it can be estimated that the common receive SNR in all the channels over the considered wideband spectrum is 2 dB. The values of SNR for any intermediate values of λ_{\max} can be found by using a suitable interpolation method.

Figure 4.10 presents the normalized MSE versus SNR for the correlated MMV scenario considering the presence and the absence of correlation knowledge at the CR receiver. From this figure, it can be noted that the normalized MSE is higher for the compressive case than for the full measurement case, decreases with the SNR for both the cases and remains almost constant for higher SNR values. While comparing the cases with and without correlation knowledge, it can be observed that the compressive case with correlation knowledge has almost 0.65 % less normalized MSE than that of the case without correlation knowledge at $\text{SNR} = 2 \text{ dB}$. Therefore, it can be concluded that the correlation knowledge improves the SNR estimation performance under the considered correlated scenario in the compressive settings. The improvement SNR estimation performance with the correlation knowledge for the full measurement case without considering sparseness has been illustrated in [65].

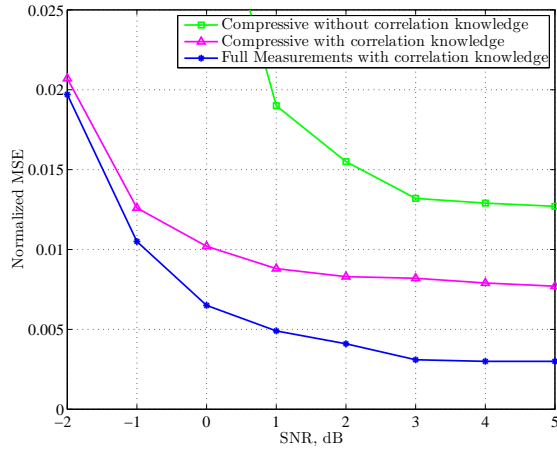


FIGURE 4.10: Normalized MSE versus SNR for the correlated MMV scenario ($\varsigma = 0.6, \rho = 0.8, \sigma = 0.6, N = 100$)

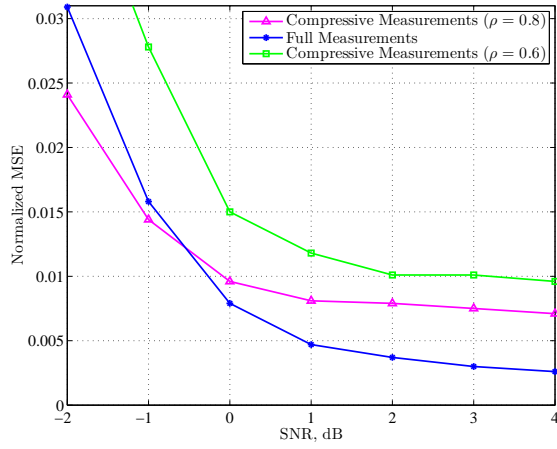


FIGURE 4.11: Normalized MSE versus SNR for the correlated noise scenario ($\varsigma = 0.6, \sigma = 0.6, N = 100$)

Similarly, Fig. 4.11 depicts the normalized MSE versus SNR for the correlated noise scenario for both the compressive and full measurement cases assuming correlation knowledge at the CR receiver. It can be observed that for SNR = 1 dB, the normalized MSE for the full measurement case is almost 5 %, for the compressive measurement case is nearly 8 % while considering $\rho = 0.8$ and it's almost 1.2 % while considering $\rho = 0.6$. Furthermore, our simulation results show that at lower values of SNR, the compressive case performs slightly better than the full measurement case in terms of the normalized MSE (below SNR value of -0.5 dB in Fig. 4.11) and the normalized MSE remains almost constant for higher SNR values. Moreover, it can be deduced that the compressive case with $\rho = 0.8$ has to sacrifice almost 3 % normalized MSE in comparison to the full measurement case at SNR = 1 dB and this estimation error increases with the decrease in the value of ρ i.e., increase in the compression. On the other hand, the advantage is that $((1 - \rho) * 100)$ % saving can be obtained in terms of hardware resources in comparison to the full measurement case.

Discussion: In this work, firstly, the theoretical expressions for a.e.p.d.f. of the measured signal's covariance matrix have been derived for two different correlated scenarios using an RMT-based approach. Subsequently, an estimation technique based on the ME of the measured signal's covariance matrix has been presented for estimating the SNR of the PU signals over a wideband spectrum. The performance of the proposed method has been evaluated in terms of the normalized MSE. It can be concluded that the proposed technique can reliably estimate the SNR for the considered scenarios even with the compressive measurements and the correlation knowledge at the CR receiver improves the SNR estimation performance. Further, it has been noted that there exists a tradeoff between the hardware sensing cost and the estimation error while using compressive measurements.

4.4 Performance Analysis

Most of the existing techniques in the literature study the throughput analysis problem considering a single radio channel. However, in practice, a CR needs to operate over a wideband channel. For this purpose, we extend the throughput analysis of a single radio channel for the wideband scenario. In this context, we consider multiple carriers over the considered wideband channel. Several Nyquist and sub-Nyquist wideband sensing approaches have been investigated in the literature [29]. The existing Nyquist wideband sensing approaches can be categorized into: (i) Wavelet detection, (ii) Multiband joint detection, (iii) Sweep-tune detection, and (iv) Filter bank detection. Out of these approaches, the first two approaches require very high-rate ADCs with high resolution and reasonable power consumption, which are difficult to implement in practice with the existing technologies [29]. In the sweep-tune approach, the sensor can use either a tunable Band Pass Filter (BPF) or tunable Local Oscillator (LO) in order to sweep across the frequency range of interest. Whereas, in the filter bank based detection, a bank of prototype filters with different shifted central frequencies can be used to sense the wideband signal [392]. Herein, we analyze the total throughput of the sweep-tune and the filter bank-based approaches.

4.4.1 Sweep-tune Approach

Let us divide the wider bandwidth W Hz into M number of sub-bands, each sub-band having bandwidth of W/M Hz. A wideband CR is assumed to operate over the entire W bandwidth. We assume that instead of sensing the whole bandwidth at a time, a CR receiver senses one sub-band at a time and then sweeps to another band in the next time slot. While using the periodic SS approach, the sensing duration τ in each frame can be divided into M number of slots with each slot having τ_m duration i.e., $\tau_m = \tau/M$. The periodic SS-based and the simultaneous SS/Tx-based frame structures with the multiple sub-band approach are shown in Figs. 4.12 and 4.13 respectively. In each specified time slot, the CR senses the presence or absence of an active primary carrier in each individual sub-band. Subsequently, the CR transmits over all the carriers during the data transmission phase. In this case, the sensing slot for each sub-band is $1/M$ of the total sensing slot allocated for one secondary frame. Based on the sensing decision of each individual sub-band, the CR transceiver applies its power allocation policy in such a way that all the vacant carriers are allocated with the full power and the occupied carriers are allocated with the reduced power considering per carrier power constraints. The reduced power is calculated based on the estimated primary SNR and the interference threshold of the PUs. The P_f expression for the m -th sub-band while using the ED technique is given by

$$P_f^{(m)}(\lambda_{th}, \tau_m) = Q \left(\left(\frac{\lambda_{th}}{\sigma_z^2} - 1 \right) \sqrt{\tau_m f_s} \right). \quad (4.33)$$

Similarly, the expression for P_d can be written as

$$P_d^{(m)}(\lambda_{th}, \tau_m) = Q \left(\left(\lambda_{th}/\sigma_z^2 - \gamma_p - 1 \right) \sqrt{\frac{\tau_m f_s}{2\gamma_p + 1}} \right). \quad (4.34)$$

The achievable secondary throughput of each sub-band for the periodic SS approach is given by

$$R^{(m)}(\lambda_{th}, \tau_m) = R_0^{(m)}(\lambda_{th}, \tau_m) + R_1^{(m)}(\lambda_{th}, \tau_m), \quad (4.35)$$

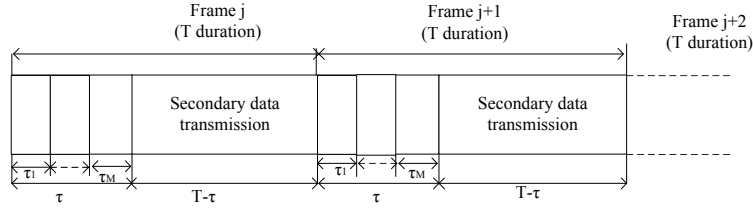


FIGURE 4.12: Frame structure of periodic SS based CR for wideband scenario

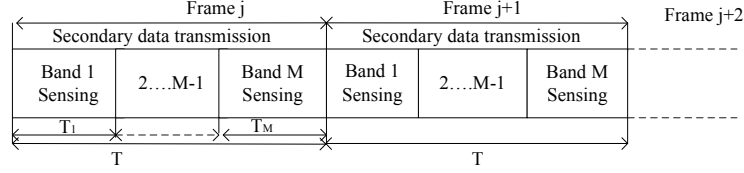


FIGURE 4.13: Frame structure of full duplex SS based CR for wideband scenario

where the values of $R_0^{(m)}(\lambda_{th}, \tau_m)$ and $R_1^{(m)}(\lambda_{th}, \tau_m)$ can be calculated using the following expressions

$$\begin{aligned} R_0^{(m)}(\lambda_{th}, \tau_m) &= \frac{T - \tau}{T} (1 - P_f(\lambda_{th}, \tau_m)) P(H_0) C_0^{(m)}, \\ R_1^{(m)}(\lambda_{th}, \tau_m) &= \frac{T - \tau}{T} (1 - P_d(\lambda_{th}, \tau_m)) P(H_1) C_1^{(m)}, \end{aligned} \quad (4.36)$$

where $C_0^{(m)}$ and $C_1^{(m)}$ denote the secondary throughput of m -th sub-band under H_0 and H_1 hypotheses respectively.

Considering the same target \bar{P}_d for each sub-band, the total throughput of the wideband CR is given by

$$R_T = \sum_{m=1}^M R^{(m)}(\lambda_{th}, \tau_m). \quad (4.37)$$

Similarly, the total achievable secondary throughput for the simultaneous SS/Tx approach can be written as

$$R_T = \sum_{m=1}^M R^{(m)}(\lambda_{th}, T_m), \quad (4.38)$$

where $T_m = T/M$ is the sensing slot for one sub-band under the simultaneous SS/Tx approach. The difference in the secondary throughput given by (4.37) and (4.38) arises due to the difference in the sensing time. The expression for $R^{(m)}(\lambda_{th}, T_m)$ is given by

$$R^{(m)}(\lambda_{th}, T_m) = R_0^{(m)}(\lambda_{th}, T_m) + R_1^{(m)}(\lambda_{th}, T_m), \quad (4.39)$$

where the values of $R_0^{(m)}(\lambda_{th}, T_m)$ and $R_1^{(m)}(\lambda_{th}, T_m)$ can be calculated as

$$\begin{aligned} R_0^{(m)}(\lambda_{th}, T_m) &= (1 - P_f(\lambda_{th}, T_m)) P(H_0) C_0^{(m)}, \\ R_1^{(m)}(\lambda_{th}, T_m) &= (1 - P_d(\lambda_{th}, T_m)) P(H_1) C_1^{(m)}. \end{aligned} \quad (4.40)$$

4.4.2 Filter-bank based Approach

In this wideband approach, the sensing slot for each sub-band is same as the sensing slot of one frame i.e., $\tau_m = \tau$ since all the sub-bands are sensed simultaneously using a parallel filter bank structure. For

the periodic SS approach, the expression for the total throughput can be written as

$$R_T = \sum_{m=1}^M R^{(m)}(\lambda_{th}, \tau), \quad (4.41)$$

where the value of $R^{(m)}(\lambda_{th}, \tau)$ is given by

$$R^{(m)}(\lambda_{th}, \tau) = R_0^{(m)}(\lambda_{th}, \tau) + R_1^{(m)}(\lambda_{th}, \tau), \quad (4.42)$$

where the values of $R_0^{(m)}(\lambda_{th}, \tau)$ and $R_1^{(m)}(\lambda_{th}, \tau)$ can be calculated using the following expressions

$$\begin{aligned} R_0^{(m)}(\lambda_{th}, \tau) &= \frac{T - \tau}{T} (1 - P_f(\lambda_{th}, \tau)) P(H_0) C_0^{(m)}, \\ R_1^{(m)}(\lambda_{th}, \tau) &= \frac{T - \tau}{T} (1 - P_d(\lambda_{th}, \tau)) P(H_1) C_1^{(m)}. \end{aligned} \quad (4.43)$$

Similar analysis follows for the simultaneous SS/Tx approach.

4.4.3 Numerical Results

The simulation set up for the wideband scenario same as presented in Section 3.4.3 except the fact that we consider different frame structures as indicated in Figs. 4.12 and 4.13. Herein, we consider 5 sub-bands within the considered bandwidth, each sub-band having bandwidth of 6 MHz. Figure 4.14 depicts the achievable throughput versus sensing time for the sweep-tune approach-based wideband scenario with parameters ($M = 5$, $I_T = -130$ dBW, $T = 100$ ms, $\text{SNR}_s = 20$ dB). From the figure, it can be noted that the optimum sensing time is 8 ms for the traditional periodic SS only approach and 9 ms for the periodic SS based hybrid approach. It can be noted that the secondary throughput with the simultaneous SS/Tx approach does not vary with the sensing time as in the narrowband context. Similarly, Fig. 4.15 presents the achievable throughput versus sensing time for filter bank detection-based wideband scenario with parameters ($M = 5$, $I_T = -130$ dBW, $T = 100$ ms, $\text{SNR}_s = 20$ dB). From the figure, it can be depicted that there occurs sensing-throughput trade-off for the conventional and hybrid periodic SS based approach and the optimum sensing time for both cases is achieved at 2.5 ms, which is equal to the optimum sensing time for the narrowband case.

While comparing the results in Fig. 4.14 and Fig. 4.15, the optimum sensing time is higher for the sweep-tune approach than for the filter bank based approach. This difference comes due to that fact that the probability of false alarm in sweep-tune approach is worse due to division of total sensing slot into mini-slots. On the other hand, the filter bank-based approach is more complex than the sweep-tune approach since it requires the number of parallel RF chains equal to the number of sub-bands. Figures 4.16 and 4.17 depict the secondary achievable throughput versus interference threshold for sweep-tune and filter bank based approaches respectively. It can be noted that the secondary throughput increases with the interference threshold for the proposed hybrid approach with both periodic SS and simultaneous SS/Tx schemes.

While comparing the considered wideband approaches, it can be depicted that the filter bank-based approach requires much less sensing time in comparison to the sweep-tune approach but it is highly complex from implementation perspectives. Therefore, there exists a tradeoff between the performance gain that can be achieved by using a wideband approach and the implementation complexity from practical perspectives.

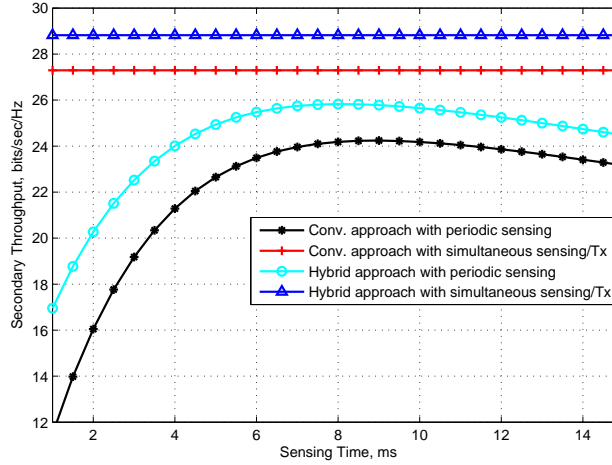


FIGURE 4.14: Secondary throughput versus sensing time for sweep-tune approach based wideband scenario ($I_T = -130$ dBW, $\bar{P}_d = 0.9$, $T = 100$ ms, $\text{SNR}_p = -24$ dB, $\text{SNR}_s = 20$ dB)

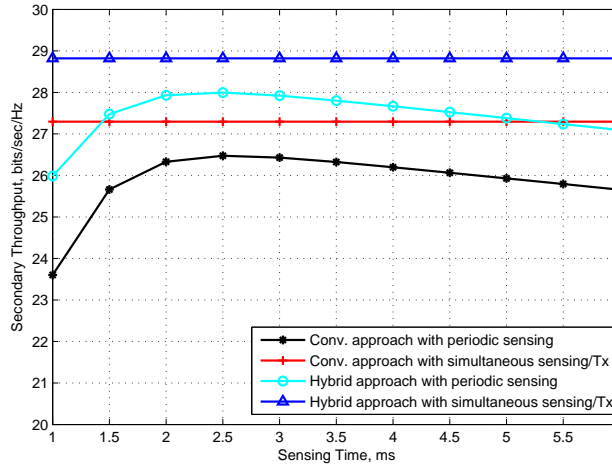


FIGURE 4.15: Secondary throughput versus sensing time for filter bank detection based wideband scenario ($I_T = -130$ dBW, $\bar{P}_d = 0.9$, $T = 100$ ms, $\text{SNR}_p = -24$ dB, $\text{SNR}_s = 20$ dB)

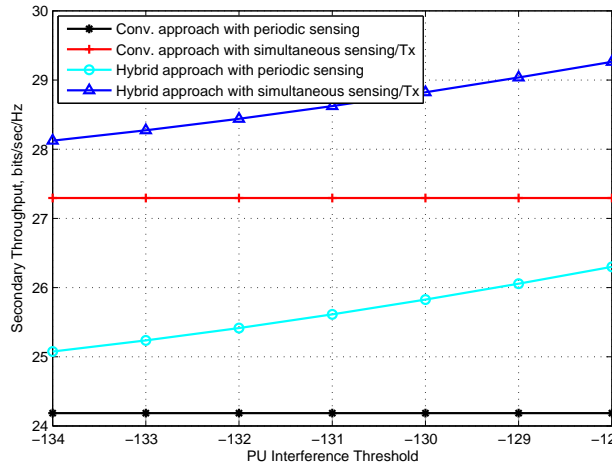


FIGURE 4.16: Secondary throughput versus interference threshold for sweep-tune approach based wideband scenario ($\tau = 8$ ms, $\bar{P}_d = 0.9$, $T = 100$ ms, $\text{SNR}_p = -24$ dB, $\text{SNR}_s = 20$ dB)

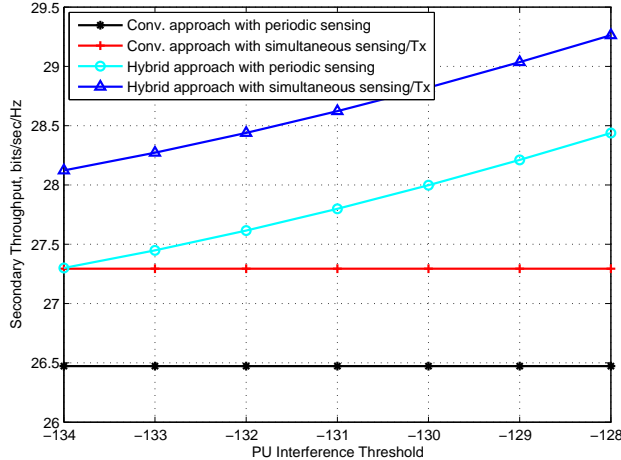


FIGURE 4.17: Secondary throughput versus interference threshold for filter bank detection based wideband scenario ($\tau = 2.5$ ms, $\bar{P}_d = 0.9$, $T = 100$ ms, $\text{SNR}_p = -24$ dB, $\text{SNR}_s = 20$ dB)

4.5 Chapter Conclusion

In this chapter, firstly, we have provided various challenges for implementing a wideband cognitive transceiver considering the aspects of wideband signal acquisition and wideband transmission. Subsequently, in Section 4.2, a compressive SOE problem has been studied for a wideband CR receiver considering the sparsity in the carrier occupancy over the considered wideband spectrum. It should be noted that the SOE needs to find the number of non-zero elements of a sparse vector and does not need to have the exact knowledge of their amplitudes or positions. As mentioned in Chapter 1, it has an important application in adjusting a suitable sampling rate for CS-based receivers in order to reduce the sensing hardware cost. To tackle this problem in this thesis, analytical expressions for the Stieltjes transforms of the measured signal's covariance matrix have been derived using an MMV model for the following scenarios: (i) constant received power, (ii) varying received power, and (ii) correlated MMV. The constant power scenario is simple from analytical perspectives but may not be realistic in practical scenarios since the received power across different carriers might be different. Although uniform distribution over a certain power range would be the most suitable choice to model the varying power scenario. Due to its analytical intractability, a modified semicircular distribution is followed while analyzing the varying power scenario. Subsequently, an estimation technique based on the ME of the measured signal's covariance matrix has been proposed for estimating the sparsity order of the PU occupancy over a wideband spectrum. Two types of errors that may occur during the estimation process i.e., randomness of the ME and residual error due to interpolation process, have been considered while evaluating the performance of the estimation process in terms of the normalized SOEE. It can be concluded that the proposed technique can reliably estimate the sparsity order for the considered scenarios even with the compressive measurements. More specifically, it has been noted that the normalized SOEE for the compressive measurement case is less than 3 % and for the full measurement case is less than 2.8 % for all the considered cases with the compression ratio (ρ) of 0.8 up to the sparsity order (σ) of 0.5. Further, it has been noted that the normalized SOEE increases with the decrease in the value of ρ i.e., increase in the compression. On the other hand, the advantage is that $((1 - \rho) * 100)$ % saving can be obtained in terms of hardware resources in comparison to the full measurement case. Thus it can be concluded that there exists a tradeoff between hardware sensing cost (number of measurements) and the estimation error while using compressive measurements.

Furthermore, in Section 4.3, similar analysis and estimation approaches have been applied for the case of compressive SNR estimation under the following two scenarios: (i) correlated noise, and (ii) correlated MMV. From the presented results, the normalized MSE is found to be higher for the compressive case than for the full measurement case, decreases with the SNR for both cases and remains almost constant beyond the SNR value of 3 dB (correlated MMV case). While comparing the cases with and without

correlation knowledge, it has been observed that the compressive case with the correlation knowledge has almost 0.65 % less normalized MSE than that of the case without correlation knowledge at SNR value of 2 dB. Therefore, it can be concluded that as in the non-compressive scenario, the correlation knowledge helps to improve the SNR estimation performance under the considered correlated scenario in compressive settings. In addition, a similar estimation-cost tradeoff has been noted while using compressive measurements for the SNR estimation purpose.

Moreover, in Section 4.4, throughput analysis carried out in Section 3.4 has been extended for wideband scenarios considering sweep-tune and filter-bank based approaches. The performances of these wideband sensing schemes has been carried out in terms of the sensing-throughput trade-off. It has been noted that the optimum sensing time is higher for the sweep-tune approach than for the filter bank based approach. This is due to the higher value of P_f in sweep-tune approach resulted from the division of total sensing slot into mini-slots. However, filter-bank based approach is more complex than the sweep-tune approach since it requires the number of parallel RF chains equal to the number of sub-bands. Therefore, it can be concluded that there exists a tradeoff between the performance gain that can be achieved by using a wideband approach and the implementation complexity from practical perspectives.

Chapter 5

Cognitive Satellite Communications

In this chapter, starting with the importance of SatCom systems, we highlight the main aspects of cognition in SatComs considering the possible frequency bands for spectral coexistence of hybrid/dual cognitive SatComs and provide a detailed overview on the existing literature related to the following three categories: (i) hybrid satellite-terrestrial systems, (ii) dual satellite systems, and (iii) spectrum sharing techniques. Further, we propose possible spectral coexistence scenarios for cognitive SatComs considering the following two main categories: (i) hybrid satellite-terrestrial coexistence, and (ii) dual satellite coexistence. Moreover, we provide the mapping of various CR techniques to the considered scenarios. Additionally, we provide the aspects of spectrum regulation and standardization activities for cognitive SatComs. Finally, we provide a discussion on various challenges from technical, regulatory and business perspectives for the effective implementation of cognitive SatComs. Some of the contributions included in this chapter have been published in [100, 101, 106].

5.1 Background

SatCom has played a key role in wireless communication field due to its wide area coverage and the ability of providing new services with different characteristics than those of terrestrial networks. It allows the extension of the coverage area of services carried today on terrestrial fixed and mobile networks. Further, SatCom has a crucial role in operations carried out to save living creatures in case of emergency situations [86]. More specifically, it has become a key communication mechanism to provide broadcast services/applications to wider coverage area. In addition, satellite technology has made it economically feasible to bring broadband communications to sparsely populated remote regions, improving access to medical, education, e-government and other services that are expensive to provide by other means. Therefore, it has played an important role in bridging the digital gap in rural communities and for economic and social development of these regions. Moreover, SatCom is the only viable option for many services in a wide range of sectors such as land mobile, aeronautical, maritime, transports, military, rescue and disaster relief, etc. Additionally, it can be an important solution to address the demand of emerging applications such as HDTV and broadband internet access.

The terrestrial wireless communication technology is advancing rapidly but at a certain point gets limited by its coverage range. Different fundamental physical constraints such as power requirements, terrain and infrastructure obstructions and antenna types etc. for wide area coverage may cause the terrestrial wireless communication to be dependent on SatComs [90]. The direct access of satellite by small, portable and even handheld terminals has been possible due to the introduction of different technologies for multi-spot beam antennas, onboard processing, and low noise receivers. However, SatCom systems have to face several challenges such as high initial investment, requirement of careful planning, capacity limitations, long manufacturing and deployment period. Further, to remain competitive with

terrestrial networks, satellite networks must provide new services and deal with various challenges such as improving reliability, efficiency, coverage and reducing costs. Several new services have emerged using SatCom technology. Aeronautical and maritime services have already been established. Further, vehicular services for cars, trains and services for sparsely populated areas are possible with the help of this technology. Moreover, the convergence of mobile, fixed and broadcasting systems with the possibility of co-existence of future satellite networks with terrestrial systems is an important research topic [89]. In this context, the hybrid/integrated system is considered as an important research field and is investigated in various literature [86, 87, 89, 90]. SatCom plays a vital role in building such heterogeneous architectures through hybrid and integrated satellite/terrestrial paradigms. Hybrid networks may coexist in the same spectrum in different ways such as two terrestrial networks or two satellite networks or satellite-terrestrial networks.

As in terrestrial systems, satellite systems are also facing the spectrum scarcity problem due to continuously increasing demand for broadcast, multimedia and interactive services. As mentioned before in Chapter 1, exploring suitable spectrum sharing mechanisms, which can enhance the spectrum utilization of the available spectrum while guaranteeing sufficient QoS to the satellite users, is becoming a key issue. In this direction, we study the importance of cognition in SatComs and various possible coexistence scenarios considering the following two main categories: (i) Hybrid satellite-terrestrial coexistence, and (ii) Dual satellite coexistence. The hybrid coexistence scenario can be beneficial to both satellite and terrestrial operators depending on which system is primary. For example, C-band spectrum is primarily licensed for FSS satellites and terrestrial cellular system can take advantage of this spectrum by operating in a secondary way. On the other hand, Ka-band spectrum 17.7 – 19.7 GHz is primarily licensed for terrestrial FS systems and the FSS satellites can operate in a secondary way if they can provide sufficient protection to the primary FS links. The details on hybrid satellite coexistence are provided in Section 5.4.1 and various enabling techniques for this coexistence are studied in Chapter 6 of this thesis.

The concept of dual satellite coexistence is motivated by several aspects such as limited satellite spectrum, orbital congestion of GEO satellites, high traffic demand in a certain coverage area, and the coexistence of two satellites for a long period during the replacement phase as highlighted in Chapter 1. Future multibeam satellites may coexist with the conventional monobeam satellite in the same coverage area in order to enhance the overall spectral efficiency of the system. These coexisting satellites can be used for providing different services to same/different categories of users over the same coverage area. Further, two multibeam satellites having different beampatterns can operate over the same spectrum with the help of proper coordination and interference avoidance/mitigation mechanisms. Moreover, LEO/MEO satellites can coexist with the GEO satellites in the same spectrum over the same coverage area and inline interference may be a serious issue in certain cases [393]. As an example, the coexistence of O3b and GEO satellite operating over the same spectrum may cause inline interference problem near the equatorial region, thus creating the need of effective CR approach to mitigate this interference. The details on dual satellite coexistence scenario are provided in Section 5.4.1 and enabling techniques for this coexistence are studied in Chapter 7 of this thesis.

5.2 Cognition in Satellite Communication

In this section, starting with the current frequency allocation for satellite services, we provide various aspects of cognition in SatComs and discuss several solutions for enhancing the spectral efficiency by referring to the existing literature. In this thesis, we define cognitive SatCom as an advanced communication technology which allows the coexistence of different satellite and terrestrial networks or two different satellite networks within the same spectrum by employing one of the suitable CR techniques. Currently, SatCom is being used in various applications such as Direct To Home (DTH), Very Small Aperture Terminals (VSATs), free and pay TV programme distribution, mobile services (MobileSat, Iridium, Globstar etc.), Satellite News Gathering (SNG), defense, radionavigation (GPS,

TABLE 5.1: Possible Frequency bands for spectral coexistence of hybrid satellite-terrestrial and dual satellite networks

Freq. Band	Link	Freq. Range (GHz)	Primary	Secondary	System Type
S	Uplink	2.17-2.20	Sat/Terr	Sat/Terr	Vehicular, Sensor Networks, Handheld
S	Uplink	1.98-2.01	Sat	Terr	Vehicular, Sensor Networks, Handheld
C	Uplink	3.4-3.8	Terr	Sat	Fixed, Nomadic, Vehicular
Ku	Uplink	13.75-14.5	Sat1	Sat2	Fixed, Nomadic
Ku	Downlink	10.7-12.75	Sat1	Sat2	Fixed, Nomadic
Ka	Uplink	27.5-29.5	Terr/Sat	Sat	Fixed, Nomadic, Maritime, Aeronautical, Interactive TV
Ka	Downlink	17.7-19.7	Sat	Terr/Sat	Fixed
Ka	Downlink	17.3-17.7	BSS Feeder	HDFSS	Fixed

TABLE 5.2: Current frequency allocation in Ka band segment (27.5 – 30 GHz uplink, 17.3 – 20.2 GHz downlink)

Frequency Range	Description
29.5 – 30 GHz (uplink) 19.7 – 20.2 GHz (downlink)	Exclusive band for High Density FSS (HDFSS)
27.5-29.5 GHz (uplink) 17.7-19.7 GHz (downlink)	Shared allocation to FS systems (Co-primary) and FSS systems
17.3-17.7 GHz	Shared allocation to FSS and BSS (Co-primary) systems (used by BSS feeder links)
28.6-29.1 GHz (uplink) 18.8 – 19.3 GHz (downlink)	Equal right to both GEO and NGEO satellite systems (originally intended for Teledesic)
29.1 – 29.5 GHz (uplink) 19.3 – 19.7 GHz (downlink)	Equal right to both GEO and NGEO satellite systems (used by NGEO feeder links e.g., Iridium)

Galileo etc.), earth observation, vehicular services, aeronautical maritime services, emergency/disaster relief communications, corporate networks, and private internet access etc. Depending on the type of the services, satellite systems can be divided into [394]: (i) FSS, (ii) MSS, (iii) Broadcasting Satellite Service (BSS), (iv) Earth Exploration Satellite Service (EES), (v) Space Research Service (SRS), (vi) Amateur Satellite Service (ASS), (vii) Radiodetermination Service, (viii) Inter-Satellite Service (ISS), and (iv) Space Operation Service (SOS). Among these systems, the main telecommunication-related systems are FSS, MSS and BSS.

In the current spectrum allocation policy, different frequency bands are allocated to different satellite services. The satellite bands are allocated either in the exclusive basis to a certain service or in the shared basis to different services. Table 5.1 provides possible frequency bands for the spectral coexistence of hybrid satellite-terrestrial and dual satellite networks. Currently, these bands are allocated to several terrestrial and satellite systems. As an example, we present current frequency allocations in (27.5 – 30 GHz uplink, 17.3 – 20.2 GHz downlink) segment of the Ka band in Table 5.2. It can be noted that some of the frequencies are exclusively allocated to FSS services and some of them are allocated in the shared basis to FSS and terrestrial FS systems¹. Further, in some of the frequencies, GEO and NGEO satellites have equal rights. In order to facilitate the coordination between different GEO/NGEO satellite systems, ITU-R footnote 5.523A related to the bands 17.8 – 19.3/28.6 – 29.1 GHz specifies that the coordination is subject to the Radio Regulations (RR) 9.11A i.e., priority based on the date of filing. In the rest of the frequency band, Effective Power Flux Density (EPFD) limits specified in the RR Article 22 should be respected for coordination with the already existing satellite systems.

As the demand for satellite services increases, the need for frequency coexistence between the new satellite systems with the already existing terrestrial/satellite networks increases rapidly due to the

¹The terminologies FSS, FS, MSS etc. are ITU definitions.

limitation in the usable satellite spectrum. The same applies for the case of terrestrial wireless networks. As detailed later in Section 5.5, satellite networks can coexist with terrestrial networks and other satellite networks using advanced dynamic access and interference mitigation techniques. This coexistence can be in the space and time domains or any other possible domains such as polarization, radiation pattern, etc. In this context, suitable CR techniques can be investigated in different uplink and downlink satellite bands, and in the bands which are allocated to the terrestrial services in the co-primary basis. Satellite and terrestrial networks can be considered as primary and secondary systems respectively or viceversa. In many scenarios, satellite transmission should be given high priority mainly due to its adverse transmission conditions and poor indoor coverage. However, in some scenarios, point to point terrestrial microwave links can be used as the primary link and the satellite link can be used as secondary by sharing the same microwave frequency band. For example, VSATs, which are commonly used for providing services in rural areas, can be used on secondary basis with a point to point microwave link being the primary one. Another application scenario can be Ultra Wideband (UWB) SatCom, in which satellite services can use the unoccupied bands of terrestrial multiband UWB spectrum on the secondary basis [395]. If some of the bands are exclusive and the rest are shared within the considered bandwidth range of interest, the carriers can be allocated dynamically in such a way that the exclusive bands will be allocated to the worst-case users and the shared bands will be allocated to other users in order to enhance the overall system throughput and the system availability.

Similar to the terrestrial CR [154, 155], a satellite CR system should be able to perform following four functions: (i) SS, (ii) spectrum management, (iii) spectrum sharing, and (iv) spectrum mobility. While sensing the spectrum, a CR user i.e., SU should monitor the available spectrum bands, capture their information, and then detect spectrum holes. Based on the spectrum availability, the SU can be allocated to a channel with the help of efficient spectrum management techniques. There may be multiple CR users trying to access the same spectrum. To manage this situation, CR network access should be coordinated to prevent multiple users seeking the overlapping portions of the spectrum, called spectrum sharing. If the specific portion of the spectrum used by a CR user is required by a PU, the CR communication must be continued in another vacant portion of the spectrum, called spectrum mobility. If none of the vacant bands are available at that time, the frequencies in the exclusive band can be allocated to the CR users. Based on the employed CR techniques, both primary and secondary systems can communicate simultaneously with the users without the need of orthogonalization (i.e., frequency division), hence minimizing the need of purchasing expensive bandwidth.

Cognitive SatCom technology can provide several advantages to industries, operators and consumers. From the global perspective, the overall spectrum usage efficiency is maximized. From the industrial point of view, a mobile market can be revitalized by the advent of a new CR equipment market and there may occur a high level of competition with low entry barriers. From the operators' perspective, they can create new revenue streams from secondary trading as well as improve the utilization of the spectrum resource that they already own. Further, consumers can be provided with a personalized and optimized mobile and broadband data service at low cost. This technology can be beneficial to both satellite and terrestrial operators depending on the scenarios. If the satellite link can be designed in a secondary way by using the spectrum licensed to the terrestrial systems, the satellite operators can get benefits in terms of the additional spectrum, hence overall system throughput. As an example, the possible deployment of Ka-band FSS terminals in the segment of the Ka-band (17.7 – 19.7 GHz downlink, 27.5 – 29.5 GHz uplink), which is primarily licensed for the terrestrial FS systems, will allow satellite operators to reuse an additional 4.4 GHz spectrum in addition to the currently available exclusive band (500 MHz in the uplink, 500 MHz in the downlink). Similarly, terrestrial systems can be designed in secondary way in order to take advantage of satellite spectrum e.g., the deployment of WiMax/LTE systems in the C-band, which is primarily licensed for the terrestrial system. In this thesis, we consider cognitive SatComs not only from the perspectives of the satellite operators but also from the mutual perspectives so that overall spectral efficiency within a certain band can be enhanced.

As mentioned in Chapter 1, cognitive SatCom has recently received important attention in different research projects and communities. The recent European Space Agency (ESA) project “ACROSS”

studied the applicability of CRs for SatComs considering the following scenarios [95]: (i) secondary use of satellite spectrum by the terrestrial system, (ii) secondary use of terrestrial spectrum by the satellite system, and (iii) a hybrid scenario where terrestrial network coverage is expanded by the use of satellite spots. In the first scenario, two separate studies have been made considering a Digital Video Broadcasting-Satellite to Handheld (DVB-SH) system operation below 3 GHz as a primary system and a FSS satellite system as a primary system. Further, the ongoing EU FP7 project CoRaSat is investigating the possibilities of applying CR techniques in the following three different scenarios [333]: (i) the coexistence of BSS feeder links and FSS downlink in the Ka band (17.3 – 17.7 GHz), (ii) the coexistence of FSS downlink with the terrestrial FS links in the Ka band (17.7 – 19.7 GHz), and (iii) the coexistence of FSS uplink with the FS links in Ka band (27.5 – 29.5) GHz.

The CR research in the satellite paradigm is different from the terrestrial context due to the following factors: (i) propagation channel (large path loss, rain fading and shadowing losses), (ii) directivity and elevation angle, (iii) larger carrier bandwidth, (iv) wide coverage area (v) power imbalance, (vi) uplink/-downlink asymmetry, (vii) polarization as an additional dof, (ix) limited onboard power and already existing intra/inter satellite interferences, (x) dynamic SS challenging due to weak signal levels, (xi) difference in spectrum occupancy, (xii) need of wideband sensing, (xiii) satellite/terrestrial terminals' sensitivity levels, (xiv) absence of feedback links in broadcasting satellites, (xv) special propagation characteristics of GEO terminals that they always face towards the equator, and (xvi) requirement of cross border agreement. More specifically, the following features, which are unique to SatComs, have differentiated the cognitive SatCom research area from the terrestrial one.

- Polarization and elevation angle can be considered as two separate degrees of freedom for enabling the coexistence of satellite and terrestrial networks. Satellite terminals with lower elevation angles tend to receive more interference from other coexisting systems than the satellite terminals with higher elevation angles.
- Implementing dynamic SS in the satellite downlink may be difficult due to large coverage areas and weak signal levels even in case of the multispot coverage.
- Wideband sensing techniques are required for detecting Ku/Ka band satellite signals and several narrowband SS techniques investigated in the context of a terrestrial CR may not be applicable.
- The directional characteristics of fixed satellite terminals can be exploited while investigating suitable coexistence techniques with the terrestrial systems.
- There exists a significant difference in the receiver sensitivity levels of the terrestrial and satellite receivers, and this can be utilized for allowing hybrid satellite-terrestrial coexistence in some scenarios.
- The resource management problem for satellite CR networks differs from the one in isolated wireless systems since resources are not uniform and they may not belong to the same operator.
- Spectrum occupancy in satellite systems is more static than in the terrestrial systems. This feature can be considered into account while designing a suitable CR approach in order to utilize the underutilized spectrum effectively. Furthermore, in most of the cases, shared frequency bands are less occupied than the exclusive satellite bands and different strategies can be followed in designing CR techniques for the systems operating in the shared and exclusive bands.

5.3 Related Literature

Several coexistence scenarios of satellite and terrestrial networks have been considered in the literature. The cases found in the literature mainly fall under three categories, which are described in detail in the following subsections.

5.3.1 Hybrid/Integrated Satellite-Terrestrial Systems

In the field of SatComs, the main available literature related to cognitive techniques has considered hybrid or integrated satellite networks [86–89]. The main difference between hybrid and integrated networks lies on whether both space and terrestrial components use a common spectrum and network or not [86]. In an integrated network, the terrestrial component can be considered as an alternative part of the satellite system in order to serve the mobile users and hence uses the same spectrum allocated to the satellite system. On the other side, in a hybrid network, satellite and terrestrial components may use different networks, frequency bands, and even air interfaces [86]. Further, in a hybrid network, terrestrial gap fillers i.e., repeaters can be employed in order to retransmit the satellite signals locally in non-LoS conditions and a local wireless system can be used to extend the coverage of satellite transmission [396]. While classifying on the basis of their match with the principles of CR techniques, many of hybrid/integrated satellite-terrestrial systems come under the category of underlay and overlay cognitive techniques. Integrated and hybrid networks have the strong potential to be an efficient and cost-effective solution to employ SatComs for mobile users. In this context, the contribution in [86] studies the satellite component of Next Generation Network (NGN) for hybrid and integrated networks taking into account of physical, MAC, and network layers issues as well as traffic engineering issues for the overflow traffic. An architecture of integrated network and a discussion on the technical challenges for its realization has been presented in [89]. In [87], resource management issues in Wireless Heterogeneous Networks (WHNs) are discussed considering the market and business cases for wireless heterogeneity and reflecting the most common radio resource management frameworks. Recently, transmit diversity techniques have been proposed for integrated networks, using repeaters as the ground components having appropriate signal processing capabilities. An efficient diversity technique using Space-Time Coding (STC) for an integrated MSS system has been proposed in [397]. In this system, ground components are terrestrial repeaters that cooperate with the satellite to transmit space-time coded signals. The cooperative diversity concept has been proposed to achieve diversity gain in the uplink of terrestrial systems, where user terminals can not support multiple antennas due to size and other constraints [155]. The synergy between terrestrial and satellite systems can be used to reduce the large fade margins in SatComs operating under fading conditions by implementing multi-radio diversity [88]. Further, there exist some research works in the direction of distributed power allocation for CR systems [398, 399]. Furthermore, power allocation strategies for CR terminals in the context of SatComs have been proposed in [400].

The concept of cognitive satellite-terrestrial radios for hybrid satellite-terrestrial systems has been presented in [90]. The basic idea presented in [90] is that the elevation angle of a satellite station can be exploited as an additional dof in order to allow the spectral coexistence with terrestrial systems. Since a satellite is seen under a high elevation angle (depending on the latitude), proper design of antenna radiation diagrams can reduce the mutual interference and enable cognitive frequency reuse. This can be considered as 3D space-time-frequency utilization rather than 2D time-frequency utilization in terrestrial CR networks [90]. An integrated system composed of a Complementary Ground Component (CGC) and a multibeam satellite based network has been considered in [401], in which both systems are considered to operate in L or S band and are assumed to be controlled by the same resource management module. Satellite system has been considered to be primary and the terrestrial system to be secondary. It has been concluded that satellite frequency can be reused by terrestrial users based on the EZ principle by defining EZs around each satellite spot beam.

In [86], two hybrid satellite-terrestrial wireless network scenarios have been considered. One scenario is SatCom network connected with WiMax terrestrial segment and another scenario is SatCom network with a WiFi terrestrial segment. In the first scenario, the considered DVB-S2 terminal is fixed while the user device is either fixed or nomadic. The satellite is GEO with Multibeam Broadband Satellite (MBS) links based on DVB-S2/-RCS. DVB-S2 has been considered for the forward link and DVB-RCS for the return link in a SatCom network. In the second scenario, the interconnection of a satellite DVB-RCS network with WiFi based on the IEEE 802.11e standard has been considered. In [402],

the considered scenario is constituted by a primary licensed system and a secondary system whose terminals implement cognitive resource allocations. A mobile satellite system compatible with DVB-SH standard [403] has been considered as primary system in the considered scenario and an infrastructured wireless terrestrial network, i.e., all the secondary terminals communicate with a local base station, is considered as a secondary system. These two systems are considered to operate in the L band frequency spectrum (0.39 – 1.55 GHz). Two approaches, namely, heuristic and game theory-based approaches, have been considered for resource allocation purpose. The results have shown that heuristic method achieves higher rates, although it can not be implemented in a distributed way like game theory-based allocation. Furthermore, a satellite/terrestrial integrated mobile communication system has been considered in [404] in which the operating frequency is assumed in between (1980 – 2010) MHz and (2170 – 2200) MHz. Two frequency allocation methods i.e., normal mode and reverse mode, have been studied and it has been concluded that normal mode is advantageous over reverse mode in terms of interference issues. In [405], the interference and the required separation distance between CGC base station and a victim Mobile Earth Station (MES) have been evaluated, which are essential for planning an integrated satellite system deployment under tolerable interference.

The Mobile Body Area Network (MBAN) is a promising solution for ubiquitous monitoring of patients in hospitals for vital signs such as temperature, pressure, blood oxygen, and electrocardiogram wirelessly [327]. MBAN communication becomes limited to transmission of data monitoring, diagnosing, and treating patients. Since continuous dedicated spectrum is not needed for this communication, MBAN and satellite network can coexist in the same frequency bandwidth using proper cognitive techniques. Furthermore, UWB technology has mainly been used for short-range terrestrial communications. There is a possibility that UWB signals can be radiated from satellites to the earth as one type of satellite radio service, leading to UWB SatCom system [395]. The key benefits of UWB system are [406]: low equipment complexity and cost, multi-path immunity, ranging and communication at the same time, low probability of intercept, and low power consumption. In this context, in [395], a FSS system, which employs UWB signals for Ku-band downlink transmission, has been considered considering the terrestrial UWB system as primary. As stated in [90], the UWB system in the (3.1 – 10.6) GHz band can be a good candidate for the introduction of cognitive solutions, given their implicit requirements for coexistence with other wireless systems. However, the following challenges exist while using UWB satellite cognitive communications: (i) higher power as compared to the the power with existing satellite transponders needs to be transmitted, (ii) UWB systems create wideband interference in the downlink, (iii) interference within the bands from other sources need to be tackled carefully, and (iv) UWB systems faces a lot of regulatory problems and no common framework is defined.

5.3.2 Dual Satellite Systems

Recently, the research towards the dual satellite coexistence using cooperative and cognitive techniques is receiving important attention due to several reasons specified in Chapter 1. As compared to the literature on hybrid/integrated systems, the existing contributions on dual satellite systems are quite limited. The available literature mainly deals with the diversity improvement purpose [407, 408]. Cooperative diversity with two satellites based on the Alamouti code is presented in [407] and it has been shown that cooperative diversity using two satellites can obtain better performance than with the traditional two satellites diversity scheme. Similarly, in [408], a simplified model for cooperative diversity using two satellites for the purpose of increasing diversity gain has been presented. In [36], a partial cooperation between two coexisting transmitters is proposed in order to reduce multiuser interferences and enhance the performance of the whole system in the context of dual satellite systems. Consequently, a heuristic, iterative and low complexity algorithm is presented to allocate users in each of the two interfering sets. In [409], the problem of distributed power control has been considered for cognitive satellite networks. Further, in [410], sharing alternatives for up to four Code Division Multiple Access (CDMA) MSS systems operating in the same spectrum have been investigated considering both

the downlink and uplink cases. It has been concluded that 4 CDMA systems may share the same band and terminal specifications are the main factors for ensuring the proper sharing.

5.3.3 Spectrum Sharing Techniques

Many GEO satellites today operate communication channels in higher frequency bands such as Ka and Ku bands but carry out Telemetry, Tracking and Control (TTC) in the C-band [411]. For the C-band interactive satellite TV and TTC services, continuous service guarantee isn't required. In this scenario, spectral holes can be detected and the detected unoccupied bands can be used for providing other terrestrial wireless services. Further, by applying proper interference mitigation techniques, underlay and overlay cognitive techniques can be applied for the coexistence of terrestrial and satellite networks to operate them in the same spectrum. The terrestrial wireless service WiMax uses the same C-band spectrum, which causes interference in the satellite downlink. In many cases, extended C band (3.4 – 3.7) GHz band has been allotted to WiMax service and some administrations are looking to deploy WiMax in standard C-band (3.7 – 4.2) GHz too. The adjacent channel interference becomes the main problem in case of the extended band allocation and co-channel interference causes problem in case of the standard C band. Today, many satellite operators claim about the interference problem in different parts of world due to the allocation of C-band frequency to WiMax services. If suitable cognitive techniques using advanced coding techniques, adaptive modulation techniques and advanced interference mitigation techniques could be investigated, the above problem can be addressed. In the C-band satellite spectrum, there exists the opportunity of using the following networks as secondary: (i) cellular networks (WiFi and WiMax Networks), (ii) smart grid networks, (iii) public safety networks, and (iv) wireless medical networks.

Since a satellite system covers a global area in nature, the frequency sharing between the satellite and terrestrial systems is essential in order to utilize the spectrum properly. The possibility of sharing the same frequency band between satellite and terrestrial networks operating in the Ka band has been studied in [91]. It has been noted that if we estimate the interference by carefully considering the antenna off-axis gain of the earth station, we can derive more realistic separation distances between the earth station and the terrestrial stations in order to allow their coexistence. Further, the contribution in [94] studies the interference impact on the FSS uplink due to High Altitude Platform Station (HAPS) gateway uplinks. With the simulation results, it has been concluded that even a large number of HAPS networks, each employing five gateway stations, would not cause harmful interference to the FSS space station.

The formation of a coordination zone around the victim receiver is one approach of sharing spectrum between two wireless systems. In this context, authors in [102] study the construction of the coordination contour around the FS receivers with respect to mobile earth stations operating in C and Ku bands. The proposed methodology is based on the velocity of the mobile stations and their frequency of passage from specific locations within the neighborhood of the FS receiver. Authors in [93] investigate the use of 2 GHz MSS frequency allocation for satellite and terrestrial mobile services based on LTE system. It has been concluded that simultaneous downlink frequency sharing between satellite and terrestrial is feasible for pedestrian microcells and vehicular macrocells, but not for the wider rural cells. Further, it has been deduced that simultaneous uplink frequency sharing is not feasible due to the aggregate interference caused by terrestrial terminals to the satellite. In this context, it is extremely important to investigate innovative CR techniques such as dynamic resource allocation in order to allow this coexistence.

As the number of terrestrial and satellite systems rises, there arises the need of spectrum sharing between these two systems in order to enhance the overall spectral efficiency. For this purpose, currently certain frequency bands above 10 GHz have been assigned to both the BSS/FSS and the terrestrial broadcasting/FS on a primary basis without providing priority to any type of the system [103]. For example, the band 10.7—12.7 GHz has been used for Direct to Home (DTH) TV reception and point to

point high capacity fixed links. In this context, authors in [103] provide an analytical methodology for the prediction of the carrier to noise plus interference ratio of broadcasting satellite systems, suffering from interference from an adjacent terrestrial link at frequencies above 10 GHz.

The reference [104] provides an overview of frequency sharing studies between IMT-advanced systems and GEO FSS systems operating in 3.4 – 4.2 GHz and 4.5 – 4.8 GHz. In order to mitigate interference between these two systems, dynamic spectrum allocation and the usage of beacon signals have been suggested. By maintaining an upto date database which contains information about all relevant information of the current services or stations such as carrier frequency, channel bandwidth etc., IMT-advanced systems can be dynamically operated by finding the holes in several domains. Similarly, periodic broadcast of beacons by one system can provide dynamic and active information on its spectrum usage to another system in order to handle the inter-system interference. Recently, European Conference of Postal and Telecommunications Administrations (CEPT) has highlighted the need of enhanced access to FSS spectrum in the 17.7 – 19.7 GHz band and identified the following approaches to enhance FSS situation in 17.7 – 19.7 GHz band [105]: (i) band segmentation, (ii) pre-coordinated areas, (iii) dynamic interference avoidance, and (iv) FS assignment database access. Moreover, the recommendation ITU-R SF.355-4 provides various sharing factors and methods that can be utilized for achieving sharing between FSS systems and terrestrial FS systems. These methods are basically based on (i) limitation of the power radiated by the FS transmitters (Recommendations ITU-R SF.406 and ITU-R SF.765), (ii) limitation of the power spectral density at the surface of the earth produced by FSS satellites (Recommendation ITU-R SF.358), and (iii) method of computing the distance within which earth station transmitters/terrestrial transmitters may produce unacceptable interference to terrestrial receivers/earth station receivers respectively sharing the same bands (Recommendation ITU-R SM.1448).

In the coexistence scenarios of GEO and NGEO networks, in-line interference may be a serious problem and it arises whenever an NGEO satellite passes through a line of sight path between an earth station and a GEO satellite. This is due to the fact that an earth station which is in line with GEO and NGEO satellites may receive and create interference through its main beam. The in-line interference causes a potential problem to the GEO networks operating near the equator while considering the case of O3b satellites. In this context, exploring efficient techniques to mitigate the in-line interference is a highly relevant and challenging problem for the spectral coexistence of GEO and NGEO satellite networks [34, 35, 412].

The interference scenario in a satellite system differs from that of terrestrial systems due to the presence of the on-board antenna which acts as a spatial filter [413]. The cochannel interference mainly arises due to the presence of side-lobes in the on-board antenna radiation pattern i.e., non-ideal angular selectivity of the spotbeams and in the radiation patterns of the earth station terminals. In NGEO satellite systems, the relative position of the cochannel spots changes over time due to the constellation dynamics. Due to this, the interference analysis between the systems operating in GEO and NGEO systems becomes more challenging. In [413], several techniques such as spot turnoff, intraorbital plane frequency division and interorbital plane frequency division have been identified in order to avoid or minimize the cochannel interference between GEO and NGEO systems. While considering these techniques, terrestrial FS networks operating in the same spectrum should also be taken into account. In the spot turnoff method, one of the two spots is turned off whenever two spots overlap too much. In the intraorbital plane frequency division method, satellites on the same orbital plane are assigned different frequency subsets up to a specified modulo R while in the interorbital plane frequency division, the available frequency spectrum is subdivided into as many subsets as the number of orbital planes in such a way that satellites on different orbital planes do not interfere with each other. The recommendation ITU-R S.1431 provides several interference mitigation techniques in order to avoid the in-line interference between NGEO satellites and these techniques are also applicable for the coexistence of GEO and NGEO satellites. Further, the recommendation ITU-R S.1325 provides the methodologies for determining statistics of short term interference between co-frequency, co-directional NGEO FSS systems and other NGEO FSS systems or GEO FSS networks.

TABLE 5.3: Possible spectral coexistence scenarios for cognitive SatComs

Scenarios	Classification basis	Types (Examples)
Hybrid Satellite-Terrestrial Coexistence	Operating frequency	FSS-FS coexistence in Ka band (17.7-19.7 GHz downlink, 27.5-29.5 GHz uplink)
		FSS-FS coexistence in Ku-band (10.7-12.75 GHz downlink, 12.75-14.5 GHz uplink)
		Multibeam satellite-Cellular coexistence in C-band (3.4-3.8 GHz downlink, 5.85-6.725 GHz uplink)
		Hybrid/integrated Sat-terrestrial networks in S-band (1.98-2.01 GHz downlink, 2.17-2.20 GHz uplink)
	Operating mode	Forward normal mode (primary and secondary both operating in forward mode)
		Return normal mode (primary and secondary both operating in return mode)
		Forward reverse mode (primary in forward mode and secondary in return mode)
		Return reverse mode (primary in return mode and secondary in forward mode)
	Link type	Single user link coexistence (e.g., FSS-FS coexistence in Ka band)
		Multiuser link coexistence (e.g., Multibeam-cellular coexistence in C band)
Dual Satellite Coexistence	Operating frequency	BSS-FSS return reverse mode coexistence in Ka band (17.3-17.7 GHz)
		Two GEO FSS satellite coexistence in Ka band (19.7-20.2 GHz downlink, 29.5-30 GHz uplink)
		Two GEO FSS satellite coexistence Ku band (10.7-12.75 GHz downlink, 12.75-14.5 GHz uplink)
		GEO-NGEO satellite coexistence in Ka band (18.8-19.3 GHz downlink, 28.6-29.1 GHz uplink)
	Operating mode	Forward normal mode
		Return normal mode
		Forward reverse mode
		Return reverse mode
	Operator's ownership	Single operator model (both primary and secondary owned by the same operator)
		Dual operator model (primary and secondary owned by different operators)
	Coverage type	Monobeam-monobeam coexistence
		Monobeam-mutibeam satellite coexistence
		Mutibeam-mutibeam satellite coexistence
	Satellite orbit	GEO-GEO satellite coexistence
		GEO-NGEO (MEO/LEO) satellite coexistence

Besides spectrum sharing between two coexisting systems, there exists the concept of optimizing the satellite spectrum by allowing the transmit and receive carriers of a full duplex link to share the same transponder space. This technology is called “DoubleTalk Carrier in Carrier” and it allows satellite users to achieve higher spectral efficiencies which cannot be achieved with the modulation and Forward Error Correction (FEC) alone [414]. This technology allows equivalent spectral efficiency using a lower order modulation and/or FEC Code, thus reducing the capital expenditure by allowing the use of a smaller block upconverter/ high power amplifier and/or antenna. The main concept behind this technology lies on the estimation and removal of the interfering signal from the local modulator prior to demodulation of the desired signal transmitted from another station.

5.4 Proposed Cognitive SatCom Scenarios

Table 5.3 provides possible spectral coexistence scenarios for cognitive SatComs. These scenarios can be broadly categorized into: (i) Hybrid satellite-terrestrial coexistence scenario, we define the systems under this scenario as hybrid cognitive SatCom systems, and (ii) Dual satellite coexistence scenario, we call the systems under this scenario as dual cognitive SatCom systems. It should be noted that although some of the combinations listed in Table 5.3 may not be feasible based on the current spectrum regulations, we assume that suitable CR techniques will be investigated in future in order to allow their coexistence. Further, if research results are satisfied enough to convince the regulators, all these combinations can be exploited in practice in order to make the efficient use of the available spectrum. In the following subsections, we provide the detailed description of two proposed coexistence scenarios and propose different CR techniques for these scenarios in subsequent chapters.

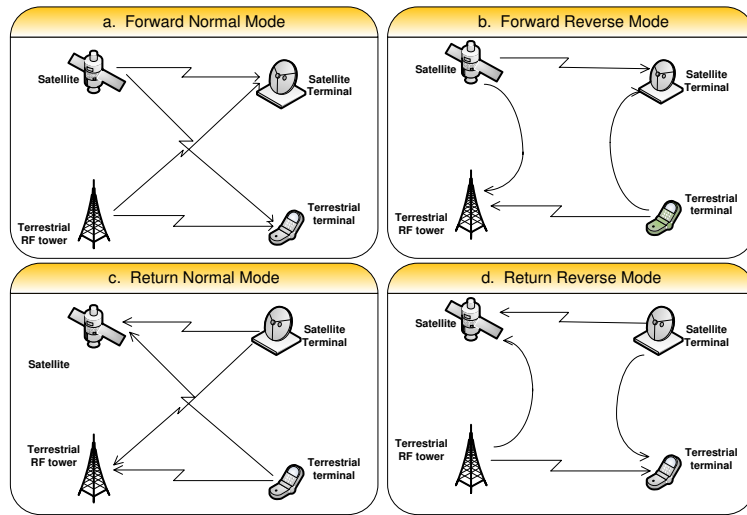


FIGURE 5.1: Different transmission modes for hybrid satellite-terrestrial cognitive scenario

5.4.1 Hybrid Satellite-Terrestrial Coexistence

This scenario deals with the coexistence of satellite and terrestrial links within the same spectrum for enhancing the overall spectral efficiency. The communication links can be i) from satellite to satellite terminals, ii) from terrestrial BS to terrestrial user terminals, iii) from satellite terminals to the satellite, iv) from terrestrial user terminals to the terrestrial BS. As noted in Table 5.3, possible hybrid satellite-terrestrial coexistence scenarios can be categorized on the basis of (i) operating frequency, (ii) operating mode, and (iii) link type. The possible examples on the basis of the operating frequency are FSS-FS coexistence in the Ka band, FSS-FS coexistence in the Ku band, multibeam satellite-cellular coexistence in the C-band, and hybrid/integrated satellite-terrestrial networks in the S-band. Further, while considering possible combinations of the operating mode of the links, the following four coexistence modes are possible [106]: i) forward normal mode (primary and secondary both operating in forward mode), ii) return normal mode (primary and secondary both operating in return mode), iii) forward reverse mode (primary in forward mode and secondary in return mode), and iv) return reverse mode (primary in return mode and secondary in forward mode). The details on these modes have been illustrated in Fig. 5.1. In this context, two priority conditions can be set i.e., by providing primary access to the satellite or to the terrestrial link. In many cases, satellite link can be considered as primary link due to adverse transmission conditions and in some of the cases, terrestrial link can be considered as primary. The latter case is beneficial for satellite operators to take advantage of the unused terrestrial spectrum in order to maximize their system capacity.

On the basis of link types, the hybrid scenario may comprise of a multi-user link coexistence (Fig. 5.2²) and a single-user link coexistence (Fig. 5.3). In the multiuser link coexistence scenario, S band (1980 – 2010 MHz downlink, 2170 – 2200MHz uplink)/C band (3.4 – 3.8 GHz downlink, 5.85 – 6.725 GHz uplink) multibeam satellite systems can coexist with terrestrial cellular systems such as WiMax, LTE using suitable CR techniques. These techniques allow the reuse of the satellite licensed spectrum in the terrestrial secondary systems or vice versa without disturbing the operation of the licensed primary systems. In the single-user link coexistence scenario, Ka band (17.3 – 19.7 GHz downlink, 27.5 – 29.5 GHz uplink) FSS satellite systems can coexist with the microwave FS links by exploiting suitable cognitive techniques. Both uplink and downlink FSS coexistence can be considered with the FS microwave link depending on the frequency of operation. The strong interfering link in this scenario is the link between satellite terminals and the microwave station. By analyzing interference between these systems, suitable CR techniques can be investigated depending on the interference level and the

²This is an example for multi-user link coexistence in the normal return mode. The spectral coexistence of the satellite downlink with terrestrial systems have been illustrated later in Figs. 6.4 and 6.19

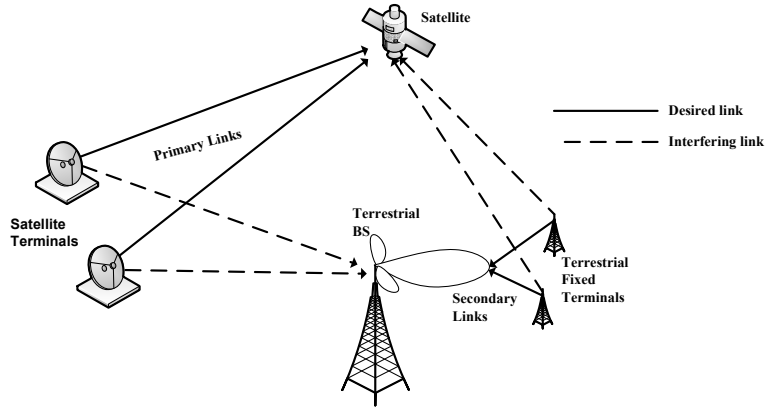


FIGURE 5.2: Hybrid satellite cognitive scenario for multiuser link coexistence

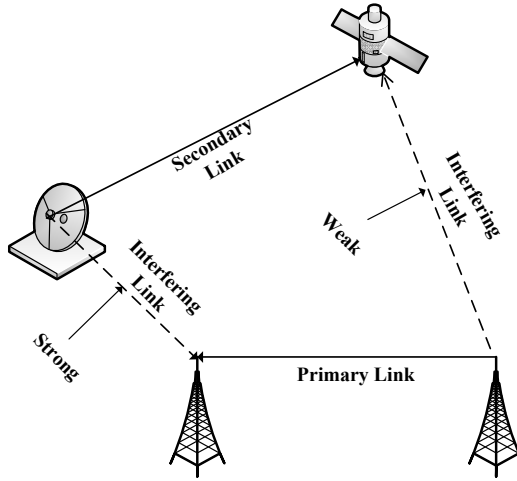


FIGURE 5.3: Hybrid satellite cognitive scenario for single user coexistence

allowable level of interaction. The following hybrid coexistence scenarios are being considered under the ongoing FP7 project CoRaSat [96]: (i) FSS downlink-FS coexistence in 17.7 – 19.7 GHz, and (ii) FSS uplink-FS coexistence in 27.5 – 29.5 GHz.

5.4.2 Dual Satellite Coexistence

Satellite systems operating in same or different orbits can be employed within the same spectrum to provide overlapping satellite services over the same frequency resources and coverage area. One satellite system can be assumed to be primary and to have priority over the shared spectrum. An example of this scenario could be an operational DTH primary service and a secondary vehicular multimedia service over a common set of frequencies. Another example could be the coexistence of GEO and Other 3 billion (O3b) satellites over the same spectrum. As mentioned in Section 5.3.2, dual satellite scenarios in the literature have been mainly investigated for diversity and user scheduling purposes [407, 408].

As noted in Table 5.3, possible dual satellite coexistence scenarios can be categorized on the basis of (i) operating frequency, (ii) operating mode, (iii) operator's ownership, (iv) coverage type, and (v) satellite orbit. On the basis of operating frequency, the following possibilities exist: (i) two GEO FSS satellite coexistence in the Ka band, (ii) two GEO FSS satellite coexistence in the Ku band, and (iii) GEO-NGEO satellite coexistence in the Ka band. Similar to the hybrid scenario, there exist four coexistence combinations on the basis of operating mode. Further, on the basis of operator's ownership, the coexistence scenarios can be of the types: (i) two operator model, and (ii) single operator model. We briefly describe these two models below.

1. Two operator model: In this application scenario, two satellites are owned by two different operators and are connected to different gateways on the earth as shown in Fig. 5.4. These satellites are assumed to be fixed multibeam satellites and are operated to provide coverage to the same geographic area in the Ka band. It can be assumed that the coverage area of two satellites can be overlapping but their multibeam patterns are not identical. The frequency reuse concept is to be used in cellular planning of both satellites to increase the capacity. The primary system shares its frequency plan to the secondary system, forming a way of cognition between them. The cognition link can be established on the ground by using a fiber optic link feeding the cognitive information from primary gateway to the secondary gateway. The secondary operator sets its frequency plan based on the primary operator's frequency plan so that the frequencies will not be repeated. In this way, effective utilization of spectrum can be obtained by forming a cognition between primary and secondary operators. Using proper scheduling techniques, both operators can provide service with limited interference. Further, advanced interference mitigation techniques can be investigated to reduce the effect of co-channel and adjacent channel interference. The main advantages of this approach over the existing multibeam satellite systems are: (i) saving in scarce spectrum resource, (ii) less interference since two satellites may use adjacent frequencies and may further employ different type of coding scheme, modulation and transmission schemes, (iii) two satellites can provide different types of services and also to serve different types of traffic. However, there exist the following challenges: (i) adjacent and co-channel interference, (ii) need of proper scheduling techniques and cognitive mechanism, and (iii) interaction between two operators for coordination and conflict handling.

2. Single Operator Model: In this scenario, two satellites are considered to be owned by a single operator and are connected to the same gateway on the earth. It can be assumed that both satellites are equipped with multibeam antennas to provide coverage to the same geographic region and frequency reuse concept is used to increase the capacity. Further, primary satellite can be considered to be equipped with antennas with larger beam patterns and secondary satellite with antennas with smaller beam patterns. The beam patterns of the secondary satellite antenna and the primary satellite antenna may form an umbrella structure as in terrestrial cellular systems. Larger cells can be used for serving vehicular traffic and smaller cells can be used for serving outdoor pedestrian traffic. Since vehicular traffic needs a lot of handovers while going from one spot beam area to another spot beam area, can be termed as spotbeam handover. A spotbeam handover involves the process of releasing the communication link between the user and the current spotbeam and acquiring a new link from the next spotbeam to continue the call, causing processing overhead in the satellite gateway. This scenario drastically reduces the processing overhead by reducing the number of handovers. The cognition between primary and secondary system can be formed by designing the secondary network based on the knowledge of the primary system. This approach has following important advantages over the existing multibeam satellite approach: (i) secondary system can operate in an opportunistic way, by using the underutilized portion of the primary licensed spectrum, (ii) less processing overhead in the satellite gateway for vehicular traffic, and (iii) a single operator can provide two different services such as vehicular multimedia service and DTH service to its coverage region by using the existing frequency band. However, there exist the following challenges to implement this model: (i) orbital congestion of satellite needs to be taken into account, (ii) the interference caused by one satellite to the satellite terminals of another satellite needs to be tackled carefully, (iii) inter-satellite interference, and (iii) satellite cost and complexity issues.

Furthermore, on the basis of the satellite orbit, dual satellite coexistence scenarios can be categorized into: (i) two GEO satellite coexistence (Fig. 5.4), and (ii) GEO-NGEO (LEO)/MEO satellite coexistence (Fig. 5.5). The primary system can be the existing GEO satellite and the secondary can be another GEO or LEO/MEO satellites depending on these scenarios. In two GEO coexistence scenario, cognitive techniques may differ for the coexistence of two multibeam systems and for the coexistence of multibeam and monobeam systems. Another scenario of GEO and LEO/MEO coexistence scenario has also received important practical consideration due to deployment of different LEO/MEO satellites within the same spectrum to improve the satellite transmission latency. The coexistence of FSS-BSS

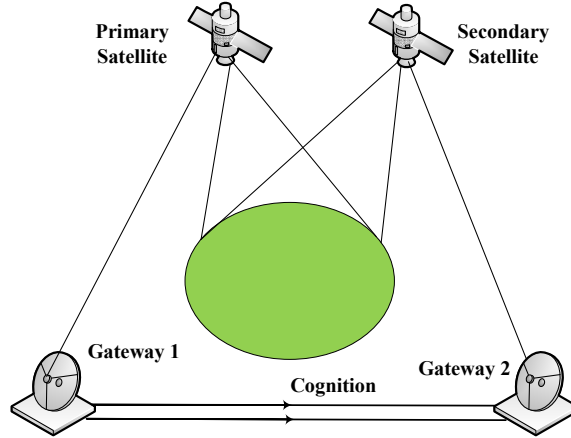


FIGURE 5.4: Dual satellite cognitive scenario for two GEO coexistence

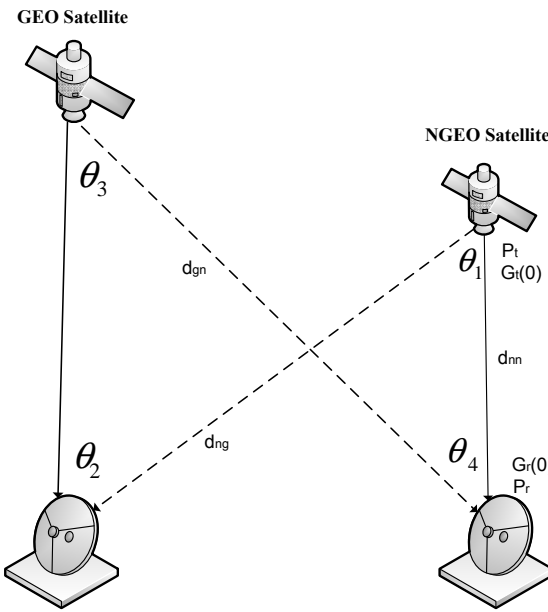


FIGURE 5.5: Dual satellite scenario for GEO and MEO/LEO coexistence

satellites i.e., BSS feeder links operating in the return mode and FSS satellite link operating in the forward mode in the Ka-band (17.3 – 17.7) GHz is being investigated in the ongoing FP7 project CoRaSat [415].

5.5 Scenarios-Techniques Mapping

Several cognitive techniques have been investigated in the literature in the context of a terrestrial CR and a review of various techniques was presented in Section 2. The main features of these techniques are presented in Table 6.2 of Chapter 6. Further, Table 5.4 presents the mapping of several conventional approaches and cognitive approaches to the considered coexistence scenarios. It can be noted that for both the coexistence scenarios, various cognitive approaches can be investigated. In practice, a suitable cognitive solution should be chosen based on the exact system type, desired performance level and allowable level of complexity. For example, a simple EZ approach based in coordination contour is simple to implement in practice but does not exploit the spectrum opportunities efficiently. Although there exists another type of CR technique, called overlay technique, the application of this approach

TABLE 5.4: Conventional approaches and possible cognitive solutions for considered coexistence scenarios

Scenarios	Conventional Approaches	Cognitive Approaches
Hybrid Satellite-Terrestrial Coexistence	<ul style="list-style-type: none"> • Time/frequency/code isolation • Coordination at ITU-R level based on date of filing • Coordination contour/zone around the victim receiver • Limits on maximum Effective Isotropic Radiated Power (EIRP) density 	<p>Interweave Techniques</p> <ul style="list-style-type: none"> • Dynamic Spectrum Sensing (SS): frequency, time, space, polarization, angular domains. • Geolocation Database • SS combined with database • Harmful interference detection and avoidance <p>Underlay Techniques</p> <ul style="list-style-type: none"> • Cognitive Beamforming/adaptive nulling • Adaptive power control • Cognitive resource allocation • Exclusion zone • Exclusion zone combined with power control
Dual Satellite Coexistence	<ul style="list-style-type: none"> • Time/frequency/code/polarization isolation • Orbital/spatial separation • Frequency channelization • Geographical separation between earth stations • Minimum look angle restrictions • Earth station and satellite antenna sidelobe minimization • GEO arc avoidance for NGEO sharing 	<p>Interweave Techniques</p> <ul style="list-style-type: none"> • Dynamic SS: frequency, time, geographical space, polarization, angular domains. • Geolocation Database • SS combined with database • Harmful interference detection and avoidance <p>Underlay Techniques</p> <ul style="list-style-type: none"> • Cognitive Interference Alignment • Cognitive beamhopping • Exclusion Zone • Adaptive Power Control • Exclusion zone combined with power control • Terminal-side beamforming

seems to be quite complex in the considered scenario due to the requirement of high level coordination between primary and secondary systems.

5.5.1 Techniques for Hybrid Coexistence Scenario

5.5.1.1 Interweave Techniques

One of the main requirements of the CR is to acquire spectrum information about its surrounding environments. In this direction, the SUs need to identify spectrum opportunities in different dimensions such as time, frequency, space, polarization and angular position in order to use the available spectrum efficiently without degrading the PU QoS. Existing spectrum awareness methods include SS, geolocation database and beacon signals. Further, existing spectrum awareness literature mostly consider exploring spectrum opportunities in the frequency, time and spatial domains. In the context of cognitive SatComs, polarization, and angular domains can also be considered as additional degrees of freedom for enabling coexistence. From the cognitive point of view, if a primary system is designed to transmit in one polarization, then the secondary system can be designed to transmit in another polarization using the polarization domain as an interference mitigation tool towards the primary systems. Dual polarization plays a significant role in satellite systems to enhance the spectral efficiency of since two independent signals can be transmitted on the same spectrum by means of two orthogonal polarizations, hence doubling the available spectrum. In contribution [114], we consider the problem of exploiting SS techniques for a dual polarized fading channel in the hybrid cognitive SatComs scenario. The sensing performance of an ED based SS technique has been analyzed in a dual polarized fading channel using different combining techniques such as SC and EGC. Further, we propose a harmful detection and avoidance scheme in the spectral coexistence of FSS uplink with the FS links operating in 17.7 – 19.7

GHz [108]. These approaches will be detailed in Chapter 6. Moreover, in practical scenarios, blind spectrum awareness techniques need to be investigated since cognitive terminal does not have prior knowledge of PU signal, channel and noise variance. In this direction, our contributions [416, 417] study eigenvalue based blind SS techniques, [54] and [53] investigate the effect of noise correlation on eigenvalue based SS techniques and the contribution [53] further purposes eigenvalue based blind SNR estimation technique for estimating the SNR of the PU signal.

Geolocation database is an alternative spectrum awareness mechanism in order to obtain the knowledge of the radio environment and can be used to determine the presence of primary systems in a certain region and to ensure that CR nodes do not operate within the occupied bands. A CR can use the database approach including history information and prediction methods to make the operation more efficient. This approach is based on maintaining a frequently updated and centrally located database with information about the regional spectrum usage, including location of PTs, coverage areas, frequencies of operation, transmission powers, radio technologies, operation requirements, etc. In this context, REM is becoming a promising architectural concept for storing environmental information for use in CR networks [158]. It can be noted that the information related to the angular, polarization and spatial domains vary slowly over the time and this information can be stored in a centralized database and then queried by a CR transmitter in order to find the spectrum opportunities in these domains. Further, the combination of preliminary database with the dynamic SS helps to reduce the number of sensors required for sensing the presence of the primary signal. Moreover, the preliminary database can be obtained from the operators and regulators and can be used for calculating interference floor and subsequently EZs. The database approach is being considered in the context of the project CoRaSat and is not further investigated in this thesis work.

5.5.1.2 Underlay Techniques

Underlay techniques such as EZ and beamforming can be applied in order to avoid harmful interference. The EZ technique defines a region around the victim receiver within which interferers are not allowed to transmit. Beamforming techniques allows the cognitive transmitters/receivers to maximize their SINRs while minimizing interference towards/from the primary receivers/transmitters. Although there are several underlay approaches which can be applicable in the considered scenario as noted in Table 5.4, in this thesis, we focus on the following two underlay approaches.

1. *Interference Modeling*: Interference analysis between the satellite and terrestrial links helps to understand the level of interference between these systems while operating within the same spectrum and provides a useful guidance on the use of suitable CR techniques. Further, interference modeling allows one to create an EZ zone around a victim receiver. In this direction, interference modeling between terrestrial BS and the satellite terminal is carried out in our contribution [106] on the basis of the interference power level. It has been observed that the satellite terminals near polar region receive more interference from a terrestrial BS than the terminals located near the equator due to the variation in the elevation angle. Further, it has been concluded that different CR techniques can be considered based on interference power level. SS and database techniques seem to provide the best performance in high interference region and in low or medium interference region, interference from secondary system to the primary system can be suppressed by using some form of underlay technique. The detailed description of this approach will be provided in Chapter 6.

2. *Cognitive Beamforming*: Existing spectrum sharing techniques mostly consider three signal dimensions i.e., frequency, time and area for sharing the available spectrum between primary and secondary systems. However, due to advancement in smart antennas and beamforming techniques, multiple users can be multiplexed into the same channel at the same time and in the same geographical area. In this context, angular dimension can be considered as a more efficient way of exploiting the underutilized primary spectrum for the SUs. In the context of considered hybrid cognitive SatComs, our contributions [145] and [119] study transmit and receive beamforming techniques using the unique transmission characteristics of GEO satellite terminals respectively. GEO satellites are located in the geosynchronous

orbit above the equator and therefore transmit in a northerly direction if we consider the European continent. The GEO satellite terminals have therefore the special propagation characteristic to always point towards the GEO satellites (south). While considering the coexistence of a satellite network with the terrestrial cellular network, the interference received by the BS is concentrated in a specific angular sector. This priori knowledge has been considered in [119] in order to investigate different receive beamforming techniques such as LCMV and MVDR for the considered scenario. Similarly, while considering transmit beamforming scenario, the reception range of all the satellite terminals is concentrated in an angular sector. This priori knowledge has been considered in [120] in order to investigate different transmit beamforming techniques such as scaled LCMV, modified LCMV and rate maximization technique for the considered scenario. The detailed description of this technique will be presented in Chapter 6.

5.5.2 Techniques for Dual Satellite Coexistence

As mentioned in the previous section, there can be possibilities of forward mode coexistence, return mode coexistence as well as hybrid coexistence of two satellite systems. In forward mode coexistence scenario, two multibeam satellites can coexist within the same spectrum using underlay CR techniques such as beamhopping and EZ. The coexistence between two monobeam satellite systems in the downlink scenario seems to be difficult since a single satellite transmission affects over the large area in the downlink. In this context, traditional satellite coexistence techniques such as orbital/spatial separation are feasible. In the return link coexistence, underlay techniques such as interference alignment can be implemented for the coexistence scenario of monobeam and multibeam satellites (discussed later in Chapter 7) and SS techniques seem to be relevant in the case of coexistence of two multibeam systems.

5.5.2.1 Interweave Techniques

Dynamic spectrum awareness techniques also can be applied for dual satellite coexistence scenario provided that the cognitive satellite terminals are equipped with the suitable RF nodes. In SS techniques, the secondary terminals can be equipped with some sensing nodes which can detect the spectrum holes in the primary satellite spectrum and can use the spectrum opportunistically. The main difficulty in this case lies in acquiring wideband satellite signal. However, instead of detecting the whole signal, some of the characteristics of the primary signal such as sparsity order, SNR, polarization can be acquired to enable the coexistence. In our contribution [145], we consider the problem of enhancing SS efficiency for the considered dual cognitive scenario exploiting the polarization domain. By deploying two orthogonally polarized antennas, any type of receive or transmit polarization can be derived. Detecting the polarization state in addition to energy of a certain carrier frequency can significantly enhance the spectrum efficiency. In this direction, different combining techniques for SS have been studied in [145] in a dual polarized AWGN channel. The detailed description of this approach will be provided in Chapter 7.

5.5.2.2 Underlay Techniques

Although there exist several underlay techniques applicable for dual satellite coexistence scenario as noted in Table 5.4, we focus on the following techniques in this thesis.

1. *Interference Alignment*: IA is an interference mitigation technique and can be used as an underlay technique for enabling coexistence of wireless networks. This technique has received important attention recently in the CR research community [1, 306]. In the context of dual satellite systems, we investigate an underlay spectral coexistence mechanism exploiting the uplink IA in order to mitigate the interference of multibeam satellite terminals towards the monobeam satellite [98]. Suitable precoding techniques can be applied at the secondary multibeam satellite terminals so that the interference

at the primary receiver can be filtered out by sacrificing some amount of the desired energy. Three different types of IA techniques, namely, coordinated, uncoordinated and static, have been investigated depending on the level of network interaction and adaptation with the channel conditions. The detailed description and analysis of this approach will be presented in Chapter 7. To enhance the spectrum efficiency further, our contribution in [418] investigates the frequency packing technique for IA based dual satellite cognitive systems.

2. Cognitive Beamhopping: A beamhopping satellite system can operate by using full frequency reuse over a certain beamhopping pattern. The main difference from conventional multibeam systems is that multiple beams within a cluster share the available spectrum in the time domain instead of the frequency domain in conventional multibeam systems. Since the primary satellite only illuminates a small fraction of beams out of a large number of beams deployed under beamhopping systems, the rest of the beams remain idle at that time waiting for their transmission slots. In this context, the overall system spectrum efficiency can be enhanced if we could deploy a secondary satellite within the same spectrum without producing harmful interference to the primary system. In this direction, we propose a novel cognitive beamhopping system with the objective of enhancing the system spectral efficiency while protecting the primary system [99, 144]. The primary satellite is assumed to be operated with larger beams and the secondary satellite with smaller beams in the same coverage area. The cognition can be achieved by sharing the beamhopping pattern and the timing information of the primary multibeam system to the secondary multibeam system using a signalling link between their corresponding gateways. The detailed analysis of this approach will be presented in Chapter 7. Recently, the performance of a cognitive beamhopping based dual satellite system has been compared with that of the coordinated dual satellite system in [419].

3. Power control: Adaptive power control at the cognitive transmitters facilitates the spectral co-existence of primary and secondary systems by guaranteeing the protection of the primary receivers. Depending on the scenarios, the power control can be applied either on the satellite-side or on the terminal-side i.e., for satellite-side power control on the forward normal mode coexistence and terminal-side power control for the return normal mode coexistence. This approach requires the knowledge of interference threshold of the victim receivers as well as channel state information in case of time varying channels. In [420], we propose an adaptive power control technique at the NGEO terminal for uplink transmissions and at the NGEO satellite for downlink transmissions. In the proposed technique, the required transmission power is determined to control interference towards the victim receiver i.e., GEO satellite in the uplink transmission and the GEO earth station terminal in the downlink transmission, taking into account of the interference threshold of these victim receivers as well as the required QoS for the NGEO link.

5.6 Spectrum Regulation and Standards

5.6.1 Spectrum Regulation

The spectrum usage must be shared among various radio services considering the provisions of national and international regulations. The current spectrum allocation process operates at both national and international levels. At the international level, the ITU is responsible for spectrum management, which divides the world into the following 3 Regions: (i) Region 1: Europe, Middle East, Russia and Africa, (ii) Region 2: The Americas, Greenland and some of the eastern Pacific islands, and (iii) Region 3: Asia, Australia and Oceania. The table of frequency allocations contained in Article 5 of the Radio Regulations (RR) allocates frequency bands in each of the three ITU Regions to radiocommunication services based on various service categories as defined in the RR. International bodies tend to set out high level guidance which national bodies adhere to in setting more detailed policies. International coordination is necessary in the cases where the zones of possible interference extend beyond the national geographical boundaries and users are inherently international such as maritime and aviation. Regional bodies such as CEPT and European Commission (EC) are responsible for making decisions,

preparing reports, recommendations, and directives at the regional level. At the national level, each administration has its own regulating agency like NTIA/FCC in USA, OFCOM in UK.

As mentioned before, in most of the current primary-only systems, international ITU-R bodies assign fixed spectrum bands to license holders on a long-term basis for large geographical regions. In these systems, the spectrum remains idle for most of the time when the services are not active and the spectrum is not utilized effectively. The exclusive spectrum usage rights are mostly implemented through transmission power caps and guard bands, which are determined by the regulators [421]. Without these two aspects, it is difficult to prevent out of band and in-band interferences. For enhancing the spectrum usage among different networks, the spectrum ownership can be transferred from spectrum owner to another party for a short time. The following different forms of spectrum ownership exist [422]: i) usage rights can be assigned to another party for short/medium term with a total transfer of rights and duties, ii) short-term spectrum leasing based on traffic variations, whereby the rights and duties may still remain with the main usage right holders, iii) spectrum trading, whereby the rights and duties may unlike other natural resources remain with the main usage rights holders, and iv) spectrum pooling. Assigning ownership in spectrum pooling technique is a challenge for the regulators. Regarding change in ownership, temporal short term change of usage right is possible. However, current administrative process is time consuming and an automated real-time system is needed. Regarding spectrum leasing and trading, no implications can be noted since an original licensee is liable for any interference/misuse. In addition, no clear assignment of ownership can be done for spectrum pooling.

With regard to the change in technology, most licensees define the BEM (Block Edge Mask) in which transmission signal must remain independent of the technology used [101]. Further, considering the change in transmission characteristics, any transmission characteristics are permitted as long as the BEM criteria are not violated. Moreover, with regard to the requirement of additional radio resources, many investigations have suggested the need for a Cognitive Pilot Channel (CPC) and it is widely discussed in regulatory bodies. Spectrum databases and trading are the current prominent techniques and they can be considered as the possible first steps towards the implementation of dynamic spectrum access techniques. Spectrum trading is an important mechanism to increase overall spectrum utilization and to open up business opportunities for access to desired spectrum. Regulatory rules for spectrum trading have been implemented in some countries for some bands, for example in the UK and US.

In the beginning, SatCom was mainly concentrated in the C-band since C-band services cover large areas and this band has less propagation and attenuation problems. C-band satellite systems facilitate intercontinental and global communications and further provide a wide range of services including critical applications such as distance learning, telemedicine, disaster recovery, and television transmission in many tropical regions. However, due to the limited C-band spectrum, the higher frequency bands such as Ku and Ka are also currently being used for commercial and military satellite applications. The ITU is responsible for proper allocation of frequency bands as well as orbital positions of the satellite. The frequency allocations are made either on an exclusive or shared basis and then are put into effect either worldwide or limited to a region. The frequency bands which are allocated internationally are again reallocated by national regulatory bodies to different services and operators.

Based on Articles 9 and 11 of the ITU Radio Regulations (RR), the unplanned FSS bands are accessed on the first-come, first-served basis. For coordinating and registering a satellite network in an unplanned band, the following three general types of submissions to ITU are followed [423]: (i) Advanced Published Information, (ii) Coordination Request, (iii) Notification and Resolution 49 (due diligence) information. In the context of cognitive SatComs, the FM44 group of CEPT Electronic Communications Committee (ECC) has recently formed 17.7 – 19.7 GHz correspondence group for sharing and compatibility study with the predefined reference system. Some of the regulatory changes which have been already considered are [97, 105]: (i) uncoordinated FSS stations in the frequency band 17.7 – 19.7 GHz should be exempt of individual license and should be allowed for free circulation within CEPT countries, (ii) any sub-band not used by the FS system in the band 17.7 – 19.7 GHz should be identified by the CEPT so that it can be used for FSS system, and (iii) knowledge of FS characteristics such as

power, locations carrier bandwidth etc. available from the database can be exploited by a employing a CR technique.

5.6.2 Standards

Standards are used in many aspects of our daily lives such as media, healthcare, food, transport, communications, energy, etc. More specifically, standards provide the following main benefits [424]: (i) the support of government policies and legislation, (ii) helps to ensure safety and reliability, (iii) interoperability, and (iv) greater choice of products to the customers. Standards are basically created in the following ways: (i) Defacto standard (ii) Industry association, and (iii) Standards bodies. On the international level, the main standardization body in the telecommunications area is the ITU. In the European context, European Telecommunication Standards Institute (ETSI) develops a variety of standards in telecommunications, broadcasting and information technology. In the context of terrestrial CR communication, several standards are either already in developed or in progress as highlighted in Section 2.5. However, in the area of cognitive Satcoms, standardization activities are still in early stage. ITU-R provides several recommendations for facilitating the sharing of FSS, MSS GEO systems with other LEO/MEO satellite systems as well as with the terrestrial FS services. Several sharing studies described in Section 5.3 are based on these recommendations. Towards the standardization direction in the Ka-band, a system reference document on “Cognitive radio techniques for SatComs operating in Ka band” is being developed in ETSI by the technical committee “Electromagnetic compatibility and radio spectrum matters” based on the activities of the ongoing CoRaSat project [97].

5.7 Discussion

Besides numerous advantages of cognitive SatComs mentioned in Section 5.2, there exist several challenges from the perspectives of the business, technical and regulatory sectors which need to be addressed for the practical implementation of this technology. In the current spectrum market, there is no cooperation between satellite and terrestrial operators. Cooperation at the international as well as at the national level is extremely important to implement this technology. In addition, incorporating satellite receivers into the terrestrial terminals may increase complexity and cost. Furthermore, suitable business models and standards for spectrum sharing between satellite and terrestrial operators need to be investigated. Limited power, wide area coverage and already existing inter-satellite as well as intra-satellite interference in satellite networks impose challenges for implementation of the CR technology in satellite networks.

Regulatory aspects also play a major role in the implementation of this technology. There is a strong need to carry out standardization activities in this area. A proper coordination among regulators, industries, academic researchers and manufacturers helps to foster its practical implementation. Due to the lack of proper regulations to facilitate sharing/trading for all spectrum bands, difficulty arises in implementing sharing/trading spectrum business. In this context, regulators should specify the threshold values for EIRP and out of band interference limits for proper operation of cognitive SatComs. Furthermore, the secondary dynamic access mechanism to government/military exclusive spectrum should be properly addressed in terms of regulations since the instant release is required when spectrum is needed in public safety and emergency scenarios. Moreover, there should be a sufficient level of interaction between national and international authorities. The collaboration between the authorities at the national level is required for the management of terrestrial spectrum while the collaboration at the international level is needed for the management of satellite spectrum. The agreement at the ITU-R level about the regulatory requirements of satellite cognitive systems is necessary. There should be sufficient interaction between technology, market and policy to implement satellite CR. Research efforts should be directed towards investigating new techniques to allow the coexistence of different networks

as well as analyzing the performance of satellite CR systems. The technological solutions should then be standardized by respecting the spectrum regulations. Furthermore, the industries should come up with viable business models by collaborating with the research institutions and they should work towards manufacturing affordable CR equipment by analyzing the market situation. Moreover, the regulators should ensure the regulation of flexible spectrum ownership properly and they should recommend different parameters such as an interference threshold to ensure that new systems do not affect the operation of the previously deployed systems.

The research challenges for cognitive SatComs can be summarized in terms of technical, regulatory and business challenges as follows.

1. Technical Challenges

1. To deal with limited power in satellites
2. To mitigate inter-satellite and/or intra-satellite interference
3. To develop innovative techniques and identify conditions for coexistence of hybrid satellite-terrestrial systems and dual satellite systems
4. To provide desired QoS to the secondary users while guaranteeing the sufficient protection of licensed primary users
5. To manage the complexity associated with CR techniques
6. Dynamic resource allocation and management in heterogeneous environments where the resources may belong to different satellite and terrestrial systems
7. To develop new techniques for handling mobility in the context of mobile scenarios
8. To investigate techniques for ensuring privacy and security
9. Dynamic SS becomes challenging in the downlink of a monobeam satellite due to large coverage area
10. Uplink transmissions with low elevation angles tend to interfere with terrestrial systems more as compared to the uplinks with higher elevation angles
11. Since the coexisting systems may not operate over the same channel bandwidths, the interference calculation from narrowband interfering transmitters to the wideband victim receivers and from wideband interfering systems to narrowband victim receivers is another issue to be addressed.
12. The interference analysis of GEO and NGEO systems operating in the same spectrum becomes challenging due to the constellation dynamics of the NGEO satellites.
13. In the coexistence of GEO and NGEO satellites within the same spectrum, inline interference may be problematic near equatorial regions.
14. In the coexistence scenario of FSS and FS links, harmful FS signal detection and avoidance at the FSS terminals is a challenge to be addressed.
15. To design adaptive beamforming and nulling techniques in order to minimize the interference from/towards interfering/victim terminals.
16. To develop suitable cooperative and spectrum management techniques in order to maximize the spectral efficiency
17. To develop adaptive power control algorithms at the cognitive transmitters in order to respect the interference threshold of the primary receivers.

2. Regulatory Challenges

1. ITU-R less susceptible to change with respect to other Regulators (e.g. FCC, OFCOM)
2. New frequency allocations to terrestrial services
3. Regulations to facilitate sharing and prevent interference
4. Regulations on procedures and requirements for country-to country coordination
5. Standardization of different aspects for cognitive SatComs
6. To ensure whether the research efforts hit the target or not.
7. Lack of regulatory policies for satellite CR
8. Private sector requesting access to government exclusive spectrum either by reallocation or increased sharing

3. Business Challenges

1. CR may further degrade the (already weak) security and privacy of SatComs
2. Increased cooperation is required between government and non-government sectors, different stakeholders and industrial partners as well as between countries.
3. Manufacturers' hesitation incorporating satellite receiver to terrestrial terminals
4. Implementing theoretical investigations in practical scenarios
5. Lack of business policies and models for dynamic access networks

In the subsequent chapters of this thesis, we address some of the above technical challenges. As mentioned in Chapter 1, we study the application of the following techniques in the considered hybrid satellite-terrestrial coexistence scenario in Chapter 6 of this thesis: (i) interference modeling, (ii) harmful interference detection, (iii) cognitive beamforming, and (iv) dual-polarized SS. Further, in Chapter 7 of this thesis, we study the application of the following techniques in the considered dual satellite coexistence scenarios: (i) cognitive IA considering the spectral coexistence of monobeam and multibeam satellite systems both operating in the normal return mode, (ii) cognitive beamhopping technique considering the spectral coexistence of two GEO multibeam satellite systems both operating in the normal forward mode, and (iii) dual-polarized SS considering the spectral coexistence of two multibeam satellites in the normal return mode. In the proposed cognitive scenarios, we assume that signal processing as well as spectrum decision and interference management mainly take place at the ground segment of the satellite system i.e, either at the gateway or at the satellite terminal.

5.8 Chapter Conclusion

Due to the peculiar features of SatCom technology such as wider coverage and the speed of delivering different services to the market, it has played a vital role in the wireless communication field. Further, its importance is expected to increase in future communication systems due to the increasing demand of satellite broadcast/broadband and interactive services as well as due to recent advances in multibeam technology and onboard digital processors. However, the main bottleneck to fulfill the aim of Terrabit/s satellite capacity within the 2020 horizon is the shortage of the usable satellite spectrum. To address this problem, cognitive SatComs can be a potential future solution to enhance the spectral efficiency like

in the terrestrial paradigm. In this context, this chapter has presented the concept of cognitive SatComs highlighting the important aspects of cognition in SatComs. From the CR communication point of view, satellite CR communication mainly differs from its terrestrial counterpart in the following aspects: (i) power imbalance due to different transmit power and receiver sensitivity levels, (ii) channel occupancy, (iii) directivity of transmission and elevation angles of the terminals, (iv) wide coverage area, (v) large propagation loss and atmospheric impairments, (vi) wider carrier bandwidth, etc. Further, a detailed review of the related existing literature has been provided in Section 5.3. Moreover, various possible spectral coexistence scenarios have been proposed considering the following two main categories: (i) hybrid satellite-terrestrial coexistence, and (ii) dual satellite coexistence. The hybrid satellite-terrestrial scenario has been further categorized on the basis of operating frequency, operating mode and the link type. Similarly, several possible dual satellite coexistence scenarios have been presented on the basis of operating frequency, operating mode, operator's ownership, coverage type and the satellite orbit.

In addition, several CR techniques have been mapped with the proposed scenarios in Section 5.5. Based on this mapping, interference modeling, interference detection, CB and dual-polarized SS solutions are proposed for hybrid cognitive SatComs in Chapter 6 of this thesis. Similarly, several solutions such as cognitive IA, cognitive beamhopping and dual-polarized SS are proposed for dual cognitive SatComs in subsequent chapters of this thesis. Further, it has been depicted that a suitable CR solution can be chosen based on the exact system type, desired performance level and allowable level of complexity. Besides, several aspects of cognitive SatComs such as spectrum regulation and standardization activities have been included in Section 5.6 while Section 5.7 has identified several business, technical and regulatory challenges for the practical deployment of cognitive SatCom technology. It can be concluded that if technology, market and policy are adapted to the requirements of this technology properly, the spectrum scarcity problem can be addressed by applying effective CR solutions in future SatCom systems.

Chapter 6

Hybrid Cognitive Satellite Communications

In this chapter, we propose several cognitive approaches for enabling the hybrid satellite-terrestrial coexistence described in Chapter 5. More specifically, we propose the following approaches: (i) Interference modeling, (ii) Interference detection, (iii) Dual-polarized SS, and (iv) CB. Among the above techniques, the first three approaches fall under the category of interweave CR techniques and the fourth one falls under the category of underlay CR techniques. Under the CB approach, we study both the receive and transmit beamforming approaches for the considered hybrid coexistence scenario. The research work included in this chapter has been published in [106, 108, 114, 119, 120, 425].

6.1 Interference Modeling

In the context of cognitive communication, interference modeling plays an important role in protecting the primary licensed system by enabling the formation of coordination contours around victim receivers (Rx). In other words, a coordination contour can be formed around the victim Rx in such a way that secondary terminals are not allowed to operate within this contour. The term coordination contour has been widely used in conventional frequency sharing literature. In the CR context, more narrower EZs can be designed by taking account of different characteristics of the primary Rx such as radiation pattern, location, direction of transmission etc. These characteristics can be obtained from the preliminary Databases (DB), which is constructed based on the information obtained from the operators, regulators or acquired with the help of measurements. Moreover, interference modeling facilitates the creation of REMs which introduces environment awareness capability to the CR network that would be difficult to acquire by individual CR capabilities through extensive spectrum analysis. Subsequently, it helps to create a geolocation DB, which is an alternative spectrum awareness mechanism to obtain the knowledge of the RF environment [158]. This geolocation DB can be used to obtain the information about the primary systems in a certain region and ensure that cognitive terminals do not attempt to operate within protected areas where cognitive transmissions would result in harmful interference levels. The difference with the EZ technique is in the fact that the DB also provides information about the current activity of the PUs while the EZ only determines the geographical restrictions without considering if the PU is active or not at a specific time. The DB information can be updated with observations from CR nodes and disseminated throughout CR networks, providing the useful awareness of environmental status to assist the CR operation. In this direction, FCC has already allowed the unlicensed operation in TVWS using the DB approach in which cognitive devices need to access a DB to obtain information on the available channels at their locations [426].

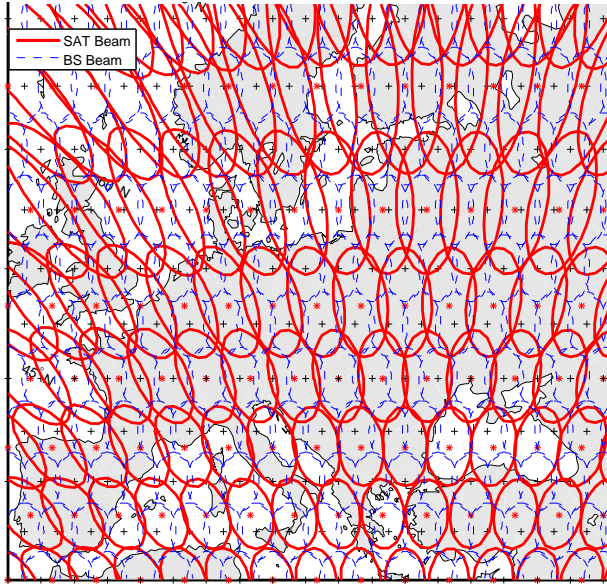


FIGURE 6.1: Coverage of Europe with multispot beams

As mentioned earlier in Chapter 1, a CR technique suitable in one geographical location under a certain condition may not be suitable for other regions, and under different conditions. In this context, this section studies an interference modeling problem in a hybrid satellite-terrestrial scenario in order to estimate the received interference level and subsequently maps suitable CR techniques based on the estimated interference power level.

6.1.1 Interference Power Level

In current GEO satellites, multiple beams can be employed instead of a single global beam in order to enhance the system capacity as in the case of the terrestrial cellular paradigm. Nowadays, tens or hundreds of beams are possible with a frequency reuse factor of three or four [427]. In this work, we consider the multibeam satellite coverage over the whole European region with 135 beams, each of radius 165 km. The 3-dB footprint coverage of a multibeam GEO satellite located at an orbital position of 28.2° E is plotted over the Europe map and is presented in Fig. 6.1. From the figure (Fig. 6.1), it can be observed that the 3-dB footprint contours become more elongated as we move from the equator to the polar region. These patterns are obtained with the help of a beamgain matrix, denoted by B . The beamgain of the j th beam for the i th user position can be written as [428]

$$B_{ij} = G_{\max} \cdot \left(\frac{J_1(u(i, j))}{2u(i, j)} + 36 \frac{J_3(u(i, j))}{u(i, j)^3} \right)^2, \quad (6.1)$$

where $u(i, j) = 2.01723 \sin(\theta(i, j)) / \sin(\theta_{3dB})$, J_m is the first kind of Bessel's function of order m , and G_{\max} is the maximum antenna gain, θ_{3dB} is the 3-dB angle and $\theta(i, j)$ represents the angular position of the i th user from the j th beam center with respect to the GEO satellite. It can be noted that the slant ranges for the spots located in the polar region are longer than those in the equatorial region. Due to this, the path loss varies as we move away from the equator to the polar region in the case of a GEO satellite. The denser grids shown in the map (Fig. 6.1) are drawn while placing terrestrial BSs and their footprint coverage areas are drawn with the circular approximation.

In SatCom systems, interference levels may vary over a large geographic region in contrast to the terrestrial wireless systems where interference is mostly localized. Depending on the positions of satellite terminals, the interference levels picked up by satellite terminals from the terrestrial interferers may vary. To illustrate this using interference modeling, we consider a simple coexistence example as

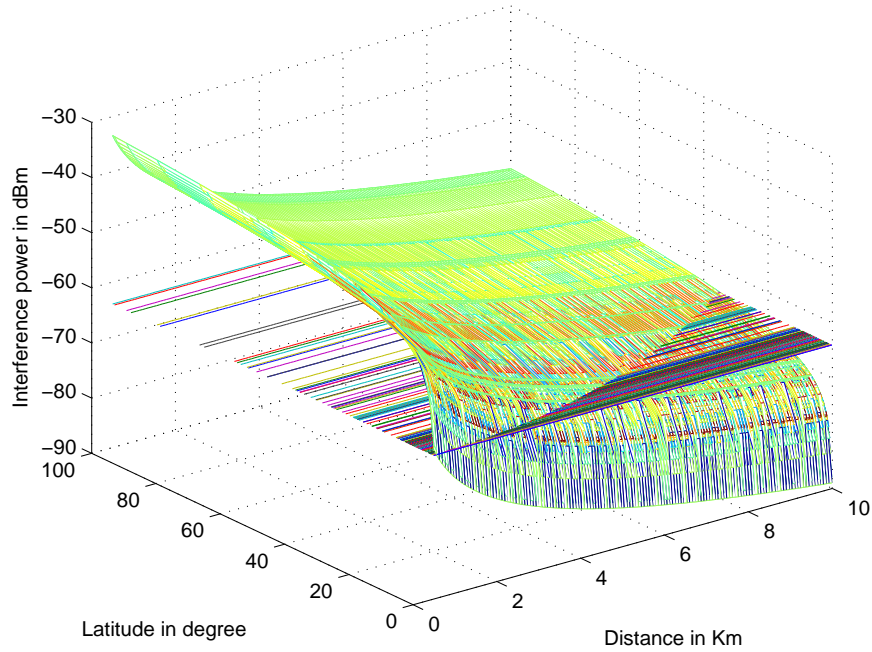


FIGURE 6.2: Interference power versus latitude and distance

described below. We consider the spectral coexistence of a C-band FSS link and a terrestrial cellular link both operating in the normal forward mode. In this scenario, the interfering paths can be (i) from the FSS satellite to the terrestrial terminals, and (ii) from the terrestrial BS to the satellite terminals. The first interference can be considered to be negligible due to that fact that satellite and terrestrial terminals have different sensitivity levels and the large propagation distance [95]. Thus, the main interfering path is from the terrestrial BS to the satellite terminals. For the sake of simplicity, we consider interference analysis between a single terrestrial BS antenna and a single satellite terminal. However, this can be generalized for multiple terrestrial BSs considering the aspect of aggregate interference since there may exist multiple BSs interfering the same satellite terminal in practical scenarios. We assume the satellite terminal to be equipped with an offset-fed parabolic dish antenna and use the radiation pattern of offset-fed parabolic antenna in the azimuth plane for interference analysis with the terrestrial BS. In order to analyze the effect of satellite terminal's geographical location on the received interference level, we repeat this task over a latitude range of 35° to 70° N. Herein, we consider the free space path loss model for calculating the interference level received at the satellite terminal considering the worst case scenario¹. Further, in order to analyze the effect of distance between BS and the satellite terminal, we consider a range of distances from 0.5 km to 10 km for each latitude position. The link budget and simulation parameters used for interference analysis are provided in Table 6.1. While analyzing the elevation angular range of the points on the Europe satellite map coverage with respect to SES ASTRA 2D GEO satellite located at 28.2° E, it has been observed that it ranges from 7.07° to 49.40° .

Figure 6.2 depicts interference power versus latitude over the considered region and the distance (between satellite terminal and the BS) in the form of a 3D plot. From the figure, it can be deduced that the interference power increases as we move towards the polar region for the considered example. This result may be different for the case of other satellite positions since the elevation angle of the satellite terminal depends on the latitude position of the terminal and the difference in the longitude position between the terminal and the satellite. For the interference region definition purpose, we consider -64 dBm as the tolerable interference threshold value i.e., interference below this value is tolerable to the satellite terminal. This threshold value has been chosen on the basis of dynamic frequency selection

¹In practice, there may occur additional loss due to the presence of obstacles and other loss mechanisms in the propagation path between a satellite terminal and the terrestrial BS. In this context, authors in [429] have recently studied the interference modeling problem considering a realistic path loss model in context of ongoing CoRaSat project.

TABLE 6.1: Simulation & Link Budget Parameters

Parameter	Value
Carrier frequency f	4 GHz
Terrestrial BS RF power P_t	66.98 dBm
Terrestrial BS antenna Gain G_t	20 dBi
EIRP BS antenna $EIRP$	86.98 dBm
Distance bet SAT Terr and BS d	0.5 km to 10 km
Path loss range $L_p \propto d^{-2}$	98.47 to 124.49 dB
Satellite Terminal Gain range G_r	20 dBi to -9.5047 dBi
Beam Radius	165 km
Satellite latitude	28.2° E
Satellite height	35786 km
Parabolic dish F/D ratio	1/2
Considered latitude range	35° N to 70° N
Considered longitude range	10° W to 45° E
Elevation angle range	7.07° to 49.40°
SAT terminal slant range	37325 km to 41070 km

(DFS) threshold² for devices having Effective Isotropic Radiated Power (EIRP) values from 23 dBm to 30 dBm [430]. From the simulation result presented in Fig. 6.2, it can be noted that interference mitigation techniques need to be considered for all the latitude range if the distance between satellite terminal and the terrestrial BS is less than 2 km and the interference becomes worse as we move further towards north. If we consider the regions having elevation angles less than 30° i.e., as we move from 52° to the north for distances between satellite terminal and BS antenna up to 5 km, the interference becomes worse. This region can be considered as a high interference region and another region below 52° can be regarded as a tolerable interference region.

Furthermore, it can be noted that satellite terminals with elevation angle less than 30° are in the risk of getting more than -64 dBm interference from the terrestrial BS for distances up to 5 km. In terms of distances, in general, the interference needs to be accounted and handled carefully if the distance between the satellite terminal and the terrestrial BS is less than 5 km. In case of satellite antennas oriented with elevation angle less than 10°, a separation distance of at least 10 km needs to be taken into account. If we want to allow the co-existence of satellite and terrestrial systems in the regions where the elevation angle is below 10°, interference mitigation techniques may not be sufficient to mitigate the interference. In this context, suitable SS and DB techniques need to be investigated as described in the following subsection.

6.1.2 Techniques Selection

1. Selection Criteria: While considering the coexistence of FSS satellite and terrestrial cellular links in the normal forward mode, a general cognitive structure can be represented as an X model as shown in Fig. 6.3. In this model, we have two desired links and two interfering links. As mentioned earlier, if we consider interference from the satellite to the terrestrial terminals to be negligible, the X network model can be reduced to Z model. This reduction is possible in the co-existence of satellite-terrestrial networks and can be taken as an advantage over the co-existence scenario of two terrestrial networks. By using the interference modeling with regard to the geographical location presented before, the Z model can be further reduced to a parallel model as shown in Fig. 6.3 for low interference regions. Parallel structure allows two networks to coexist independently in the same spectrum. In low interference regions, there is possibility of co-existence of satellite and terrestrial networks in the same spectrum with very less interaction, whereas, in high interference regions, Z model needs to be considered by allowing a sufficient level of interaction between satellite and terrestrial systems.

²This threshold has been chosen as a reference for illustrating interference modeling method and suitable models can be used in practical scenarios.

In the above context, the following two interference models can be considered: (i) low interaction model for the regions below 52° and distances more than 5 km, and (ii) high interaction model for the regions above 52° and distances less than 5 km. In each scenario, one link may be considered as strong and the other as weak, primary links always being strong. If the interference level is high, there arises less possibility of suppressing interference by using existing interference mitigation techniques and complex interference mitigation techniques need to be investigated. In this context, it's better to use SS and DB techniques for achieving the best performance. Out of these two techniques, DB technique can be used from long-term perspective and SS from short-term perspective. If the interference level is low or medium, interference from one system to another system can be suppressed by using some form of underlay techniques. Overlay techniques can be used in both high interference and low interference scenario by using advanced coding and modulation techniques. Since a sufficient level of interaction between primary and secondary system is required in overlay systems, this technique appears to be complicated from practical aspects in the considered scenario.

2. Applicable Techniques: The salient features of the main CR techniques discussed in the literature and their challenges for cognitive SatComs are summarized in Table 6.2. Regarding SS techniques, several techniques such as ED, matched filter based detection, cyclostationary feature detector, covariance/eigenvalue based detector etc. are studied in the literature and research works are being carried out towards exploiting new domains such as elevation angle, polarization, radiation pattern etc. Since SS in the satellite cognitive scenario needs to be carried out over a wide coverage area, collaboration of terrestrial BSs to aid in satellite SS can be one important approach in the considered scenario. In this context, exploring the applicability of collaborative SS to solve the HNP in SatCom systems. Furthermore, different cooperative sensing techniques can be applied in practical scenarios which may help the satellite users which are in deep fade region and reduce the HNP caused by failure in detecting the presence of PU due to presence of blocking obstacles and fading. Among many available SS techniques, ED is the most common because of its low computational and implementation complexities [13]. The optimal way for any signal detection is a matched filter since it maximizes the received SNR and it requires less time to achieve high processing gain due to its coherent nature. However, the main drawback of this method is that a CR needs a dedicated Rx for every PU class. In a cyclostationary feature-based detection technique, the prior knowledge on certain features of the PU signals is required for performing detection [10].

In the DB technique, STs query a DB in order to find the unoccupied frequency bands and transmit in these bands. The main drawback with this technique is that it mainly considers the static allocation of free bands and dynamic channel allocation needs the frequent update of the DB, which seems to be difficult to implement in the considered scenario. Regarding overlay techniques, encoding techniques may depend up on the level of interference between primary and secondary systems i.e., based on the geographical location.

Regarding underlay techniques, several interference mitigation and resource allocation techniques can be applied. The interference constraint in an underlay scenario can be met by using the following approaches: (i) Multiple antennas: suitable beamforming techniques can be applied to reduce interference to the PUs, (ii) Wide Bandwidth: cognitive signal can be spread below the noise floor and de-spread at the secondary Rx, and (iii) Power control: suitable power levels can be applied at the STs to ensure that the interference is below the PU interference threshold. Furthermore, various techniques such as transmit beamforming, IA, user scheduling in combination with beamforming can be employed to mitigate interference to the PUs. Moreover, underlay techniques can be applied in satellite cognitive scenario by exploiting additional dofs such as polarization, radiation pattern of antenna, elevation angle etc. In general, satellite antennas use circular polarization and terrestrial BS antennas use linear polarization. In this context, polarization domain can be considered as an additional dof to isolate the interference between primary and secondary systems. If the polarization types of the signal and receiving antenna are matched with each other, then maximum power of arriving signal is transferred to the antenna. Therefore, the polarization domain can be used from the perspective of sensing the

TABLE 6.2: Features of main CR techniques

Cognitive Techniques	Spectrum Sensing	Underlay	Overlay	Database
Cognitive Information	Power spectral density	Channel State Information (CSI)	CSI and data	Geolocation data/history information
QoS Constraints	Probability of detection Probability of false alarm	Interference Threshold	Rate limit threshold	Access Time
Applicable Techniques	<ul style="list-style-type: none"> Single node sensing/ Multi-antenna sensing Collaborative sensing (centralized/distributed) Energy detection Matched filter based detection Cyclostationary feature detector Autocorrelation/Covariance /Eigenvalue based detection Polarization/DoA sensing Wideband sensing (Compressive sensing) Interference modeling Interference detection 	<ul style="list-style-type: none"> Beamforming Exclusion Zone Resource allocation (power/carrier) Interference alignment and cancellation Scheduling Beamhopping Polarization/SNR-aware techniques 	<ul style="list-style-type: none"> Superposition coding Rate splitting Relaying: amplify and forward, decode and forward Known Interference precancellation Coordinated power control 	<ul style="list-style-type: none"> Localization assisted techniques Storage and access techniques Prediction techniques
Challenges for Cognitive SatComs	<ul style="list-style-type: none"> Wide area sensing Weak signal detection LoS interference Hidden node problem Sensor complexity 	<ul style="list-style-type: none"> Adaptive resource allocation/power control Interference control Synchronization LoS slow fading channel 	<ul style="list-style-type: none"> High level of coordination Efficient coding and transmission techniques Synchronization 	<ul style="list-style-type: none"> Requirement of third party for DB management Wide satellite footprint Data acquisition

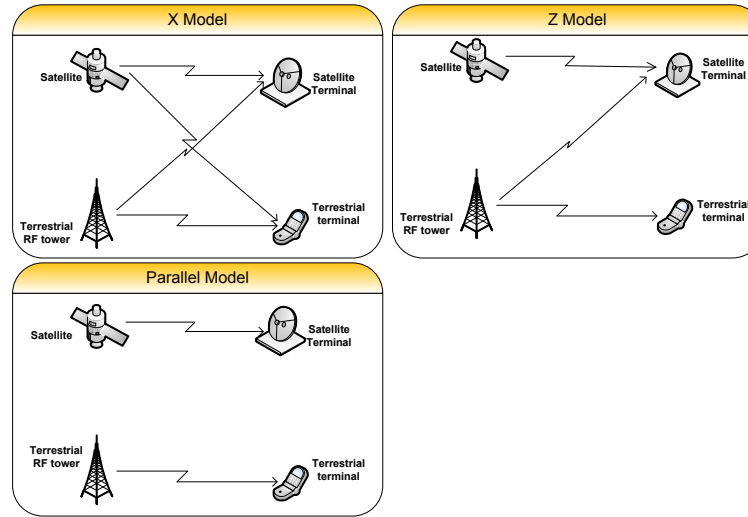


FIGURE 6.3: Different co-existence models

PU signal as well as increasing the throughput of primary and secondary systems. In this context, we study the performance of an ED-based SS in a dual-polarized fading channel in Section 6.3.

Additionally, GEO satellite terminal antennas have the special feature to always look to the equator. This feature can be used as an additional dof in analyzing the interference. Further, it can be used for DoA aware beamforming-based underlay techniques by using a priori knowledge of DoA of satellite signals as illustrated in Section 6.4. Moreover, proper design of radiation patterns can exploit another degree of freedom for the coexistence of satellite and terrestrial networks on the same spectrum. Depending on the latitude, satellite is seen under a high elevation angle and proper design of radiation patterns can allow the reduction of interference between primary and secondary systems. This fact facilitates 3D space-time-frequency utilization in satellite CR networks rather than 2D time-frequency utilization in terrestrial CR networks [90].

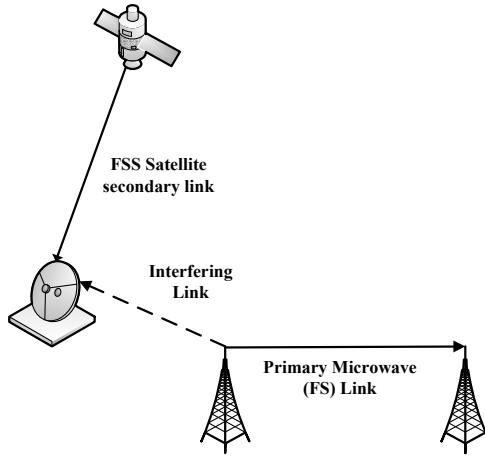


FIGURE 6.4: Coexistence of FSS satellite downlink and microwave link

6.2 Interference Detection

In this section, we study an interference detection problem for a cognitive Rx considering an example of hybrid satellite-terrestrial scenario as described in the following subsection.

6.2.1 Scenario and Problem Description

We consider the coexistence of a GEO FSS downlink with terrestrial FS links both operating in the Ka band (17.7 – 19.7 GHz) as represented in Fig. 6.4. This is one of the scenarios considered under the framework of European FP7 project CoRaSat [96]. In the considered scenario, the primary and secondary links are FS link and FSS downlink, respectively. In the considered scenario (Fig. 6.4), the downlink interference from the FSS satellite to the FS links is taken into account by system planning and can be kept below the defined regulatory limitations in terms of the maximum power flux-density (pfд) at the earth's surface [431]. According to Article 21 of ITU-R radio regulations, the pfд at the earth's surface produced by emissions from a space station, including emissions from a reflecting satellite shall not exceed the limit provided in Table 21.4 of [431] for all conditions and for all modulation schemes. For example, a FSS satellite operating in 17.7 – 19.7 GHz frequency range should respect the pfд limit of $-15 \text{ dBW/m}^2/\text{MHz}$ for 0° to 5° angles of arrivals above the horizontal plane. However, the interference from FS Transmitters (Txs) to the secondary satellite terminal needs to be taken into account in order to guarantee sufficient QoS of the SUs.

The satellite link (in DVB-S2 and DVB-SX standards) from a central hub station to the terminals generally employs the ACM scheme in order to adapt the transmission modulation and coding to the terminal's Signal to Interference plus Noise Ratio (SINR) [432]. Depending on the link setup, the rain fading at the location of the FSS terminals may affect both the carrier as well as the FS interference level at the FSS Rx input with different magnitudes. We can define this margin as the amount the carrier power can be faded to reach a specific threshold level of the used modulation and coding. This margin parameter is consequently systematically underestimated in case the interference could not be distinguished from the noise level at the FSS Rx input. This would be the case if we could not detect and estimate the interference received from the terrestrial FS links. However, the detection and estimation of the FS interference is feasible in principle and we investigate this aspect in this work. We consider the problem of detecting the FS link interference presence at the FSS Rx input and compute the performance of a practical detector. It can also be treated as a sense and avoidance scheme since the cognitive satellite terminal attempts to detect the harmful FS signal using suitable sensing techniques, and based on the result, it tries to avoid using active harmful FS carriers. In other words, the FSS terminal tries to avoid activity in the bands where the interference received from the FS Tx's exceeds a

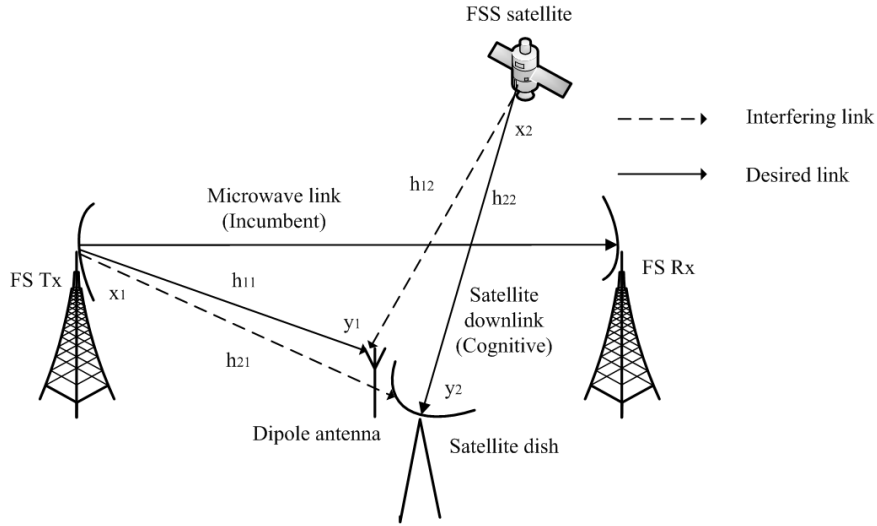


FIGURE 6.5: Front end of satellite terminal with additional dipole antenna and corresponding desired/interfering links

predetermined threshold. The important application of this technique in the considered scenario comes from the fact that after detecting the FS interference, the cognitive system does not need to concern about the location of the FS Rxs during its transmission [96]. For this purpose, different CR techniques such as EZ, combination of DB and SS, and sense and avoidance schemes can be investigated. In this work, we study the feasibility of applying sensing and avoidance schemes to allow this coexistence.

The main challenges for implementing SS in the considered scenario are to detect the weak levels of the FS interference, and to define an appropriate sensing threshold in order to decide whether a harmful FS carrier is present or not. Since all the FS transmissions are not harmful to the FSS terminal, we define the harmful FS carrier as the active FS carrier which affects the normal operation of the FSS terminal by creating interference above its interference tolerance threshold. In the existing SS literature, the commonly used assumption is that all the SUs are silent during the period of sensing and the sensor receives only PUs' signal during the sensing interval. Unlike the above assumption, the FSS terminal under the considered scenario receives downlink transmission from its satellite beam as well as the FS transmission simultaneously. In this context, the main challenge is how to detect the presence of a primary signal from the received signal which can be a combination of the desired signal (FSS downlink signal), interference signal (transmit signal from the FS Tx), and the Rx thermal noise.

To address the above issues, we can exploit the use of an additional RF chain with a dipole antenna having a donut shaped gain pattern across the horizon in addition to the existing satellite dish antenna. The difference between two antennas is that the dish antenna used for receiving a satellite signal is directed towards the satellite and the additional dipole antenna can be dedicated for detecting the FS signal coming from the horizontal direction. Based on ITU-R S.456, the dish antenna receiving gain towards the horizon varies from 7 to -6.6 dB while considering GEO satellite terminals located in European continent with 10° to 35° elevation angles. Since a purely omnidirectional antenna is not practically realizable, we consider a half wave dipole antenna which has a gain of 2.15 dB [433]. Other options can be (i) a rotating horn antenna, (ii) a Uniform Linear Array (ULA) with electronic steering, (iii) a 4/6 horn circular detector looking over the horizon, and (iv) several detectors on the back of the reflector. However, these options are quite costly in comparison to the inclusion of a dipole antenna. In the above context, we assume that the FSS terminal is equipped with a dipole antenna, which is dedicated for the sensing purpose as depicted in Fig. 6.5.

Let $x_1(t)$ be the signal transmitted by the FS Tx at time instant t and $x_2(t)$ be the signal transmitted by the FSS satellite. Further, let h_{11} denote the channel gain from the FS Tx towards the dipole antenna, h_{21} be the channel gain from the FS Tx towards the dish antenna, h_{12} be the channel gain

from the FSS satellite towards the dipole antenna and the h_{22} as the channel gain from the FSS satellite towards the dish antenna. It can be noted that these channel gains depend on the gains of the transmit and receive antennas and the path loss of the corresponding link. It should be noted that from the view of detecting the harmful FS signal, Line of Sight (LoS) path between the FS Tx and the dipole antenna is the worst-case since these effects further reduce the interference level. Therefore, we do not consider the effects of rain fading and shadowing in this contribution. As depicted in Fig. 6.5, the dipole antenna receives two signals: one signal from the FS Tx and another one from the FSS downlink transmission. Since the purpose of this antenna is to sense the FS transmission, the signal received from the FS Tx is the desired one, and the signal received from the FSS transmission is the interfering one. Similarly, the satellite dish receives two signals: the desired signal from the FSS satellite and the interfering signal from the FS Tx. In the aforementioned scenario, different individual or joint signal processing techniques can be applied in order to separate the intended signal from the FS interfering signal [106]. In this work, we study individual signal processing using an ED technique as described in the following subsection.

6.2.2 Problem Formulation

In an individual signal processing method, two RF chains of the cognitive satellite terminal process the received signals separately. The RF chain with the dipole antenna is responsible for sensing the presence of the FS signal. Basically, this process detects the power level received by the dipole antenna and applies decision threshold in order to decide the presence or absence of the FS signal. Let H_0 denote the hypothesis for the absence of the FS harmful transmission and H_1 denote the hypothesis for the presence of the FS harmful transmission, then the binary hypothesis testing problem for detecting the presence of the FS signal can be written as

$$\begin{aligned} H_0 : y_1(n) &= h_{12}x_2(n) + z(n), \text{ FS absent} \\ H_1 : y_1(n) &= h_{11}x_1(n) + h_{12}x_2(n) + z(n), \text{ FS present}, \end{aligned} \quad (6.2)$$

where $z(n)$ denotes the AWGN at the dipole receive chain. In order to test the above hypothesis, we need to find a decision statistic whose distribution sufficiently differs under the H_0 and the H_1 hypotheses. If the energy of the FSS received signal at the dipole antenna remains more or less the same and is known by performing link budget analysis, then the sensing threshold can be solely based on the distribution of the noise energy. Subsequently, the sensing threshold calculated from the distribution of the noise energy can be scaled based on the known value of the FSS received signal level. In the above hypothesis testing problem, if the hypothesis H_0 is satisfied, then it can be decided that the FS signal over a certain band is absent and then the FSS system can use this band in the secondary basis. Whereas, if the hypothesis H_1 is satisfied, the decision is the presence of the FS signal and the FSS transmission should be switched to another band. In case, other bands in the FS specific allocated band are not available or their quality is not better enough, the FSS transmission should be moved to the exclusive band. These decisions are to be taken centrally by the satellite network management system based on the feedback it receives by the terminals.

In the considered FS link detection problem, we treat the FSS signal as the noise. This is due to the fact that the FSS received signal at the dipole antenna is well below the harmful FS signal corresponding to the Interference to Noise (I/N) target of -10 dB and is very close to the noise level at the dipole antenna as verified by numerical analysis in 6.2.4. In this case, (6.2) reduces to the following conventional hypothesis testing problem

$$\begin{aligned} H_0 : y_1(n) &= z(n), \text{ FS absent} \\ H_1 : y_1(n) &= h_{11}x_1(n) + z(n), \text{ FS present}. \end{aligned} \quad (6.3)$$

In the following subsection, we apply an ED technique in order to solve the above binary hypothesis problem (6.3).

After sensing the FS signal using an energy detector, the sensed power level has to be translated into the interference level received by the dish antenna. To do this accurately, the offset angle of the FSS satellite receiving antenna in the direction of FS transmission should be known. In practice, this information can be obtained from the DB by knowing the direction of FS transmission, and the exact locations of the FS Tx and FSS terminal. However, it may be difficult to acquire this information for all cases. In this context, we can follow the worst-case approach considering the elevation angle of the FSS terminal, which is the lowest possible off-axis angle to the horizon, as the offset angle towards the FS transmission. Furthermore, due to high directivity of the FS transmission, we assume only a single FS as a major interferer towards the FSS terminal.

The sensing of the harmful FS transmission can be done either in the DVB-S2 receive chain or in the dipole chain. The main differences between these two approaches are: (i) sensing with the satellite dish requires to detect low SNR i.e., -10 dB for I/N target of -10 dB whereas the dipole antenna receives better SNR as illustrated in Section 6.2.4, (ii) sensing with the satellite dish requires the cancelation of the DVB-S2 signal before deciding the presence or absence of the FS signal whereas the DVB-S2 signal is negligible in comparison to the harmful FS interference while sensing with the dipole (illustrated in Section 6.2.4). Due to these reasons, we focus on the dipole sensing for our analysis in the following subsection and later we evaluate the performance of the sensing with both approaches in our numerical results.

6.2.3 Energy Detection-based Interference Detection

In this subsection, we provide theoretical expressions for probability of false alarm (P_f) and probability of detection (P_d) for the ED based sensing in the considered scenario. Let us consider that the transmitted FS signal $x(n)$ is an independent and identically distributed (i.i.d.) Gaussian random process with mean zero and variance $E[x(n)]^2 = \sigma_x^2$ and the noise $z(n)$ is a Gaussian i.i.d. random process with zero mean and variance $E[z(n)]^2 = \sigma_z^2$. Furthermore, we assume that the primary FS signal $x(n)$ is independent from the noise $z(n)$. Let τ be the sensing time and N be the number of samples collected within this duration i.e., $N = \lceil \tau \rceil f_s$. The test statistic for the ED technique is given by $T = \frac{1}{N} \sum_{n=1}^N |y(n)|^2$. It can be noted that the test statistic T is a random variable and under the H_0 hypothesis, for very large values of N , the probability density function (p.d.f.) of T can be approximated by a Gaussian distribution with mean $\mu = \sigma_z^2$ and variance $\sigma_0^2 = \frac{1}{N} [E[z(n)]^4 - \sigma_z^2]$ [107]. Using binary hypothesis testing, the expressions for P_f and P_d can be computed by (2.5). For Circularly Symmetric Complex Gaussian (CSCG) noise case, the expression for P_f can be written as [107]

$$P_f(\lambda_{th}, \tau) = Q \left(\left(\frac{\lambda_{th}}{\sigma_z^2} - 1 \right) \sqrt{\tau f_s} \right), \quad (6.4)$$

where $Q(\cdot)$ is the complementary distribution function of the standard Gaussian random variable, given by $Q(x) = \frac{1}{\sqrt{2\pi}} \int_x^\infty \exp(-\frac{t^2}{2}) dt$. Similarly, under the H_1 hypothesis, the expression for P_d is given by

$$P_d(\lambda_{th}, \tau) = Q \left((\lambda_{th}/\sigma_z^2 - \gamma_{FS} - 1) \sqrt{\frac{\tau f_s}{2\gamma_{FS} + 1}} \right), \quad (6.5)$$

where γ_{FS} is the received SNR of the primary signal measured at the dipole chain, which can be written as $\gamma_{FS} = P_r/\sigma_z^2$, where P_r is the received power at the dipole antenna, given by $P_r = P_t G_t(\theta) G_r \left(\frac{\lambda}{4\pi d} \right)^2$, where P_t is the FS transmit power, θ is the offset angle (from the boresight direction) of the FS transmitting antenna in the direction of satellite terminal and $G_t(\theta)$ is the corresponding gain, G_r is

the fixed gain of the dipole antenna, λ is the wavelength, d is the distance between FS Tx and the satellite terminal.

Let \bar{P}_f be the target P_f and \bar{P}_d be the target P_d . Then combining (6.4) and (6.5), P_d is related to \bar{P}_f as follows

$$P_d = Q \left(\frac{1}{\sqrt{2\gamma_{FS} + 1}} (Q^{-1}(\bar{P}_f) - \sqrt{\tau f_s \gamma_{FS}}) \right). \quad (6.6)$$

Using the above expressions, for a given pair of target false alarm and detection probabilities (\bar{P}_f, \bar{P}_d) , the minimum number of samples required to achieve these targets can be determined using the following relation

$$N_{\min} = \frac{1}{\gamma_{FS}^2} [Q^{-1}(\bar{P}_f) - Q^{-1}(\bar{P}_d) \sqrt{2\gamma_{FS} + 1}]^2. \quad (6.7)$$

In the above analysis, it is assumed that the noise variance is perfectly known to the detector. However, in practice, the noise is neither perfectly Gaussian, perfectly white, nor perfectly stationary [15]. Therefore, the noise variance in practice has to be estimated by using a proper noise calibration method. The noise calibration can be done either during the manufacturing process or by carrying out on-site Out of Bands (OoB) measurements. Another option for noise calibration is to use in-band measurements at the frequencies where the pilot is absent so that the noise statistics can be calibrated at the pilot frequencies [217]. Further, in the considered FS detection problem, the noise variance can also be estimated by carrying out sequential measurements over the band of interest if we know the spectrum grids used by the terrestrial links.

In [15], it has been shown that it's not possible to achieve the robust detection performance beyond a certain SNR value even by increasing the sensing duration in the presence of noise variance uncertainty. The distributional uncertainty of the noise can be represented with a interval $\sigma^2 \in [(1/\rho)\sigma_z^2, \rho\sigma_z^2]$, where σ_z^2 is the nominal noise power and the parameter $\rho > 1$ indicates the uncertainty level. Following the procedure in [15], to achieve target P_f and P_d robustly for the considered CSCG noise case, (6.4) and (6.5) in the presence of noise uncertainty can be written as

$$P_f(\lambda_{th}, \tau) = Q \left(\left(\frac{\lambda_{th}}{\rho\sigma_z^2} - 1 \right) \sqrt{\tau f_s} \right). \quad (6.8)$$

$$P_d(\lambda_{th}, \tau) = Q \left(\left(\frac{\lambda_{th}}{\frac{1}{\rho}\sigma_z^2} - \gamma_{FS} - 1 \right) \sqrt{\frac{\tau f_s}{2\gamma_{FS} + 1}} \right). \quad (6.9)$$

The minimum number of samples required to achieve target \bar{P}_d and target \bar{P}_d in presence of noise variance uncertainty can be obtained after eliminating λ_{th} from (6.8) and (6.9), given by

$$N_{\min 1} = \frac{[Q^{-1}(\bar{P}_f) - Q^{-1}(\bar{P}_d) \sqrt{2\gamma_{FS} + 1}]^2}{[\gamma_{FS} - (\rho - \frac{1}{\rho})]^2}. \quad (6.10)$$

By assuming $2\gamma_{FS} + 1 \approx 1$ for low SNR values in (6.10), it can be noted that $N \rightarrow \infty$ as γ_{FS} decreases with the value of ρ . This particular value of SNR is called as SNR wall [15] and it reflects that the ED can not robustly detect the signal if $\gamma_{FS} \leq (\rho - \frac{1}{\rho})\sigma_z^2$. Further, the value of SNR equal to $\frac{\rho^2 - 1}{\rho}$ is SNR wall of an energy detector.

6.2.4 Numerical Results

In this section, we study the sensing performance of the ED-based sensing and avoidance scheme in the considered scenario. While analyzing the detector sensitivity, we can use the worst-case condition considering the lowest possible EIRP of the FS transmitting antenna. Whereas, while analyzing the

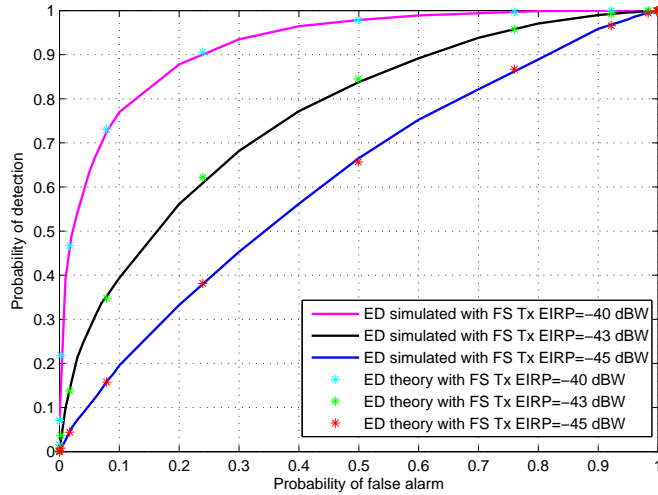


FIGURE 6.6: Probability of detection versus probability of false alarm ($\tau = 2$ ms, $d = 1$ km)

interference effect on the FSS terminal, we need to consider the highest possible EIRP value of the FS Tx. In Table 6.3, we present simulation parameters used for producing the presented results. In our results, we consider that the FSS signal received by a dipole antenna is well below the noise level at the dipole chain as well as the received harmful FS signal level corresponding to the I/N target of -10 dB at the satellite dish. For example, using the link budget parameters specified in Table 6.3, the harmful interference power threshold at the dipole chain is -146.6 dBW/MHz and the received FSS satellite signal level at the dipole chain corresponding to the maximum transmit power is -151.8 dBW/MHz which is 9.8 dB below the dipole chain noise level of -142 dBW/MHz and 5.2 dB below the harmful interference power threshold. It should be noted that this received FSS level further reduces when considering fading and atmospheric effects in the FSS downlink channel. From Table 6.3, based on ITU-R F.758-5 and ITU-R F.699, the worst-case EIRP and the maximum possible EIRP for FS transmission are found to be -44.79 dBW and 36.29 dBW respectively.

Since we are interested in protecting the FSS terminal from the FS harmful interference, the hypothesis testing problem (6.3) while considering the I/N threshold of -10 dB at the DVB-S2 receive chain can be written as

$$\begin{aligned} H_0 : I(\text{dBW}) &\leq -10 \text{ dB} + N(\text{dBW}), \text{ harmful FS absent,} \\ H_1 : I(\text{dBW}) &> -10 \text{ dB} + N(\text{dBW}), \text{ harmful FS present,} \end{aligned} \quad (6.11)$$

where N denotes the receiver noise power in dBW over the considered bandwidth. In our detection problem, the FS interference level greater than -10 dB + N (dBW) should be successfully detected.

Figure 6.6 shows the performance of the ED-based sensing in the considered scenario in terms of Receiver Operating Characteristic (ROC) curves ($\tau = 2$ ms, $d = 1$ km). In this result, we have considered different lower values of EIRPs including the worst-case EIRP (-45 dBW). From the figure, it can be noted that the P_d increases with the increase in the value of P_f and better detection is achieved for higher values of FS EIRPs. The theoretical results plotted in Fig. 6.6 were obtained using (6.6). To evaluate the sensing performance with respect to the distance between FSS terminal and FS Tx, we plot P_d versus distance between FS terminal and the FSS terminal in Fig. 6.7 with parameters ($\tau = 2$ ms, $P_f = 0.01$). From the figure, it can be noted that the value of P_d decreases with the increase in the distance. Furthermore, the sensing performance increases with the increase in the value of FS EIRP. In order to evaluate the level of FS interference on the satellite terminal, we consider a Ka band FSS link with a satellite terminal situated in Betzdorf, Luxembourg (49.68° N, 6.35° E) communicating with the SES ASTRA 2D GEO satellite located at 28.2° E. The elevation angle of the considered terminal is found to be 29.36° . As stated earlier, we can follow the worst-case approach to find the offset angle of the FSS receiving antenna in the direction of the FS Tx. For the elevation angle of 29.36° in the

TABLE 6.3: Simulation and link budget parameters

Parameter	Value
Carrier frequency	18 GHz
<i>Parameters for FS Tx</i>	
Tx output range	-37 to -3.0 dBW (ITU-R F.758-5)
Feeder loss range	0 to 2 dB (ITU-R F.758-5)
Antenna Radiation Pattern	ITU-R F.699-7
Antenna diameter	0.6 m
Lowest possible gain	-5.79 dBi
Lowest EIRP	-44.79 dBW
Maximum gain	39.29 dBi
Maximum EIRP	36.29 dBW
FS carrier Bandwidth	5 MHz
<i>Parameters for dipole chain</i>	
Antenna type	Half wave dipole
Antenna Gain	2.15 dB
Sampling Rate	10 MHz
Rx Noise Temperature	460 K
Noise power at dipole Rx	-142 dBW/MHz
<i>Parameters for DVB-S2 chain</i>	
FSS carrier BW	27 MHz
FSS ES antenna	42.1 dBi
Rx Noise temperature	262 K
Noise power	-143.4 dBW/MHz
I/N target at dish	-10 dB
Interference Threshold	-153.4 dBW/MHz
Maximum rx antenna gain	42.1 dBi
Antenna Radiation pattern	ITU-R S.456
Antenna diameter	0.75 m
FSS site height	100 m
Terminal location	49.68° N, 6.35° E
<i>Parameters for FSS satellite</i>	
GEO satellite location	28.2° E
Satellite Altitude	35786 km
Tx power @saturation	80 W
Max. antenna gain	50 dBi
Path loss to terminal	-208.67 dB

TABLE 6.4: Sensing time calculation for ED detector

Parameter	Value
I/N target at the dish (FSS Rx LNB input)	-10 dB
FSS carrier bandwidth	27 MHz
Rx noise temperature at the dish (FSS LNB I/P)	262 K
Link noise contribution	1 dB
Noise power (N) at the dish (LNB input)	-143.4 dBW/MHz
Interference threshold at the dish (LNB input)	-153.4 dBW/MHz
Received power threshold at dipole (P_r)	-146.6 dBW/MHz
Rx noise temperature at dipole (LNB input)	460 K
FS carrier bandwidth	5 MHz
Noise Power at dipole chain (LNB input) (N_o)	-142 dBW/MHz
$\gamma_{FS} = P_r/N_o$ threshold at dipole	-4.59 dB
Target probability of detection	0.9
Target probability of false alarm	0.01
Minimum number of samples N_{\min}	$132.13 \approx 132$
Sampling rate at dipole chain f_s	10 MHz
Sampling time $\tau = N_{\min}/f_s$	0.0132 ms

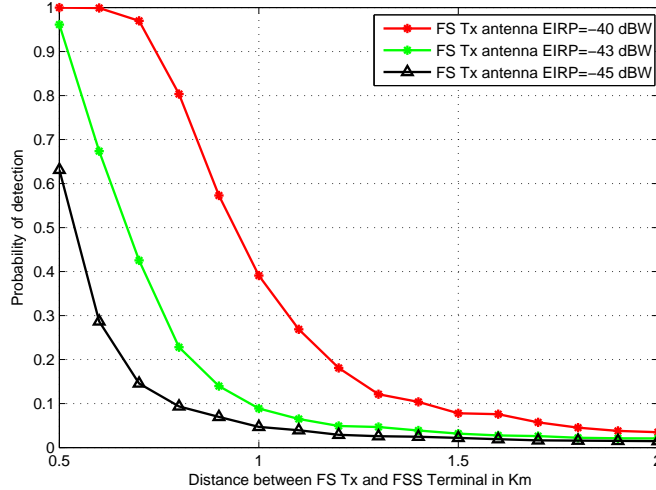


FIGURE 6.7: Probability of detection versus distance between FS Tx and FSS terminal ($\tau = 2$ ms, $P_f = 0.01$)

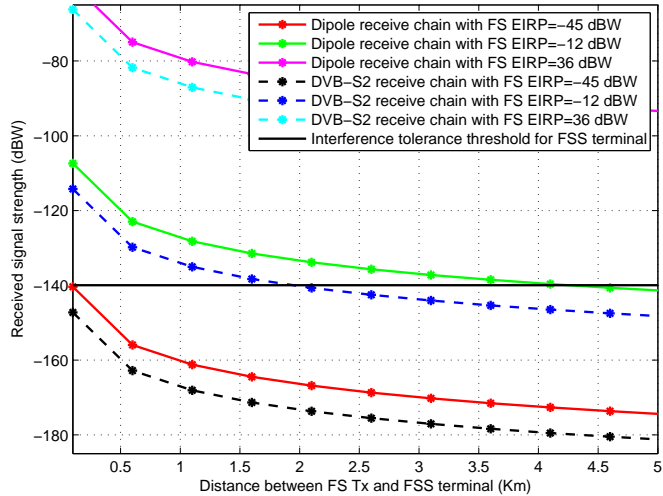


FIGURE 6.8: Total signal strengths received by dipole and DVB-S2 chains for different EIRP values

considered use case, the gain of FSS receiving antenna in the direction of the FS transmission is equal to -4.69 dB, based on ITU-R S.456. The received power level detected by the dipole antenna can be converted to the interference strength received by the dish antenna in the following way. Interference level picked up by satellite dish antenna (dBW)=signal strength detected by the dipole antenna (dBW) -2.15 dB+Gain of the FSS antenna towards the FS Tx (dB). Figure 6.8 depicts the signal strengths received by the dipole and satellite dish antennas for different values of FS transmit EIRP. From the figure, it can be noted that for the highest value of FS EIRP (36 dBW), the interference level picked up by the satellite dish antenna is well above the interference threshold and the use of shared spectrum band is not possible (even for very large separation distances) in this scenario. Furthermore, for the lowest EIRP value (-45 dBW), the interference level picked up by the satellite dish is well below the interference threshold and the sharing is feasible (even for very small separation distances). For the EIRP value of -12 dBW, it can be observed that the received interference level exceeds the interference threshold for separation distances less than 1 km. However, for the separation distances above 2 km, the received interference level is less than the interference threshold and frequency sharing between FSS downlink and FS link is possible. Therefore, it can be concluded that there exists a range of EIRP values of FS transmission for which frequency sharing is possible between FSS downlink and the FS link.

In Table 6.4, we present calculations for obtaining sensing time for the ED technique considering the I/N target of -10 dB at the DVB-S2 chain of the satellite terminal. It can be noted that the minimum

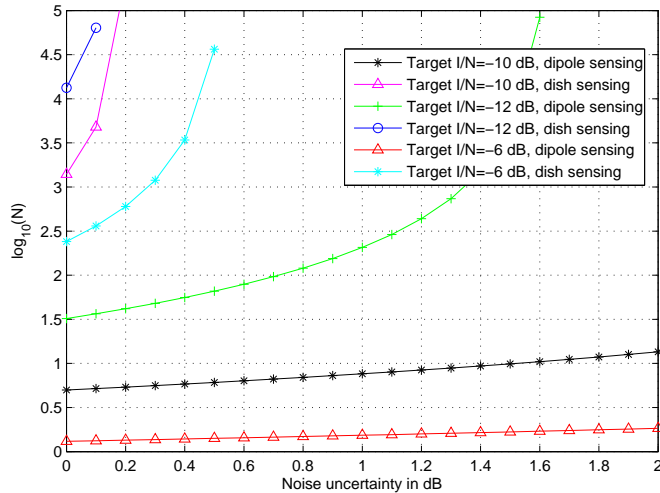


FIGURE 6.9: Sample complexity versus noise uncertainty while using the ED technique (target $P_d = 0.9$, target $P_f = 0.01$)

number of samples required to satisfy the constraints of $P_f = 0.01$, $P_d = 0.9$ and I/N target of -10 dB is around 132. Furthermore, considering the sampling rate of 10 MHz at the dipole chain, the sensing time comes to be 0.0132 ms as depicted in Table 6.4. To analyze the effect of noise uncertainty in the considered problem, we consider the noise uncertainty range from 0 dB to 2 dB and evaluate the detection performance using the analysis presented in Section 6.2.3.

Figure 6.9 analyzes the sample complexity (in terms of $\log_{10}(N)$) of the ED technique with the noise uncertainty level for different I/N target values at the DVB-S2 receive chain. Further, we present the results of dipole sensing and dish sensing for the considered target values of I/N . From the figure, it can be noted that with dipole sensing, the number of samples for I/N target values of -10 dB and -6 dB are practically feasible and there occurs no SNR wall problem for the considered noise uncertainty range. If we want to guarantee the $I/N = -12$ dB, the detector faces the SNR wall problem at 1.6 dB noise uncertainty value even with the dipole sensing. However, for the single interferer case, the I/N value of -10 dB is quite practical and the dipole sensing provides the desired performance with realizable number of samples. Moreover, if we look at the dish sensing part, SNR wall problem occurs for all the I/N target values within the considered noise uncertainty zone. From this result, it can be noted that the dipole sensing performs well in terms of sensing the FS signal while maintaining the desired I/N target whereas the dish sensing fails within the considered noise uncertainty zone.

6.3 Dual Polarized Spectrum Sensing

Dual polarized channels have been considered in satellite links and terrestrial links to enhance the spectrum efficiency as well as to remove the practical difficulty of spatial separation required by antennas in MIMO links [109] [112]. The use of dual polarized antennas has become a promising cost-effective and space-effective alternative for enhancing the reliability of transmission by creating polarization diversity [434]. However, wireless fading channels may reduce the orthogonality of dual polarized channels causing cross polarization effects. The performance of an ED based SS technique has been carried out in Rayleigh, Rician and Nakagami fading channels in [13, 14, 184] but the dual polarized fading channel has received limited attention. The dual polarized channel is gaining more importance in the cognitive communication [112] [113], and there remain challenges to explore suitable SS techniques for this channel. Further, cross polarization effects impose a challenge to carry out SS in a dual polarized fading channel. This is the main motivation for this work. We carry out the performance analysis of an ED based SS technique in a dual polarized fading channel using different combining techniques. Starting with the single antenna case, we review analytical expressions for P_d and P_f for AWGN and

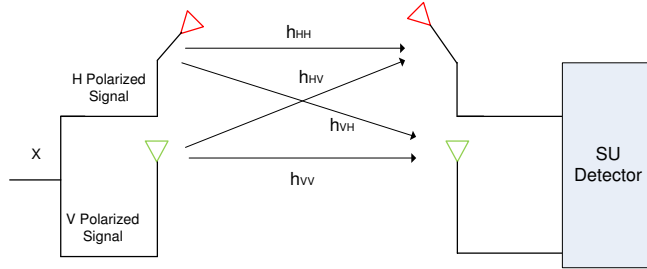


FIGURE 6.10: System Model for the considered dual-polarized SS

Rayleigh fading channels. Subsequently, we deal with uni-polarized MIMO channel which acts as a building block for the dual polarized channel and we include the cross correlation in channel to include the effect of XPD in a dual polarized fading channel.

6.3.1 System and Signal Model

1. Use Case: The hybrid satellite-terrestrial system presented in Fig. 5.3 can be considered as one practical scenario. In this scenario, a microwave backhaul link between terrestrial BSs i.e., FS link can be used as a primary link and the FSS satellite uplink as the secondary. The frequency of operation may range from Ku band to Ka band depending on the deployment of FS links in a certain geographical location. This scenario can be beneficial for satellite operators to take advantage of terrestrial licensed spectrum on the secondary basis. As mentioned before, the use of dual polarization has been exploited for creating polarization diversity in various satellite and terrestrial literature [112, 435, 436]. Hence, dual polarized antennas can be considered on both satellite and terrestrial networks for studying this cognitive scenario. In the considered scenario, the interference from terrestrial FS Tx to the satellite can be considered to be negligible due to large propagation distance as well as due to different directive nature of the FS transmission, whereas interference from the satellite terminal to the terrestrial FS Rx needs to be taken into account to respect the interference constraint of the licensed FS users. This can be done either by using dynamic SS or underlay approaches which guarantee the protection of FS Rxs. In this work, we focus on SS approach considering a dual polarized fading channel.

2. Signal Model: We consider a cognitive scenario with a SU Rx and a PU Tx both equipped with dual polarized antennas. Under this model, it can be considered that the same symbol can be aligned to two orthogonal polarization states and be transmitted through different dimensions from a PU Tx. The system model is illustrated in Fig. 6.10. The received signal at SU Rx can be written in the following form

$$\mathbf{y} = \mathbf{H}_d \mathbf{x} + \mathbf{w}, \quad (6.12)$$

where \mathbf{H}_d is (2×2) channel matrix, \mathbf{x} is (2×1) dual polarized signal and \mathbf{w} is an AWGN vector including independent noise coefficients at two branches of dual polarized antenna. The channel matrix \mathbf{H}_d can be written as

$$\mathbf{H}_d = \begin{bmatrix} h_{HH} & h_{HV} \\ h_{VH} & h_{VV} \end{bmatrix}, \quad (6.13)$$

where h_{mn} denotes the channel coefficient on channel mn . Let H_0 denote the hypothesis of PU being absent and H_1 denotes hypothesis of active PU. The PU signal detection problem can be formulated in terms of following binary hypothesis testing problem.

$$\begin{aligned} H_0 : \mathbf{y}(n) &= \mathbf{w}(n), & \text{PU absent} \\ H_1 : \mathbf{y}(n) &= \mathbf{H}_d \mathbf{x}(n) + \mathbf{w}(n), & \text{PU present} \end{aligned} \quad (6.14)$$

where $n = 1, 2, \dots, u$, u being the product of observation duration T and bandwidth B i.e., $u = TB$. We consider Rayleigh fading channel since the channel between the satellite terminal and the terrestrial

Tx/Rx may not be a LoS channel. We consider SC and EGC techniques in the energy level instead of co-phasing and adding the signals from different antennas as in conventional diversity schemes. These definitions are similar to the square law selection and square law combining terms used in [184]. Further, it can be noted that conventional diversity combining techniques such as MRC technique seem to be difficult to apply for unknown PU signal detection due to weak PU signal as well as no co-operation from the source in the context of cognitive SatComs.

6.3.2 Energy Detection for Single Antenna Case

The ED problem was first studied in [437] for deterministic signals transmitted over a flat band-limited Gaussian noise channel. The performance of SS methods degrades due to fading effects in a wireless channel. The ED problem for signals transmitted over a variety of fading channels using different receive diversity schemes has been considered in [13], [184], [14] [438]. In practical scenarios, the total fading involves the combined effect of two independent processes: small-scale fading and large scale fading i.e., multi-path and shadowing effects [214]. In case of a satellite channel, lognormal fading due to shadowing, rain fading and other atmospheric effects should be taken into consideration [439]. Since we are considering our system model with respect to satellite-terrestrial hybrid scenario, we focus on terrestrial wireless channel which is the sensing channel between satellite cognitive terminal and the terrestrial Tx.

Before considering fading scenarios, let's start with the AWGN case. The decision statistic (T_{ED}) of the energy detector follows a central chi-square (χ^2) distribution with $2u$ dofs under the H_0 hypothesis. Under the H_1 hypothesis, T_{ED} follows a non-central χ^2 distribution with $2u$ dofs and non-centrality parameter 2γ , γ being SNR of the PU signal i.e.,

$$T_{ED} \sim \begin{cases} \chi_{2u}^2, & H_0 \\ \chi_{2u}^2(2\gamma), & H_1 \end{cases} \quad (6.15)$$

The p.d.f. of T_{ED} under H_0 and H_1 can be written as [184]

$$T_{ED} = \begin{cases} \frac{1}{2^u \Gamma(u)} y^{u-1} e^{-\frac{y}{2}}, & H_0 \\ \frac{1}{2} \left(\frac{y}{2\gamma}\right)^{\frac{u-1}{2}} e^{-\frac{2\gamma+y}{2}} I_{u-1}(\sqrt{2\gamma}y), & H_1 \end{cases} \quad (6.16)$$

where $\Gamma(\cdot)$ is the gamma function and $I_n(\cdot)$ is the n -th order modified Bessel function of first kind. Then P_f and P_d can be computed using (2.5). The expression for P_f can be computed using (6.16) to evaluate the P_f expression in (2.5) and can be written as

$$P_f = \frac{\Gamma(u, \frac{\lambda_{th}}{2})}{\Gamma(u)}, \quad (6.17)$$

where $\Gamma(\cdot, \cdot)$ is the incomplete gamma function. Similarly, the expression for P_d can be computed using (6.16) to evaluate P_d expression in (2.5) and can be written as

$$P_d = Q_u(\sqrt{2\gamma}, \sqrt{\lambda_{th}}), \quad (6.18)$$

where $Q_u(\cdot, \cdot)$ is the generalized Marcum Q-function. The expressions in (6.17) and (6.18) do not include the effect of channel fading. For the fading scenario, the expression for P_f becomes same as (6.18) since it is independent of the SNR, hence, independent of any fading. The expression for P_d in any fading channel can be obtained by averaging the conditional P_d as given by (6.18) over the fading distribution [13]. For the case of small-scale fading, the distribution of the envelope of the received signal is generally considered to be Rayleigh distributed, which makes the received power distribution to be exponential [438]. The instantaneous SNR γ of a signal having Rayleigh distributed amplitude

follows an exponential p.d.f. given by [13]

$$f(\gamma) = \frac{1}{\bar{\gamma}} \exp\left(-\frac{\gamma}{\bar{\gamma}}\right), \quad \gamma \geq 0, \quad (6.19)$$

where $\bar{\gamma}$ is the average SNR. The average P_d in Rayleigh fading case, denoted as \bar{P}_{dr} , can be calculated by averaging (6.18) over (6.19), which can be written as

$$\bar{P}_{dr} = \int_0^\infty Q_u\left(\sqrt{2\gamma}, \sqrt{\lambda_{th}}\right) f(\gamma) d\gamma. \quad (6.20)$$

Letting $x = \sqrt{2\gamma}$, the above expression can be written as

$$\bar{P}_{dr} = \frac{1}{\bar{\gamma}} \int_0^\infty Q_u\left(x, \sqrt{\lambda_{th}}\right) x e^{-\frac{x^2}{2\bar{\gamma}}} dx. \quad (6.21)$$

By solving above integral problem using (12) from [440], the closed form solution for \bar{P}_{dr} can be written as

$$\bar{P}_{dr} = e^{-\frac{\lambda_{th}}{2}} \sum_{n=0}^{u-2} \frac{1}{n!} \left(\frac{\lambda_{th}}{2}\right)^n + \left(\frac{1+\bar{\gamma}}{\bar{\gamma}}\right)^{u-1} \left[e^{-\frac{\lambda_{th}}{2(1+\bar{\gamma})}} - e^{-\frac{\lambda_{th}}{2}} \sum_{n=0}^{u-2} \frac{1}{n!} \left(\frac{\lambda_{th}\bar{\gamma}}{2(1+\bar{\gamma})}\right)^n \right]. \quad (6.22)$$

6.3.3 Proposed Energy Detection Approach for Dual Antenna Case

1. *Uni-polarized MIMO channel*: In this channel, all antennas are identically polarized and this channel can be considered as a building block for dual polarized channels. The MIMO channel matrix \mathbf{H} can be defined as

$$\mathbf{H} = \begin{bmatrix} h_{11} & h_{12} \\ h_{21} & h_{22} \end{bmatrix}. \quad (6.23)$$

The channel coefficients h_{11} , h_{12} , h_{21} , and h_{22} are considered to be c.c.s. i.i.d. random variables modeling Rayleigh fading. From the polarization point of view, the matrix \mathbf{H} denotes uni-polarized channel matrix i.e., all antennas are identically polarized. Then the binary hypothesis testing problem can be written as

$$\begin{aligned} H_0 : \mathbf{y}(n) &= \mathbf{w}(n), & \text{PU absent} \\ H_1 : \mathbf{y}(n) &= \mathbf{Hx}(n) + \mathbf{w}(n), & \text{PU present} \end{aligned} \quad (6.24)$$

where $\mathbf{x}(n) = \begin{bmatrix} X(n) \\ X(n) \end{bmatrix}$, $X(n)$ being n -th transmitted symbol. In this scenario, fading signal amplitude is found to be Rayleigh distributed with parameter $\sigma = 2$ instead of Rayleigh distribution with parameter $\sigma = 1$ in single antenna case. We consider this factor to derive the theoretical expression for P_d in case of a MIMO channel in the next subsection.

2. *Dual polarized channel*: Two branches of a dual polarized antenna can be considered to receive H-polarized and V-polarized signals coming from the PU transmit antenna. In this work, we consider the enhancement of diversity rather than multiplexing using diversity combining techniques. For this purpose, the same symbol can be aligned to horizontal and vertical orthogonal polarization while transmitting through the PU's Tx. The dual polarized channel can be regarded as a 2×2 MIMO spatial channel if we exclude polarization effects. The exact modeling of a dual polarized channel is quite complex and it depends on the following factors [113]

1. Spatial separation between two antennas at both Tx and Rx sides.
2. Cross-polar isolation (XPI) of Tx and Rx antennas: Its value is taken as infinite for perfect antennas.

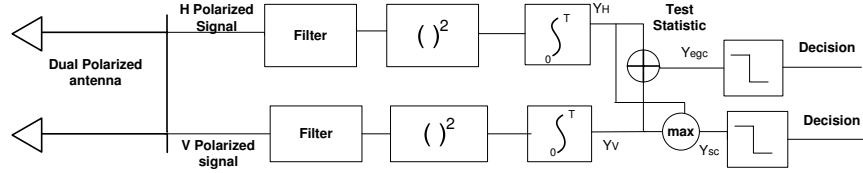


FIGURE 6.11: Block diagram of SC and EGC techniques for SS

3. Spatial separation in channel: This is taken into account as in an uni-polarized MIMO channel.
4. Cross-polar ratio (XPR) of the channel: This becomes zero for perfect orthogonality of two polarized channels.
5. Cross Polarization discrimination (XPD): It is the combined effect of XPI and XPR.

In our analysis, we assume that co-located orthogonally polarized antennas are placed on both transmit and receive sides and XPI factor of both antennas is infinite. By making these assumptions, we are removing the effects of spatial correlation due to antenna separation and cross-polar reception due to imperfection of antennas on both sides. The channel matrix in this condition can be modeled in the following way

$$\mathbf{H}_d = \begin{bmatrix} h_{HH} & h_{HV} \\ h_{VH} & h_{VV} \end{bmatrix} = \mathbf{X} \odot \mathbf{H}, \quad (6.25)$$

where \mathbf{H} is a uni-polarized channel matrix as considered in the above section, \odot denotes the Hadamard product, $E[|h_{HH}|^2] = E[|h_{VV}|^2] = 1$, $E[|h_{VH}|^2] = E[|h_{HV}|^2] = \sqrt{\chi_{cx}}$, χ_{cx} being XPR and

$$\mathbf{X} = \begin{bmatrix} 1 & \sqrt{\chi_{cx}} \\ \sqrt{\chi_{cx}} & 1 \end{bmatrix}. \quad (6.26)$$

The variable χ_{cx} quantifies the inverse of XPD in case of infinite XPI and varies in range $[0, 1]$ since $0 \leq XPD < \infty$ [111]. It can be expressed as: $\chi_{cx} = \frac{\chi_{cx,H} + \chi_{cx,V}}{2}$ with $\chi_{cx,V} = \frac{E|h_{HV}|^2}{E|h_{VV}|^2}$ and $\chi_{cx,H} = \frac{E|h_{VH}|^2}{E|h_{HH}|^2}$. The decision statistic to check the hypothesis problem given in (6.24) for a dual polarized channel depends on the type of combining technique used in combining two branch signals.

6.3.4 Combining Techniques for Dual Polarized Channel

The block diagram of the SC and EGC techniques for SS using a dual polarized antenna is shown in Fig. 6.11. As noted in the figure, two branch signals are passed through the filter to limit the noise power and then passed through squared and integrator devices. Then a test statistic is calculated based on the employed technique. In the following subsections, we study the application of SC and EGC techniques in the considered dual polarized channel using ED-based detection discussed in Section 6.3.3. Further, we derive theoretical expressions for P_d and P_f for these techniques in the considered channel.

6.3.4.1 Selection Combining

In this technique, the energies of the received signals in each branch are computed by taking samples within a certain period T and the detector selects the highest energy between them. The decision statistic for the SC can be expressed as: $T_{sc} = \max(T_H, T_V)$, where T_H and T_V are decision statistics calculated for H-polarized branch and V-polarized branch respectively. Under H_0 , the expression for

P_f for the SC, $P_{f,sc}$, becomes different than that for single antenna case and can be evaluated using c.d.f. of T_{sc} given H_0 i.e., $F_{T_{sc}}$, can be written as [184]

$$P_{f,sc} = 1 - F_{T_{sc}}(\lambda_{th} | H_0) = 1 - \left[1 - \frac{\Gamma(u, \frac{\lambda_{th}}{2})}{\Gamma(u)} \right]^2. \quad (6.27)$$

Similarly, P_d for the SC i.e., $P_{d,sc}$ in an AWGN channel under the H_1 hypothesis can be written as

$$P_{d,sc} = 1 - \left[1 - Q_u \left(\sqrt{2\gamma_H}, \sqrt{\lambda_{th}} \right) \right] \left[1 - Q_u \left(\sqrt{2\gamma_V}, \sqrt{\lambda_{th}} \right) \right]. \quad (6.28)$$

The average value of $\bar{P}_{d,sc}$ over 2 independent Rayleigh branches can be evaluated in the following way [184]

$$\bar{P}_{d,sc} = 1 - \int_0^\infty \left[1 - Q_u \left(\sqrt{2\gamma_H}, \sqrt{\lambda_{th}} \right) \right] f(\gamma_H) d\gamma_H \times \int_0^\infty \left[1 - Q_u \left(\sqrt{2\gamma_V}, \sqrt{\lambda_{th}} \right) \right] f(\gamma_V) d\gamma_V. \quad (6.29)$$

The above equation when combined with the \bar{P}_{dr} expression from (6.22) can be written as

$$\bar{P}_{d,sc} = 1 - (1 - \bar{P}_{dr}(\bar{\gamma}_H, 2u)) \times (1 - \bar{P}_{dr}(\bar{\gamma}_V, 2u)). \quad (6.30)$$

In the considered dual polarized scenario, the expression for P_f remains same as (6.27) because the noise processes are same as in Single Input Multiple Output (SIMO) scenario. The distribution of amplitude of both H-polarized and V-polarized signals is Rayleigh with varying parameter $\sigma = 1 + \sqrt{\chi_{cx}}$ instead of Rayleigh distribution with parameter $\sigma = 1$ in SIMO scenario. Since the value of χ_{cx} ranges from 0 to 1, the value of σ ranges from 1 for the SIMO case to 2 for the ideal MIMO case. This effect can be reflected in P_d expression by scaling $\bar{\gamma}_H$ and $\bar{\gamma}_V$ by the factor σ in (6.30) and can be written as

$$\bar{P}_{d,sc} = 1 - (1 - \bar{P}_{dr}(\sigma\bar{\gamma}_H, 2u)) \times (1 - \bar{P}_{dr}(\sigma\bar{\gamma}_V, 2u)). \quad (6.31)$$

6.3.4.2 Equal Gain Combining

This technique combines the energy of two branches with equal gain i.e., it simply adds energies of two branches of a dual polarized antenna. The final decision statistic using this technique can be written as: $T_{egc} = T_H + T_V$. Under the H_0 hypothesis in an AWGN channel, adding 2 i.i.d. central chi-square variates, each with $2u$ dof and unit variance results in another central chi-square variate with $4u$ dof with the same variance [184]. Therefore, P_f for EGC, $P_{f,egc}$ can be written as

$$P_{f,egc} = \frac{\Gamma \left(2u, \frac{\lambda_{th}}{2} \right)}{\Gamma(2u)}. \quad (6.32)$$

The decision statistic T_{egc} under hypothesis H_1 in an AWGN channel follows a non-central chi-square χ^2 distribution with $4u$ dofs and non-centrality parameter $2\gamma_{egc}$. The expression for P_d in AWGN channel for EGC, $P_{d,egc}$, can be written as

$$P_{d,egc} = Q_{2u}(\sqrt{2\gamma_{egc}}, \sqrt{\lambda_{th}}), \quad (6.33)$$

where γ_{egc} is the SNR of the combined signal. For Rayleigh fading scenario, considering 2 i.i.d. Rayleigh fading branches of a dual polarized antenna, the p.d.f. of γ_{egc} can be written as [13]

$$f(\gamma_{egc}) = \frac{1}{\bar{\gamma}_{egc}^2} \gamma_{egc} \exp \left(-\frac{\gamma_{egc}}{\bar{\gamma}_{egc}} \right). \quad (6.34)$$

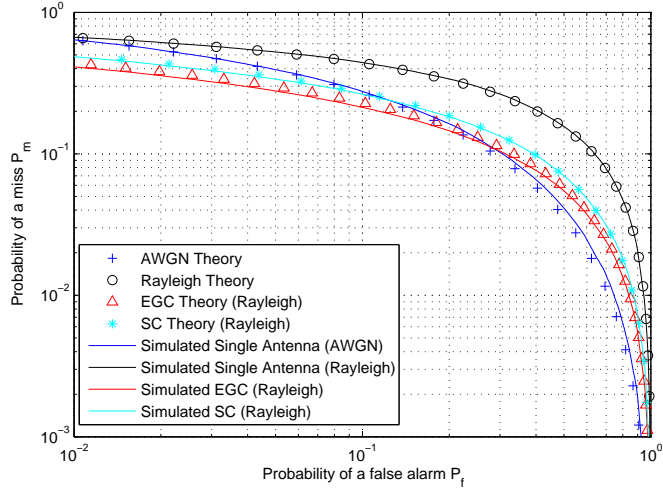


FIGURE 6.12: P_m versus P_f for different cases (SNR = -4 dB, dof = 60, Number of Monte Carlo realizations (N) = 10^4)

The average value of $\bar{P}_{d,egc}$ in Rayleigh fading channels can then be obtained by averaging (6.34) over (6.33) as

$$\bar{P}_{d,egc} = \int_0^\infty Q_{2u} \left(\sqrt{2\gamma_{egc}}, \sqrt{\lambda_{th}} \right) f(\gamma_{egc}) d\gamma_{egc}. \quad (6.35)$$

The closed form for above equation can be written in the following form³.

$$\bar{P}_{d,egc} = G + K^2 e^{-\frac{\lambda_{th}}{2}} \left[\sum_{i=1}^{2u-1} \frac{\left(\frac{\lambda_{th}}{2}\right)^i}{i!} {}_1F_1 \left(2; i+1; \frac{\lambda_{th}(1-K)}{2} \right) \right], \quad (6.36)$$

where ${}_1F_1$ is the confluent hypergeometric function, $K = \frac{1}{1+\bar{\gamma}_{egc}}$ and $G = e^{-\frac{\lambda_{th}K}{2}} \left[1 + \frac{K\lambda_{th}(1-K)}{2} \right]$. In the considered dual polarized scenario, the expression for P_f remains same as (6.32). The expression for P_d then becomes (6.36) with the modified value of K which can be written as: $K' = \frac{1}{1+\sigma\bar{\gamma}_{egc}}$, where $\sigma = 1 + \sqrt{\chi_{cx}}$ as defined in earlier subsection. Therefore, the value of $\bar{P}_{d,egc}$ in a dual polarized channel depends on the value of XPR and ranges from upper bound for an ideal MIMO channel to lower bound for a SIMO channel.

6.3.5 Numerical Results

To analyze the sensing performance of the considered approach, Complementary ROC (CROC) curves (probability of a miss, P_m versus P_f) are plotted based on both theoretical and simulation results. We consider the following cases in our numerical analysis. 1) First case considers single antenna reception in an AWGN channel for the reference purpose. 2) Second case considers the single antenna reception with a flat fading Rayleigh channel. 3) In this case, we consider receive diversity with two receiving antenna in a SIMO Rayleigh fading channel considering SC and EGC techniques to combine the signals coming from two branches. 4) This case considers 2 transmit and 2 receive antenna with a 2×2 Rayleigh fading channel to resemble the channel structure of dual polarized wireless channel. 5) In this case, we include power imbalance in the MIMO channel in order to reflect XPD effect in a dual polarized channel. Figure 6.12 shows the performance comparison of cases 1, 2 and 3 in terms of CROC curves. Both theoretical and simulation results of SC and EGC techniques in a Rayleigh fading channel are presented. From the figure, it can be noted that EGC performs only slightly better than SC technique

³It should be noted that we present $\bar{P}_{d,egc}$ for 2 branch scenario of a dual polarized antenna instead of L-branch scenario considered in [184].

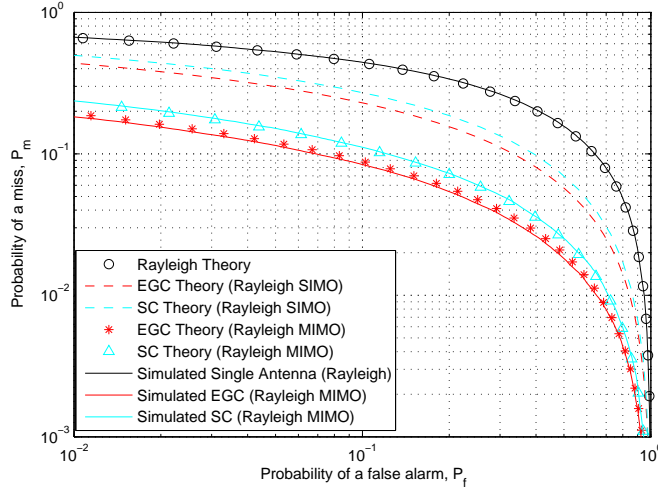
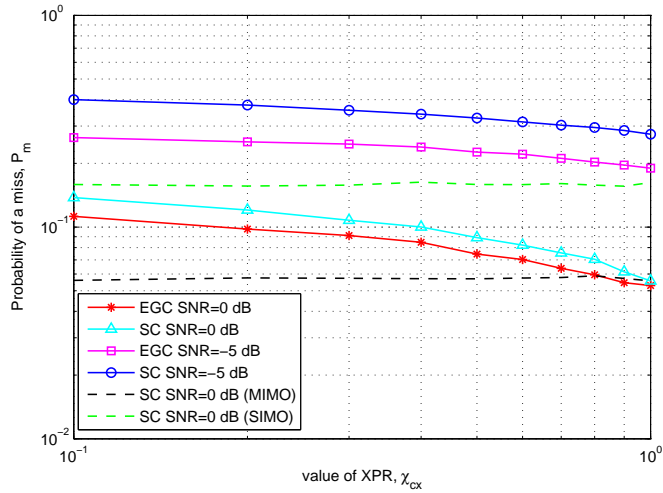


FIGURE 6.13: P_m versus P_f for SC and EGC techniques in MIMO Rayleigh fading channel (SNR = -4 dB, dof = 60, $N = 10^4$)

in a Rayleigh fading channel. Both techniques perform better than single antenna reception. These results are consistent with the results obtained in literature [13] and we are considering low value of SNR to reflect the weak nature of signals in cognitive SatComs. Further, Fig. 6.13 depicts the comparison of SC and EGC techniques in MIMO and SIMO Rayleigh fading channels for cases 2, 3 and 4. Both theoretical and simulation results for EGC and SC techniques in the considered MIMO Rayleigh fading channel have been plotted. From the results, it can be noted that both techniques perform better in a MIMO Rayleigh fading channel than in SIMO scenario. Further, the EGC technique performs better than the SC as in the SIMO scenario.

Figure 6.14 presents P_m versus XPR value for SC and EGC techniques for P_f value of 0.07 at two different SNR values of 0 dB and -5 dB. From the simulation results, it can be noted that for both the techniques, P_m decreases with the value of χ_{cx} and they provide closer detection performance at higher values of SNR. The value of P_m becomes minimum for unity value of χ_{cx} and it becomes maximum when χ_{cx} equals zero. From these results, it can be inferred that the sensing performance in a dual polarized channel increases with the value of χ_{cx} and it ranges from the minimum for SIMO channel to the maximum for an ideal MIMO channel. Furthermore, in terms of XPD, the detection performance decreases with the value of XPD since χ_{cx} quantifies the inverse of XPD. Therefore, it can be concluded that the detection performance in a dual polarized fading channel increases with the value of XPR and its lower and upper bounds occur for a SIMO fading channel and an ideal MIMO fading channel respectively.

Discussion: The performance of an ED-based SS technique has been analyzed in a dual polarized fading channel in the context of cognitive Satcoms. EGC and SC techniques have been considered to enhance the SS efficiency by combining the received signals from two branches of a dual-polarized antenna at the energy level. The theoretical expressions for P_d and P_f have been provided for these techniques in AWGN, SIMO and MIMO Rayleigh fading channels. The simulation as well as theoretical results show that the performance of the ED technique in a MIMO fading channel is much better than in SIMO and SISO fading channels. Further, the effect of XPR on SS efficiency has been analyzed and it can be concluded that the detection performance in a dual polarized fading channel increases with the value of XPR and its lower and upper bounds occur for a SIMO fading channel and an ideal MIMO fading channel respectively.

FIGURE 6.14: P_m versus XPR for $P_f = 0.07$ (dof = 60, $N = 2 \times 10^4$)

6.4 Cognitive Beamforming

Towards exploiting the sharing of available spectrum between primary and secondary systems, existing techniques mostly focus on three dimensions i.e., frequency, time and area. However, due to advancements in smart antennas and beamforming techniques, it has been possible to multiplex multiple users into the same channel at the same time and in the same geographical area [441]. In the context of cognitive communications, an angular dimension or a directional dimension of spectral space can be considered as an efficient way of exploiting the space dimension to exploit the underutilized primary spectrum. Recently, the spatial dimension has received important attention for different spectrum sharing applications [441–443].

Beamforming is a signal processing technique used in antenna arrays with the advantages of spatial discrimination and spatial filtering capabilities [238]. Multi-antenna beamforming has been widely used in traditional fixed spectrum-based wireless systems as an effective means to mitigate the co-channel interference [444, 445]. In the CR literature, beamforming has been applied as an underlay CR technique in order to maximize the SINR towards its desired users while guaranteeing the aggregate interference to the PUs to be below the interference threshold. The main difference between a conventional beamforming problem and the Cognitive Beamforming (CB) problem is the introduction of interference constraints imposed by primary network while designing the beamformer. The existing CB techniques have been considered mostly in the coexistence scenarios of two terrestrial networks [115–117, 253, 254] but has received less attention in the satellite paradigm.

In this work, we focus on hybrid satellite-terrestrial coexistence scenario considering a satellite link as the primary and a terrestrial link as the secondary. As an example, the practical coexistence of an FSS system with fixed ground terminals (i.e., dishes) operating in C-band and a terrestrial WiMax network providing broadband services to the fixed users can be considered. This coexistence scenario is beneficial for the terrestrial operators in terms of enhancing the system throughput by reusing the satellite spectrum. By exploiting the prior knowledge of the GEO satellites, we propose different receive beamforming techniques for the uplink coexistence scenario in [119] and different transmit beamforming techniques for the downlink coexistence scenario in [120]. GEO satellite terminals have a special propagation characteristic to always point towards the GEO satellites (South if we consider the European continent excluding the regions near to the equator). This comes from the fact that GEO satellites are located in the geosynchronous orbit above the equator and therefore transmit in a northerly direction. While considering the coexistence of a satellite network with the terrestrial cellular network in the normal forward mode, the reception range of all the satellite terminals is concentrated in an angular sector. Similarly, in the coexistence of satellite network with the terrestrial network

in the normal return mode, the interference received by the terrestrial BS is also concentrated in an specific angular sector. Further, this interference becomes more prominent as we move towards the polar region from the equator due to lower elevation angles of the satellite terminals [106]. Therefore, the interference provided/received by the BS to/from the satellite terminals depends on the directional properties of the transmitted beam designed at the BS. Similar scenario was considered in [118] while reusing the satellite broadcast spectrum for terrestrially broadcast signals in the United States and the use of different directional antennas at the user location was proposed to allow the spectrum reuse. In our contribution, we apply LCMV and MVDR beamformers for the considered scenario and analyze their performances in terms of the pattern response and the output SINR. The prior knowledge that all the ground satellite terminals are pointing south is the cognition that we exploit in this study. Since this is an inherent characteristic of SatComs, no interaction is needed between primary and secondary systems.

6.4.1 Cognitive Beamforming for Uplink Coexistence Scenario

Figure 5.2 (Chapter 5) shows a practical coexistence scenario of satellite and terrestrial networks with both networks operating in the normal return mode. The satellite link is considered as primary and the terrestrial link as secondary i.e., satellite terminals are PUs and terrestrial terminals are SUs. The interference from terrestrial terminals to the satellite may be weak due to large propagation distance and less directive nature of the terrestrial terminals. However, the aggregate interference from the terrestrial terminals to the satellite may become problematic if there exist several terrestrial terminals reusing the satellite spectrum at the same time and needs to be taken into account. Further, the interference from the satellite terminals to the terrestrial BS should be taken into account in order to guarantee the QoS of the secondary links. In this work, we are interested in mitigating the second interference i.e., from the satellite terminals to the BS using a spatial filtering technique. As mentioned before, the interference received by the BS is concentrated in a specific angular sector due to unique propagation characteristic of GEO satellite terminals and the BS receives interference from its northern sector. In this context, our aim is to design receive beamforming at the terrestrial BS in order to fulfill the following objectives: (i) to maximize the SINR towards the desired user (located in the south), and (ii) to mitigate the interference coming from the northern sector. The detailed layout of this scenario is shown in Fig. 6.15. It should be noted that a terrestrial terminal located in an interfering sector (northern) for a particular BS can be served by other BSs situated norther to this terminal. Furthermore, by using some form of user scheduling techniques, multiple terrestrial users can be supported under this system model. In the considered receive beamforming approach, the exact locations and the number of the interfering satellite terminals may be unknown to the beamformer.

6.4.1.1 Signal Model

Let M be the number of antennas in the BS antenna array and K be the number of users in the considered system including both PUs and SUs. Under this scenario, each user can be viewed as a transmit antenna in a point to point MIMO system and the same Rx architecture can be used at the BS to separate each user's data by employing a receive beamforming technique. The received signal vector \mathbf{y} at the BS can be written as

$$\mathbf{y} = \sum_{k=1}^K h_k \mathbf{a}(\theta_k) s_k + \mathbf{z}, \quad (6.37)$$

where h_k represents the channel gain towards the k th user and remains constant for all sensors in the array assuming that there is a strong line of sight path between the array antenna and user antennas, s_k is the transmitted symbol by k th user, $\mathbf{a}(\theta_k)$ is an $M \times 1$ response vector θ_k being the angle of arrival

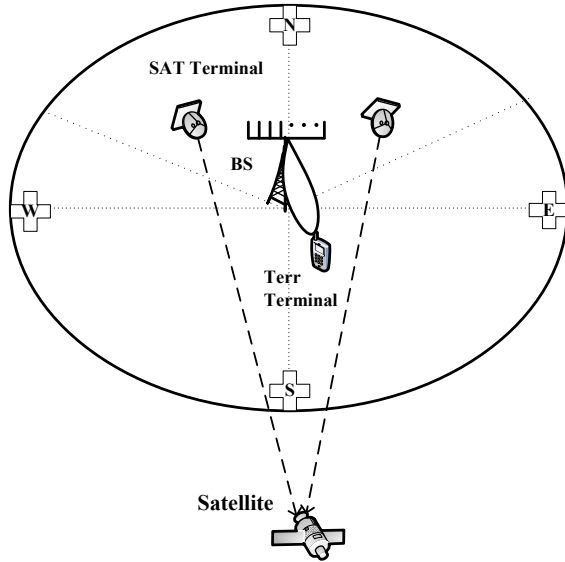


FIGURE 6.15: Layout of the considered scenario (N,W,S and E denote North, West, South and East)

for the k th user, \mathbf{z} is an $M \times 1$ i.i.d. Gaussian noise vector. The array response vector $\mathbf{a}(\theta_k)$ can be written as [445]

$$\mathbf{a}(\theta_k) = \left[1, e^{\frac{-j2\pi d \sin(\theta_k)}{\lambda}}, \dots, e^{\frac{-j2\pi(M-1)d \sin(\theta_k)}{\lambda}} \right]^T, \quad (6.38)$$

where d is the inter-element spacing of the antennas at the BS array and λ represents the wavelength of a radio frequency signal. The Rx at the BS can separate signals transmitted from different spatially located users because of their different response vectors on the received antenna array. Let's consider that there is only one desired user i.e., a single SU and $(K-1)$ interfering users i.e., PUs. Then \mathbf{y} can be expressed as

$$\mathbf{y} = h_1 \mathbf{a}(\theta_1) s_1 + \mathbf{q}, \quad (6.39)$$

where h_1 is the channel towards the desired user, $\mathbf{a}(\theta_1)$ is the array response vector for the desired user, s_1 is desired user's transmitted symbol and

$$\mathbf{q} = \sum_{k=2}^K h_k \mathbf{a}(\theta_k) s_k + \mathbf{z}. \quad (6.40)$$

For the purpose of receive beamforming, the received signal vector \mathbf{y} is then linearly combined through a complex weight vector $\mathbf{w} \in \mathcal{C}^M$ to yield the array output \hat{s}_1 as $\hat{s}_1 = \mathbf{w}^\dagger \mathbf{y}$. The beamforming weight vector \mathbf{w} should be chosen in such a way that the first term of (6.39) is maximized while the second term is minimized.

6.4.1.2 Applicable Techniques

1. *MVDR Technique*: The received signal at the BS antenna array from (6.37) can also be written as

$$\mathbf{y} = \mathbf{As} + \mathbf{z}, \quad (6.41)$$

where $\mathbf{A} = [\mathbf{a}(\theta_1), \mathbf{a}(\theta_2), \dots, \mathbf{a}(\theta_K)]$ is called the Signal Direction Matrix (SDM), $\mathbf{s} = [s_1, s_2, \dots, s_K]^T$, each s_k being the symbol associated with the k th user. The beamformer's response to the desired user located at an angle θ_d is given by; $\mathbf{w}^\dagger \mathbf{a}(\theta_d)$. The optimization problem for the MVDR beamformer can

be written as

$$\begin{aligned} & \min_{\mathbf{w}} \mathbf{w}^\dagger \mathbf{R}_{i+n} \mathbf{w} \\ & \text{subject to } \mathbf{w}^\dagger \mathbf{a}(\theta_d) = 1. \end{aligned} \quad (6.42)$$

Since in practical scenarios, \mathbf{R}_{i+n} is unavailable and only the sample covariance matrix \mathbf{R}_y is available, given by; $\mathbf{R}_y = \frac{1}{N} \sum_{i=1}^N \mathbf{y}(n) \mathbf{y}^\dagger(n)$. Using \mathbf{R}_y instead of \mathbf{R}_{i+n} , the optimization problem for the MVDR beamformer can be written as

$$\begin{aligned} & \min_{\mathbf{w}} \mathbf{w}^\dagger \mathbf{R}_y \mathbf{w} \\ & \text{subject to } \mathbf{w}^\dagger \mathbf{a}(\theta_d) = 1. \end{aligned} \quad (6.43)$$

When the desired signal is uncorrelated to the interference, the minimization problem in (6.43) is same as the minimization problem in (6.42) [446]. The solution of the constrained optimization problem (6.43) can be obtained by using Lagrange multiplier method and is given by

$$\mathbf{w} = \frac{\mathbf{R}_y^{-1} \mathbf{a}(\theta_d)}{\mathbf{a}^\dagger(\theta_d) \mathbf{R}_y^{-1} \mathbf{a}(\theta_d)}. \quad (6.44)$$

2. LCMV Technique: In this beamformer, the weights are chosen to minimize the output variance or power subject to multiple response constraints. Unlike the MVDR beamformer, this includes multiple response constraints with a unity response in the desired direction and null responses in the interfering directions. To include multiple constraints in the above variance minimization problem (6.43), the following constraint equation can be written

$$\mathbf{C}^\dagger \mathbf{w} = \mathbf{f}, \quad (6.45)$$

where \mathbf{C} is an $M \times L$ constraint matrix and \mathbf{f} is an $L \times 1$ response vector, $L = K$ is the number of constraints. The above equation (6.45) can be further rewritten as

$$\begin{bmatrix} \mathbf{a}^\dagger(\theta_1) \\ \mathbf{a}^\dagger(\theta_2) \\ \vdots \\ \mathbf{a}^\dagger(\theta_K) \end{bmatrix} \mathbf{w} = \begin{bmatrix} 1 \\ 0 \\ \vdots \\ 0 \end{bmatrix}. \quad (6.46)$$

Then the LCMV beamforming problem can be written as

$$\begin{aligned} & \min_{\mathbf{w}} \mathbf{w}^\dagger \mathbf{R}_y \mathbf{w} \\ & \text{subject to } \mathbf{C}^\dagger \mathbf{w} = \mathbf{f}. \end{aligned} \quad (6.47)$$

The solution of the above problem (6.47) is given by [447]

$$\mathbf{w} = \mathbf{R}_y^{-1} \mathbf{C} (\mathbf{C}^\dagger \mathbf{R}_y^{-1} \mathbf{C})^{-1} \mathbf{f}. \quad (6.48)$$

6.4.1.3 Proposed Spatial Filtering Approach

We assume that BS antenna array is oriented horizontally i.e., East-West direction as shown in Fig. 6.15. As mentioned before, the angular sector in which interfering satellite terminals are located is known to the beamformer beforehand while the number of interfering terminals and their exact locations are unknown under the considered scenario. In this context, the objective of a receive beamformer at the BS is to mitigate the interference coming from the interfering sector and to maximize the SINR towards the desired user. Following assumptions are made during the analysis:

- The DoA of the desired user is known⁴.
- The incident wave arrives at the array in the horizontal plane $\phi = \pi/2$ so that azimuthal direction completely determines the DoA.
- The distance between BS and the user is large enough for the user to be in the far field region so that spherical waves approximate the plane waves.

Let us define DoA range for the interfering signals from the satellite terminals to lie in the range $[\theta_{\min}, \theta_{\max}]$. The values of θ_{\max} and θ_{\min} at a particular geographical location can be calculated by performing the geometric analysis of a GEO satellite link [106]. To design a beamformer, we uniformly sample this range in the interval of $\theta_i = \Delta/(K-1)$, where $\Delta = \theta_{\max} - \theta_{\min}$. The position of satellite terminals are generated randomly with uniform distribution in the angular sector of 0° to 90° . Based on the received signal's covariance matrix, beamforming weights for the MVDR and the LCMV beamformers are calculated using (6.44) and (6.48) respectively. Subsequently, these weights are used for calculating SINRs for the considered simulation environment. If the received SINR at the BS is above the target SINR, the desired user can be served by that particular BS. Otherwise, the desired user has to be served by some other nearby BS.

The performance of a beamformer can be specified in the form of its response pattern and the output SINR. The response pattern specifies the response of the beamformer to an incoming signal as a function of DoA and frequency. The response pattern in θ direction (considering a single radio frequency channel) can be calculated as

$$G(dB) = 20\log_{10}(|\mathbf{w}^\dagger \mathbf{a}(\theta)|). \quad (6.49)$$

In the considered scenario, the actual array response vectors for the interfering users differ from the array response vectors used while designing the beamformer, resulting in uncertainties in the array response vectors of the interfering users. In this context, firstly, we calculate the beamformer weights considering one interferer in each quantized angle and based on the assumption that the array response vectors for the desired user and the interfering users are exactly known. Subsequently, these weights can be applied to the considered scenario in order to evaluate the performance of LCMV and MVDR beamformers. For a particular beamformer, the average SINR can be calculated by considering several Monte-Carlo realizations as

$$\overline{SINR} = \frac{1}{N_s} \sum_{n=1}^{N_s} \frac{\gamma |\mathbf{w}^\dagger \mathbf{a}(\theta_d)|^2}{\mathbf{w}^\dagger \mathbf{R}_{i+n} \mathbf{w}}, \quad (6.50)$$

where N_s is the number of Monte-Carlo realizations. Using Friis transmission formula, the received power (P_r) at the BS from the satellite/terrestrial terminal located at a distance d is calculated as

$$P_r = \frac{P_t G_t G_r}{(4\pi d/\lambda)^2} = P_t G_t G_r L_p^{-1}, \quad (6.51)$$

where G_t and G_r are gains of transmit and receive antennas respectively, P_t is the transmitted power and the term $L_p = (4\pi d/\lambda)^2$ represents the free space path loss. Let us define β_k be the path loss coefficient of the link between the k th user and the terrestrial BS. While considering the path loss into account, (6.41) can be rewritten as

$$\mathbf{y} = \mathbf{A} \text{diag}(\boldsymbol{\beta}) \mathbf{s} + \mathbf{z}, \quad (6.52)$$

where $\boldsymbol{\beta} = [\beta_1 \ \beta_2 \ \cdots \ \beta_K]$.

⁴In practice, the DoA of desired user can be estimated by using some DoA estimation algorithms such as MUSIC algorithm.

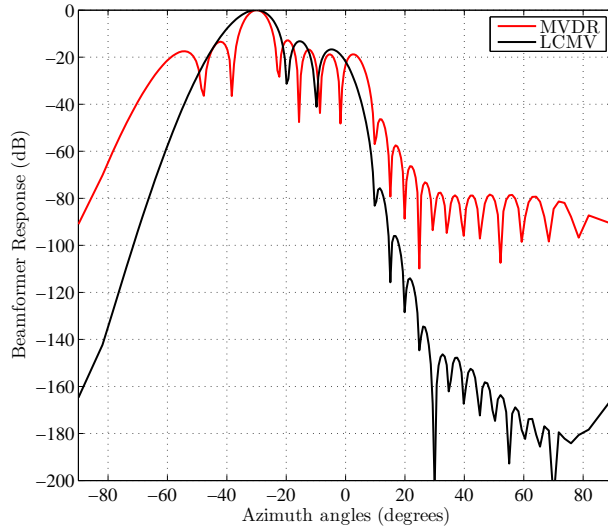


FIGURE 6.16: Response versus azimuth angle for LCMV and MVDR beamformers, $M = 20$, $K = 17$

6.4.1.4 Numerical Results

Let us consider that all the satellite terminals are seen at azimuth angle range of 10° to 85° from the BS. We consider a single desired user at an angle of -30° and a ULA at the BS with the layout shown in Fig. 6.15. The simulation and link budget parameters for both the links (i.e., link between SAT terminal and the BS and the link between terrestrial terminal and the BS) are provided in [119]. To design a LCMV beamformer, we need DoAs of the interfering users. For this purpose, we quantize the considered interfering sector in the interval of 5° and consider one terminal in each quantized angle. It can be noted that the pattern generated in 0° to 90° quarter is repeated in another quarter 90° to 180° due to symmetric nature of the ULA pattern. Therefore, the response pattern generated within the region 10° to 85° is repeated over the region 170° to 95° . Figure 6.16 shows the array response versus azimuth angles plot for MVDR and LCMV beamformers. The number of interferers considered was 16 and the transmit power for each interfering terminal was considered to be 30 dBm. From the figure, it can be observed that by considering the interfering range from 10° to 85° , we can create the array response about -50 dB to -110 dB down the desired response for the MVDR beamformer and about -80 to -200 dB down the desired response for the LCMV beamformer. Figure 6.17 shows the SINR versus azimuth angles plot of LCMV and MVDR beamformers for $M = 20$ and $K = 17$ in the considered simulation environment in which the random interfering users are generated with uniform distribution and the interfering power at the BS from these terminals is different due to different DoAs and distances to the BS. From the figure, it can be observed that the LCMV beamformer provides similar SINR as that of MVDR beamformer towards the desired user and can provide very low SINR towards the interfering sector than the MVDR beamformer. From this result, it can be concluded that LCMV beamformer can reject the interference more effectively than the MVDR beamformer in the considered scenario.

Figure 6.18 shows the SINR versus number of interferers for $M = 18$ and $K = 17$. The SINR for both beamformers decreases as the number of interfering users increases in the considered interfering sector. From the figure, it can be noted that the LCMV beamformer shows better performance compared to MVDR for low number of interferers (< 9 in the figure) and for higher number interferers, MVDR shows better performance than the LCMV beamformer. Further, as noted in [119], MVDR beamformer's SINR performance becomes worse than that of the LCMV beamformer when the mismatch angle of the desired user increases beyond 3° .

Discussion: In the considered scenario, the DoA of the desired user and the range in which interferers are located is known while the exact locations of the interferers are unknown to the beamformer. Simulation results show that performance of both the beamformers is similar in the desired direction

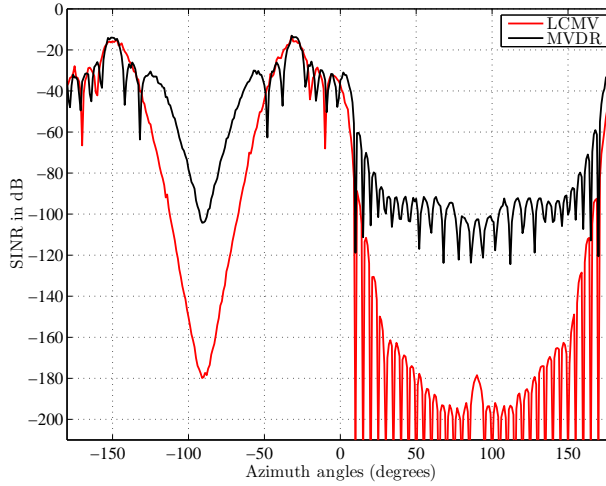


FIGURE 6.17: SINR versus Azimuth angles plot of LCMV and MVDR beamformers for the considered scenario, $M = 20$, $K = 17$

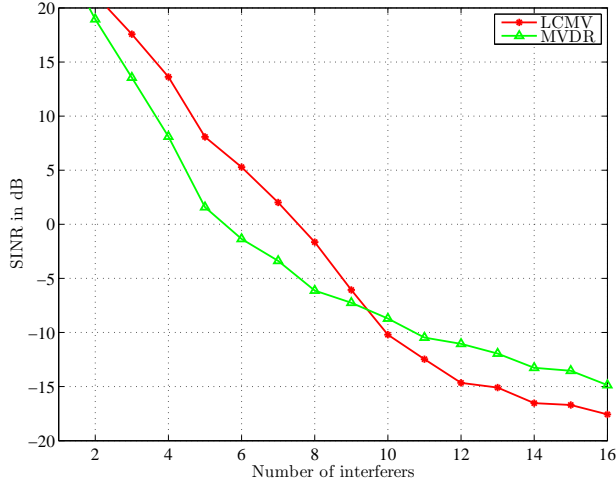


FIGURE 6.18: SINR versus number of interferers for proposed scenario with beamformers designed for $M = 18$

while the performance of the LCMV beamformer is much better in terms of rejecting interference coming from the interfering sector. Furthermore, it has been noted from the results that even in case of uncertainty of the exact locations of the interfering users, the LCMV beamformer is capable of creating low response towards the considered interfering region. In practical situations, exact DoA of the desired signal may deviate from the estimated one causing DoA mismatch of the desired signal. The response of the LCMV beamformer in case of angular mismatch can be maximized by placing multiple unit response directional constraints while the performance of MVDR beamformer becomes worse in this case. However, the performance of LCMV beamformer becomes worse for large number of interferers and it deteriorates rapidly when the number of antennas becomes less than the number of interferers while the performance of the MVDR beamformer is better than that of the LCMV in this condition. Therefore, the LCMV beamformer is suitable in terms of rejecting interference effectively for a small number of interferers and MVDR beamformer is suitable for a large number of interferers.

6.4.2 Cognitive Beamforming for Downlink Coexistence Scenario

Figure 6.19 shows a practical coexistence scenario of satellite and terrestrial networks with both networks operating in the normal forward mode. The detailed layout of the considered scenario is presented

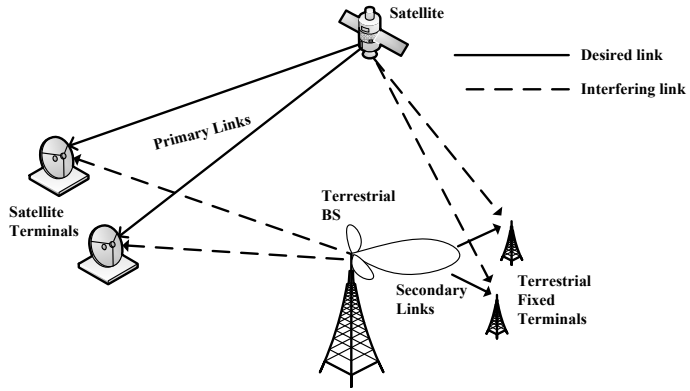


FIGURE 6.19: Hybrid satellite-terrestrial downlink coexistence scenario

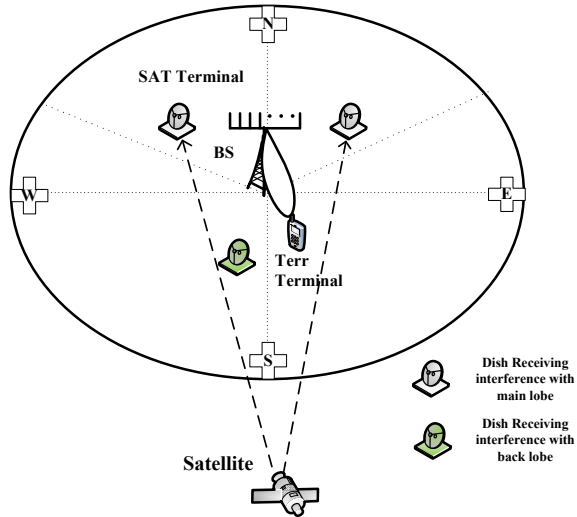


FIGURE 6.20: Layout of the considered scenario (N,W,S and E denote North, West, South and East)

in Fig. 6.20. Under this scenario, the reception range of a satellite terminal is concentrated in an angular sector and it receives terrestrial interference from the BSs located at its south. In this work, our main objective is to mitigate interference from the terrestrial BS towards satellite terminals by applying transmit beamforming techniques at the terrestrial BS. Furthermore, we consider the situation of protecting satellite terminals located beyond the considered angular sector from the secondary interference picked up by their backlobes. The layout of the considered scenario is shown in Fig. 6.15. The interference channel we are dealing in this scenario is the channel from terrestrial BS to the satellite terminals and the secondary channel is from terrestrial BS to the terrestrial terminals. By using some form of scheduling techniques, multiple terrestrial users can be supported under this system model. One way of mitigating interference towards the PU terminals is by controlling the power of secondary transmission. However, the secondary rate has to be sacrificed while protecting the PU terminals. In this context, we formulate an optimization problem to maximize the SU rate by guaranteeing sufficient protection of PU terminals with a given transmit power budget.

6.4.2.1 Signal Model

For the uplink coexistence scenario of Fig. 6.19, we consider a single SU over a terrestrial link, multiple PUs within the considered interfering sector and one PU beyond this sector. Furthermore, we consider the SU and PU terminals to be equipped with a single antenna. Let M be the number of antennas in the secondary BS antenna array and K be the number of PUs in the considered sector. Let s be a symbol which is to be transmitted from the secondary BS antenna at a particular time instant

with $E[ss^\dagger] = 1$ and \mathbf{w} be the $M \times 1$ beamforming weight vector at the BS antenna array. Then the transmitted signal vector from the secondary BS antenna array can be written as: $\mathbf{x}_s = \mathbf{w}s$. The value of \mathbf{w} can be written as: $\mathbf{w} = \sqrt{p}\mathbf{v}$, p representing the power supplied to each antenna of the array and $\|\mathbf{v}\| = 1$.

Let \mathbf{h}_p be the channel vector from the BS to the satellite terminal i.e., PU and \mathbf{h}_s be the channel vector from the BS to the terrestrial terminal i.e., SU. Then the received signal at the SU can be written as

$$y_s = \mathbf{h}_s^\dagger \mathbf{x}_s + z_s, \quad (6.53)$$

where \mathbf{h}_s is given by; $\mathbf{h}_s = \alpha_s \mathbf{a}(\theta_s)$. Similarly, the interfering signal at the PU terminal can be written as

$$y_p = \mathbf{h}_p^\dagger \mathbf{x}_s + z_s, \quad (6.54)$$

where \mathbf{h}_p is given by; $\mathbf{h}_p = \alpha_p \mathbf{a}(\theta_p)$, where $\mathbf{a}(\theta_p)$ represents the array response vector for DoA θ_p with θ_p being DoA for the PU signal and $\alpha_p \propto d_p^{-n}$ is the path loss coefficient between the secondary BS and the PU terminal with d_p being the distance and n being a path loss exponent.

6.4.2.2 Proposed Techniques

Based on the above system model, we try to address the following problems in this work.

1. How to mitigate the interference towards a certain angular sector based on the a priori knowledge of the propagation characteristics of GEO satellite terminals ? The beamforming weights at the BS should be designed in such a way that the transmitted power towards this angular sector is minimized.
2. Another problem is to design beamforming weights such that the SINR towards the desired SU is maximized. In other words, the SUs also should maximize the utilization of cognitive transmission.
3. Furthermore, it may be the case that the satellite terminals located beyond the sector of interest may receive the interfering signal from their backlobes. This may hamper the operation of the primary system. To solve this problem, we need to ensure that the interfering signal strength picked up by the backlobe of the satellite terminal is below the interference threshold level of the terminal.
4. Problem (3) can be solved by controlling transmitted power at the BS. However, this may affect the SU rate. This leads to defining and solving an optimization problem which we describe in the next section.

To address the aforementioned problems, we propose the following three different techniques.

1. *Scaled LCMV Technique*: The standard LCMV beamforming problem can be written as

$$\begin{aligned} & \min_{\mathbf{w}} \mathbf{w}^\dagger \mathbf{R}_d \mathbf{w} \\ & \text{subject to } \mathbf{C}^\dagger \mathbf{w} = \mathbf{f}. \end{aligned} \quad (6.55)$$

where \mathbf{R}_d is an $M \times M$ downlink spatial covariance matrix [448]. We assume that \mathbf{R}_d is perfectly known⁵ while designing the beamformer. In this work, we calculate it based on the knowledge of the

⁵In practice, the downlink covariance matrix can be calculated from uplink covariance matrix by using different transformation approaches [449].

array response vectors of the desired SU and the PU terminals⁶. The solution of the above problem can be written as [447]

$$\mathbf{w}_{\text{LCMV}} = \mathbf{R}_d^{-1} \mathbf{C} (\mathbf{C}^\dagger \mathbf{R}_d^{-1} \mathbf{C})^{-1} \mathbf{f}. \quad (6.56)$$

If the primary satellite terminals are present beyond the sector of interest, the back lobe of the terminals may pick up the interference power transmitted from the BS. To protect the PUs from this interference with a certain threshold, we can design a scaled LCMV beamformer by sacrificing some amount of transmit power in the desired direction. For the scaled LCMV, the weights of the LCMV beamformer given by (6.56) can be scaled as: $\mathbf{w}_{\text{LCMV}_s} = \epsilon * \mathbf{w}_{\text{LCMV}}$, ϵ being a scaling parameter. The value of ϵ may range from a nonzero small positive value to 1. When $\epsilon = 0$, the beamformer response to all the directions becomes zero and therefore, the value of ϵ should be greater than zero. It can be noted that as the value of ϵ increases, the higher transmit power has to be sacrificed in the desired direction.

2. Modified LCMV Technique: In the standard LCMV technique, the response constraints towards the PUs are set as zeros and the response constraint towards the desired user is set as unity. In this scenario, the PUs are assumed to be located within an angular sector and the BS designs its beam pattern to mitigate the interference towards this sector. To consider the scenario of protection towards the backlobes of the PUs, we modify the standard LCMV optimization by putting one more constraint and formulate a new optimization problem. The new constraint is set in such a way that the interference picked up by the backlobe of the satellite terminals is below the interference threshold of the terminal. Let I_T be the interference threshold set by the designers for the satellite terminals from the perspective of the interference picked up by the backlobe. Then the modified LCMV optimization problem is defined as

$$\begin{aligned} & \min_{\mathbf{w}} \mathbf{w}^\dagger \mathbf{R}_d \mathbf{w} \\ & \text{subject to } \mathbf{C}^\dagger \mathbf{w} = \mathbf{f} \\ & \mathbf{w}^\dagger \mathbf{R}_p \mathbf{w} \leq I_T, \end{aligned} \quad (6.57)$$

where $\mathbf{R}_p = \mathbf{a}(\theta_b) \mathbf{a}^\dagger(\theta_b)$ is the matrix containing the response vector towards the PU at the DoA of θ_b located beyond the sector of interest. Using Lagrangian multiplier method for solving the optimization problem (6.57), the Lagrangian can be written as

$$L(\mathbf{w}, \lambda, \eta) = \mathbf{w}^\dagger \mathbf{R}_d \mathbf{w} + \lambda (\mathbf{C}^\dagger \mathbf{w} - \mathbf{f}) + \eta (\mathbf{w}^\dagger \mathbf{R}_p \mathbf{w} - I_T) = 0. \quad (6.58)$$

Using further steps mentioned in [120], the value of \mathbf{w} can be written as

$$\mathbf{w} = (\mathbf{R}_d + \eta \mathbf{R}_p)^{-1} \mathbf{C} [\mathbf{C}^\dagger (\mathbf{R}_d + \eta \mathbf{R}_p)^{-1} \mathbf{C}]^{-1} \mathbf{f}. \quad (6.59)$$

The above solution presents the value of \mathbf{w} in terms of the Lagrangian multiplier η . Furthermore, the complementary slackness condition for inequality constraint can be written as: $\eta (\mathbf{w}^\dagger \mathbf{R}_p \mathbf{w} - I_T) = 0$. If $\eta = 0$, the solution (6.59) reduces to the solution of standard LCMV optimization problem given by (6.56). If $\eta \neq 0$, the following condition should be satisfied

$$\mathbf{w}^\dagger \mathbf{R}_p \mathbf{w} - I_T = 0. \quad (6.60)$$

The optimal value of \mathbf{w} can be found using (6.60) and (6.59) but the process involves complex steps. Therefore, based on above derived expressions, we present a simple iterative algorithm in [120] to solve the problem (6.57).

3. SU Rate Maximization: Let us denote the transmit signal covariance matrix by \mathbf{R}_t , which can be defined as

$$\mathbf{R}_t = E[\mathbf{x}_s \mathbf{x}_s^\dagger] = p \mathbf{v} \mathbf{v}^\dagger = \mathbf{w} \mathbf{w}^\dagger. \quad (6.61)$$

⁶To have the knowledge of DoAs of the PUs while designing the beamforming weights, we quantize the known angular sector in the uniform interval as described later in the following paragraph.

The optimization problem for maximizing the rate of SUs by allowing the sufficient protection for the PU can be written as

$$\begin{aligned} \max_{p \geq 0, \|\mathbf{v}\|=1} \log(1 + \text{SINR}(\theta_s, p, d_s)) \\ \text{subject to } \sum_{i=1}^M p_i \leq P_T, \\ I_p(\theta_p^{(j)}, p, d_p) \leq I_{TH}, j = 1, \dots, K \end{aligned} \quad (6.62)$$

where $\text{SINR}(\theta_s, p, d_s)$ represents the SINR of the desired SU and it is a function of θ_s , transmit power across each antenna p , and the distance d_s between the BS and the desired SU, P_T is the total power budget. Furthermore, $I_p(\theta_p^{(j)}, p, d_p)$ is the interference received at the j th PU due to secondary transmission and it is a function of θ_p , p , and the distance d_p between the BS and the PU, I_{TH} is the interference threshold required by the PUs. The SINR for the desired SU considering the case of a single BS with uniform power allocation across multiple antennas can be written as

$$\text{SINR}(\theta_s, p, d_s) = \mathbf{h}_s^\dagger \mathbf{R}_t \mathbf{h}_s = \frac{p\lambda^2 d_s^{-n}}{(4\pi)^2} \{ \mathbf{a}^\dagger(\theta_s) \mathbf{v} \mathbf{v}^\dagger \mathbf{a}(\theta_s) \}, \quad (6.63)$$

where λ is the wavelength of electromagnetic signal. Similarly, the interference received at the PU due to secondary transmission can be written as

$$I(\theta_p^{(j)}, p, d_p) = \mathbf{h}_p^\dagger \mathbf{R}_t \mathbf{h}_p = \frac{p\lambda^2 d_p^{-n}}{(4\pi)^2} \{ \mathbf{a}^\dagger(\theta_p^{(j)}) \mathbf{v} \mathbf{v}^\dagger \mathbf{a}(\theta_p^{(j)}) \}. \quad (6.64)$$

Using (6.63) and (6.64), the optimization problem in (6.64) can be written as

$$\begin{aligned} \max_{p \geq 0, \|\mathbf{v}\|=1} \log(1 + \alpha_s^2 p \{ \mathbf{a}^\dagger(\theta_s) \mathbf{v} \mathbf{v}^\dagger \mathbf{a}(\theta_s) \}) \\ \text{subject to } \sum_{i=1}^M p_i \leq P_T, \\ \frac{p\lambda^2}{(4\pi d_p)^2} \{ \mathbf{a}^\dagger(\theta_p^{(j)}) \mathbf{v} \mathbf{v}^\dagger \mathbf{a}(\theta_p^{(j)}) \} \leq I_{TH}, j = 1, \dots, K \end{aligned} \quad (6.65)$$

To solve the above optimization problem, firstly, we convert into a simple form as described below. Maximizing the term $\log(1 + \alpha_s^2 p \{ \mathbf{a}^\dagger(\theta_s) \mathbf{v} \mathbf{v}^\dagger \mathbf{a}(\theta_s) \})$ is equivalent to maximizing $|\sqrt{p} \mathbf{a}^\dagger(\theta_s) \mathbf{v}|$. Since $\mathbf{w} = \sqrt{p} \mathbf{v}$, the objective function can be written as: $|\mathbf{a}^\dagger(\theta_s) \mathbf{w}|$. Similarly, the interference power to the PU can be written as: $\alpha_p^2 |\mathbf{a}^\dagger(\theta_p) \mathbf{w}|^2$. Furthermore, we design \mathbf{w} in such a way that the term $\mathbf{a}^\dagger(\theta_s) \mathbf{w}$ has a real value without loss of any generality. Therefore, the optimization problem in (6.65) after including an additional constraint for the PU located beyond the considered sector can be written as

$$\begin{aligned} \max_{\mathbf{w}} \text{Re}[\mathbf{a}^\dagger(\theta_s) \mathbf{w}] \\ \text{subject to } \|\mathbf{w}\| \leq \sqrt{P_T} \\ \text{Im}[\mathbf{a}^\dagger(\theta_s) \mathbf{w}] = 0 \\ |\alpha_b \mathbf{a}^\dagger(\theta_b) \mathbf{w}| \leq \sqrt{I_T} \\ |\alpha_p \mathbf{a}^\dagger(\theta_p^{(j)}) \mathbf{w}| \leq \sqrt{I_{TH}}, j = 1, \dots, K \end{aligned} \quad (6.66)$$

The above optimization problem is in the form of Second Order Cone Programming (SOCP) problem [450] and can be solved using standard convex optimization software CVX [451].

6.4.2.3 Numerical Results

Let us consider a geographic sector which lies in the angular range from 10° to 85° with reference to the secondary BS. We consider a single desired user at an angle of -30° and a ULA at the BS with

the layout shown in Fig. 6.20. Further, we consider a single satellite terminal at an angle of -15° to analyze the effect of secondary transmission on the backlobe of the satellite terminal. The simulation and link budget parameters for both the links (i.e., link between the BS and satellite terminal and the link between the BS and terrestrial terminal) are provided in [120].

Figure 6.21 shows the beam patterns of the standard LCMV, scaled LCMV, modified LCMV and the SU rate maximization approach. For the scaled LCMV technique, the scaling parameter $\epsilon = 0.1$ was considered. From the figure, it can be noted that the beam pattern for scaled LCMV has a gain of 20 dB below the beam pattern for standard LCMV for all the considered angular range. In this way, we can reduce the transmitted signal towards the backlobe of the PU terminal by 20 dB with the sacrifice of 20 dBW transmit power in the desired direction. This method may be suitable for terrestrial systems with terminals having higher sensitivity and for satellite systems with terminals having higher front to back ratio. The beamforming weights for the standard LCMV were computed using (6.56) and for the modified beamformer using the algorithm presented in [120]. Furthermore, the beamforming weights for the SU rate maximization approach were obtained by solving optimization problem (6.66) using CVX software [451]. The interference threshold towards the backlobe of the PU terminal (I_T) located at -15° was set to be -50 dBW and the interference threshold towards the PU terminals (I_{TH})⁷ located in the considered angular region was set as -80 dBW.

Figure 6.22 shows the performance comparison of the modified LCMV and the standard LCMV beamformers in terms of the SINR. The beamforming weights calculated as described above were applied in the considered simulation environment where the exact positions and number of the PU terminals were unknown to the beamformer. During simulation, the value of I_T was considered to be 80 dB less than the power transmitted in the desired direction. From the figure, it can be noted that modified beamformer reduces the SINR towards the direction of the satellite terminal located at DoA of -15° , thus protecting the satellite terminal from secondary interference. The reduced value of SINR in the direction of the primary satellite terminal depends on the choice of the parameter I_T . This parameter should be chosen so as to meet the permissible interference level picked up by the backlobe of the satellite terminal in practical scenarios.

In the SU rate maximization approach, the transmit power in the desired direction depends on the chosen power threshold constraint in the direction of the PU terminals. To evaluate the performance of beamformer's response in the desired direction with respect to the change in the power threshold, simulations were carried by varying power threshold from -50 dBW to 0 dBW in the DoAs of the PUs. For this purpose, the PU terminals were considered within the angular sector from 45° to 85° with each terminal at 5° interval. Figure 6.23 presents the plot of transmitted power in the desired direction versus power threshold in the PU's direction. Furthermore, different plots have been presented considering desired users in different angular positions ($30^\circ, 20^\circ, 10^\circ, 0^\circ$). It can be noted that the transmit power in the desired user's direction is the maximum when the constrained threshold power is kept at -10 dBW for all the cases. Furthermore, it can be noted that the transmit power in the desired direction increases as the angular difference between the desired SU and the considered sector becomes large (i.e., maximum at 0° in Fig. 6.23).

To evaluate the performance of the beamformer with respect to the distance of the PU terminal from the BS, simulations were carried out considering the interference threshold of -150 dBW. Figure 6.24 shows the worst case SU rate versus PU distance from the BS. The distance of the PU was varied from 0.5 km to 10 km, transmit power constraint was considered to be 20 W and the desired user was considered at -30° . From the figure, it can be noted that the SU rate increases with the increase in the PU distance. The rate of increase is fast at the lower values of the distance and slow at the higher values of the distance. To show the overall effect of PU distance from the BS and the angular deviation from the considered sector, we have presented a three dimensional plot in Fig. 6.25. The distance range is considered from 0.5 km to 5 km and the angular deviation range was considered from 5° to 30° i.e.,

⁷It should be noted that the response constraint towards these PU terminals in case of LCMV based approaches is zero.

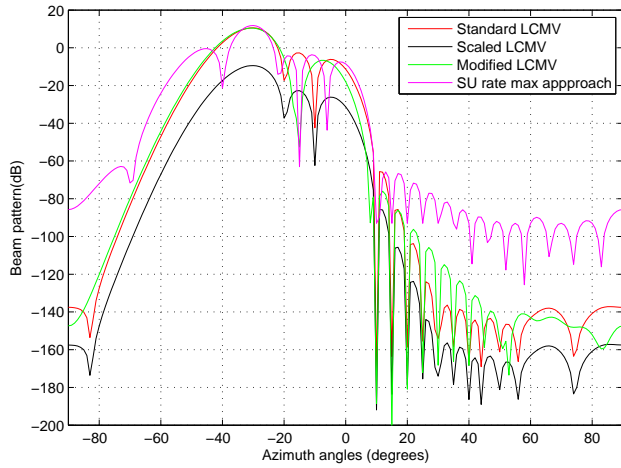


FIGURE 6.21: Beam patterns of different transmit beamforming techniques

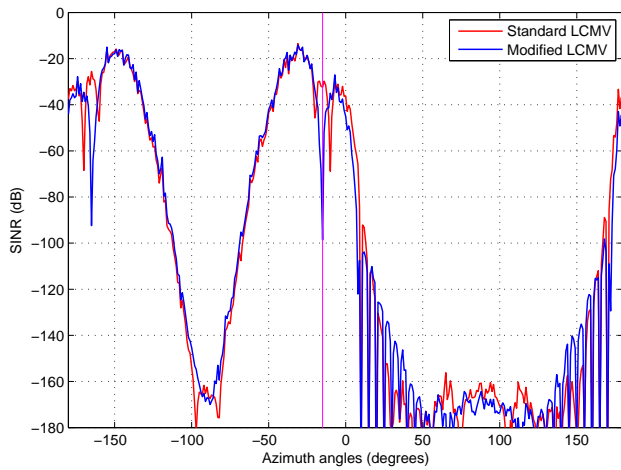


FIGURE 6.22: SINR comparisons of the modified LCMV and standard LCMV in the considered scenario

the DoAs of the SUs were considered in the range from 40° to 15° . The interference power threshold at the PU terminal⁸ was considered to be -150dBW . The SU rate was calculated by considering the worst case placement of the SU i.e., at a distance of 5km from the BS. As the interference threshold towards the PU is decreased, the beamformer has to reduce its transmitted power and in turn the secondary rate is reduced.

Discussion: While comparing the LCMV approaches with the SU rate maximization approach from Fig. 6.21, it can be noted that the later technique can provide slightly higher transmit power in the desired direction while the LCMV techniques can create very low interference towards the PU terminals located in the region of interest. It can be noted that there is less flexibility of introducing additional constraints such as power budget, interference threshold etc. in the LCMV based approaches. Furthermore, another difficulty for LCMV approach lies in acquiring the downlink covariance matrix. In SU rate maximization approach, there is more flexibility of introducing new constraints although the SU rate is dependent on the PU distance, interference threshold as well as the angular deviation from the sector of interest. It can be deduced that the choice of a particular technique mainly depends on the required performance level, the flexibility of introducing new constraints and the complexity of the technique.

⁸It should be noted that this is the maximum tolerable interference power at the PU terminal including the effect of path loss.

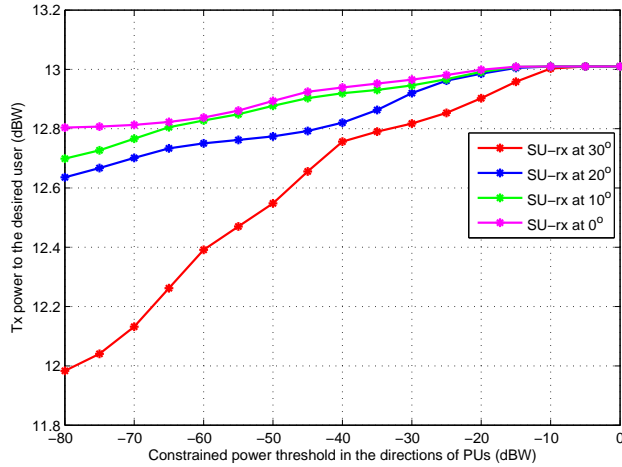


FIGURE 6.23: Transmit power in the desired direction versus power threshold using optimization problem (6.66)

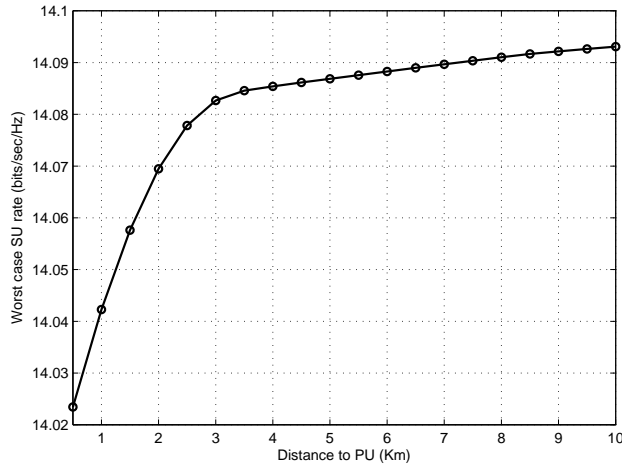


FIGURE 6.24: Worst case SU rate versus PU distance from the BS

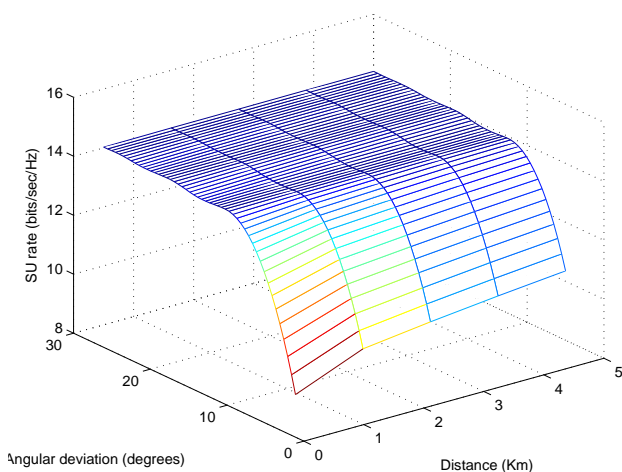


FIGURE 6.25: Worst case SU rate versus PU distance and angular deviation from the sector of interest

6.5 Chapter Conclusion

In this chapter, the application of various cognitive approaches such as interference modeling, interference detection, dual polarized SS, cognitive beamforming has been studied in the context of hybrid cognitive SatComs. From the interference modeling carried out between a terrestrial BS and a satellite terminal in the spectral coexistence of a C-band FSS link and a terrestrial cellular link both operating in the normal forward mode (Section 6.1), it has been observed that satellite terminals near the polar region receive more interference from a terrestrial BS than the satellite terminals the interference level varies significantly over a large geographical region due to the variation in the elevation angle of GEO satellite terminals. Further, it has been concluded that a suitable CR technique can be selected based on the interference power level obtained from the interference modeling. For example, interweave approaches such as SS and DB techniques seem to provide the best performance in high interference regions whereas in low or medium interference regions, interference from the secondary system to the primary can be suppressed using some form of underlay approach. Although the overlay approach can be applicable in both high and low interference scenarios, it seems to be suitable only for integrated systems with a very high level of interaction. Further, from the study of harmful detection problem for the coexistence scenario of FSS-FS coexistence in 17.7 – 19.7 GHz band (Section 6.2), it can be concluded that FS harmful interference can be reliably detected with the help of an additional dipole antenna equipped in the satellite terminal even using a simple ED-based approach. In addition, it has been shown that this solution can overcome the noise uncertainty problem which arises while sensing with the satellite dish.

Furthermore, in Section 6.3, the application of a dual-polarized SS in a dual polarized fading channel has been studied and theoretical expressions for P_d and P_f have been derived for SIMO and MIMO Rayleigh fading channels. From the theoretical as well as numerical analysis, it can be concluded that the performance of the ED technique in a MIMO fading channel is much better than in SIMO and SISO fading channels. Furthermore, the effect of XPR on SS efficiency has been analyzed and it can be concluded that the detection performance in a dual polarized fading channel increases with the value of XPR and its lower and upper bounds occur for a SIMO fading channel and an ideal MIMO fading channel respectively.

Moreover, in Section 6.4, the application of an underlay CB technique has been studied for the spectral coexistence scenario of satellite and terrestrial networks in both downlink and uplink coexistence scenarios. By using the priori knowledge about the interfering/victim sector which arises due to special propagation characteristics of the satellite terminals, different receive/transmit beamforming methods have been studied. In the considered scenarios, the DoA of the desired user and the range in which interferers are located is known while the exact locations of the interferers may not be unknown while designing the beamformer. From the performance comparison of MVDR and LCMV beamformers in the uplink coexistence scenario, it can be concluded that their performances are similar in the desired direction while the performance of the LCMV beamformer is much better in terms of rejecting interference coming from the interfering sector. Further, it has been noted that LCMV beamformer is better suited in case of the desired signal's DoA mismatch while the MVDR beamformer is better in presence of a large number of interferers. In the downlink coexistence scenario, various approaches such as scaled LCMV, modified LCMV and SU rate maximization approaches have been proposed. It can be concluded that the modified LCMV technique can provide the increased SINR towards the desired terminal and can mitigate the interference towards the specific angular sector by also providing sufficient protection towards the primary terminals located beyond the sector of interest. Further, the considered SU rate maximization technique provides the flexibility of applying different constraints while maximizing the SU rate. Further, it has been noted that the worst case SU rate is dependent on the PU distance, the permissible interference threshold at the PU terminals as well as the angular deviation of the desired user from the considered angular sector. It can be deduced that the choice of a particular technique mainly depends on the required performance level, the flexibility of introducing new constraints and the complexity of the technique.

Chapter 7

Dual Satellite Cognitive Communications

In this chapter, we propose several cognitive approaches for enabling the dual satellite coexistence described in Chapter 5. More specifically, we propose the following approaches: (i) Interference Alignment (IA), (ii) Cognitive beamhopping, and (iii) Dual-polarized SS. The IA technique is applied for the spectral coexistence of monobeam-multibeam GEO satellite coexistence in the normal return mode. The cognitive beamhopping technique is applied for the spectral coexistence of two GEO multibeam satellites in the normal forward mode considering the EZ and power control approaches. Further, dual-polarized sensing has been applied for the spectral coexistence of multibeam satellites in the normal return mode. The research work reported in this chapter has been published in [98, 99, 139, 144, 145, 425].

7.1 Cognitive Interference Alignment

Interference is an inevitable phenomenon in wireless communication systems when multiple uncoordinated links share a common wireless channel. The spectral coexistence of two satellite systems can be modeled as a CR network with interference channels between primary and secondary systems. The operation of the primary network usually follows a predefined standard and should not be degraded, while the secondary network should employ advanced communication techniques in order to exploit the underutilized dimensions in the frequency, time and space domains. Depending on the level of interference between primary and secondary systems, different interference management approaches can be applied and subsequently, different CR techniques techniques can be employed [106]. If the interference is weaker than the noise floor, the interference signal can be treated as noise [452] and the single user encoding/decoding mechanisms can be applied. Because of its simplicity and ease of implementation, this approach is widely used in practice, but does not achieve interference-free capacity even for the simple case of a broadcast channel [453]. If the interference level is strong in comparison to the noise floor, it is possible to decode the interference and then subtract it from the received signal. This method is less common in practice due to its complexity and security issues. However, when the interference level is comparable to the desired signal, treating it as noise is not effective because of the interference constraints involved while decoding and the cancelation of the interference may require complex primary receivers. In this case, one approach is to orthogonalize channels so that transmitted signals are chosen to be non-overlapping in the time, frequency or space domain, leading to Time Division Multiple Access (TDMA), Frequency Division Multiple Access (FDMA) or Space Division Multiple Access (SDMA) respectively. Furthermore, in multiuser interference networks, applying the above techniques is problematic since the aggregate interference may be stronger than the noise floor in many cases and decoding may also be complex due to involvement of several interfering users. Although the orthogonalization approach effectively eliminates multiuser interference in wireless

networks, it may lead to under-utilization of communication resources and it also does not achieve the capacity of interference channels [292]. In this context, IA has received important attention as an interference mitigation tool in interference-limited wireless systems such as cellular wireless networks, CR systems and ad-hoc networks [121–124].

7.1.1 Related Literature and Contributions

In multibeam joint processing, multiple users can be jointly processed by a single gateway and Multiuser Detection (MUD) is possible. In this context, several literature have studied the problem of multiuser/-multibeam joint decoding for satellite channels [454–456]. The capacity analysis of multibeam joint decoding over composite satellite channels has been carried out in [455] and joint multiuser processing techniques for multibeam satellites for both forward link and return link have been investigated in [456]. Further, the studies in [454, 457, 458] consider reverse link scenarios. Authors in [457] proposed an iterative multiuser decoding algorithm for the return link of multibeam satellites. Moreover, the return link of a multibeam satellite with Rician fading has been analyzed in [458] under the framework of Wyner’s Gaussian cellular MAC.

As noted in Chapter 2, the application of IA technique in legacy wireless networks and CR networks has been studied in different settings [121, 125, 126, 135–138, 306]. Further, IA technique has also been investigated in multicarrier systems in different settings [128, 131–133]. A projection based IA technique including the concepts of signal alignment and channel alignment has been investigated in [131]. The IA technique for an interference network with the multicarrier transmission over parallel sub-channels has been tackled in [132]. The signal alignment for multicarrier code division multiple access (MC-CDMA) in two way relay systems has been studied in [133]. Despite various literature about IA in terrestrial cellular networks, only a few studies have been reported about IA in the satellite literature. The feasibility of implementing subspace interference alignment (SIA) in a multibeam satellite system has been studied in [134] and it has been concluded that the SIA using frequency domain is advantageous for a multibeam satellite.

As mentioned earlier in Chapter 1, there exists no contribution on the application of IA technique in the dual satellite coexistence scenario. Further, most of the IA literature focus on IA over the spatial domain, which does not seem to be applicable in the satellite paradigm. In the above context, this work investigates an underlay spectral coexistence mechanism which exploits an uplink IA over the carrier domain in order to mitigate the interference of multibeam satellite terminals towards the monobeam satellite in a monobeam-multibeam dual satellite coexistence scenario. The performances of different IA techniques, namely static, uncoordinated and coordinated, are evaluated and compared with primary only, resource division and no-mitigation techniques in terms of the sum-rate capacity, primary to secondary rate ratio and primary rate protection ratio. With the help of theoretical and numerical analyses, it is shown that the coordinated IA approach perfectly protects the primary rate.

7.1.2 System Model

Let us consider a monobeam satellite (SAT1) and a multibeam satellite (SAT2) serving the same coverage area as shown in Fig. 7.1. These satellites are assumed to be connected to different gateways. We consider the monobeam system as primary and the multibeam system as secondary with both satellites operating in normal return mode. The monobeam and multibeam satellites can be adjacent or even colocated in terms of orbital slots. The cognition between these two systems can be achieved with the help of a high speed signalling link (i.e., microwave or optical fiber) between their gateways. Furthermore, we consider a single monobeam satellite terminal (ST1), N number of multibeam satellite terminals (ST2s) served by N beams of the SAT2. This coexistence scenario resembles the spectral

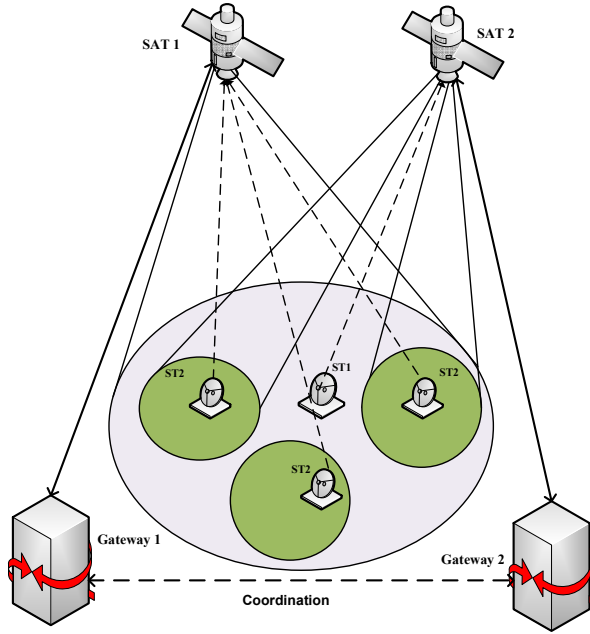


FIGURE 7.1: Graphical representation of the considered dual satellite coexistence system

coexistence scenario of heterogeneous networks in the context of 4G and 5G terrestrial wireless communications i.e., the spectral coexistence of small cells and a macro cell as illustrated in [98, 306]. In the considered scenario (Fig. 7.1), multibeam joint processing is considered at the gateway of SAT2 to decode the received signals from ST2s jointly [427]. Since a single gateway is responsible for processing the transmitted and received signals corresponding to a large geographical area, the application of joint processing techniques in the satellite context is centralized. After scheduling, we consider that one ST1 and N number of ST2s are transmitting simultaneously in a single slot over a common spectrum band. In this context, the IA technique can be applied at the multibeam satellite terminals to mitigate the interference towards the primary satellite.

Furthermore, we consider that all the satellite terminals use multicarrier transmission scheme and the IA is employed at the ST2s over $L = M + 1$ carriers, affected by Adjacent Carrier Interference (ACI). In this context, we consider a narrowband FDMA system which can be applicable for L/S band mobile satellite systems. We consider that M number of symbols are transmitted by ST1 and 1 symbol per ST2 is transmitted by spreading across all the carriers. Furthermore, it should be noted that ST1 sends M symbols over M subcarriers whereas each ST2 sends 1 symbol over L subcarriers. To suppress the interference caused by ST2s using IA technique, CSI towards the SAT1 is required and we assume that this CSI can be acquired at the ST2s by listening to the pilot signals broadcasted from the gateway. In this context, we assume Time Division Duplex (TDD) mode of operation and for a satellite system with Frequency Division Duplex (FDD) mode of operation, an alternative way of acquiring CSI should be investigated since uplink CSI can not be derived from the downlink pilots in FDD mode. As an example, for satellite scenarios where FDD is used, the uplink CSI can be derived from uplink pilots and then can be fed back with the help of a gateway.

In addition to CSI, ST2s and the SAT1 should be aware of the predefined IA vector in order to perform IA. Depending on how IA vector is calculated, we consider three different IA techniques: static, coordinated, and uncoordinated in our analysis. These techniques depend on the level of coordination between primary and secondary systems. The concept behind cognitive IA is to employ precoding at the ST2s so that the received secondary signals at the PR are all aligned across the alignment vector. In this way, interference can be filtered out by sacrificing one dof and some part of the desired received energy. For this purpose, the ST1 utilizes only M out of L dofs and reserves one dof which is devoted to IA filtering. However, after filtering the signal is interference free and can be easily decoded using conventional detection techniques. The term cognitive comes from the fact that the ST2s have to be

aware of the CSI and the alignment vector to perform the precoding. On the other hand, the PR needs only to perform filtering adapted to alignment vector and no additional awareness or intelligence is required.

7.1.3 Signal and Channel Model

1. *Signal Model*: The received signal at the primary receiver i.e., SAT1 can be written as

$$\mathbf{y}_p = \mathbf{H}\mathbf{x} + \sum_{i=1}^N \mathbf{F}_i \mathbf{x}_i + \mathbf{z}_p, \quad (7.1)$$

where \mathbf{y}_p is the $L \times 1$ received symbol vector, \mathbf{x} and \mathbf{x}_i are the $M \times 1$ and $L \times 1$ transmitted symbol vectors from the ST1 and the i th ST2 respectively, and \mathbf{z}_p is the receiver noise. The input signals \mathbf{x}, \mathbf{x}_i are assumed to be Gaussian and obey the following sum power constraints: $E[\mathbf{x}^\dagger \mathbf{x}] \leq \gamma_p M$ and $E[\mathbf{x}_i^\dagger \mathbf{x}_i] \leq \gamma_s L$, γ_p and γ_s being the transmit SNR of the primary and secondary systems respectively. The $L \times M$ matrix \mathbf{H} represents the channel gains between the SAT1 and the ST1 while the $L \times L$ matrix \mathbf{F}_i represents the channel gains between the SAT1 and i th ST2. To simplify notations, all \mathbf{F}_i are grouped into a single $L \times NL$ matrix $\mathbf{F} = [\mathbf{F}_1 \dots \mathbf{F}_N]$. The received signal at the joint processor of the SAT2 gateway can be written as

$$\mathbf{y}_s = \sum_{i=1}^N \tilde{\mathbf{F}}_i \mathbf{x}_i + \tilde{\mathbf{H}}\mathbf{x} + \mathbf{z}_s, \quad (7.2)$$

where \mathbf{y}_s is the $NL \times 1$ received symbol vector and \mathbf{z}_s is the receiver noise. The $NL \times M$ channel matrix $\tilde{\mathbf{H}}$ represents the channel gains between all SAT2 beams and the ST1 while the $NL \times L$ channel matrix $\tilde{\mathbf{F}}_i$ represents the channel gains between all SAT2 beams and the i th ST2. For notational simplicity, we group all $\tilde{\mathbf{F}}_i$ into a single $NL \times NL$ matrix $\tilde{\mathbf{F}} = [\tilde{\mathbf{F}}_1 \dots \tilde{\mathbf{F}}_N]$.

2. *Channel Model*: We consider a spectral coexistence network of multibeam and monobeam satellite systems with interference channels between them. Each transmitter/receiver node consists of a single antenna and uses multicarrier transmission so that the channels can be represented as diagonal matrices, where the diagonal entries correspond to the different sub-channels. The multicarrier model considered in this scenario differs from MIMO (spatial) channel matrix with full entries as considered in the terrestrial scenario.

Due to imperfect bandpass filters¹, weak copies of adjacent carrier signals may leak into the central carrier causing adjacent carrier interference. Therefore, we consider a multicarrier channel model with ACI. We assume that each carrier goes through independent flat-fading channels. The multi-carrier channel matrix with ACI for the i th satellite link for L number of carriers can be written as

$$\mathbf{H} = \begin{bmatrix} h_1 & \sqrt{\rho}h_2 & \dots & 0 \\ \sqrt{\rho}h_1 & h_2 & \dots & 0 \\ 0 & \sqrt{\rho}h_2 & \dots & 0 \\ \vdots & \vdots & \vdots & \vdots \\ 0 & 0 & h_{L-1} & \sqrt{\rho}h_L \\ 0 & 0 & \sqrt{\rho}h_{L-1} & h_L \end{bmatrix}, \quad (7.3)$$

¹The main reason for ACI is due to imperfect bandpass filters since we consider a narrowband FDMA system in this study.

where ρ represents the fraction of carrier power leaked to adjacent carriers and the parameter h_i represents the Rician fading coefficient, given by

$$h_i = \left(\sqrt{\frac{K}{K+1}}l + \sqrt{\frac{1}{K+1}}g_i \right), \quad (7.4)$$

where K is the Rician factor, l is a deterministic parameter representing the line of sight (LoS) component and g_i is a c.c.s. i.i.d. element for the i th satellite link representing the Rayleigh fading coefficient. The channel matrix between the SAT1 and the i th ST2 can be written as

$$\mathbf{F}_i = \alpha_i \mathbf{D}_i, \quad (7.5)$$

where α_i is the beam gain coefficient between the SAT1 and the i th SAT2 and \mathbf{D}_i has similar structure as \mathbf{H} . As a result,

$$\mathbf{F} = (\boldsymbol{\alpha}^T \otimes \mathbb{I}_{L \times L}) \odot \mathbf{D}, \quad (7.6)$$

with $\boldsymbol{\alpha} = [\alpha_1 \dots \alpha_N]^T$ and $\mathbf{D} = [\mathbf{D}_1 \dots \mathbf{D}_N]$. It is assumed that the fading coefficients are independent across block matrices \mathbf{D}_i . In addition, the channel matrix between SAT2 and the ST1 can be written as

$$\tilde{\mathbf{H}} = (\boldsymbol{\beta} \otimes \mathbb{I}_{L \times M}) \odot \mathbf{P}, \quad (7.7)$$

where $\boldsymbol{\beta} = [\beta_1 \dots \beta_N]^T$ includes beam gain coefficients between SAT2 and the ST1 and $\mathbf{P} = [\mathbf{P}_1 \dots \mathbf{P}_N]^T$ is a block matrix with each \mathbf{P}_i having similar structure as \mathbf{H} . Similarly, the channel matrix between SAT2 and the i th ST2 can be written as

$$\tilde{\mathbf{F}}_i = (\boldsymbol{\beta}_i \otimes \mathbb{I}_{L \times L}) \odot \mathbf{S}_i, \quad (7.8)$$

where $\boldsymbol{\beta}_i$ contains the beam gain coefficient between SAT2 and the i th ST2 and \mathbf{S}_i has similar structure as \mathbf{H} . As a result,

$$\tilde{\mathbf{F}} = (\mathbf{B} \otimes \mathbb{I}_{L \times L}) \odot \mathbf{S}, \quad (7.9)$$

with $\mathbf{B} = [\boldsymbol{\beta}_1 \dots \boldsymbol{\beta}_N]$ and the block matrix \mathbf{S} given by

$$\mathbf{S} = \begin{bmatrix} \mathbf{S}_{11} & \mathbf{S}_{12} & \cdots & \mathbf{S}_{1N} \\ \mathbf{S}_{21} & \mathbf{S}_{22} & \cdots & \mathbf{S}_{2N} \\ \ddots & & & \\ \mathbf{S}_{N1} & \mathbf{S}_{N2} & \cdots & \mathbf{S}_{NN} \end{bmatrix}, \quad (7.10)$$

where each block \mathbf{S}_{ij} follows the similar structure as \mathbf{H} .

Higher gain can be achieved with a multibeam satellite in comparison to a monobeam satellite since each of the beams is narrower than a beam which would cover the whole of the region to be served. For the considered coexistence scenario, the monobeam and multibeam satellites can be adjacent or even collocated in terms of orbital slots. The beam gain of the satellite link in all the above cases are evaluated based on following expression [459]

$$B(m, k) = G_T \cdot FL \cdot G_{\max} \cdot \left(\frac{J_1(u(m, k))}{2u(m, k)} + 36 \frac{J_3(u(m, k))}{u(m, k)^3} \right)^2, \quad (7.11)$$

where $B(m, k)$ represents the beam gain of k th beam for m th terminal position, J_i is the first kind of Bessel's function of order i , $u(m, k) = 2.01723 \sin(\theta(m, k))/\theta_{3dB}$, G_T is the terminal antenna gain, FL is the free space path loss for the satellite link, G_{\max} is the maximum satellite antenna gain, θ_{3dB} is the 3 dB angle and $\theta(m, k)$ represents the nadir angle to m th terminal position from k th beam center position with respect to the satellite.

7.1.4 Coexistence Techniques

In this section, we provide capacity expressions for different coexistence techniques including the IA approach. Let us consider the following input-output relation for a MIMO system.

$$\mathbf{y} = \mathbf{H}\mathbf{x} + \mathbf{z} \quad (7.12)$$

with $E[\mathbf{x}\mathbf{x}^\dagger] = \gamma\mathbf{I}$. The capacity of a MIMO channel is then given by [460]

$$C = \log \det \left(\mathbf{I} + \gamma \mathbf{H} \mathbf{H}^\dagger \right). \quad (7.13)$$

In the presence of cochannel interference, the input-output relation for a MIMO system can be written as

$$\mathbf{y} = \mathbf{H}\mathbf{x} + \mathbf{H}_c\mathbf{x}_c + \mathbf{z} \quad (7.14)$$

with $E[\mathbf{x}_c\mathbf{x}_c^\dagger] = \gamma_c\mathbf{I}$, where \mathbf{x}_c is a Gaussian vector transmitted by an interfering cochannel terminal. Then the capacity of a MIMO channel with input-output relation given by Equation (7.14) can be written as [461]

$$C = \log \det \left(\mathbf{I} + \gamma_c \mathbf{H} \mathbf{H}^\dagger \mathbf{R}^{-1} \right), \quad (7.15)$$

where the term \mathbf{R}^{-1} includes the effect of cochannel interference and \mathbf{R} can be written as:

$$\mathbf{R} = E[\tilde{\mathbf{z}}\tilde{\mathbf{z}}^\dagger] = \mathbf{I} + \gamma_c \mathbf{H}_c \mathbf{H}_c^\dagger \quad (7.16)$$

with $\tilde{\mathbf{z}} = \mathbf{H}_c\mathbf{x}_c + \mathbf{z}$. It should be noted that (7.13) and (7.15) are used repeatedly in the following subsection to study the throughput of considered techniques.

1. *Primary only*: In this technique, we consider only the presence of a primary system and there is no interference from the secondary system. This case corresponds to current frequency allocations, according to which each band is allocated only to a primary system. For the considered system, the primary throughput, let us denote by C_{po} , can be written as

$$C_{po} = E \left[\log \det \left(\mathbf{I}_L + \frac{\gamma_{ps}}{M} \mathbf{H} \mathbf{H}^\dagger \right) \right], \quad (7.17)$$

where \mathbf{I}_L is the identity matrix of dimension L and γ_{ps} represents the SNR at the transmit antenna of the primary system.

2. *No Mitigation*: In this technique, we assume that the available resource is split into two in order to allow the interference free parallel operation of primary and secondary systems. The orthogonalization is considered in the time domain for the considered multi-carrier scenario. In this case, the primary throughput, denoted by C_{ps} , can be written as

$$C_{ps} = E \left[\log \det \left(\mathbf{I}_L + \frac{\gamma_{ps}}{M} \mathbf{H} \mathbf{H}^\dagger \left(\mathbf{I}_L + \frac{\gamma_{ss}}{L} \mathbf{F} \mathbf{F}^\dagger \right)^{-1} \right) \right], \quad (7.18)$$

where γ_{ss} represents the SNR at the transmit antenna of the secondary system. The secondary throughput with this technique can be written as

$$C_{ss} = E \left[\log \det \left(\mathbf{I}_{NL} + \frac{\gamma_{ss}}{L} \tilde{\mathbf{F}} \tilde{\mathbf{F}}^\dagger \left(\mathbf{I}_{NL} + \frac{\gamma_{ps}}{M} \tilde{\mathbf{H}} \tilde{\mathbf{H}}^\dagger \right)^{-1} \right) \right]. \quad (7.19)$$

In both cases, the second term represents the cochannel interference.

3. *Resource Division*: In this technique, we assume that the available resource is split into two in order to allow the interference free parallel operation of primary and secondary systems. The orthogonalization is considered in the time domain for the considered multi-carrier scenario. In this case, the

primary throughput, denoted by \hat{C}_{pr} , can be written as

$$\hat{C}_{pr} = \frac{1}{2} E \left[\log \det \left(\mathbf{I}_L + \frac{2\gamma_{ps}}{M} \mathbf{H} \mathbf{H}^\dagger \right) \right] \quad (7.20)$$

while the secondary throughput can be written as

$$\hat{C}_{sr} = \frac{1}{2} E \left[\log \det \left(\mathbf{I}_{NL} + \frac{2\gamma_{ss}}{L} \tilde{\mathbf{F}} \tilde{\mathbf{F}}^\dagger \right) \right]. \quad (7.21)$$

4. Interference Alignment: In this technique, IA is employed at all the ST2s towards the SAT1 and interference is filtered out at the SAT1 by using the IA vector. In this case, the primary throughput, denoted by \bar{C}_{ps} , can be written as:

$$\bar{C}_{ps} = E \left[\log \det \left(\mathbf{I}_M + \frac{\gamma_p}{M} \bar{\mathbf{H}} \bar{\mathbf{H}}^\dagger \right) \right], \quad (7.22)$$

where $\bar{\mathbf{H}}$ is the equivalent channel matrix after IA filtering. For the SAT2, the interference coming from the ST1 has to be tolerated and thus secondary throughput, \bar{C}_{sp} , can be written as

$$\bar{C}_{sp} = E \left[\log \det \left(\mathbf{I}_{NL} + \frac{\gamma_s}{L} \bar{\mathbf{F}} \bar{\mathbf{F}}^\dagger \left(\mathbf{I}_{NL} + \frac{\gamma_p}{M} \tilde{\mathbf{H}} \tilde{\mathbf{H}}^\dagger \right)^{-1} \right) \right], \quad (7.23)$$

where $\bar{\mathbf{F}}$ is the equivalent channel matrix including precoding. We follow the alignment and filtering procedure proposed in [306] in order to evaluate the performance of multicarrier IA in the considered scenario. Interested readers may refer to [98, 306] for the detailed mathematical formulations of filtering and alignment procedure.

7.1.5 Interference Alignment Types

In this section, we describe three different IA approaches and their performances are compared with the help of numerical results in Section 7.1.6.

1. Static approach: In this approach, \mathbf{v} is predefined and does not depend on the channel state. It can be noted that this is quite static but also a simple solution which assumes no coordination in the network. The disadvantage of this approach that a large amount of received power may be filtered out since the IA direction may be aligned with one of the strong eigenvectors of the random SAT1-ST1 channel.

2. Uncoordinated approach: In this approach, there is no coordination between primary and secondary satellite systems. Furthermore, ST2s are aware of their CSI towards the SAT1 but have no information about the CSI of the ST1. In this context, the ST2s select \mathbf{v} in order to maximize the secondary throughput. Subsequently, the SAT1 senses the \mathbf{v} and applies the appropriate filter \mathbf{Q} . In this context, the following optimization problem can be defined [306]

$$[\mathbf{v}, \mathbf{Q}] = \arg \max_{\mathbf{v}, \mathbf{Q}} (\bar{C}_{ss}), \quad \text{s.t. } \mathbf{Q}\mathbf{v} = 0, \mathbf{Q}\mathbf{Q}^\dagger = 1. \quad (7.24)$$

Since the interference channel coefficients $\tilde{\mathbf{H}}$ are unknown, the following simplified objective function can be employed

$$[\mathbf{v}, \mathbf{Q}] = \arg \max_{\mathbf{v}, \mathbf{Q}} \text{trace}(\bar{\mathbf{F}} \bar{\mathbf{F}}^\dagger). \quad (7.25)$$

The solution of (7.25) is hard to tackle analytically. In this context, a heuristic approach can be followed by selecting the eigenvector corresponding to the largest eigenvalue of the equivalent channel covariance matrix $\sum_{i=1}^L \tilde{\mathbf{F}}_i (\mathbf{F}_i^{-1}) (\mathbf{F}_i^\dagger)^{-1} \tilde{\mathbf{F}}_i^\dagger = \mathbf{T}$. The matrix \mathbf{T} can be decomposed using the eigenvalue

decomposition as: $\mathbf{T} = \mathbf{U}^\dagger \mathbf{\Lambda} \mathbf{U}$ with $\mathbf{U} = [\mathbf{u}_1, \mathbf{u}_2, \dots, \mathbf{u}_M]$ and $\mathbf{\Lambda}$ being a diagonal matrix with the eigenvalues in descending order. Therefore, one simple heuristic solution is to choose the eigenvector corresponding to the largest eigenvalue, i.e., $\mathbf{v} = \mathbf{u}_1$ and to design a truncated unitary matrix \mathbf{Q} so that the condition $\mathbf{Q}\mathbf{v} = 0$ is satisfied.

3. *Coordinated approach*: In this approach, the primary and secondary systems coordinate to exchange the CSI information and the alignment vector. The selection of \mathbf{v} takes place at the SAT1 and is subsequently communicated to the ST2s. It is assumed that the channel coherence time is adequate for the alignment direction to be fed back and used by the ST2s. This is an egoistic approach since the SAT1 dictates the behavior of the ST2s in order to maximize the performance of the primary system. In this context, the following optimization problem can be defined

$$[\mathbf{v}, \mathbf{Q}] = \arg \max_{\mathbf{v}, \mathbf{Q}} \bar{\mathbf{C}}_{ps}, \quad \text{s.t. } \mathbf{Q}\mathbf{v} = 0, \mathbf{Q}\mathbf{Q}^\dagger = 1. \quad (7.26)$$

Now let $\mathbf{H}\mathbf{H}^\dagger = \mathbf{U}\mathbf{\Lambda}\mathbf{U}^\dagger$ be the eigenvalue decomposition of $\mathbf{H}\mathbf{H}^\dagger$ and $\mathbf{\Lambda}(\mathbf{H}\mathbf{H}^\dagger) = [0 \ \lambda_1 \ \dots \ \lambda_M]$ are the M ordered eigenvalues. The eigenvectors define an orthonormal basis of the MIMO/multicarrier sub-channels. In this direction, the optimal strategy is to select the eigenvector which corresponds to the zero eigenvalue as the alignment direction.

Theorem 7.1. *For $L = M + 1$, coordinated IA fully protects the primary rate, namely:*

$$\bar{\mathbf{C}}_{ps} = \mathbf{C}_{po}. \quad (7.27)$$

Proof. From (7.17) and (7.22), it can be observed that the throughput for primary only technique is a function of eigenvalues of $\mathbf{H}\mathbf{H}^\dagger$ and the throughput for coordinated IA technique is a function of eigenvalues of $\bar{\mathbf{H}}\bar{\mathbf{H}}^\dagger$. The objective here is to show that both $\mathbf{H}\mathbf{H}^\dagger$ and $\bar{\mathbf{H}}\bar{\mathbf{H}}^\dagger$ have the same non-zero eigenvalues.

Since $\bar{\mathbf{H}} = \mathbf{Q}\mathbf{H}$, $\bar{\mathbf{H}}\bar{\mathbf{H}}^\dagger = \mathbf{Q}\mathbf{H}\mathbf{H}^\dagger\mathbf{Q}^\dagger$, using the property $\det(\mathbf{I} + \gamma\mathbf{AB}) = \det(\mathbf{I} + \gamma\mathbf{BA})$, $\log \det(\mathbf{I}_M + \frac{\gamma_{ps}}{M}\bar{\mathbf{H}}\bar{\mathbf{H}}^\dagger) = \log \det(\mathbf{I}_M + \frac{\gamma_{ps}}{M}\mathbf{Q}^\dagger\mathbf{Q}\mathbf{H}\mathbf{H}^\dagger)$. Using the eigenvalue decomposition, $\mathbf{Q}^\dagger\mathbf{Q}$ and $\mathbf{H}\mathbf{H}^\dagger$ can be written as: $\mathbf{Q}^\dagger\mathbf{Q} = \mathbf{V}\mathbf{B}\mathbf{V}^\dagger$, $\mathbf{H}\mathbf{H}^\dagger = \mathbf{U}\mathbf{\Lambda}\mathbf{U}^\dagger$, where \mathbf{U} and \mathbf{V} are unitary matrices. Hence,

$$\log \det\left(\mathbf{I}_M + \frac{\gamma_{ps}}{M}\mathbf{Q}^\dagger\mathbf{Q}\mathbf{H}\mathbf{H}^\dagger\right) = \log \det\left(\mathbf{I}_M + \frac{\gamma_{ps}}{M}\mathbf{V}\mathbf{B}\mathbf{V}^\dagger\mathbf{U}\mathbf{\Lambda}\mathbf{U}^\dagger\right). \quad (7.28)$$

Since \mathbf{Q} is truncated unitary, \mathbf{B} can be written as:

$$\mathbf{B} = \begin{bmatrix} 1 & 0 & \cdots & 0 & 0 \\ 0 & 1 & \cdots & 0 & 0 \\ & & \ddots & & \\ 0 & 0 & \cdots & 1 & 0 \\ 0 & 0 & \cdots & 0 & 0 \end{bmatrix}, \quad (7.29)$$

and $\mathbf{\Lambda}$ is also a diagonal matrix with the following structure.

$$\mathbf{\Lambda} = \begin{bmatrix} \lambda_M & 0 & \cdots & 0 & 0 \\ 0 & \lambda_{M-1} & \cdots & 0 & 0 \\ & & \ddots & & \\ 0 & 0 & \cdots & \lambda_1 & 0 \\ 0 & 0 & \cdots & 0 & 0 \end{bmatrix}, \quad (7.30)$$

where $\lambda_1, \lambda_2, \dots, \lambda_M$ corresponds to M eigenvalues. Using the property $\det(\mathbf{I} + \gamma\mathbf{AB}) = \det(\mathbf{I} + \gamma\mathbf{BA})$, (7.28) can be written as

$$\log \det\left(\mathbf{I}_M + \frac{\gamma_{ps}}{M}\bar{\mathbf{H}}\bar{\mathbf{H}}^\dagger\right) = \log \det\left(\mathbf{I}_M + \frac{\gamma_{ps}}{M}\mathbf{B}\mathbf{V}^\dagger\mathbf{U}\mathbf{\Lambda}\mathbf{U}^\dagger\mathbf{V}\right). \quad (7.31)$$

Since the truncated unitary matrix \mathbf{Q} in the coordinated approach is constructed using the eigenvectors in \mathbf{U} , which correspond to non-zero eigenvalues, $\mathbf{V}^\dagger \mathbf{U}$ gives a new unitary matrix $\tilde{\mathbf{V}}$ and has the following structure

$$\mathbf{V}^\dagger \mathbf{U} = \begin{bmatrix} & & & & 0 \\ & & & & 0 \\ & & \tilde{\mathbf{V}} & & \vdots \\ & & & & 0 \\ 0 & 0 & \cdots & 0 & 1 \end{bmatrix}. \quad (7.32)$$

After removing one dimension, (7.31) can be written as

$$\log \det \left(\mathbf{I}_M + \frac{\gamma_{ps}}{M} \mathbf{B} \mathbf{V}^\dagger \mathbf{U} \Lambda \mathbf{U}^\dagger \mathbf{V} \right) = \log \det \left(\mathbf{I}_M + \frac{\gamma_{ps}}{M} \mathbf{V} \tilde{\Lambda} \tilde{\mathbf{V}}^\dagger \right) = \log \det \left(\mathbf{I}_M + \frac{\gamma_{ps}}{M} \tilde{\Lambda} \right), \quad (7.33)$$

where $\tilde{\Lambda}$ contains the non-zero eigenvalues of $\mathbf{H} \mathbf{H}^\dagger$. Hence, $\bar{\mathbf{H}} \bar{\mathbf{H}}^\dagger$ and $\mathbf{H} \mathbf{H}^\dagger$ have identical non-zero eigenvalues in this approach and this completes the proof. \square

Remark 7.2. Due to the fact that we reserve one dof for interference alignment, the coordinated IA technique perfectly preserves the primary rate. Optimally there can be L data streams at the PT and if we use all L degree of freedoms for signal transmission, there exists no zero eigenvalue and in that case, even the coordinated approach will have small gap as compared to the primary only technique.

7.1.6 Numerical Results

In this section, we present a number of numerical results in order to provide a comparative evaluation of the considered schemes.

1. Performance Metrics: The sum-rate capacity of the considered coexistence system is dictated by the primary throughput and the secondary average per-link throughput, let us denote by C_{sys} , and define as

$$C_{\text{sys}} = C_{\text{ps}} + \frac{C_{\text{ss}}}{N}, \quad (7.34)$$

where C_{ps} is the throughput of the primary system in the presence of the secondary system, C_{ss} is the average per-link rate of the secondary system in the presence of the primary system, and N is the number of SUs. It should be noted that in (7.34), we consider secondary average per-link throughput i.e., $\frac{C_{\text{ss}}}{N}$ in order to reflect the secondary per-user throughput as we increase the number of SUs in the system, as illustrated later with the help of numerical results.

Subsequently, the primary to secondary rate ratio can be denoted by PSR and is defined as

$$\text{PSR} = \frac{C_{\text{ps}}}{C_{\text{ss}}/N}. \quad (7.35)$$

Finally, the primary rate protection ratio is denoted by PR and defined as

$$\text{PR} = \frac{C_{\text{ps}}}{C_{\text{po}}}, \quad (7.36)$$

where C_{po} denotes the primary only capacity in the absence of the secondary system.

2. Results: While simulating the considered coexistence scenario, ST1 and ST2s are assumed to be uniformly distributed within the coverage area of the beams of SAT1 and SAT2, respectively. Furthermore, the beams of the multibeam antennas are also uniformly distributed within the coverage area of the monobeam satellite, emulating a beam hopping pattern. We consider a multicarrier channel model

TABLE 7.1: Simulation parameters for capacity results

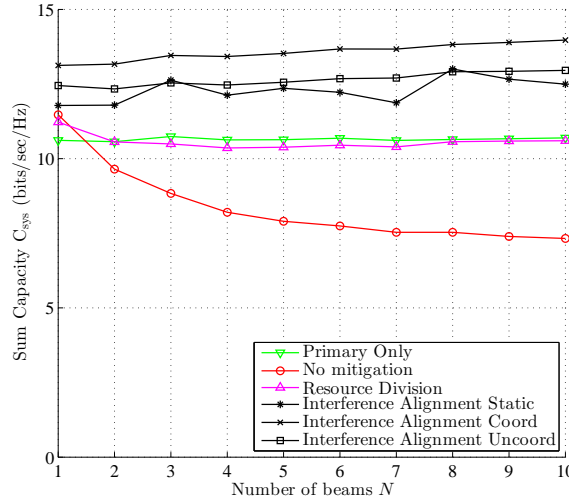
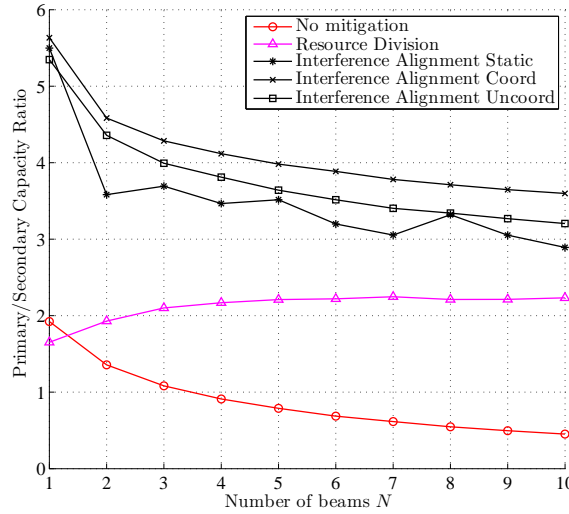
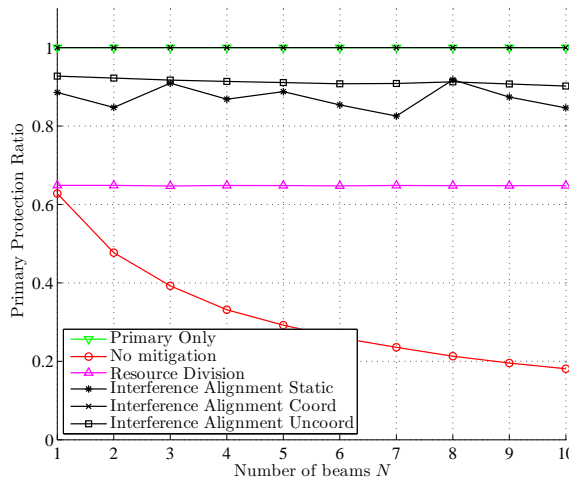
Parameter	Symbol	Value	Range
Number of ST2s	N		1 – 10
Number of carriers used by ST1	M	4	
Number of symbols transmitted by ST1		4	
Number of carriers used by ST2	L	5	
Number of symbols transmitted by each ST2		1	
Monobeam Radius	R_{ps}	520 km	
Multibeam Radius	R_{ss}	165 km	
ST1 Transmit Power	P_{ps}	10 dBW	
ST2 Transmit Power	P_{ss}	3.98 dBW	
Receiver Noise Power @ 5 MHz	N_0	-137 dBW	
Monobeam 3-dB Beamwidth	BW_{ps}	0.82°	
Multibeam 3-dB Beamwidth	BW_{ss}	0.26°	
Intercarrier interference component	ρ	0.15	
Rician factor	K	12 dB	
Freee Space Path loss	FL	190 dB	
Max Satellite Antenna Gain	G_{max}	48 dBi	
Terminal Antenna Gain	G_T	5 dB	
Number of Monte Carlo realizations		10^3	

with ACI and each non-zero component of the channel matrix being independent Rician fading coefficient. The ergodic metrics are then evaluated by averaging over a large number of channel realizations and positions. Table 7.1 presents the parameter values and ranges used for producing the numerical results in this scenario. For the resource division approach, we consider resource sharing between the primary and secondary systems in the time domain.

Figure 7.2 depicts the normalized system rate (C_{sys}) versus number of SAT2 beams N for different techniques and it can be observed that the coordinated IA technique performs better than all other techniques and the sum-rate slowly increases with N for this technique. The sum-rate for uncoordinated IA technique is worse than the coordinated IA technique and is still better than other considered techniques and it increases slowly with the value of N . Furthermore, the sum-rate for no mitigation technique decreases with the value of N , remains more or less constant with the value of N for resource division and remains constant for the primary only technique. The increased sum-rate capacity for the IA techniques is due to the combined effect of multibeam joint processing and the applied IA technique. The variation in the results in this scenario from the previous scenario is due to the different nature of the channel. In satellite coexistence scenario, the channel is non-zero mean and we consider a tridiagonal channel matrix with 3 correlated entries.

Figure 7.3 shows the PSR versus N for the considered techniques. It can be observed that the maximum PSR is achieved with the coordinated IA technique and it decreases with the value of N . This happens due to the introduction of more number of beams in the considered coverage area. The PSR for IA uncoordinated, IA static and no-mitigation also decreases when more beams are introduced into the system. Furthermore, the PSR for the resource division technique increases slightly for lower values of N and remains constant at higher values of N . This is because the secondary throughput reduces with N due to the channel structure.

Figure 7.4 depicts the PR versus N plot for the considered schemes. It can be observed that the coordinated IA technique is optimal and matches with the primary only technique. This means that the coordinated IA technique fully protects the primary rate. Furthermore, all techniques except the no-mitigation technique shows a constant protection rate with the value of N , while the performance of no-mitigation decreases monotonically as in previous scenario. Moreover, the uncoordinated IA technique protects almost 90% of the total primary rate and the resource division protects about 65% of the total primary rate.

FIGURE 7.2: Normalized system rate versus number of SAT2 beams N .FIGURE 7.3: Primary to secondary rate ratio versus number of SAT2 beams N .FIGURE 7.4: Primary protection ratio versus number of SAT2 beams N .

3. *Discussion:* In this contribution, the spectral coexistence of multibeam and monobeam satellites with multicarrier transceivers has been studied in the satellite paradigm. The main conclusion of this study is that multicarrier based IA can be applied for allowing the coexistence of monobeam and

multibeam satellites in the normal return mode. From the comparison of the considered IA techniques in the considered scenario, it is noted that the coordinated IA technique can provide perfect protection to the monobeam satellite and matches with the primary only rate i.e., the rate that would be achieved in the absence of the secondary multibeam system. This has been verified with the help of both theoretical analysis and numerical results. Further, from the viewpoint of protecting primary rate as well as achieving the highest rate, the coordinated IA technique is the best among all other techniques in considered satellite coexistence scenario. In the considered analysis and simulation environment, a multicarrier channel model with the ACI has been considered with each channel coefficient modeled as a Rician fading coefficient. From the practical perspectives, the coordinated scheme requires the exchange of CSI and alignment vector between the gateways of two satellite systems. This can be achieved with the help of a high speed link between their gateways. If this coordination mechanism is not available in practice, the uncoordinated approach can be followed with some sacrifice in the sum-rate and the primary rate protection as compared to the coordinated scheme. If the interference caused by the uncoordinated approach to the monobeam satellite is below the interference tolerance limit set by the regulatory bodies and the secondary rate is sufficient in order to guarantee the QoS of the link, the uncoordinated approach can be applied.

7.2 Cognitive Beamhopping

In conventional multibeam systems, partial frequency reuse can be used to enhance the system capacity. However, it may be impractical to apply full frequency reuse due to excessive co-channel interference which is difficult to remove using existing interference mitigation techniques. A beamhopping satellite system can operate by using full frequency reuse over a certain beamhopping pattern [140]. The main difference between conventional multibeam and beamhopping systems is that frequency sharing among multiple beams within a cluster takes place in different domains, i.e., frequency and time domains respectively. Several contributions exist in the literature in the context of beamhopping systems [140–143]. Since in a beamhopping system, only a single beam of a cluster is active during a particular time slot, there exists an opportunity to reuse the full frequency using smaller beams of another secondary satellite in the same time slot. In this direction, we propose a cognitive beamhopping system with the objective of enhancing the system Spectral Efficiency (SE) while protecting the PUs. We consider a dual satellite spectral coexistence scenario of two multibeam satellites with a primary satellite having larger beams and a secondary satellite having smaller beams. The cognition is achieved by sharing the beamhopping pattern and the timing information of the primary multibeam system to the secondary multibeam system using a signalling link between their corresponding gateways. The timing information is exchanged to guarantee the proper synchronization of the primary and secondary transmissions. The primary multibeam system is considered to be an already deployed system and its performance should not be degraded beyond the prescribed threshold by the deployment of the secondary satellite systems. The secondary satellite dynamically adapts its beampattern and transmit power ensuring the unobstructed operation of the primary system. In this context, the performance of the proposed cognitive beamhopping system is evaluated and compared with the performance of conventional multibeam and beamhopping satellite systems in terms of SE (bits/sec/Hz). Furthermore, we consider a scenario where multiple SUs are present within an inactive primary beam and evaluate the system performance of the proposed system. For this purpose, we consider full frequency reuse and frequency sharing among the SUs. Furthermore, a power control technique is considered at the secondary satellite to protect the primary satellite terminals using a predetermined interference threshold. Moreover, we apply the EZ principle to investigate the opportunity for secondary transmission in the switched-off regions of the primary satellite system. The main objective is to find the regions in which secondary satellite can operate ensuring protection against harmful interference for the primary systems. In addition, the power control and the EZ techniques are compared in terms of the total system throughput considering the same aggregated secondary interference.

7.2.1 Existing Multibeam Systems

1. Conventional Multibeam System: In conventional multibeam systems, the total available bandwidth (W) in the forward link is divided into K segments, where the parameter K is the frequency reuse factor. Then the bandwidth allocated to the i -th user beam (W_i) can be written as: $W_i = W/K$. The set of the beams which share the total bandwidth defines a beam cluster. The total gain in terms of frequency reuse obtained by using a multibeam satellite in comparison with a monobeam satellite depends on the number of clusters in that region which would be covered by a single beam of the monobeam satellite. The bandwidth allocated per beam can be written as: $W_i = N_i W_c$, where N_i is the number of carriers in the i -th beam and W_c is the bandwidth of each carrier. As the value of K decreases, the available bandwidth per beam increases but the co-channel interference also increases. Since the system capacity depends on both the available bandwidth and the co-channel interference, the value of K should be chosen in such a way that the maximum system capacity is achieved.

2. Flexible Multibeam System: In comparison to the conventional systems, the flexible system uses a non-regular frequency reuse pattern and non-uniform power/carrier allocation. In practical situations, at least one carrier per beam is allocated i.e., $N_i \in \{1, 2, \dots, N_{\max}\}$, where $N_{\max} = N_c - (K - 1)$ and $N_c = W/W_c$ is the total number of available carriers. Let N_b be the total number of beams in the system, then the $N_c \times N_b$ bandwidth allocation matrix \mathbf{C} can be defined as [143]

$$\mathbf{C} = \begin{bmatrix} C_{11} & C_{12} & \dots & C_{1N_b} \\ C_{21} & C_{22} & \dots & C_{2N_b} \\ \vdots & \vdots & \ddots & \vdots \\ C_{N_c 1} & C_{N_c 2} & \dots & C_{N_c N_b} \end{bmatrix}, \quad (7.37)$$

where C_{ij} represents the i -th carrier allocated to the j -th beam. The number of carriers allocated to the j -th beam can be calculated as: $N_j = \sum_{i=1}^{N_c} C_{ij}$, where $C_{ij} \in \{0, 1\}$ indicates whether the i -th carrier is allocated to the j -th beam or not.

3. Beamhopping Multibeam System: In this system, a limited number of beams are simultaneously illuminated with a regular repetition pattern. This is referred to as a beamhopping technique. Such a technique helps to reduce the number of amplifiers on board as well as the power demands on the payloads [462]. This technique can be implemented with full frequency or partial frequency reuse. In case of full frequency reuse, a regular time window is periodically applied to the beamhopping system and the entire available bandwidth is allocated to each illuminated beam. The duration for each illuminated beam should be selected to satisfy the user transmission delay requirement. In case of partial frequency reuse, the total bandwidth is segmented and each beam can be illuminated with a fraction of W . Let N_t be the number of time slots in each time window, then the $N_t \times N_b$ beam illumination matrix \mathbf{T} can be written as:

$$\mathbf{T} = \begin{bmatrix} T_{11} & T_{12} & \dots & T_{1N_b} \\ T_{21} & T_{22} & \dots & T_{2N_b} \\ \vdots & \vdots & \ddots & \vdots \\ T_{N_t 1} & T_{N_t 2} & \dots & T_{N_t N_b} \end{bmatrix}, \quad (7.38)$$

where T_{ij} indicates that the i -th time slot is allocated to the j -th beam. The total number of time slots allocated to the j -th beam can be written as: $N_{j,t} = \sum_{i=1}^{N_t} T_{ij}$, where $T_{ij} \in \{0, 1\}$ indicates whether the i -th time slot is allocated to the j -th beam or not.

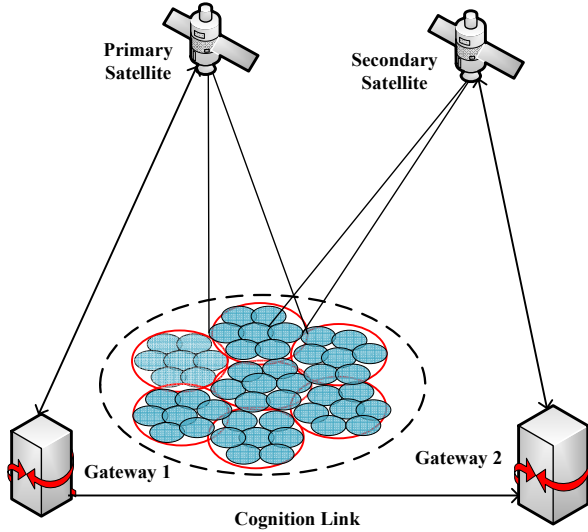


FIGURE 7.5: Spectral coexistence scenario of two multibeam satellites in the same geographical region

7.2.2 Proposed System and Techniques

7.2.2.1 System Model

We consider a dual satellite coexistence scenario as shown in Fig. 7.5. We consider both satellites to be multibeam satellites covering the same geographical region and operating in the normal forward mode. Both satellites are assumed to be co-located in the same GEO orbit and are connected to different gateways on Earth. These gateways are connected with the help of a high speed terrestrial link (e.g., optical fiber, microwave). In addition, both satellites operate in the Ka-band frequencies (20 – 21 GHz forward link). The primary satellite is an already deployed satellite for providing high priority broadband multimedia services to the fixed users. The secondary satellite can be used for providing services requiring low QoS such as interactive services to the fixed users. In this context, we assume the proposed cognitive beamhopping system to be compatible with the second generation of DVB-S2 or the next generation of DVB (DVB-Sx) standards.

The primary satellite is operated with larger beams and the secondary satellite with smaller beams in the same coverage area². We consider a coverage area with larger primary beams and many spot-beams within each primary beam and these spot-beams are the beams of the secondary satellite. The cognition is achieved by sharing the beamhopping pattern and the timing information of the primary satellite to the secondary satellite with the help of a signalling link between the gateways. Based on this a priori knowledge of the beamhopping pattern, the secondary satellite's beamhopping pattern is designed so that it does not degrade the primary's operation. Furthermore, the primary and secondary transmissions can be synchronized with the help of the exchanged timing information. The secondary satellite is supposed to be more dynamic and be equipped with smaller transponders (as reflected by link budget parameters presented in Table 7.2). We consider a Single Feed per Beam (SFPB) type antenna sub-system for the primary system and an array fed reflector i.e., Multiple Feeds per Beam (MFPB) type antenna sub-system for the secondary system. As noted in [464], although both the SFPB and MFPB architectures are comparable in terms of the cost and mass, the MFPB architecture is preferable for smaller satellites due to the requirement of only two reflectors, one for transmission and the another for reception [464, 465]. Furthermore, it is possible to design the secondary link to have low SNR at the center of the beam (in comparison to the receive SNR at the primary beam center) due

²Due to recent advances in multibeam antenna technology, it is feasible to create coverage cells of less than 0.5° diameter [463, 464].

to smaller coverage areas of the secondary beams while meeting the same edge requirements [466, 467]. Moreover, partitioning a beam into many sub-beams performs well towards the spot beam edge meeting the edge gain requirements. In this context, the importance of spot-beams is increasing due to their low peak gains and low contour levels resulting in smaller antenna aperture and lower hardware costs [466]. Although it is possible to illuminate a portion of beams simultaneously with the full frequency reuse or the fractional frequency reuse in a beamhopping system, we focus on the full frequency reuse approach in our considered scenario. In the following subsection, we present different techniques which can be applied for the spectral coexistence of two multibeam satellites.

7.2.2.2 Applicable Techniques

Since the primary satellite only illuminates a small fraction of beams out of a large number of beams deployed under the beamhopping system, the rest of the beams remain idle at that time waiting for their transmission slots. If we could deploy a secondary satellite within the same spectrum in such a way that it has a beamhopping sequence different from that of the primary one and it does not produce harmful interference with the primary system, the overall system spectrum efficiency can be enhanced. The idea is that the primary satellite shares its beamhopping pattern to the secondary satellite and based on this knowledge, the secondary satellite's beamhopping pattern is designed so that it does not affect the primary system's operation. For this purpose, interaction between primary and secondary systems is required as the secondary system has to be aware of the primary satellite's beamhopping pattern. This can be achieved with the help of a cognition link between the gateways. This scheme can be considered as a Beamhopping Pattern Planning (BPP) scheme. In this context, different techniques such as an EZ principle [61, 326] and a power control method can be applied.

1. Power Control Method: In the context of terrestrial CR networks, this method has been applied in various settings [468, 469]. In this work, we apply this method for the considered dual satellite coexistence scenario. The power of the secondary satellite can be calculated based on the aggregate interference level provided by the secondary system to the primary. This can be applied to all the secondary beams over the considered region or only the secondary beams which are located within a certain range from the primary receiver. For power control within a certain region, this method can be combined with the EZ method. If the secondary satellite beams lie in between the white region and the black region i.e., in the grey region³ [326], we can implement power control in those secondary beams to maintain the interference threshold level of the PUs. In this combined method, the beams which are located in the black region are not activated and the beams which are located in the white region can be supplied with full power within a particular beamhopping slot. The sequence of active and inactive secondary beams should be changed in different time slots. This can be carried out easily based on the knowledge of primary beamhopping pattern. Furthermore, it is possible to apply dynamic power control method based on the distance from the primary active beam. In this method, less power is allocated to the secondary beams which are near the primary active beam and the transmitted power of the secondary beams can be increased as the distance from the primary active beam increases. It should be noted that there is a trade-off between power control and the achievable secondary throughput.

2. Exclusion Zone Method: This method has been investigated in the literature in various settings. The EZ principle is applied in [325] in the context of integrated satellite and terrestrial mobile systems. In [61], the primary exclusive region for a CR network is proposed using the spatial spectrum holes. A CR network consisting of a single PT and multiple SUs has been considered and bounds on the radius of the PER has been proposed based on the aggregated secondary interference and outage guarantee to the PU. In [326], the bounds for black, grey and white regions have been investigated. These contributions have considered a single PT scenario considering the application of TVWSs. In this scenario, the EZ region is confined within a certain region and the secondary system is allowed to operate beyond this specific region. However, in terrestrial cellular systems as well as in the multibeam satellite systems, there exist multiple co-channel PTs within a coverage region. In this context, secondary systems should

³Readers are referred to [61] and [326] for the definitions of different regions.

not be allowed to operate within the EZ regions of all the co-channel primary beams to ensure sufficient protection for all the PUs.

In this work, we apply the EZ principle to investigate the operating region for the secondary satellite. The secondary satellite operates in such a way that its active beam lies beyond the EZ of all the primary active beams. The EZ concept can be used to find out the region in which the secondary satellite can transmit with full power and the regions in which the secondary satellite has to adjust its power. The secondary satellite beams are activated with full power in the region from which the aggregate interference to the primary satellite terminal is below some acceptable limit. Furthermore, the secondary beams which fall in the EZ of the primary beams can be activated with the limited power depending on how far they are from the beam centre position of the active primary beams⁴. The size of the EZ has a great impact on the QoS of the primary satellite since it affects the level of secondary interference that needs to be tolerated and on the secondary satellite capacity since it affects the available amount of primary spectrum at a given location.

7.2.3 Signal and Channel Model

Let us consider a multibeam satellite system that employs a satellite antenna with N_b beams using a beamhopping pattern. At a particular time slot, only $M = N_b/K$ beams are active transmitting independent information streams to M fixed terminals located in different active main beams. During a particular time slot, each satellite terminal suffers from the interference from other co-channel beams. This multibeam satellite channel can be modeled with $M \times M$ channel matrix \mathbf{H} , each element of \mathbf{H} , h_{ij} representing the channel coefficient from beam j to user i .

For the cognitive coexistence of two satellites within the same spectrum while covering the same geographical region, the footprint of these satellites should be taken into account. The beam gain of the j -th beam for the i -th user position can be denoted by B_{ij} and is given by (6.1).

Let N_{b1} be the total number of beams in the primary satellite and M be the total number of users to be served by the network. The received power at the output of the decoder of user i , denoted by $P_{r,i}$, is related to the input power at beam j as

$$P_{r,i} = h_{ij} P_{t,j}, \quad (7.39)$$

where $j = \{1, \dots, N_{b1}\}$, $i = \{1, \dots, M\}$, $P_{t,j}$ is the input power to beam j . Under clear sky conditions, this channel coefficient can be calculated as [470]

$$h_{ij} = \frac{B_{ij} G_{r,ij}}{(4\pi d_{ij})^2}, \quad (7.40)$$

where $G_{r,ij}$ is the gain of the i -th user antenna towards the j -th beam and can be considered to be constant as it does not show significant variation in time. The parameter d_{ij} is the slant distance of the i -th user from the satellite which can be written as: $d_{ij}^2 = r_{ij}^2 + D_j^2$, where r_{ij} is the distance of i -th user position from the j -th beam centre position and D_j is the height of the geostationary satellite from the j -th beam center position.

For each user i , the following condition should be satisfied to have a reliable link: $\gamma_i \geq \gamma_{th}$, where γ_i is the SINR of the i -th user, γ_{th} is the minimum SINR required by the user to have the desired QoS.

⁴We use the beam center position as the reference point but the interference threshold is adjusted in order to guarantee the sufficient protection to the beam edge PUs as well.

Therefore, the power allocated to each beam should be calculated in the following way

$$P_{t,j} = \frac{\gamma_{\text{th}} \cdot I_{\text{cn}}}{\min_{i \in j} |h_{ij}|^2}, \quad (7.41)$$

where I_{cn} is a parameter including the noise and the interference from co-channel beams, the notation $i \in j$ means that i -th user is served by the j -th beam. The above equation represents the power allocated to the j -th beam under clear sky conditions.

7.2.4 System Performance

The following coexistence scenarios may be considered: (i) operating SUs only in the white region where no secondary interference is present, (ii) implementing power control in the secondary transmission, and (iii) by carrying out dynamic spectrum sensing and allocating idle bands to the SUs. In this work, we focus on the first two scenarios. Furthermore, we consider scenarios where a single SU and multiple SUs are present within each inactive primary beam.

7.2.4.1 Throughput Analysis

In this section, we present the theoretical expressions for evaluating the performance of different systems. In this analysis, we assume fixed carrier and power allocation for conventional multibeam and beamhopping systems. Furthermore, we assume a band-limited Gaussian line of sight channel contaminated with cochannel interference and consider that the interference is uncorrelated with the desired signal. It can be noted in [471] that while considering DVB-S2 with ACM, the spectral efficiency curve follows the Shannon curve with a certain gap. Assuming that suitable modulation and coding is available to recover the supported SNR range, the Shannon capacity can be used as a suitable metric for evaluating the system performance⁵.

1. Conventional Multibeam System: In this case, the multibeam satellite coverage with frequency reuse factor of K is considered. The dominant interference in this case is the co-channel interference from neighboring co-channel cells. The SINR of the i -th user is given by

$$\gamma_{\text{CV},i} = \frac{|h_{ii}|^2 P_t}{P_t \sum_{j \in S_p} |h_{ij}|^2 + \sigma^2}, \quad (7.42)$$

where σ^2 denotes the noise power, P_t represents the transmitted power and S_p represents the set of co-channel beams. It can be noted that we include all possible co-channel cells in a given area and adjacent channel interference is not included in (7.42). The system throughput for this system can be written as [83]

$$C_{\text{CV}} = \frac{W}{K} \sum_{i=1}^{N_b} \log_2(1 + \gamma_{\text{CV},i}), \quad (7.43)$$

where N_b is the number of beams in the system.

2. Beamhopping System: In this case, a beamhopping system with slot reuse factor of K is considered. Each active beam uses full frequency instead of fractional frequency reuse in the conventional multibeam systems. This is equivalent to frequency reuse factor in the frequency domain. The SINR of the i -th user is given by

$$\gamma_{\text{BH},i} = \frac{|h_{ii}|^2 P_t}{P_t \sum_{j \in S_B} |h_{ij}|^2 + \sigma^2}, \quad (7.44)$$

⁵In practice, we need to take account of channel fading, coding and modulation parameters depending on the type of modulation and coding scheme employed while evaluating the overall system capacity [471].

where S_B represents the set of beams which are active in a particular beamhopping slot. The system throughput for this system can be written as

$$C_{BH} = W \sum_{i=1}^{N_b/K} \log_2(1 + \gamma_{BH,i}), \quad (7.45)$$

where N_b/K represents the number of beams which are active per beam slot.

3. Cognitive Beamhopping System: Since only a certain fraction of total available beams are active in a particular time slot, we can explore the possibility of using those frequencies in the secondary satellite system in a secondary way. The primary system is a beamhopping system with larger beams with slot reuse factor of K . The secondary system can also be considered to be a beamhopping system with smaller beams and lower transmit power. The total system throughput in this system can be expressed as

$$C_{CB} = C_{PS} + C_{SP} = W \left(\sum_{i=1}^{N_b/K} \log_2(1 + \gamma_{CP,i}) + \sum_{i=1}^{N_s} \log_2(1 + \gamma_{CS,i}) \right), \quad (7.46)$$

where C_{PS} and C_{SP} denote primary/secondary throughput in the presence of secondary/primary system respectively, $\gamma_{CP,i}$ represents the SINR of the PU, $\gamma_{CS,i}$ represents the SINR of the SU and N_s denotes the number of active secondary beams. The expression for $\gamma_{CP,i}$ can be written as

$$\gamma_{CP,i} = \frac{|h_{P,ii}|^2 P_{pt}}{P_{pt} \sum_{j \in S_p} |h_{p,ij}|^2 + P_{st} \sum_{j \in S_s} |h_{ij,s}|^2 + \sigma^2}, \quad (7.47)$$

where P_{pt} is the transmit power of the primary system, P_{st} is the transmit power of the secondary system, S_s represents the set of secondary active beams in a particular slot. The parameter $h_{p,ij}$ represents the channel gain of the i -th PU from the j -th primary beam and $h_{ij,s}$ denotes the channel gain of the i -th PU from the j -th secondary beam. Similarly, the expression for $\gamma_{CS,i}$ can be written as

$$\gamma_{CS,i} = \frac{|h_{S,ii}|^2 P_{st}}{P_{pt} \sum_{j \in S_p} |h_{ij,p}|^2 + P_{st} \sum_{j \in S_s} |h_{s,ij}|^2 + \sigma^2}, \quad (7.48)$$

where $h_{ij,p}$ is the channel gain of i -th SU from the j -th primary beam and $h_{s,ij}$ is the channel gain of i -th SU from the j -th secondary beam.

7.2.4.2 Power Control Method

In this method, firstly, the aggregate interference from the secondary satellite beams to the PU is calculated and based on this interference level, the transmit power of the secondary satellite is adjusted to meet the interference threshold level of the PU. Let I_T be the interference threshold level of the PU to have sufficient protection⁶ and I_{AGG} be the aggregate interference from secondary beams to the PU. Then the expression for I_{AGG} at a particular slot can be written as: $I_{AGG} = P_{st} \sum_{j \in S_s} |h_{ij,s}|^2$. The transmit power of the secondary satellite can be adjusted in the following way to guarantee sufficient protection for the PU

$$P_{st} = \frac{I_T}{\sum_{j \in S_s} |h_{ij,s}|^2}. \quad (7.49)$$

It can be noted that as the number of SUs within an primary inactive beam increases, the denominator term of the above equation increases and the secondary satellite has to reduce its transmission power.

⁶It can be noted that primary system has to sacrifice some throughput corresponding to this interference tolerance level.

7.2.4.3 Exclusion Zone Method

Investigating the exact EZ for the primary active beam in our considered scenario is one important research problem. Furthermore, by sacrificing a certain tolerable primary throughput, the secondary satellite can coexist with the primary depending on the EZ radius. If the EZ radius is too small, the primary terminals need to tolerate more interference from the secondary satellite and if the EZ radius is too large, the total SE of the system needs to be sacrificed. In this context, we address the trade-off problem of primary throughput sacrifice and the total SE of cognitive beamhopping system. Furthermore, our interest is to investigate the minimum distance from the primary active beam center at which the secondary satellite can serve its users ensuring perfect protection to the PUs. The application of the EZ principle in our proposed cognitive beamhopping system is described below.

We consider a geographic region covered with the beampatterns of the primary and secondary satellites. Each primary beam consists of N_s number of secondary beams and only a fraction of total primary beams are active within a particular time slot. Let θ_{3dB} be 3 dB beamwidth of the primary beam and can be calculated as:

$$\theta_{3dB} = \tan^{-1}(r/D), \quad (7.50)$$

where r is the radius of the primary beam corresponding to the 3 dB beamwidth and the D is the height of the satellite from the center of the beam. By increasing the value of θ_{3dB} by some amount Δ i.e., $\theta_{\text{new}} = \theta_{3dB} + \Delta$, we can calculate the new value of r corresponding to the particular value of θ_{new} . During a particular time slot, only the secondary beams which lie outside the EZ of the active primary beams are made active⁷. This is done by comparing the nearest distance of the secondary beam from the center of the primary active beam with the EZ radius. While doing this, distances from all the active primary co-channel beams is taken into consideration to ensure the protection for all the PU terminals in the considered region.

7.2.5 Results and Discussion

We consider the following three systems for comparison: (i) conventional multibeam system⁸, (ii) beamhopping system, and (iii) proposed cognitive beamhopping system. The simulation parameters are presented in Table 7.2. In the proposed cognitive beamhopping system, each beam of the primary system includes 7 sub-beams which are served by the secondary satellite.

1. *Performance Metrics*: The system performance is evaluated using total SE in bits/sec/Hz and primary rate protection ratio. The total SE of the conventional multibeam, beamhopping and the proposed cognitive beamhopping systems are obtained using (7.43), (7.45) and (7.46) respectively. The primary rate protection ratio, denoted by PR, is defined as $\text{PR} = \frac{C_{\text{ps}}}{C_{\text{po}}}$ as in (7.36).

2. *Methodology*: We evaluate the performance of the proposed cognitive beamhopping system using two different approaches. The primary system is supposed to be a beamhopping system with a fixed beamhopping pattern and the secondary system is supposed to be an intelligent system which can adjust its beampattern based on the primary beamhopping sequence. In the first approach, the secondary system applies power control to the active beams in order to provide the sufficient protection to the primary users. In this context, we investigate both the full frequency reuse and frequency sharing-based approaches among the secondary users in each primary inactive beam. In the second approach, we apply the exclusion zone principle, in which only the secondary beams which lie inside the exclusion zone of all the active primary beams at a particular time instant are switched off. It should be noted that in the EZ approach, the secondary system does not need to implement power control in order to protect the PUs. Furthermore, the proposed solution can be considered as a special case of overlapping coverage of

⁷It can be noted that a secondary beam should not be active even if a part of it lies within the EZ of active primary beams since we are considering normal forward scenario.

⁸This denotes the static beam case with the conventional frequency reuse system and is considered here for the throughput comparison purpose.

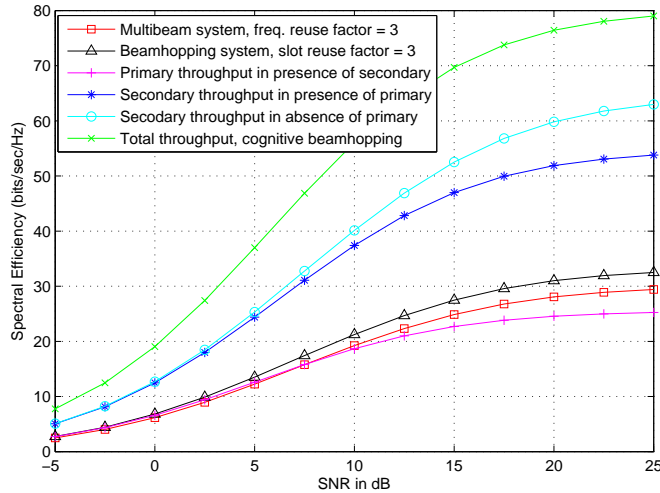
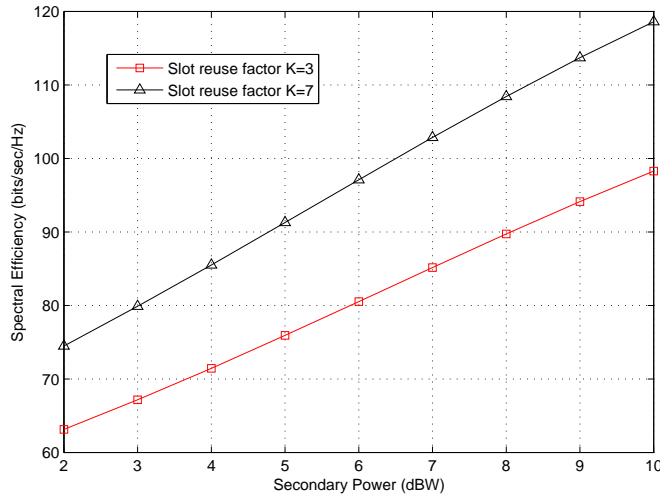
multibeam systems which is closer to a real implementation on integrated satellite-terrestrial systems for multibeam satellites combined with ground complementary components [325].

We calculate the beamwidth using the expression given by (7.50), in which the corresponding cell radius i.e., the value of r can be found by accommodating the N_b number of beams in the considered coverage area (5000 km) and N_s number of secondary beams in each primary beam. Then we calculate the peak antenna gain values for primary and secondary systems using $G(\text{dB}) = 10\log(29,000/(\theta_{3\text{dB}})^2)$ considering antenna efficiency to be 60 % [394], which results in higher antenna peak gain for the secondary system in comparison to the primary system. This allows system designers the flexibility of using less transmit power per beam for the secondary system than that in the primary system meeting the same edge gain requirements. Since the size of the satellite is partially determined by the required transmit power, designers can save payload weight on the secondary satellite. In our analysis, we divide our considered area into smaller cells with the considered number of beams and consider the maximum SNR in the center of the beam closer the receive SNR value provided by the link budget calculation in Table 7.2. For interference calculation, we calculate 4 different beam matrices using (6.1) for the following scenarios: (i) from primary beams to the SUs, (ii) from secondary beams to the PUs, (iii) from primary beams to the PUs, and (iv) from secondary beams to the SUs. Then we evaluate the system performance using capacity expressions provided in Section 7.2.4 and present results in the following subsections.

TABLE 7.2: Simulation and link budget parameters

Parameter	Symbol	Value
Orbit		GEO
Satellite height	D	35800 km
Frequency band		Ka (20 GHz)
User link bandwidth	W	500 MHz
Coverage area radius	R	5000 km
<i>Parameters for primary Satellite</i>		
Interference tolerance threshold	I_0	-123 dBW
Slot reuse factor	K	3.7
Number of primary Beams	N_b	37
3 dB beamwidth	$\theta_{3\text{dB}1}$	1.3125°
TWTA RF power @ saturation	P_{pt}	20 dBW
Max satellite antenna gain	G_t	42.26 dBi
Free space path loss	FL	209.5 dB
Fading margin		3 dB
Noise power @ 500 MHz	N_o	-117 dBW
Max user antenna gain	G_r	45 dBi
Receive SNR at the beam center		11.76 dB
<i>Parameters for Secondary satellite</i>		
Number of secondary beams per primary beam	N_s	7
3 dB beamwidth	$\theta_{3\text{dB}2}$	0.5052°
TWTA RF power @ saturation	P_{st}	10 dBW
Max satellite antenna gain	G_t	50.55 dBi
Free Space Path loss	FL	209.5 dB
Fading Margin		3 dB
Noise Power @ 500 MHz	N_o	-117 dBW
Max user antenna gain	G_r	45 dBi
Receive SNR at the beam center		10.05 dB

3. *Throughput Comparison*: Figure 7.6 shows the SE (bits/sec/Hz) versus SNR for different systems for $K = 3$, $N_b = 19$ and $P_{\text{st}} = P_{\text{pt}}$. During this simulation setting, only one SU was considered at the center of each inactive primary beam. From the figure, it can be noted that the SE for the beamhopping system is slightly greater than for the conventional multibeam system. Furthermore, it can be noted that the primary only SE slightly decreases at higher values of SNR in the presence of secondary system whereas the total SE of the cognitive beamhopping system increases. The increase in the secondary throughput in comparison to the primary throughput in Fig. 7.6 comes from the fact that there are

FIGURE 7.6: Throughput comparison of different systems ($K = 3, N_b = 19, P_{st} = P_{pt}$)FIGURE 7.7: Spectral efficiency versus secondary power in cognitive beamhopping system ($N_b = 37, P_{pt} = 10\text{dBW}$)

more number of active secondary beams (smaller) with the same transmit power during a particular beamhopping slot. Moreover, it should be noted that the value of the SE plotted in our results is the SE obtained over the considered area instead of the SE of a single link.

Figure 7.7 shows the SE versus secondary transmit power (P_{st}) for $K = 3, 7$ and $N_b = 37$. The primary transmit power (P_{pt}) was considered to be 10dBW. From the figure, it can be noted that the total SE of the cognitive beamhopping system for $K = 7$ is higher than for $K = 3$ and it increases with the secondary transmit power for both the values of K . Figure 7.8 shows the PR versus secondary power for $K = 3, 7$ and $N_b = 37$. From this figure, it can be noted that the primary rate protection ratio is higher for the case of $K = 3$ than for the case of $K = 7$. While comparing Figs. 7.7 and 7.8, it can be concluded that for lower value of reuse factor e.g., $K = 3$, less number of primary inactive beams are available resulting in less number of secondary active beams in a particular time slot. Therefore, the total SE for the case of $K = 7$ is higher than the case of $K = 3$ due to large increase in secondary SE. On the otherhand, the primary system is more protected for $K = 3$ case than for $K = 7$ since only few secondary beams are active in the former case than in the later case. Therefore, the choice of the factor K should be made in order to make a trade-off between the total SE and the PR. It should be noted that there is a lower bound on the size of the beams due to electromagnetic properties of satellite antenna arrays and propagation characteristics of satellite channels.

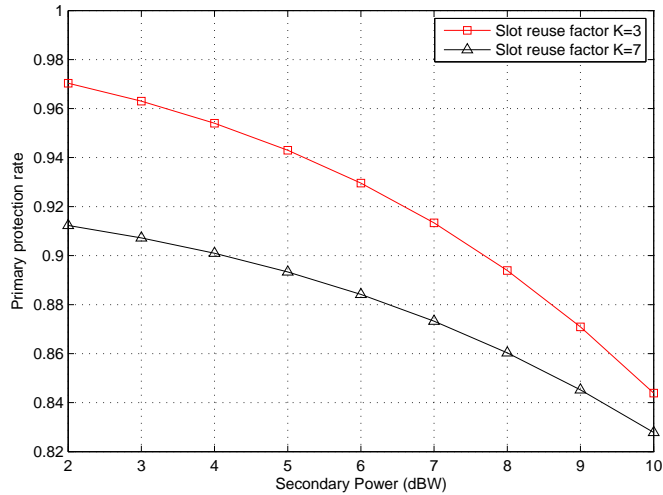


FIGURE 7.8: Primary rate protection ratio versus secondary power in cognitive beamhopping system ($N_b = 37, P_{pt} = 10\text{dBW}$)

TABLE 7.3: Throughput comparison for different scenarios in a cognitive beamhopping system

K	N_b	Power ($P_{pt} = 10\text{dBW}$)	$C_{PO}(\text{bps}/\text{Hz})$	$C_{PS}(\text{bps}/\text{Hz})$	$C_{PR}(\text{bps}/\text{Hz})$	$C_{SP}(\text{bps}/\text{Hz})$	$C_{CB}(\text{bps}/\text{Hz})$
3	37	$P_{st} = P_{pt}/2$	37.53	34.29	0.913	50.86	85.16
3	37	$P_{st} = P_{pt}$	37.53	31.69	0.84	66.63	98.32
3	37	$P_{st} = 2 \times P_{pt}$	37.53	27.68	0.73	80.76	108.44
7	37	$P_{st} = P_{pt}/2$	22.61	20.18	0.89	67.63	87.82
7	37	$P_{st} = P_{pt}$	22.61	18.34	0.81	85.28	103.62
7	37	$P_{st} = 2 \times P_{pt}$	22.61	15.67	0.69	99.68	115.35
3	19	$P_{st} = P_{pt}/2$	21.21	19.83	0.93	28.44	48.27
3	19	$P_{st} = P_{pt}$	21.21	18.66	0.88	37.47	56.14
3	19	$P_{st} = 2 \times P_{pt}$	21.21	16.78	0.79	45.91	62.69
7	19	$P_{st} = P_{pt}/2$	9.88	8.47	0.86	51.98	60.45
7	19	$P_{st} = P_{pt}$	9.88	9.10	0.92	40.61	49.72
7	19	$P_{st} = 2 \times P_{pt}$	9.88	7.48	0.76	61.82	69.31

Table 7.3 shows the primary only throughput C_{PO} , primary throughput in presence of the secondary C_{PS} , secondary throughput in presence of the primary C_{SP} , primary rate protection ratio C_{PR} and total throughput C_{CB} of the cognitive beamhopping system. This table presents the above mentioned performance metrics for the values of $K = 3, 7$ and $N_b = 19, 37$ for the following power ratio cases: (i) secondary power half of the primary power i.e., $P_{st} = P_{pt}/2$, (ii) secondary power equal to the primary power i.e., $P_{st} = P_{pt}$ and (iii) secondary power double than that of the primary power i.e., $P_{st} = 2 \times P_{pt}$. From the table, it can be noted that the value of C_{PS} decreases from the case (i) to (ii) and further decreases from case (ii) to case (iii) for all combinations of K and N_b . As a result, the primary rate protection ratio also decreases from case (i) to case (iii) for all combinations of K and N_b . For example, for $K = 3$ and $N_b = 37$, the primary protection rate is 0.913 for case (i), 0.84 for case (ii) and 0.73 for case (iii). Furthermore, it can be noted from the table that the value of C_{SP} as well as the value of C_{CB} increases from the case (i) to the case (iii) for all the combinations of K and N_b . From these comparative results, it can be concluded the primary rate is more protected with less secondary power in comparison to the primary power while secondary throughput and the total throughput is the maximum for the highest secondary transmitted power. While comparing the cases for $K = 3$ and $K = 7$ for a specific value of N_b , it can be noted that the primary rate protection ratio for $K = 7$ is less than for $K = 3$ while the secondary throughput as well as the total throughput increases for the $K = 7$ case than for the $K = 3$ case for all the considered power ratio cases.

4. *Power Control Method:* To calculate the number of SUs which can be served in switched off region of the primary beams, simulations were carried out considering the presence of multiple SUs

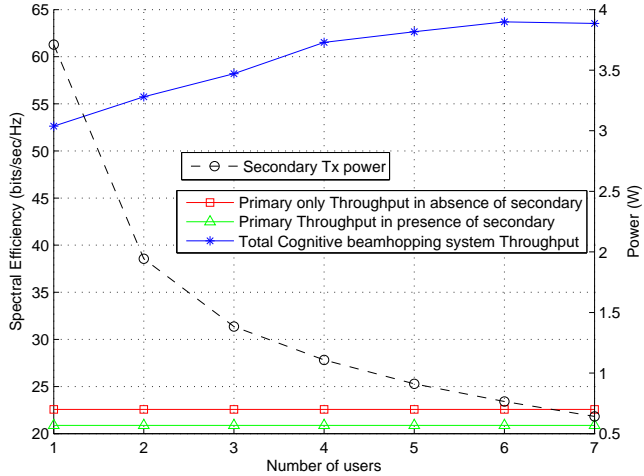


FIGURE 7.9: SE versus number of SUs in cognitive beamhopping system with full frequency reuse ($K = 7, N_b = 37, P_{pt} = 10\text{dBW}$)

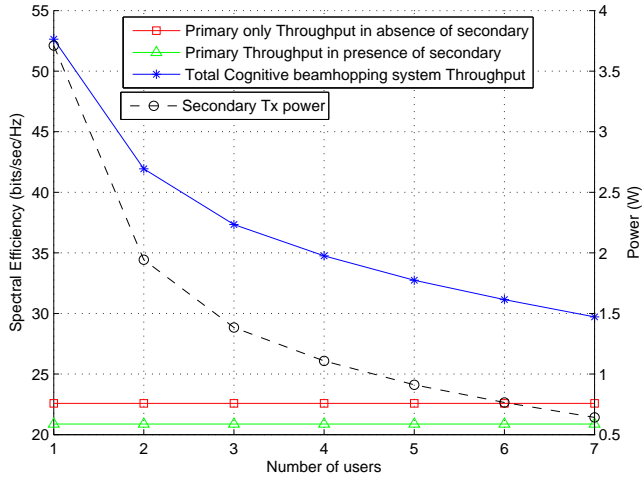


FIGURE 7.10: SE versus number of SUs in cognitive beamhopping system with frequency sharing among the SUs ($K = 7, N_b = 37, P_{pt} = 10\text{dBW}$)

per inactive primary beam. Figure 7.9 shows SE versus number of users for cognitive beamhopping system. In this simulation settings, the SUs were placed at the center of sub-beams in each inactive primary beam and the number of users was varied from 1 to 7. The full frequency reuse is considered for both primary and secondary systems. For the result in Fig. 7.9, the parameters considered were $K = 7, N_b = 37, P_{pt} = 10\text{dBW}$. The interference tolerance threshold of each PU for the considered user link bandwidth (500 MHz) was considered to be -123dBW ⁹ and based on this interference threshold, power of the secondary satellite was calculated for considered number of SUs. From the figure, it can be noted that SE increases with the number of users and it almost saturates while increasing the user number from 6 to 7. Furthermore, it can be noted that the secondary satellite has to reduce its transmitted power as the number of SUs increases in order to protect the primary rate with tolerable level of interference. Moreover, the simulations were carried for the cases of $K = 3, N_b = 37$, $K = 7, N_b = 19$ and $K = 3, N_b = 19$. It has been noted from the results that for a specific value of N_b , the total cognitive beamhopping throughput is greater for $K = 7$ case for all the considered number of users but the primary throughput for the primary system is higher for $K = 3$ case. Furthermore, the primary protection rate is slightly less in $K = 3$ case than in $K = 7$ case provided the same interference threshold limit for each PU.

To evaluate the performance of proposed cognitive beamhopping system in the presence of multiple users with frequency sharing, simulations were carried out by sharing the spectrum resource among the SUs

⁹This value was chosen to ensure that the aggregated interference to noise ratio does not exceed -6dB [472].

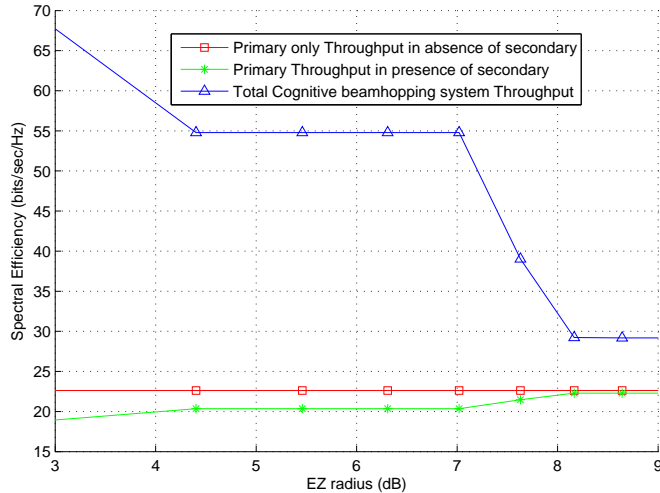


FIGURE 7.11: SE versus EZ radius (dB) for cognitive beamhopping system considering single SU in the center of inactive primary beam ($K = 7, N_b = 37, P_{pt} = P_{st} = 10\text{dBW}$)

in the same inactive primary beam. In this case, each SU uses only a fraction of the spectrum resource and this fraction depends on the considered number of users. Figure 7.10 shows SE versus number of users for cognitive beamhopping system with frequency sharing among the SUs in the secondary system with $K = 7, N_b = 19, P_{st} = 10\text{dBW}$. From the figure, it can be noted that the total throughput of the cognitive system decreases as the number of SUs increases. Furthermore, the power of secondary user has to be adjusted as per black line drawn in the figure to meet the interference threshold limit of the PUs. Similarly, the simulation experiment was carried out for the case of $K = 3, N_b = 19, P_{pt} = 10\text{dBW}$ and it is noted that overall throughput decreases in this case for all number of SUs but the primary throughput increases for $K = 3$ case. Furthermore, the primary rate is slightly less protected in $K = 3$ case than in $K = 7$ case provided the same interference threshold limit for each PU.

From the comparison of two cases with full frequency reuse and frequency sharing in the secondary system, it can be concluded that the SE increases with the number of users in the frequency reuse case and the SE decreases with the number of users in the frequency sharing case. Furthermore, the frequency sharing among users is not that much suitable from practical perspectives. Therefore, the cognitive beamhopping system can achieve significant enhancement in the total throughput than the primary only system by using full frequency reuse in secondary system in practical scenarios.

5. *EZ Method*: Figure 7.11 shows the SE versus EZ radius (dB) for $K = 7, N_b = 37, P_{pt} = P_{st} = 10\text{dBW}$. In this simulation settings, one SU was considered at the center of each inactive primary beam. For a particular beamhopping slot, all the secondary beams which are inside the EZ of all the primary active beams were not taken into account for calculating interference as well as the total SE of the system i.e., only the beams which lie outside the EZ regions of the all the active primary beams were considered. The EZ radius of the beam was varied from 3 dB to 9 dB. From the figure, it can be noted that the primary throughput in the presence of secondary increases i.e., the primary protection rate is increased with the increase in the EZ radius as expected whereas the total SE decreases. It can be noted that after the EZ radius of 8.5 dB, the primary rate is almost protected with a significant gain in the total SE. In this aspect, we can enhance the total SE using the EZ principle in the proposed cognitive beamhopping system ensuring sufficient protection to the primary system.

Figure 7.12 depicts the SE versus EZ radius (dB) for $K = 7, N_b = 37, P_{pt} = P_{st} = P_{pt}/2$ considering the case of multiple SUs in each inactive primary beam. The following three scenarios have been considered for comparison (i) Best position of the SUs (Beam centre), (ii) Random position of the SUs, and (iii) Worst position of the SUs (Beam edge). While simulating the best case scenario, SUs were placed at the centers of secondary beams within each inactive primary beam. For the random scenario, positions of the SUs were generated randomly with uniform distribution while for the worst case scenario, the SUs were placed just on the border of the secondary beams within each inactive

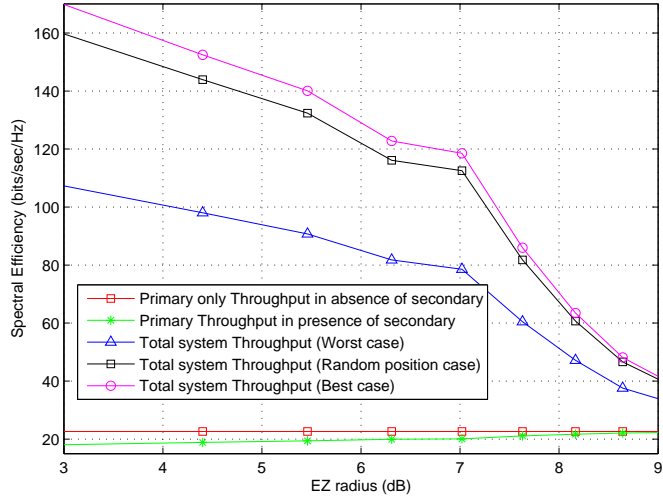


FIGURE 7.12: Comparison of SE versus EZ radius (dB) for different SU positions (considering multiple SUs within each inactive primary beam) ($K = 7, N_b = 37, P_{pt} = 10\text{dBW}, P_{st} = P_{pt}/4$)

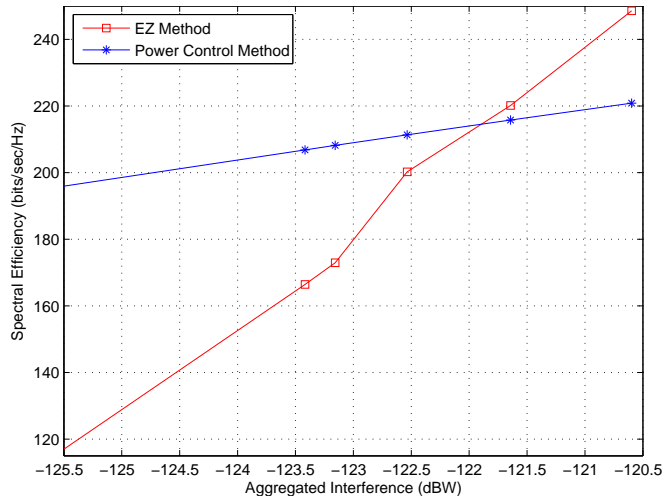


FIGURE 7.13: Comparison of power control and EZ methods $K = 7, N_b = 37$

primary beam. From the figure, it can be depicted that the best case scenario achieves the highest total system throughput in comparison to other scenarios. Furthermore, the performance of the random users scenario is closer to the best case scenario as depicted in the figure. From practical perspectives, the worst case scenario is more realistic than other scenarios.

6. Comparison of EZ and power control Methods: In order to compare the above two methods, simulations were carried out with parameters $K = 7, N_b = 37$. To have a fair comparison of these two methods, the aggregated interference from the secondary system to the primary system was kept fixed in both systems. While simulating the EZ method, the value of P_{st} was considered to be half of the value of $P_{pt} = 10\text{dBW}$ and the power control was applied on the secondary transmission using the same aggregated interference obtained in EZ method. Figure 7.13 shows the comparison of SE obtained using these methods versus aggregated interference. The aggregated interference was varied from -125.5dBW to -120.5dBW . It can be noted that power control method shows less variation in SE over the considered range than the EZ method. Furthermore, it can be deduced that the power control method achieves higher SE than the EZ method for low values of the aggregated interference and after a certain value of aggregated interference (-121.9dBW in Fig. 7.13) the EZ method achieves higher SE than the power control method. Therefore, it can be concluded that the power control method achieves higher system throughput in the presence of low secondary aggregated interference while the EZ method is better suited for high secondary aggregated interference.

5. Discussion and Technical Challenges: We have proposed a novel cognitive beamhopping technique

allowing the coexistence of multibeam satellite systems. The primary system can be a multibeam satellite with a predetermined beamhopping pattern. In this context, the application of beamhopping in multibeam satellite systems has been already discussed in various contributions [140–143]. In this thesis, we studied the feasibility of using another multibeam satellite system having smaller beams in a secondary way in order to enhance the overall spectral efficiency of the system. The system performance of the proposed system has been evaluated using the theoretical expressions presented in Section 7.2.4. It was noted that operating the SUs in the inactive regions of the primary system significantly enhances the spectral efficiency of the overall system. However, the secondary cochannel beams may provide harmful interference to the active primary users, hence degrading the quality of primary links. To address this issue, we have considered two different techniques, more specifically, power control and EZ based approaches, in order to protect the PUs considering the tolerable interference threshold of the PUs. In the power control based approach, the secondary system has to reduce transmission power of its active beams ensuring that the aggregated interference towards the PUs remains below the PU interference threshold limit. Whereas, in the EZ based approach, only the secondary beams which lie outside the EZ of the primary beams are active without reduction in the transmission power. Besides presenting results for individual cases, we have compared these two approaches in terms of the SE. It should be noted that we have not discussed the combined case of these approaches in this thesis. The combination of power control and EZ based approaches may lead to further increase in the SE since different power control strategies can be applied on different regions while protecting the PUs. Furthermore, the combination of dynamic spectrum sensing with these techniques may lead to better spectrum utilization by exploiting spectrum holes in both the temporal and spatial domains.

Despite the significant advantages of the proposed cognitive beamhopping system for enhancing overall spectral efficiency of the satellite systems, there are several technical challenges in order to fully implement this system in practice. In this context, we present technical challenges of implementing the proposed system from practical perspectives below.

1. In order to operate the secondary system in the switched off regions of the primary system, the secondary system should be aware of the primary beamhopping sequence as mentioned in Section 7.2.2. For this purpose, a high speed backhaul link needs to be established between the gateways of primary and secondary systems.
2. The operation of primary and secondary systems should be synchronized in time for proper operation of both the systems. For this purpose, timing information needs to be exchanged with the help of the backhaul link between the gateways or intersatellite links between two satellites.
3. In case the primary system employs flexible beamhopping system whose beamhopping pattern changes based on the traffic demand, the beamhopping pattern should be updated frequently to the secondary system in order to avoid interference between the two systems.
4. For the secondary system, there exists a flexibility to choose lower transmit power while meeting the edge gain requirements since the antenna peak gain becomes higher for smaller beams. The requirement of low transmit power results in smaller transponder size, hence reducing the payload cost. However, the complexity of the antenna sub-system may increase while designing the spot beams depending on the technique used for creating multiple spot beams. Therefore, a trade-off is required between the smallest possible beamsize and the complexity of the antenna sub-system.
5. Designing smaller beams of the secondary system over the coverage area of each primary beam seems to be challenging. However, due to recent progress in the spot beam technologies, it is feasible to create smaller coverage cells having less than 0.5° diameter as mentioned in Section 7.2.2. Furthermore, it is also possible to divide one spot beam into many sub-beams with the reduction in peak antenna gain, hence resulting in smaller antenna aperture, while maintaining the edge gain requirements [466, 467]. Besides these possibilities, there still exist challenges to design low complexity antenna structures for multiple spot beams.

6. Since the secondary system employs smaller beams in comparison to the primary system, faster handover is needed for serving mobile users.
7. If the secondary system can use significantly smaller beams, the coexistence of the two multibeam systems can be related to the case of a new generation system being deployed on top of existing legacy systems. In this context, the time to market of the proposed system seems to be long since the beamhopping technique is not widely employed in current satellite systems.
8. Although it may appear redundant if both satellites belong to the same operator, the primary and secondary satellites can be used for providing different services to same/different categories of users, hence enhancing the overall spectral efficiency of the system. As an example, the primary satellite can be used to provide high priority broadband multimedia services and the secondary satellite to provide low QoS services such as interactive services as stated in Section 7.2.2. Further, there may arise a situation where the operator has to launch another satellite to meet the increased traffic demand in order to enhance capacity in the same coverage area. On the other hand, if primary and secondary satellites belong to different operators, the primary operator may not share the beamhopping sequence with the secondary operator. In this context, different strategies can be used depending on the employed spectrum assignment policy. For example, if the spectrum is exclusively licensed to the primary system, some financial and regulatory incentives can be provided to the primary operator in order to facilitate the spectrum sharing provided that sufficient QoS is guaranteed for both systems. If the spectrum is allocated on co-primary basis, the secondary operator can use sensing measurements in order to sense the multibeam pattern as well as the beamhopping pattern and subsequently use underlay approaches such as exclusion zone and power control based techniques in order to protect the primary system. However, sensing the primary beamhopping pattern may be challenging requiring dense sensor deployment and handling delayed measurements. In this context, exploring innovative sensing mechanisms in order to address the above issues is an important research challenge.

7.3 Dual Polarized Sensing

Existing SS literature mainly considers the use of amplitude, frequency or phase characteristics of the signals, which can be referred as scalar signal processing [473]. Among many available SS techniques in the literature, ED is the most common way of SS because of its low computational and implementation complexities [13, 183]. The electromagnetic (EM) signal propagating through space is polarized with some polarization state. The polarization state of a signal, a basic vector characteristic of an EM signal, is the orientation of the electric field vector at a given point in space, during one period of oscillation. Since traditional ED techniques only consider amplitude information of one component of signal and neglect the information from another orthogonal component, information provided by the vector nature of EM signals is not fully exploited.

Furthermore, the concepts of spectrum sharing in the frequency, time and spatial domains have been considered in much literature but the polarization domain has not been fully exploited. In the existing literature, the polarization domain has been used for diversity and multiplexing purposes [109–111]. The use of the polarization domain for SS has not been investigated extensively and few research works have been reported in literature. The concept of Reconfigurable Polarization Detection (RPD) for increasing the detection capability of a radar system by using vector signal processing has been proposed in [473]. A SS technique based on RPD method has been proposed in [474] as a means to enhance SS performance of SUs, making use of vector polarization states. A polarization sensing technique exploiting the transmit and receive polarization states has been proposed in [475], which takes into account the interference constraint of PU and the SINR demands of SUs. An optimal polarization receiving scheme for CRs has been proposed in [476] to improve the SINR demands of SUs.

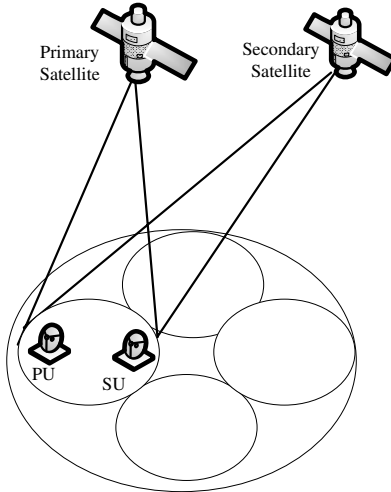


FIGURE 7.14: Dual satellite cognitive scenario

In this work, the polarization domain has been exploited as an additional dof to explore efficient SS and transmission schemes in the context of cognitive SatComs using the concept of RPD technique introduced in [473]. Generally, FSS and terrestrial BS antennas use horizontal (H) and vertical (V) polarization, whereas Direct Broadcast Satellites (DBS) may use left and right hand circular polarization as well as H/V polarization. The state of polarization is important in determining the energy transfer efficiency between transmit and receive antenna [477]. By deploying two orthogonally polarized antennas, any type of receive or transmit polarization can be derived. Detecting the polarization state in addition to energy of a certain carrier frequency can significantly increase the spectrum efficiency by investigating suitable cognitive techniques in polarization domain. Different combining techniques considered in this work exploit both H-polarized and V-polarized components using vector signal processing. Since a dual polarized antenna receives both polarized components but it receives noise with identical average power, increased SS performance can be expected because of better signal reception.

7.3.1 System and Signal Model

1. Use Case: In Chapter 6.3, we analyzed the performance of the ED technique in a dual polarized fading channel. In this chapter, the focus is on a dual-polarized AWGN channel. The practical scenario for its application is depicted in Fig. 7.14. The considered scenario is the dual satellite cognitive scenario consisting of two multibeam satellites providing coverage to the same geographic area and both operating in the normal return mode. It can be assumed that frequency reuse concept is used to increase the capacity. The secondary terminal i.e., satellite terminal can be equipped with a dual polarized antenna. This acts as a receive terminal of an $M \times 2$ MIMO or 1×2 Single Input Multiple Output (SIMO) channel and the difference from general MIMO or SIMO channels is that two antennas are orthogonally polarized instead of uni-polarized antennas in MIMO or SIMO channels. The channel created due to the presence of a dual polarized antenna in the radio link can be regarded as a dual-polarized channel. In the considered scenario, the channel can be considered as a dual polarized AWGN channel since the satellite channel remains static for most of the time. The cognitive satellite terminal to be connected to the secondary satellite within a particular beam can sense the polarization used by the primary satellite and use the opposite sense of polarization to transmit its data using the same carrier frequency in the secondary basis.

2. Signal Model: Two branches of dual polarized antenna can be considered to receive H-polarized and V-polarized signals coming from PU transmit antenna to the SU receive antenna. In the considered use cases, a single SU and a single PU can be considered for the sake of simplicity. Let \mathbf{s}_p be PU transmit vector signal and \mathbf{y}_{ps} be the signal vector arriving at the dual polarized antenna of SU. The transmit signal vector \mathbf{s}_p can be generated from H-polarized component s_{pH} and V-polarized component s_{pV} ,

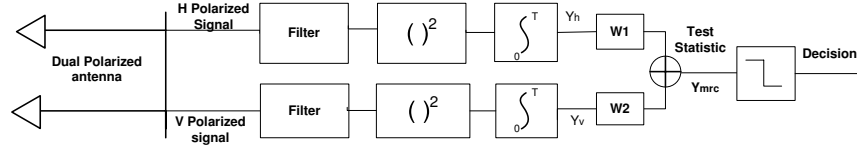


FIGURE 7.15: Block diagram of MRC technique for SS

which are orthogonal to each-other. Let us consider that \mathbf{X}_t and \mathbf{X}_r are polarization states of primary transmit and receive antennas respectively, and \mathbf{C}_t and \mathbf{C}_r are polarization states of secondary transmit and receive antennas respectively. The transmit signal vector \mathbf{s}_p can be represented in terms of Jones vector as [474]

$$\mathbf{s}_p = \begin{bmatrix} s_{pH} \\ s_{pV} \end{bmatrix} = \begin{bmatrix} s_{pH}^i + j s_{pH}^q \\ s_{pV}^i + j s_{pV}^q \end{bmatrix}, \quad (7.51)$$

where i and q are in-phase and quadrature phase components. Then the polarization state of transmit antenna in terms of Jones vector can be written as [475]

$$\mathbf{X}_t = \begin{bmatrix} \cos\alpha_p \\ \sin\alpha_p e^{j\phi_p} \end{bmatrix}, \quad (7.52)$$

where $\alpha_p \in (0, \pi/2)$, $\phi_p \in (0, 2\pi)$ can be calculated using the following equations

$$\begin{aligned} \alpha_p &= \arctan \frac{|s_{pV}|}{|s_{pH}|} \\ \phi_p &= \phi_{pV} - \phi_{pH} = \arctan \frac{|s_{pV}^q|}{|s_{pV}^i|} - \arctan \frac{|s_{pH}^q|}{|s_{pH}^i|}. \end{aligned} \quad (7.53)$$

The components s_{pH} and s_{pV} can then be weighted by using a power imbalance factor $a = \tan(\alpha_p)$ to impact the practical scenario of power imbalance in two branches of dual polarized antenna in the following way to make total energy unity.

$$\mathbf{s}_p = \begin{bmatrix} \frac{1}{1+a^2} s_{pH} \\ \frac{a}{1+a^2} s_{pV} \end{bmatrix}. \quad (7.54)$$

Assuming that the channel conditions between PU and SU remain ideal during the observation time interval t , the detection problem can be stated in terms of following binary hypothesis.

$$\begin{aligned} H_0 : \mathbf{y}_{ps}(t) &= \mathbf{n}(t), \quad \text{PU absent} \\ H_1 : \mathbf{y}_{ps}(t) &= \mathbf{s}_p(t) + \mathbf{n}(t), \quad \text{PU present} \end{aligned} \quad (7.55)$$

where $\mathbf{n}(t)$ represents the zero mean complex Gaussian noise vector. The decision statistic to check the above hypothesis problem depends on the type of combining technique used in combining H-polarized and V-polarized signals.

7.3.2 Combining Techniques

In the following subsection, we analyze the performance of the following combining techniques in the considered AWGN channel with the help of numerical analysis: (i) SC, (ii) EGC, (iii) MRC, and (iv) OPBC. The block diagrams and details of SC and EGC are presented in Chapter 6. Therefore, we only describe the following techniques in this section.

1. *Maximum Ratio Combining*: This technique combines the energies of two branches with different weights as depicted in Fig. 7.15. The branch with higher energy is weighted with greater factor than

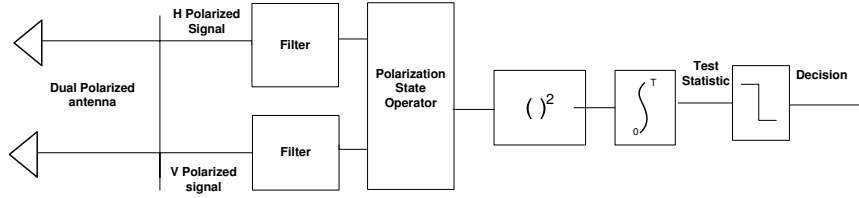


FIGURE 7.16: Block diagram of OPBC technique for SS

the branch having lower energy. The decision statistic using MRC technique can be written as

$$T_{mrc} = w_1 T_h + w_2 T_v, \quad (7.56)$$

where w_1 and w_2 are the weights applied to decision metrics T_h and T_v respectively. The decision statistic T_{mrc} under hypothesis H_1 follows a non-central chi-square χ^2 distribution with $2TB$ degrees of freedom with non-centrality parameter $\bar{\gamma}_{mrc}$, which can be written as

$$\bar{\gamma}_{mrc} = 2 \frac{w_1}{(w_1 + w_2)} \bar{\gamma}_h + 2 \frac{w_2}{(w_1 + w_2)} \bar{\gamma}_v. \quad (7.57)$$

The expression for P_d can be written as

$$P_d = Q_u \left(\sqrt{\bar{\gamma}_{mrc}}, \sqrt{\lambda_{th}} \right), \quad (7.58)$$

where $\bar{\gamma}_{mrc} = 2\gamma_{mrc}$, γ_{mrc} being SNR of the PU signal after performing MRC.

2. Optimum Polarization Based Combining: In scalar signal sensing methods such as energy detection, vector signals of PUs are converted to scalar quantities, whereas, in OPBC technique, both H and V components of primary signals are combined based on the polarization states of received signals. The signal power at receiving antenna becomes maximum for an incoming field if the receiver has conjugate polarization state as the transmitter and it becomes minimum at orthogonal polarization state to that at transmitter [476]. The block diagram of OPBC technique has been shown in Fig. 7.16. In cognitive SatCom scenario, polarization state can be adjusted as follows: transmit polarization state of a satellite terminal can be chosen in order to protect the terrestrial PUs from interference caused by it and then its receive polarization state can be optimized to ensure its QoS, mitigating interference from terrestrial PUs to its receiver.

In practical cognitive scenarios, there may be presence of multiple PUs and SU needs to adapt its receiving polarization state \mathbf{C}_r to receive different PU signals with different polarization states. Since it is not practical to change the hardware structure of antenna to adapt to different polarization states, virtual polarization adaptation scheme can be used to get the same phenomena as stated in [473]. In this scheme, the polarization adaptation takes place within the processor not in the antenna hardware. It can be noted that OPBC technique involves per-sample processing in contrast to other combining techniques and it needs one combining operation per sensing period. The horizontal and vertical reception of vector signal \mathbf{y}_{ps} through dual polarized antenna can be written in terms of Jones vector as

$$\mathbf{y}_{ps} = \begin{bmatrix} y_{psH} \\ y_{psV} \end{bmatrix}. \quad (7.59)$$

The received signal vector \mathbf{y}_{ps} can then be weighted by polarization state vector, which is constrained by power. Polarization state vector can be constructed by multiplying phase weighting operator \mathbf{P} and amplitude weighting operator \mathbf{A} , which are given by [474]

$$\begin{aligned} \mathbf{P} &= \begin{bmatrix} 1 & 0 \\ 0 & e^{j\phi_s} \end{bmatrix} \\ \mathbf{A} &= \begin{bmatrix} \cos\alpha_s \\ \sin\alpha_s \end{bmatrix}. \end{aligned} \quad (7.60)$$

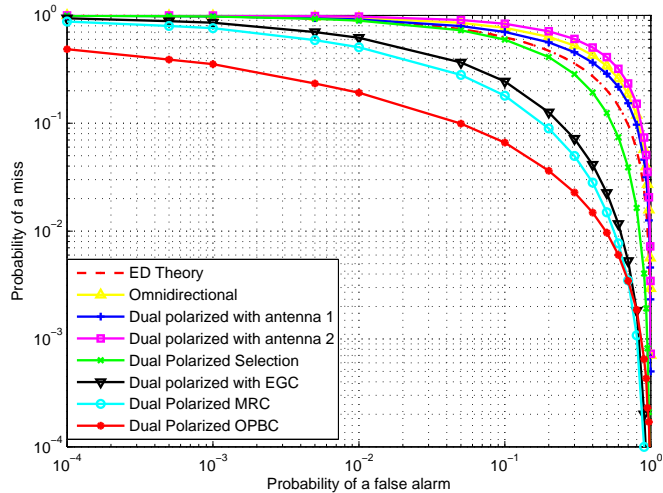


FIGURE 7.17: Comparison of CROC curves for different combining techniques

The polarization state of the SU receive antenna \mathbf{C}_r can be considered to be equivalent to the following form

$$\mathbf{C}_r = \mathbf{PA} = \begin{bmatrix} \cos\alpha_s \\ \sin\alpha_s e^{j\phi_s} \end{bmatrix}, \quad (7.61)$$

where α_s and ϕ_s are parameters defining the polarization state and can be calculated from (7.53) by replacing \mathbf{s}_p with \mathbf{y}_{ps} . The decision for the presence or absence of PU signal can be made based on the following decision metric

$$T_{opbc} = \sum_{i=1}^{N_s} |\mathbf{C}_{r,i}^\dagger \mathbf{y}_{ps,i}|^2 \gtrless_{H_0}^{H_1} \lambda_{th}, \quad (7.62)$$

where N_s is the number of samples. The value of threshold λ_{th} can be determined by using the preset value of P_f . Since \mathbf{y}_{ps} is a complex Gaussian vector and \mathbf{C}_r is a linear transformation, the decision statistic T_{opbc} follows χ^2 distribution [16]. Subsequently, the expression for P_d can be written as

$$P_d = Q_u \left(\sqrt{\bar{\gamma}_{opbc}}, \sqrt{\lambda_{th}} \right), \quad (7.63)$$

where $\bar{\gamma}_{opbc} = 2\gamma_{opbc}$, γ_{opbc} being the received SNR obtained after applying the polarization state operator.

7.3.3 Results and Discussion

1. Simulation Results: We consider the following six different cases for comparing the sensing performance. 1) First case considers the omnidirectional antenna, which senses the signals coming from all directions independent of polarization state of received signal. 2) Second case considers dual polarized antenna. One radiator of dual polarized antenna is dedicated to receive only H-polarized signal and another dedicated to receive only V-polarized signal. The received signals from these two different antennas are considered for detection individually. 3) Third case considers SC technique to combine the signals received from two radiators of dual polarized antenna. 4) Fourth case considers EGC technique. 5) Fifth case considers MRC technique. 6) Sixth case considers OPBC technique using the polarization states of received signals. Complementary Receiver Operating Characteristic (CROC) curves (probability of a miss P_m versus P_f) have been presented to compare the sensing performance of these cases. In the considered simulation environment, two orthogonal polarized signals are generated and they are weighted with variable $a = \tan(\alpha_p)$. Since $\alpha_p \in (0, \pi/2)$, the value of a ranges from 0 to ∞ . The value of variable a determines the power levels of two orthogonally polarized signals and it is responsible for determining whether the resultant signal is horizontal or vertical or near to any of these polarization

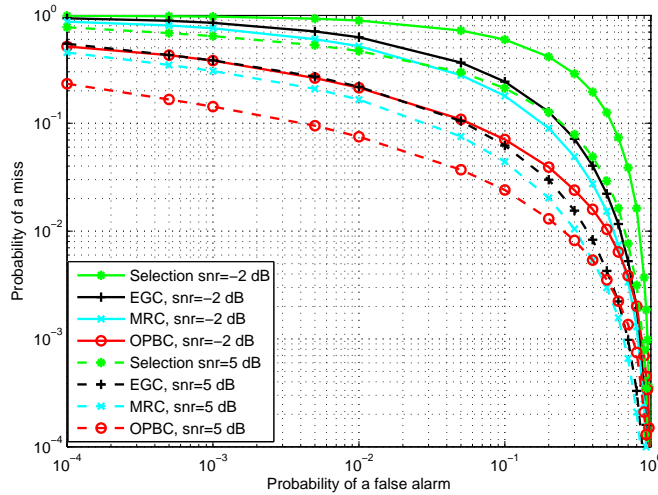
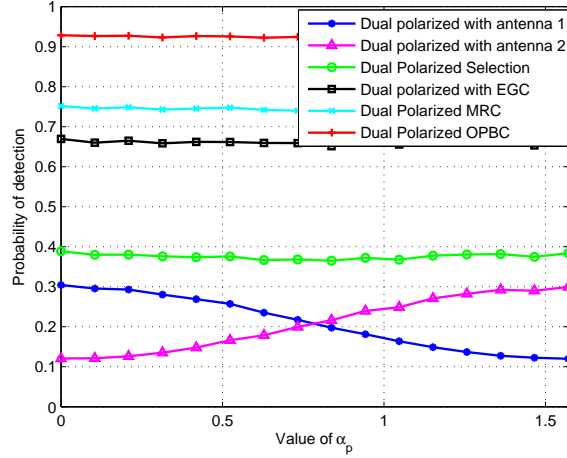


FIGURE 7.18: Comparison of CROC curves for different values of SNR

states. For example: when $a = 1$, both H and V components have same half power and when $a = 0$, the signal transmitted from transmit antenna is totally H-polarized, V-polarized signal being absent. Dual polarized AWGN channel has been considered due to lack of scattering in SatComs. Fig. 7.17 shows the comparison of CROC curves for six different cases at SNR value of -2 dB, degree of freedom (dof) value 6 and 3×10^5 number of iterations (N). The value of α_p in this case is $\pi/6$ and corresponding value of power imbalance factor a is 0.5777. The dof value determines the time bandwidth product i.e., it is equal to $2TB$. The received SNR of the omnidirectional antenna has been considered to be half than that of dual polarized antenna to carry out fair comparison between single antenna and two antenna cases. From the simulation results, it can be observed that OPBC technique performs much better than all the other cases and MRC performs slightly better than EGC and EGC performs better than SC technique. SC performs better than case 1 and case 2 due to selection of larger decision metric in each iteration while calculating P_d . Moreover, the sensing performance of dual polarized with antenna 1 is observed to be better than that of single omnidirectional antenna case and dual polarized with antenna 2 because antenna 1 in this case receives higher strength signal than antenna 2 due to power imbalance factor a applied to two orthogonal signals. The theoretical ED curve has been drawn using (5.19) and (5.20) as a reference. Furthermore, it has been noted during simulation that theory ED curve closely matches with the single antenna case when full received SNR has been considered.

Figure 7.18 presents the comparison of CROC curves of considered 3, 4, 5 and 6 cases in terms of different values of SNR (dof=6, $\alpha_p = \pi/6$, $N=3 \times 10^5$). SNR values of -2 dB and 5 dB have been considered for comparison. It can be observed from the figure that the probability of missing the PU presence for each case gets decreased as SNR is increased. Figure 7.19 shows the plot of P_d versus α_p angle (SNR= -2 dB, dof=6, $N=10^4$). The range of α_p has been taken from 0 to $\pi/2$ and the value of P_f has been taken as 0.1. It can be observed from the result that P_d with dual polarized antenna 1 exceeds the value of P_d of dual polarized antenna 2 up to the value of $\pi/4$ and the relation gets reverse after this value. Furthermore, it can be observed that P_d versus α_p curve becomes approximately flat for SC, EGC, MRC and OPBC cases i.e. P_d is independent of value of α_p .

2. *Discussion* From the simulation results, it can be observed that for the same value of P_f and SNR, OPBC technique can sense the primary signals with higher efficiency than other considered cases. From system complexity point of view, the OPBC technique appears to be more complex than other combining techniques since polarization operator is applied on per sample basis. The cost of complexity increases linearly with the number of samples N as compared to SC, EGC and MRC combining techniques. In practical scenarios, XPD may affect the performance of this technique. The effect of XPD on sensing performance in a dual polarized fading channel has been evaluated in Chapter 6. Analysis of polarization based cognitive techniques in different practical channels need to be carried out to implement this technique practically. Furthermore, the following conclusions can be drawn by analyzing the simulation results. Picking any one of radiators of the dual polarized antenna provides

FIGURE 7.19: Probability of detection versus value of α_p

better sensing performance than single omnidirectional antenna. The SC technique provides better performance than individual cases of dual polarized antenna due to the advantage in selecting the decision statistic. MRC and EGC techniques provide more efficient SS due to power gain obtained by combining two signals in different ways. The OPBC technique increases the SS efficiency significantly by optimally combining two signals received from branches of dual polarized antenna at the cost of system complexity.

7.4 Chapter Conclusion

In this chapter, several cognitive approaches such as IA, cognitive beamhopping and dual-polarized SS have been studied in the context of dual satellite cognitive SatComs. In Section 7.1, the spectral coexistence of multibeam and monobeam satellites with multicarrier transceivers has been studied considering a monobeam satellite as the primary and a multibeam satellite as the secondary. The main conclusion of this study is that multicarrier based IA can be applied for allowing the coexistence of monobeam and multibeam satellites in the normal return mode i.e., to mitigate the interference from the multibeam satellite terminals to the monobeam satellite. From the comparison of the considered IA techniques in the considered scenario, it is noted that the coordinated IA technique can provide perfect protection to the monobeam satellite and matches with the primary only rate i.e., the rate that would be achieved in the absence of the secondary multibeam system. This has been verified with the help of both theoretical analysis and numerical results. Further, from the viewpoint of protecting primary rate as well as achieving the highest rate, the coordinated IA technique is the best among all other techniques in considered satellite coexistence scenario. In the considered analysis and simulation environment, a multicarrier channel model with the ACI has been considered with each channel coefficient modeled as a Rician fading coefficient. From the practical perspectives, the coordinated scheme requires the exchange of CSI and alignment vector between the gateways of two satellite systems. This can be achieved with the help of a high speed link between their gateways. If this coordination mechanism is not available in practice, the uncoordinated approach can be followed with some sacrifice in the sum-rate and the primary rate protection as compared to the coordinated scheme.

Additionally, in Section 7.2, a novel cognitive beamhopping system has been proposed for the spectral coexistence of two multibeam satellites operating in the normal forward mode. The performance of the proposed system has been evaluated and compared with the conventional multibeam and beamhopping systems. It can be concluded that the proposed system significantly improves the SE over other techniques. In addition, based on the comparison of the full frequency reuse and frequency sharing approaches, it can be concluded that the SE increases with the number of SUs in the former approach

but decreases with the number of SUs in the later approach. Further, EZ and power control techniques have been investigated in order to provide sufficient protection to the primary satellite users. It has been noted that in most of the cases that primary rate is perfectly protected after the EZ radius of 8.5 dB for the set of considered parameters with a significant gain in the total SE. Moreover, it has been observed that the power control approach is suitable for the case of low secondary aggregated interference while the EZ approach for the case of high aggregated interference.

Besides, in Section 7.3, the application of an ED-based detection has been studied in a dual polarized AWGN channel using different combining techniques. The performance of an OPBC technique has been compared with SC, EGC and MRC techniques and it has been noted that this technique outperforms the other techniques in terms of the sensing performance. Further, the following conclusions can be drawn by analyzing the simulation results. Picking any one of radiators of the dual polarized antenna provides better sensing performance than a single omnidirectional antenna. The SC technique provides better performance than individual cases of dual polarized antenna due to the advantage in selecting the decision statistic. MRC and EGC techniques provide more efficient SS due to power gain obtained by combining two signals in different ways. In addition, the OPBC technique increases the SS efficiency significantly by optimally combining two signals received from branches of dual polarized antenna at the cost of system complexity.

Chapter 8

Conclusions, Discussion and Future Recommendations

8.1 Conclusive Summary

Cognitive radio communication is considered a promising solution in order to address the spectrum shortage problem in both terrestrial and satellite systems. Out of three main CR paradigms considered in the literature, this thesis has focussed on interweave and underlay approaches. The detailed concluding remarks for each considered problem have been provided at the end of the corresponding chapter, and hence we briefly summarize the main conclusions of this study, important impacts and possible future extensions in the following paragraphs. Further discussion on the contributed domains as well as future recommendations are provided in Sections 8.2 and 8.3, respectively.

One of the main functions of a CR is to acquire the knowledge about its operating radio environment. After acquiring this knowledge, it can adapt its radio operating parameters such as transmit power, modulation and coding scheme, operating frequency, etc. in order to utilize the available spectrum opportunities effectively. The higher the level of information it can acquire, the better spectrum exploitation mechanisms can be implemented. In this context, one of the main aims of this thesis was to study spectral awareness techniques considering spectrum awareness as a multidimensional problem in contrast to the commonly used single dimensional problem in the literature. In the above context, the first part of this thesis has provided contributions in the areas of spectrum sensing, signal to noise ratio estimation and sparsity order estimation which are useful for realizing interweave and underlay cognitive transceivers as well as a hybrid cognitive transceiver. Furthermore, these problems have been studied taking channel and noise correlations into account whose effects are often neglected in the existing contributions. Moreover, in practice, a CR may not have the knowledge of the primary channel, message and the noise variance. In this context, an eigenvalue based approach was followed which does not require the knowledge of the primary message and channel and some of the techniques under this approach are even insusceptible to the noise variance uncertainty. The considered approach is applicable for a variety of multidimensional scenarios ranging from an oversampling-based single node sensing to the cooperative sensing scenario. In the area of spectrum sensing, this thesis has proposed new sensing thresholds and demonstrated that the existing sensing thresholds fail under correlated scenarios and the proposed ones can provide better sensing performance. It should be noted that this thesis has studied only SCN and ME based approaches under correlated scenarios using an asymptotic approach and it is an interesting future aspect to evaluate and compare all the possible eigenvalue-based approaches using deterministic methods in order to find a better decision statistic. Additionally, this thesis has proposed an eigenvalue-based SNR estimation method in order to estimate the SNR of the primary signal received at the CR in both narrowband and wideband scenarios considering the effects of channel and noise correlations into account. It has been noted the knowledge of correlation significantly helps in improving

the SNR estimation performance. In this context, a suitable method needs to be investigated in practice in order to measure noise/channel correlation while applying the proposed approach. Besides, considering the sparsity order as an important parameter to realize efficient CS-based receivers, an sparsity order estimation problem has been studied in the context of a wideband cognitive transceiver. More importantly, theoretical expressions for the Stieltjes transform of the received signal's covariance matrix have been provided for different uncorrelated and correlated scenarios which can be subsequently used for obtaining the a.e.p.d.f. of the received signal and used to estimate the operating parameters of the primary system. One possible future extension can be to define a common platform in order to compare the proposed eigenvalue based techniques with the existing approaches and to select the best algorithm for the considered practical scenario. Towards more practical realisation, the next step can be to demonstrate the performance of the proposed sensing thresholds and SNR/sparsity order estimation algorithms in a software defined platform or Field Programmable Gate Array (FPGA) test bed in a laboratory environment.

Another main focus of this study was to propose suitable CR approaches and evaluate their performances in SatCom systems. Similar to the terrestrial context, SatCom systems are also facing the spectrum scarcity problem in order to meet the increasing spectrum demands for interactive, broadband and broadcast multimedia satellite services. To address this issue, dynamic spectrum access and spectrum sharing are fundamental approaches for utilizing the available spectrum effectively. Although terrestrial research is quite mature in this domain, it is rather unexplored in the satellite paradigm. In this context, this thesis has introduced the concept of cognitive SatComs highlighting the important aspects of cognition in SatComs and challenges from technical, regulatory and business perspectives. Further, various possible spectral coexistence scenarios have been presented considering the following two main categories: (i) hybrid satellite-terrestrial coexistence, and (ii) dual satellite coexistence. The hybrid satellite-terrestrial coexistence scenario is beneficial for both satellite and terrestrial operators depending on which system is primarily licensed in a particular spectrum band while the dual satellite coexistence scenario is advantageous for satellite operators in order to increase their revenues by providing higher data rates and better QoS to their valued customers. Understanding transmission/reception characteristics of satellite and terrestrial systems significantly helps in employing a suitable CR technique for the spectral coexistence of these networks. This thesis has followed the above approach while selecting the mapping of the techniques to the scenarios. Several peculiar features of the satellite systems such as variation of elevation angle over a large geographical region, GEO terminal's directive characteristics, difference in the receiver sensitivity levels, etc. have been utilized for choosing a suitable CR technique. Besides, the polarization domain has been considered as an additional degree of freedom for spectrum sharing purpose as highlighted in Chapter 1. Recently, there has been an increasing interest in cognitive SatCom area from EC, ESA, SatNex community, CEPT, academic institutions as well as from satellite operators and manufacturers. Several national and European projects are ongoing in this area as highlighted in Chapter 1. In this domain, this thesis has provided contributions in the following two main aspects: (i) Spectrum awareness/exploitation techniques for hybrid cognitive SatComs, and (ii) Spectrum awareness/exploitation techniques for dual cognitive SatComs. The main aspects of these contributions and impacts are summarized in the following paragraphs.

In the context of hybrid cognitive SatComs, various enabling techniques have been studied in this thesis considering a suitable practical scenario. Out of four possible modes of coexistence, this thesis has focussed on the normal operational modes considering the normal forward mode and the normal return mode. One interesting future aspect in this area is to study the hybrid mode of coexistence and to compare its performance with that of normal mode coexistence in order to decide on the proper mode selection. From the interference modeling carried out between a terrestrial BS and a satellite terminal in the spectral coexistence of a C-band FSS link and a terrestrial cellular link both operating in the normal forward mode (Section 6.1), it has been observed that the terrestrial interference level picked up by the satellite terminals varies significantly over a large geographical area due to the variation in the elevation angle of satellite terminals. Further, it has been concluded that interference modeling helps in selecting a suitable CR technique in a particular geographical region based on the interference

power level utilizing the specific features of CR approaches. It should be noted that the interference modeling presented in this thesis is based on the free space path loss channel and a single interferer. This study has been already extended to the scenario with more realistic path loss model and multiple interferers in the context of ongoing CoRaSat project [429]. Furthermore, from the study of harmful detection problem for the coexistence scenario of FSS-FS coexistence in 17.7 – 19.7 GHz band (Section 6.2), it can be concluded that FS harmful interference can be reliably detected with the help of an additional dipole antenna equipped in the satellite terminal even using a simple ED-based approach. Additionally, it has been shown that this solution can overcome the noise uncertainty problem which arises while sensing with the satellite dish. It should be noted that this study was conducted considering a worst-case approach from the harmful interference detection perspective and it becomes interesting to find a suitable antenna structure (corresponding to the required gain) which can detect the harmful interference in a practical scenario with more realistic path loss model. Moreover, the application of an ED-based SS in a dual polarized fading channel has been studied with the help of both theoretical as well as numerical analysis (Section 6.3). Additionally, the effect of XPD on SS efficiency has been analyzed. Towards more practical realization of this approach, the next step can be to acquire measurements from a dual polarized antenna and to test the performance of different SS techniques in order to find a suitable approach in terms of complexity and sensing efficiency. Moreover, by using the priori knowledge about the interfering/victim sector which arises due to special propagation characteristics of the satellite terminals, different receive/transmit beamforming methods have been studied (Section 6.4) for the spectral coexistence of GEO satellite and terrestrial cellular networks. The terminal-based beamforming at the FSS terminal in order to avoid the interference from the BSS/FS interferers is being studied in the context of ongoing CoRaSat project [478]. In addition, ESA has already started its activity for terminal-based adaptive nulling/beamforming techniques in order to mitigate interference in the spectral coexistence of FSS and FS systems in the Ka-band [479].

In addition to the spectral coexistence of satellite and terrestrial networks, there may exist the spectral coexistence of two satellite systems over the same coverage area in different ways as detailed in Chapter 5. The concept of dual satellite coexistence is motivated due to several aspects such as the orbital congestion of GEO orbits, high traffic demand in a certain area, etc. as highlighted in Chapter 1. In this context, this thesis has proposed enabling techniques for two satellite systems considering both normal return mode coexistence and normal forward mode coexistence. In the normal return mode scenario, this thesis has applied the IA approach by exploiting the multicarrier nature of satellite transmission for the spectral coexistence of a monobeam (primary) and a multibeam (secondary) satellites (Section 7.1). It has been concluded that the multicarrier based IA can be applied for allowing the coexistence of monobeam and multibeam satellites in the normal return mode i.e., to mitigate the interference from the multibeam satellite terminals to the monobeam satellite. Further, from the viewpoint of protecting primary rate as well as achieving the maximum rate, the coordinated IA technique has been found to be the best among all other techniques in the considered dual-satellite coexistence scenario. It should be noted that the multibeam satellite terminals have to be aware of the CSI and the alignment vector to perform precoding. This awareness may not be perfect in practice and it is an interesting future aspect to study the performance degradation caused due to imperfection in the CSI as well as in the alignment vector. In addition, this thesis has proposed a novel cognitive beamhopping system for the normal normal mode coexistence of two multibeam beamhopping satellites by exploiting the additional degree of freedom available from the time slot reuse concept of beamhopping systems in contrast to the frequency reuse concept used in conventional multibeam systems (Section 7.2). Further, exclusion zone and power control techniques have been investigated in order to provide sufficient protection to the primary satellite users in the considered coexistence scenario. One of the possible future extensions for this work is to find the proper beamhopping sequence for the secondary system based on the knowledge of the primary beamhopping pattern in order to maximize its throughput while providing sufficient protection to the primary system. In the context of dual cognitive SatComs, the ongoing CoRaSat project is studying the spectral coexistence of BSS feeder links and FSS downlink in the band 17.3 – 17.7 GHz. Additionally, the coexistence of GEO satellite networks and O3b satellites operating

in the MEO orbit is an important practical dual satellite coexistence scenario as highlighted in our recent contributions [393, 420].

8.2 Discussion

Future wireless systems should be able to address the increasing capacity demands of currently deployed wireless technologies. In this context, the main challenge is the scarcity of the available spectrum. This challenge can be addressed either by the exploitation of additional usable spectrum in higher frequency bands or by the effective utilization of the currently available spectrum. Towards exploiting the additional spectrum, recently several research contributions are examining the usage of millimeter wave (mm-wave) for cellular communications [480] and optical communication for satellite applications [481]. However, these possibilities are limited to specific radio environments and the research is still in its infancy. On the other hand, another promising solution is the exploitation of the available spectrum band by accessing the primary licensed spectrum in an opportunistic way or by exploiting suitable spectral sharing mechanisms. This solution does not require the acquisition of the additional expensive spectrum resource, hence reducing the overall capital and operational expenditure for an operator. In this context, CR communication has received important attention and studied in several literature.

Interweave and underlay CR approaches have their own advantages and disadvantages in the view of practical implementation. The interweave system is based on the assumption that there exist spectral holes in the primary spectrum band and may not be suitable in heavily occupied spectrum regions. Further, in this system, the SUs are allowed to transmit in a band only when a PU is not using that particular band. However, in practice, the PRs have some interference tolerance capability which is totally neglected in interweave systems [33]. It should be noted that the interference caused by the STs is not harmful to a PR all the time since it becomes harmful only if the interference exceeds the interference threshold of the PR. In this context, underlay systems can make better utilization of the available frequency resources in spectrum sharing scenarios. On the other hand, in underlay systems, the possibility of having secondary transmission with full power is neglected since the secondary transmission is limited by the transmit power constraint based on the interference threshold of the PRs. In this context, a hybrid approach of spectrum access seems to be a promising future solution. Although several existing contributions have considered power control in the underlay systems, the SNR estimation aspect has received less attention. As mentioned earlier, SNR estimation of the primary signals is important not only in choosing an appropriate threshold in switching interweave and underlay transmission strategies but also in selecting suitable transmit power of the CRs in order to guarantee the sufficient protection of the PRs based on the estimated channel between the CR and the PR. In this direction, this thesis has highlighted the importance of SNR estimation for a CR and identified various practical scenarios for its applications. Further, the aspect of simultaneous SS/Tx approach has been considered assuming the possibility of future full duplex CRs. It should be noted that the implications of the SNR estimation errors as well as self interference issues for a full duplex CR on the performance of the cognitive transceiver have not been analyzed in this thesis and are considered as future works.

The CR techniques within the same taxonomy can be compared in terms of their performances and complexity of implementation. For example, the performance of several SS approaches can be compared in terms of the ROC curve for a fixed SNR or P_d versus SNR for a fixed P_f . Since this comparison has been carried out in several existing literature [11, 29], this was out of scope of this thesis work. Further, SS techniques can be knowledge-based, blind or semi-blind depending on the requirement of the knowledge about the PU signal, channel and noise variance at the CR receiver. Although eigenvalue based techniques are usually considered to be blind in the literature, it should be noted that only those techniques such as SCN and SLE, whose decision statistics are based on the ratio, are blind to the noise variance and other approaches such as the ME still require the knowledge of the noise variance at the CR receiver for the decision process. In this context, this thesis studied the SCN-based approach as a

blind approach and the ME-based approach as semi-blind. Furthermore, different underlay approaches can be compared in terms of the primary rate protection ratio and achievable secondary throughput. Moreover, interweave systems may not work in the context of delay sensitive traffic while underlay systems can still work by creating constant SNR penalty.

As mentioned earlier, the CR research is still in its infancy in the context of SatComs. Both satellite and terrestrial operators can take advantage of the spectrum assigned to other systems by exploiting suitable CR techniques. Despite current development of multibeam technology, there is still a large gap in order to achieve the target of Terrabit/s capacity within the 2020 horizon. Cognitive SatComs can be one option to break this gridlock. In this context, this thesis has studied various aspects of Cognitive SatComs with its applications in different scenarios. The hybrid satellite-terrestrial coexistence scenario considered in this thesis is different from that of the hybrid/integrated systems considered in the literature in the sense that the considered scenario is more general and applicable for independent satellite and terrestrial networks operating in all the bands instead of the most commonly used L/S band hybrid satellite-terrestrial system in the literature. Similar hybrid scenarios are recently being investigated in the context of CoRaSat project in the Ka-band [96].

Although GEO satellites have been given importance in this thesis, we have studied an inline interference mitigation problem in [393, 420] considering the spectral coexistence of a GEO satellite and O3b satellite. In this direction, future research should further exploit advanced cognitive solutions in order to allow the coexistence of GEO FSS and NGEO FSS/MSS systems considering the constellation dynamics of the NGEO orbit into account. Although current frequency sharing research in the Ka-band is examining the solutions of the coexistence problems either on GEO satellite-terrestrial FS coexistence scenario or GEO-NGEO coexistence scenario, one of the future research challenges is to consider these three systems i.e., GEO, NGEO and terrestrial systems operating under the same spectrum while studying the frequency coexistence problems. Further, most of the ongoing studies focus on the fixed satellite terminals for the FSS systems and it can be an interesting future aspect to investigate suitable cognitive approaches in the context of mobile platforms e.g., aircraft-mounted/ship-mounted/land-based Earth Stations on Mobile Platforms (ESOMPs) and for the MSS systems.

Although the aspects of frequency, time and space domains have been widely treated in the CR literature, exploring the additional benefit which can be achieved using polarization and all these sharing dimensions simultaneously remains an open problem. Further, the main challenge for implementing polarization-based exploitation is XPD. The polarization of the transmitted signals may change due to XPD caused by multipath fading and other environmental impairments. Therefore, it's crucial to investigate techniques which are less susceptible to XPD effects or which can mitigate this effect. Several contributions in the literature have demonstrated the feasibility of using polarization domain as an additional dof for different spectrum sharing applications but the additional gain that can be achieved by implementing this technique in practice over the complexity overhead introduced while implementing this technique is not clearly understood. In this context, future research should focus on finding the tradeoff between performance gain and the system complexity while using polarization domain in order to understand the practical feasibility of the polarization-based technique. Besides, there is an emerging concept of polarization modulation technique for carrying information bearing signals [482], which can be further explored from sensing perspectives in order to detect the polarization modulated signals.

Currently, beamforming is considered as one of the important techniques and is under extensive research and development to improve the capacity of cellular networks, thus improving the SE as well as reducing interference by introducing intelligence inside the network. The same aspect can be realized in terms of the CB for future CR networks which may coexist with the primary licensed systems. The main challenge in realizing this is to obtain the accurate DoA information of the desired and interfering users. In practice, this information can be obtained either from the databases or by estimating it at the radio side with a suitable DoA estimation algorithm. In Chapter 6 of this thesis, it has been noted that by employing CB at the terrestrial BS, interference towards/from the satellite terminals can be effectively

mitigated. Evaluating the performance of the satellite system due to the employed CB at the system level could be an interesting aspect to explore in order to understand the system-level performance of the proposed CB approach.

In SatCom systems, the channel occupancy is constant in many cases and it may be argued that dynamic SS does not provide much advantage over its complexity of implementation. However, in hybrid cognitive systems in which satellite systems want to operate over the terrestrial licensed spectrum, dynamic SS is also necessary in order to find spectral holes in the terrestrial licensed spectrum. For the cases in which satellite spectrum is primary and another satellite/terrestrial system wants to operate in a secondary way, database approach seems to be more promising in comparison to the dynamic SS approach. Further, in many cases, SS and database approaches can be considered as complementary to each other. In other words, the SS approach helps in building a REM required for the database approach and a preliminary database obtained from regulators/operators may help in finding the geographical regions where SS can be useful. In addition, a suitable CR technique can also be selected based on the interference power level as detailed in Section 6.1.2.

As detailed in Chapter 5, there exist several technical, regulatory and business challenges in the realization of CR technology in SatCom systems. To achieve the aim of future cognitive SatComs, industries, operators, regulatory bodies and research institutions should carry out more collaborative works. Further, international collaboration among these bodies is essential in the SatCom context due to its inherent nature of wider coverage. Due to different inherent characteristics of SatComs such as limited power, wide coverage area, strong LoS, large path loss and shadowing losses, existing terrestrial CR techniques may not be directly applicable in realizing cognitive SatComs. In this context, this thesis work has contributed in exploring some important CR approaches suitable for SatComs. Besides, a significant amount of future research work is needed to address many technical challenges and to implement satellite CR networks.

8.3 Future Recommendations

In the following subsections, we present open research problems related to the topics discussed in the first and the second parts of this thesis.

8.3.1 Research Issues (Part I)

Spectrum Awareness under Practical Constraints

- In practical scenarios, the signal awareness problem at the CR receiver is affected by several factors such as noise uncertainty, interference/channel uncertainty, signal uncertainty, power amplifier nonlinearity, quantization errors, frequency, time and phase offsets, etc. Although several researchers have attempted to address these problems, the solutions are either applicable for specific scenarios or only mitigate the effect of one specific type of impairments. In this context, it remains an open challenge to explore one common awareness approach/framework which can combat the aforementioned issues and is applicable for a wide range of scenarios.

Signal Detection using Multiple Decision Statistics

- The main drawback of the eigenvalue based SS approach is its complexity, which is mainly dependent on the sample covariance matrix computation and the EVD operation as mentioned in Chapter 2. It can be noted that all the decision statistics in the context of eigenvalue based techniques can be calculated based on a single EVD operation on the received signal's sample

covariance matrix. In this context, it may be advantageous to take the combined decision using different decision statistics instead of considering only a single decision statistics without adding further complexity to the CR receiver. In this context, it would be interesting to investigate a suitable fusion approach which can provide better sensing performance from the joint decision statistics.

Cooperative Spectrum Sensing in Heterogeneous Networks

- Existing cooperative SS methods mostly focus on homogeneous cooperating nodes considering identical node capabilities, equal number of antennas, equal sampling rate and identical received SNR. However, in practice, nodes with different capabilities can be deployed at different stages and are very much likely to be heterogeneous in terms of the aforementioned features. For example, some of the nodes may be equipped with legacy ED sensors and others may be equipped with eigenvalue based sensors. In this context, it remains an open research challenge to investigate suitable data fusion schemes which can combine multiple decision statistics effectively at the FC. Furthermore, another interesting future aspect is to study adaptive decision forwarding in cooperative sensing scenario where each node can forward the best decision statistic to the fusion centre based on the received primary SNR, number of acquired samples. etc. Moreover, the extension of this problem for the scenarios with correlated multiple decision statistics is another important topic to be explored.

Cognitive Transceiver Design

- In an interweave system, sensing-throughput tradeoff exists while using the periodic sensing/Tx approach by the CR receiver as noted in various literature. A similar tradeoff exists in hybrid interweave/underlay systems as noted in Chapter 3 of this thesis. In the considered hybrid transceivers, SNR estimation errors have not been taken into account. However, in practice, there may occur SNR estimation errors due to inaccuracy of the estimation process and this may affect the performance of the power control-based underlay scheme. In this context, it's an interesting aspect to analyze the effect of SNR estimation errors in the performance of the underlay scheme, which may lead to the tradeoff between estimation time and throughput.
- Further, simultaneous SS/transmission can be one approach to solve the sensing-throughput tradeoff issue. One possible option to realize this approach is to use a full duplex transceiver. However, the main issue in realizing this transceiver is the self interference. Although several self interference mitigation schemes have been studied in the literature, there may occur some level of self interference in practice depending on the employed mitigation mechanism, hence degrading the throughput performance. In this context, it is important to study the effect of self interference on the performance of the full duplex transceiver.
- The application of the estimated sparsity order for implementing adaptive CS at the CR receiver can be an interesting future work since the required sampling rate (number of measurements) to achieve a successful recovery or detection rate varies with the sparsity order of the considered wideband spectrum. If the sampling rate at the CR receiver is adjusted based on the estimated SOE instead of the fixed sparsity order, a significant saving in the hardware resources can be achieved.

Applications of Compressive Sensing in CR Communications

- The reconstruction process in a CS-based CR receiver requires significant computational complexity. From the detection/estimation point of view, it is not necessary to reconstruct the entire

original sparse signal. The decision on the presence or the absence of PU signals over the considered spectrum can be made based on the compressed measurements only and the reconstruction step of the commonly used CS technique can be completely illuminated [74]. Although the existing literature considers signal detection/estimation over the whole considered band using compressive measurements, it is an open research issue to determine the occupancy status of each carrier within the considered wideband spectrum while utilizing only these compressive measurements.

- Another issue in designing practical CS-based receivers is to investigate suitable practical sensing matrices. Furthermore, the compression of a non-sparse signal depends on the proper selection of the measurement matrix [483]. The well-known family of CS matrices is a random projection or a matrix of i.i.d. random variables from a sub-Gaussian distribution such as Gaussian or Bernoulli since this family is universally incoherent with all other sparsifying bases [484]. However, in practical applications, the unstructured nature of random matrices make their realizations highly complex and the memory requirement also increases. In this context, it is an open challenge to investigate practical sensing matrices required for compressive detection/estimation applications.
- As discussed in Chapter 2, REMs are useful for the implementation of database-based cognitive communication over a wide coverage area and wide bandwidth. They can be created with the help of distributed sensor measurements. However, due to the constraints on the sensor hardware and energy, it is necessary to keep the number of sensor measurements low. In this context, the application of compressed SS by exploiting the sparsity in the frequency and spatial domains can be considered as an interesting future research problem.

Performance-Complexity Tradeoff

Several interweave and underlay techniques considered in the literature as well as in this thesis have different levels of implementation complexity. From a system designer's perspective, one important aspect is to choose a suitable technique based on the performance-complexity tradeoff. Although several contributions [11, 12] in the literature have attempted to compare the techniques under the same taxonomy, the detailed investigation of performance-complexity tradeoff for all the existing CR techniques within a particular taxonomy is still an open research issue.

8.3.2 Research Issues (Part II)

Interference Modeling and Analysis in Heterogeneous Systems

- Interference analysis between two heterogeneous systems with different carrier bandwidths is an important issue to be addressed. The existing literature mostly assumes the same carrier bandwidth between victim and interfering receivers. However, in spectrum coexistence scenarios such as FSS-FS coexistence in the Ka band, two coexisting systems can have separate carrier bandwidths. Further, in terms of the time domain, interference criteria are generally specified as long-term interference and short-term interference based on the interference power levels that can only be exceeded no more than specified percentages of the time. The long term interference usually affects the radio link performance by degrading the fade margin of the receiver whereas the short-term interference may degrade bit error rate performance even if the signal is unfaded [485]. The short-term interference criteria is quite important in analyzing the receiver performance of spectrum sharing systems and it may vary widely for different services. In this context, it is an open research challenge to investigate suitable interference criteria for the considered coexisting heterogeneous systems/services.
- Based on the interference power level received by the victim receivers, a suitable CR solution can be applied as mentioned in Chapter 6. In this context, interference modeling using a unified

framework by considering the aggregate secondary network interference and analyzing its impact on the performance of the primary system is a relevant research issue in the context of cognitive SatComs.

- In cognitive SatCom scenarios studied in this thesis, the interference occurs between two coexisting links either in the normal forward mode or in the normal return mode. In these scenarios, the application of blind source separation techniques [486] can be considered as an important future topic for interference management between the coexisting systems.

Terrestrial Cellular-Multibeam Satellite Coexistence

- In the uplink coexistence of satellite and terrestrial cellular networks considered in Chapter 6, the aggregate interference from terrestrial terminals to the satellite might be problematic. In this context, it is an interesting future work in order to find the maximum number of terrestrial terminals which can be served within a particular region without providing harmful interference to the primary satellite.
- Furthermore, C-band coexistence scenarios studied in this thesis consider both terrestrial cellular and satellite networks operating either in the normal forward mode or in the normal return mode. It is an interesting future aspect to analyze the coexistence scenarios of terrestrial cellular and satellite networks with hybrid modes i.e., terrestrial cellular in the uplink and satellite network in the downlink.

FSS-FS System Coexistence

- For the harmful detection problem studied in Chapter 6 for the downlink FSS-FS coexistence scenario (17.7 – 19.7 GHz), only individual signal processing has been studied in this thesis work. Several other approaches such as joint signal processing, Rise over Thermal (RoT) measurement, and exploitation of plot signals as discussed in [108] can be investigated for their applicability in this scenario.
- FS transmissions are highly directive in the Earth's horizontal plane and the GEO FSS transmissions are also directive but in different directions which depend on the elevation angle of the terminal with respect to the satellite. In this context, it is an interesting aspect to explore three dimensional approach considering two angular components i.e., azimuth and elevation into account while designing a beamformer at the satellite terminal. The beamforming weights can be designed in such a way that the interference coming from/towards the plane in which the FS transmissions are concentrated is mitigated. Further, if the FS stations are close to each other, they can be grouped into a cluster and a suitable beamformer can be designed in order to mitigate interference towards/from a specified cluster. Moreover, designing range-based beamformers based on the principle of bandpass/band stop filter is an interesting aspect to explore in the future.

Dual Satellite Coexistence

- In the cognitive beamhopping system proposed in Chapter 7, it is assumed that the secondary satellite is capable of adjusting its beamhopping sequence based on the primary beamhopping pattern obtained via a feedback link. In this context, it is an interesting future work to find a proper switching sequence for the secondary satellite system in such a way that its throughput is increased while respecting the interference threshold of the PUs.

- In the spectral coexistence of GEO-NGEO networks, the inline interference is the main issue as discussed in Chapter 5. In our recent works [393, 420], we have proposed power control-based approach in order to mitigate this interference considering the spectral coexistence of a GEO satellite and the O3b satellite. It would be interesting to investigate other suitable solutions for mitigating this interference in the considered scenario and also to study the coexistence scenario of Iridium satellite network with other satellite networks operating in the polar region where inline interference situation might be different.

Spectrum Aggregation

- Spectrum aggregation is one of the key issues for dynamic resource allocation in future SatComs. The motivation behind this approach is to utilize discrete spectrum bands efficiently in order to support high bandwidth requirements of satellite services. After acquiring information about the vacant channels either in the satellite band or terrestrial band which the secondary satellite system wants to share, it may not be possible to allocate the available spectrum segment to the secondary satellite system due to different carrier bandwidths used by two systems. For example, in the FSS-FS coexistence scenario, carrier bandwidth of the existing FS links ranges from 1.25 MHz to 220 MHz (ITU-R Recommendation F.758-5) whereas the FSS satellite system generally uses the carrier bandwidth of 36 MHz. In this context, aggregation of the available spectrum before allocation can significantly enhance the utilization of the available spectrum.

Intelligence in SatCom Systems

- The payload complexity in future multibeam satellites can be reduced by providing some form of intelligence to the satellite space station. For example, by knowing the activity of channels in the uplink in the case of interactive satellite services, only the corresponding downlink channels can be amplified/transmitted from the satellite instead of processing the whole transponder bandwidth, thus reducing the processing power as well as the transponder size. Furthermore, other novel signal processing techniques can be investigated in the satellite transponder in order detect and filter harmful interference/jammer detection. Additionally, the sensing intelligence can be incorporated into the satellite terminals in order to reuse the licensed terrestrial spectrum effectively.

FSS-FS-NGEO Coexistence

- It should be noted that ongoing and past studies have considered only the coexistence of two systems i.e., either FS and FSS or GEO FSS and MEO systems within a frequency band. However, in some portions of the Ka band spectrum, there may occur the spectral coexistence of three different systems. For example, in the Ka band segments, 18.8 – 19.7 GHz (downlink) and 28.6 – 29.5 GHz (uplink), GEO and NGEO satellites have equal-right allocations. Since this spectrum segment is primarily allocated to FS systems, there may occur the coexistence of GEO FSS, FS and NGEO systems. In this context, it is an important future aspect to carry out interference modeling and to investigate suitable CR approaches for the coexistence of these different systems operating over the same band.

Satellite-assisted CR

- Due to its wide coverage area, satellite could be an option for facilitating CR implementation in the terrestrial paradigm. In this context, satellite-assisted CR can be one promising area to be explored in the future. The satellite based sensor networks are already in operation for different

purposes such as weather monitoring, earth observation, etc. The application of these sensor networks can be extended for the acquisition of spectrum occupancy information over a wider coverage area which can be subsequently exploited by the other networks in order to enhance the overall spectral efficiency.

Appendix A

Random Matrix Theory Preliminaries

Let $F_{\mathbf{X}}(x)$ be the eigenvalue probability density function of a matrix \mathbf{X} .

Theorem A.0.1. The Stieltjes transform $\mathcal{S}_{\mathbf{X}}(z)$ of a positive semidefinite matrix \mathbf{X} is defined by [43]

$$\mathcal{S}_{\mathbf{X}}(z) = E \left[\frac{1}{\mathbf{X} - z} \right] = \int_{-\infty}^{\infty} \frac{1}{\lambda - z} dF_{\mathbf{X}}(\lambda). \quad (\text{A.1})$$

Theorem A.0.2. The η transform of a positive semidefinite matrix \mathbf{X} can be defined as [43]

$$\eta_{\mathbf{X}}(\gamma) = E \left[\frac{1}{1 + \gamma \mathbf{X}} \right], \quad (\text{A.2})$$

where γ is a nonnegative real number and thus $0 \leq \eta_{\mathbf{X}}(\gamma) \leq 1$.

Theorem A.0.3. The Σ transform of the density of eigenvalues of \mathbf{X} can be defined using η transform in the following way [43]

$$\Sigma_{\mathbf{X}}(z) = -\frac{1+z}{z} \eta_{\mathbf{X}}^{-1}(1+z). \quad (\text{A.3})$$

Theorem A.0.4. The R transform is related to the inverse of Stieltjes transform as [43]

$$\mathcal{R}_{\mathbf{X}}(z) = \mathcal{S}_{\mathbf{X}}^{-1}(-z) - \frac{1}{z}. \quad (\text{A.4})$$

Theorem A.0.5. For a Wishart random matrix \mathbf{X} , the R transform of the density of eigenvalues of \mathbf{X} is defined as [43]

$$\mathcal{R}_{\mathbf{X}}(z) = \frac{\beta}{1-z}. \quad (\text{A.5})$$

For any $a > 0$,

$$\mathcal{R}_{a\mathbf{X}}(z) = a\mathcal{R}_{\mathbf{X}}(az). \quad (\text{A.6})$$

Theorem A.0.6. For a Wishart random matrix \mathbf{X} , the Σ transform of the density of eigenvalues of \mathbf{X} is defined as [43]

$$\Sigma_{\mathbf{X}}(z) = \frac{1}{z + \beta}. \quad (\text{A.7})$$

Theorem A.0.7. The η transform of the density of eigenvalues of \mathbf{X} is related to the Stieltjes transform by the following relation [43]

$$\eta_{\mathbf{X}}(z) = \frac{\mathcal{S}_{\mathbf{X}}(-\frac{1}{z})}{z}. \quad (\text{A.8})$$

Theorem A.0.8. The Stieltjes transform of the semicircular law (4.15) is given by [23]

$$\mathcal{S}(z) = \frac{1}{2}[-z + \sqrt{z^2 - 4}] \quad (\text{A.9})$$

Theorem A.0.9. The Stieltjes transform of the semicircular law (4.15) is given by [23]

$$\mathcal{S}(z) = \frac{1}{2}[-z + \sqrt{z^2 - 4}] \quad (\text{A.10})$$

Appendix B

Proofs of Theorems

Proof of Theorem 3.3.1

Assuming that signal and noise are independent, for very large value of N , (3.2) leads to the following approximation for the white noise scenario

$$\lim_{N \rightarrow \infty} \hat{\mathbf{R}}_{\mathbf{Y}}(N) \approx p\mathbf{H}\mathbf{H}^\dagger + \hat{\mathbf{R}}_{\mathbf{Z}}. \quad (\text{B.1})$$

In this scenario, the sample covariance of received signal under assumed conditions can be realized as the sum of two Wishart matrices i.e., $p\hat{\mathbf{R}}_{\mathbf{H}} = p\mathbf{H}\mathbf{H}^\dagger$ and $\hat{\mathbf{R}}_{\mathbf{Z}}$ with same degree of freedom and different covariance structures. In this condition, MP law holds true for both matrices. Although it is possible to find another Wishart matrix from the the addition of $p\hat{\mathbf{R}}_{\mathbf{H}}$ and $\hat{\mathbf{R}}_{\mathbf{Z}}$ approximately (see Lemma 6, [487]) and then apply scaled MP law by scaling with variance $(1+p^2)$ for the new Wishart matrix, we use free probability theory for more accurate analysis. The R transform of eigenvalue density function of $\hat{\mathbf{R}}_{\mathbf{Y}}$ can be found by adding the R transforms of density functions of $p\hat{\mathbf{R}}_{\mathbf{H}}$ and $\hat{\mathbf{R}}_{\mathbf{Z}}$ using free probability theory. Using (A.6), the R transform of $p\hat{\mathbf{R}}_{\mathbf{H}}$ can be written as

$$\mathcal{R}_{p\hat{\mathbf{R}}_{\mathbf{H}}}(z) = p\mathcal{R}_{\hat{\mathbf{R}}_{\mathbf{H}}}(pz) = \frac{p\beta}{1-pz}. \quad (\text{B.2})$$

Since the R transform of $\hat{\mathbf{R}}_{\mathbf{Z}}$ is $\mathcal{R}_{\hat{\mathbf{R}}_{\mathbf{Z}}}(z) = \frac{\beta}{1-z}$ from (A.5), the combined R transform can be written as

$$\mathcal{R}_{\hat{\mathbf{R}}_{\mathbf{Y}}}(z) = \frac{p\beta}{1-pz} + \frac{\beta}{1-z}. \quad (\text{B.3})$$

The inverse Stieltjes transform can be obtained by applying (B.3) on (A.4). Then the Stieltjes transform $\mathcal{S}_{\hat{\mathbf{R}}_{\mathbf{Y}}}$ of the asymptotic distribution of $\frac{1}{N}\mathbf{Y}\mathbf{Y}^\dagger$ under white noise scenarios can be obtained for any $z \in \mathbb{C}$ by solving the following cubic polynomial

$$(pz)\mathcal{S}_{\hat{\mathbf{R}}_{\mathbf{Y}}}^3(z) + (p(-2\beta + z + 1) + z)\mathcal{S}_{\hat{\mathbf{R}}_{\mathbf{Y}}}^2(z) + ((1 - \beta)(1 + p) + z)\mathcal{S}_{\hat{\mathbf{R}}_{\mathbf{Y}}}(z) + 1. \quad (\text{B.4})$$

Subsequently, the a.e.p.d.f. of $\hat{\mathbf{R}}_{\mathbf{Y}}$ under H_1 hypothesis in the presence of white noise is obtained by using the Stieltjes inversion expression given by (3.34).

Proof of Theorem 3.3.2

Using the similar arguments as in the above subsection, the following approximation can be written for the correlated noise scenario

$$\lim_{N \rightarrow \infty} \hat{\mathbf{R}}_{\mathbf{Y}}(N) \approx p\mathbf{R}\mathbf{R}_1 + \Theta^{1/2}\hat{\mathbf{R}}_{\mathbf{Z}}\Theta^{1/2}. \quad (\text{B.5})$$

In the above expression, the expression $\Theta^{1/2}\hat{\mathbf{R}}_{\hat{\mathbf{Z}}}\Theta^{1/2}$ follows the Mestre law and its Stieltjes transform of $\hat{\mathbf{R}}_{\hat{\mathbf{Z}}}$ can be written as [147]

$$\mathcal{S}_{\hat{\mathbf{R}}_{\hat{\mathbf{Z}}}}(z) = \frac{z + 2z\mu + 1 - \beta + \sqrt{[z - (1 + \beta)]^2 - 4\beta(1 + \mu z)}}{2z(1 + \mu z)}. \quad (\text{B.6})$$

Then the R transform for $\hat{\mathbf{R}}_{\hat{\mathbf{Z}}}$ is calculated using (A.4) and can be expressed as

$$\mathcal{R}_{\hat{\mathbf{R}}_{\hat{\mathbf{Z}}}}(z) = -\frac{1}{2} \frac{(z - 1 + \sqrt{(z^2 - 2z + 1 - 4\mu\beta z)})}{\mu z}. \quad (\text{B.7})$$

In correlated noise scenarios, the sample covariance of the received signal under assumed conditions can be realized as a sum of one Wishart matrix i.e., $p\hat{\mathbf{R}}_{\mathbf{H}}$ and another correlated Wishart matrix $\hat{\mathbf{R}}_{\hat{\mathbf{Z}}}$. In this condition, MP law can be applied for $p\hat{\mathbf{R}}_{\mathbf{H}}$ and the analysis carried out under H_0 hypothesis in Section 3.2.4.1 can be applied for $\hat{\mathbf{R}}_{\hat{\mathbf{Z}}}$. Subsequently, the R transform of density function of the received signal can be found by adding the R transforms of density functions of $p\hat{\mathbf{R}}_{\mathbf{H}}$ and $\hat{\mathbf{R}}_{\hat{\mathbf{Z}}}$. This way, the Stieltjes transform of $\hat{\mathbf{R}}_{\hat{\mathbf{Z}}}$ can be written as [147]

$$\mathcal{S}_{\hat{\mathbf{R}}_{\hat{\mathbf{Z}}}}(z) = \frac{z + 2z\mu + 1 - \beta + \sqrt{[z - (1 + \beta)]^2 - 4\beta(1 + \mu z)}}{2z(1 + \mu z)}. \quad (\text{B.8})$$

Next, the R transform for $\hat{\mathbf{R}}_{\hat{\mathbf{Z}}}$ is calculated using (A.4) and can be expressed as

$$\mathcal{R}_{\hat{\mathbf{R}}_{\hat{\mathbf{Z}}}}(z) = -\frac{1}{2} \frac{(z - 1 + \sqrt{(z^2 - 2z + 1 - 4\mu\beta z)})}{\mu z}. \quad (\text{B.9})$$

The combined R transform then becomes

$$\mathcal{R}_{\hat{\mathbf{R}}_{\mathbf{Y}}}(z) = \frac{p\beta}{(1 - pz)} - \frac{1}{2} \frac{(-1 + z + \sqrt{(1 - 2z + z^2 - 4\mu\beta z)})}{z\mu}. \quad (\text{B.10})$$

The inverse Stieltjes transform can be obtained by applying (B.10) on (A.4). Finally, the Stieltjes transform $\mathcal{S}_{\hat{\mathbf{R}}_{\mathbf{Y}}}$ of the asymptotic distribution of $\frac{1}{N}\mathbf{Y}\mathbf{Y}^\dagger$ under correlated noise scenarios can be obtained for any $z \in \mathbb{C}$ by solving the quartic polynomial (3.36).

Proof of Theorem 3.3.3

Assuming that signal and noise are uncorrelated to each other, for very large value of N , the following approximation can be written for correlated channel and uncorrelated noise scenario

$$\lim_{N \rightarrow \infty} \hat{\mathbf{R}}_{\mathbf{Y}}(N) \approx p\hat{\mathbf{H}}\hat{\mathbf{H}}^\dagger + \hat{\mathbf{R}}_{\mathbf{Z}}(N). \quad (\text{B.11})$$

The Stieltjes transform of $\hat{\mathbf{R}}_{\hat{\mathbf{H}}} = \frac{1}{N}\hat{\mathbf{H}}\hat{\mathbf{H}}^\dagger$ can be written as [147]

$$\mathcal{S}_{\hat{\mathbf{R}}_{\hat{\mathbf{H}}}}(z) = \frac{z + 2z\mu + 1 - \beta + \sqrt{[z - (1 + \beta)]^2 - 4\beta(1 + \mu z)}}{2z(1 + \mu z)}. \quad (\text{B.12})$$

The R transform of $\hat{\mathbf{R}}_{\hat{\mathbf{H}}}$ can be found by using (A.4). Furthermore, the R transform of $p\hat{\mathbf{R}}_{\hat{\mathbf{H}}}$ can be found by using (A.6) and can be written as

$$\mathcal{R}_{p\hat{\mathbf{R}}_{\hat{\mathbf{H}}}}(z) = -\frac{p}{2} \frac{(pz - 1 + \sqrt{(p^2z^2 - 2pz + 1 - 4\mu\beta pz)})}{\mu pz}. \quad (\text{B.13})$$

Subsequently, the combined R transform for $\hat{\mathbf{R}}_Y$ can be written as

$$\mathcal{R}_{\hat{\mathbf{R}}_Y}(z) = -\frac{p}{2} \frac{(pz - 1 + \sqrt{(p^2 z^2 - 2pz + 1 - 4\mu\beta pz)})}{\mu pz} + \frac{\beta}{(1-z)}. \quad (\text{B.14})$$

The inverse Stieltjes transform can be obtained by applying (B.14) on (A.4) and then the Stieltjes transform can be obtained by solving the quartic polynomial given by (3.37).

Proof of Theorem 3.3.4

Using the similar arguments as in previous proofs, the following approximation can be written for the case of presence of both channel/noise correlation

$$\lim_{N \rightarrow \infty} \hat{\mathbf{R}}_Y(N) \approx p\hat{\mathbf{H}}\hat{\mathbf{H}}^\dagger + \hat{\mathbf{R}}_{\hat{\mathbf{Z}}}(N). \quad (\text{B.15})$$

The Stieltjes transform of $\hat{\mathbf{R}}_{\hat{\mathbf{Z}}}$ and $\hat{\mathbf{R}}_{\hat{\mathbf{H}}}$ are same and can be written as [147]

$$\mathcal{S}_{\hat{\mathbf{R}}_{\hat{\mathbf{H}}}}(z) = \mathcal{S}_{\hat{\mathbf{R}}_{\hat{\mathbf{Z}}}}(z) = \frac{z + 2z\mu + 1 - \beta + \sqrt{[z - (1 + \beta)]^2 - 4\beta(1 + \mu z)}}{2z(1 + \mu z)}. \quad (\text{B.16})$$

The R transforms of $\hat{\mathbf{R}}_{\hat{\mathbf{H}}}$ and $\hat{\mathbf{R}}_{\hat{\mathbf{Z}}}$ can be found by using (A.4) and (B.16). The matrices $\hat{\mathbf{R}}_{\hat{\mathbf{H}}}$ and $\hat{\mathbf{R}}_{\hat{\mathbf{Z}}}$ are independent and any of these matrices can be written using eigenvalue decomposition as $\mathbf{U}\Lambda\mathbf{U}^\dagger$, where the elements of Λ are the eigenvalues which are distributed according to Theorem 5.1 with compact supports. As a result, $\hat{\mathbf{R}}_{\hat{\mathbf{H}}}$ and $\hat{\mathbf{R}}_{\hat{\mathbf{Z}}}$ are unitarily invariant and asymptotically free. Then the R transform of $p\hat{\mathbf{R}}_{\hat{\mathbf{H}}}$ can then be found by using (A.6) and can be written as

$$\mathcal{R}_{p\hat{\mathbf{R}}_{\hat{\mathbf{H}}}}(z) = -\frac{p}{2} \frac{(pz - 1 + \sqrt{(p^2 z^2 - 2pz + 1 - 4\mu\beta pz)})}{\mu pz}. \quad (\text{B.17})$$

Next, the combined R transform for $\hat{\mathbf{R}}_Y$ can be written as

$$\mathcal{R}_{\hat{\mathbf{R}}_Y}(z) = -\frac{p}{2} \frac{(pz - 1 + \sqrt{(p^2 z^2 - 2pz + 1 - 4\mu\beta pz)})}{\mu pz} - \frac{1}{2} \frac{(z - 1 + \sqrt{(z^2 - 2z + 1 - 4\mu\beta z)})}{\mu z}. \quad (\text{B.18})$$

The inverse Stieltjes transform can be obtained by applying (B.18) on (A.4) and then the Stieltjes transform can be obtained by solving the quartic polynomial given by (3.38).

Proof of Theorem 4.2.1

Since $\hat{\mathbf{R}}$ and $\hat{\mathbf{R}}_1$ are independent Wishart matrices, they are asymptotically free [43]. As a result, the combined aepdf of the term $\hat{\mathbf{R}}\hat{\mathbf{R}}_1$ in (4.7) can be obtained by applying multiplicative free convolution property of Σ transform in the following way [350]

$$\Sigma_{\hat{\mathbf{R}}\hat{\mathbf{R}}_1}(z) = \Sigma_{\hat{\mathbf{R}}}(z) \cdot \Sigma_{\hat{\mathbf{R}}_1}(z). \quad (\text{B.19})$$

The η transform corresponding to $\Sigma_{\hat{\mathbf{R}}\hat{\mathbf{R}}_1}(z)$ in (B.19) can be obtained using (A.3) and its polynomial can be written as

$$z(\eta(z) + 1)(\eta(z) + \rho)(\eta(z) + \sigma) - \eta(z). \quad (\text{B.20})$$

Then using the relation between η and Stieltjes transform given by (A.8), the polynomial for Stieltjes transform of the asymptotic distribution of the eigenvalues of the product of $\hat{\mathbf{R}}$ and $\hat{\mathbf{R}}_1$ can be written as

$$z^2\mathcal{S}^3(z) + z(2 - \rho - \sigma)\mathcal{S}^2(z) + (-z + (\rho - 1)(\sigma - 1))\mathcal{S}(z) - 1 = 0. \quad (\text{B.21})$$

Let $\mathcal{R}_{\hat{\mathbf{R}}_c}$ be the R transform of the product term $\hat{\mathbf{R}}\hat{\mathbf{R}}_1$ and is calculated using (B.21) and (A.4), which is given by

$$\mathcal{R}_{\hat{\mathbf{R}}_c}(z) = \frac{-(1/2)(z\rho + z\sigma - 1 + \sqrt{(z^2\rho^2 - 2z^2\rho\sigma - 2z\rho + z^2\sigma^2 - 2z\sigma + 1)})}{z^2}. \quad (\text{B.22})$$

Subsequently, the R transform of $p\hat{\mathbf{R}}\hat{\mathbf{R}}_1$ in the second term of (4.7) becomes $p\mathcal{R}_{\hat{\mathbf{R}}_c}(pz)$. Since the term $\hat{\mathbf{R}}_Z$ in (4.7) follows the MP distribution, the R transform of $\hat{\mathbf{R}}_Y$ using additive free convolution property can be written as

$$\mathcal{R}_{\hat{\mathbf{R}}_Y}(z) = p\mathcal{R}_{\hat{\mathbf{R}}_c}(pz) + \mathcal{R}_{\hat{\mathbf{R}}_Z}(z). \quad (\text{B.23})$$

Finally, the polynomial for the Stieltjes transform of the density of $\hat{\mathbf{R}}_Y$ in (4.13) is obtained using (A.4).

Proof of Theorem 4.2.2

Since \mathbf{P} is a square matrix, $\mathbf{P}^{1/2}\hat{\mathbf{R}}_1\mathbf{P}^{1/2}$ and $\mathbf{P}\hat{\mathbf{R}}_1$ have identical eigenvalues [43]. Therefore, the Σ transform of the term $\hat{\mathbf{R}}\mathbf{P}^{1/2}\hat{\mathbf{R}}_1\mathbf{P}^{1/2}$ in (4.14) can be written as

$$\Sigma_{\hat{\mathbf{R}}\mathbf{P}\hat{\mathbf{R}}_1}(z) = \Sigma_{\hat{\mathbf{R}}}(z) \cdot \Sigma_{\mathbf{P}}(z) \cdot \Sigma_{\hat{\mathbf{R}}_1}(z). \quad (\text{B.24})$$

Since $\hat{\mathbf{R}}$ and $\hat{\mathbf{R}}_1$ follow the MP distribution, their Σ transforms are given by (4.12) and the Σ transform of \mathbf{P} is given by (4.18). Subsequently, using (B.24), the following expression can be written.

$$\Sigma_{\hat{\mathbf{R}}\mathbf{P}\hat{\mathbf{R}}_1}(z) = \frac{1}{\rho + z} \cdot \frac{1}{\sigma + z} \cdot \frac{1}{2} \frac{g(g\bar{p} + \sqrt{g^2\bar{p}^2 - 8 - 4z})}{z}. \quad (\text{B.25})$$

Then using (B.25), (A.8) and (A.3), the Stieltjes transform of the asymptotic distribution of eigenvalues of $\hat{\mathbf{R}}\mathbf{P}^{1/2}\hat{\mathbf{R}}_1\mathbf{P}^{1/2}$ in (4.19) is obtained. Using free probability theory, the R transform of the density of the eigenvalues of $\hat{\mathbf{R}}_Y$, given by (4.14), can be written as [43]

$$\mathcal{R}_{\hat{\mathbf{R}}_Y}(z) = \mathcal{R}_{\mathbf{W}}(z) + \mathcal{R}_{\hat{\mathbf{R}}_Z}(z). \quad (\text{B.26})$$

Finally, the expression for the Stieltjes transform in (4.20) is obtained using the definitions of transforms in the Appendix A and (4.19).

Proof of Theorem 4.2.3

We use R transform and Σ transform to derive the aepdf of $\hat{\mathbf{R}}_Y$ using free probability theory. Since $\hat{\mathbf{R}}$ and $\hat{\mathbf{R}}_1$ follow the MP law, their Σ transforms can be calculated using (4.12). The Σ transform of Θ , which follows the tilted semicircular law (4.21) is given by [147]

$$\Sigma_{\Theta}(z) = 1 - \mu z. \quad (\text{B.27})$$

It can be noted that since Θ and $\hat{\mathbf{R}}_1$ are square matrices, the terms $\Theta^{1/2}\hat{\mathbf{R}}_1\Theta^{1/2}$ and $\Theta\hat{\mathbf{R}}_1$ have identical eigenvalues [43]. Then the Σ transform of the product of $\hat{\mathbf{R}}$, Θ and $\hat{\mathbf{R}}_1$ can be written as

$$\Sigma_{\hat{\mathbf{R}}\Theta\hat{\mathbf{R}}_1}(z) = \frac{1}{\rho + z} \cdot (1 - \mu z) \cdot \frac{1}{\sigma + z}. \quad (\text{B.28})$$

Subsequently, the polynomial for the corresponding η transform is obtained using (A.3) and (B.28), which is given by

$$\eta(\rho + \eta - 1)(\eta + \sigma - 1)z + (\eta - 1)(1 - \mu(\eta - 1)) = 0. \quad (\text{B.29})$$

The Stieltjes transform of the density of the eigenvalues of the product of $\hat{\mathbf{R}}$ and $\Theta\hat{\mathbf{R}}_1$ can be obtained using (B.29) and (A.8) and is given by

$$\begin{aligned} & z^2\mathcal{S}^3(z) + (-\mu z^2 - \sigma z + 2z - \rho z)\mathcal{S}^2 \\ & + (-\rho + 1 + \rho\sigma - 2\mu z - \sigma - z)\mathcal{S}(z) - 1 - \mu. \end{aligned} \quad (\text{B.30})$$

The R transform of the density of the eigenvalues of the product of $\hat{\mathbf{R}}$ and $\Theta\hat{\mathbf{R}}_1$ is calculated using (A.4) and (B.30) and is given by

$$\mathcal{R}_{\hat{\mathbf{R}}\Theta\hat{\mathbf{R}}_1}(z) = -\frac{1}{2} \frac{(-1 + z\sigma + z\rho + \sqrt{1 - 2z\sigma - 2z\rho + z^2\sigma^2 - 2z^2\rho\sigma + z^2\rho^2 - 4\rho\sigma z\mu})}{(z(z + \mu))}. \quad (\text{B.31})$$

Since the term $\hat{\mathbf{R}}_Z$ in (4.22) follows the MP distribution, the R transform of $\hat{\mathbf{R}}_Y$ using additive free convolution property can be written as

$$\mathcal{R}_{\hat{\mathbf{R}}_Y}(z) = p\mathcal{R}_{\hat{\mathbf{R}}\Theta\hat{\mathbf{R}}_1}(pz) + \mathcal{R}_Z(z). \quad (\text{B.32})$$

Finally, the Stieltjes transform of the density of $\hat{\mathbf{R}}_Y$ can be calculated using (B.32) and (A.4).

Bibliography

- [1] K. Patil, R. Prasad, and K. Skouby, “A survey of worldwide spectrum occupancy measurement campaigns for cognitive radio,” in *Int. Conf. Devices and Commun. (ICDeCom)*, Feb. 2011, pp. 1–5.
- [2] FCC, “Spectrum policy task force report,” ET Docket 02-155, Nov. 02 2002.
- [3] J. Mitola and G. Maguire, “Cognitive radio: making software radios more personal,” *IEEE Personal Commun.*, vol. 6, no. 4, pp. 13–18, Aug. 1999.
- [4] FCC, “Notice of proposed rule making and order,” ET Docket 03-322, 2003.
- [5] FCC, “Second report and order and memorandum opinion and order: In the matter of unlicensed operation in the TV broadcast bands,” Doc. 08-260, Nov. 2008.
- [6] FCC, “Third memorandum opinion and order,” Doc. 12-36, Apr. 2012.
- [7] OFCOM, “Regulatory requirements for white space device in the UHF TV band,” Tech. Rep., July 2012.
- [8] C.-S. Sum and et al, “Cognitive communication in TV white spaces: An overview of regulations, standards, and technology,” *IEEE Commun. Mag.*, vol. 51, no. 7, pp. 138–145, July 2013.
- [9] M. Nekovee, “Cognitive radio access to TV white spaces: Spectrum opportunities, commercial applications and remaining technology challenges,” in *IEEE Symp. DySPAN*, April 2010, pp. 1–10.
- [10] A. Goldsmith, S. Jafar, I. Maric, and S. Srinivasa, “Breaking spectrum gridlock with cognitive radios: An information theoretic perspective,” *Proc. IEEE*, vol. 97, no. 5, pp. 894–914, May 2009.
- [11] T. Yucek and H. Arslan, “A survey of spectrum sensing algorithms for cognitive radio applications,” *IEEE Commun. Surveys & Tutorials*, vol. 11, no. 1, pp. 116–130, 2009.
- [12] E. Axell, G. Leus, E. Larsson, and H. Poor, “Spectrum sensing for cognitive radio: State-of-the-art and recent advances,” *IEEE Signal Process. Magazine*, vol. 29, no. 3, pp. 101–116, May 2012.
- [13] F. Digham, M.-S. Alouini, and M. Simon, “On the energy detection of unknown signals over fading channels,” in *IEEE Int. Conf. Commun.*, vol. 5, May 2003, pp. 3575–3579.
- [14] S. Herath, N. Rajatheva, and C. Tellambura, “Energy detection of unknown signals in fading and diversity reception,” *IEEE Trans. Commun.*, vol. 59, no. 9, pp. 2443–2453, Sept. 2011.
- [15] R. Tandra and A. Sahai, “SNR walls for signal detection,” *IEEE J. Sel. Topics Signal Process.*, vol. 2, no. 1, pp. 4–17, Feb. 2008.
- [16] S. M. Kay, *Fundamentals of Statistical Signal Processing: Detection Theory*, 1st ed. Prentice-Hall PTR, 1998, vol. II.
- [17] Y. Zeng, C. L. Koh, and Y.-C. Liang, “Maximum eigenvalue detection: Theory and application,” in *IEEE Int. Conf. Commun.*, May 2008, pp. 4160–4164.
- [18] Y. Zeng and Y.-C. Liang, “Eigenvalue-based spectrum sensing algorithms for cognitive radio,” *IEEE Trans. Commun.*, vol. 57, no. 6, pp. 1784–1793, June 2009.
- [19] M. Fujii and Y. Watanabe, “A study on SNR estimation for cognitive radio,” in *IEEE Int. Conf. Ultra-Wideband (ICUWB)*, Sept. 2012, pp. 11–15.
- [20] W. Ejaz, N. Hasan, and H. S. Kim, “SNR-based adaptive spectrum sensing for cognitive radio networks,” *Int. J. Innovative Computing, Info. and Control*, vol. 8, no. 9, pp. 6095–6105, 2012.
- [21] D.-S. Shiu, G. Foschini, M. Gans, and J. Kahn, “Fading correlation and its effect on the capacity of multielement antenna systems,” *IEEE Trans. Commun.*, vol. 48, no. 3, pp. 502–513, Mar 2000.

- [22] H. Hui, "Influence of antenna characteristics on MIMO systems with compact monopole arrays," *IEEE Antennas and Wireless Propag. Letters*, vol. 8, pp. 133–136, 2009.
- [23] R. Couillet and M. Debbah, *Random Matrix Methods for Wireless Communications*, 1st ed. Cambridge University Press, 2011.
- [24] T. Yucek and H. Arslan, "MMSE noise plus interference power estimation in adaptive OFDM systems," *IEEE Trans. Veh. Technol.*, vol. 56, no. 6, pp. 3857–3863, 2007.
- [25] T. Tian, H. Iwai, and H. Sasaoka, "Pseudo BER based SNR estimation for energy detection scheme in cognitive radio," in *IEEE 75th Veh. Technol. Conf. (Spring)*, May 2012, pp. 1–5.
- [26] V. Chavali and C. da Silva, "Collaborative spectrum sensing based on a new SNR estimation and energy combining method," *IEEE Trans. Veh. Technol.*, vol. 60, no. 8, pp. 4024–4029, 2011.
- [27] D. Cabric and R. Brodersen, "Physical layer design issues unique to cognitive radio systems," in *IEEE PIMRC*, vol. 2, Sept. 2005, pp. 759–763.
- [28] H. Tang, "Some physical layer issues of wide-band cognitive radio systems," in *First IEEE DySPAN*, Nov. 2005, pp. 151–159.
- [29] H. Sun, A. Nallanathan, C.-X. Wang, and Y. Chen, "Wideband spectrum sensing for cognitive radio networks: a survey," *IEEE Wireless Commun.*, vol. 20, no. 2, pp. 74–81, April 2013.
- [30] Z. Tian and G. Giannakis, "Compressed sensing for wideband cognitive radios," in *IEEE ICASSP*, vol. 4, April 2007, pp. 1357–1360.
- [31] H. Sun, W.-Y. Chiu, J. Jiang, A. Nallanathan, and H. Poor, "Wideband spectrum sensing with sub-Nyquist sampling in cognitive radios," *IEEE Trans. Signal Process.*, vol. 60, no. 11, pp. 6068–6073, Nov. 2012.
- [32] J. Meng, W. Yin, H. Li, E. Hossain, and Z. Han, "Collaborative spectrum sensing from sparse observations in cognitive radio networks," *IEEE J. Sel. Areas Commun.*, vol. 29, no. 2, pp. 327–337, Feb. 2011.
- [33] X. Jiang, K.-K. Wong, Y. Zhang, and D. Edwards, "On hybrid overlay-underlay dynamic spectrum access: Double-threshold energy detection and markov model," *IEEE Trans. Veh. Technol.*, vol. 62, no. 8, pp. 4078–4083, 2013.
- [34] C. Park, C. Kang, Y. Choi, and C. Oh, "Interference analysis of geostationary satellite networks in the presence of moving non-geostationary satellites," in *2nd Int. Conf. Info. Technology Convergence and Services (ITCS)*, Aug. 2010, pp. 1–5.
- [35] J. Fortes and R. Sampaio-Neto, "An analytical method for assessing interference in interference environments involving NGSO satellite networks," *Int. J. Satellite Commun. and Networking*, vol. 17, no. 6, pp. 399–419, Dec. 1999.
- [36] D. Christopoulos, S. Chatzinotas, and B. Ottersten, "User scheduling for coordinated dual satellite systems with linear precoding," in *IEEE ICC*, June 2013, pp. 4498–4503.
- [37] L. Shen, H. Wang, W. Zhang, and Z. Zhao, "Blind spectrum sensing for cognitive radio channels with noise uncertainty," *IEEE Trans. Wireless Commun.*, vol. 10, no. 6, pp. 1721–1724, June 2011.
- [38] M. Orooji, R. Soosahabi, and M. Naraghi-Pour, "Blind spectrum sensing using antenna arrays and path correlation," *IEEE Trans. Veh. Technol.*, vol. 60, no. 8, pp. 3758–3767, Oct. 2011.
- [39] S. Bokharaiee, H. Nguyen, and E. Shwedyk, "Blind spectrum sensing for OFDM-based cognitive radio systems," *IEEE Trans. Veh. Technol.*, vol. 60, no. 3, pp. 858–871, March 2011.
- [40] P. De and Y.-C. Liang, "Blind spectrum sensing algorithms for cognitive radio networks," *IEEE Trans. Veh. Technol.*, vol. 57, no. 5, pp. 2834–2842, Sept. 2008.
- [41] W. Zhang, G. Abreu, M. Inamori, and Y. Sanada, "Spectrum sensing algorithms via finite random matrices," *IEEE Trans. Commun.*, vol. 60, no. 1, pp. 164–175, Jan. 2012.
- [42] A. Kortun and et al, "On the performance of eigenvalue-based cooperative spectrum sensing for cognitive radio," *IEEE J. Sel. Topics Signal Process.*, vol. 5, no. 1, pp. 49–55, Feb. 2011.
- [43] A. M. Tulino and S. Verdu, "Random matrix theory and wireless communications," *Foundations and Trends in Communications and Information Theory*, vol. 1, no. 1, pp. 1–182, 2004.
- [44] L. Cardoso, M. Debbah, P. Bianchi, and J. Najim, "Cooperative spectrum sensing using random matrix theory," in *3rd Int. Symp. Wireless Pervasive Computing*, May 2008, pp. 334–338.

[45] F. Penna, R. Garello, and M. Spirito, "Cooperative spectrum sensing based on the limiting eigenvalue ratio distribution in Wishart matrices," *IEEE Commun. Letters*, vol. 13, no. 7, pp. 507–509, July 2009.

[46] A. Taherpour, M. Nasiri-Kenari, and S. Gazor, "Multiple antenna spectrum sensing in cognitive radios," *IEEE Trans. Wireless Commun.*, vol. 9, no. 2, pp. 814–823, February 2010.

[47] K. Hassan and et al, "Predicted eigenvalue threshold based spectrum sensing with correlated multiple-antennas," in *IEEE VTC (Spring)*, May 2012, pp. 1–5.

[48] L. Wei and O. Tirkkonen, "Spectrum sensing in the presence of multiple primary users," *IEEE Trans. Commun.*, vol. 60, no. 5, pp. 1268–1277, May 2012.

[49] P. Wang, J. Fang, N. Han, and H. Li, "Multiantenna-assisted spectrum sensing for cognitive radio," *IEEE Trans. Veh. Technol.*, vol. 59, no. 4, pp. 1791–1800, May 2010.

[50] P. Bianchi, M. Debbah, M. Maida, and J. Najim, "Performance of statistical tests for single-source detection using random matrix theory," *IEEE Trans. Info. Th.*, vol. 57, no. 4, pp. 2400–2419, 2011.

[51] L. Wei and O. Tirkkonen, "Analysis of scaled largest eigenvalue based detection for spectrum sensing," in *IEEE ICC*, June 2011, pp. 1–5.

[52] M. Matthaieu, M. Mckay, P. Smith, and J. Nossek, "On the condition number distribution of complex wishart matrices," *IEEE Trans. Commun.*, vol. 58, no. 6, pp. 1705–1717, June 2010.

[53] S. K. Sharma, S. Chatzinotas, and B. Ottersten, "Eigenvalue based sensing and SNR estimation for cognitive radio in presence of noise correlation," *IEEE Trans. Veh. Technol.*, vol. 62, no. 8, pp. 1–14, Sept. 2013.

[54] S. K. Sharma, S. Chatzinotas, and B. Ottersten, "The effect of noise correlation on fractional sampling based spectrum sensing," in *IEEE ICC*, June 2013, pp. 2589–2594.

[55] S. K. Sharma, S. Chatzinotas, and B. Ottersten, "Maximum eigenvalue detection for spectrum sensing under correlated noise," in *IEEE ICASSP*, May 2014, pp. 4464–4468.

[56] C. Tepedelenlioglu and R. Challagulla, "Low-complexity multipath diversity through fractional sampling in OFDM," *IEEE Trans. Signal Process.*, vol. 52, no. 11, pp. 3104–3116, Nov. 2004.

[57] H. Nishimura, M. Inamori, and Y. Sanada, "Sampling rate selection for fractional sampling in OFDM," in *IEEE PIMRC*, Sept. 2007, pp. 1–5.

[58] S. K. Sharma, M. Patwary, and M. Abdel-Maguid, "Enhanced information throughput in multiple input multiple output orthogonal frequency division multiplexing based systems using fractional sampling and iterative signal processing", *Trans. Emerging Tel. Tech.*, vol. 5, no. 12, pp. 1208–1218, Oct. 2013.

[59] B. Li, Q. Wang, G. Lu, Y. Chang, and D. Yang, "Linear MMSE frequency domain equalization with colored noise," in *IEEE 66th Veh. Technol. Conf.*, Sept. 30-oct. 3 2007, pp. 1152–1156.

[60] R. Couillet, J. Silverstein, Z. Bai, and M. Debbah, "Eigen-inference for energy estimation of multiple sources," *IEEE Trans. Info. Th.*, vol. 57, no. 4, pp. 2420–2439, 2011.

[61] M. Vu, N. Devroye, and V. Tarokh, "On the primary exclusive region of cognitive networks," *IEEE Trans. Wireless Commun.*, vol. 8, no. 7, pp. 3380–3385, July 2009.

[62] S. Senthuran, A. Anpalagan, and O. Das, "Throughput analysis of opportunistic access strategies in hybrid underlay and overlay cognitive radio networks," *IEEE Trans. Wireless Commun.*, vol. 11, no. 6, pp. 2024–2035, 2012.

[63] X. Kang, Y.-C. Liang, H. K. Garg, and L. Zhang, "Sensing-based spectrum sharing in cognitive radio networks," in *IEEE GLOBECOM*, Nov. 2008, pp. 1–5.

[64] M. Khoshkholgh, K. Navaie, and H. Yanikomeroglu, "Access strategies for spectrum sharing in fading environment: Overlay, underlay, and mixed," *IEEE Trans. Mobile Computing*, vol. 9, no. 12, pp. 1780–1793, Dec. 2010.

[65] S. K. Sharma, S. Chatzinotas, and B. Ottersten, "SNR estimation for multi-dimensional cognitive receiver under correlated channel/noise," *IEEE Trans. Wireless Commun.*, vol. 12, no. 12, pp. 6392–6405, Dec. 2013.

[66] S. K. Sharma, S. Chatzinotas, and B. Ottersten, "Eigenvalue based SNR estimation for cognitive radio in presence of channel correlation," in *IEEE Globecom*, Dec. 2013, pp. 3419–3424.

[67] S. K. Sharma, S. Chatzinotas, and B. Ottersten, "A hybrid cognitive transceiver architecture: Sensing-throughput tradeoff," in *9th Int. Conf. Cognitive Radio Oriented Wireless Networks (CROWNCOM)*, June 2014.

[68] R. Walden, "Analog-to-digital converter survey and analysis," *IEEE J. Sel. Areas Commun.*, vol. 17, no. 4, pp. 539–550, April 1999.

[69] M. Ariaudo and et al, "Green radio despite Dirty RF front-end", *EURASIP J. Wireless Commun. Networking*, vol. 146, April 2012.

[70] R. Baraniuk, "Compressive Sensing," *IEEE Signal Process. Mag.*, vol. 24, no. 4, pp. 118–121, July 2007.

[71] D. Donoho, "Compressed sensing," *IEEE Trans. Info. Th.*, vol. 52, no. 4, pp. 1289–1306, April 2006.

[72] E. Candes and M. Wakin, "An introduction to compressive sampling," *IEEE Signal Process. Mag.*, vol. 25, no. 2, pp. 21–30, March 2008.

[73] Y. Wang, A. Pandharipande, Y. Polo, and G. Leus, "Distributed compressive wide-band spectrum sensing," in *Info. Theory and Applications Workshop*, Feb. 2009, pp. 178–183.

[74] M. Davenport, P. Boufounos, M. Wakin, and R. Baraniuk, "Signal processing with compressive measurements," *IEEE J. Sel. Topics Signal Process.*, vol. 4, no. 2, pp. 445–460, April 2010.

[75] J. E. Vila-Forcen, A. Artes-Rodriguez, and J. Garcia-Frias, "Compressive sensing detection of stochastic signals," in *42nd Annual Conf. Info. Sciences and Systems, 2008*, March 2008, pp. 956–960.

[76] S. Hong, "Direct spectrum sensing from compressed measurements," in *Military Commun. Conf.- MILCOM*, Oct 2010, pp. 1187–1192.

[77] Y. Wang, Z. Tian, and C. Feng, "Sparsity order estimation and its application in compressive spectrum sensing for cognitive radios," *IEEE Trans. Wireless Commun.*, vol. 11, no. 6, pp. 2116–2125, June 2012.

[78] S. K. Sharma, S. Chatzinotas, and B. Ottersten, "Compressive sparsity order estimation for wideband cognitive radio receiver," *IEEE Trans. Signal Process.*, vol. 62, no. 19, Oct. 2014.

[79] S. K. Sharma, S. Chatzinotas, and B. Ottersten, "Compressive SNR estimation for wideband cognitive radio under correlated scenarios," in *IEEE Wireless Commun. and Networking Conf. (WCNC)*, April 2014, pp. 713–718.

[80] S. K. Sharma, S. Chatzinotas, and B. Ottersten, "Compressive sparsity order estimation for wideband cognitive radio receiver," in *IEEE ICC*, June 2014, pp. 1361–1366.

[81] K. Becher, "The European case for satellite communications," Knowledge and Analysis LLP under ESA Contract 21596/08/NL/AD, Tech. Rep., May 2009.

[82] P. Chini, G. Giambene and S. Kota, "A survey on mobile satellite systems," in *Int. J. Satellite Commun.*, vol. 2010, no. 28, 2010, pp. 29–57.

[83] R. Alegre-Godoy, N. Alagha, and M. Vazquez-Castro, "Offered capacity optimization mechanisms for multi-beam satellite systems," in *IEEE ICC*, June 2012, pp. 3180–3184.

[84] A. Kyrgiolas, B. Evans, P. Thompson, P. Mathiopoulos, and S. Papaharalabos, "A terabit/second satellite system for european broadband access: A feasibility study," *Int. J. Satellite Commun. and Networking*, vol. 32, no. 2, pp. 63–92, 2014.

[85] O. Vidal and et al, "Next generation high throughput satellite system," in *2012 IEEE First AESS European Conf. Satellite Telecommun. (ESTEL)*, Oct. 2012, pp. 1–7.

[86] S. Kota, G. Giambene, and S. Kim, "Satellite component of NGN: Integrated and hybrid networks," *Int. J. Satellite Commun. and Networking*, 2010.

[87] L. Gavrilovska and V. Atanasovski, "Resource management in wireless heterogeneous networks (WHNs)," in *9th Int. Conf. on Telecommun. in Modern Satellite, Cable, and Broadcasting Services*, Oct. 2009, pp. 97–106.

[88] A. Khan, M. Adda, and T. Khan, "Multi radio diversity for satellite-terrestrial mobile communications," in *IEEE Int. Conf. Circuits and Systems for Commun.*, May 2008, pp. 673–677.

[89] B. Evans and et al, "Integration of satellite and terrestrial systems in future multimedia communications," *IEEE Wireless Comm.*, vol. 12, no. 5, pp. 72 – 80, Oct. 2005.

[90] S. Kandeepan, L. De Nardis, M.-G. Di Benedetto, A. Guidotti, and G. Corazza, "Cognitive satellite terrestrial radios," in *IEEE GLOBECOM*, Dec. 2010, pp. 1 –6.

[91] D.-S. Oh, S.-M. Lee, D.-S. Ahn, and S. Kim, "A study on the separation distance for frequency sharing between GSO network and terrestrial network in Ka band," in *IEEE Veh. Technol. Conf.*, May 2008, pp. 2967–2971.

[92] Y. H. Yun and J. H. Cho, "An orthogonal cognitive radio for a satellite communication link," in *IEEE 20th Int. Symp. PIMRC*, Sept. 2009, pp. 3154–3158.

[93] A. B. Awoseyila and B. G. Evans, "Frequency sharing between satellite and terrestrial in the 2 GHz MSS band," in *31st AIAA ICSSC*, May 2009, pp. 117–123.

[94] J. Park, S. Nam, and D. Oh, "Coexistence of gateway uplinks for high altitude platform station with uplink for the fixed-satellite service in 6 GHz band," in *17th Asia-Pacific Conf. on Commun. (APCC)*, Oct. 2011, pp. 715–719.

[95] M. Hoyhtya and et al, "Applicability of cognitive radio to satellite systems (ACROSS)," VTT technical research centre, Finland, Tech. Rep., 2012. [Online]. Available: <http://telecom.esa.int/telecom>

[96] K. Liolis and et al, "Cognitive radio scenarios for satellite communications: The CoRaSat approach," in *FutureNetworkSummit*, July 2013, pp. 1–10.

[97] N. Chuberre, B. Evans, A. Vanelli-Coralli, J. Krause, J. Grotz, and S. K. Sharma, "FP7 project CoRaSat intermediate results and standardization strategy," in *European Conf. Networks and Commun.*, June 2014.

[98] S. K. Sharma, S. Chatzinotas, and B. Ottersten, "Interference alignment for spectral coexistence of heterogeneous networks," *EURASIP J. Wireless Commun. and Networking*, vol. 2013, no. 46, 2013.

[99] S. K. Sharma, S. Chatzinotas, and B. Ottersten, "Cognitive beamhopping for spectral coexistence of multibeam satellites," in *Int. J. Satellite Commun. and Networking*, March 2014.

[100] S. K. Sharma, S. Chatzinotas, and B. Ottersten, "Cognitive radio techniques for satellite communication systems," in *IEEE VTC*, Sept. 2013, pp. 1–5.

[101] S. K. Sharma, S. Chatzinotas, and B. Ottersten, "Satellite cognitive communications and spectrum regulation," in *Internaitonal Regulations of Space Communications: Current Issues*, M. Hofmann, Ed. Larcier, 2013, ch. 11, pp. 201–214.

[102] M. Koletta, V. Milas, and P. Constantinou, "Analysis of the interference environment generated by mobile earth stations operating in frequency bands shared with the fixed service," in *7th Int. Conf. Telecommun. in Modern Satellite, Cable and Broadcasting Services*, vol. 2, Sept. 2005.

[103] A. Panagopoulos, P.-D. Arapoglou, G. Chatzarakis, J. Kanellopoulos, and P. Cottis, "Coexistence of the broadcasting satellite service with fixed service systems in frequency bands above 10 GHz," *IEEE Trans. Broadcasting*, vol. 52, no. 1, pp. 100–107, March 2006.

[104] ITU-R, "Sharing studies between IMT-advanced systems and geostationary satellite networks in the fixed satellite service in 3400-4200 and 4500-4800 MHz frequency bands," ITU-R M.2109, Tech. Rep., 2007.

[105] CEPT, "FM44(11)057 annex 5, working document on Ka band 17.7-19.7 GHz band," Available online: www.cept.org/Documents/FM-44/3105.

[106] S. K. Sharma, S. Chatzinotas, and B. Ottersten, "Satellite cognitive communications: Interference modeling and techniques selection," in *6th Advanced Satellite Multimedia Systems Conference (ASMS) and 12th Signal Processing for Space Communications (SPSC) Workshop*, Sept. 2012, pp. 111–118.

[107] Y.-C. Liang, Y. Zeng, E. Peh, and A. T. Hoang, "Sensing-throughput tradeoff for cognitive radio networks," *IEEE Trans. Wireless Commun.*, vol. 7, no. 4, pp. 1326–1337, April 2008.

[108] S. K. Sharma, S. Maleki, S. Chatzintoas, J. Grotz, and B. Ottersten, "Implementation issues of cognitive radio techniques for Ka band (17.7-19.7 GHz) SatComs," in *7th ASMS/13th SPSC*, Sept. 2014.

[109] B. S. Collins, "Polarization-diversity antennas for compact base stations," *Microwave J.*, vol. 43, no. 1, pp. 76–88, Jan. 2000.

[110] C. B. Dietrich and et al, "Spatial, polarization, and pattern diversity for wireless handheld terminals," *IEEE Trans. Antennas and Propag.*, vol. 49, no. 9, pp. 1271–1281, Sep 2001.

[111] S. Chatzinotas, D. Christopoulos, and B. Ottersten, "Coordinated multi-point decoding with dual-polarized antennas," in *7th IWCMC*, July 2011, pp. 157–161.

[112] N. Zorba, M. Realp, M. Lagunas, and A. Perez-Neira, "Dual polarization for MIMO processing in multi-beam satellite systems," in *10th Int. Workshop SPSC*, Oct. 2008, pp. 1–7.

[113] C. Oestges, B. Clerckx, M. Guillaud, and M. Debbah, "Dual-polarized wireless communications: from propagation models to system performance evaluation," *IEEE Trans. Wireless Commun.*, vol. 7, no. 10, pp. 4019–4031, Oct. 2008.

[114] S. K. Sharma, S. Chatzinotas, and B. Ottersten, "Spectrum sensing in dual polarized fading channels for cognitive SatComs," in *IEEE GLOBECOM*, Dec. 2012, pp. 3419–3424.

[115] S. Yiu, M. Vu, and V. Tarokh, "Interference and noise reduction by beamforming in cognitive networks," *IEEE Trans. Commun.*, vol. 57, no. 10, pp. 3144–3153, Oct. 2009.

[116] T. Luan, F. Gao, X.-D. Zhang, J. Li, and M. Lei, "Rate maximization and beamforming design for relay-aided multiuser cognitive networks," *IEEE Trans. Veh. Technol.*, vol. 61, no. 4, pp. 1940–1945, May 2012.

[117] K. Cumanan, L. Musavian, S. Lambotharan, and A. Gershman, "SINR balancing technique for downlink beamforming in cognitive radio networks," *IEEE Signal Process. Lett.*, vol. 17, no. 2, pp. 133–136, Feb. 2010.

[118] Bryson, "Northpoint Technology Ltd. v. MDS America," Inc. and MDS International S.A.R.L. (Fed. Cir. 2005-06-28).

[119] S. K. Sharma, S. Chatzinotas, and B. Ottersten, "Spatial filtering for underlay cognitive satcoms," in *Personal Satellite Services*, ser. Lecture Notes of the Institute for Computer Sciences, Social Informatics and Telecommun. Engg., R. Dhaou and et al, Eds. Springer International Publishing, 2013, vol. 123, pp. 186–198.

[120] S. K. Sharma, S. Chatzinotas, and B. Ottersten, "Transmit beamforming for spectral coexistence of satellite and terrestrial networks," in *8th Int. Conf. CROWNCOM*, July 2013, pp. 275–281.

[121] V. Cadambe and S. Jafar, "Interference alignment and spatial degrees of freedom for the K user interference channel," in *IEEE ICC*, May 2008, pp. 971–975.

[122] V. Cadambe and S. Jafar, "Interference alignment and the degrees of freedom of wireless X networks," *IEEE Trans. Info. Th.*, vol. 55, no. 9, pp. 3893–3908, Sept. 2009.

[123] H. Zhou, T. Ratnarajah, and Y.-C. Liang, "On secondary network interference alignment in cognitive radio," in *IEEE Symp. New Frontiers in Dynamic Spectrum Access Networks (DySPAN)*, May 2011, pp. 637–641.

[124] S. Kaimalelu, R. Krishnan, S. Kalyani, N. Akhtar, and B. Ramamurthi, "Cognitive interference management in heterogeneous femto-macro cells networks," in *IEEE ICC*, June 2011, pp. 1–6.

[125] S. Chatzinotas and B. Ottersten, "Interference alignment for clustered multicell joint decoding," in *IEEE Wireless Commun. and Networking Conf.*, March 2011, pp. 1966–1971.

[126] C. Suh and D. Tse, "Interference alignment for cellular networks," in *46th Annual Allerton Conf. Commun., Control, and Computing*, 23-26 2008, pp. 1037–1044.

[127] R. Tresch, M. Guillaud, and E. Riegler, "On the achievability of interference alignment in the K-user constant MIMO interference channel," in *IEEE/SP 15th Workshop on Statistical Signal Process.*, Aug. 2009, pp. 277–280.

[128] B. Da and R. Zhang, "Exploiting interference alignment in multi-cell cooperative ofdma resource allocation," in *IEEE Global Telecommun. Conf.*, Dec. 2011, pp. 1–5.

[129] S. Chatzinotas and B. Ottersten, "Interference mitigation techniques for clustered multicell joint decoding systems," *EURASIP Journal on Wireless Communications and Networking, Special Issue on Multicell Cooperation for Next Generation Communication Systems*, vol. 132, 2011.

[130] A. Masucci, A. Tulino, and M. Debbah, "Asymptotic analysis of uplink interference alignment in ricean small cells," in *IEEE Global Telecommunications Conference*, Houston, Texas, USA, 2011.

[131] R. Ganesan and A. Klein, "Projection based space-frequency interference alignment in a multi-carrier multi-user two-way relay network," in *8th International Symposium on Wireless Communication Systems*, Nov. 2011, pp. 266–270.

[132] C. Shi, R. Berry, and M. Honig, "Interference alignment in multi-carrier interference networks," in *IEEE International Symposium on Information Theory Proceedings*, Aug. 2011, pp. 26–30.

[133] T. Liu and C. Yang, "Signal alignment for multicarrier code division multiple user two-way relay systems," *IEEE Transactions on Wireless Communications*, vol. 10, no. 11, pp. 3700–3710, Nov. 2011.

[134] P. Jain and M. Vazquez-Castro, "Subspace interference alignment for multibeam satellite communications systems," in *5th ASMS and the 11th SPSC*, Sept. 20010, pp. 234–239.

[135] S. Perlaza, N. Fawaz, S. Lasaulce, and M. Debbah, "From spectrum pooling to space pooling: Opportunistic interference alignment in MIMO cognitive networks," *IEEE Trans. Signal Process.*, vol. 58, no. 7, pp. 3728–3741, 2010.

[136] B. Abdelhamid, M. Elsabrouty, and S. Elramly, "Novel interference alignment in multi-secondary users cognitive radio system," in *IEEE Symp. Computers and Communications (ISCC)*, 2012, pp. 785–789.

[137] M. Amir, A. El-Keyi, and M. Nafie, "Constrained interference alignment and the spatial degrees of freedom of MIMO cognitive networks," *IEEE Trans. Info. Th.*, vol. 57, no. 5, pp. 2994–3004, 2011.

[138] G. Chen, Z. Xiang, C. Xu, and M. Tao, "On degrees of freedom of cognitive networks with user cooperation," *IEEE Wireless Commun. Letters*, vol. 1, no. 6, pp. 617–620, July 2012.

[139] S. K. Sharma, S. Chatzinotas, and B. Ottersten, "Cognitive interference alignment for spectral coexistence," in *Cognitive Radio and Networking for Heterogeneous Wireless Networks*, D. Benedetto and et al, Eds. Springer, 2014, ch. 2.

[140] J. Anzalchi and et al, "Beam hopping in multi-beam broadband satellite systems: System simulation and performance comparison with non-hopped systems," in *5th ASMS conf. and the 11th SPSC workshop*, Sept. 2010, pp. 248–255.

[141] A. Mokhtar and M. Azizoglu, "On the downlink throughput of a broadband LEO satellite network with hopping beams," *IEEE Commun. Letters*, vol. 4, no. 12, pp. 390–393, Dec. 2000.

[142] N. Fonseca and J. Sombrin, "Multi-beam reflector antenna system combining beam hopping and size reduction of effectively used spots," *IEEE Antennas and Propagation Magazine*, vol. 54, no. 2, pp. 88–99, April 2012.

[143] L. Jiang, "Multi-beam satellite resource optimization for beam hopping transmission," PhD thesis, Department of Telecommun. and systems Engineering, Universitat Autonoma de Barselona, 2010.

[144] S. K. Sharma, S. Chatzinotas, and B. Ottersten, "Cognitive beamhopping for spectral coexistence of multibeam satellites," in *Future Network and Mobile Summit (FutureNetworkSummit), 2013*, July 2013, pp. 1–10.

[145] S. K. Sharma, S. Chatzinotas, and B. Ottersten, "Exploiting polarization for spectrum sensing in cognitive SatComs," in *7th ICST Conf. CROWNCOM*, Sept. 2012, pp. 36–41.

[146] S. Chatzinotas, M. Imran, and R. Hoshayr, "On the multicell processing capacity of the cellular MIMO uplink channel in correlated Rayleigh fading environment," *IEEE Trans. Wireless Commun.*, vol. 8, no. 7, pp. 3704–3715, July 2009.

[147] X. Mestre, J. Fonollosa, and A. Pages-Zamora, "Capacity of MIMO channels: asymptotic evaluation under correlated fading," *IEEE J. Sel. Areas Commun.*, vol. 21, no. 5, pp. 829–838, June 2003.

[148] J. Mattingley and S. Boyd, "Real-time convex optimization in signal processing," *IEEE Signal Process. Mag.*, vol. 27, no. 3, pp. 50–61, May 2010.

[149] S. K. Sharma, S. Chatzinotas, and B. Ottersten, "Cognitive Beamforming for Spectral Coexistence of Hybrid Satellite Systems," in *Cooperative and Cognitive Satellite Systems*, S. Chatzintoas and et al, Eds. Elsevier, 2014, ch. 13, to appear.

[150] J. Mitola, *Cognitive Radio Architecture: The Engineering Foundations of Radio XML*, 1st ed. Wiley, Oct. 2006.

[151] R. S. Groups, "Working document towards a preliminary draft new report: Software defined radio in land mobile services (question 230-1/8)," ITU, Tech. Rep. 8A/121-E, Sept. 2004.

[152] T. R. Shields, "SDR update," Global Standards Collaboration, Sophia Antipolis, France, Tech. Rep., Sept. 2005.

[153] A. Shukla and et al, "Cognitive radio technology: A study for OFCOM," QinetiQ, Tech. Rep. QINETIQ/06/00420 Issue 1.1, Feb. 2007.

[154] I. Akyildiz, W.-Y. Lee, M. C. Vuran, and S. Mohanty, "A survey on spectrum management in cognitive radio networks," *IEEE Commun. Mag.*, vol. 46, no. 4, pp. 40–48, April 2008.

[155] K. Letaief and W. Zhang, "Cooperative communications for cognitive radio networks," *Proceedings of the IEEE*, vol. 97, no. 5, pp. 878–893, May 2009.

[156] S. Haykin, "Cognitive radio: brain-empowered wireless communications," *IEEE J. Sel. Areas Commun.*, vol. 23, no. 2, pp. 201–220, Feb 2005.

[157] J. Palicot, C. Moy, and R. Hachemani, "Multilayer sensors for the sensorial radio bubble," *Physical Communication*, vol. 2, no. 1-2, pp. 151–165, Sep. 2009.

[158] J. Riihijarvi, P. Mahonen, M. Petrova, and V. Kolar, "Enhancing cognitive radios with spatial statistics: From radio environment maps to topology engine," in *4th Int. Conf. CROWNCOM*, June 2009, pp. 1–6.

[159] Y. Zhao, L. Morales, J. Gaeddert, K. Bae, J.-S. Um, and J. Reed, "Applying radio environment maps to cognitive wireless regional area networks," in *IEEE Int. Symp. DySPAN*, April 2007, pp. 115–118.

[160] J. wu Zhang, Q. Zhao, and J. yuan Zou, "The IEEE 802.22 wran system based on radio environment map (rem)," in *First Int. Workshop on Education Technology and Computer Science*, vol. 1, March 2009, pp. 98–101.

[161] S. Kawade and M. Nekovee, "Wireless options for high data-rate indoor users: Cognitive access to TV white space," in *First UK-India Int. Workshop on Cognitive Wireless Systems*, April 2011.

[162] S. Subramani and et al, "Towards practical rem-based radio resource management," in *Future Network Mobile Summit (FutureNetw)*, 2011, June 2011, pp. 1–8.

[163] J. Riihijarvi, P. Mahonen, and S. Sajjad, "Influence of transmitter configurations on spatial statistics of radio environment maps," in *20th Int. Symp. PIMRC*, Sept 2009, pp. 853–857.

[164] L. Bolea, J. Perez-Romero, R. Agusti, and O. Sallent, "Context discovery mechanisms for cognitive radio," in *IEEE 73rd VTC (Spring)*, May 2011, pp. 1–5.

[165] M. Buddhikot and et al, "Dimsumnet: new directions in wireless networking using coordinated dynamic spectrum," in *6th Int. Symp. WoWMoM*, June 2005, pp. 78–85.

[166] M. Filo, A. Hossain, A. Biswas, and R. Piesiewicz, "Cognitive pilot channel: Enabler for radio systems coexistence," in *2nd Int. Workshop CogART*, May 2009, pp. 17–23.

[167] R. Haines, "Cognitive pilot channels for femto-cell deployment," in *7th Int. Symp. Wireless Commun. Systems (ISWCS)*, Sept 2010, pp. 631–635.

[168] D. Pauluzzi and N. Beaulieu, "A comparison of SNR estimation techniques for the AWGN channel," *IEEE Trans. Commun.*, vol. 48, no. 10, pp. 1681–1691, Oct 2000.

[169] A. Ijaz, A. Awoseyila, and B. Evans, "Improved SNR estimation for BPSK and QPSK signals," *Electronics Letters*, vol. 45, no. 16, pp. 858–859, July 2009.

[170] A. Ijaz, A. Awoseyila, and B. Evans, "Signal-to-noise ratio estimation algorithm for advanced DVB-RCS systems," *IEEE Trans. Broadcasting*, vol. 58, no. 4, pp. 603–608, Dec 2012.

[171] A. Ijaz, A. Awoseyila, and B. Evans, "Signal-to-noise ratio estimation algorithm for adaptive coding and modulation in advanced digital video broadcasting-radar cross section satellite systems," *IET Commun.*, vol. 6, no. 11, pp. 1587–1593, July 2012.

[172] S. Srinivasa and S. Jafar, "The throughput potential of cognitive radio: A theoretical perspective," *IEEE Commun. Magazine*, vol. 45, no. 5, pp. 73–79, May 2007.

[173] J. Palicot (edited by), *Radio Engineering: From Software radio to Cognitive Radio*. Wiley, 2011.

[174] A. Ghasemi and E. S. Sousa, "Fundamental limits of spectrum-sharing in fading environments," *IEEE Trans. Wireless Commun.*, vol. 6, no. 2, pp. 649–658, Feb. 2007.

[175] FCC, "Establishment of an interference temperature metric to quantify and manage interference and to expand available unlicensed operation in certain fixed, mobile and satellite frequency bands," ET Docket 0-289, 2003.

[176] T. W. Ban, W. Choi, B. C. Jung, and D. K. Sung, "Multi-user diversity in a spectrum sharing system," *IEEE Trans. Wireless Commun.*, vol. 8, no. 1, pp. 102–106, Jan. 2009.

[177] M. Costa, "Writing on dirty paper (corresp.)," *IEEE Trans. Info. Th.*, vol. 29, no. 3, pp. 439–441, May 1983.

[178] S. I. Gel'fand and M. S. Pinsker, "Probl. contr. and inform. theory," *Coding for channel with random parameters*, vol. 9, no. 1, pp. 19–31, 1980.

[179] Y. H. Yun and J. H. Cho, "An orthogonal cognitive radio for a satellite communication link," in *IEEE PIMRC*, Sept. 2009, pp. 3154–3158.

[180] L. Li, F. Khan, M. Pesavento, and T. Ratnarajah, "Power allocation and beamforming in overlay cognitive radio systems," in *IEEE 73rd Veh. Technol. Conf.*, May 2011, pp. 1–5.

[181] Y. Zeng and Y.-C. Liang, "Maximum-minimum eigenvalue detection for cognitive radio," in *IEEE 18th Int. Symp. PIMRC*, Sept. 2007, pp. 1–5.

[182] R. Tandra and A. Sahai, "Fundamental limits on detection in low SNR under noise uncertainty," in *Int. Conf. Wireless Networks, Commun. and Mobile Computing*, vol. 1, June 2005, pp. 464–469.

[183] D. Cabric, A. Tkachenko, and R. Brodersen, "Spectrum sensing measurements of pilot, energy, and collaborative detection," in *IEEE Military Commun. Conf.*, Oct. 2006, pp. 1–7.

[184] F. F. Digham, M.-S. Alouini, and M. K. Simon, "On the energy detection of unknown signals over fading channels," *IEEE Trans. Commun.*, vol. 55, no. 1, pp. 21–24, Jan. 2007.

[185] J. Proakis, *Digital Communications*, 3rd ed. McGraw-Hill, 1995.

[186] D. Cabric, S. Mishra, and R. Brodersen, "Implementation issues in spectrum sensing for cognitive radios," in *Thirty-Eighth Asilomar Conf. on Signals, Systems and Computers*, vol. 1, Nov. 2004, pp. 772–776.

[187] J. Lunden, V. Koivunen, A. Huttunen, and H. Poor, "Spectrum sensing in cognitive radios based on multiple cyclic frequencies," in *2nd Int. Conf. CROWNCOM*, Aug. 2007, pp. 37–43.

[188] A. Dandawate and G. Giannakis, "Statistical tests for presence of cyclostationarity," *IEEE Trans. Signal Process.*, vol. 42, no. 9, pp. 2355–2369, Sep. 1994.

[189] K. Maeda, A. Benjebbour, T. Asai, T. Furuno, and T. Ohya, "Recognition among OFDM-based systems utilizing cyclostationarity-inducing transmission," in *IEEE Int. Symp. DySPAN*, April 2007, pp. 516–523.

[190] Y. Zeng and Y.-C. Liang, "Robustness of the cyclostationary detection to cyclic frequency mismatch," in *IEEE Int. Symp. PIMRC*, Sept 2010, pp. 2704–2709.

[191] Z. Khalaf and J. Palicot, "On the use of the sparse property of the cyclic autocorrelation function to blindly estimate the cyclostationarity," *Frequenz*, vol. 66, no. 9-10, pp. 279–292, Sep. 2012.

[192] Z. Khalaf, A. Nafkha, and J. Palicot, "Blind spectrum detector for cognitive radio using compressed sensing and symmetry property of the second order cyclic autocorrelation," in *7th Int. Conf. CROWNCOM*, June 2012, pp. 291–296.

[193] Z. Khalaf, J. Palicot, A. Nafkha, and H. Zhang, "Blind free band detector based on the sparsity of the cyclic autocorrelation function," in *Proc. 21st European Signal Process. Conf. (EUSIPCO)*, Sept 2013, pp. 1–5.

[194] H. Wang, W. Jouini, R. Hachemani, J. Palicot, L. Cardoso, and M. Debbah, "Blind bandwidth shape recognition for standard identification using USRP platforms and SDR4all tools," in *6th Advanced Int. Conf. Telecommun.*, May 2010, pp. 147–152.

[195] F. Bhatti, G. Rowe, and K. Sowerby, "Spectrum sensing using feature vectors," in *IEEE Int. Conf. Commun. Systems*, Nov. 2012, pp. 448–452.

[196] J. Palicot and C. Roland, "A new concept for wireless reconfigurable receivers," *IEEE Commun. Magazine*, vol. 41, no. 7, pp. 124–132, July 2003.

[197] R. Hachemani, J. Palicot, and C. Moy, "A new standard recognition sensor for cognitive radio terminals," in *The European Signal Process. Conf.*, Sept. 2007, pp. 856–860.

[198] P. Zhang, R. Qiu, and N. Guo, "Demonstration of spectrum sensing with blindly learned features," *IEEE Commun. Letters*, vol. 15, no. 5, pp. 548–550, May 2011.

[199] R. Sharma and J. Wallace, "Improved spectrum sensing by utilizing signal autocorrelation," in *IEEE 69th Veh. Technol. Conf.*, April 2009, pp. 1–5.

[200] R. Sharma and J. Wallace, "Improved autocorrelation-based sensing using correlation distribution information," in *Int. ITG Workshop on Smart Antennas (WSA)*, Feb 2010, pp. 335–341.

[201] M. Naraghi-Pour and T. Ikuma, "Autocorrelation-based spectrum sensing for cognitive radios," *IEEE Trans. Vehicular Technol.*, vol. 59, no. 2, pp. 718–733, Feb 2010.

[202] Y. Zeng and Y.-C. Liang, "Spectrum-sensing algorithms for cognitive radio based on statistical covariances," *IEEE Trans. Vehicular Technol.*, vol. 58, no. 4, pp. 1804–1815, May 2009.

[203] M. Jin, Y. Li, and H.-G. Ryu, "On the performance of covariance based spectrum sensing for cognitive radio," *IEEE Trans. Signal Process.*, vol. 60, no. 7, pp. 3670–3682, July 2012.

[204] A. Kortun, T. Ratnarajah, M. Sellathurai, C. Zhong, and C. Papadias, "On the performance of eigenvalue-based cooperative spectrum sensing for cognitive radio," *IEEE J. Sel. Topics in Signal Process.*, vol. 5, no. 1, pp. 49–55, Feb 2011.

[205] W. Zhang, G. Abreu, M. Inamori, and Y. Sanada, "Spectrum sensing algorithms via finite random matrices," *IEEE Trans. Commun.*, vol. 60, no. 1, pp. 164–175, January 2012.

[206] I. Akyildiz, B. Lo, and R. Balakrishnan, "Cooperative spectrum sensing in cognitive radio networks: A survey," *Physical Communication*, vol. 4, no. 2011, pp. 40–62, 2011.

[207] X. Chen, H. Chen and W. Meng, "Cooperative communications for cognitive radio networks-from theory to applications," *IEEE Comm. Surveys & Tutorials*, no. 99, pp. 1–13, 2014.

[208] Z. Quan, S. Cui, H. Poor, and A. Sayed, "Collaborative wideband sensing for cognitive radios," *IEEE Signal Process. Mag.*, vol. 25, no. 6, pp. 60–73, Nov. 2008.

[209] C. Sun, W. Zhang, and K. Letaief, "Cooperative spectrum sensing for cognitive radios under bandwidth constraints," in *IEEE WCNC*, March 2007, pp. 1–5.

[210] Z. Tian and G. Giannakis, "A wavelet approach to wideband spectrum sensing for cognitive radios," in *Int. Conf. CROWNCOM*, June 2006, pp. 1–5.

[211] Z. Quan, S. Cui, A. Sayed, and H. Poor, "Optimal multiband joint detection for spectrum sensing in cognitive radio networks," *IEEE Trans. Signal Process.*, vol. 57, no. 3, pp. 1128–1140, March 2009.

[212] Z. Quan, S. Cui, A. Sayed, and H. Poor, "Spatial-spectral joint detection for wideband spectrum sensing in cognitive radio networks," in *IEEE ICASSP*, March 2008, pp. 2793–2796.

[213] M. Davenport, J. Laska, J. Treichler, and R. Baraniuk, "The pros and cons of compressive sensing for wideband signal acquisition: Noise folding versus dynamic range," *IEEE Trans. Signal Process.*, vol. 60, no. 9, pp. 4628–4642, Sept 2012.

[214] S. Atapattu, C. Tellambura, and H. Jiang, "Performance of an energy detector over channels with both multipath fading and shadowing," *IEEE Trans. Wireless Commun.*, vol. 9, no. 12, pp. 3662 –3670, Dec. 2010.

[215] T. Shehata and M. El-Tanany, "A novel adaptive structure of the energy detector applied to cognitive radio networks," in *11th Canadian Workshop on Info. Th.*, May 2009, pp. 95–98.

[216] X. Ling and et al, "Adaptive threshold control for energy detection based spectrum sensing in cognitive radios," *IEEE Wireless Commun. Letters*, vol. 1, no. 5, pp. 448–451, October 2012.

[217] R. Tandra and A. Sahai, "Noise calibration, delay coherence and SNR walls for signal detection," in *3rd IEEE Int. Symp. DySPAN*, Oct. 2008, pp. 1–11.

[218] T. Bogale and L. Vandendorpe, "Max-min SNR signal energy based spectrum sensing algorithms for cognitive radio networks with noise variance uncertainty," *IEEE Trans. Wireless Commun.*, vol. 13, no. 1, pp. 280–290, January 2014.

[219] H. Farag and E. Mohamed, "Improved cognitive radio energy detection algorithm based upon noise uncertainty estimation," in *31st National Radio Science Conf. (NRSC)*, April 2014, pp. 107–115.

[220] D. Joshi, D. Popescu, and O. Dobre, "Adaptive spectrum sensing with noise variance estimation for dynamic cognitive radio systems," in *44th Annual Conf. Info. Sciences and Systems*, March 2010, pp. 1–5.

[221] C. Lim, "Adaptive energy detection for spectrum sensing in unknown white Gaussian noise," *IET Commun.*, vol. 6, no. 13, pp. 1884–1889, Sept. 2012.

[222] A. Mariani, A. Giorgetti, and M. Chiani, "Effects of noise power estimation on energy detection for cognitive radio applications," *IEEE Trans. Commun.*, vol. 59, no. 12, pp. 3410–3420, Dec. 2011.

[223] S. Maleki, A. Pandharipande, and G. Leus, "Two-stage spectrum sensing for cognitive radios," in *IEEE ICASSP*, March 2010, pp. 2946–2949.

[224] Z. Khalaf, A. Nafkha, J. Palicot, and M. Ghazzi, "Low complexity enhanced hybrid spectrum sensing architectures for cognitive radio equipment," *Int. J. Advances in Telecommun.*, vol. 3, no. 3-4, pp. 214–227, 2010.

[225] F. Penna, R. Garello, D. Figlioli, and M. Spirito, "Exact non-asymptotic threshold for eigenvalue-based spectrum sensing," in *4th Int. Conf. CROWNCOM*, June 2009, pp. 1 –5.

[226] M. Haddad, A. M. Hayar, M. H. Fetoui, and M. Debbah, "Cognitive radio sensing information-theoretic criteria based," in *2nd Int. Conf. CROWNCOM*, Aug. 2007, pp. 241–244.

[227] G. de Abreu, W. Zhang, and Y. Sanada, "Spectrum sensing algorithms via finite random matrix theory," in *IEEE ICC*, June 2011, pp. 1–5.

[228] L. Wang, B. Zheng, J. Cui, and W. Yue, "Spectrum sensing using non-asymptotic behavior of eigenvalues," in *Int. Conf. Wireless Communications and Signal Process.*, Nov. 2011, pp. 1–5.

[229] K. Cao and Z. Yang, "A novel cooperative spectrum sensing algorithm based on random matrix theory," in *6th Int. Conf. Wireless Communications Networking and Mobile Computing (WiCom)*, Sept. 2010, pp. 1–4.

[230] C. Zhong, M. McKay, T. Ratnarajah, and K.-K. Wong, "Distribution of the Demmel condition number of wishart matrices," *IEEE Trans. Commun.*, vol. 59, no. 5, pp. 1309–1320, May 2011.

[231] A. Kortun, M. Sellathurai, T. Ratnarajah, and C. Zhong, "Distribution of the ratio of the largest eigenvalue to the trace of complex wishart matrices," *IEEE Trans. Signal Process.*, vol. 60, no. 10, pp. 5527–5532, Oct. 2012.

[232] L. Wang, B. Zheng, J. Cui, S. Tang, and H. Dou, "Cooperative spectrum sensing using free probability theory," in *IEEE Global Telecommun. Conf.*, Dec. 2009, pp. 1–5.

[233] L. Wang, B. Zheng, J. Cui, and Q. Meng, "Cooperative MIMO spectrum sensing using free probability theory," in *5th Int. Conf. WiCom*, Sept. 2009, pp. 1–4.

[234] S. Chatzinotas, S. K. Sharma, and B. Ottersten, "Asymptotic analysis of eigenvalue-based blind spectrum sensing techniques," in *IEEE ICASSP*, May 2013, pp. 4464–4468.

[235] S. Kim, J. Lee, H. Wang, and D. Hong, "Sensing performance of energy detector with correlated multiple antennas," *IEEE Signal Process. Letters*, vol. 16, no. 8, pp. 671–674, Aug. 2009.

[236] V. Banjade, N. Rajatheva, and C. Tellambura, "Performance analysis of energy detection with multiple correlated antenna cognitive radio in Nakagami-m fading," *IEEE Commun. Letters*, vol. 16, no. 4, pp. 502–505, April 2012.

[237] B. Nadler, F. Penna, and R. Garello, "Performance of eigenvalue-based signal detectors with known and unknown noise level," in *IEEE Int. Conf. Commun.*, 2011, pp. 1–5.

[238] B. Van Veen and K. Buckley, "Beamforming: a versatile approach to spatial filtering," *IEEE ASSP Magazine*, vol. 5, no. 2, pp. 4–24, April 1988.

[239] H. Krim and M. Viberg, "Two decades of array signal processing research: the parametric approach," *IEEE Signal Process. Magazine*, vol. 13, no. 4, pp. 67–94, July 1996.

[240] A. Gershman, N. Sidiropoulos, S. Shahbazpanahi, M. Bengtsson, and B. Ottersten, "Convex optimization-based beamforming," *IEEE Signal Processing Mag.*, vol. 27, no. 3, pp. 62–75, 2010.

[241] H. Cox, R. Zeskind, and M. Owen, "Robust adaptive beamforming," *IEEE Trans. Acoustics, Speech and Signal Process.*, vol. 35, no. 10, pp. 1365–1376, 1987.

[242] R. Lorenz and S. Boyd, "Robust minimum variance beamforming," *IEEE Trans. Signal Process.*, vol. 53, no. 5, pp. 1684–1696, 2005.

[243] S.-J. Kim, A. Magnani, A. Mutapcic, S. Boyd, and Z.-Q. Luo, "Robust beamforming via worst-case sinr maximization," *IEEE Trans. Signal Process.*, vol. 56, no. 4, pp. 1539–1547, 2008.

[244] S. Vorobyov, Y. Rong, and A. Gershman, "Robust adaptive beamforming using probability-constrained optimization," in *IEEE/SP 13th Workshop on Statistical Signal Process.*, 2005, pp. 934–939.

[245] S. Vorobyov, H. Chen, and A. Gershman, "On the relationship between robust minimum variance beamformers with probabilistic and worst-case distortionless response constraints," *IEEE Trans. Signal Process.*, vol. 56, no. 11, pp. 5719–5724, 2008.

[246] M. Kobayashi and G. Caire, "A practical approach for weighted rate sum maximization in MIMO-OFDM broadcast channels," in *Conference Record of the Forty-First Asilomar Conf. on Signals, Systems and Computers*, Nov 2007, pp. 1591–1595.

[247] H. Park, S.-H. Park, J.-S. Kim, and I. Lee, "SINR balancing techniques in coordinated multi-cell downlink systems," *IEEE Trans. Wireless Commun.*, vol. 12, no. 2, pp. 626–635, February 2013.

[248] R. Masmoudi, E. Belmega, I. Fijalkow, and N. Sellami, "A closed-form solution to the power minimization problem over two orthogonal frequency bands under qos and cognitive radio interference constraints," in *Int. Symp. DySPAN*, Oct. 2012, pp. 212–222.

[249] S. He, Y. Huang, S. Jin, F. Yu, and L. Yang, "Max-min energy efficient beamforming for multicell multiuser joint transmission systems," *IEEE Commun. Letters*, vol. 17, no. 10, pp. 1956–1959, Oct. 2013.

[250] S. Yiu, M. Vu, and V. Tarokh, "Interference and noise reduction by beamforming in cognitive networks," *IEEE Trans. Commun.*, vol. 57, no. 10, pp. 3144–3153, 2009.

[251] F. Sun and E. De Carvalho, "A leakage-based MMSE beamforming design for a MIMO interference channel," *IEEE Signal Process. Letters*, vol. 19, no. 6, pp. 368–371, June 2012.

[252] L. Zhang, Y.-C. Liang, Y. Xin, and H. Poor, "Robust cognitive beamforming with partial channel state information," *IEEE Trans. Wireless Commun.*, vol. 8, no. 8, pp. 4143–4153, August 2009.

[253] A. Tajer, N. Prasad, and X. Wang, "Beamforming and rate allocation in MISO cognitive radio networks," *IEEE Trans. Signal Process.*, vol. 58, no. 1, pp. 362–377, 2010.

[254] K. Cumanan, L. Musavian, S. Lambotharan, and A. Gershman, "SINR balancing technique for downlink beamforming in cognitive radio networks," *IEEE Signal Processing Letters*, vol. 17, no. 2, pp. 133–136, 2010.

[255] K. Phan, S. Vorobyov, N. Sidiropoulos, and C. Tellambura, "Spectrum sharing in wireless networks via qos-aware secondary multicast beamforming," *IEEE Trans. Signal Process.*, vol. 57, no. 6, pp. 2323–2335, 2009.

[256] E. Gharavol, Y.-C. Liang, and K. Mouthaan, "Robust downlink beamforming in multiuser MISO cognitive radio networks with imperfect channel-state information," *IEEE Trans. Veh. Technol.*, vol. 59, no. 6, pp. 2852–2860, July 2010.

[257] H. Du, T. Ratnarajah, M. Pesavento, and C. Papadias, "Joint transceiver beamforming in MIMO cognitive radio network via second-order cone programming," *IEEE Trans. Signal Process.*, vol. 60, no. 2, pp. 781–792, 2012.

[258] K. Hamdi, W. Zhang, and K. Letaief, "Joint beamforming and scheduling in cognitive radio networks," in *IEEE GLOBECOM*, 2007, pp. 2977–2981.

[259] L. Zhang, Y.-C. Liang, and Y. Xin, "Joint beamforming and power allocation for multiple access channels in cognitive radio networks," *IEEE J. Sel. Areas in Commun.*, vol. 26, no. 1, pp. 38–51, 2008.

[260] S. Yiu, M. Vu, and V. Tarokh, "Interference reduction by beamforming in cognitive networks," in *IEEE GLOBECOM*, 2008, pp. 1–6.

[261] M. Pesavento, D. Ciochina, and A. Gershman, "Iterative dual downlink beamforming for cognitive radio networks," in *Int. Conf. CROWNCOM*, 2010, pp. 1–5.

[262] A. Zarrebini-Esfahani, T. A. Le, and M. R. Nakhai, "A power-efficient coverage scheme for cell-edge users using cognitive beamforming," in *IEEE PIMRC*, 2013, pp. 3028–3032.

[263] R. Zhang and Y.-C. Liang, "Exploiting multi-antennas for opportunistic spectrum sharing in cognitive radio networks," *IEEE J. Sel. Topics Signal Process.*, vol. 2, no. 1, pp. 88–102, 2008.

[264] R. Zhang, F. Gao, and Y.-C. Liang, "Cognitive beamforming made practical: Effective interference channel and learning-throughput tradeoff," *IEEE Trans. Commun.*, vol. 58, no. 2, pp. 706–718, 2010.

[265] W. Zong, S. Shao, Q. Meng, and W. Zhu, "Joint user scheduling and beamforming for underlay cognitive radio systems," in *15th Asia-Pacific Conf. on Commun.*, 2009, pp. 99–103.

[266] A. Massaoudi, N. Sellami, and M. Siala, "A two-phase scheduling scheme for cognitive radio networks based on opportunistic beamforming," in *IEEE VTC Spring*, 2013, pp. 1–5.

[267] A. T. Hoang, Y.-C. Liang, and M. Islam, "Power control and channel allocation in cognitive radio networks with primary users' cooperation," *IEEE Trans. Mobile Computing*, vol. 9, no. 3, pp. 348–360, 2010.

[268] W. Su, J. Matyjas, and S. Batalama, "Active cooperation between primary users and cognitive radio users in heterogeneous ad-hoc networks," *IEEE Trans. Signal Process.*, vol. 60, no. 4, pp. 1796–1805, 2012.

[269] J. Liu, W. Chen, Z. Cao, and Y. Zhang, "An opportunistic scheduling scheme for cognitive wireless networks with cooperative beamforming," in *IEEE GLOBECOM*, 2010, pp. 1–5.

[270] R. Mudumbai, D. Brown, U. Madhow, and H. Poor, "Distributed transmit beamforming: challenges and recent progress," *IEEE Commun. Mag.*, vol. 47, no. 2, pp. 102–110, 2009.

[271] Y. Deng, A. Burr, D. Pearce, and D. Grace, "Distributed beamforming for cognitive radio networks," in *3rd Int. Conf. Commun. and Networking in China*, 2008, pp. 1206–1210.

[272] A. Minturn, D. Vernekar, Y. Yang, and H. Sharif, "Distributed beamforming with imperfect phase synchronization for cognitive radio networks," in *IEEE ICC*, 2013, pp. 4936–4940.

[273] G. Zheng, S. Ma, K.-K. Wong, and T.-S. Ng, "Robust beamforming in cognitive radio," *IEEE Trans. Wireless Commun.*, vol. 9, no. 2, pp. 570–576, 2010.

[274] G. Zheng, K.-K. Wong, and B. Ottersten, "Robust cognitive beamforming with bounded channel uncertainties," *IEEE Trans. Signal Process.*, vol. 57, no. 12, pp. 4871–4881, Dec. 2009.

[275] L. Zhang, Y.-C. Liang, Y. Xin, and H. Poor, "Robust cognitive beamforming with partial channel state information," *IEEE Trans. Wireless Commun.*, vol. 8, no. 8, pp. 4143–4153, 2009.

[276] I. Wajid, M. Pesavento, Y. Eldar, and A. Gershman, "Robust downlink beamforming for cognitive radio networks," in *IEEE GLOBECOM*, 2010, pp. 1–5.

[277] A. Lozano, "Long-term transmit beamforming for wireless multicasting," in *IEEE ICASSP*, vol. 3, 2007, pp. 417–420.

[278] A. Phan, H. Tuan, H. Kha, and D. T. Ngo, "A reverse convex programming for beamforming in cognitive multicast transmission," in *Third Int. Conf. Commun. and Electronics (ICCE)*, 2010, pp. 211–215.

[279] Y. Huang, Q. Li, W.-K. Ma, and S. Zhang, "Robust multicast beamforming for spectrum sharing-based cognitive radios," *IEEE Trans. Signal Process.*, vol. 60, no. 1, pp. 527–533, 2012.

[280] M. Beko, "Efficient beamforming in cognitive radio multicast transmission," *IEEE Trans. Wireless Commun.*, vol. 11, no. 11, pp. 4108–4117, 2012.

[281] A. H. Phan, H. D. Tuan, H. H. Kha, and D. T. Ngo, "Nonsmooth optimization for efficient beamforming in cognitive radio multicast transmission," *IEEE Trans. Signal Process.*, vol. 60, no. 6, pp. 2941–2951, 2012.

[282] S. A. Jafar, "Interference alignment- a new look at signal dimentions in a communication network," *Foundations and Trends in Communication and Info. Th.*, vol. 7, no. 1, pp. 1–134, 2010.

[283] E. Telatar, "Capacity of multi-antenna Gaussian channels," *European Trans. on Telecomm. (ETT)*, vol. 10, no. 6, pp. 585–596, Nov. 1999.

[284] C. Vaze and M. Varanasi, "The degree-of-freedom regions of MIMO broadcast, interference, and cognitive radio channels with no CSIT," *IEEE Trans. Info. Th.*, vol. 58, no. 8, pp. 5354–5374, Aug. 2012.

[285] B. C. Jung, D. Park, and W.-Y. Shin, "Opportunistic interference mitigation achieves optimal degrees-of-freedom in wireless multi-cell uplink networks," *IEEE Trans. Commun.*, vol. 60, no. 7, pp. 1935–1944, July 2012.

[286] W. Shin, N. Lee, J.-B. Lim, C. Shin, and K. Jang, "On the design of interference alignment scheme for two-cell MIMO interfering broadcast channels," *IEEE Trans. Wireless Commun.*, vol. 10, no. 2, pp. 437–442, Feb. 2011.

[287] B. Koo and D. Park, "Interference alignment with cooperative primary receiver in cognitive networks," *IEEE Commun. Letters*, vol. 16, no. 7, pp. 1072–1075, 2012.

[288] O. El Ayach, S. Peters, and J. Heath, R.W., "The practical challenges of interference alignment," *IEEE Wireless Commun.*, vol. 20, no. 1, pp. 35–42, 2013.

[289] V. Cadambe and S. Jafar, "Interference alignment and degrees of freedom of the K-user interference channel," *IEEE Trans. Info. Th.*, vol. 54, no. 8, pp. 3425 –3441, Aug. 2008.

[290] S. Jafar and S. Shamai, "Degrees of freedom region of the MIMO X channel," *IEEE Trans. Info. Th.*, vol. 54, no. 1, pp. 151 –170, Jan. 2008.

[291] H. Li, "Linear interference alignment based on signal and interference space ranks," in *4th IET Int. Conf. on Wireless, Mobile Multimedia Networks*, 2011, pp. 169–172.

[292] M. Razaviyayn, M. Sanjabi, and Z.-Q. Luo, "Linear transceiver design for interference alignment: Complexity and computation," *IEEE Trans. Info. Th.*, vol. 58, no. 5, pp. 2896–2910, 2012.

[293] C. Wang, T. Gou, and S. Jafar, "Subspace alignment chains and the degrees of freedom of the three-user MIMO interference channel," in *IEEE ISIT*, 2012, pp. 2471–2475.

[294] K. Gomadam, V. Cadambe, and S. Jafar, "A distributed numerical approach to interference alignment and applications to wireless interference networks," *IEEE Trans. Info. Th.*, vol. 57, no. 6, 2011.

[295] S. Jafar, "Exploiting channel correlations - simple interference alignment schemes with no CSIT," in *IEEE Globecom*, 2010, pp. 1–5.

[296] T. Gou, C. Wang, and S. Jafar, "Aiming perfectly in the dark-blind interference alignment through staggered antenna switching," *IEEE Trans. Signal Process.*, vol. 59, no. 6, pp. 2734–2744, 2011.

[297] B. Nazer, M. Gastpar, S. Jafar, and S. Vishwanath, "Ergodic interference alignment," *IEEE Trans. Info. Th.*, vol. 58, no. 10, pp. 6355–6371, 2012.

[298] M. Kang and W. Choi, "Ergodic interference alignment with delayed feedback," *IEEE Signal Processing Letters*, vol. 20, no. 5, pp. 511–514, 2013.

[299] Y. Lejosne, D. Slock, and Y. Yuan-Wu, "Degrees of freedom in the MISO BC with delayed-CSIT and finite coherence time: Optimization of the number of users," in *6th Int. Conf. on NetGCoop*, 2012, pp. 80–85.

[300] G. Bresler, A. Parekh, and D. Tse, "The approximate capacity of the many-to-one and one-to-many Gaussian interference channels," *IEEE Trans. Info. Th.*, vol. 56, no. 9, pp. 4566–4592, 2010.

[301] O. Ordentlich and U. Erez, "On the robustness of lattice interference alignment," *IEEE Trans. Info. Th.*, vol. 59, no. 5, pp. 2735–2759, 2013.

[302] L. Yang and W. Zhang, "Asymmetric interference alignment and cancelation for 3-user MIMO interference channels," in *IEEE ICC*, 2012, pp. 2260–2264.

[303] T. M. Nguyen, T. Quek, and H. Shin, "Opportunistic interference alignment in MIMO femtocell networks," in *IEEE ISIT*, 2012, pp. 2631–2635.

[304] S. Perlaza, M. Debbah, S. Lasaulce, and J.-M. Chaufray, "Opportunistic interference alignment in MIMO interference channels," in *IEEE PIMRC*, 2008, pp. 1–5.

[305] S. Jafar, V. Cadambe, and C. Wang, "Interference alignment with asymmetric complex signaling," in *47th Annual Allerton Conf. on Commun., Control, and Computing*, 2009, pp. 991–996.

[306] S. Chatzinotas and B. Ottersten, "Cognitive interference alignment between small cells and a macrocell," in *Int. Conf. Telecommun. (ICT)*, April 2012, pp. 1–6.

[307] M. Maso, L. S. Cardoso, M. Debbah, and L. Vangelista, "Orthogonal precoder for lte small-cells networks," *IEEE J. on Sel. Areas Commun.*, 2011.

[308] L. Huang, G. Zhu, and X. Du, "Cognitive femtocell networks: an opportunistic spectrum access for future indoor wireless coverage," *IEEE Wireless Commun.*, vol. 20, no. 2, pp. 44–51, 2013.

[309] B. Guler and A. Yener, "Interference alignment for cooperative MIMO femtocell networks," in *IEEE GLOBECOM*, 2011, pp. 1–5.

[310] F. Pantisano, M. Bennis, W. Saad, M. Debbah, and M. Latva-aho, "Interference alignment for cooperative femtocell networks: A game-theoretic approach," *IEEE Trans. Mobile Computing*, , no. 99, 2012.

[311] L. B. Le and E. Hossain, "Resource allocation for spectrum underlay in cognitive radio networks," *IEEE Trans. Wireless Commun.*, vol. 7, no. 12, pp. 5306–5315, Dec. 2008.

[312] R. Zhang, Y.-C. Liang, and S. Cui, "Dynamic resource allocation in cognitive radio networks," *IEEE Signal Process. Magazine*, vol. 27, no. 3, pp. 102–114, May 2010.

[313] C.-H. Chen and C.-L. Wang, "Power allocation for OFDM-based cognitive radio systems under primary user activity," in *IEEE 71st VTC Spring*, May 2010, pp. 1–5.

[314] C.-H. Chen, C.-L. Wang, and C.-T. Chen, "A resource allocation scheme for cooperative multiuser OFDM-based cognitive radio systems," *IEEE Trans. Commun.*, vol. 59, no. 11, pp. 3204–3215, November 2011.

[315] S. Ekin, M. Abdallah, K. Qaraqe, and E. Serpedin, "Random subcarrier allocation in OFDM-based cognitive radio networks," *IEEE Trans. Signal Process.*, vol. 60, no. 9, pp. 4758–4774, Sept 2012.

[316] D. Niyato and E. Hossain, "Radio resource management games in wireless networks: an approach to bandwidth allocation and admission control for polling service in IEEE 802.16," *IEEE Wireless Commun.*, vol. 14, no. 1, pp. 27–35, Feb 2007.

[317] C.-H. Ko and H.-Y. Wei, "Game theoretical resource allocation for inter-BS coexistence in IEEE 802.22," *IEEE Trans. Veh. Technol.*, vol. 59, no. 4, pp. 1729–1744, May 2010.

[318] G. Zhang, K. Yang, P. Liu, E. Ding, and Y. Zhong, "Joint channel bandwidth and power allocation game for selfish cooperative relaying networks," *IEEE Trans. Veh. Technol.*, vol. 61, no. 9, pp. 4142–4156, Nov 2012.

[319] Y. Zhang, D. Niyato, P. Wang, and E. Hossain, "Auction-based resource allocation in cognitive radio systems," *IEEE Commun. Magazine*, vol. 50, no. 11, pp. 108–120, November 2012.

[320] A. De Domenico, E. Strinati, and M. Di Benedetto, "A survey on mac strategies for cognitive radio networks," *IEEE Commun. Surveys and Tutorials*, vol. 14, no. 1, pp. 21–44, First 2012.

[321] V. Swarup, V. Ribeiro, and A. Gupta, "A comparative study of scheduling schemes for cognitive radio networks: A quality of service perspective," in *Fifth Int. Conf. Commun. Systems and Networks*, Jan 2013, pp. 1–6.

[322] B. Wang and D. Zhao, "Scheduling for long term proportional fairness in a cognitive wireless network with spectrum underlay," *IEEE Trans. Wireless Commun.*, vol. 9, no. 3, pp. 1150–1158, March 2010.

[323] ITU, "Determination of the coordination area around an earth station in the frequency bands between 100 MHz and 105 GHz," 2000, ITU-R SM.1448.

[324] B. Evans and et al, "Deliverable D3.2: Performance evaluation of existing cognitive techniques in satellite context," Available at <http://www.ict-corasat.eu>, 2014.

[325] V. Deslandes, J. Tronc, and A.-L. Beylot, "Analysis of interference issues in integrated satellite and terrestrial mobile systems," in *5th ASMS conf. and 11th SPSC workshop*, Sept. 2010, pp. 256 –261.

[326] Z. Wei, Z. Feng, Q. Zhang, and W. Li, "Three regions for space-time spectrum sensing and access in cognitive radio networks," in *IEEE Globecom Conf.*, Dec. 2010, pp. 1 –6.

[327] J. Wang, M. Ghosh, and K. Challapali, "Emerging cognitive radio applications: A survey," *IEEE Commun. Magazine*, vol. 49, no. 3, pp. 74–81, March 2011.

[328] F. P. Group, "Rethinking spectrum scarcity: Database driven cognitive radio," A Fair point Group White Paper, Tech. Rep., Sept. 2010.

[329] D. Lekomtcev and R. Marsalek, "Comparison of 802.11af and 802.22 standards – physical layer and cognitive functionality," *Elektrorevue J.*, vol. 3, no. 2, pp. 12–18, 2012.

[330] Ecma, "Mac and phy for operation in tv white space," online, June 2012, available online: <http://www.ecma-international.org/publications/files/ECMA-ST/ECMA-392.pdf>, Access date: 06/10/2014.

[331] M. Murroni and et al, "IEEE 1900.6: spectrum sensing interfaces and data structures for dynamic spectrum access and other advanced radio communication systems standard: technical aspects and future outlook," *IEEE Commun. Magazine*, vol. 49, no. 12, pp. 118–127, December 2011.

[332] "IEEE standard for spectrum sensing interfaces and data structures for dynamic spectrum access and other advanced radio communication systems - amendment 1: Procedures, protocols, and data archive enhanced interfaces," *P1900.6a/D0.7*, June 2014.

[333] K. Liolis and et al, "Deliverable D2.2: Regulatory, standardization and technology framework," Available at <http://www.ict-corasat.eu>, 2013.

[334] J. Sydor, "Coral: A wifi based cognitive radio development platform," in *Int. Symp. Wireless Communication Systems (ISWCS)*, Sept 2010, pp. 1022–1025.

[335] K. Amiri and et al, "Warp, a unified wireless network testbed for education and research," in *IEEE Int. Conf. Microelectronic Systems Education*, June 2007, pp. 53–54.

[336] S. Zarrin and T. J. Lim, "Throughput-sensing tradeoff of cognitive radio networks based on quickest sensing," in *IEEE ICC*, 2011, pp. 1–5.

[337] M. Cardenas-Juarez and M. Ghogho, "Spectrum sensing and throughput trade-off in cognitive radio under outage constraints over nakagami fading," *IEEE Commun. Letters*, vol. 15, no. 10, pp. 1110–1113, 2011.

[338] S. Stotas and A. Nallanathan, "On the throughput and spectrum sensing enhancement of opportunistic spectrum access cognitive radio networks," *IEEE Trans. Wireless Commun.*, vol. 11, no. 1, pp. 97–107, 2012.

[339] W. Cheng, X. Zhang, and H. Zhang, "Full duplex spectrum sensing in non-time-slotted cognitive radio networks," in *IEEE Military Commun. Conf.*, 2011, pp. 1029–1034.

[340] E. Ahmed, A. Eltawil, and A. Sabharwal, "Rate gain region and design tradeoffs for full-duplex wireless communications," *IEEE Trans. Wireless Commun.*, vol. 12, no. 7, pp. 3556–3565, 2013.

[341] M. Duarte, C. Dick, and A. Sabharwal, "Experiment-driven characterization of full-duplex wireless systems," *IEEE Trans. Wireless Commun.*, vol. 11, no. 12, pp. 4296–4307, 2012.

[342] J. Vartiainen, H. Saarnisaari, J. Lehtomaki, and M. Juntti, "A blind signal localization and SNR estimation method," in *IEEE Military Commun. Conf.*, 2006, pp. 1–7.

[343] A. Ghasemi and E. Sousa, "Interference aggregation in spectrum-sensing cognitive wireless networks," *IEEE J. Sel. Topics Signal Process.*, vol. 2, no. 1, pp. 41–56, Feb. 2008.

[344] M. Grimm, R. K. Sharma, M. Hein, and R. Thoma, "Non-linearly induced interference and its mitigation in cognitive wideband receivers," *18th European Wireless Conf.*, pp. 1–6, April 2012.

[345] R. Janaswamy, "Effect of element mutual coupling on the capacity of fixed length linear arrays," *IEEE Antennas and Wireless Propag. Letters*, vol. 1, no. 1, pp. 157–160, 2002.

[346] A. Vasilopoulos, G. Vitzilaios, G. Theodoratos, and Y. Papananos, "A low-power wideband reconfigurable integrated active RC filter with 73 dB SFDR," *IEEE J. Solid-State Circuits*, vol. 41, no. 9, pp. 1997–2008, Sept. 2006.

[347] H. Shin and Y. Kim, "A CMOS active RC low-pass filter with simultaneously tunable high and low cutoff frequencies for IEEE 802.22 applications," *IEEE Trans. Circuits and Systems II: Express Briefs*, vol. 57, no. 2, pp. 85–89, Feb. 2010.

[348] S. Haykin, *Communication Systems*, 4th ed. John Wiley & Sons, Inc.

[349] O. Tirkkonen and L. Wei, *Foundation of Cognitive Radio Systems: Exact and asymptotic analysis of largest eigenvalue based spectrum sensing*. InTech, 2012, no. 978-953-51-0268-7, ch. 1.

[350] D. Voiculescu, "Multiplication of certain non-commuting random variables," *J. Operator Theory*, vol. 18, pp. 223–235, 1987.

[351] W. Z. Zhigang Bao, Guangming Pan, "Universality for the largest eigenvalue of a class of sample covariance matrices," online, July 2013, <http://arxiv.org/abs/1304.5690v4>.

[352] I. M. Johnstone, "On the distribution of the largest eigenvalue in principal component analysis," *Annals of Statistics*, vol. 29, no. 2, pp. 295–327, 2001.

[353] C. Tracy and H. Widom, "On the distribution of the largest eigenvalue in principal component analysis," *Comm. Math. Phys.*, vol. 177, pp. 727–754, 1996.

[354] N. E. Karoui, "Tracy-widom limit for the largest eigenvalue of a large class of complex sample covariance matrices," *Ann. Probab.*, vol. 35, no. 2, pp. 663–714, 2007.

[355] Y.-C. Chen and Y.-T. Su, "Mimo channel estimation in correlated fading environments," *IEEE Trans. Wireless Commun.*, vol. 9, no. 3, pp. 1108–1119, 2010.

[356] D. Voiculescu, "Addition of certain non-commuting random variables," *J. Funct. Analysis*, vol. 66, pp. 323–346, 1986.

[357] S. J. Shellhammer, "Spectrum sensing in IEEE 802.22," in *IAPR Workshop Cognitive Info. Processing*, June 2008.

[358] M.-H. Yoon, Y. Shin, H.-K. Ryu, and J.-M. Woo, "Ultra-wideband loop antenna," *Electronics Letters*, vol. 46, no. 18, pp. 1249–1251, September 2010.

[359] Z.-C. Hao and J.-S. Hong, "Highly selective ultra wideband bandpass filters with quasi-elliptic function response," *IET Microwaves, Antennas & Propag.*, vol. 5, no. 9, pp. 1103–1108, June 2011.

[360] J. Laska and et al, "Compressive sensing for dynamic spectrum access networks: Techniques and tradeoffs," in *IEEE Symp. New Frontiers in DySPAN*, May 2011, pp. 156–163.

[361] B. Farhang-Boroujeny, "OFDM versus filter bank multicarrier," *IEEE Signal Process. Magazine*, vol. 28, no. 3, pp. 92–112, May 2011.

[362] D. Wasden, H. Moradi, and B. Farhang-Boroujeny, "Design and implementation of an underlay control channel for cognitive radios," *IEEE J. Sel. Areas Commun.*, vol. 30, no. 10, pp. 1875–1889, Nov. 2012.

[363] R. Mahesh, A. Vinod, C. Moy, and J. Palicot, "A low complexity reconfigurable filter bank architecture for spectrum sensing in cognitive radios," in *Int. Conf. CROWNCOM*, May 2008, pp. 1–6.

[364] A. Sahin, I. Güvenç, and H. Arslan, "A survey on prototype filter design for filter bank based multicarrier communications," *CoRR*, vol. abs/1212.3374, 2012.

[365] E. J. Candes, "Compressive sampling," in *Proc. Int. Congress of Mathematicians*, vol. 3, 2006, pp. 1433–1452.

[366] J. Tropp and A. Gilbert, "Signal recovery from random measurements via orthogonal matching pursuit," *IEEE Trans. Info. Th.*, vol. 53, no. 12, pp. 4655–4666, Dec. 2007.

[367] W. Dai and O. Milenkovic, "Subspace pursuit for compressive sensing signal reconstruction," *IEEE Trans. Info. Th.*, vol. 55, no. 5, pp. 2230–2249, May 2009.

[368] Z. Zeinalkhani and A. Banihashemi, "Iterative recovery algorithms for compressed sensing of wideband block sparse spectrums," in *IEEE ICC*, June 2012, pp. 1630–1634.

[369] S. Mistry and V. Sharma, "New algorithms for wideband spectrum sensing via compressive sensing," in *IEEE ICC*, June 2013, pp. 2595–2600.

[370] B. Rao, S. Chatterjee, and B. Ottersten, "Detection of sparse random signals using compressive measurements," in *IEEE ICASSP*, March 2012, pp. 3257–3260.

[371] A. Tulino, G. Caire, S. Verdu, and S. Shamai, "Support recovery with sparsely sampled free random matrices," *IEEE Trans. Info. Th.*, vol. 59, no. 7, pp. 4243–4271, July 2013.

[372] Y. Eldar, "Compressed sensing of analog signals in shift-invariant spaces," *IEEE Trans. Signal Process.*, vol. 57, no. 8, pp. 2986–2997, Aug. 2009.

[373] M. Mishali and Y. Eldar, "From theory to practice: Sub-nyquist sampling of sparse wideband analog signals," *IEEE J. Sel. Topics Signal Process.*, vol. 4, no. 2, pp. 375–391, April 2010.

[374] D. Malioutov, S. Sanghavi, and A. Willsky, "Compressed sensing with sequential observations," in *IEEE ICASSP*, March 2008, pp. 3357–3360.

[375] D. Malioutov, M. Cetin, and A. Willsky, "A sparse signal reconstruction perspective for source localization with sensor arrays," *IEEE Trans. Signal Process.*, vol. 53, no. 8, pp. 3010–3022, 2005.

[376] C. Qi, X. Wang, and L. Wu, "Underwater acoustic channel estimation based on sparse recovery algorithms," *IET Signal Process.*, vol. 5, no. 8, pp. 739–747, 2011.

[377] S. Wright, R. Nowak, and M. A. T. Figueiredo, "Sparse reconstruction by separable approximation," *IEEE Trans. Signal Process.*, vol. 57, no. 7, pp. 2479–2493, 2009.

[378] S.-J. Kim, K. Koh, M. Lustig, S. Boyd, and D. Gorinevsky, "An interior-point method for large-scale l_1 -regularized least squares," *IEEE J. Sel. Topics Signal Process.*, vol. 1, no. 4, pp. 606–617, 2007.

[379] Z. He, A. Cichocki, A. Cichocki, R. Zdunek, and S. Xie, "Improved focuss method with conjugate gradient iterations," *IEEE Trans. Signal Process.*, vol. 57, no. 1, pp. 399–404, 2009.

[380] H. Zhu, G. Leus, and G. Giannakis, "Sparsity-cognizant total least-squares for perturbed compressive sampling," *IEEE Trans. Signal Process.*, vol. 59, no. 5, pp. 2002–2016, 2011.

[381] Y. Eldar and M. Mishali, "Robust recovery of signals from a structured union of subspaces," *IEEE Trans. Info. Th.*, vol. 55, no. 11, pp. 5302–5316, nov. 2009.

[382] S. Cotter, B. Rao, K. Engan, and K. Kreutz-Delgado, "Sparse solutions to linear inverse problems with multiple measurement vectors," *IEEE Trans. Signal Process.*, vol. 53, no. 7, pp. 2477–2488, 2005.

[383] D. Wipf and B. Rao, "An empirical bayesian strategy for solving the simultaneous sparse approximation problem," *IEEE Trans. Signal Process.*, vol. 55, no. 7, pp. 3704–3716, 2007.

[384] J. Romberg, "Compressive sensing by random convolution," *SIAM J. Imag. Sci.*, vol. 2, no. 4, p. 1098–1128, 2009.

[385] J. Tropp, J. Laska, M. Duarte, J. Romberg, and R. Baraniuk, "Beyond nyquist: Efficient sampling of sparse bandlimited signals," *IEEE Trans. Info. Th.*, vol. 56, no. 1, pp. 520–544, Jan. 2010.

[386] W. Wang, M. Wainwright, and K. Ramchandran, "Information-theoretic limits on sparse signal recovery: Dense versus sparse measurement matrices," *IEEE Trans. Info. Th.*, vol. 56, no. 6, pp. 2967–2979, 2010.

[387] A. Fletcher, S. Rangan, and V. Goyal, "Necessary and sufficient conditions for sparsity pattern recovery," *IEEE Trans. Info. Th.*, vol. 55, no. 12, pp. 5758–5772, 2009.

[388] Y. Jin and B. Rao, "Support recovery of sparse signals in the presence of multiple measurement vectors," *IEEE Trans. Info. Th.*, vol. 59, no. 5, pp. 3139–3157, May 2013.

[389] G. Reeves and M. Gastpar, "The sampling rate-distortion tradeoff for sparsity pattern recovery in compressed sensing," *IEEE Trans. Info. Th.*, vol. 58, no. 5, pp. 3065–3092, 2012.

[390] X. Yu and S. J. Baek, "Sufficient conditions on stable recovery of sparse signals with partial support information," *IEEE Signal Process. Letters*, vol. 20, no. 5, pp. 539–542, 2013.

[391] Z. Zhang and B. Rao, "Sparse signal recovery in the presence of correlated multiple measurement vectors," in *IEEE ICASSP*, March, pp. 3986–3989.

[392] B. Farhang-Boroujeny, "Filter bank spectrum sensing for cognitive radios," *IEEE Trans. Signal Process.*, vol. 56, no. 5, pp. 1801–1811, May 2008.

[393] S. K. Sharma, S. Chatzinotas and B. Ottersten, "Inline interference mitigation techniques for spectral coexistence of GEO and NGEO satellites," in *Int. J. Sat. Commun. and Networking*, Sep. 2014.

[394] G. Maral and M. Bousquet, *Satellite Communication Systems: systems, techniques and technology*, 5th ed. Wiley, 2009.

[395] W. Yong and H. Yihua, "UWB SATCOM towards cognitive radio," in *4th Int. Conf. WiCOM*, Oct. 2008, pp. 1–3.

[396] S. Singh and R. Ramola, "Physical layer technologies and challenges in mobile satellite communications," *ACEEE Int. J. Communication*, vol. 1, no. 3, pp. 28–32, Dec. 2010.

[397] S. Kim, H. W. Kim, K. Kang, and D. S. Ahn, "Performance enhancement in future mobile satellite broadcasting services," *IEEE Commun. Magazine*, vol. 46, no. 7, pp. 118–124, July 2008.

[398] E. Del Re, G. Gorni, L. Ronga, and R. Suffritti, "A power allocation strategy using game theory in cognitive radio networks," in *Int. Conf. Game Theory for Networks*, May 2009, pp. 117–123.

[399] M. Haddad, M. Debbah, and A. Hayar, "Distributed power allocation for cognitive radio," in *9th Int. Symp. Signal Process. and Its Applications*, Feb. 2007, pp. 1–4.

[400] E. D. Re and et al, "Power allocation strategy for cognitive radio terminals," in *First Int. Workshop Cognitive Radio and Advanced Spectrum Management*, , Feb. 2008, pp. 1–5.

[401] V. Deslandes, J. Tronc, and A.-L. Beylot, "Analysis of interference issues in integrated satellite and terrestrial mobile systems," in *5th ASMS/SPSC*, Sept. 2010, pp. 256–261.

[402] E. Del Re, G. Gorni, L. Ronga, and R. Suffritti, "Resource allocation in cognitive radio networks: A comparison between game theory based and heuristic approaches," *Wireless Personal Commun.*, vol. 49, pp. 375–390, 2009.

[403] ETSI, "Digital video broadcasting (DVB); framing structure, channel coding and modulation for satellite services to handheld devices (SH) below 3 GHz, Tech. Rep. EN 302 583, v 1.1.1, March 2008.

[404] Y. Fujino and et al, "Satellite terrestrial integrated mobile communication system as a disaster counter-measure," in *XXXth URSI General Assembly and Scientific Symp.*, Aug. 2011, pp. 1–4.

[405] H. Gam, D. Oh, and B. Ku, "Compatibility of integrated satellite systems with another satellite system operating in adjacent beam," in *World academy of Science, Engineering and Technol.*, vol. 71, Nov. 2010, pp. 1–11.

[406] C. Stallo and et al, "On the use of UWB radio interface for EHF satellite communications," in *IEEE Aerospace Conf.*, March 2010, pp. 1–11.

[407] Z. Guo-zhen, H. Bao-hua, and M. Jing, "One scheme of cooperative diversity with two satellites based on the alamouti code," in *IET 3rd Int. Conf. Wireless, Mobile and Multimedia Networks (ICWMNN)*, Sept. 2010, pp. 151–154.

[408] J. Xiao, F. Shaodong, L. Wei, Z. Gengxin, and Z. Guozhen, "Research on cooperative diversity in mobile satellite communication system," in *Second Int. Workshop on Education Technology and Computer Science (ETCS)*, vol. 1, March 2010, pp. 304–307.

[409] L. N. Wang and B. Wang, "Distributed power control for cognitive satellite networks," *Advanced Materials Research: Mechatronics and Intelligent Materials II*, vol. 71, pp. 1156–1160, March 2012.

[410] L. Bambace and D. Ceballos, "Sharing possibilities amongst CDMA mobile satellite systems, and impacts of terminal characteristics on sharing," *Acta Astronautica*, vol. 41, pp. 649–659, March 2012.

[411] M. Irfan and A. Qadir, "Spectrum sharing studies in C band between IMT 2000 (WIMAX) & satellite networks," in *IEEE 9th Malaysia Int. Conf. Commun. (MICC)*, Dec. 2009, pp. 497–500.

[412] P. Noschese, S. Porfili, and S. Di Girolamo, "ADS-B via Iridium NEXT satellites," in *Tyrrhenian Int. Workshop Digital Commun. - Enhanced Surveillance of Aircraft and Vehicles*, Sept. 2011, pp. 213–218.

[413] F. Vatalaro, G. Corazza, C. Caini, and C. Ferrarelli, "Analysis of LEO, MEO, and GEO global mobile satellite systems in the presence of interference and fading," *IEEE J. Sel. Areas Commun.*, vol. 13, no. 2, pp. 291–300, Feb. 1995.

[414] Comtech, "Optimizing satellite communications using DoubleTalk Carrier-in-Carrier & CDM-625 advanced satellite MODEM," online, Dec. 2010, comtech EF Data Corporation, Available online: <http://www.comtechefdata.com/files/>, Last access date: 10/11/2014.

[415] D3.2, "Corasat deliverable: Technology analysis and mapping," Available at <http://www.ict-corasat.eu>, 2014.

[416] S. Chatzinotas, S. K. Sharma, and B. Ottersten, "Asymptotic analysis of eigenvalue-based blind spectrum sensing techniques," in *IEEE ICASSP*, May 2013, pp. 4464–4468.

[417] S. Chatzinotas, S. K. Sharma, and B. Ottersten, "Multiantenna signal processing for cognitive communications," in *IEEE ChinaSIP*, July 2013, pp. 293–297.

[418] S. Chatzinotas, S. K. Sharma, and B. Ottersten, "Frequency packing for interference alignment-based cognitive dual satellite systems," in *Vehicular Technology Conference (VTC Fall), 2013 IEEE 78th*, Sept. 2013, pp. 1–7.

[419] S. K. Sharma, D. Christopoulos, S. Chatzinotas, and B. Ottersten, "New generation cooperative and cognitive dual satellite systems: Performance evaluation," in *32nd AIAA ICSSC*, Aug. 2014.

[420] S. K. Sharma, S. Chatzinotas, and B. Ottersten, "Inline interference mitigation techniques for spectral coexistence of GEO and NGEO satellites," in *31st AIAA Int. Commun. Satellite Systems Conf. (ICSSC)*, Oct. 2013, pp. 1–12.

[421] M. Weiss and C. Liu, "Spectrum trading with interference rights," in *7th Int. Conf. CROWNCOM*, June 2012, pp. 135–140.

[422] ITU, "Radio spectrum management for a converging world," in *Workshop on Radio Spectrum Management for a Converging World*, Feb. 2004.

[423] J. Christensen, "ITU regulations for Ka-band satellite networks," Available online: <http://www.itu.int/md/> Last accessed date: 19/05/2014.

[424] ETSI, "Why we need standards," online, available online: <http://www.etsi.org/standards>, Access date: 10/10/2014.

[425] S. K. Sharma, S. Chatzinotas, and B. Ottersten, "Exploiting polarization for spectrum awareness in cognitive satellite communications," in *Software-Defined and Cognitive Radio Technologies for Dynamic Spectrum Access and Management*, N. Kaabouch and W.-C. Hu, Eds. IGI Global, 2014, to appear.

[426] FCC, "Unlicensed operation in the TV broadcast bands," ET Docket No. 04-186, Sept. 2010.

[427] S. Chatzinotas, G. Zheng, and B. Ottersten, "Joint precoding with flexible power constraints in multibeam satellite systems," in *IEEE GLOBECOM*, Dec. 2011, pp. 1–5.

[428] M. Diaz, N. Courville, C. Mosquera, G. Liva, and G. Corazza, "Non-linear interference mitigation for broadband multimedia satellite systems," in *Int. Workshop Satellite and Space Commun.*, Sept. 2007, pp. 61–65.

[429] A. Mohamed, M. Lopez-Benitez, and B. Evans, "Frequency sharing between Ka-band satellite and terrestrial systems," in *20th Ka band Conference*, Oct. 2014.

[430] W. Perkins, "FCC interference temperature gives licensees a fever," online, <http://www.avw.co.nz/catalogue/images/andrew/docs/TP-100323-EN.pdf>.

[431] ITU-R, "Radio regulations," ITU-R Article 21, Tech. Rep., 2004.

[432] E. Alerty and et al, "Adaptive coding and modulation for the DVB-S2 standard interactive applications: Capacity assessment and key system issues," *IEEE Wireless Commun.*, vol. 14, no. 4, pp. 61–69, August 2007.

[433] J. D. Kraus and R. J. Marhefka, *Antennas for all applications*. McGraw-Hill, 2001.

[434] R. Nabar, H. Bolcskei, V. Erceg, D. Gesbert, and A. Paulraj, "Performance of multiantenna signaling techniques in the presence of polarization diversity," *IEEE Trans. Signal Process.*, vol. 50, no. 10, pp. 2553–2562, Oct 2002.

[435] W. Lee and Y. Yeh, "Polarization diversity system for mobile radio," *IEEE Trans. Commun.*, vol. 20, no. 5, pp. 912 – 923, Oct. 1972.

[436] B. Lindmark and M. Nilsson, "On the available diversity gain from different dual-polarized antennas," *IEEE J. Sel. Areas Commun.*, vol. 19, no. 2, pp. 287–294, Feb. 2001.

[437] H. Urkowitz, "Energy detection of unknown deterministic signals," *Proc. IEEE*, vol. 55, no. 4, pp. 523–531, April 1967.

[438] R. K. Sharma and J. W. Wallace, "Analysis of fusion and combining for wireless source detection," in *Int. ITG workshop on Smart Antennas-WSA*, Feb. 2009.

[439] D. Roddy, *Satellite Communications*, 4th ed. McGraw-Hill, 2006.

[440] A. Nuttall, "Some integrals involving the function (corresp.)," *IEEE Trans. Inf. Th.*, vol. 21, no. 1, pp. 95–96, Jan. 1975.

[441] H. Sarvanko, M. Hoyhtya, M. Matinmikko, and A. Mammela, "Exploiting spatial dimension in cognitive radios and networks," in *6th Int. Conf. CROWNCOM*, June 2011, pp. 360–364.

[442] J. Xie, Z. Fu, and H. Xian, "Spectrum sensing based on estimation of direction of arrival," in *Int. Conf. on Computational Problem-Solving (ICCP)*, Dec. 2010, pp. 39–42.

[443] E. Tsakalaki, D. Wilcox, E. Carvalho, C. Papadias, and T. Ratnarajah, "Spectrum sensing using single-radio switched-beam antenna systems," in *7th Int. Conf. CROWNCOM*, June 2012.

[444] F. Rashid-Farrokhi, K. Liu, and L. Tassiulas, "Transmit beamforming and power control for cellular wireless systems," *IEEE J. Sel. Areas Commun.*, vol. 16, no. 8, pp. 1437–1450, Oct. 1998.

[445] V. Katkovnik, M.-S. Lee, and Y.-H. Kim, "Performance study of the minimax robust phased array for wireless communications," *IEEE Trans. Commun.*, vol. 54, no. 4, pp. 608–613, April 2006.

[446] E. Santos, M. Zoltowski, and M. Rangaswamy, "Indirect dominant mode rejection: A solution to low sample support beamforming," *IEEE Trans. Signal Process.*, vol. 55, no. 7, pp. 3283–3293, July 2007.

[447] R. Lorenz and S. Boyd, "Robust minimum variance beamforming," *IEEE Trans. Signal Process.*, vol. 53, no. 5, pp. 1684–1696, May 2005.

[448] D. Filho, C. Cavalcante, J. Romano, and L. Resende, "An LCMV-based approach for downlink beamforming in fdd systems in presence of angular spread," in *Proc. EUSIPCO*, June 2002.

[449] B. Chalise, L. Haering, and A. Czylwik, "Robust uplink to downlink spatial covariance matrix transformation for downlink beamforming," in *IEEE ICC*, vol. 5, June 2004, pp. 3010–3014 Vol.5.

[450] W. Zhi, Y.-C. Liang, and M. Y. W. Chia, "Robust transmit beamforming in cognitive radio networks," in *IEEE Singapore Int. Conf. Commun. Systems*, Nov. 2008, pp. 232–236.

[451] M. Grant, S. Boyd, and Y. Ye, "CVX: Matlab software for disciplined convex programming," online, Nov. 2007, www.stanford.edu/~boyd/cvx.

[452] C. Geng, N. Naderializadeh, A. Avestimehr, and S. Jafar, "On the optimality of treating interference as noise," in *51st Annual Allerton Conference on Communication, Control, and Computing*, Oct 2013, pp. 1166–1173.

[453] H. Weingarten, Y. Steinberg, and S. Shamai, "The capacity region of the Gaussian multiple-input multiple-output broadcast channel," *IEEE Trans. Info. Th.*, vol. 52, no. 9, pp. 3936–3964, 2006.

[454] M. L. Moher, "Multiuser decoding for multibeam systems," *IEEE Trans. Veh. Technol.*, vol. 49, no. 4, pp. 1226–1234, July 2000.

[455] D. Christopoulos, S. Chatzinotas, M. Matthaiou, and B. Ottersten, "Capacity analysis of multibeam joint decoding over composite satellite channels," in *Forty Fifth Asilomar Conference on Signals, Systems and Computers*, Nov. 2011, pp. 1795–1799.

[456] D. Christopoulos, S. Chatzinotas, G. Zheng, J. Grotz, and B. Ottersten, "Linear and nonlinear techniques for multibeam joint processing in satellite communications," *EURASIP J. Wireless Commun. and Networking*, vol. 2012, no. 162, 2012.

[457] M. Debbah and et al, "Interference mitigation for the reverse-link of interactive satellite networks," in *9th Int. Workshop signal process. for space commun.*, 2006.

[458] N. Letzepis and A. Grant, "Capacity of the multiple spot beam satellite channel with rician fading," *IEEE Trans. Info. Th.*, vol. 54, no. 11, pp. 5210–5222, Nov. 2008.

[459] M. Diaz, N. Courville, C. Mosquera, G. Liva, and G. Corazza, “Non-linear interference mitigation for broadband multimedia satellite systems,” in *Int. Workshop on Satellite and Space Commun.*, Sept. 2007, pp. 61–65.

[460] A. Lozano and A. Tulino, “Capacity of multiple-transmit multiple-receive antenna architectures,” *IEEE Trans. Info. Th.*, vol. 48, no. 12, pp. 3117–3128, Dec. 2002.

[461] R. Blum, “MIMO capacity with interference,” *IEEE J. Sel. Areas Commun.*, vol. 21, no. 5, pp. 793–801, June 2003.

[462] S. Scalise and et al, “Integral satcom initiative european technology platform strategic research and innovation agenda-edition 2011,” Seventh Framework Programme (FP), 2011, available online: www.isi-initiative.org.

[463] Y. Demers and et al, “Very large reflectors for multibeam antenna missions,” Available online: <http://www.northropgrumman.com/BusinessVentures/AstroAerospace/Pages/TechnicalPapers/>, 2009.

[464] M. Schneider, C. Hartwanger, and H. Wolf, “Antennas for multiple spot beam satellites,” *CEAS Space Journal*, vol. 2, no. 1, pp. 59–66, Dec. 2011.

[465] S. Yun and et al, “Multibeam reflector antenna fed by few elements for Ka-band communication satellite,” in *Int. Symp. Antennas and Propagation Society*, July 2012, pp. 8–14.

[466] O. Kilic and A. I. Zaghloul, “Antenna aperture size reduction using subbeam concept in multiple spot beam cellular satellite systems,” *Radio Science*, vol. 44, no. 1, Jan. 2009.

[467] O. Kilic and A. I. Zaghloul, *Satellite Communications*. InTechOpen, 2010, ch. Interference in Cellular Satellite Systems, pp. 299–322.

[468] E. Dall’Anese, S.-J. Kim, G. Giannakis, and S. Pupolin, “Power control for cognitive radio networks under channel uncertainty,” *IEEE Trans. Wireless Commun.*, vol. 10, no. 10, pp. 3541–3551, Oct. 2011.

[469] G. Zhao, G. Li, and C. Yang, “Proactive detection of spectrum opportunities in primary systems with power control,” *IEEE Trans. Wireless Commun.*, vol. 8, no. 9, pp. 4815–4823, Sept. 2009.

[470] A. Destounis and A. Panagopoulos, “Dynamic power allocation for broadband multi-beam satellite communication networks,” *IEEE Commun. Letters*, vol. 15, no. 4, pp. 380–382, April 2011.

[471] R. Rinaldo and R. D. Gaudenzi, “Capacity analysis and system optimization for the forward link of multi-beam satellite broadband systems exploiting adaptive coding and modulation,” *Int. J. Sat. Commun., and Networking*, vol. 2004, no. 22, pp. 401–423, 2004.

[472] A. Paul and et al, “Interference protection criteria, phase 1-compilation from existing sources,” Available online, url: <http://www.ntia.doc.gov/files/ntia/publications/>, 2005.

[473] A. J. Poelman, “Virtual polarisation adaptation a method of increasing the detection capability of a radar system through polarisation-vector processing,” *IEEE Commun., Radar and Signal Process.*, vol. 128, no. 5, pp. 261–270, Oct. 1981.

[474] F. Liu and et al, “Virtual polarization detection: A vector signal sensing method for cognitive radios,” in *IEEE Veh. Technol. Conf. (Spring)*, May 2010, pp. 1–5.

[475] F. Liu and et al, “Polarization spectrum sensing scheme for cognitive radios,” in *5th Int. Conf. Wireless Commun., Networking and Mobile Comput.*, Sept. 2009, pp. 1–4.

[476] D. Wei and et al, “A SINR improving scheme based on optimal polarization receiving for the cognitive radios,” in *IEEE Int. Conf. Network Infrastructure and Digital Content*, Nov. 2009, pp. 100–104.

[477] D. Stapor, “Optimal receive antenna polarization in the presence of interference and noise,” *IEEE Trans. Antennas and Propag.*, vol. 43, no. 5, pp. 473–477, May 1995.

[478] S. K. Sharma, S. Maleki, S. Chatzinotas, J. Grotz, J. Krause, and B. Ottersten, “Joint carrier allocation and beamforming for cognitive SatComs in Ka-band (17.3 – 18.1 GHz),” submitted to *Int. Conf. Communications*, 2015.

[479] ESA, “Antennas and signal processing techniques for interference mitigation in next generation Ka band high throughput satellites,” ESA tender no. A07821, 2014.

[480] T. S. Rappaport and et al, “Millimeter wave mobile communications for 5G cellular: It will work!” *IEEE Access*, vol. 1, pp. 335–349, 2013.

- [481] B. Edwards and D. Israel, "A geosynchronous orbit optical communications relay architecture," in *IEEE Aerospace Conference*, March 2014, pp. 1–7.
- [482] Z. Abidin, P. Xiao, M. Amin, and V. Fusco, "Circular polarization modulation for digital communication systems," in *Int. Symp. on Commun. Systems, Networks Digital Signal Process. (CSNDSP)*, July 2012, pp. 1–6.
- [483] S. K. Sharma, M. Patwary, and M. Abdel-Maguid, "Spectral efficient compressive transmission framework for wireless communication systems," *IET Signal Processing*, vol. 7, no. 7, pp. 558–564, Sep. 2013.
- [484] T. T. Do, G. Lu, N. H. Nguyen, and T. D. Tran, "Fast and efficient compressive sensing using structurally random matrices," *IEEE Trans. Signal Process.*, vol. 60, no. 1, pp. 139–154, Jan. 2012.
- [485] G. Kizer, *Digital Microwave Communication*, John Wiley & Sons Inc., New Jersey, 2013.
- [486] S. Choi, A. Cichocki, H. Park, and S. Lee, "Blind source separation and independent component analysis: A review," *Neural Information Processing - Letters and Reviews*, vol. 6, no. 1, pp. 1–57, 2005.
- [487] B. Nosrat-Makouei, J. Andrews, and R. Heath, "MIMO interference alignment over correlated channels with imperfect CSI," *IEEE Trans. Signal Process.*, vol. 59, no. 6, pp. 2783 –2794, June 2011.